Extruder Principles and Operation

Extruder Principles and Operation

Second edition

M. J. Stevens

Formerly, Institute of Polymer Technology
Loughborough University of Technology, UK

and

J. A. Covas

Department of Polymer Engineering
University of Minho, Braga, Portugal



SPRINGER-SCIENCE+BUSINESS MEDIA, B.V.

First editon 1985

Second edition 1995

© 1995 Springer Science+Business Media Dordrecht
Originally published Chapman & Hall in 1995
Softcover reprint of the hardcover 2nd edition 1995

Typeset in 10/12 pt Times by Thomson Press (I) Ltd., New Delhi, India

ISBN 978-94-010-4247-5 ISBN 978-94-011-0557-6 (eBook)
DOI 10.1007/978-94-011-0557-6

Apart from any fair dealing for the purposes of research or private study, or criticism or review, as permitted under the UK Copyright Designs and Patents Act, 1988, this publication may not be reproduced, stored, or transmitted, in any form or by any means, without the prior permission in writing of the publishers, or in the case of reprographic reproduction only in accordance with the terms of the licences issued by the Copyright Licensing Agency in the UK, or in accordance with the terms of licences issued by the appropriate Reproduction Rights Organization outside the UK. Enquiries concerning reproduction outside the terms stated here should be sent to the publishers at the London address printed on this page.

The publisher makes no representation, express or implied, with regard to the accuracy of the information contained in this book and cannot accept any legal responsibility or liability for any errors or omissions that may be made.

A catalogue record for this book is available from the British Library

Library of Congress Catalog Card Number: 95-68494



Printed on acid-free text paper, manufactured in accordance with ANSI/NISO Z39.48-1992 (Permanence of Paper).

Contents

Preface ix
Acknowledgements xi

1 Introduction **1**
1.1 Scope and limitations 1
1.2 Method 2

2 Practical extrusion processes and their requirements **4**
2.1 Shaping processes and their requirements 6
2.2 Other applications and their requirements 19

3 Flow behaviour relevant to extrusion **27**
3.1 Viscosity 27
3.2 Shear flow 33
3.3 Extensional flow 47
3.4 Elastic effects 48
3.5 Measurement of viscosity and elasticity 51

4 Thermal and energy properties in processing **54**
4.1 Thermal properties 54
4.2 Thermal conduction 56
4.3 Non-isothermal flow and heat transfer 59
4.4 Mixing 62

5 Extrusion dies **65**
J. A. Covas
5.1 Introduction 65
5.2 Factors influencing the performance of an extrusion die 67
5.3 Extrusion dies for some profiles 77
5.4 General principles of die design 91
5.5 Specific aspects of die design 103
5.6 Operational strategies for problem-solving 119

6 Principles of melt flow in single-screw extruders **127**
6.1 Functions of the extruder 127
6.2 Derivation of flow equation 129
6.3 Leakage flow 140
6.4 Output equations and longitudinal pressure profiles for common screw types 142
6.5 Graphical representation of output for screw/die combinations, including venting 151
6.6 Output corrections 164
6.7 Pseudoplastic flow 167
6.8 Non-isothermal flow 173

7 Solids conveying and melting in single-screw extruders **175**
J. A. Covas
7.1 The relevance of solids conveying and melting 175
7.2 Phenomenological description of solids conveying and melting 179
7.3 Theoretical analysis 189

8 Principles of energy balance **225**
8.1 Energy balance and efficiency 225
8.2 Power consumption in the screw: Newtonian isothermal case 229
8.3 Pseudoplastic isothermal approximation 235
8.4 Power in non-isothermal flow 236
8.5 Effect of variables on energy balance 251

9 Operation of single-screw extruders **270**
9.1 Overall performance of the screw 270
9.2 Effects of controlled variables 282
9.3 Polymer properties 288
9.4 Screw design 291
9.5 Operational strategies 295

10 Twin-screw extruders **316**
10.1 Non-intermeshing screws 318
10.2 Partial intermeshing 320
10.3 Full intermeshing: counterrotation 323
10.4 Full intermeshing: corotation 330
10.5 Comparison of machine types 348

11 Extruder operation as part of a total process **352**
11.1 Quality 352
11.2 Stability 359

11.3 Shear history 364
11.4 Control 366
11.5 Scale-up 376

12 Practical extruder operation 384
12.1 Steady operation 384
12.2 Colour and grade changing 387
12.3 Start-up and shut-down 389
12.4 Dismantling and cleaning 392
12.5 Waste recovery 397

13 Application to the individual machine 399

Appendices 405
A Properties of polymers for heat and flow 405
B Derivations of flow and pressure 413
B.1 Alternative derivation of flow equation 413
B.2 Estimation of leakage flows 415
B.3 Longitudinal pressure profiles 418
B.4 Pressure gradients in a stepped screw 420
B.5 Further examples of Q–P diagrams 423
C Energy consumption and energy balance 427
C.1 Experimental determination of energy balance 427
C.2 Derivation of power absorbed in screw 435
C.3 Heat flows in melt pumping section 438
C.4 Distribution of shear heating and transverse circulation 450
C.5 Temperature variation in the flight clearance 458
D Stability of melt pumping section 467

E List of tables 469
References 471

Index 475

Preface

This book is intended to fill a gap between the theoretical studies and the practical experience of the processor in the extrusion of thermoplastic polymers. The former have provided a basis for numerical design of extruders and their components, but generally give scant attention to the practical performance, especially to the conflict between production rate and product quality. In practice extruders are frequently purchased to perform a range of duties; even so, the operator may have to use a machine designed for another purpose and not necessarily suitable for the polymer, process or product in hand. The operator's experience enables him to make good product in unpromising circumstances, but a large number of variables and interactions often give apparently contradictory results. The hope is that this book will provide a logical background, based on both theory and experience, which will help the industrial processor to obtain the best performance from his equipment, to recognize its limitations, and to face new problems with confidence. Mathematics is used only to the extent that it clarifies effects which cannot easily be expressed in words; if it is passed over, at least a qualitative understanding should remain. The approximate theory will not satisfy the purist, but this seems to the authors less important than a clear representation of the physical mechanisms on which so much of the polymer processing industry depends.

M. J. STEVENS
J. A. COVAS

Acknowledgements

The authors are responsible for statements and opinions expressed in this book, which are their own, but would like gratefully to acknowledge the assistance over many years from the staff of the Institute of Polymer Technology, Loughborough University of Technology and, respectively, from Imperial Chemical Industries PLC, Petrochemicals and Plastics Division and the staff of the Department of Polymer Engineering, University of Minho, Braga, Portugal.

The contributions of O. S. Carneiro and A. G. Cunha who, during their research projects, obtained some of the information presented in Chapters 5 and 7, are also gratefully acknowledged.

Introduction

1

1.1 SCOPE AND LIMITATIONS

The objective of this book is to summarize the principles of screw extrusion processes for plastics and rubbers, the practical performance and its theoretical explanation, and operating procedures to exploit this performance. Unlike design, the latter are not well covered in existing literature. This book aims to make an original contribution to effective practical operation and so does not attempt comprehensively to review the literature, but only to refer to those works which contribute to an understanding of operation.

The scope of the work includes the principles and operation of the screw extruder as a machine, as a combination with a die, and as part of a total fabrication process, including subsidiary functions such as compounding and venting. It includes the special requirements for the extruder of individual processes such as wire covering, tubular film blowing and blow moulding, but does not attempt to cover other aspects of these processes. In order that the objective may be adequately covered in a book of reasonable size, certain matters are excluded, and the reader's attention is directed to the references at the back of the book for further information. In particular, the mechanical construction and adaptation for special purposes of screw extruders is governed partly by the process requirements described in Chapter 2, but also by standardization, manufacturing methods and mechanical reliability. Mechanical construction is dealt with in Chapter 6 of Fisher (1976) and Chapter 6 of Schenkel (1966). Commercial models and unconventional types of extruder are also covered by Fisher and Schenkel, as well as by periodic reviews such as *Plastics and Rubber Weekly**. As this book is primarily concerned with operation, it does not purport to be a manual for the precise dimensional design of machine, screw or die for a specific performance. This is covered by several authors, including Fenner (1970).

**Plastics and Rubber Weekly*, Maclaren and Sons Ltd, London.

1.2 METHOD

First a number of practical extrusion processes are described in outline, together with the requirements they impose on the extruder and die. The relevant general equations of mass and heat flow are then presented and their application to extrusion problems developed. The significance is explained of the properties of plastics and rubber materials suitable for extrusion, especially the flow and thermal properties of polymer melts. Then the flow equations are developed for the design and operation of dies. A simplified extrusion theory is developed for both mass flow and energy consumption in single-screw machines and presented in both algebraic and graphical form to demonstrate the effects of dimensional and operational variables on output, energy balance, melt temperature and product uniformity. These effects are used to propose strategies for operation to optimize the performance of the extruder. The general principles and operation of twin-screw extruders are then briefly described. A discussion follows on the operation of the extruder and control to eliminate faults in the total system. In particular, the problem of scaling up an extrusion process from the development laboratory to large-scale production is studied. Although the simplified theory is approximate, its predictions are largely borne out in practice. It is used in preference to more exact methods since the algebraic form of the solutions permits a ready identification and understanding of the effects of separate variables on extruder and die performance; this tends to be obscured in the more exact methods, which usually involve digital computation.

As a complement to the analysis of steady-state operation, recommendations for start-up, shut-down, dismantling and cleaning are given, based on practical experience.

The total commercial process of extrusion of plastics and rubbers covers the conversion of a raw polymer, usually in the form of powder or pellets, into a saleable finished or semi-finished product. This will include matters of management and plant organization common to many other materials and processes. It will also include polymer handling and storage, product specification and quality control, plant layout, installation and maintenance, product finishing, assembly, packing and distribution, all of which are general to many plastics processes and only indirectly concerned with the actual operation of extrusion. The intention of this volume is to provide the specific requirements of extrusion, and their explanations, which form the technical background to the total process and its peripheral aspects.

In its simplest terms, extrusion consists of forcing a polymer in liquid form (usually molten) under pressure through a die to produce a continuous section or profile. This may then be sized, drawn down, corrugated, etc., to modify and control the shape and dimensions of the section and in some cases the properties (mechanical, optical, etc.). In the case of thermoplastics, the product or **extrudate** must be cooled to retain its shape, while rubbers are

chemically cross-linked (**cured**) to achieve properties such as elasticity and resistance to chemicals and heat. In some processes, e.g. blow moulding, injection moulding and in-line vacuum forming, the extrudate may be shaped into a discontinuous or intermittent form before cooling or curing. Other subsidiary processes, such as printing, slitting and on-line testing, may precede coiling or cutting into handleable lengths. The detail of these operations after the die (collectively **post-forming**) is highly specific to the material and product, much of it confidential to each company, so space precludes exhaustive study here. However, it is just as important as the extruder to the 'quality', dimensions and surface finish of the product; an understanding of the effects of, say, the ratio of haul-off rate to extruder output is essential to economic production. The effects of changes after the die are usually visible, if not self-evident, but one cannot see what is going on inside the extruder, and this book aims to provide the basic mechanisms which help to explain the performance of the screw(s) and die, and hence their interactions with post-forming operations. The book also introduces strategies for operation (Chapters 9 and 10) and control (Chapter 11), as well as some practical experience on selection of screws, start-up, cleaning and fault-finding (Chapters 11 and 12).

An important subject for development engineers is the prediction of the performance of full-scale production plant from that of a small laboratory process, since by its nature heavy moving machinery is expensive to modify or replace and, owing to special materials and manufacture, changes cause lengthy and costly production delays; this is given special attention. Literature references are given at the end of the book in alphabetical order. Mathematical equations are numbered in order of appearance, separately for each chapter and appendix. SI units are used throughout, with c.g.s. or f.p.s. units in brackets where appropriate. Unless otherwise stated, numerical constants are dimensionless, and therefore the same in any consistent system of units.

2 Practical extrusion processes and their requirements

This chapter makes a brief survey of the common applications of screw extruders. It also attempts an explanation of why the requirements of these applications differ, at least in degree, so that when the implications of the general theory in Chapters 5–10 are applied to practice in Chapter 11, it is clear why different materials, processes and products may require different operational and control strategies. These requirements must necessarily be stated in qualitative terms, and users will no doubt be able to give examples where practice appears to contradict statements made here; the author's hope is that the deductions in later chapters will be helpful in the majority of cases and in the remainder will provide a guide to the correct methods and criteria, based on sound analysis.

The single-screw extruder is primarily a drag pump, suitable for working with highly viscous fluids and capable of operation at the high pressures and temperatures consequently required for processing high molecular weight polymers in their thermoplastic state. As explained in section 6.2, the drag mechanism leads to an output which is more or less influenced by back pressure, and section 8.5 shows that this also leads to changes in energy balance, so the interdependence of variables is a vital aspect of performance. The single-screw machine is also mechanically simple and robust, permitting high-energy inputs at relatively low speeds.The usual screw configuration, having 20 or more turns with a pitch similar to screw diameter, gives a long slender machine in which substantial longitudinal temperature gradients can be maintained and controlled, and an appreciable residence time permitting a degree of end-to-end mixing. In addition to this distributive mixing, high shear stresses, especially over the flight tip, give a degree of dispersive mixing for breaking up solid agglomerates, e.g. pigments. As explained in section 6.2, the complex flow within a relatively narrow channel leads to side-to-side mixing and a fair uniformity of composition and temperature. Coincidentally, the single screw is also an effective conveyor of particulate solids, at approximately the rate required by the melt section, so that gravity feeding is usually sufficient.

The drag mechanism also causes internal shearing of the viscous material being pumped, leading to additional power consumption and temperature rise in the polymer. This inefficiency as a pump may be utilized beneficially by assisting external heating in melting the polymer and in heating it internally rather than by conduction, with consequent reduction of internal temperature gradients. The single-screw extruder may be used as a continuous stirred reactor for highly viscous materials, e.g. polymerization and intentional degradation, though differing viscosities of components and products may lead to slip and pumping problems. The end-to-end mixing mentioned previously may also lead to a wide distribution of residence times, undesirable in chemical reaction.

In contrast, the twin-screw extruder (Chapter 10) has a much narrower distribution of residence times and is less sensitive to slip, making this type more suitable for reaction processes and dissimilar viscosities. It approaches more nearly a positive-displacement action, largely independent of back pressure for both output and energy balance. Unlike the single-screw machine,

Table 2.1 Thermoplastics used in extrusion

Abbreviation	*Base polymer*
	AMORPHOUS
ABS	acrylonitrile-butadiene-styrene
PMMA	polymethylmethacrylate
CAB	cellulose acetate butyrate
PC	polycarbonate
PS	polystyrene
PVAC	polyvinyl acetate
PVAL	polyvinyl alcohol
SAN	styrene-acrylonitrile
UPVC	unplasticized (rigid) polyvinyl chloride
PPVC	plasticized (flexible) polyvinyl chloride
HIPS	high impact polystyrene (rubber-toughened)
	SEMI-CRYSTALLINE
POM	polyoxymethylene; polyformaldehyde (polyacetal)
EVAC	ethylene vinyl acetate copolymer
PA	polyamide (nylon)
PETP	polyethylene terephthalate (saturated polyester)
PBTP	polybutylene terephthalate
LDPE	low density polyethylene
LLDPE	linear low density polyethylene
HDPE	high density polyethylene
PP	polypropylene (homo- and copolymers)
PEEK	polyether ether ketone
PTFE	polytetrafluoroethylene (ram extrusion only)

Based on BS 3502: Pt 1 (1978), with additions.

in the twin-screw extruder mixing, both distributive and dispersive, takes place largely in the various clearance gaps. Internal shearing in the screw channels is also less, leading to lower mechanical power inputs, and the polymer is melted more by heat conduction through the barrel wall.

The extruder performs a number of other functions, and these are used either principally or incidentally in a wide range of specialized applications. The extruder is essentially suitable for continuous operation; however, it is widely used in many blow moulding machines and most injection moulding machines on an intermittent basis. It performs surprisingly well in this mode, though factors addtional to those presented in this book must be taken into account; the former are not readily represented in analytical terms.

The screw extruder is thus highly suitable for continuously processing a wide range of synthetic thermoplastic polymers into an equally wide range of finished or semi-finished products. Table 2.1 lists the principal thermoplastics used in extrusion, together with the standard abbreviations. A large number of 'specialty' polymers are extruded for specific applications; these include some fluoropolymers, but PTFE is usually ram extruded because of volume changes and decomposition at high temperatures and extremely high viscosity at lower temperatures. In addition, many raw and unvulcanized rubbers are processed on screw extruders and in special cases, e.g. injection and dough moulding, linear prepolymers of phenolic and polyester thermosetting polymers are successfully handled. The true thermoplastics are often processed, either precompounded with stabilizers, fillers, plasticizers, pigments, processing lubricants, fire-retardants, etc., or these additives are incorporated within the extruder as part of the shaping process. When required in a final cross-linked form (e.g. HDPE by radiation), this is usually by a process following the extrusion operation. Rubbers and thermosets are usually precompounded with cross-linking (vulcanizing) agents as well as fillers, pigments, etc., so that heating in the extruder commences the cross-linking reaction; it is then a matter of controlling temperature, residence time, etc., so that the material remains sufficiently thermoplastic in the extruder and die, while cross-linking is completed in subsequent operations.

2.1 SHAPING PROCESSES AND THEIR REQUIREMENTS

2.1.1 Solid sections

The first of the shaping processes is for solid sections, e.g. rod, strip, profiles and sections. These are used as stock for subsequent machining, gaskets, structural sections (angles, channels, etc.), rainwater guttering, curtain rail, lighting diffusers and many other purposes. Shaping is principally by the melt die, in which uniform flow rate and uniform die swell (elastic recovery) are pre-eminent. This involves uniform melt and metal temperatures, and control of

land length and shear history. Drawdown, if any, is usually no more than to the extent of negativing die swell, and cooling is usually in air or waterbath while supported on a band conveyor or rollers. Sizing is usually only for fine control of shape or dimensions and is frequently omitted. Elastic memory in the polymer and flow patterns in the die may give rise to twisting or lengthwise curling, and attempts to remove these by guides or tension, rather than by correcting the cause, will usually distort the shape and/or dimensions, or give residual stress which may cause distortion in service. Except for small and simple sections, which if flexible may be coiled, these products are usually stored and transported in cut straight lengths.

2.1.2 Hollow sections

These include circular tube and pipe, square tube for racking and light furniture, and complex hollow sections such as window framing, in some cases incorporating metal sections which are sheathed during extrusion (Fig. 2.1). Applications for tube and pipe include medical, food, chemical, hydraulic, gas and water distribution, effluent and drainage, and conduit and sleeving, e.g. for electrical and telephone cables. Sizes range from medical tubing less than 1 mm in diameter to water and drainage pipe 600 mm in diameter. The die cores or mandrels forming the internal shape may be supported on a 'spider' which divides the flow, or at the rear of a crosshead or side-entry die. Note that this also carries the thrust due to the drag of the polymer on the core. Complex sections involve difficulties in achieving uniform flow and avoiding distortion due to non-uniform elastic strain and thermal contraction. In this case, as with open sections, drawdown will be a minimum to control die swell. However, with symmetrical sections, especially circular tube, drawdown does not distort the section, but reduces both diameter and thickness. It is often used for small diameters, permitting a larger die with lower resistance and higher throughput. Sizing during cooling is almost universal, fixing *either* the internal or external diameter. The dimensions of the (melt) die and the relation between output and haul-off rate then determine the final thickness and consequently the other (external or internal) diameter. Precise internal diameter is required for metering and sliding seals, e.g. in disposable hypodermics and beer pumps, and precise external diameter is required for use with injection moulded fittings in compression and solvent jointing. In larger pressure pipes, e.g. for gas and water distribution, internal surface finish may also be important in minimizing crack initiation and, in chemical applications, to reduce environmental stress cracking. In both cases residual stress in the pipe should be minimized. With large pipes, say over 300 mm in diameter, the linear speed during extrusion tends to be low unless a very large extruder is used, and consequently the time for thermal degradation in the die is large. If this is minimized, e.g. with UPVC, by reducing die length, then rapid changes of cross-section occur leading to

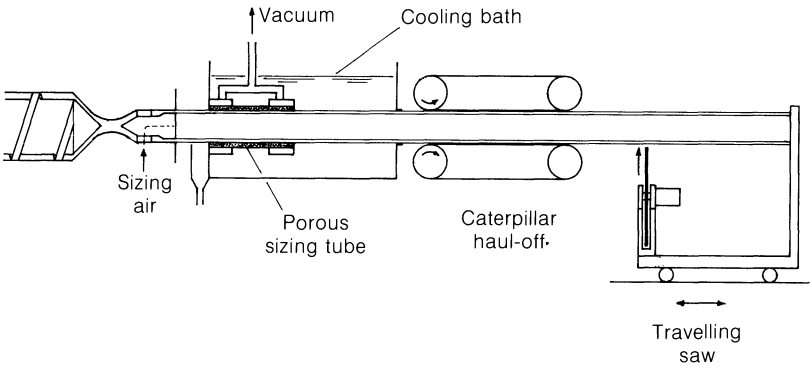


Figure 2.1 Tube extrusion.

residual stress, excessive die swell and transverse orientation of the polymer, instead of the normal longitudinal orientation which tends to occur, especially at low extrusion temperatures. Sizing may be by one or more sizing plates, by internal pressure (through the die spider) against a lubricated sizing tube or by external vacuum on a porous or perforated sizing tube. Since sizing must be accompanied by cooling, the former usually occurs while the product is submerged in a waterbath. Wherever possible, tubes are coiled in lengths of 30 m or more to reduce subsequent jointing. Large rigid pipes are cut in straight lengths up to 20 m long, depending on transport facilities.

Die adjustment, to achieve concentricity and uniform wall thickness in tube, is discussed in Chapter 5. Such adjustment should only be used for fine control, since substantial circumferential variations, e.g. in die gap or land length, are likely to lead to non-axial flow and non-uniform swelling, and possibly to lateral pressure differences on the die mandrel, which distorts, tending to negative the adjustment. In such cases, the cause of non-uniform flow or viscosity from the extruder should be corrected. As with the choker bars used for flat sheet dies (p. 83), a restrictor ring with a narrow annular gap may also be used well before the die lips to remove uneven flow inherent in the design of the die or adaptor. Low velocities in the die may be used to give good surface finish and low residual strain (and swelling). The consequent low resistance permits use of long die lips, which also promotes good surface and low swelling; even so, pressure may be too low for adequate melting and mixing in the extruder, and screen packs may be added to increase the back pressure.

Corrugated tube may be produced in line by a shaping operation following or in place of sizing and during cooling. Reinforced tube may be extruded by passing the reinforcement through the die and extruding around it, as in wire covering, or by plaiting or winding the reinforcement on to the cooled lining tube. Further polymer (possibly of different composition) may then be wrapped or extruded over the assembly. The former, integrated process uses die pressure to force the polymer into intimate contact with the reinforcement

but places limitations on the type and arrangement of reinforcement and the use of layers of different polymers.

2.1.3 Wire covering

In wire covering, which includes both electrical insulation and sheathing of cables for protection, the wire or assembly of insulated cores is pulled by the haul-off through the die, usually of the crosshead type (Fig. 2.2), where the polymer is forced round it by die pressure and into intimate contact before leaving the die lips. The polymer coating is drawn along by the wire and the thickness of the coating depends on the balance between polymer flow rate and wire speed. A typical 'single' may consist of a copper conductor 0.45 mm in diameter with an insulating covering of LD polyethylene 0.22 mm thick, and extrusion rates in excess of 1500 m min^{-1} have been reported. One limitation is the tension in the conductor, which may cause cold drawing and loss of accuracy; the other is melt fracture of the polymer causing a rough or distorted surface of poor appearance and liable to give problems in subsequent processes, e.g. coil winding. For fine wires, high speed is desirable to give a reasonable mass flow rate; to offset consequent high die pressures, land lengths are usually minimized and greater die swell is allowed for. Note that the shear conditions in the polymer differ from those in solid rod extrusion in that the inner surface is moving with the conductor causing an additional drag flow, as distinct from the pressure flow in a simple capillary. Cooling is usually in air, sometimes in a festoon, but waterbaths have been used for the highest speeds. At high speeds, haul-off speed relative to extrusion speed is especially important for insulation thickness, which must be a minimum for economy and uniform for subsequent lay-up or winding. Relative speeds and/or tension between pay-off reel and the various components of haul-off and wind-up are important for smooth operation, and must be maintained during acceleration at start-up. Continuity of insulation is obviously vital, but in many cases adhesion to the wire is also important to reduce breakdown due to corona

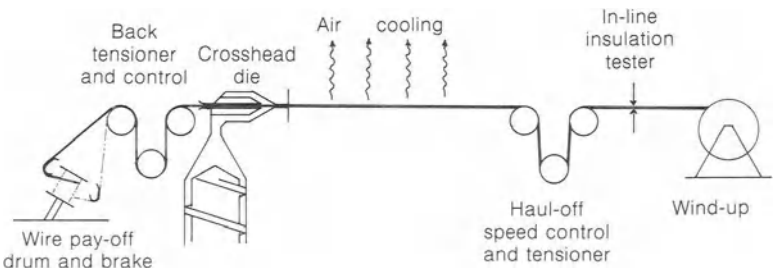


Figure 2.2 Wire covering.

discharge in high-voltage AC applications and ingress of moisture in non-electrical applications, where the polymer provides corrosion protection. Thus in submarine telephone cables, where a 15 mm conductor may be covered with a 25 mm thickness of LDPE (to minimize signal loss) extrusion rates will be relatively slow, with water cooling in stages, sometimes with programmed temperatures, to minimize temperature and shrinkage differentials within the insulation and maintain adhesion to the core. With such thick insulation or sheathing, haul-off tension will not be critical, but haul-off speed will determine thickness and a constant speed is essential to avoid surface lumps or ripples. These, apart from appearance and performance aspects, are likely to be detrimental in both handling and subsequent operations such as armouring.

2.1.4 Flat sheet

Flat sheet extrusion, primarily in UPVC, ABS and polystyrene, is fundamentally similar to that for solid sections; however, as widths between 1 and 2 m are frequently required, uniform distribution of the polymer melt across the die and mechanical rigidity of the latter become major problems. Design for uniform flow is considered in Chapter 5, but it should be noted that a deflection of only 0.1 mm in each die lip will cause approximately 20% variation in thickness of a nominal 1 mm sheet. If the simple fishtail die is used, with a small divergence angle to give essentially axial flow, then for wide sheet the die will be massive, residence time of the polymer (*re* degradation) will be large and the die area subjected to polymer pressure and liable to distortion will be large. Maintenance of uniform die temperature will also be difficult, and uniform flow will not be assured. The coathanger or manifold die, in which the polymer flows transversely in a relatively wide passage before flowing axially through a short thin passage to the die lips, is more compact, has shorter residence time and smaller pressure area. Uniform heating remains difficult. Adjustable die lips and fixed or adjustable restrictor (choker) bars are commonly used to control local flow rates and thickness, but because of die swell and drawdown effects, and the substantial thermal lag in the massive die, these adjustments are tedious and interact in a complex way. Thus uniformity and constancy of temperature and viscosity of the polymer at the die inlet are essential for good distribution. The author recalls a 150 mm extruder feeding polypropylene to a fishtail die approximately 400 mm wide with a multistrand die plate. When the strands were hauled off at uniform speed, the outer strands were found to be of visibly larger diameter than those in the centre. This was contrary to normal experience, where the longer flow path to the ends causes greater resistance and a lower flow rate. It was discovered that the larger pellets were of higher Melt Flow Rate (lower viscosity; see section 3.5) than the smaller pellets from the centre. It was concluded that the temperature of the melt leaving the extruder was higher at the outer diameter than at the centre; this, coupled with the greater residence time, gave greater degradation and lower final viscosity.

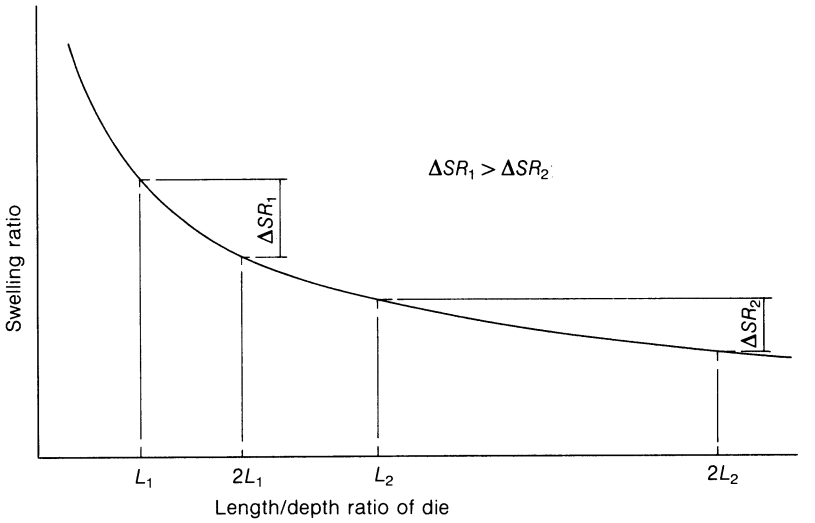


Figure 2.3 Effect of land length adjustments on swelling ratio varations (cf. Fig. 3.10).

The combined effects of temperature and degradation on viscosity outweighed the greater die resistance, leading to a greater flow rate to the outer strands. As described in section 11.1, any change in output or other operating conditions is likely to alter the spatial temperature distribution from the screw, so that correction by die adjustments would only be valid for one polymer and set of conditions. Die land lengths are usually large to improve surface finish and reduce tendency to swelling. The land length may be varied across the die to compensate for pressure differences due to different path lengths in the manifold; because of the shape of the curve of swelling ratio against land length (Fig. 2.3), such variation in land length may cause less variation in die swell than with small land lengths. Sheet is commonly drawn down from the die, leading to a greater reduction in thickness than in width, offsetting to some extent spatial variations in thickness and swelling at the die (due to variations in shear history). However, since the draw-in in width is mainly at the edges, these tend to be of a bulbous form, thicker than the rest of the sheet, and are thus frequently trimmed off. Lateral constraint away from the edges prevents elimination of thickness variation, and if drawdown is too small (slow haul-off) those parts of the sheet which are extruding fast will ripple to conform to the lower linear speed of the remainder. Time variations of flow rate from the extruder will of course lead to fluctuating thickness of the finished sheet despite drawdown. Haul-off speed in relation to extruder output is thus important in determining average thickness and, to some extent, thickness variations. Cooling may be by air, on one side while supported on a band conveyor for thin sheets or on both sides while supported on rollers for thicker sheets. Cooling

may also be by waterbath or by passing over/between water-cooled drums. These may have polished, matt or patterned surfaces to give a corresponding surface finish to the plastic sheet, or profiled to give longitudinal corrugations, or lobed to give transverse corrugation. Multilayer sheet of different polymers, grades or colours may be produced by coextrusion from separate extruders through a common die or through separate dies, the webs then being laminated together between rolls. In the latter case the surface temperature and freedom from defects and degradation are important in achieving good interlayer adhesion and absence of bubbles, etc. In the former case similar viscosities and velocities are necessary where the streams meet, as well as streamlined flow paths and sufficient pressure before the die exit, to give good adhesion and avoid interpenetration of the layers. Sheet extrusion may also form the first stage of a continuous plant for vacuum-formed products, though the extruded sheet will usually be cooled and reheated to give accurate temperature control for the vacuum forming operation.

2.1.5 Flat film

Extrusion of flat film in almost all thermoplastics is in many respects similar to that of sheet, though thickness variations due to mechanical distortion of the die asssume even greater importance, since a given absolute die deflection represents a greater percentage on a thinner sheet, and the increased die resistance leads to higher pressures. Higher velocities are also required to give similar mass outputs, and the problem is usually resolved by using high drawdown ratios of 10:1 or more on thickness, giving wider die gaps (say 0.5 mm), lower die velocity and pressure, and improved percentage thickness tolerance. The thinner films are also more flexible, so the unsupported gap between die lips and haul-off/cooling must also be much reduced (20–50 mm). Often this is achieved by shaping the die so that the extruded web is led directly on to the upper surface of a driven and cooled 'chill' roll (Fig. 2.4). Cooling in contact with the polished surface of the roll imparts a good lower surface to the film, while the upper surface relaxes as it cools in air. The roll forms a means of haul-off by surface friction, and its speed controls drawdown and final film thickness. The high degree of drawdown over a short distance requires high elongation to break in the melt, and thus generally high melt temperatures. As many films are manufactured from semi-crystalline polymers, the rapid cooling tends to suppress crystallization. This is beneficial in giving high elongation of the cooled film for subsequent drawing/orientation processes. In the case of polymers which crystallize fairly slowly, e.g. LDPE, this leads to small spherulites in a substantially amorphous matrix which has high clarity but low stiffness compared with more crystalline films produced by the tubular process. An alternative process is to extrude vertically downwards into water with a roller haul-off on the cooled film (Fig. 2.5). By keeping the coolant surface close to the die lips, both drawdown and cooling are rapid, with results

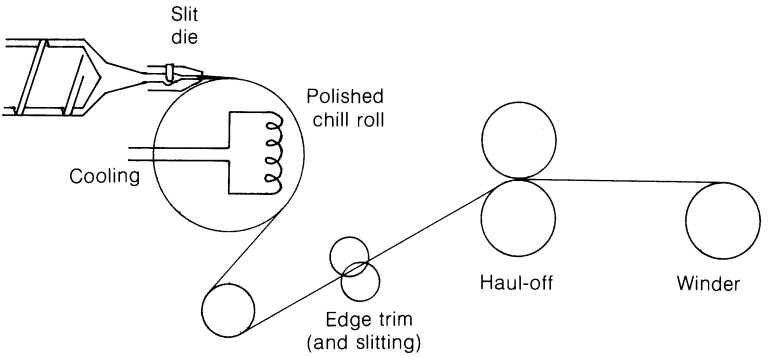


Figure 2.4 Chill-roll extrusion of flat film.

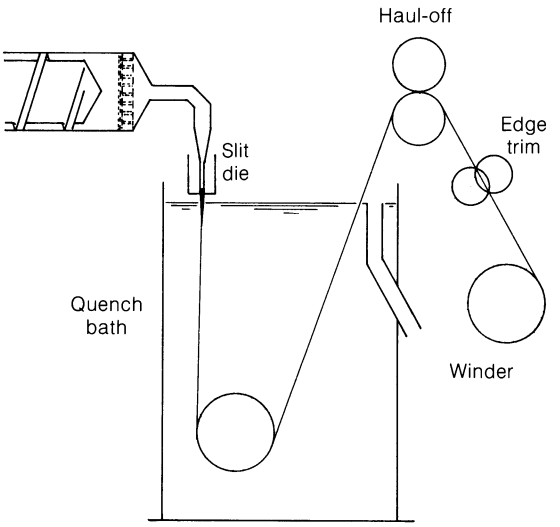


Figure 2.5 Waterbath flat film extrusion.

similar to the chill-roll process. Thus water level and temperature control affect clarity and stiffness, while the haul-off rate controls thickness. Rapid drawing probably assists stability, but uniform extrusion rate and absence of mechanical vibration (affecting the water surface) are also vital. Uniform and constant melt temperature assists not only uniform flow in the die, but also uniform drawing, both of which influence final thickness variation. Since film dies are easily blocked or damaged by solid matter in the polymer, fine filter packs are usually used, further increasing the back pressure on the extruder. It is worth noting that 'gels' of high molecular weight polymer are appreciably

elastic and will often elongate to pass through filters and dies, only to recover their shape and cause 'fisheyes', etc., in the finished film. If these cannot be eliminated, it is probably wise to use either a filter mesh appreciably smaller than the die gap to break up any gels passing through so that they are less likely to produce apparent surface defects, or a continuously changed filter with back flushing to remove the gels before the pressure drop across the filter builds up sufficiently to force the gels through.

Multilayer flat films may be made by similar methods to those for sheet, but the greater importance of optical properties makes the elimination of interfacial defects more vital. Subsequent handling in wrapping machinery makes adhesion more important, especially where one strong or stiff component provides mechanical support for another layer providing mainly chemical resistance or barrier properties. Reduced thicknesses of the layers also makes flow- and viscosity-matching more important where two or more components are brought together within the die. The chill-roll process is also used extensively for melt extruding a thin film on to a paper or textile substrate to form a supported coating. The substrate is passed over the roll and the film extruded on top of it, with or without a second roll to improve penetration and surface finish of the film. This surface coating may be only a few micrometres thick so that very high melt temperatures (e.g. in excess of 300°C for LDPE) may be required to give low viscosity and uniform thickness to this polymeric film.

2.1.6 Tapes

Tapes for sound and video recording, package strapping, etc., especially in polypropylene and PETP, are usually highly oriented in the longitudinal direction. The initial tape, which may be up to 40 × 1.5 mm, is made by vertical extrusion into a waterbath, as for flat film, but with limited drawdown. Water temperature is kept low and the distance of the surface from the die is as small as 5 mm to give rapid cooling and low crystallinity. The tape is then reheated to a temperature well below the crystalline melting point and drawn lengthwise by 10:1, or greater, to produce a high degree of uniaxial orientation. It is then 'heat set' by heating to a somewhat higher temperature while held under tension to crystallize in the oriented state and then cooled. The low initial crystallinity gives high elongation to break which permits sufficient drawing to orient, a low modulus which reduces tension required to draw at high strain rate, and less tendency to reversion (disorientation) before heat setting. Evidently the melt temperature at extrusion must be high enough to eliminate crystallinity present in the feed material, but low enough to permit rapid cooling throughout the relatively thick initial tape. For consistent properties, melt and waterbath temperature must be closely controlled, while for consistent dimensions, extrusion rate and haul-off speed must be kept in proportion.

2.1.7 Fibres and monofilaments

Fibres and monofilaments are widely extruded in polypropylene, nylon 66 and PETP. In the finer gauges this is usually vertically downwards into water or a countercurrent of air with a substantial degree of drawdown. Multihole spinarets are used as dies, usually immediately preceded by a filter pack of graded sand or porous metal (Fig. 2.6). To give a reasonable mass output, extrusion speeds are high and consequently pressure drops through the filter pack and spinaret are also high. However, as the filter pack blocks up during a run, its pressure drop will increase and this would normally cause a decrease in extruder output; but to maintain drawdown and properties and minimize tension, which would break the thread-line, the output must be kept closely in step with the haul-off and winding equipment, which would be difficult by adjusting the speed of either the extruder screw or the winders. The extruder is therefore usually used as a source of melt which is then metered by gear pumps whose output is insensitive to back pressure. This indicates a requirement for high and constant melt temperature to minimize viscosity and pressure drops (cooling is not such a limiting factor with fine threads) and an output which changes rapidly with small changes of pressure (see appendix B.5). On the contrary, where the extruder feeds the spinaret directly the output should change little with pressure, and speed control must be precise but readily adjustable.

The orientation of fibres by reheating and drawing may usually be done at much higher linear speeds than melt spinning and is therefore usually a separate operation out of line.

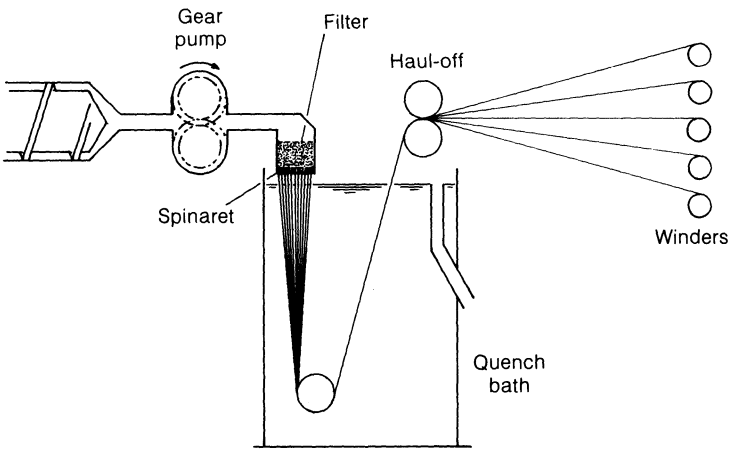


Figure 2.6 Melt spinning of fibres.

2.1.8 Netting and mesh

In addition to adaptations of conventional weaving and knitting processes from filament or tape, netting may be made by several melt processes. Possibly the most common uses an annular die in which the outer element and mandrel can be rotated or oscillated in relation to each other. Each element contains a number of longitudinal or helical grooves producing a series of strands. As either or both of the elements are rotated, welds forming a mesh are produced when the grooves in the two halves coincide. Another patented method (Briston, 1974) passes an extruded sheet between grooved rollers, and the indented sheet is then stretched to break the thin portions and create a net – this is capable of economic production of much finer meshes than by an oscillating die.

2.1.9 Tubular film (blown film)

In addition to the processes previously described for flat film, thin films are made by the tubular process, especially from low density and high density polyethylenes, polypropylene and PETP. An annular die of the in-line or crosshead type forms a thin tube of 50 mm–2 m diameter and 0.2–1.0 mm thickness. This is inflated by blowing in air, either through the centre of the die or through a flattened tube between the haul-off rolls. The blown tube is cooled and solidified by high-velocity air from an annular ring surrounding the tube and some distance from the die; the tube is flattened by converging guide boards or sets of rollers and led into a pair of driven haul-off nip rollers (Fig. 2.7). It may be wound directly as layflat tube, slit at both sides and wound into two flat reels, or, especially for the widest film 2–15 m wide, slit at one side only, so that in use it can be opened to the full circumference, though with a visible centreline due to the fold. Extrusion is usually vertically upwards, avoiding buoyancy effects on the blown tube and permitting the heavy extruder and wind-ups to be floor-mounted and easing handling of raw material and finished product. In small plants the extruder is frequently vertical with an in-line die, both being continuously oscillated to distribute any irregularities in thickness. Thickness variations may be reduced by adjusting a flexible outer die lip; whether this is exaggerated or reduced by blowing depends on the cooling conditions. Where the extruder is horizontal, a crosshead die is convenient, but to improve polymer distribution to the die, an in-line die is sometimes coupled to the extruder by a simple pipe bend of small diameter, or a spiral-mandrel die may be used. The ratio blown tube diameter/die diameter (**blow ratio**) is usually 1.5:1 to 6:1 and typically 3:1; since the bubble is stretched both transversely and longitudinally, the thickness reduction is approximately 10:1, corresponding to a blow ratio of 3.3:1. The blow ratio is a balance between the hoop stress produced by the internal air pressure and the increase in tensile viscosity due to the air ring cooling; if the latter is very effective, the blown tube diameter will be

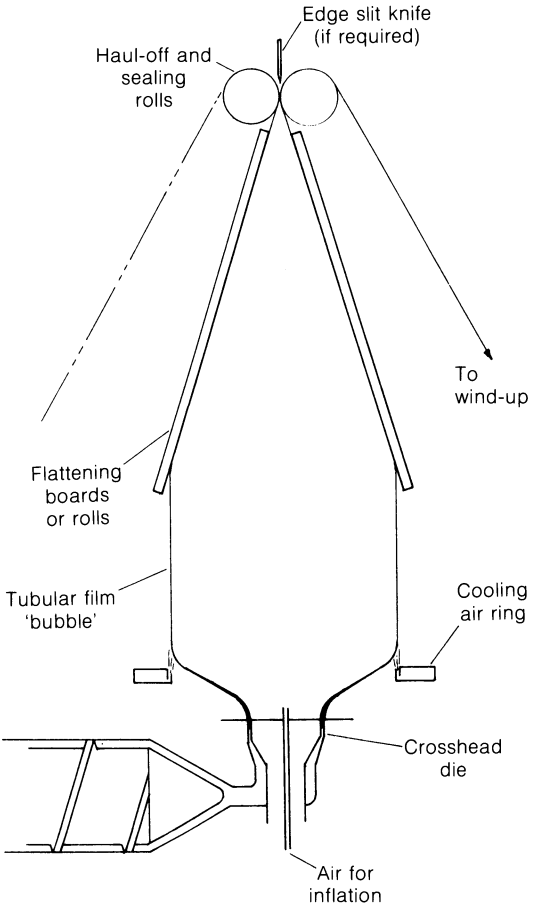


Figure 2.7 Tubular film extrusion.

close to that of the air ring, but otherwise it may continue to expand with less certain control. Since the process is essentially melt shaping, little orientation is normally produced; however, if the haul-off speed is increased beyond that required to avoid sagging of the blown tube, a degree of longitudinal orientation may be developed. Because of the distance necessary for blowing between die and air ring (**freeze line height**), cooling is relatively slow and the crystallinity of LDPE film will be greater than for chill-roll or waterbath cast film, and will increase with freeze line height. This generally gives a stronger and stiffer film, but of poorer clarity than the chill-roll film. However, slower cooling allows more time for surface defects, e.g. die lines, originating at the die to relax, so optimum optical properties require a compromise in freeze line height. For a fixed freeze line height, increased output rate, increased melt temperature and decreased blow ratio all tend to give slower cooling and

increased crystallinity – in the last case the resulting greater thickness also delays cooling. With HDPE and UPVC films, the rates of crystallization are, respectively, considerably faster and slower than with LDPE. As a result, the crystallinity and film properties are much less affected by these variables.

If oriented film is required, this may be done out of line from either chill or blown film, or similarly to tape and fibre, in-line from a 'cast' tube. The latter may be extruded vertically upwards, or downwards into water, without blowing (increase in diameter) and limited longitudinal drawing, but rapidly cooled to suppress crystallization. For improved temperature control, the tube is then reheated and blown at well below melt temperature to produce balanced or unbalanced orientation, depending on haul-off rate, and an increase in width and decrease in thickness. Evidently tubular film requires complete melting and homogenization in the extruder, absence of dirt or gels, and a very constant extrusion rate to avoid thickness variations and surface ripples. For blown film, the melt temperature must be high enough to permit the required blow ratio, whereas for cast tube for orientation a compromise is necessary between rapid cooling and avoidance of flow and surface defects. To achieve economic mass flow rates, linear extrusion speeds must be high, and raising melt temperature will raise the threshold speed for onset of melt fracture and give more rapid relaxation of surface defects. Long die lands are usually required to give uniform thickness, good surface finish and elimination of 'spider' lines. These, together with high output rates and narrow die gaps, involve high die pressures, often of the order of 40–50 MN m^{-2}.

2.1.10 Foams

One of the incidental functions of the screw extruder is in the processing of thermoplastic foams into most of the forms previously mentioned. This may be by mixing in the feed material a proportion of solid foaming agent which decomposes, typically to nitrogen and carbon dioxide, at the temperatures within the extruder. Owing to the high pressure, these gases remain in solution or as small bubbles until pressure is reduced at the die exit, when foaming occurs. The pore size and distribution is governed by the number and distribution of nucleating points, sometimes achieved by a small percentage of undecomposed foaming agent. Another method is to inject a liquid foaming agent into the melt section of the extruder, which then distributes it throughout the melt. The pressure in the machine maintains the foaming agent as a liquid despite the increase in temperature, until it volatilizes and foams the product with the reduction in pressure at the die. Foaming requires fairly constant output for control of product density, especially with liquid injection, which is independently metered, where melt mixing is also required. Close control of temperature, both of the final melt and along the barrel, is required to achieve the correct degree of decomposition of the foaming agent, and at the correct

point in the screw. Pressures do not require close control, but must be kept between predetermined limits if output is varied.

2.2 OTHER APPLICATIONS AND THEIR REQUIREMENTS

The screw extruder fulfils a number of useful functions which do not directly lead to saleable products, although in certain cases these may be integrated with the preceding processes.

2.2.1 Compounding

The commonest of these is compounding of stabilizers, antioxidants, fillers, plasticizers, lubricants, pigments and other additives. This is further discussed in sections 9.1.5, 10.3.4, 10.4.5 and 11.1; here general considerations will be outlined. As a continuous process, the long-term uniformity of product depends on a consistent composition in the feed material; although the extruder provides a degree of end-to-end mixing, the mean residence time in the melt is of the order of only 10 s, i.e. the hold-up volume is small in relation to the hourly throughput, thus the extruder can only mix and even out variations within the hold-up volume. As shown in section 6.2, distributive mixing in the single-screw channel occurs due to the cross-channel component of flow, and also in a down-channel direction with increasing back pressure, as well as in any devices attached to the screw or preceding the die included specifically to increase mixing. Such devices often impose back pressure on the screw, and part of any improvement in mixing occurs within the screw and could be achieved merely by increasing the back pressure with a screenpack. Shear stresses within the screw channel are usually less than required to fracture agglomerates of particulate solids, including pigments; thus little dispersive mixing occurs in the channel. In the flight clearance, shear rates and stresses are approximately two orders of magnitude greater than in the channel and dispersion readily occurs. However, as shown in section 6.3, the leakage flow per turn is normally only a few per cent of the total flow and, even if each portion of the melt only passed once through the clearance, it is unlikely that every portion would experience this in the length of a usual melt section. In fact, the leakage flow is redistributed in the channel flow, from which the leakage flow at a later stage is taken randomly, so that some polymer will be sheared two or more times and other portions not at all. In addition, the clearance is typically only 0.10–0.15 mm for a 100 mm diameter screw, so that larger solid particles are unlikely to enter the flight clearance; also the time of shearing is very short – of the order of 0.1 s at 1 rps. In contrast, both distributive and dispersive mixing in the twin-screw extruder is primarily in the gaps between screws and thus more uniformly distributed through the material mass. In

addition, mixing sections are frequently introduced at intermediate points to promote uniformity further.

Patented designs of 'barrier' screw and mixers of the smearhead and Dulmage type ensure that all the polymer passes at least once through a close clearance. Thus the single-screw extruder is not usually adequate for dispersive mixing without special screws or mixing attachments, but, especially at high back pressures, it is quite effective as a distributive mixer on a small scale, and forms a useful compounding unit when fed with a blend including masterbatch, or following an 'intensive' high-speed mixer for powders. The flow patterns in the screw (see Figs 6.6 and 6.7) give a wide range of residence times, which is undesirable for heat- or shear-sensitive polymers and additives, since some part of the polymer experiences heat or shear for a much greater time than the average. The closer range of residence times and smaller shear heating in the twin-screw machine make it especially suitable for heat-sensitive polymers such as UPVC and PP and it often gives adequate mixing without special attachments.

As output is increased, residence time decreases and the use of distributive mixing attachments becomes desirable. These usually entail substantial pressure drops, giving high back pressure on the extruder, which also increases the mixing effectiveness of the screw (at the expense in the single screw of low output and additional shear heating). Large machines running at low speed are desirable to increase the residence time and increase surface for cooling, providing shear stresses are not reduced unduly. To keep viscosities and shear stresses high, low melt temperatures are desirable, but it may not be possible to apply sufficient cooling to maintain these low temperatures despite shear heating. It is, of course, possible to use the same extruder for compounding and product shaping, but the above requirements for compounding may be incompatible with those for shaping, so that the extruder cannot give its best performance for both functions simultaneously.

Many variants of extruder compounding have been attempted, with varying degrees of success. In one case a dispersion of pigment in a volatile liquid was metered by a piston pump under pressure into the melt pumping section of a single-screw extruder fitted with a patented design of mixing head. Microtoming of the cross-section of the cooled extrudate showed that circumferential distribution was good, but annular rings of different pigment content were observable, due to lack of a radial mixing component in the mixing head and the point of injection being too near the end of the screw for the latter to achieve thorough mixing. In another case, polyethylene masterbatch containing a high proportion of slip agent was solid-fed to a small single-screw extruder, which melted and pumped it through a restrictor into the melt pumping section of a larger single-screw machine handling base polymer. The former gave problems of low and erratic flow rates, until cooling was applied to the screw in the feed section only, but otherwise the process operated steadily with adequate distribution at the end of the large extruder. Proportional

control of the speeds of the two machines and monitoring of the pressure at the end of the masterbatch machine gave sufficiently consistent content of slip agent in the final film compound.

2.2.2 Melt blending

Other mixing operations related to compounding include melt blending, structure modification and intentional degradation. Melt blending includes mixing two polymers of the same type but different molecular weight, mixing two polymers of similar mean molecular weight but different distributions, and more recently two different polymers, e.g. low density polyethylene with high density polyethylene or polypropylene. The latter has gained in importance, especially blends of other polymers with LLDPE in order to exploit the properties of both polymers. In all cases, if the melt viscosities are similar at processing temperature little difficulty need be anticipated, provided the constituents are miscible, though if shear sensitivity (non-Newtonian flow index n) is very different for the two components, radial segregation into zones of differing shear rate may occur. If the temperature coefficient of viscosity is substantially different for the two components, processing temperature ranges may be limited. If viscosities at processing temperature are very different, e.g. due to widely differing molecular weights, the mixture may tend to behave as a suspension of relatively solid, high-viscosity component in low-viscosity second component. As discussed in Chapter 7 in respect of the melting stage, when a suspension is sheared, the shear rate and viscous heating are higher in the low-viscosity component, causing a temperature rise in the latter which further reduces its viscosity, whereas the high-viscosity component is heated mainly by conduction. Thus initial segregation is liable to continue, with poor mixing. A strategem employed with batch melt mixers in this case is to feed the high molecular weight component first, and add the cold second component only when the former has been sheared and heated to reduce its viscosity; to operate this on the extruder would require special equipment such as an intermediate feed pocket with force feeder.

In all blending operations, as in compounding, large-scale uniformity in the product requires proportional feeding of the components to at least a similar accuracy, and the avoidance of demixing. The latter is most likely to occur due to segregation of the feed in the hopper or first part of the screw, e.g. due to different particle shapes or densities causing selective feeding by the screw.

Structure modification and degradation may include many chemical reactions, either homogeneous or promoted by additives or catalysts; in addition to its normal functions of melting and pumping, the extruder is usually required to do mechanical (e.g. shear) work on the polymer, to maintain energy balance and to ensure at least a degree of mixing of the product. One example is the selective breakdown by mechanical shearing of a high molecular weight constituent of LDPE to reduce molecular weight spread and improve product

properties. This required considerable mechanical drive power and resulted in appreciable temperature rise of the polymer, but the resulting energy input to the polymer was largely absorbed in heating the polymer to a melt temperature suitable for granulation. A second example involved the thermal and shear degradation of polypropylene from a high molecular weight as polymerized to a lower value suitable for melt processing. Exclusion of oxygen was important in minimizing the oxidative element of degradation, as was accurate temperature control – a change of temperature of a single barrel zone of 1°C produced a measurable change in Melt Flow Rate of the product. The molecular weight distribution of the product was significantly different from that resulting from polymerization direct to the same average value, giving different mechanical properties, e.g. impact strength, as well as different processability. Vacuum extraction was used in the extruder to remove as much as possible of the very low molecular weight products of degradation, as well as catalyst residues, which adversely affected colour and odour of the product.

2.2.3 Degassing and drying

Vacuum extraction for degassing and/or drying is also frequently used for contaminated or damp feed material, but of itself would be an energy-expensive process of limited effectiveness, because of the restricted residence time and surface area for devolatilization. It is therefore commonly used in conjunction with an extrusion compounding or fabrication process, as discussed in section 6.5, where the volatiles do not exceed, say, 5% by mass of the polymer flow rate. Note that extraction in the melt is of limited value, e.g. with damp PETP, which will partially hydrolyse at melt temperatures, if these occur upstream of the vent position.

2.2.4 Filtering

Filtering of solid contamination from the melt, usually between the screw and die, is also commonly associated with fabrication processes, especially those with narrow die gaps such as film and fibre extrusion and thin wire covering, where contamination would dramatically affect electrical insulation. It is sometimes used as a separate process, e.g. with raw natural rubbers and with scrap recovery; the economic case for the latter is discussed in section 12.5. Scrap is sometimes re-extruded to obtain a suitable particle shape for re-feeding to the main process (especially sprues and runners in injection moulding). More commonly it is mixed as a proportion of new feed material, either to make a homogeneous granular feed, or directly into sheet for vacuum forming or tube for blow moulding; it may also include additives (especially stabilizers) to replace losses between the original feed and the scrap. Thus scrap recovery may include one or more of the steps of blending, compounding, degassing, filtering and granulation. As discussed in Chapter 7, satisfactory

feeding of irregular-shaped scrap and avoidance of segregation are probably the most common problems, especially when scrap, alone or blended, is refed directly to an extrusion fabrication process.

2.2.5 Dewatering

A special application of extrusion, which has been used commercially with rubbers and often associated with filtering and granulation, makes use of the tendency of the screw to pump high-viscosity materials in preference to lower-viscosity. This is seen in the rearward displacement of air entrapped in the feed, but in this case is used for dewatering wet rubber. The feed pocket is replaced by a perforated section, for example with a series of narrow longitudinal slits through which the displaced water drains, while substantially dry rubber is conveyed along the screw to be heated and extruded.

2.2.6 Polymerization

The twin-screw extruder has also been used for continuous polymerization, using its mixing and heat transfer functions as a high-temperature, high-pressure reactor. The single-screw machine is less satisfactory for this purpose since widely differing viscosities of monomer and polymer may cause slip and loss of pumping, and as mentioned in section 2.2.1, the spectrum of residence times is broad, tending to an undesirably wide molecular weight distribution in the polymer.

2.2.7 Blow moulding

The screw extruder is widely used in blow moulding of bottles and other hollows, including toys and ducting. In some cases, short lengths of extruded tube are stored and reheated for blowing out-of-line from extrusion. More usually, one or more tubes are extruded, cut off and pinched at one end and blown inside sets of moulds where they cool by contact with the cold mould. The first requirement is for a uniform flow with low elastic memory; the melt temperature should be low to give rapid cooling and reduce 'parison' sag, and for large containers, extrusion should also be rapid to reduce time for sagging. For large containers, where extruder output would form a limitation, the extruder may continuously fill an accumulator, which discharges intermittently and rapidly through the die. In some small machines with a single mould, the extruder screw is run only for the time required to form the parison, and then stopped while blowing and cooling occurs; this intermittent operation gives more time for melting, but departs from steady-state conditions and may give spatial variations of temperature, strain history, etc., in the parison.

2.2.8 Injection moulding

Modern injection moulding is heavily dependent on the single-screw extruder, although twin screws are also used. Again, the screw usually runs intermittently, though the 'rest' period may only be a few seconds during actual injection. This is necessary where the screw also act as the ram for injection, a ring non-return valve being fitted at the end of the screw to prevent reverse flow in the screw during injection, which is generally under much higher pressure (up to $200\,MN\,m^{-2}$) than during refilling by the screw (usually less than $5\,MN\,m^{-2}$). An additional complication is that the screw is displaced rearward as it pumps melt into the reservoir formed by the injection cylinder, and since the feed opening is usually fixed, the effective length of the screw progressively decreases during each filling cycle. This does not usually apply to piggy-back machines where the screw preplasticizing unit is separate from the injection ram, though a non-return valve and intermittent rotation are still usual. In modern machines under computer control, the screw speed and/or the back pressure against which the screw acts may be programmed to vary during the filling cycle. The first requirement is that the screw should refill the cylinder with the necessary volume of molten polymer within the cooling and 'dead' times of the particular moulding and machine, so that plasticization does not extend the overall cycle time. The screw must provide a homogeneous melt, frequently including the incorporation of pigments or coloured granular masterbatch, 'screw-back' pressure being adjustable to assist the mixing in the screw. For thermoplastics, the required melt temperature will tend to be high, giving a low viscosity for thin mouldings and/or long flow paths in the runners and mould, which because of cooling during mould filling must in any case be filled fast, so that high temperature reduces the injection pressure required. However, melt temperature also has important effects on the structure and mechanical properties of the final moulding, while thermally sensitive polymers like UPVC may be subject to degradation, especially of the 'cushion' material left in the cylinder between shots.

Phenolic-type thermosets require very precisely controlled low temperatures (e.g. water/steam heating) to avoid curing of the cushion material before the next shot, while giving sufficient fluidity for the shot to be injected into the hot mould at high velocity so that shear heating in the nozzle raises the temperature of the shot to give rapid curing. Unsaturated polyester thermosets may be injected cold so that the screw does little more than convey the premix to the cylinder.

Thus polymer, machine and product all influence the required temperature; it is important that this is as uniform as possible throughout the shot volume, which varying screw speed or back pressure seeks to achieve, despite the changing effective screw length. It should be noted particularly that during injection the flow within the cylinder is unlikely to be similar to that during refilling, (Pearson, 1944, Figs 87, 89, 92, 94; Tanev, 1975) so that any

temperature variation during the latter will not appear in the same sequence in injection. Moisture removal by venting is also included in some plasticizing units, with further problems due to axial screw movement. The steady-state theory is only qualitatively applicable to this situation of intermittent rotation, changing effective length and possibly changing speed and back pressure during the cycle, and predicted effects may be overridden by transients including elasticity of the melt, non-steady-state heat transfer and mechanical/hydraulic inertia in the machine.

Table 2.2 Comparison of process requirements

	Uniform/constant							*Maximum* (×) *or minimum* (✓)							
Process	*Output, Q*	*Pressure, P*	*Melt temperature, T_m*	*Mixing*	*Residence time, t_{res}*	*Specific power, E/Q*	*Elastic memory*	*Output, Q*	*Pressure, P*	*Melt temperature, T_m*	*Mixing*	*Residence time, t_{res}*	*Specific power, E/Q*	*Shear history*	*Elastic memory*
Rod, section, profile		×					×								✓
Tube, hollows		×						×[a]	✓						✓
Wire covering, sheathing				×			×		×	×					
Sheet, laminating		×	×					×							✓
Flat film[b]	×		×	×			×		×		×				
Paper coating	×		×						×	×	×				
Tape	×		×	×											
Fibres, filament, netting	×		×							×	×				
Tubular film	×		×	×			×		×		×				
Foam		×	×	×	×					✓	×				
Compounding[c]			×	×		×[d]		×		✓	×	×[e]		×	
Blending, degrading			×	×	×	×		×		×[f]	×	×	×	×	
Degassing, drying								×		✓	×	×	✓		
Filtering		×						×		✓			✓		
Scrap recovery				×				×		✓	×		✓	✓	
Dewatering								×		✓			✓	✓	
Polymerizing	×		×	×	×						×	×	✓	✓	
Blow moulding	×		×				×	×		✓					✓
Injection moulding			×	×				×			×				

[a] Large pipes.
[b] Incl. multilayer and laminating.
[c] Incl. pumping of additives.
[d] And shear.
[e] Usually.
[f] Degrading (×), Blending (✓).

2.2.9 Comparison of requirements

The foregoing brief survey includes many of the commercial applications of the screw extruder, sufficient to show its wide importance and the differing requirements of processes of which it forms a part. Thus it is impossible to define an ideal design or method of operation for all purposes, and to make the discussion in Chapters 9, 10 and 11 more specific, Table 2.2 attempts to summarize the important requirements for each process and product type. Of course, high output, uniform temperature, etc., are desirable in all processes; only the more critical items are indicated, and even these will be qualified by the product, e.g. thick tube and sheet require high output, whereas for thin tube and sheet minimum elastic memory may be more critical – the indications should be taken to refer to the more critical product. The table suggests that the non-fabrication processes generally have a wider range of requirements than do those which are primarily shaping, especially in respect of maximum/minimum values. In some cases the requirements of the two groups are contradictory, emphasizing that compounding or scrap recovery may be more effective as a separate operation rather than integrated with a shaping process, although requiring more labour, energy and overheads. It appears, not unreasonably, that temperature is the most common criterion, for both uniformity and maximum/minimum value; in several cases not indicated, e.g. film and injection moulding, the temperature must be controlled at a prerequisite value for an individual polymer or operating condition, even though this is not the maximum or minimum achievable.

Flow behaviour relevant to extrusion

3

In this chapter the principles and basic equations relating to fluid flow of polymers will be stated, with emphasis on those which are relevant to melt extrusion. In general, for proofs and other applications, reference should be made to standard works on rheology such as that by Brydson (1981). Design of extruder dies is specifically covered in Chapter 5.

3.1 VISCOSITY

When a liquid is subjected to stress, it deforms continuously as long as the stress is applied, unlike a perfect solid which deforms a fixed amount, independent of time. On removal of stress, the liquid remains in its deformed state, whereas an elastic solid recovers its original dimensions instantaneously and completely (Fig. 3.1). Thus the stiffness or modulus, which is the relation between stress and deformation (strain), is unique for a solid, but for a liquid is dependent on time and so does not define a property of the material. However, under a constant stress, the rate of deformation with time is constant and the ratio is the **viscosity**. In direct stress σ (tension, compression), the ratio extension/original length is defined as the **strain** ε (Fig. 3.2) and the ratio stress/strain as the **modulus of elasticity** E, which is constant for a Hookean solid. For a liquid, the **strain rate** is:

$$\frac{d\varepsilon}{dt} = \dot{\varepsilon} = \frac{1}{L} \cdot \frac{dL}{dt} \tag{3.1}$$

and the **extensional viscosity**:

$$\frac{\sigma}{\dot{\varepsilon}} = \Lambda \tag{3.2}$$

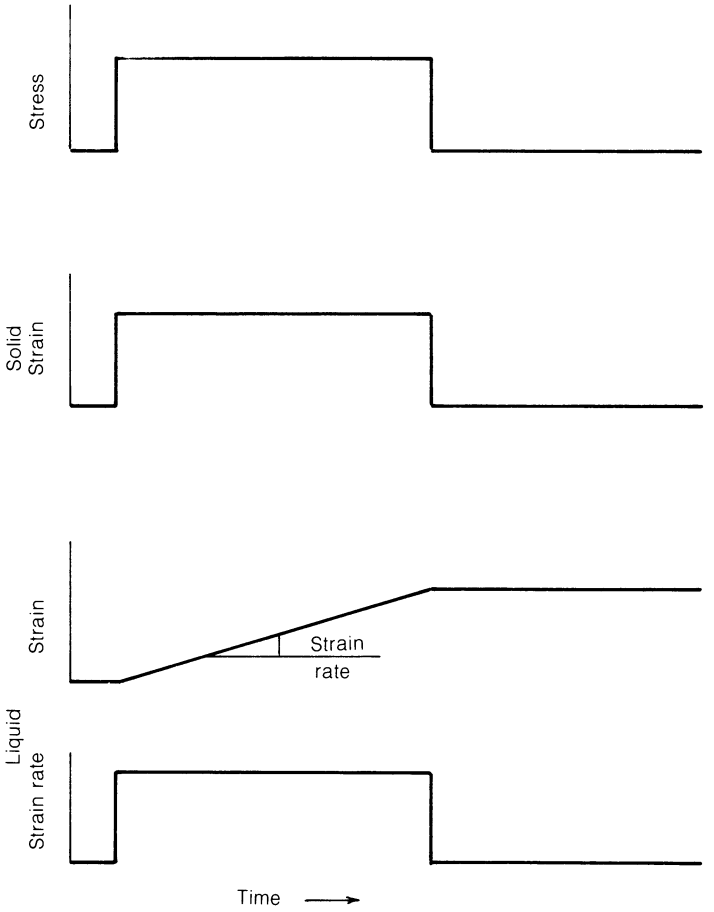


Figure 3.1 Deformation under stress.

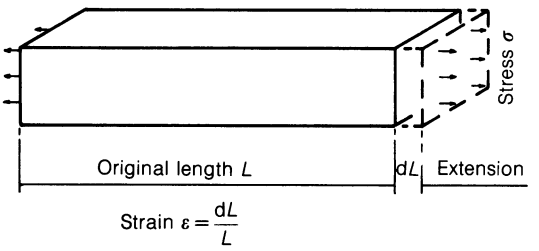
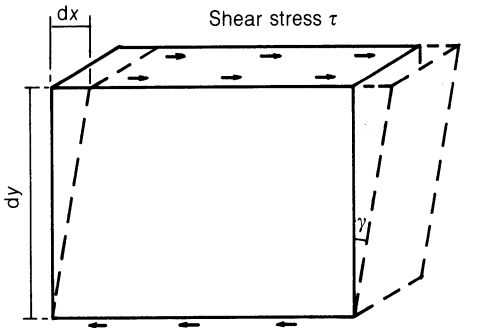


Figure 3.2 Extensional strain.



Shear strain $\frac{dx}{dy} = \tan\gamma \simeq \gamma$

Figure 3.3 Shear strain.

In shear, stress τ causes a deformation dx in the direction of the stress, but **shear strain** is defined (Fig. 3.3) as:

$$\frac{dx}{dy} = \tan\gamma \simeq \gamma \tag{3.3}$$

for small strains. **Shear modulus** G (modulus of rigidity) is τ/γ. For a liquid, the strain rate is:

$$\frac{d\gamma}{dt} = \dot{\gamma} = \frac{d}{dt}\left(\frac{dx}{dy}\right) = \frac{d}{dy}\left(\frac{dx}{dt}\right) = \frac{dw}{dy} \tag{3.4}$$

where $w = dx/dt$ is the velocity. The **shear viscosity** is:

$$\frac{\tau}{\dot{\gamma}} = \eta \tag{3.5}$$

Strain is a pure ratio and therefore dimensionless. Thus the units of stress and modulus are both $N\,m^{-2}$. Strain rate has dimensions 1/time, expressed as s^{-1}, and so the unit of viscosity is $N\,s\,m^{-2}$. In a Newtonian fluid, the relation between shear stress and shear strain rate is linear (Fig. 3.4), i.e. the viscosity is constant, independent of the values of stress and strain (shear) rate, but

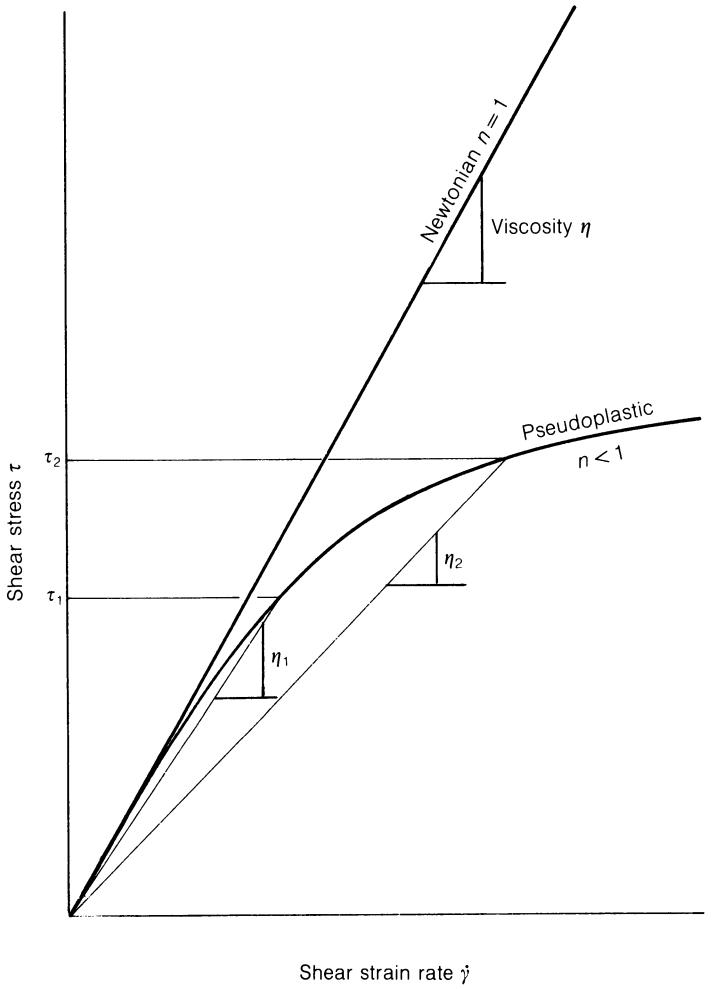


Figure 3.4 Shear viscosity.

dependent on temperature. Many molten polymers are to a lesser or greater extent non-Newtonian, i.e. shear rate is no longer proportional to shear stress, the viscosity usually decreasing with increasing shear stress or shear rate, when they are said to be **pseudoplastic** (Fig. 3.4). The definition of viscosity (equation (3.5)) is still used, but this is now a function of shear stress or shear rate as well as temperature. An approximation which is frequently used expresses shear stress as a simple power of shear rate:

$$\tau = K\dot{\gamma}^n \tag{3.6}$$

where K is a constant for a specified material and temperature. Combining equations (3.6) and (3.5) gives:

$$\eta \propto \dot{\gamma}^{n-1} \propto \tau^{(n-1)/n} \tag{3.7}$$

where for a pseudoplastic fluid, $n < 1$, and evidently Newtonian behaviour is equivalent to $n = 1$. Both of these approximations facilitate mathematical analysis, but it must be realized that the 'power law' has little physical basis; it is a convenient approximation over a limited range of shear rates.

The index n is known as the **pseudoplasticity index**, and a decrease in its value from unity towards zero indicates further departure from the Newtonian relation, i.e. shear stress rises more slowly with shear rate. Figure 3.4 indicates that at very high shear rates, shear stress tends to a limiting value and viscosity continuously decreases, giving a curve similar to Fig. 3.5 (log/log scales). If viscosity is plotted against shear rate, the curve has a negative slope of $n - 1$ (equation (3.7)) on log/log scales, with a maximum value of -1 (45°) when $n = 0$. In both cases Newtonian flow is represented by a horizontal line. As indicated by Fig. 3.5, many polymer melts approach this condition at very low shear rates, giving what is often referred to as **zero-shear viscosity**.

Viscosity (at fixed shear rate for pseudoplastic flow) decreases with increase of temperature; the best approximation is probably an Arrhenius relation:

$$\eta = A \exp(E/RT) \tag{3.8}$$

where A and E are constants, the latter being the activation energy for flow in J mol^{-1}, R is the gas constant in J K^{-1} mol^{-1} and T the absolute temperature in kelvin. Other approximations used over limited ranges of temperature are:

$$\eta = B \exp(-bT) \tag{3.9}$$

and

$$\eta = \eta_0[1 - \beta(T - T_0)] \tag{3.10}$$

Equation (3.8) would imply that curves of $\log \eta$ against $\log \dot{\gamma}$ were parallel, i.e. that the effect of temperature was independent of shear rate. For many real polymers this is not the case and either n must be varied with temperature or E must be a function of shear rate; this leads to complex mathematical equations and, for the present purpose, where small changes are concerned, it is sufficient in most cases to use equations (3.7) and (3.10) with an experimental mean value at an appropriate shear rate and temperature. It is important for any useful calculation that these data are obtained, preferably in the form of viscosity versus shear rate and temperature, for the grade of material in use. These may be available on request from the raw material supplier, but to permit useful process control, the processor should have facilities to obtain his own data (see section 11.4). Typical flow curves for some common polymers are given in

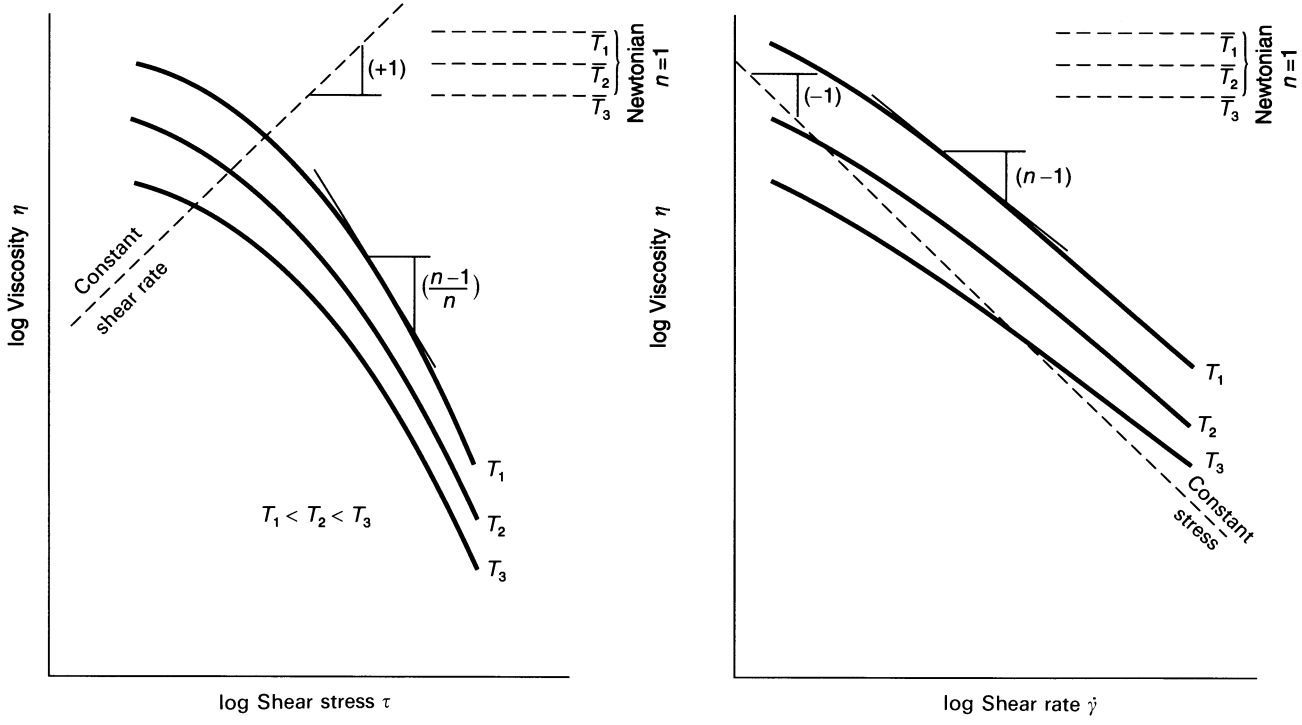


Figure 3.5 Typical viscosity curves.

Cogswell (1981). A limited amount of data has been published (Westover, 1961) on the effect of pressure on viscosity; the increase at high pressures is considerable for polystyrene, but may probably be neglected for polyolefines at normal extrusion pressures.

3.2 SHEAR FLOW

3.2.1 Simple shear

If a layer of polymer of uniform temperature and thickness h (Fig. 3.6) is sheared by tangential forces F on the opposing faces, causing relative motion of its boundaries $W = \mathrm{d}x/\mathrm{d}t$, the shear stress $\tau = F/xz$ will be constant (by balance of forces) at all sections, and if viscosity is a material property, it will also be constant at constant stress. Then by equation (3.5), the shear rate will also be constant:

$$\dot{\gamma} = \frac{\mathrm{d}w}{\mathrm{d}y} = \frac{W}{h} \tag{3.11}$$

Note that this is independent of the relation between τ and $\dot{\gamma}$, i.e. it applies to both Newtonian and pseudoplastic behaviour.

3.2.2 Circular capillary (Newtonian)

The flow is considered to be fully developed, i.e. it is purely axial and the velocity profile is independent of axial position. Then the pressure may be

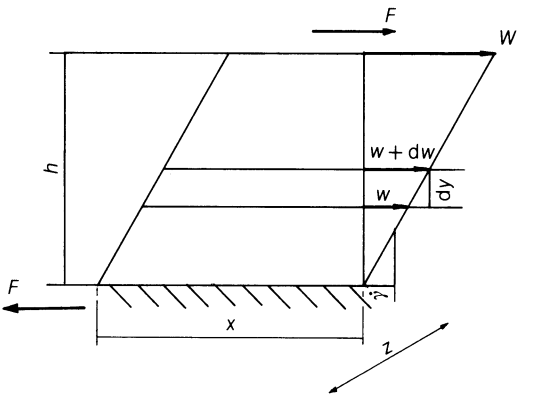


Figure 3.6 Simple shear.

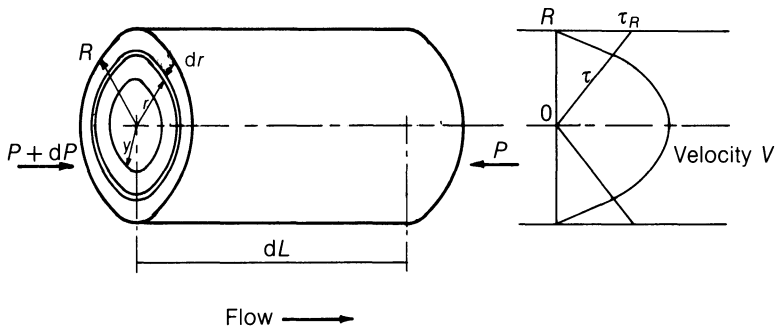


Figure 3.7 Capillary flow.

considered uniform across a normal cross-section, and will fall in the direction of flow. Using the subscripts y, r and R for values at the corresponding radii, the shear stress and shear rate at radius y are τ_y and $\dot{\gamma}_y = \mathrm{d}V_y/\mathrm{d}y$, respectively. If the pressure falls from $P + \mathrm{d}P$ to P over a length $\mathrm{d}L$, then equating forces on a cylinder radius y and length $\mathrm{d}L$ (Fig. 3.7):

$$[(P + \mathrm{d}P) - P]\pi y^2 = 2\tau_y \pi y \,\mathrm{d}L \tag{3.12}$$

Therefore

$$\tau_y = \frac{\mathrm{d}P}{\mathrm{d}L} \cdot \frac{y}{2} \tag{3.13}$$

Note that:

- shear stress is proportional to pressure gradient;
- shear stress is proportional to radius, since $\mathrm{d}P/\mathrm{d}L$ is independent of radius;
- shear stress is independent of fluid properties;
- shear stress at the wall $\tau_R = (R/2) \cdot \mathrm{d}P/\mathrm{d}L$.

Since pressure decreases as L increases, τ takes the opposite sign to $\dot{\gamma}$, and by definition:

$$\tau_y = -\eta \frac{\mathrm{d}V_y}{\mathrm{d}y} \tag{3.14}$$

Therefore

$$\begin{aligned} \dot{\gamma}_y &\equiv \frac{\mathrm{d}V_y}{\mathrm{d}y} \\ &= -\frac{\tau_y}{\eta} \\ &= -\frac{\mathrm{d}P}{\mathrm{d}L} \cdot \frac{y}{2\eta} \end{aligned} \tag{3.15}$$

so that shear rate is also proportional to radius. Then:

$$\begin{aligned} dV_y &= -\frac{\tau_y}{\eta}\,dy \\ &= -\frac{dP}{dL}\cdot\frac{y\,dy}{2\eta} \end{aligned} \tag{3.16}$$

Integrating:

$$\int_0^r dV = -\frac{1}{2\eta}\cdot\frac{dP}{dL}\int_0^r y\,dy \tag{3.17}$$

giving:

$$V_r - V_0 = -\frac{r^2}{4\eta}\cdot\frac{dP}{dL} \tag{3.18}$$

Assuming the fluid adheres to the wall (no slip), $V_R = 0$. Then:

$$V_0 = \frac{R^2}{4\eta}\cdot\frac{dP}{dL} \tag{3.19}$$

and

$$\begin{aligned} V_r &= \frac{1}{4\eta}\cdot\frac{dP}{dL}(R^2 - r^2) \\ &= V_0\left(1 - \frac{r^2}{R^2}\right) \end{aligned} \tag{3.20}$$

giving a paraboloidal velocity profile.

The volume flow in an annulus dr wide at radius r is:

$$dQ_r = V_r \cdot 2\pi r\,dr \tag{3.21}$$

and total volumetric flow:

$$\begin{aligned} Q &= \frac{2\pi}{4\eta}\cdot\frac{dP}{dL}\int_0^R (R^2 - r^2)r\,dr \\ &= \frac{\pi R^4}{8\eta}\cdot\frac{dP}{dL} \end{aligned} \tag{3.22}$$

Rearranging:

$$dP = \frac{8\eta Q\,dL}{\pi R^4} \tag{3.23}$$

Taking equation (3.15) for shear rate at the capillary wall, and substituting for dP/dL from equation (3.22):

$$\begin{aligned} \dot{\gamma}_R &= -\frac{dP}{dL}\cdot\frac{R}{2\eta} \\ &= \frac{4Q}{\pi R^3} \end{aligned} \tag{3.24}$$

which gives the wall shear rate in terms of flow rate and die dimensions.

3.2.3 Infinite slit (Newtonian)

With the same assumptions as for the capillary, the infinite slit is T wide by H deep, where $T \gg H$, so the drag at the end surfaces can be neglected, so that flow is one-dimensional and velocity varies in the H direction only. The subscripts are y, h and X, where $X = H/2$, for the corresponding dimensions measured from the centreline (Fig. 3.8). By force balance on a region T wide by y from the centre:

$$\mathrm{d}P\, yT = \tau_y T\, \mathrm{d}L \tag{3.25}$$

Then:

$$\begin{aligned} \frac{\mathrm{d}P}{\mathrm{d}L} \cdot y &= \tau_y \\ &= -\eta \dot{\gamma}_y \\ &= -\eta \frac{\mathrm{d}V_y}{\mathrm{d}y} \end{aligned} \tag{3.26}$$

Again, shear stress is proportional to distance from the centre, to the pressure gradient, and is independent of the fluid properties. Then:

$$\begin{aligned} \mathrm{d}V_y &= -\frac{\tau_y}{\eta}\, \mathrm{d}y \\ &= -\frac{1}{\eta} \cdot \frac{\mathrm{d}P}{\mathrm{d}L}\, y\, \mathrm{d}y \end{aligned} \tag{3.27}$$

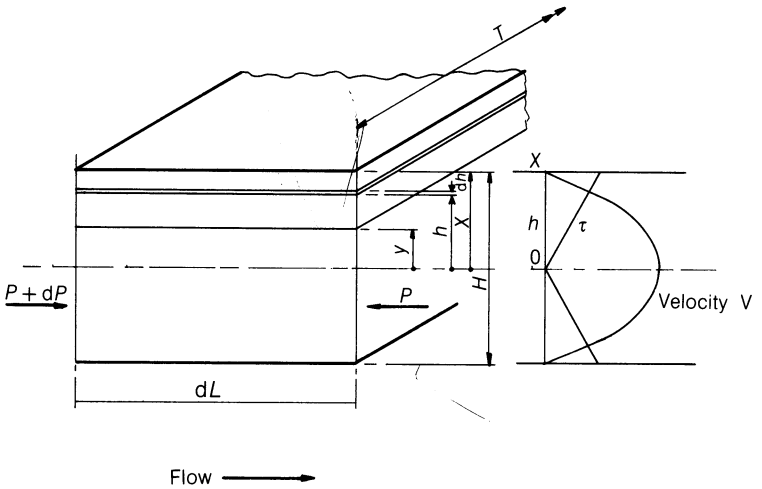


Figure 3.8 Flow in infinite slit.

Integrating:

$$\int_0^h \mathrm{d}V = -\frac{1}{\eta}\cdot\frac{\mathrm{d}P}{\mathrm{d}L}\int_0^h y\,\mathrm{d}y \tag{3.28}$$

giving:

$$V_h - V_0 = -\frac{h^2}{2\eta}\cdot\frac{\mathrm{d}P}{\mathrm{d}L} \tag{3.29}$$

But $V_X = 0$. Then:

$$\begin{aligned} V_0 &= \frac{X^2}{2\eta}\cdot\frac{\mathrm{d}P}{\mathrm{d}L} \\ &= \frac{H^2}{8\eta}\cdot\frac{\mathrm{d}P}{\mathrm{d}L} \end{aligned} \tag{3.30}$$

and

$$\begin{aligned} V_h &= \frac{1}{2\eta}\cdot\frac{\mathrm{d}P}{\mathrm{d}L}(X^2 - h^2) \\ &= \frac{1}{8\eta}\cdot\frac{\mathrm{d}P}{\mathrm{d}L}(H^2 - 4h^2) \end{aligned} \tag{3.31}$$

giving a parabolic velocity profile (uniform in the T direction).

The volume flow in a lamina $\mathrm{d}h$ thick at h from the centre is:

$$\mathrm{d}Q_h = V_h T\,\mathrm{d}h \tag{3.32}$$

and total volumetric flow:

$$\begin{aligned} Q &= 2\int_0^X \frac{T}{2\eta}\cdot\frac{\mathrm{d}P}{\mathrm{d}L}(X^2 - h^2)\,\mathrm{d}h \\ &= \frac{T}{\eta}\cdot\frac{\mathrm{d}P}{\mathrm{d}L}\left[X^2 h - \frac{h^3}{3}\right]_0^X \\ &= \frac{2T}{3\eta}\cdot\frac{\mathrm{d}P}{\mathrm{d}L}X^3 \\ &= \frac{TH^3}{12\eta}\cdot\frac{\mathrm{d}P}{\mathrm{d}L} \end{aligned} \tag{3.33}$$

where $H = 2X$. Rearranging:

$$\mathrm{d}P = \frac{12\eta Q\,\mathrm{d}L}{TH^3} \tag{3.34}$$

The wall shear rate is:

$$\begin{aligned} \dot{\gamma}_X &= -\frac{X}{\eta}\cdot\frac{\mathrm{d}P}{\mathrm{d}L} \\ &= -\frac{H}{2\eta}\cdot\frac{\mathrm{d}P}{\mathrm{d}L} \\ &= \frac{6Q}{TH^2} \end{aligned} \tag{3.35}$$

Table 3.1 Summary of flow equations

	Shear stress at wall, $\tau_w(\mathrm{N\,m^{-2}})$	*Shear rate at wall,* $\dot{\gamma}_w(\mathrm{s^{-1}})$	*Ratio* V_{max}/V_{mean}	*Pressure drop,* $dP(\mathrm{N\,m^{-2}})$	*Volumetric flow rate,* $Q(\mathrm{m^3\,s^{-1}})$
NEWTONIAN $\tau = \eta\dot{\gamma}$					
Round tube					
Radius R	$\frac{dP}{dL}\cdot\frac{R}{2}$	$\frac{4Q}{\pi R^3}$	2.0	$\frac{8\eta Q dL}{\pi R^4}$	$\frac{\pi R^4}{8\eta}\cdot\frac{dP}{dL}$
'Infinite' slit					
Width T Depth H	$\frac{dP}{dL}\cdot\frac{H}{2}$	$\frac{6Q}{TH^2}$	1.5	$\frac{12\eta Q dL}{TH^3}$	$\frac{TH^3}{12\eta}\cdot\frac{dP}{dL}$
POWER LAW $\tau \propto \dot{\gamma}^n$ $\eta = \eta_0\left(\frac{\dot{\gamma}}{\dot{\gamma}_0}\right)^{n-1}$					
Round tube					
Radius R	$\frac{dP}{dL}\cdot\frac{R}{2}$	$\frac{3n+1}{n}\cdot\frac{Q}{\pi R^3}$	$\frac{3n+1}{n+1}$	$\frac{2(3n+1)}{n}\cdot\frac{\eta_w Q dL}{\pi R^4}$	$\left(\frac{n}{3n+1}\right)\cdot\frac{\pi R^4}{2\eta_w}\cdot\frac{dP}{dL}$
'Infinite' slit					
Width T Depth H	$\frac{dP}{dL}\cdot\frac{H}{2}$	$\frac{4n+2}{n}\cdot\frac{Q}{TH^2}$	$\frac{2n+1}{n+1}$	$\frac{4(2n+1)}{n}\cdot\frac{\eta_w Q dL}{TH^3}$	$\frac{n}{4(2n+1)}\cdot\frac{TH^3}{\eta_w}\cdot\frac{dP}{dL}$

The results of these two cases of pressure flow, together with the corresponding results for flow of a power-law fluid, are given in Table 3.1. From equation (3.23) it is seen that in a capillary of constant radius, and providing viscosity is not dependent on pressure, the pressure gradient dP/dL is constant and equal to P/L. Equation (3.22) may then be rewritten:

$$Q = \frac{\pi R^4}{8\eta}\cdot\frac{P}{L} \tag{3.36}$$

or, putting $K = \pi R^4/8L$ for a die of constant dimensions:

$$Q = \frac{KP}{\eta} \tag{3.37}$$

The flow equations (3.22) and (3.33) and the corresponding power-law equations (Table 3.1) may be used to determine the effects of varying dimensions on pressure flow. For two capillaries in series, as in a stepped die, the volumetric flow rate is evidently the same in each part. Then for a Newtonian fluid, from equation (3.22):

$$\frac{\pi R_2^4}{8\eta}\cdot\frac{dP_2}{dL} = \frac{\pi R_1^4}{8\eta}\cdot\frac{dP_1}{dL}$$

or

$$\frac{dP_2}{dL} = \left(\frac{R_1}{R_2}\right)^4 \cdot \frac{dP_1}{dL} \tag{3.38}$$

If, for example, $R_2 = 0.95R_1$,

$$\frac{dP_2}{dL} = 1.228 \frac{dP_1}{dL} \tag{3.39}$$

i.e. a 5% decrease in radius gives a 22.8% increase in pressure gradient.

For a pseudoplastic power-law fluid, Table 3.1 gives for wall shear rates:

$$\dot{\gamma}_{w2} = \frac{R_1^3}{R_2^3} \dot{\gamma}_{w1} \tag{3.40}$$

and

$$\eta_{w2} = \left(\frac{R_1}{R_2}\right)^{3n-3} \cdot \eta_{w1} \tag{3.41}$$

Then for equal flow rate Q,

$$\frac{dP_2}{dL} = \frac{dP_1}{dL} \cdot \left(\frac{R_1}{R_2}\right)^4 \left(\frac{R_1}{R_2}\right)^{3n-3}$$

$$= \frac{dP_1}{dL} \cdot \left(\frac{R_1}{R_2}\right)^{3n+1} \tag{3.42}$$

Then for $R_2 = 0.95R_1$ and $n = 0.3$,

$$\frac{dP_2}{dL} = 1.102 \frac{dP_1}{dL} \tag{3.43}$$

i.e. for a highly pseudoplastic fluid, a 5% decrease in radius gives a 10.2% increase in pressure gradient.

The corresponding values for a 5% reduction in depth H of a slit of uniform width T would be 16.6% and 8.5% for $n = 1$ and $n = 0.3$, respectively.

For two capillaries of equal length in parallel, as in a multistrand die, the pressure drop and pressure gradient across each is the same. Then for a Newtonian fluid, from equation (3.23):

$$\frac{8\eta Q_2}{\pi R_2^4} = \frac{8\eta Q_1}{\pi R_1^4}$$

or

$$Q_2 = Q_1 \left(\frac{R_2}{R_1}\right)^4 \tag{3.44}$$

If $R_2 = 0.95R_1$,

$$Q_2 = 0.814Q_1 \tag{3.45}$$

i.e. a 5% reduction in radius gives an 18.6% reduction in flow rate. The mean velocity $Q/\pi R^2$ is reduced by 9.75%. This is important with, for example, a common haul-off from a multistrand die.

For a pseudoplastic power-law fluid, Table 3.1 gives:

$$\dot{\gamma}_{w2} = -\frac{1}{\eta_{w2}} \cdot \frac{R_2}{2} \cdot \frac{dP}{dL}$$

$$= \dot{\gamma}_{w1} \frac{\eta_{w1}}{\eta_{w2}} \cdot \frac{R_2}{R_1} \tag{3.46}$$

But by equation (3.7):

$$\eta_{w2} = \eta_{w1} \left(\frac{\dot{\gamma}_{w2}}{\dot{\gamma}_{w1}} \right)^{n-1} \tag{3.47}$$

Therefore

$$\frac{\dot{\gamma}_{w2}}{\dot{\gamma}_{w1}} = \frac{R_2}{R_1} \left(\frac{\dot{\gamma}_{w2}}{\dot{\gamma}_{w1}} \right)^{1-n}$$

or

$$\frac{\dot{\gamma}_{w2}}{\dot{\gamma}_{w1}} = \left(\frac{R_2}{R_1} \right)^{1/n} \tag{3.48}$$

and

$$\eta_{w2} = \eta_{w1} \left(\frac{R_2}{R_1} \right)^{(n-1)/n} \tag{3.49}$$

Then

$$Q_2 = Q_1 \left(\frac{R_2}{R_1} \right)^4 \left(\frac{R_2}{R_1} \right)^{(1-n)/n}$$

$$= Q_1 \left(\frac{R_2}{R_1} \right)^{(3+1/n)} \tag{3.50}$$

If $R_2 = 0.95R_1$ and $n = 0.3$,

$$Q_2 = 0.723Q_1 \tag{3.51}$$

i.e. a 5% reduction in radius gives a 27.7% reduction in flow rate and a 19.9% reduction in mean velocity – greater than in the Newtonian case. The corresponding values for two slits of equal width T in parallel, the depth H_2 of one being $0.95H_1$, would be a 14.3% and 23.9% reduction in flow rate for $n = 1$ and $n = 0.3$, respectively. The mean velocity is reduced by the same proportion as for the circular capillary for both values of n.

The implications of these calculations for tolerances in practical extrusion dies will be discussed in Chapter 5. In addition to pressure loss within a capillary, there is frequently an entrance loss, especially with square-entry dies, which may be equivalent to an additional die length of between $4L/R$ and $6L/R$ at low shear rates, increasing at higher rates; this is discussed in section 3.5.

A difficult aspect of shear flow occurs when shearing takes place simultaneously in more than one direction. This arises in the channel of an extruder screw, where polymer melt is simultaneously sheared along the channel, with a net flow rate dependent on the back pressure, and across the channel, with zero net flow rate. The resultant varies in both magnitude and direction, leading to lengthy equations for Newtonian fluids (see section 8.4). For non-Newtonian fluids the results are too complex to be of service in analysing industrial operation. Another case occurs when a mixing device is attached to the delivery end of the screw, e.g. a smearhead or Dulmage head. The rotation of the device causes a simple shear flow transverse to the axis (linear velocity distribution), whereas the useful output is represented by an axial pressure flow, as in a narrow slit (equation (3.33)), giving a curved, e.g. parabolic, velocity distribution; the resultant again varies in magnitude and direction. It is stated that the effective viscosity (assumed to be isotropic) at a point is governed by the maximum shear rate at that point. Experiments by Cogswell (Cogswell and Lamb, 1970) with LDPE showed a reduction in viscosity in a die following a rotating head when the speed of the latter was increased; this was attributed to a temporary chain disentanglement, possibly peculiar to this polymer.

3.2.4 Strain energy in shear

Referring to Fig. 3.6, consider a lamina dy thick parallel to the direction of shear stress and moving with velocity w. Then the shear force acting over the interface between this and an adjacent lamina having velocity $w + dw$ is:

$$F = \tau xz \tag{3.52}$$

The distance over which this acts in time t is:

$$[(w + dw) - w]t \tag{3.53}$$

and the work done in time t:

$$Ft[(w + dw) - w] = \tau xz\, t\, dw \tag{3.54}$$

But the volume of the lamina is $xz\, dy$, so the work done in time t per unit volume is:

$$\frac{\tau xz\, t\, dw}{xz\, dy} = \tau \frac{dw}{dy} t \tag{3.55}$$

and the strain energy per unit volume:

$$\tau \frac{dw}{dy} = \tau\dot{\gamma}\,\mathrm{N\,s^{-1}\,m^{-2}} \tag{3.56}$$

Substituting viscosity from equation (3.5) gives:

$$\text{Strain energy per unit volume} = \frac{\tau^2}{\eta}$$
$$= \eta\,\dot{\gamma}^2\,\text{N s}^{-1}\,\text{m}^{-2} \text{ or } \text{W m}^{-3} \tag{3.57}$$

In the case of simple shear, substituting from equation (3.11) gives:

$$\text{Strain energy per unit volume} = \frac{\eta W^2}{h^2}\,\text{W m}^{-3} \tag{3.58}$$

or

$$\text{Strain energy per unit surface area} = \frac{\eta W^2}{h}\,\text{W m}^{-2} \text{ (in simple shear)} \tag{3.59}$$

For a power-law fluid, substitution of equation (3.6) in equation (3.56) gives:

$$\text{Strain energy per unit volume} = K\dot{\gamma}^{n+1}$$
$$= K\left(\frac{W}{h}\right)^{n+1} \text{ (simple shear)} \tag{3.60}$$

In a circular capillary, from equation (3.15):

$$\dot{\gamma}_r = -\frac{\mathrm{d}P}{\mathrm{d}L}\cdot\frac{r}{2\eta} \tag{3.61}$$

Then for a Newtonian fluid, combining equation (3.57) and (3.61), the strain energy in an annulus r to $r + \mathrm{d}r$ is:

$$\left(\frac{\mathrm{d}P}{\mathrm{d}L}\right)^2\frac{r^2}{4\eta}\cdot 2\pi rL\,\mathrm{d}r = \frac{\pi L}{2\eta}\left(\frac{\mathrm{d}P}{\mathrm{d}L}\right)^2\cdot r^3\,\mathrm{d}r \tag{3.62}$$

Total strain energy in the capillary is:

$$\frac{\pi L}{2\eta}\left(\frac{\mathrm{d}P}{\mathrm{d}L}\right)^2\int_0^R r^3\,\mathrm{d}r = \frac{\pi L}{8\eta}\left(\frac{\mathrm{d}P}{\mathrm{d}L}\right)^2\cdot R^4 \tag{3.63}$$

The distribution of local strain energy in a capillary, given by equation (3.62), is plotted in Fig. 3.9.

Substituting from flow equation (3.22):

$$\text{Total strain energy} = \frac{8\eta LQ^2}{\pi R^4}$$
$$= Q\,\mathrm{d}P \text{ (in circular capillary)} \tag{3.63}$$

where $\mathrm{d}P$ is the pressure drop in length L.

Similarly in an infinite slit, from equation (3.26):

$$\dot{\gamma}_h = -\frac{\mathrm{d}P}{\mathrm{d}L}\cdot\frac{h}{\eta} \tag{3.64}$$

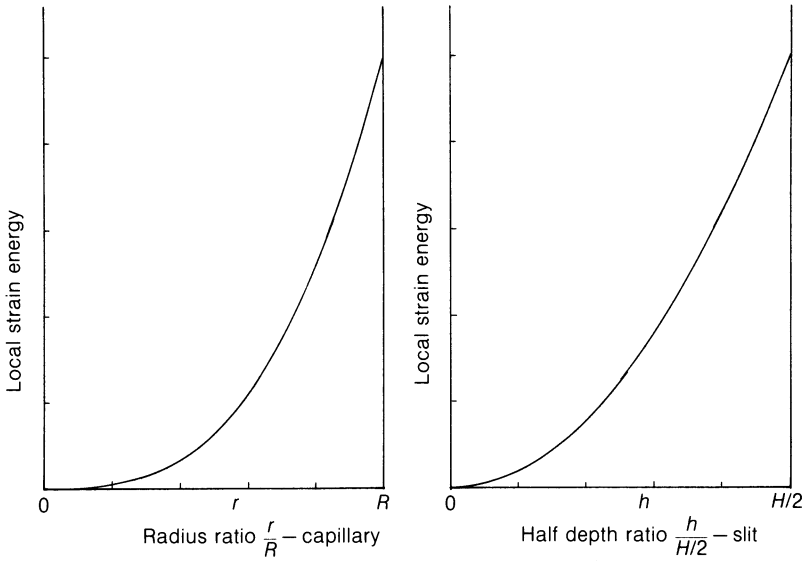


Figure 3.9 Transverse variation of local strain energy.

The strain energy in lamina h to $h + \mathrm{d}h$ is:

$$\left(\frac{\mathrm{d}P}{\mathrm{d}L}\right)^2 \frac{h^2}{\eta} \cdot TL\,\mathrm{d}h = \frac{TL}{\eta}\left(\frac{\mathrm{d}P}{\mathrm{d}L}\right)^2 \cdot h^2\,\mathrm{d}h \tag{3.65}$$

Total strain energy is:

$$\frac{2TL}{\eta}\left(\frac{\mathrm{d}P}{\mathrm{d}L}\right)^2 \int_0^X h^2\,\mathrm{d}h = \frac{2TL}{3\eta}\left(\frac{\mathrm{d}P}{\mathrm{d}L}\right)^2 X^3$$

$$= \frac{TL}{12\eta}\left(\frac{\mathrm{d}P}{\mathrm{d}L}\right)^2 H^3 \tag{3.66}$$

since $X = H/2$ as shown in Fig. 3.8. Substituting from flow equation (3.33):

$$\text{Total strain energy} = \frac{12\eta Q^2 L}{TH^3}$$

$$= Q\,\mathrm{d}P \text{ (in infinite slit)} \tag{3.67}$$

where $\mathrm{d}P$ is the pressure drop in length L.

The distribution of local strain energy in a wide slit, given by equation (3.65), is also plotted in Fig. 3.9.

The order of magnitude of strain energy and viscous heating is illustrated by the following example. In a 100 mm diameter extruder screw, with channel 100 mm wide, at 1 rps, the velocity is approximately $0.3\,\mathrm{m\,s^{-1}}$. If the channel depth is 10 mm, the shear rate W/h is approx. $0.3/0.01 = 30\,\mathrm{s^{-1}}$. Then from

Chapter 6, the drag flow rate is given by:

$$Q_D = \frac{Wbh}{2}$$
$$= \frac{\pi \times 0.1 \times 0.1 \times 0.01}{2}$$
$$= 1.57 \times 10^{-4}\,m^3\,s^{-1} \quad (6.9)$$

Assume that viscosity is $10^3\,N\,s\,m^{-2}$. Then considering the downchannel velocity only, which in drag flow is simple shear:

$$\text{Strain energy} = \eta\,\dot{\gamma}^2$$
$$= 10^3 \times 30^2$$
$$= 9 \times 10^5\,W\,m^{-3}$$

and

$$\text{Volume of one turn} \simeq \pi Dbh$$
$$= \pi 0.1 \times 0.1 \times 0.01$$
$$\simeq 3 \times 10^{-4}\,m^3$$

Then

$$\text{Strain energy per turn} = 9 \times 10^5 \times 3 \times 10^{-4}$$
$$= 2.7 \times 10^2\,W$$

Taking from Table 4.1 density and specific heat as $750\,kg\,m^{-3}$ and $2500\,J\,kg^{-1}\,K^{-1}$, respectively, the heating rate is:

$$\frac{dT}{dt} = \frac{9 \times 10^5}{750 \times 2500}$$
$$\simeq 0.5°C\,s^{-1}$$

In a capillary, say a die 5 mm in diameter by 10 mm long, and taking the flow rate $Q = 0.1 \times 10^{-4}\,m^3\,s^{-1}$ and a Newtonian viscosity of $10^3\,N\,s\,m^{-2}$,

$$dP = \frac{8\eta Q dL}{\pi R^4}$$
$$= \frac{8 \times 10^3 \times 0.1 \times 10^{-4} \times 0.01}{\pi (2.5)^4 \times 10^{-12}}$$
$$= 6.5 \times 10^6\,N\,m^{-2}$$

The wall shear rate is:

$$\dot{\gamma}_R = \frac{4Q}{\pi R^3}$$
$$= \frac{4 \times 0.1 \times 10^{-4}}{\pi \times 2.5^3 \times 10^{-9}}$$
$$= 815\,s^{-1}$$

and volume of die

$$= \pi \times 2.5^2 \times 10^{-6} \times 0.01$$
$$= 19.6 \times 10^{-8}\,\text{m}^3$$

The energy dissipated in passing die is

$$Q \cdot dP = 0.1 \times 10^{-4} \times 6.5 \times 10^6$$
$$= 65\,\text{W}$$

Then

$$\text{Strain energy} = \frac{65}{19.6 \times 10^{-8}}$$
$$= 3.32 \times 10^8\,\text{W m}^{-3}$$

Note that this is half that given by $\eta\dot{\gamma}_R^2$, i.e. as if the strain energy at the wall persisted over the whole capillary – see Fig. 3.9. The time to pass die is:

$$\frac{19.6 \times 10^{-8}}{0.1 \times 10^{-4}} = 19.6\,\text{ms}$$

and the heating rate is:

$$\frac{dT}{dt} = \frac{3.32 \times 10^8}{750 \times 2500}$$
$$= 177°\text{C s}^{-1}$$

Thus the temperature rise in passing die is:

$$dT = 177 \times 19.6 \times 10^{-3}$$
$$= 3.97°\text{C}$$

To compare these shear strain energies with that in elongational flow, consider a die entrance, reducing in diameter from 50 mm to 5 mm in 20 mm length – a sharp taper in order to exaggerate the elongational component. Evidently, due to the lower average shear rate, the shear strain energy in the taper entry will be less than in the capillary. Now

$$\text{Volume of entrance} = \frac{\pi}{3} \times 25^2 \times 10^{-6} \times 20 \times 10^{-3}$$
$$= 13.09 \times 10^{-6}\,\text{m}^3$$
$$\text{Half angle of taper} = \tan^{-1}\left(\frac{50-5}{2 \times 20}\right)$$
$$= \tan^{-1} 1.125$$
$$= 48.4°$$

From equation (3.69) we have:

$$\text{Elongational strain} = \log_e \left(\frac{50}{5}\right)^2$$
$$= 4.605$$

The flow rate, as before, is:

$$Q = 0.1 \times 10^{-4}\,\text{m}^3\,\text{s}^{-1}$$

and the time to pass taper is:

$$\frac{\text{Volume}}{Q} = \frac{13.09 \times 10^{-6}}{0.1 \times 10^{-4}}$$
$$= 1.309\,\text{s}$$

Then average strain rate is given by:

$$\dot{\varepsilon} \equiv \frac{d\varepsilon}{dt}$$
$$= \frac{4.605}{1.309}$$
$$= 3.518\,\text{s}^{-1}$$

Assume a tensile viscosity of:

$$\Lambda = 3\eta$$
$$= 3 \times 10^3\,\text{N s m}^{-2}$$

By analogy with shear strain energy, elongational strain energy is given by:

$$\Lambda\dot{\varepsilon}^2 = 3 \times 10^3 \times 3.518^2$$
$$= 37.1 \times 10^3\,\text{W m}^{-3}$$

Note that the shear strain energy in the die is of the order of 10^4 times this elongational energy. The elongational energy stored in the taper will be:

$$37.1 \times 10^3 \times 13.09 \times 10^{-6} = 0.486\,\text{W}$$

Much of this energy is stored elastically and will be released by elastic recovery at the die exit, giving lateral swelling and retraction in length. However, if this energy is dissipated by internal friction in the parallel channel, e.g. in a very long die, the rate of temperature rise will be

$$\frac{dT}{dt} = \frac{37.1 \times 10^3}{750 \times 2500}$$
$$= 0.0198°\text{C}\,\text{s}^{-1}$$

which is negligible compared with that due to shear in the capillary.

Strain energy and viscous heating can be derived in more complex cases where an analytical expression is available for shear rate (or shear stress) and (in non-isothermal or non-Newtonian cases) for viscosity. Combined drag and pressure flow is studied in section 8.4.

3.3 EXTENSIONAL FLOW

Extensional flow with a free surface occurs in many downstream processes such as fibre drawing, film blowing and bottle blowing. These, and the associated changes in morphology, e.g. strain-induced crystallization and uniaxial or biaxial orientation, are beyond the scope of this book and the reader is referred to the extensive literature. In steady operating conditions, extensional flow within the channel of the extruder screw is likely to be masked by drag and pressure shear flows. Extensional flow within the geometry defined by solid boundaries occurs in the die adaptor between the screw and the die and within converging sections of the die. In these cases it is accompanied by shear (capillary) flow due to boundary friction, the energy for both of these coming from the longitudinal pressure gradient. By analogy with equation (3.57), the strain energy is $\Lambda\dot{\varepsilon}^2$ per unit volume, and unless the transition is very rapid (when non-axial flow may occur), the elongational strain rates are modest. As mentioned on p. 46, much of the elongational strain energy is stored elastically within the polymer, and on release from the constraint of the die is recovered, causing swelling of the extrudate and retraction in length. However, as the melt is only partially elastic, the balance of the energy is transformed into heat by viscous dissipation within the die; the longer the residence time in the die, e.g. by increasing die length, the greater the dissipation and the less the die swell (Fig. 3.10).

For a circular converging channel, the extensional strain at constant volume V (Fig. 3.2) is:

$$\begin{aligned}\varepsilon &= \frac{L+\mathrm{d}L}{L} - 1 \\ &= \frac{V}{\pi r^2} \cdot \frac{\pi(r+\mathrm{d}r)^2}{V} - 1 \\ &= \frac{(r+\mathrm{d}r)^2}{r^2} - 1 \\ &\simeq \frac{2\,\mathrm{d}r}{r}\end{aligned} \tag{3.68}$$

The total strain between r_0 and r_1 is given by:

$$\begin{aligned}\varepsilon_{\text{total}} &= 2\int_{r_0}^{r_1} \frac{\mathrm{d}r}{r} \\ &= [2\log_e r]_{r_0}^{r_1} \\ &= \log_e \left(\frac{r_1}{r_0}\right)^2\end{aligned} \tag{3.69}$$

If the volumetric flow rate is $Q\,\mathrm{m^3\,s^{-1}}$ and the velocity at channel radius r is:

$$\frac{\mathrm{d}L}{\mathrm{d}t} = \frac{Q}{\pi r^2} \tag{3.70}$$

then

$$Q\,dt = \pi r^2\,dL$$
$$= \pi[(r + dr)^2 - r^2]\,L$$
$$= 2\pi r L\,dr$$

or

$$\frac{dr}{dt} = \frac{Q}{2\pi r L} \tag{3.71}$$

But the total time is expressed as:

$$\frac{\text{Volume of channel}}{\text{Volumetric flow rate}} = \frac{V}{Q} \tag{3.72}$$

Thus average elongational strain rate is given by:

$$\dot{\varepsilon} = \frac{Q}{V} \log_e \left(\frac{r_1}{r_0}\right)^2 \tag{3.73}$$

Note that a constant strain rate and constant extensional stress require a parabolic rather than linear convergence, and the former is preferably approximated in practice by a series of decreasing taper angles, as explained in Chapter 5.

The pressure drop in a convergent channel due to extensional flow is given by Powell (1974) in terms of the shear rate at the exit:

$$dP_{Ec} = \frac{\Lambda\dot{\gamma}F_3(R_0 - R_1)}{3\,dL} \tag{3.74}$$

where Λ is the extensional viscosity (equation (3.2)) and $F_3 = 1 - (R_1/R_0)^3$. He also states that this extensional pressure drop is small for small taper angles. The extensional viscosity is, on theoretical grounds, frequently taken as three times the zero-shear viscosity. For many polymer melts, with the notable exception of LDPE (Cogswell, 1968), experiment indicates that the extensional viscosity is independent of stress or strain rate. Powell (1974) also states that where shear and extensional flows are concurrent, as in a tapered channel, they may be treated separately and the total pressure drop will be the sum of the two.

3.4 ELASTIC EFFECTS

The principal effect of melt elasticity is in recovery from shear and/or elongational strain imposed at the entrance or in flow through the die. In the absence of intentional drawing, it appears as a lateral swelling at the die exit and associated retraction in length, especially during a slow extrusion of parisons for blow moulding. The elasticity may be demonstrated by pulling

sharply on the extrudate, when the extruder has just stopped or is extruding slowly, and then releasing it, when it will (partly) spring back. Polymer melts are also partially elastic in shear flow e.g. partial recovery after shearing in a cone and plate viscometer. It might also be seen as a momentary peak in screw torque during start-up, but in practice would be difficult to distinguish from mechanical inertia. As with elongational flow, the elastic strain is, with time, converted into viscous dissipation, and when the extruder is slowed or stopped the recovery of the remaining strain would be difficult to distinguish from the slow 'drooling' from the die due to expansion on release of residual pressure. The most significant effect within the extruder is probably when polymer enters the flight clearance from the channel and is suddenly subjected to much greater shear rate; if the melt is non-Newtonian and appreciably elastic, the viscosity

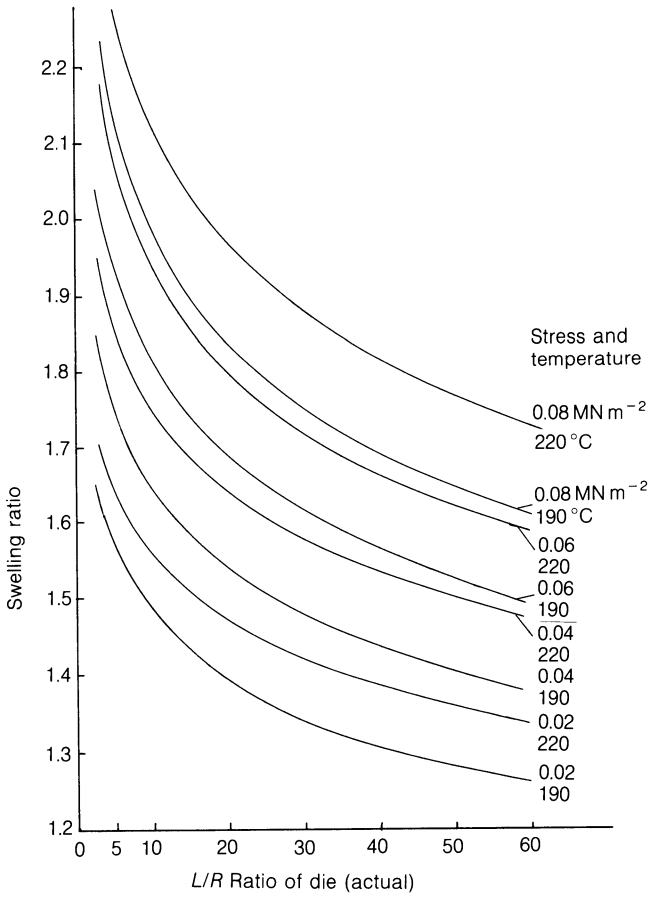


Figure 3.10 Swelling ratio vs die length – polystyrene.

will not fall instantaneously to that corresponding to the higher shear rate, giving a transient high stress and accompanying shear heating. Conversely, at the exit from the flight clearance, the viscosity will not instantaneously rise to match the sudden reduction of shear rate; these effects, spaced by an interval of 0.1 s or less, may not be identical and mutually cancelling.

The swelling ratio from a circular capillary, defined as the ratio of the extrudate diameter to the die diameter, depends on the polymer, the melt temperature, the die length (L/R ratio), the die entry geometry and the shear stress or shear rate within the die. The extrudate diameter is usually measured after contraction on cooling to room temperature, but some optical methods have been used to measure the diameter 'on-line' while still near melt temperature. The swelling ratio decreases as die length is increased, giving more time for relaxation, tending to a constant value for very long dies (Fig. 3.10). The effect of melt temperature is minimized by correlating on a basis of shear stress rather than shear rate, and the author's data in Fig. 3.11 for a sample of crystal polystyrene suggest that the effect of an increase in temperature is then an almost constant small increase in swelling ratio over a considerable range of shear stress and L/R ratio. In this case the increase is between 0.05 and 0.15 for a 30°C increase in temperature. Powell (1974) presents generalized curves for swelling ratio in thickness and width from slit dies, as well as circular capillaries, in terms of recoverable shear strain. The latter, however, must be determined experimentally for each polymer and temperature.

A number of flow defects which appear related to elastic behaviour of polymer melts have been observed and studied extensively (Cogswell, 1981). Surface roughness on the extrudate (sharkskin, orange peel etc.) appears to be related to surface effects within the die, due to excessive shear stress near the wall or to 'stick-slip' intermittent adhesion to the die surface, aggravated by low metal temperatures and influenced to some extent by the surface finish and nature of the metal surface. As with die swell, these may be modified or minimized by drawing the extrudate from the die. Other flow defects have been shown to disturb the whole flow, of which melt fracture is probably the most familiar and most studied. This seems to originate when a critical shear stress is exceeded in the die, independent of temperature and die length, though a critical extensional strain rate at the die entry has also been proposed. The effect may be minimized, but without appreciably altering the threshold, by use of finely tapered die entrances (equation (3.73)).

Intentional mono- or biaxial orientation by drawing after the die has been mentioned in Chapter 2 in connection with fibre and film production. Within the extruder and die orientation may be produced by flow, e.g. longitudinally during flow through a long die or in wire covering or transversely during rapid divergence in a large tube die. The low stresses possible at melt temperatures, coupled with more rapid relaxation, lead to generally low levels of orientation in the product, compared with fibre and film drawing. The effects may well be

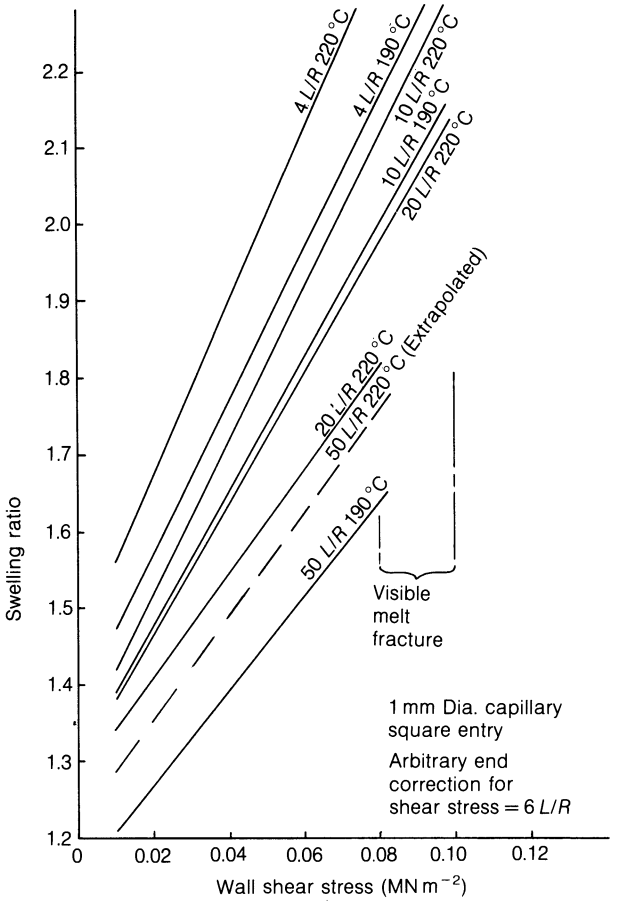


Figure 3.11 Swelling ratio vs shear stress – GP polystyrene.

undesirable, being manifested in directional loss of impact strength. Associated with the orientation may also be strain-induced crystallization if the strain is maintained while the product cools through the appropriate temperature range.

3.5 MEASUREMENT OF VISCOSITY AND ELASTICITY

A detailed survey of rheometers and viscometers would be inappropriate; only the main requirements and limitations for practical processing will be discussed. Measurement of (shear) viscosity is required at the temperatures and shear rates encountered in the extruder and die, and ready means of checking that these characteristics are maintained (section 11.4). The

processing temperature range for a particular polymer and product is usually known, but data over a range of at least 50°C are desirable so that the temperature coefficient of viscosity (e.g. β in equation (3.10)) can reliably be determined. Obviously the viscometer must be capable of attaining, and accurately holding, the required temperatures, and be mechanically robust enough to withstand the pressures and torques required by high viscosities. Shear rates in the screw channel are normally in the range 10–100 s^{-1}, which approximates to that of the capillary specified in BS 2782 (1970) Method 720A. However, both in the die and over the flight clearance the shear rates may be as high as 2000–3000 s^{-1}, where the Melt Flow Rate gives little indication, owing to non-Newtonian variation of viscosity with shear rate. For similar reasons parallel plate rotational viscometers are of little use, since they represent a range of shear rates from centre to circumference and so for non-Newtonian fluids give only a (weighted) average viscosity over that shear rate range. The cone and plate viscometer gives a uniform shear rate over the radius, but must be capable of operating over a substantial speed range to cover the required shear rates. Although these instruments are capable of producing accurate research data, including elastic recovery in some cases, they are limited to rather low shear rates and stresses, partly due to slippage at the surfaces. The capillary viscometer involves a range of shear rates simultaneously across the capillary radius (equation (3.15)) but reproduces the shear conditions in simple dies; data are normally produced in terms of the shear rate at the wall (the maximum value) as represented by equation (3.24) (apparent shear rate) or the pseudoplastic 'true' shear rate (Table 3.1). The corresponding apparent and 'true' viscosities are determined to satisfy equation (3.5). In capillary flow, either viscosity and corresponding shear rate may be used, as long as the same equation is used in calculating the production die as was used in determining the viscosity from experimental data. A number of corrections may be required, of which the most important is the Bagley end correction, which requires preliminary measurements with dies of at least two L/R ratios. The capillary viscometer is capable of operating over a wide range of predetermined shear rates, with mechanical constant speed drive to the piston, or predetermined shear stresses with adjustable gas pressure. The upper limit is generally set by the onset of melt fracture, which although it nominally occurs at constant shear stress, may cause severe distortion in a square-entry viscometer die which would hardly be apparent in a well-streamlined production die. The viscometer may also be used for determining swell ratios over a range of temperatures and shear stresses, as illustrated by Figs 3.10 and 3.11.

Accurate extensional data in the ranges useful for extruder die design are difficult to obtain without sophisticated laboratory equipment. Many research workers have used 'zero-length' or orifice plate dies to obtain data on end corrections, recoverable strain, etc., though there remains a question as to whether the flow conditions to the die entry are modified by the different exit

flow pattern (profile and velocity distribution) compared with a die of finite length. Another possibility is to use tapered dies once the parameters for shear flow have been determined (section 3.3); the example on p. 46 indicates that the extensional component of flow may be too small for accurate results.

4 Thermal and energy properties in processing

4.1 THERMAL PROPERTIES

The specific volume of polymers in the solid state increases approximately linearly with temperature, so that a coefficient of (cubic) expansion may usefully be used. In the melt state, expansion is also approximately linear with temperature, but usually at a higher rate than in the solid. Semi-crystalline polymers including polyolefines, nylons, polyoxymethylene (POM) and polyethylene terephthalate (PETP) also show a fairly sudden increase in specific volume just below the melting point, due to disordering of the crystalline regions to the completely amorphous state in the melt; the magnitude of this increase will depend on the degree of crystallinity in the solid polymer, which, especially with low density polyethylene and polypropylene, is a function, *inter alia*, of the preceding cooling rate. The degree of crystallinity is normally unknown, being only one factor affecting solid density. However, this does not affect density ρ ($kg\,m^{-3}$) and specific volume in the melt, though data on the latter are not always available. The melt density of LDPE at 190°C, for example, is approximately $760\,kg\,m^{-3}$ ($0.76\,g\,cm^{-3}$) compared with 920–940 $kg\,m^{-3}$ at room temperature, so it is important that the appropriate value is used in converting mass to volumetric flow and vice versa at processing temperature (Fig. A.1).

Specific heat C_p ($J\,kg^{-1}\,K^{-1}$) varies little with temperature in the solid state but is somewhat higher in the melt state. As is mentioned in section 8.1, a constant specific heat is adequate in calculating the effects, e.g. on energy balance, of small changes in operating conditions. However, when heating semi-crystalline polymers additional heat is absorbed near the melting point in melting the crystallites, giving rise to a sharp peak in the curve of specific heat; it is thus preferable to use the integrated form which is internal energy (sensible heat) in $J\,kg^{-1}$ versus temperature (Fig. A.2), where the total energy I

at the die is required. This has similar shape to the specific volume curve, and similarly the lower end depends on initial crystallinity in the solid state. At constant pressure, as proposed in section 8.1, changes in enthalpy may be regarded as equal to corresponding changes in internal energy.

Polymers in both solid and molten states are good thermal insulators, i.e. values of thermal conductivity k ($W\,m^{-1}\,K^{-1}$) are very low in comparison with metals used in construction of extruders and dies. Thermal conductivity of insulators is difficult to measure with accuracy, especially in liquids, and published data on conductivity of polymers at melt temperatures are scarce and conflicting. Some previously unpublished data (Adamski, 1974) are presented in Figs A.4 and A.5.

Table 4.1 Thermal properties: conversion factors and typical values

Property	*SI*	*c.g.s*	*f.p.s*
Density	1000 kg m^{-3}	1 g/cm^3	62.35 lb/ft^3 0.0361 lb/in^3
Viscosity	1 N s m^{-2}	10 poise (P)	2420 lb/h · ft
Specific heat	1 MJ kg^{-1} K^{-1}	238.9 cal/g · °C	–
	4.19 × 10^3 J kg^{-1} K^{-1}	1 cal/g · °C	1 BTU/lb · °F 1 CHU/lb · °C
Thermal conductivity	1 W m^{-1} K^{-1}	0.002 39 cal/cm · s · °C	6.93 BTU · in/ft^2 · h · °F 0.5775 BTU · ft/ft^2 · h · °F
	0.0419 W m^{-1} K^{-1}	1 × 10^{-4} cal/cm · s · °C	–
Heat transfer coefficient	1 W m^{-2} K^{-1}	0.239 × 10^{-4} cal/cm^2 · s · °C	0.176 BTU/ft^2 · h · °F 0.176 CHU/ft^2 · h · °C
Work	1 J	0.239 g · cal	9.48 × 10^{-4} BTU 5.27 × 10^{-4} CHU

	Air (at NTP)	*Water (at 15°C)*	*Steel*	*LDPE*
Density ($kg\,m^{-3}$)	1.224	1000	7800	760 (at 180°C)
Viscosity ($N\,s\,m^{-2}$)	1.80 × 10^{-5}	1.12 × 10^{-3}	–	10^2–10^3
Specific heat ($J\,kg^{-1}\,K^{-1}$)	1005	4190	503	2300–2850
Thermal conductivity ($W\,m^{-1}\,K^{-1}$)	0.0255	0.585	50 (Copper 400)	0.33–0.50
Prandtl No. ($C_p\eta/k$)	0.70	8.0	–	5 × 10^6
Latent heat ($J\,kg^{-1}$)	–	22.6 × 10^5 (steam)	–	1.3 – 1.7 × 10^5
Thermal diffusivity ($m^2\,s^{-1}$)	–	–	1.3 × 10^{-5}	1.5 – 3 × 10^{-7}

As discussed below, the low values of conductivity mean that heat conduction within the polymer may be neglected in comparison with conduction in the metal barrel wall, e.g. longitudinally from zone to zone. Its main significance is in limiting heat transfer, e.g. from the barrel heaters in the melting process (Chapter 7) and dissipating heat generated by internal shear heating (section 8.4). Where such heat flows take place, substantial temperature gradients and temperature differences will be established, especially in thick sections, and these will be slow to disappear.

Thermal diffusivity $\alpha = k/\rho C_p$ ($m^2 s^{-1}$) is significant in transient heat conduction (section 8.4) and may be more simply measured directly from (transient) cooling experiments than by calculation from the constituent values. However, doubt has been cast on its significance where the latter are varying. It is used in section 8.4 in relation to dissipation within the metal barrel of viscous heating from the flight clearance. Since much of the existing data are in f.p.s. or c.g.s. units, conversion factors and some typical values are given in Table 4.1.

4.2 THERMAL CONDUCTION

Steady thermal conduction in one dimension is given by the Fourier equation:

$$q = -kA \frac{dT}{dx} \tag{4.1}$$

where q is the rate of heat flow (W), k is the thermal conductivity ($W m^{-1} K^{-1}$), A is the cross-section through which heat is conducted (m^2) and $-dT/dx$ is the temperature gradient ($K m^{-1}$) in the direction of heat flow, the negative sign indicating that the heat flows in the direction of falling temperature. This equation illustrates that heat flow is necessarily accompanied by, and proportional to, a temperature gradient. It is also proportional to the conductivity, so that the low thermal conductivity of polymers implies small heat flows and/or large temperature gradients. At a given heat flow, the temperature difference increases with distance (thickness) through which heat is conducted, so that the temperature difference may be appreciable through a thick extruder barrel. An increase of thickness at constant temperature difference implies a smaller heat flow – hence cooling passages are kept close to the mould surface in injection and blow moulds. Where heat is conducted through layers of two or more materials of different conductivity, the heat flow is constant so that:

$$\begin{aligned} q &= -k_1 A_1 \frac{dT_1}{dx_1} \\ &= -k_2 A_2 \frac{dT_2}{dx_2} \end{aligned} \tag{4.2}$$

and if the cross-sections are the same, the **heat flux** is expressed as:

$$\frac{q}{A} = -k_1 \frac{dT_1}{dx_1}$$

$$= -k_2 \frac{dT_2}{dx_2} \tag{4.3}$$

Then:

$$\frac{dT_1/dx_1}{dT_2/dx_2} = \frac{k_2}{k_1} \tag{4.4}$$

that is, the temperature gradients are inversely proportional to the conductivities. Taking the temperature of the interface as T', this can be rewritten as:

$$\frac{T_1 - T'}{T' - T_2} = \frac{k_2\, dx_1}{k_1\, dx_2} \tag{4.5}$$

so that the total temperature difference $T_1 - T_2$ is subdivided in proportion to the respective thicknesses dx_1, dx_2 and inversely as the conductivities.

If heat is conducted from barrel heaters through a 30 mm thick barrel (k for steel is 50 $W\,m^{-1}\,K^{-1}$) and a 5 mm thickness of LDPE ($k = 0.5\,W\,m^{-1}\,K^{-1}$) with an overall temperature difference of 100°C, the temperature differences across barrel and polymer will be 5.7 and 94.3°C, respectively. Heat conduction in two or three dimensions generally requires digital computation, which is rarely justified in steady-state extrusion. However, in the particular case of radial conduction through a cylinder of length L, e.g. an extruder barrel, the heat flow q is constant but the area is proportional to radius and hence the temperature gradient must increase towards the centre. Integration of equation (4.1) between inner and outer radii R_1 and R_2 gives:

$$q = \frac{2\pi kL(T_2 - T_1)}{\log_e (R_2/R_1)} \tag{4.6}$$

In transient conduction, as in the initial warm-up of a machine, heat is simultaneously gained (or lost) by each element and conducted through it to and from adjacent elements. The former changes the temperature of the element which in turn modifies the temperature gradients determining conduction. By use of the conduction equation (4.1) for the instantaneous conduction into and out of an element and a heat balance in which the difference of these equals the sensible heat gained (or lost) by the element, the following equation is obtained for one-dimensional transient conduction in the absence of internal heat generation, such as chemical reaction or internal shearing:

$$\frac{dT}{dt} = \alpha \frac{d^2T}{dx^2} \tag{4.7}$$

where t is time, x is distance in direction of heat flow, and thermal diffusivity $\alpha = k/\rho C_p$ ($m^2\,s^{-1}$).

A common case is where a solid body at uniform temperature T_b is suddenly placed in contact with surroundings at a uniform and constant temperature T_a. Graphical solutions are available (McAdams, 1954, pp. 33ff.) for temperature T at time t and distance r from the centre of a body of thickness/diameter $2r_m$, in terms of an unaccomplished temperature change

$$Y = \frac{T_a - T}{T_a - T_b}$$

a relative time

$$X = \frac{\alpha t}{r_m^2}$$

a resistance ratio

$$m = \frac{k}{hr_m}$$

and a radius ratio

$$n = \frac{r}{r_m}$$

In the special case of an infinite slab and where the surface heat transfer coefficient h^* is very large (negligible resistance), $m \simeq 0$ and

$$\frac{T_a - T}{T_a - T_b} = \frac{4}{\pi}\left(e^{-a_1 X}\sin\frac{\pi x}{2r_m} + \frac{1}{3}e^{-9a_1 X}\sin\frac{3\pi x}{2r_m} + \frac{1}{5}e^{-25a_1 X}\sin\frac{5\pi x}{2r_m} + \cdots\right) \quad (4.8)$$

where a_1 equals $(\pi/2)^2$ (from McAdams 1954, equation (3.3)). The total heat absorbed, $Q = 2r_m A\rho C_p(T_{avg} - T_b)$, by the body up to time t is given by a space-average temperature rise, $T_{avg} - T_b$, where:

$$\frac{T_{avg} - T_b}{T_a - T_b} = 1 - \frac{8}{\pi^2}\left(e^{-a_1 X} + \frac{1}{9}e^{-9a_1 X} + \frac{1}{25}e^{-25a_1 X} + \cdots\right) \quad (4.9)$$

(from McAdams 1954, equation (3.4)). It should be noted that in this case the surface temperature of the solid rises instantaneously to T_a of the surroundings, with progressively smaller and slower rises towards the centre.

The complications of two- or three-dimensional transients in simple solid shapes can be avoided by approximate corrections (McAdams 1954, pp. 40–43) to the one-dimensional methods.

Where the surface heat transfer coefficient h is small ($m \to \infty$) and the surface resistance controls the heat flow, this and the temperature increases in the solid at a given time will evidently be smaller. If the temperature gradient in the solid is ignored, for an infinite slab the temperature of the solid as a function

* The symbol h is conventional, but must be distinguished from screw channel depth in Chapters 6,7 and 8.

of time is given by:

$$-\log_e Y = \frac{X}{m} \tag{4.10}$$

(McAdams 1954, equation (3.5)) and the heat transferred is evidently $(T - T_b)$ multiplied by the mass and specific heat of the slab.

For conditions not covered by the above analytical relations, numerical or graphical methods may be utilized. An example of a numerical method and the analytic methods are given in appendix C.5 for the transient local heating of the extruder barrel due to the high shear heat generation in the flight clearance.

Heat radiation may be significant in the cooling of films and sheets; in the extruder it makes a small contribution to the heat losses from the outer surfaces of the barrel and die, bearing in mind that the temperature of the heaters may fluctuate well above the nominal barrel or die temperature.

The Stefan–Boltzmann law of radiation from a 'black' body is:

$$W = \sigma T^4 \tag{4.11}$$

where W is the emissive power ($W\,m^{-2}$), T the absolute temperature (K) and the Stefan–Boltzmann constant $\sigma = 5.67 \times 10^{-8}\,W\,m^{-2}\,K^{-4}$. This equation was used as part of the calculation for values in Table C.1. For small temperature differences, the radiant heat transmission from a body at T_1 to surroundings at T_0 may be taken as approximately proportional to $T_1 - T_0$.

4.3 NON-ISOTHERMAL FLOW AND HEAT TRANSFER

4.3.1 Velocity distribution

In Chapter 3 it was shown (equation (3.13)) that in capillary flow, shear stress increases in direct proportion to radius, from zero at the centre to a maximum at the wall, and independent of the fluid properties. In isothermal flow of a Newtonian fluid, viscosity is constant and, by equation (3.5), shear rate is similarly proportional to radius. When this is integrated to give velocities, the distribution of velocity is parabolic (strictly, paraboloidal – see mean velocity in Table 3.1). If the fluid is heated from the wall equation (4.1) indicates a (downward) temperature gradient towards the centre, and thus viscosity will be lower at the wall than in the centre. Thus the shear rate will be increased near the wall and decreased near the centre in comparison with the isothermal case, giving a flattened profile – b in Fig. 4.1 compared with the parabolic curve a. If the fluid is cooled, the temperature and viscosity gradients will be reversed, leading to a lower shear rate at the wall and a more peaked profile (Fig. 4.1, curve c). The curves are drawn in Fig. 4.1 to indicate approximately the same mean velocity and volumetric flow rate. In isothermal pseudoplastic flow, the viscosity decreases with increasing shear stress, again giving higher shear rates near the wall and a velocity profile similar to curve b in Fig. 4.1. Heating and

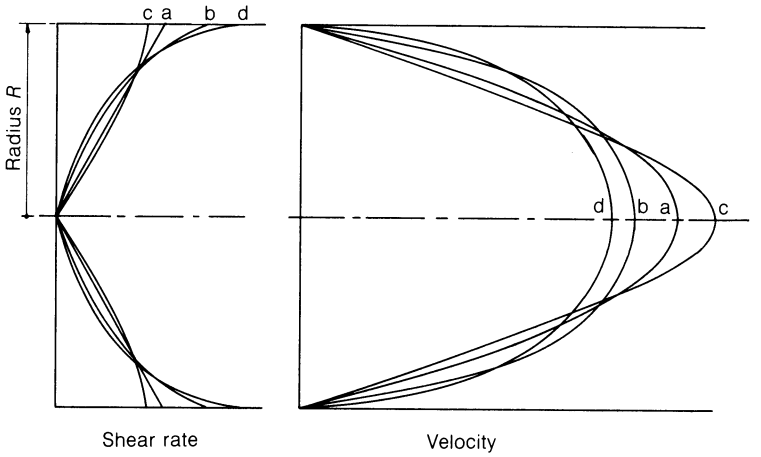


Figure 4.1 Effects of viscosity variation on velocity distribution. (a) isothermal Newtonian; (b) heating Newtonian; (c) cooling Newtonian; (d) heating pseudoplastic.

cooling of a pseudoplastic fluid again modifies the isothermal velocity profile, e.g. heating will give a profile similar to curve d in Fig. 4.1, which in the extreme tends towards 'plug' or 'rod-like' flow. It is these interactions between temperature and velocity profiles which complicate heat transfer calculations (see below).

4.3.2 Surface heat transfer

Where heat is transferred through a surface to or from a fluid, an additional thermal resistance occurs. The effective thickness cannot be determined, so surface heat transfer is usually related to a temperature difference between fluid and solid surface, instead of to a temperature gradient, and the corresponding heat flow is given by:

$$q = hA\,\mathrm{d}T \tag{4.12}$$

where $\mathrm{d}T$ is the temperature difference and h^* is a surface coefficient of heat transfer in $\mathrm{W\,m^{-2}\,K^{-1}}$. Evidently where temperature gradients in the solid are significant, equation (4.1) and (4.12) may be combined:

$$q = \frac{kA}{x}(T_2 - T') = hA(T' - T_1) \tag{4.13}$$

For heat transfer to cooling water (usually in turbulent flow), the reader is referred to standard works on heat transfer (McAdams, 1954; Kay and

*See footnote p. 58.

Nedderman, 1974) for determination of heat transfer coefficients and, where fluid or metal temperatures vary, e.g. from temperature rise between inlet and outlet, for determination of the appropriate mean temperature difference. The Reynolds number for flow of polymers in extruders is always much less than 2100, so flow is always laminar. Heat transfer to or from a Newtonian fluid is given in terms of the dimensionless Nusselt number hD/k, where h is based on arithmetic average temperature difference and D is the diameter of a capillary.

The mass flow rate w^* and length of the capillary L are combined in a second dimensionless group, the Graetz number wC_p/kL. For values of Graetz number greater than 10, the theoretical curve is closely approximated by:

$$\frac{hD}{k} = 1.75\left(\frac{wC_p}{kL}\right)^{1/3} \tag{4.14}$$

For a wide slit, this equation may be used, where the thickness H of the slit is equal to $D/2$ and the mass flow rate w is through a width πH, i.e. the same mass velocity ($kg\,s^{-1}\,m^{-2}$) as in a capillary of diameter D. At values of Graetz number less than 10, i.e. small mass flow rate w or great length L, the final fluid temperature approaches that of the wall, and at Graetz number less than 3 the Nusselt number for a capillary diameter D approximates:

$$Nu = \frac{2}{\pi} Gz \tag{4.15}$$

with a gradual transition in the range $3 < Gz < 10$.

For molten polymers, several corrections are necessary; radial temperature gradients modify the velocity profile from the parabolic form assumed for isothermal Newtonian flow, as does non-Newtonian behaviour (see p. 60). Heat generation due to shear heating and thermal expansion may also be significant; many workers have examined this problem including Forrest and Wilkinson (1973; 1974) and Abedi (1975). Figure 4.2, which is reproduced from Abedi's work, shows both computed and experimental results to give an approximate indication of the range of values to be expected. The reader is referred to the original work for further detail, including the definitions of the variables. The differences in heat transfer between heating (curve 3 of Fig. 4.2) and cooling (curve 2) are primarily due to the effects of coupled temperature and velocity profiles. Curves 4 and 1 show the additional effects of thermal expansion and viscous heating, which according to Abedi tend to oppose each other. It should be noted that the Nusselt number in Fig. 4.2 is based on the temperature rise or fall of the polymer melt, including viscous heating, and not solely on the heat to or from the solid surface.

In Fig. 3.9 the variation of strain energy is shown for a Newtonian fluid due to pressure flow in two simple geometries. This strain energy is converted into

*The symbol w is conventional, but must be distinguished from local downstream velocity in Chapters 6 and 8.

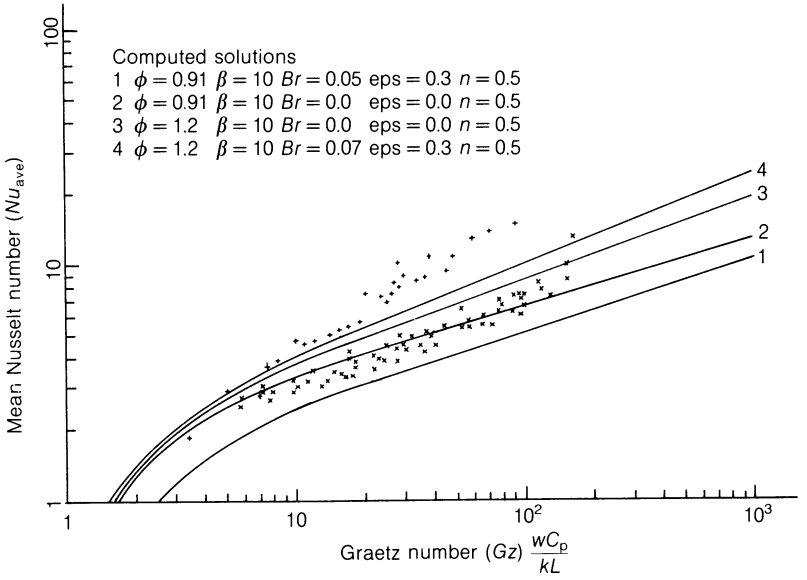


Figure 4.2 Convective heat transfer to/from polymer melts. + published experimental data (heating); × Abedi's experimental data (cooling).

viscous heating, leading to local temperature increases. If the density is ρ and specific heat C_p, the rate of local temperature rise in the absence of conduction will be (for unit volume):

$$\frac{dT}{dt} = \frac{\eta \dot{\gamma}^2}{\rho C_p} \tag{4.16}$$

Equation (4.16) was used in the example on p. 45.

As mentioned above, in non-isothermal and non-Newtonian conditions, the shear stress/shear rate relations (equations (3.15) and (3.26)) will be modified and viscosity is no longer a constant. Thus, aside from changes in the total strain energy, the distributions will change, and consequently so will the local temperature differences – which may persist to the end of the screw. These differences are reduced by transverse circulation and thermal conduction within the polymer, whose rate is controlled by the thermal diffusivity (p. 58); this is examined in section 8.4.

4.4 MIXING

In flow at high velocity of low viscosity fluids (Reynolds number greater than 2100), turbulence gives rapid and intimate mixing of the stream. In laminar flow, kinetic energy effects are negligible and, as seen in Chapter 3, adjacent layers slide relative to each other without interpenetration. Thus mixing between one location and another, which may initially have different

compositions, is by this relative motion transferring part of the material from one location to another, so tending to mix the material from the two locations and achieve a more uniform composition. This is known as **distributive** mixing and is characterized by how far two fluid particles, initially adjacent, are separated by the mixing process. Referring to Fig. 4.3, which illustrates a small element of material subjected to uniform simple shear in one direction, points in two laminae (layers) dy thick are adjacent at time t_0. If their velocities in the direction of shear are w and $w + dw$, respectively, their relative movement at time $t_0 + dt$ will be:

$$[(w + dw) - w](t_0 + dt - t_0) \tag{4.17}$$

and the total shear strain will be:

$$\frac{dw}{dy}(t_0 + dt - t_0) \tag{4.18}$$

If the shear stress is uniform, the relative movement of laminae $2dy$ apart will be:

$$[(w + 2dw) - w](t_0 + dt - t_0) \tag{4.19}$$

and the shear strain will be:

$$\frac{2dw}{2dy}(t_0 + dt - t_0) \tag{4.20}$$

Thus evidently total shear strain is an appropriate measure of mixing, taking account of both the relative movement and the initial separation of the particles. As shown by equations (4.18) and (4.20), total shear strain is given by the product of shear rate and the time for which it acts:

$$\frac{dw}{dy}dt = \dot{\gamma}_y\,dt \tag{4.21}$$

and this is the measure of distributive mixing in laminar flow; if motion occurs in more than one direction, then at any location the shear strain is the time of action multiplied by the vector sum of (local) shear rates. This mechanism of mass transfer not only promotes uniformity of composition but also of

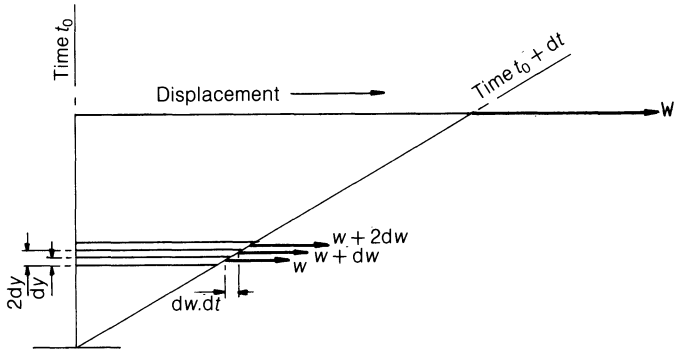


Figure 4.3 Distributive mixing in shear flow.

temperature, assisting the thermal mechanisms of heat conduction or diffusion. However, in the extruder screw channel the flow velocities are primarily parallel to the cylindrical surface of the barrel, whereas conduction is primarily radial; the former promotes end-to-end and side-to-side uniformity while the latter assists temperature uniformity in a radial direction. The exception is at the sides of the channel (Fig. 6.7) where continuity requires a degree of radial flow – see section 8.4.

The foregoing analysis refers to fluids, which deform continuously under a finite (shear) stress. If solid particles, e.g. fillers or pigments, are present, they will deform initially and elastically under stress, and recover their original dimensions on removal of stress. To effect mixing of solids or Bingham fluids having a finite yield stress, it is necessary to exceed this stress and cause permanent deformation or fracture, before distributive mixing can occur. In this **dispersive** mixing, it is the stress which must exceed a minimum value for mixing to occur, and this minimum is usually not achieved in the single-screw extruder, except possibly over the flight clearance, and then only for a short time interval, and not uniformly through the extruded mass. In contrast, in the twin-screw extruder the clearances between the two screws represent a larger area of shearing and the flow paths ensure that a greater proportion of the total mass is subjected to shear; the level of stress depends on the width of the clearances, and this may vary widely along the length of a machine as well as between different types and designs of machine.

Extrusion dies

5

J. A. Covas

5.1 INTRODUCTION

Despite its apparent geometrical simplicity, the extrusion head plays a fundamental role in the extrusion line. It is aimed at shaping the melt pumped by the extruder into the desired cross-section at the specified rate, but it also contributes decisively to the final physical and aesthetical characteristics of the extrudate. Since the various post-extrusion phenomena taking place induce variations in the extrudate cross-section along the extrusion line, the die-lip dimensions are generally different from those of the final product. Not only is this difference extremely difficult to predict theoretically, but it also varies with the operating conditions and with the rheological properties of the material being processed. Thus, in practice, extrusion dies are usually provided with adjusting systems that, directly or indirectly, change the local thickness of the flow channel, thus providing the possibility of producing extrudates with the adequate dimensional tolerances. The operator's skill is also determinant for this purpose.

Nowadays, extrusion dies have reached a high level of sophistication and efficiency as a result of advances in control and automation technologies. Correction actions can be taken automatically, whenever the control system detects changes in the extrudate quality. Computational techniques capable of simulating the viscoelastic pressure flow of polymer melts through the channels of typical dies have also been developed, supporting the design of new tools or the assessment of the performance of existing ones. These programs improve the accuracy of the design and reduce the amount of time spent on adjustments. Unfortunately, with the exception of some specific geometries, such as spiral mandrel, flat film and cable covering, the general strategy to be adopted for die design purposes remains to be fully integrated. As a consequence, the effective mass throughput of some extrusion lines may be significantly lower than could be attained with an efficient design

methodology, unless the operator's process knowledge is sufficient to implement operational strategies compensating for the limitations of the design.

The output of an extrusion line is defined by the lowest capacity of its various constitutive elements:

- The output capacity of the extruder, which is dictated by the volumetric output, the melting capacity and the power available;
- The calibrating and cooling capacities (which are determined by the time for heat transfer, the heat transfer coefficient and the temperature difference between the polymer and the cooling media);
- The capacity for manipulating the extrudate (for example, time needed for post-extrusion shaping operations, or changing spools in winders);
- The performance of the extrusion head (stress, pressure, velocity and temperature fields induced);
- The rheological properties of the melt.

Replacing and/or modifying the extruder, increasing the number and/or the length of the cooling/calibration zones, and further automating the line (fully automatic winders, with automatic change of the full spools, have been available for some time) will increase the capacity of the first three parameters. The design of the extrusion head should consider the rheology of the polymer in order to minimize the total pressure drop and the viscous dissipation, to ensure adequate melt homogeneity, and to keep the normal stresses below the critical values. Therefore, the performance of an extrusion line is directly dependent upon both the efficiency of the extrusion head, and the ability of the processor to optimize the corresponding operating conditions. Ideally, the maximum throughput should be dictated by the processability of the material (onset of rheological defects, molecular orientation – hence, anisotropy – induced, and degradation caused by unavoidable heating and viscous dissipation).

In conclusion, an efficient extrusion head should be able to produce a specific cross-section with tight tolerances at high rate, with good melt homogeneity, an acceptable pressure drop and good surface characteristics. These tools frequently have three distinct geometrical zones. In the **entrance zone** the inlet melt eventually crosses a filter pack and breaker plate. Melt filtering and pressurization, and the destruction of the previous helicoidal pattern of flow along the extruder screw, are accomplished. In the **adaptor** (or **transition zone**), the channel gradually changes from a circular cross-section into the shape of the die lips. This zone may have a relatively complex geometry and may take a wide variety of shapes, including a spiral mandrel, or a 'torpedo'-shaped mandrel with the corresponding supporting legs. In the **parallel zone** the melt acquires its final characteristics before exiting the die, and some parameters such as the die swell, the average residence time, flow uniformity and back pressure may be controlled to some extent.

Since the viscoelastic characteristics of polymer flow play a dominant role in the correct design and operation of an extrusion head, the frequently limited knowledge of these matters by processors makes this a semi-empirical process, with the operator making unnecessary use of correction mechanisms and operating at rates frequently well below the values that could be attained. In the following sections of this chapter the main factors influencing the performance of extrusion dies will be identified, some general considerations on die design will be presented, and practical operational/troubleshooting actions will be discussed.

5.2 FACTORS INFLUENCING THE PERFORMANCE OF AN EXTRUSION DIE

The extrusion head, together with the calibration sleeve, when used, is frequently considered as the only unit of the extrusion line which is responsible for shaping the melt pumped by the extruder into the desired cross-section. The other equipment, such as cooling bath(s), haul-off, cutting or winding units, are often regarded as having minor importance, being devoted to the cooling down and/or the manipulation of the extrudate. In fact, there is an overall strong interrelationship between the various elements of an extrusion line and the dimensional and physical characteristics of the extrudate being produced. Consequently, a number of functional, geometrical and operational parameters influence the performance of an extrusion die.

5.2.1 Die construction

Although the geometry and the dimensions of the several components of an extrusion head are obviously related to the shape and size of the profile being extruded, the construction system adopted must generally ensure easy maintenance (assembling, disassembly and cleaning operations should be expedited), low manufacturing costs, efficient sealing between elements, fast coupling to the extruder, sufficient mechanical resistance to minimize deformations and the corresponding distortion of the previously adequate flow channels, and the correct location and power of the heating system. As will be demonstrated throughout this chapter, for a given material, application and set of operating conditions (e.g. temperatures and screw speed), there are only a limited number of geometries of the die optimizing the process in terms of the mass flow rate, dimensions and shape of the extrudate, as well as balanced physical properties across the profile. However, in practice, the rheological characteristics of the melt vary locally and with time, either randomly or periodically, both due to fluctuations in the temperature field (relating to the precision and sensitivity of the heating control system) and due to variations from polymer batch to batch. Moreover, the processor might wish to use the

same tool for a group of polymers/compounds to produce the same or similar extrudates (this can be accomplished by inserting the adequate calibrator and modifying the operating conditions, such as the haul-off speed and the screw rotation frequency).

It is worth recalling that one of the most stringent prerequisites of a die is that it can produce an extrudate with uniform average velocity across its width. The resistance to flow, defined as

$$R = \frac{\Delta P}{Q} = f(geometry,\ rheology), \tag{5.1}$$

where ΔP is the pressure drop needed to generate a flow rate Q, must be identical for every flow path in the die. According to equation (5.1), changes in the temperature field and/or local modifications in the geometry will affect the resistance, introducing variations in the throughput. For example, when producing a profile, it is important to balance the flows of the various subsections, thus preventing severe distortions of the extrudate, or the presence of serious residual stresses in the profile. Usually, uniform flow resistance is guaranteed by changing the die land length locally.

Therefore, in practice, for correction purposes or to increase operational flexibility, it is important to provide the extrusion head with the capability of modifying locally, and in a controlled manner, some relevant profile dimension, or the temperature field. This is usually accomplished via the use of adjustable mandrels and choker bars, whose displacement or deflection is controlled by several individual bolts. The location of these systems depends on their main objective. For example, if the flow uniformity of flat film is to be improved, choker bars are usually inserted somewhere in the parallel zone, and some flow relaxation is sought. Adjustment of the die lips influences the local throughput and increases the utility range of the die. More recently, the mechanical adjustment of the channel gap may be replaced by thermal systems that locally modify the temperature field (hence the viscosity, the pressure drop and the local mass flow rate) of the polymer melt flow. The dimensions of the extrudate can also be corrected by acting on the post-extrusion parameters, for example by controlling the local cooling conditions. In fact, it will be seen that the calibration system guarantees the appropriate external (or, more rarely, the internal) contour of the profile at a specific location on the extrusion line, but variations may eventually occur there after.

5.2.2 Material rheology

The polymer melt must flow along the die without creating stagnation zones or developing secondary flows. The viscous dissipation should be controlled, particularly in the case of the extrusion of heat-sensitive polymers such as

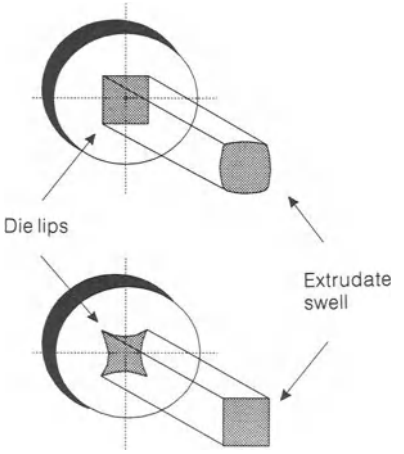


Figure 5.1 The effect of the extrudate swelling on the extrudate shape. Top: A square die will produce a distorted extrudate. Bottom: a square extrudate will require a particular die-lip cross-section.

PVC, the adequate welding of eventual individual flows should be ensured, and the extrudate should emerge with uniform average velocity throughout the exit cross-section, exhibiting good surface characteristics. This means that for a particular production rate the polymer rheology determines the geometry of the flow path. While the shear stresses, and the corresponding shear thinning character of the fluid, contribute significantly to the total pressure drop, the normal stresses are related to the extrudate quality and, in a sense, they determine the effective limits of the polymer extrudability. In fact, the occurrence of sharkskin melt fracture phenomena is frequently associated with the development of extensional flows, although their origins and mechanism are still being debated intensely in the literature (Cogswell, 1977; Kurtz, 1984; Ramamurthy, 1986). This anomaly can be described as a rough surface, often with a distinct pattern, occurring during the steady-state extrusion of specific polymer melts through dies. For practical purposes, the normal stresses developed during convergent flows or near to the die exit, where a significant extensional flow component develops, should be kept below a critical value, which is material-intrinsic. Normal stresses also develop along the extrusion line, as a consequence of stretching. A number of other rheological anomalies with practical significance, such as fisheyes, plate-out and die-lip build-up, are difficult not only to account for but also to predict. Fisheyes are specks of hard polymer protruding from the surface of the extrudate. They are believed to originate in the course of polymer production, but could also be formed upon processing, as a consequence of non-uniform fusion. Plate-out and die-lip build-up are sticky deposits of (lower molecular weight?) polymer on the surfaces of the equipment (e.g. on the legs of the

spider mandrel), or on the die surface, respectively. They appear to be associated with interactions between some formulation components, breadth of the molecular weight distribution, ambient humidity, and some geometrical features of the die.

The extrudate swell at the die exit is a well-known manifestation of polymer elasticity. As shown in Fig. 5.1, not only the size of the cross-section is increased but also, in the case of non-axisymmetric profiles, distortion of the shape occurs. The practical implications of the latter seem obvious: when defining the shape of the die lips, one should try to compensate for the distortion that will take place upon processing (Fig. 5.1, bottom). The equilibrium extrudate swell depends on operational and geometrical parameters. Increasing shear rates and lower melt temperatures favour elasticity, whereas longer die land lengths and lower reservoir-to-capillary ratios reduce the swell. Hence, a vast combination of die geometries and processing conditions can produce the same extrudate cross-section. The theoretical prediction of the die-swell behaviour is very complex. Recently, computations of the non-isothermal die swell for long capillaries and slits produced good predictions, by solving numerically, using a Galerkin upwind finite element method (FEM), the momentum and energy equations coupled to a Kaye–Bernstein–Kearsley–Zapas (K-BKZ) integral constitutive equation (Barakos and Mitsoulis, 1994). Initial attempts to predict the shape distortion were not entirely successful (Huang and White, 1979; White and Huang, 1981), but recently an inverse die formulation scheme was developed, enabling the prediction of the shape of the die lips for a given cross-section of the extrudate, by means of an implicit Newton–Raphson iterative technique (Legat and Marchal, 1993).

Unfortunately, the above methodologies are very elaborate (involving the manipulation of complex constitutive equations) and costly in terms of computational requirements and/or of computing time. Thus, they are not usually accessible to the average processor, who frequently has to rely upon the scarce rheological data supplied by the polymer manufacturer. This reduces to shear flow curves for a limited number of melt temperatures, and average extrudate-swell data for long capillaries, either in tabular or graphical form (recoverable shear strain values are sometimes presented). Tensile flow data and/or conditions at which flow defects occur are very difficult to obtain. Alternatively, it is possible to use methodologies that provide an estimation of the extensional and elastic behaviours from experimental shear flow data acquired by capillary rheometry which, as seen above, can be obtained from the polymer manufacturers (Covas, Carneiro and Brito, 1991; Covas and Carneiro, 1992). For example, the phenomenological analysis of convergent flow patterns (occurring in capillary rheometry), developed by Cogswell (1972) uses information contained in the fraction of pressure drop due to end effects, P_0 (computed via the well-known Bagley correction), to estimate the material's extensional

behaviour. In the case of circular dies, the relevant equations are:

$$\sigma = 3(n+1)P_0/8 \tag{5.2}$$

$$\dot{\varepsilon} = 4\tau\dot{\gamma}/[3(n+1)P_0] \tag{5.3}$$

where σ and $\dot{\varepsilon}$ are the average normal stress and extensional strain rate respectively, τ is the shear stress and $\dot{\gamma}$ is the corresponding shear rate. If the maximum shear rate of the available shear flow data corresponds to the onset of rheological defects, the above expressions may be used to determine the critical normal stress and strain rate. This can be related to the maximum admissible convergence angle, α,through the relationship:

$$\alpha = 2\tan^{-1}(2\dot{\varepsilon}/\dot{\gamma}) \tag{5.4}$$

For wedge tapered sections:

$$\alpha = 3\tan^{-1}(3\dot{\varepsilon}/\dot{\gamma}) \tag{5.5}$$

where $\dot{\gamma}$ represent the shear rate at the exit of the taper. It is also possible to adopt correlations between the first normal stress difference, N_1 (which is a measure of the polymer elasticity), and the shear viscosity function, $\eta(\dot{\gamma})$, and between the former and the equilibrium die swell, DS (given by the ratio extrudate diameter/die diameter). Good results have been obtained when describing the viscosity function by a Munstedt-type polynomial (of degree 2) (Munstedt, 1978), and Wagner (1977) and Tanner (1970) formulations, relating N_1 with η and N_1 with DS respectively, are coupled (Covas, Carneiro and Brito, 1991):

$$DS = \left[1 + \frac{1}{8}\left(\frac{a_1 - 1 + 2a_2\log(a_T\dot{\gamma})}{n}\right)^2\right]^{1/6} \tag{5.6}$$

In the above equation, a_1 and a_2 are the first- and second-order coefficients of the Munstedt polynomial, a_T is a shift factor that considers the effect of the temperature on the viscosity, and n is a material's intrinsic damping constant, with values typically between 0.13 and 0.20. Table 5.1 shows the average values of n, obtained at the indicated temperature range, for some polymers. Since the

Table 5.1 Values of the damping constant, n

Material	*Temperature range* (°C)	n
PS	175–205	0.18
HDPE (pipes)	190–240	0.18
LDPE (film)	170–210	0.05
LLDPE	150–160	0.14
UPVC	190–210	0.19–0.26
PPVC	150–180	0.38

swelling ratio generally depends not only on the shear rate but also on the direction in which it is measured, it is necessary to modify the values predicted for capillaries with equation (5.6) to other shapes. Taking a slit as an example, the percentage of swell in area is roughly the same for the two geometries. Then, the area swell ratio, determined by squaring the diameter swell ratio, is multiplied by a factor for either the slit width or thickness. Whereas for polyolefines the swelling ratio in the thickness direction is approximately equal to the square of that across the width (Powell, 1974) in PVC extrusion it has been speculated that the amount of swell is inversely proportional to the width to thickness ratio (Brown, Kim and Summers, 1979). For flow between parallel plates, equation (5.6) is modified into (Tanner, 1970):

$$DS = \frac{H}{H_0} = \left[1 + \frac{1}{12}\left(\frac{a_1 - 1 + 2a_2 \log(a_T\dot{\gamma})}{n}\right)^2\right]^{1/4} \tag{5.7}$$

Commercial PVC compounds are known to exhibit anomalous rheological characteristics, due to the development of supermolecular flow at the usual processing conditions. One of the practical implications of this is the increase in melt elasticity with increasing temperature, i.e. extrudate swell increases with increasing temperature. This behaviour is associated with the well-known 'gelation' process of progressively changing the particulate structure of the material into a network of entanglements and of three-dimensional order. Since equations (5.6) and (5.7) were derived for true melt flow, they should be modified in order to accommodate this unusual response (it should be noted that at higher temperature true melt flow and conventional rheological behaviour are observed). For capillaries (Covas and Carneiro, 1992):

$$DS = \left[1 + \frac{1}{8}\left(\frac{a_1 - 1 + 2a_2 \log(a_T\dot{\gamma})}{n' a_T}\right)^2\right]^{1/6} \tag{5.8}$$

where n' is the damping function at the reference temperature, which typically takes values between 0.19 and 0.26 for compounds for rigid pipes and profiles.

5.2.3 Extruder–die interaction

The operating point of an extrusion process is given by the values of the output and pressure at which the characteristic curves of the extruder and die meet (see Chapter 6). At constant extruder geometry and operating conditions, the location of the operating point depends on the die resistance, which is a function of its geometry, and of the polymer viscosity. In other words, the output of the extrudate depends both on the die cross-section and flow channel geometry, and on the operating conditions. While the lower limit of the die resistance relates to poor melt homogeneity and the eventual survival of solids, its maximum dictates excessive viscous dissipation, or power consumption.

5.2.4 Post-extrusion phenomena

As discussed in section 5.1, the output of an extrusion line may be limited by the available cooling and extrudate manipulation capacities. Taking the extrusion of pipes as an example, the required length of the calibration and cooling bath(s) depends on the heat transfer coefficient and on the temperatures of the melt and of the cooling fluid. The cutting speed or the time required for changing spools in the winder are also relevant. Figure 5.2 illustrates such a line, and shows the appropriate extrudate transversal temperature profiles at several locations (Kleindienst, 1973). The melt is considered to emerge from the die at uniform temperature. While the pipe's nominal diameter is calibrated, an outer layer of material must solidify, in order to withstand the forces acting on the profile along the remaining length of the line, without distorting its external contour. These include normal and friction forces due to various guides and the haul-off, stretching (or drawdown, given by the ratio of the velocity of the caterpillar to the extrudate velocity at the die exit), internal pressure used for calibration and buoyancy forces. Since the normal forces applied by the haul-off are important, when the profile leaves the cooling bath a considerable percentage of its thickness should have solidified, if ovalization is to be avoided. Finally, a good-quality cut requires that the entire section is solid. Under these conditions, the nominal diameter of the pipe could well be within the specified tolerances. However, other phenomena may alter the average or the local thicknesses of the pipe. As a matter of fact, even when all the equipment is correctly designed and operated, the extrudate is subjected to irreversible dimensional changes along the line. These should be anticipated when defining the die lips, since calibration and/or modifications in the operating variables may not be effective in controlling these phenomena.

Griffith and Tsai (1980) and Stevenson (1985) investigated the influence of the operating conditions, die geometry and material properties on the dimensions of the extrudates along several locations on the extrusion line. Die swell and drawdown were identified as parameters of prime importance. In practice, the

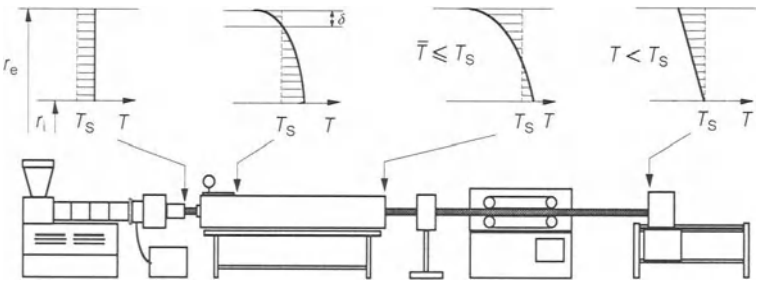


Figure 5.2 Required extrudate temperature profiles at specific locations along an extrusion line (adapted from Kleindienst, 1973).

extrudate never reaches the equilibrium swell state, because swell and stretch occur simultaneously as it emerges from the die, inducing size and shape changes. Although calibration will ensure the adequate profile external contour, residual stresses and thickness gradients may develop. Since the swelling of the extrudate is restricted by the calibrator, the internal stresses, together with the pressure difference for calibrating, are manifested as friction forces along the wall. For example, if during the extrusion of pipes the calibrating unit is positioned at a distance L from the die, the tube deformation includes ε_1, representing the deformation taking place between the die and the calibration unit (this is a function of the degree of stretching and of the polymer elasticity), and ε_2, representing the deformation taking place inside the calibrator. These have been computed by Halasz (1993), who advises adjusting the melt deformation so that the degree of stretching and ε_2 are similar. From the process modelling point of view, this problem is similar to a biaxial stretching viscoelastic flow, but without the possibility of applying the membrane theory, since the tube is thick. Furthermore, there is a contact point dividing the outer boundary of the expanded tube, i.e. the free inflated surface and the friction boundary, whose location is unknown when the numerical simulation is initiated (Sun, Luo and Tanner, 1994). This type of situation is considered to be one of the open questions in rheology and computation. Only recently, Sun, Luo and Tanner (1994) have undertaken the isothermal simulation of a thick tube expansion and extension by traction, ignoring friction in the calibrator.

If one considers the production of filaments, with each individual rod being stretched in air for a short distance before being cooled down in a waterbath, the effect of the drawdown on the extrudate cross-section can be clearly established. Taking the stretching process as isothermal, neglecting extrudate swell and considering the flow as Newtonian, a simple mass balance will yield:

$$DR = A_o/A_e = V_e/V_o \tag{5.9}$$

where DR is the drawdown ratio, A denotes cross-section and V represents velocity; the indices o and e refer to locations near the die exit, and before the pulling rolls, respectively. The corresponding stretching force is (Agassant, Avenas and Sergent, 1986):

$$F = 3\eta_e Q \log (DR/L) \tag{5.10}$$

where η_e is the extensional viscosity, Q is the volumetric output and L the stretching length. When the viscoelastic nature of the polymer is taken into account the computation of F is much more complex, but it can evidence the existence of operating conditions when it is not possible to stretch the polymer (Agassant, Avenas and Sergent, 1986). In any case, despite the many criteria proposed for defining the 'spinnability' of a particular polymer, it is well known that the material must exhibit extensional strain hardening character-

istics, i.e. that the increase in the extensional viscosity must be greater than the decrease in the cross-section (resulting from the rate at which the filament is extended). These rheological conditions may also be met by playing with the cooling conditions.

Gravity-induced slump, i.e. flow of melt under its own weight, leading to uneven wall thickness distribution in the profile, cannot be avoided by calibration. It gains practical significance in large-thickness profiles, where the cooling conditions, associated with low thermal conductivity of the polymer, generally allow a significant amount of plastic to remain in the melt state for long periods. Measurements during the production of HDPE pipe at 335 kg h^{-1} (Pittman *et al.*, 1992), revealed that a significant melt slump had occurred, with the thickness at the top being 7.1% less than the mean value, and at the base being 7.9% greater. During the same experiments, the pipe diameter decreased from 325 mm at the sizing sleeve to a final value of 315 mm

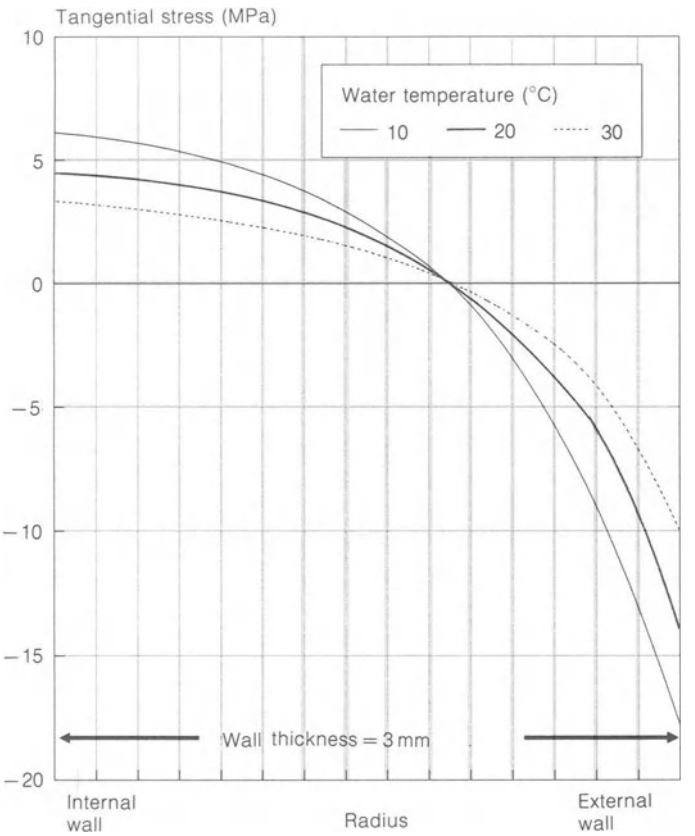


Figure 5.3 Distribution of stresses in the walls of a 3 mm thick pipe, due to exteral cooling, for different water temperatures (Berger and Krämer, 1975).

(a reduction of 3.1%), whereas the wall thickness decreased about 20%. The effects of slump are usually overcome by manually adjusting the die eccentricity, but on-line automatic control is also possible. Giacomin and Doshi (1988) and Pittman *et al.* (1992) have simulated this phenomenon numerically (using finite element methods) and developed computer-aided methods for setting up the die correctly to compensate for slump.

Shrinkage upon cooling occurs both transversely and lengthwise and it also induces residual stresses in the extrudate. It is given by:

$$\delta = \beta(T_N - T_k) \tag{5.11}$$

where β is the heat expansion coefficient and the term in brackets is the temperature difference in the environment. Due to the temperature gradient across the thickness of the extrudate, the corresponding differences in deformation cause a stress gradient, thus promoting internal stresses in the product. In the case of pipes, which are usually subjected to external sizing/cooling, residual compressive stresses near the outer wall and tensile stresses near the internal wall arise. Figure 5.3 shows the distribution of stresses in the walls of a 3 mm thick tube for various cooling conditions (Berger and Krämer, 1975). In the case of pipes subjected to internal pressure, this stress field is not favourable, as the total circumferential stress developing at the inner wall is the sum of the tensile stress arising from the applied pressure (which reaches a maximum at this location), and the tensile residual stress. One way of keeping the internal stresses as low as possible is to incorporate annealing zones, by allowing air convection between two consecutive cooling units, or using higher cooling-medium temperatures. As shown experimentally by measuring the pipe wall temperatures in different thickness depths upon cooling, there is a steep rise in the temperature of the outer layers during exposure to the annealing zones, which reduces the temperature gradient in the pipe and relieves internal stresses (Kamp and Kurz, 1980; Pittman *et al.*, 1992). Practice has shown that these zones could extend through 5–10% of the total cooling section, without affecting the heat transfer efficiency (Kamp and Kurz, 1980; Kurz, 1988).

Figure 5.4 schematizes an extrusion line and identifies the main variables affecting the size and shape of the extrudate. These include extrudate swell, shrinkage upon cooling, uniaxial drawdown and normal forces induced by the caterpillar, slump and buoyancy forces. The latter may be important when extruding low-density and relatively thin profiles. The final properties of the extrudate are affected by the polymer processing history in the extruder, by the flow conditions within the die, by the rates of stretching and temperature change upon cooling (which influence the surface and bulk morphology and crystallinity), and by the dimensional uniformity and surface quality of the profile. A correlation between the extruder screw speed and geometry, die geometry, set temperatures, output, polymer properties (which vary with the polymer type, grade and composition), cooling conditions, haul-off velocity and the final morphology (which means a specific mechanical performance) of

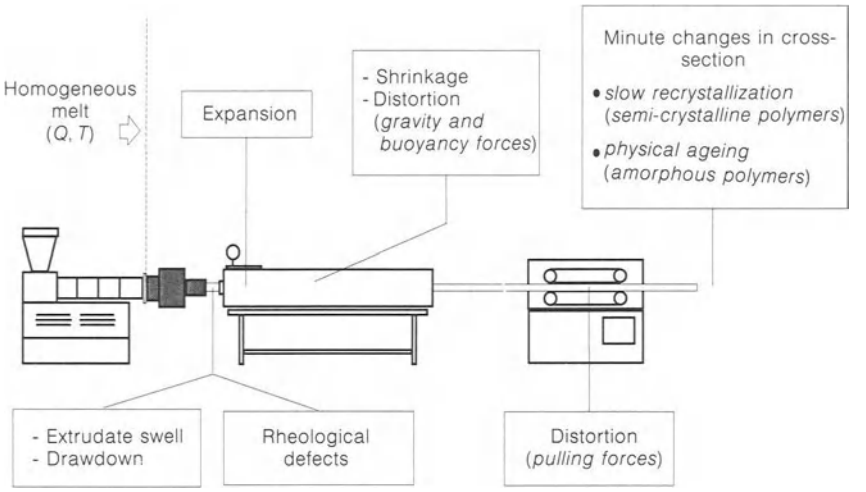


Figure 5.4 Variables affecting the shape and size of an extrudate along an extrusion line.

an extrudate is to be expected. It is possible to use the same extrusion head for the production of a range of products and/or materials with the required properties, within the specified tolerances. However, this flexibilty is often compensated by the difficulty in establishing the required operational strategies leading to the optimization of the process in terms of the output and/or of the product performance.

5.3 EXTRUSION DIES FOR SOME PROFILES

This section discusses the general design features of the extrusion heads most commonly used to produce some popular extrudates. A more detailed analysis can be found in the relevant literature (Henson, 1988; Levy and Carley, 1989; Michaeli, 1992; Halasz,1993). The nature and extent of this chapter precludes the discussion of recent developments for specific applications. New concepts, such as the oscillating die, which superimposes longitudinal and transverse oscillations (Casulli *et al.*, 1990), the shear controlled orientation die, for management of the extrudate's microstructure (Allan and Bevis, 1991), and the production of corners and curved extrudates (Miller, Lee and Stevenson, 1991) will not be further discussed.

5.3.1 Tubing and pipes

Pipe extrusion involves converting the circular flow at the extrusion head inlet into an annular flow at the die exit. Among the various solutions to this problem, one (Fig. 5.5, top) uses a mandrel encompassing the adapter and the

parallel zone, supported by legs (so-called **spider legs**). These legs divide the incoming flow into several streams that are subsequently reunited into a single annular flow. The resulting welding lines are easily detectable in the internal (non-calibrated) surface of the pipe, reducing the pipe resistance. Consequently, not only should the axial profile of the legs be carefully defined, minimizing the flow disturbance, but also conditions favouring adequate welding should be guaranteed. This means that the residence time in the subsequent conical zone of the die should be several times the polymer relaxation time. By forcing a compression ratio the polymer molecules are stretched in the axial direction and the corresponding stress causes a strong decrease in the relaxation time. Thus, a good quality weld is possible during a short residence time (Overeijnder, 1982). In the parallel zone, with a characteristic length/thickness ratio of 15–30, the melt is further homogenized, and the extrudate swell and the total pressure drop are controlled. The

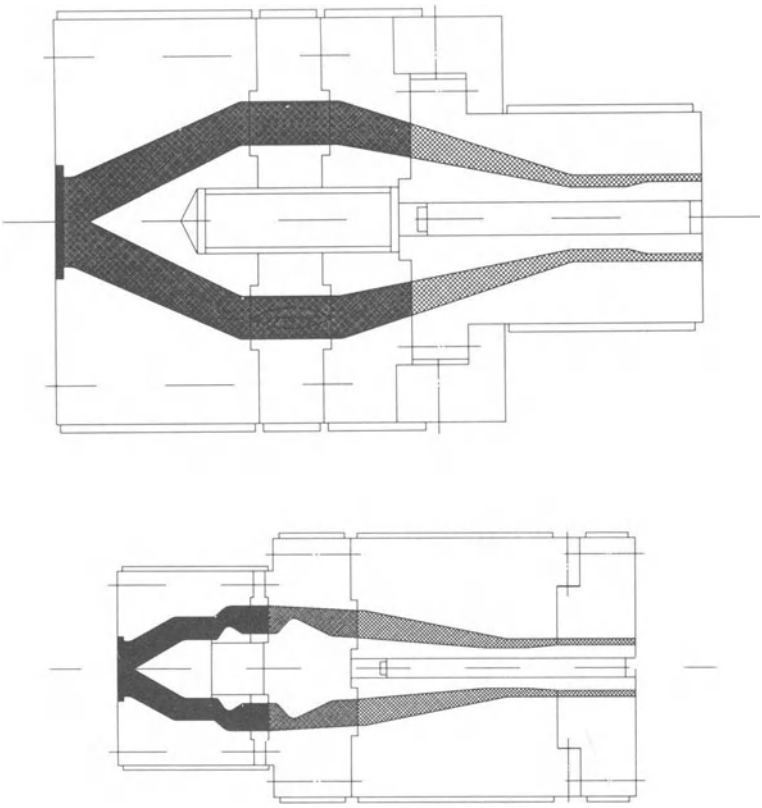


Figure 5.5 Pipe mandrel dies. The spider-supported mandrel solution is used in the extrusion of UPVC (top), whereas the perforated ring is adequate for the processing of polyolefines (bottom) (Battenfeld).

head is usually provided with a die ring whose eccentricity relative to the mandrel can be adjusted through centring screws.

As discussed above, each type of pipe requires, in principle, a specific extrusion head. However, as the economics of the process would be strongly questionable, dies of different sizes can usually be coupled to the same extrusion head. In practice, and considering the production of UPVC pipes as an example, it is typically possible to cover the standard range of diameters ranging from 10 to 710 mm using eight extrusion heads, coupled to the individual specific dies. For certain dimensions an overlap exists, so that the same product can be produced by two different extrusion heads. This principle is also valid for other products, such as blown film or blow moulded containers.

A number of design solutions avoiding, or minimizing, the effects of the weld lines have been envisaged. For example, the mandrel can be supported by a **perforated ring** instead of a number of legs, as multiple welds between the various flows will be preferable to a single weak line across the entire pipe thickness (Fig. 5.5, bottom). In the case of the **filter basket extrusion head** (developed by Hoechst AG, Germany), the perforated basket creates a flow radially outwards. This type of construction saves space, but faces a number of problems (Henson, 1988). The **spiral mandrel extrusion head** uses the concept that became popular in blown film extrusion. The incoming melt is radially distributed through several individual channels cut on the mandrel surface, initiating a helicoidal flow pattern towards the die exit. Since the gap between the die body and the mandrel increases in the downchannel direction, whereas the depth of the helical grooves decreases, that flow mode is progressively changed into an axial flow. If the geometry of the die is conveniently designed by taking into consideration the rheological characteristics of the polymer, the melt is evenly distributed through the entire annular cross-section (thus exiting the die with uniform velocity) and no weld lines are present. Perhaps surprisingly, this concept has not been adopted by processors manufacturing pipes as frequently as its advantages would justify.

The application of the recent advances in instrumentation and control technologies to pipe extrusion has allowed significant improvements in the consistency of the process and also in material savings, as narrower tolerances became possible (savings of 2–4% in polymer costs are usually claimed by equipment manufacturers). Simultaneously with the general trend towards complete process automation, since the early 1980s it has been possible to measure (frequently by an ultrasonic technique) the average pipe diameter and the thickness variations along the perimeter, and to correct eventual anomalies automatically. This is usually known as **automatic die centring** (this designation is not entirely correct since, in practice, when the operator adjusts the die lips in order to ensure the production of a pipe with uniform thickness, he is compensating for local flow anomalies induced, for example, by temperature fluctuations, or gravity slump, and thus he may be in fact decentring the die). This operation was initially accomplished with mechanical systems that would

physically modify the geometry of the die. More recently, thermal centring systems, using dies where various zones in the circumferential direction are thermally isolated and separately controlled, can locally vary the melt temperature, and consequently the pressure drop and the flow velocity, have become popular.

5.3.2 Blown film

Since producing blown films requires shaping the melt into an annular flow, one might anticipate finding solutions similar to those discussed above. As the film is usually extruded vertically upwards, vertical extruders are coupled to tools with central feeding. When the extruder is positioned horizontally, the extrusion head can work with either lateral or central feeding. Conventional mandrel dies exhibit two limitations. One is associated with the welding of the individual flow fronts uniting after surrounding the mandrel, thus creating an important longitudinal weakness in the film. The other consists in the development of flow streamlines with different lengths in the downchannel direction (due to the change from horizontal to vertical flow), creating total pressure drop differences across the die circumference and hence a gradient in the film thickness (see equation (5.1)). It is possible to equalize the flow path length by diverting or rerouteing portions of the material, but this solution is seldom adopted due to manufacturing, maintenance and cleaning difficulties. One strategy that is usually adopted in such extrusion lines is to allow for some

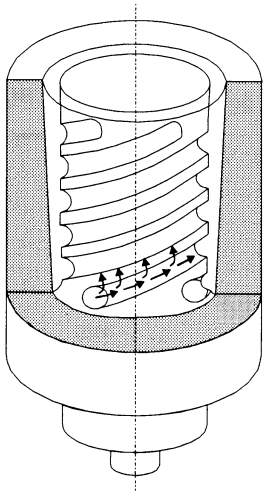


Figure 5.6 Schematic representation of the spiral mandrel die, with half the body cut away.

means of spreading the anomalies throughout the film perimeter, to avoid well-defined weak lines or areas. Usually the die, the extruder/head ensemble, or the haul-off unit rotate, or oscillate, slowly. When the die rotates, a dedicated drive has to be incorporated and efficient sealings have to be carefully designed. Non-rotating die systems are advantageous, since the die is smaller, thus requiring shorter residence times.

The above difficulties associated with weld lines and film thickness variations led to the development of the spiral mandrel extrusion head (Fig. 5.6), described in section 5.3.1. The melt is usually fed either through a central channel connected to a system of radial runners (sometimes called ports), or through a ring. The latter provides easier access to the central zone of the tool, which may be important for the purposes of internal bubble cooling. The number of radial channels is often identical to the number of helical channels. However, it is possible to have one radial channel feeding two spirals (with a triangular transition), or one radial channel feeding half of two spiral channels (Rauwendaal, 1991b). The performance of a blown film die is dictated by its capacity to produce a uniform flow rate around the circumference of the die, free of weld and haze lines. The residence time distribution should be narrow, with a short average residence time, and the pressure required to pump the melt should be low (Coyle, 1991). The uniformity of the exit flow will depend essentially on the design of the spiral. A poorly designed die will produce periodic flow variations, equal to the number of spiral grooves (Vlcek, Vlachopoulos and Perdikoulios, 1988). Generally, the flow uniformity improves significantly by increasing the number of helical channels. In industry, it is common practice to use 1–2 grooves per inch of die diameter (Rauwendaal, 1991b). An important part of the total pressure drop occurs in the die land. Consequently, widened gaps are used for polymers of high and narrowly distributed molecular weight, such as LLDPE and certain types of HDPE. A relaxation zone between the spirals and the die exit may also be incorported.

In recent years, there have been important developments in output capacities, production speeds and thicknesses in the film sector. It is now possible to produce 6 μm polyethylene film at winding speeds reaching 140 m min^{-1} (Schafer, 1994). This obviously requires high levels of advancement in equipment design and process control. For example, a number of techniques for controlling the average and circumferential diameters are currently available. Mechanical and thermal centring systems use the same principles as developed for pipes. Mechanical systems are frequent for this geometry, as some processors believe that it is risky to cope with a film exhibiting temperature differences upon emerging from the die. One important manufacturer uses die bolts to adjust a flexible die lip, and hence the die gap. The bolts are mechanically driven by stepper motors. Recently, control systems acting on the cooling diaphragm have been proposed. For example, one system includes a segmented automatic secondary air ring, located just

before the point where the bubble begins to shape, which provides less air flow to the thicker sections of the film and vice versa. The stretching of the film will then actuate differently in these sections and any thickness differences are evened out. Other systems use individually heated or unheated air to adjust the film gauge.

5.3.3 Flat film/sheet

Extruding a flat sheet or film with a relatively large width and uniform thickness requires shaping the circular melt at the end of the extruder into a rectangular cross-section with the various elementary flow elements facing similar residence times and flow resistances. This is not easy, since the length of the flow streamline near the centre of the profile is obviously shorter than that closer to the periphery. Thus, and according to equation (5.1), either a specific temperature field is defined (inducing distinct rheological characteristics at different locations), or the flow geometry must be varied locally. In the simpler extrusion heads a distribution channel, perpendicular to the main flow direction, distributes the incoming melt across the width of the head. Subsequently, the melt advances uniformly towards the die exit. This construction is usually known as **T-type** (Fig. 5.7, top). Although the cross-section of the distribution channel is significantly larger than the thickness of the parallel

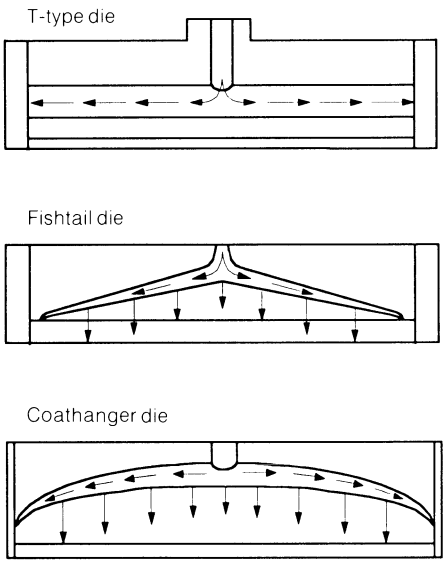


Figure 5.7 Schematic representation of dies for flat film. The different configurations aim at guaranteeing uniform melt distribution across the width.

flow, the system does not really guarantee an even flow distribution, the resistance still varying with the location along the width. In practice, this type of design can only work satisfactorily with relatively low-viscosity materials (which justifies the fact that this solution is at present mainly used for coating purposes). Thus, the existence of correcting devices, such as choker bars and flexible lips, which allow the adjustment of the local thickness of the channel, is particularly important to ensure the proper tolerances of the extrudate. These systems can also deal with process or material variations.

It is possible to design these dies rheologically, thus theoretically ensuring an even flow distribution, i.e. uniform average exit velocity across the extrudate width. The corresponding solutions include the **fishtail** and the **coathanger** dies, in which the distributor changes its cross-section gradually in the transversal direction (in a linear and in a nonlinear mode respectively, frequently with a drop-shaped cross-section), and the parallel zone has varying length across the width (Fig. 5.7). Consequently, an element of fluid near to the centre of the die spends little time in the distributor, but will have to flow within a narrow gap for most of the length of the die, whereas another fluid element closer to the periphery will flow along a substantial part of the distributor (which has a bigger cross-section, hence causing less pressure drop), and then towards the exit between narrow parallel plates, but for a shorter period. Deflection of the die under the pressures developed may significantly alter the flow path and should, therefore, be considered during the design stage. From the above reasoning, one may again conclude that these dies must be created with a specific flow rate and polymer (or polymer rheology) in mind or, in other words, that the optimum performance is only attained for one particular viscosity and throughput.

In practice, the material rheology may vary, due to local fluctuations in the temperature, or in the actual characteristics of the material. These tools must also exhibit some flexibility in terms of the width and, especially, the thickness of the extrudate, and of the range of materials that can be processed. Apart from the adjustment systems referred to above, it may be possible to use replaceable lower lips, flexible lips and/or locally deflectable channel walls, or systems that vary the extrudate width. With any of these solutions it is possible to manufacture a good-quality extrudate, but the performance of the die is not maximized. Hydraulic, electromechanical and thermal systems are used for automatically reducing film profile variations. Thermal systems, based upon the expansion or contraction of adjusting members induced by changes in the temperature, are probably the most widely used.

5.3.4 Profiles

The term **profile** refers to a wide variety of shapes and, in fact, includes the extrudates previously discussed. However, it usually denotes non-circular or non-axisymmetric cross-sections. Generally, the design of this type of dies

depends on whether the product is hollow (for example, a window profile) or compact (a 'T' contour), and on whether the cross-section is simple or elaborate. The difficulty in establishing the most appropriate flow channel (in terms of streamlining, residence time distribution and prevention of rheological anomalies) is directly related to the need to shape the incoming circular flow into a cross-section similar to that of the profile (the need to compensate for the post-extrusion distortions requires, as discussed, the extrusion of a melt with a specific contour), with all the 'subsections' of the profile emerging with the same average speed. Thus, if producing a rectangular or circular cross-section is not very difficult, designing an extrusion head for the manufacture of a window frame requires a lot of experience and know-how. Many processors try to neutralize the effects of a poorly designed die with the careful manipulation of the profile cooling conditions. However, this often leads to the development of important residual stresses in the extrudate, or to serious distortions of the product in service.

Flat or **plate dies** are the simplest. The required opening is placed at the exit of the flow channel, sometimes with a minimum amount of streamlining. This solution, although cheap, may obviously induce the development of stagnant zones, or of unbalanced heat dissipation. Nowadays, these dies are usually made of brass, or low-grade tool steel, and are used for short-run productions with thermally stable polymers. Different profiles can be extruded simply by changing the plate. The semi-streamlined or **multistage dies** consist of a number

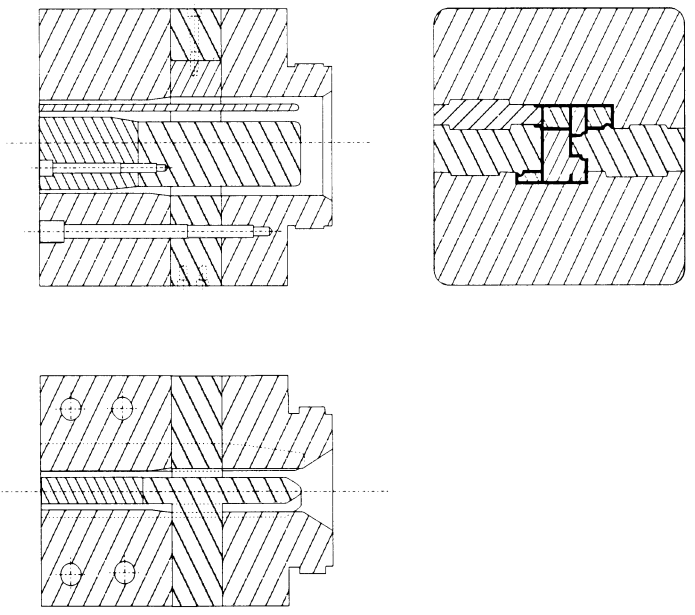


Figure 5.8 Streamlined window profile die (Schiedrum, 1975).

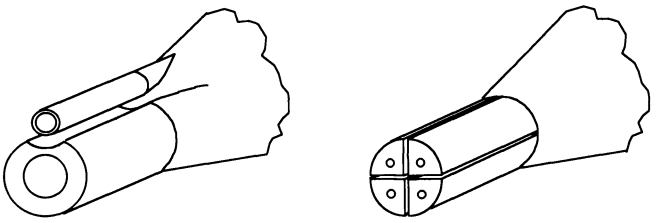


Figure 5.9 Partial representation of profile dies for medical applications, using a conical adaptor and removable inserts (Beddus, 1989).

of discrete plates, each with a specific cross-section, but successively approaching the shape and the dimensions of the outlet. These are longer-run dies, and adequate streamlining may overcome problems with material stagnation and degradation. **Streamlined profile dies** use (conical or trumpet-shaped) adaptors that gradually shape the flow up to the parallel zone, whose length may vary locally, to ensure uniform flow at the die exit (Fig. 5.8). When the adaptor's cross-section reduces linearly, the flow speed will be initially slow and then increases significantly. In certain circumstances, this may result in overheating of the material. Trumpet-shaped adaptors can be designed to increase the speed linearly, or to maintain a constant accelerating flow in the axial direction (Sors, 1974). However, this solution is not used consistently due to difficulties in machining the channel.

The production of hollow profiles requires the insertion of mandrel(s) and the corresponding retainer plates. In this region the elementary melt streams become mainly one-dimensional, and the resistance to flow increases. However, in corners, or where two or more individual flow channels unite, the average flow velocity becomes higher, since the zero (or slip) velocity at the metallic wall is now replaced by the average velocity of the polymer between parallel plates. Certain profiles, such as double-wall sheet or catheters for medical applications, are generally extruded using heads based upon the geometry of the simpler similar profiles (coathanger and conical mandrel, respectively), which are then adapted to the specific geometry being manufactured (Fig. 5.9).

The internal surfaces of many profile extrusion dies are plated or coated with chrome to provide good lubricity and facilitate cleaning the die. Chrome plating provides a hard surface layer that can be polished to a fine finish. Several companies supply a PTFE-impregnated nickel or chrome coating. In this case the surface becomes slippery. When processing at higher temperatures, tungsten disulphide or titanium nitride coatings are advisable (Rauwendaal, 1991c). Generally, this type of solution induces slip at the wall (an effect similar to that of incorporating external lubricants in PVC compounds), thus favouring the development of plug flow conditions (which is equivalent to low power-law indexes, n). Under these circumstances, extrudate swell and, consequently,

the profile distortion, are diminished, and lower normal stresses make the occurrence of rheological defects less probable (section 5.2.2).

5.3.5 Wire and cable

In wire coating a thin layer of polymer is extruded around a copper wire through a **crosshead die**, at speeds often above 2000 m min^{-1}. In the case of a high-voltage cable, the centre conductor may, for example, be covered by three separate layers. The innermost layer will function as an electric screen, the intermediate layer is usually a polyethylene insulation material, and the outer layer serves as an electric screen. Therefore, the technique can be used for primary and secondary coating, i.e. covering metallic conductors, or coating previously insulated wires.

The polymer enters the die by a side-fed supply and is distributed around the mandrel, inside which the pre-heated conductor advances at constant speed. Thus, the melt is deviated 90° in relation to the initial flow direction. Subsequently, the melt flows in an annular gap towards the die exit, where it covers the conductor. Two coating techniques are generally used (Michaeli, 1992) (Fig. 5.10). One is pressure insulation, where the melt is pushed against the wire before exiting the die. The eventual encapsulation of air bubbles

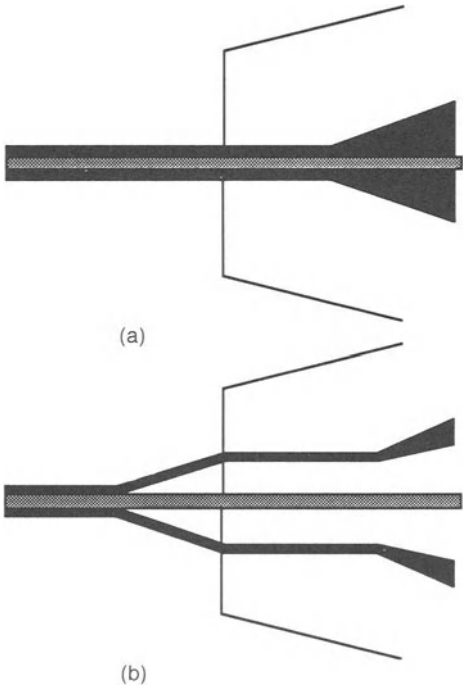


Figure 5.10 Pressure, or compression (top), and tube (bottom) wire coating processes.

between the individual conductors, which would affect the cable performance, is avoided. In the other, tube coating, the extruded tube is pushed against the conductor immediately after emerging from the die, either by the velocity difference between the two, or through the use of a vacuum. This technique is mainly used in secondary coating, i.e. to coat previously insulated wires.

A well-known problem related to cable covering is void formation. This is due to the fact that since the outer part of the polymer solidifies first, it becomes impossible for the inner region to shrink freely upon its solidification. The adhesion of the plastic to the metal decreases, and macroscopic voids can form within the polymer, reducing the dielectric strength of the cable. Also, side-feeding produces differences in the length of the various flow streamlines and, consequently, in the insulation thickness distribution (which, ultimately, may affect the prescribed electric cable performance). As for other annular extrudates and for flat film, it is possible to design rheologically a flow distribution system ensuring uniform flow velocity throughout the circumference of the die. One of the most popular techniques uses **heart-shaped distribution systems**, where the incoming material from the extruder is split into two channels becoming wider and shallower as the flow progresses in the axial direction, as seen in Fig. 5.11. The contour of the heart is calculated to induce similar flow resistances near the external and the internal walls. Following the principles applied to other geometries, the appropriate flow channel is computed for specific rheological and operational characteristics. Thus, to ensure some flexibility in terms of the range of dimensions and materials that can be processed, or to compensate for changes in the processing conditions, die interchangeable centring systems are widely used.

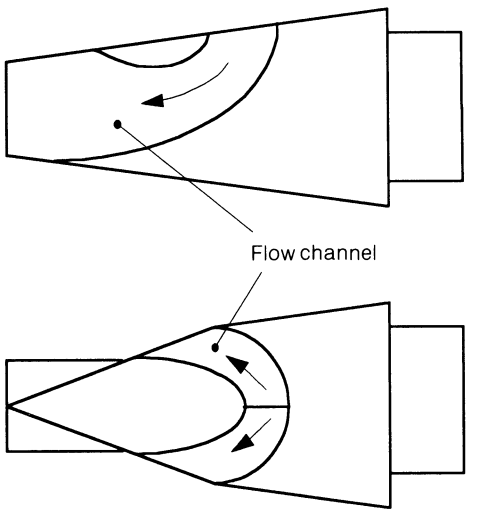


Figure 5.11 Heart-shaped distribution system for wire coating (adapted from Michaeli, 1992).

5.3.6 Multilayer extrudates

Multilayer extrudates, generally combining two or more different polymers, or compounds based on the same polymer, can be produced by lamination (this is a multistep extrusion process, where each layer is extruded separately and partially – or totally – cooled before the next one is applied), or via coextrusion, where the various melt layers emerge simultaneously from the die lips. Michaeli (1992) has classified the existing coextrusion techniques according to the flow mode of the individual streams along the die. Accordingly, these can progress in three ways.

First, they can progress separately throughout the entire length of the die. The various polymer melts move in individual channels inside the die and are pushed together at the die exit. The process is usually assisted by pressure rolls, or by positive pressure. Materials having markedly different rheological properties (and/or that should flow at different temperatures) can be processed with this technique.

Second, they can progress separately throughout most of the die, then come into contact under pressure along the adaptor or in the parallel zone. The principle behind this technique is illustrated in Fig. 5.12, which shows the joining of three different materials, denoted A, B and C. The three-layer flow pattern is determined by the rheology of each polymer, and by the relative differences in thickness and velocity. In the example considered, materials A and B exhibit similar rheology, whereas the characteristics of polymers B and C are significantly different. This may cause instability in the interface between B and C, which may be observed on the extrudate surface as a parabolic pattern. Relatively high shear stresses (typically between 0.03 and 0.06 MPa) favour this phenomenon. Thus, it is particularly relevant to adapt the geometry of the flow channels and the operating conditions to the specific set of polymers to be

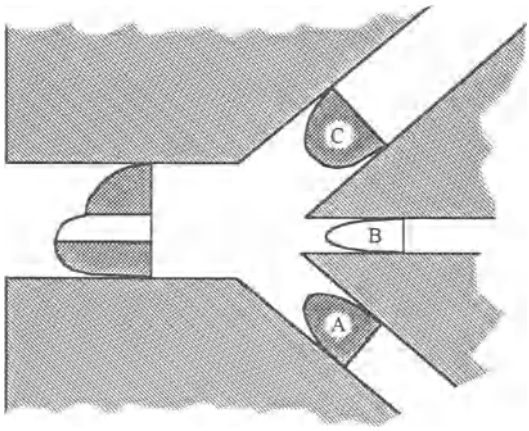


Figure 5.12 Joining of three individual flow fronts in coextrusion.

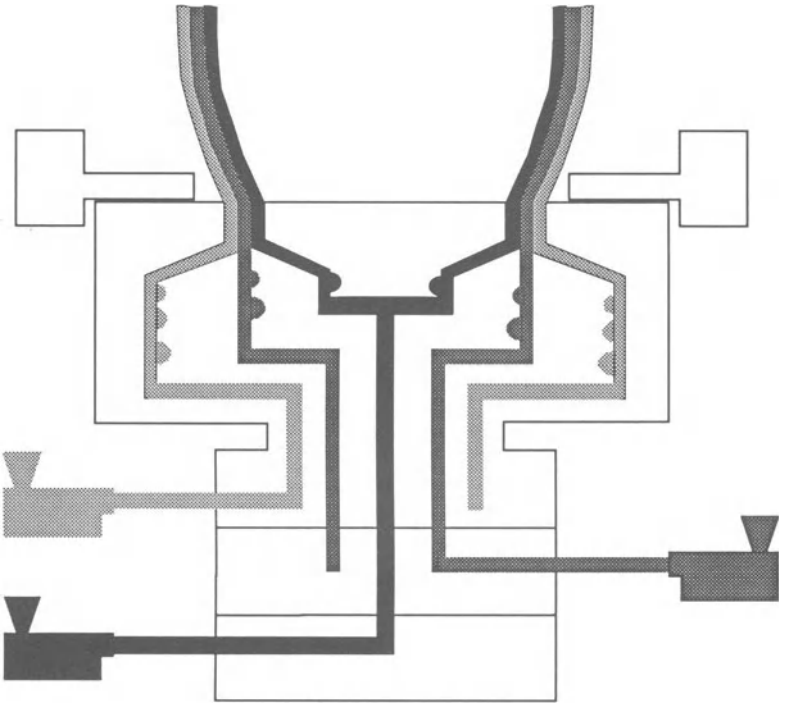


Figure 5.13 Working principle of a blown film coextrusion die.

processed. The individual channels are usually kept next to each other, to optimize the temperature control and to minimize the individual streamlines length differences. However, the construction is complicated and therefore expensive. Nevertheless, this technique is very popular and has been adapted to the production of the majority of the geometries available by extrusion. As an example, Fig. 5.13 shows a three-layer blown film coextrusion die. The individual melts flow in conventional spiral mandrel geometries before uniting at the entrance of the parallel zone. As in single-melt extrusion, a die centring system can be provided and the entire tool can rotate slowly to disperse any anomalies. Furthermore, flexibility in application is promoted by using a system of interchangeable modular manifolds, which can alter the sequence of combination of materials used in the film (ABA, BAB, ABC, CBA, etc.). It should also be noted that the number of film layers does not have to match the number of feeding extruders. Through proper manifold or die design one of the materials – generally a bonding agent – can be inserted as more than one film layer.

Finally, the streams can progress together throughout the entire length of the die (**feed-block process**). This technique is often used in flat film production and allows the use of conventional extrusion dies for a single melt in

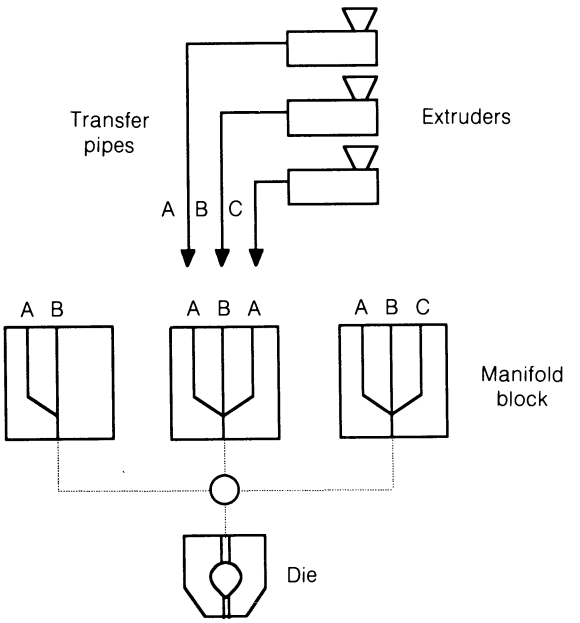


Figure 5.14 Working principle of a modular flat film coextrusion system.

coextrusion. The **manifold block** unites in the specified order the incoming melts, fed from the various extruders by **transfer pipes** (see Fig. 5.14). Replacing the manifold block, inserted between the die and the transfer pipes, enables the distribution of the layers to be changed whenever necessary.

The melts should have similar viscosities, because their segregation is then ensured by the laminar nature of the flow. Figure 5.15(a) shows that when the volumes, or the viscosities, of layers A and B are similar, the distribution of the layers is stable and uniform. When there is an appreciable difference between the cross-section or between the relative viscosities of the different layers, the distribution changes as the flow develops. In Fig. 5.15(b) the less viscous fluid A begins encapsulating the more viscous melt B. This process progresses as the residence time increases. On the other hand, if the volume of A is much lower than the volume of B, it is very difficult to ensure an interface extending throughout the entire width of the extrudate. Material A will accumulate as a strip on the surface of B (Fig. 5.15(c)). Other problems related to differences in the viscosity of the various layers include extrudate bending, and changes in the thickness of the layers across the extrudate width. The first is caused by overflow of the less viscous layer. The second is typical in flat film coextrusion, and is explained by the progressive rearrangement of the layers as they progress in the manifold. Minimization of these problems requires correct design of the die and the transfer pipes (which should have rectangular cross-section), and promotion of adequate rheology. It is important to reduce the interfacial shear

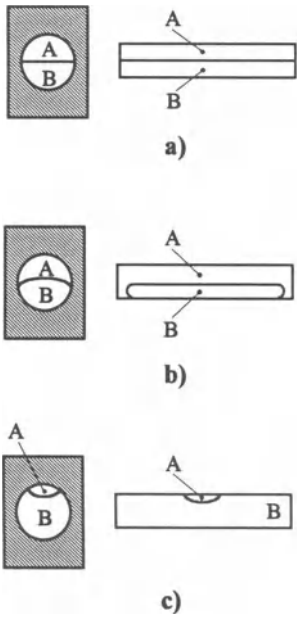


Figure 5.15 Layer rearrangement in coextrusion, due to differences in the viscosities, or flow volumes, of the individual polymers.

stress, and to match both the interfacial viscosity and the interfacial elasticity (which dictate the normal stresses at the interface).

5.4 GENERAL PRINCIPLES OF DIE DESIGN

Although this book is primarily concerned with the operation of extruders and shaping heads, it seems relevant to introduce some general principles of die design, as these will not only illustrate the interrelationship between the various intervening parameters, both inside and outside the die, but will also hopefully provide a guide to some of the design problems often encountered by processors (such as making a new die land, and scaling an existing die up or down). Moreover, understanding the principles and limitations of die design will also help to identify the possibilities and the practical effects of operational actions.

The design of extrusion dies consists mainly in the definition of an appropriate flow path for the material, ensuring streamlining, good melt homogeneity and temperature distribution, an acceptable pressure drop, a narrow residence time distribution, the absence of any flow defects, and the production of a cross-section with the required shape and dimensional

tolerances at the highest possible flow rate. Thus, for any particular application (product, material and typical operating conditions) it is necessary to define geometrical parameters such as convergences, compression ratios, relative channel lengths, and flow restriction contours, in terms of the adequate velocity, temperature, stress, shear rate, pressure drop and residence time profiles developed. The designer should also consider, as completely as possible, the effect of the post-extrusion phenomena on the distortion of the extrudate along the extrusion line. As seen previously, these include extrudate swell, drawdown, shrinkage, and gravity, compression and buoyancy forces. Although extrusion is a forgiving process in the sense that it allows dimensional corrections to be made during the calibration stage, it is convenient to take these phenomena into account when establishing the cross-section of the die lips to avoid the consequences of the building up of residual stresses in the extrudate. Other relevant design steps include the mechanical design of the tool's constitutive parts, the location and power requirements of the heating system, the design of the calibrator and the determination of the minimum length for the cooling zone. Michaeli (1992) has given attention to these aspects in his unique book on die design.

The complexity of each of these tasks and the rapid development of the capacity and performance of computers favoured the application of the computer-aided engineering (CAE) approach to die design. This has resulted in the availability of many commercial die design packages. As a consequence, this trend will be used in this section both to explain the current limitations of the approach, and to introduce die design strategies. Obviously, any calculation sequence can be implemented into a computer program. The commercial packages currently available simulate the flow inside the die with varying degrees of sophistication, providing quantitative information (such as temperature and velocity fields, pressure drop and residence time) that can be used by an experienced operator to evaluate the performance of an existing die, or to assess the adequacy of a new design (O'Brien, 1992). Since new sections can be added, or the current geometrical configuration may be easily modified, and the processing conditions and the material rheology can be altered with little effort, time-consuming or difficult experiments are minimized, and a few design alternatives can be selected for prototyping. The programs solve the general equations of motion and energy, with a particular set of boundary conditions, coupled to a constitutive equation describing the rheological behaviour of the fluid (either non-Newtonian viscous or viscoelastic fluids are usually considered). Nowadays, spiral mandrel blown film and coathanger and fishtail dies are often designed via this type of approach.

Two types of package are available. General-purpose programs, able to offer a wide variety of constitutive models, simulate the flow along the geometry input by the operator. A numerical (often sophisticated and computer-intensive) approach, using either finite elements, finite differences, or volume control techniques, is adopted. The operator defines the

geometry, chooses the boundary conditions and inputs the material and the operational characteristics, and the program automatically generates the mesh, and solves the flow equations through successive increments towards a converged solution. Results such as velocity and temperature profiles, streamlines, and values along a streamline, can be presented either numerically or graphically for many different practical problems. The various programs differ mainly in the numerical algorithm implemented, in the type of constitutive models available, in the graphical capabilities exhibited and in user friendliness. Another family of software has been developed with a specific die geometry in mind, namely flat and blown film, blow moulding and wire coating. These programs generally use a straightforward screen data input system, and employ simpler flow-simulation techniques. In some cases, the algorithm is able to compute the geometry of the flow channel that produces a perfectly uniform extrudate.

One of the main difficulties associated with simulating the polymer melt flow for die design purposes is keeping computation times within reasonable limits, especially for complex flow channels. For example, Rakos, Kiani and Sebastian (1989) developed a three-dimensional finite-element solution technique to obtain the velocity and pressure distributions in the adaptor and parallel zones of a non-axisymmetric profile die. In the case of a simple 'L'-shaped profile, using 27 noded brick elements, the flow simulation took approximately 45 CPU minutes when running on an ETA10 supercomputer and 48 CPU hours on a VAX GPX/II workstation. Therefore, it is important to develop adequate approximation methods to simplify the geometry and/or the flow equations. The real three-dimensional flow should be reduced, whenever possible, to a two- or one-dimensional problem (2.5 and 1.5 dimensions are sometimes considered, when three or two velocity components depend upon two or one spatial coordinates, respectively) as follows (Vergnes and Agassant, 1986):

- Dies may often be considered as narrow channels, i.e. one dimension is generally significantly narrow when compared with the other two. The flow is then described by the equations for a fully developed flow between parallel plates, with a gap equal to the local gap; this may be applied to the exit region of pipes, or of flat film dies.
- Annular flow geometries can conveniently be unrolled without inducing significant errors, to use a Cartesian coordinate system, when the channel depth is small in comparison with the outer radius. This technique is very often used to study the crosshead of a wire coating die.
- A complex flow may be divided into different elementary flows. Coathanger, profile and spiral mandrel dies are usually studied in this way.
- Since in extrusion the flow velocity is low and the polymer temperature is similar to the die wall temperature, it is often feasible to use a mean temperature over the channel depth.

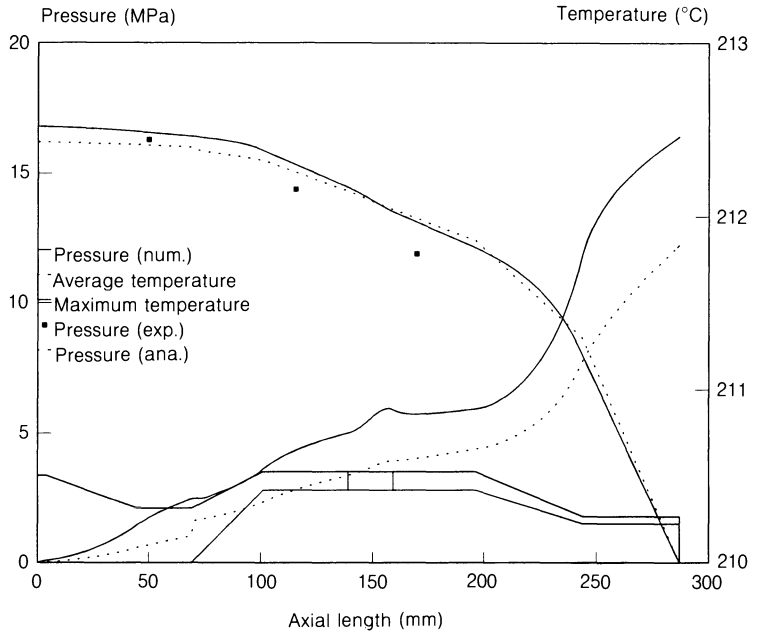


Figure 5.16 Temperature and pressure axial profiles in a pipe mandrel die (Carneiro, 1994).

As an example, Fig. 5.16 compares the predictions of a simple analytical isothermal analysis with the results of a numerical non-isothermal simulation (performed with a finite-differences technique) of the flow of a typical HDPE melt through a conventional mandrel-type pipe extrusion die (Carneiro, 1994). The average temperature increased less than 2 °C due to viscous dissipation, whereas the maximum temperature rose approximately 2.5 °C. Similar results have been obtained with other numerical schemes (Sebastian and Rakos, 1985). The pressure drops computed analytically and numerically are very similar. The effect of the viscous dissipation is obviously related to the dimensions of the die, to the polymer rheology, and to the mass throughput. Nevertheless, the calculated temperature increases are generally below 10 °C (Sebastian and Rakos, 1985). Thus the most appropriate CAE tool (or computing scheme) to be applied by an industrial company in the study of the flow of molten polymers through extrusion dies depends upon the nature of the problem (product shape, specified tolerances, throughput, material), on the amount of time allowed for development purposes, on the existing technical and scientific know-how and on the available computing resources.

With few exceptions, and regardless of their sophistication, the currently available programs are essentially evaluation tools. The results of the flow simulation for a particular set of conditions minimize the need for experimental work, but they are only indirectly used for die design purposes. In fact, it is the operator who should decide whether the flow conditions (or,

alternatively, the die geometry) are adequate or should be improved, and where the required changes should be implemented. Finally, most programs can only deal with the stream of fluid inside the die, ignoring the effect of all the post-extrusion phenomena. One exception is the MICROPUS software, which is able to perform the thermal design of dies (Menges, Kalwa and Schmidt, 1987). Further developments in CAE for extrusion die design should combine the know-how achieved in the understanding of the individual aspects of the process (viscoelastic flow through relatively complicated geometries, extrudate swell at the die exit, cooling of elaborate hollow profiles, microstructure and morphology development) and unite them in a package able to solve practical engineering problems. Two prerequisites are necessary if this is to be achieved.

One is the study of the *inverse formulation* of processing problems. As seen above, in the conventional simulation techniques the equations describing the flow are coupled to constitutive equations describing the material properties and solved for a given set of operational and geometrical conditions. Information on the flow conditions is obtained. The inverse formulation technique corresponds to solving the equations of the problem coupled to the constitutive equations, but now in order to determine the die geometry or the operating conditions that would induce a pre-specified flow pattern, or product geometry. Since this approach is particularly complicated, an alternative solution consists in developing **optimization schemes**, involving the implementation of decision mechanisms, and of some know-how on the problem, in the program.

The other prerequisite is the establishment of a fully integrated general strategy for die design, which would consider in the appropriate sequence the various physical, thermal, rheological and mechanical aspects of the design. Such a scheme would require the use of thorough rheological and physical material information, which is unfortunately rarely available, because of the need for extensive experimental work. Thus, the existence of data banks, or the use of techniques for speedily generating the relevant data (such as those presented in section 5.2.2) is essential.

Figure 5.17 depicts a possible general strategy for designing extrusion dies (Covas, Carneiro and Brito, 1991; Michaeli, 1992). The steps involved comprise mainly: an initial definition of the die lips; establishing the flow path layout; designing the breaker plate and filters, if present; evaluating the mechanical resistance of the die components; computing the influence of the post-extrusion phenomena on the extrudate shape; and designing the heating system. The die is divided into a series of geometrically simpler modules that can be more easily studied, namely in terms of the relationship between pressure drop and flow rate. Moreover, starting the design procedure by outlining the cross-section of the die lips allows the consistent definition of the tentative shape of any adjacent module (in the extruder direction). Apart from the rheological and thermophysical properties of the polymer, typical required input data comprise the mechanical and thermal properties of the material(s)

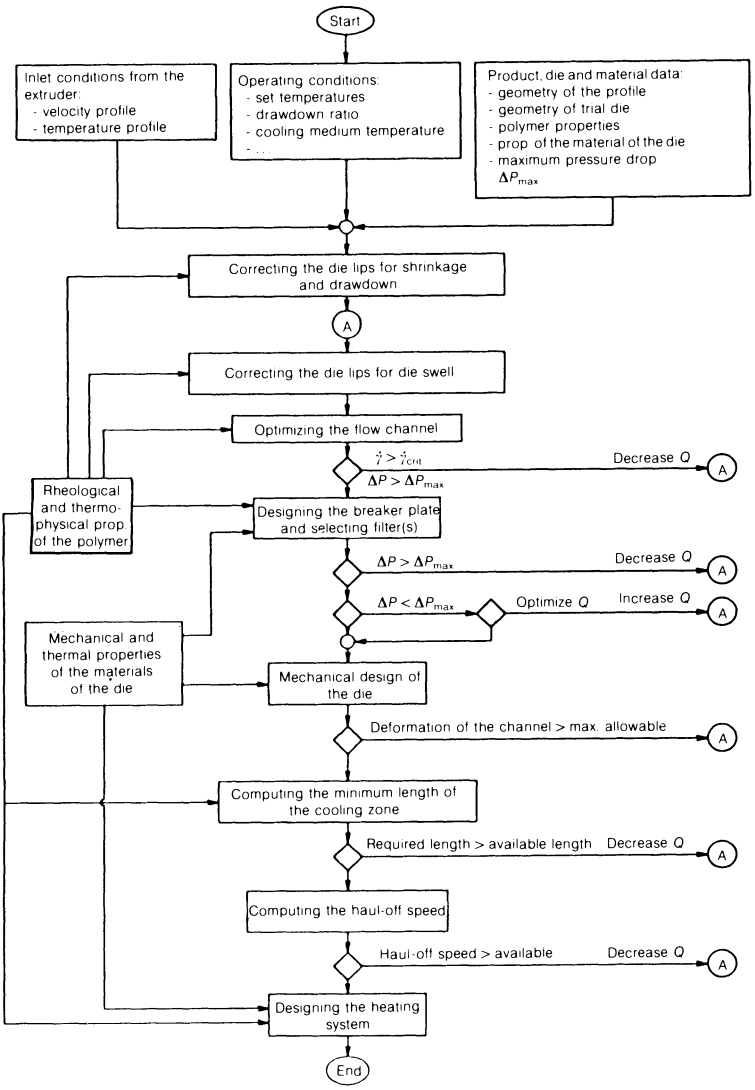


Figure 5.17 General strategy for designing extrusion dies (Covas, Carneiro and Brito, 1991).

of the die, an initial guess at the die geometry, the operating conditions (these include the boundary conditions at the extruder/die interface – temperature and velocity field), and some practical boundary operating values (such as the maximum extruder output or power available, maximum total pressure drop, and local maximum temperatures).

1. **Initial definition of the die lips.** Since any post-extrusion of the extrudate should be compensated by redesigning the die lips, which in turn alters the

dimensions of the flow channel, and consequently the die swell, an iterative procedure should be sought. This will be dealt with in greater detail in section 5.5.4.

2. The **rheological design of the die** (definition of the flow channel) should guarantee:

- *the non-existence of any flow anomalies.* Critical normal stresses cannot be reached; temperature and velocity fields should be determined and carefully evaluated; conditions for the adequate welding of the individual melt streams should be promoted.
- *an acceptable pressure drop.* A minimum pressure drop is required for adequate flow mixing and melting inside the extruder. The highest limit value is related to the mechanical work of the polymer (which may induce its degradation), to the effect on the output of the process, to the available power of the extruder motor and to the mechanical resistance of several die and extruder components (namely the extruder screw and the die fixing bolts).

Figure 5.18 presents the calculation sequence corresponding to the rheological design of a die, consisting of a parallel zone, an adaptor, breaker plate and filters (Covas, Carneiro and Brito, 1991; Carneiro, 1994). The calculations are performed from the die lips towards the adaptor, as seen above. After compensating for the change in size of the extrudate due to draw-down and shrinkage upon cooling, the extrudate swell is estimated. In the case of non-axisymmetric profiles, the analysis should include a mass balance over the entire cross-section, in order to determine the local die land ratios that ensure the extrusion of a product with uniform average speed. The converging taper of the adaptor (either linear or trumpet-shaped) should be validated in terms of normal stresses, by confronting the values reached with the critical limit. If necessary, correction procedures include decreasing the convergence and/or the mass throughput. The breaker plate and filters must also be accounted for in terms of pressure drop. The total pressure drop should be compared periodically with the limit specified, to decide whether the operational conditions should be updated.

As discussed above, the simulation of the polymer flow through the several channels constituting the die requires solution of the continuity, momentum and energy equations for a set of boundary conditions, coupled to a relevant constitutive model. Although the approximation methods referred to simplify this task, the use of numerical techniques is still required. These are often not easily accessible to the average processor/designer, nor justifiable at this stage of the designing sequence. However, if the isothermal non-Newtonian flow in ducts with simple shapes (e.g. circular or annular channels, parallel plates) is treated abundantly in the literature, methods for predicting the flow–pressure relationship for an arbitrary cross-sectional shape are rarely reported. Nevertheless, certain analytical equations apparently produce fair predictions and can, therefore, be adopted for die

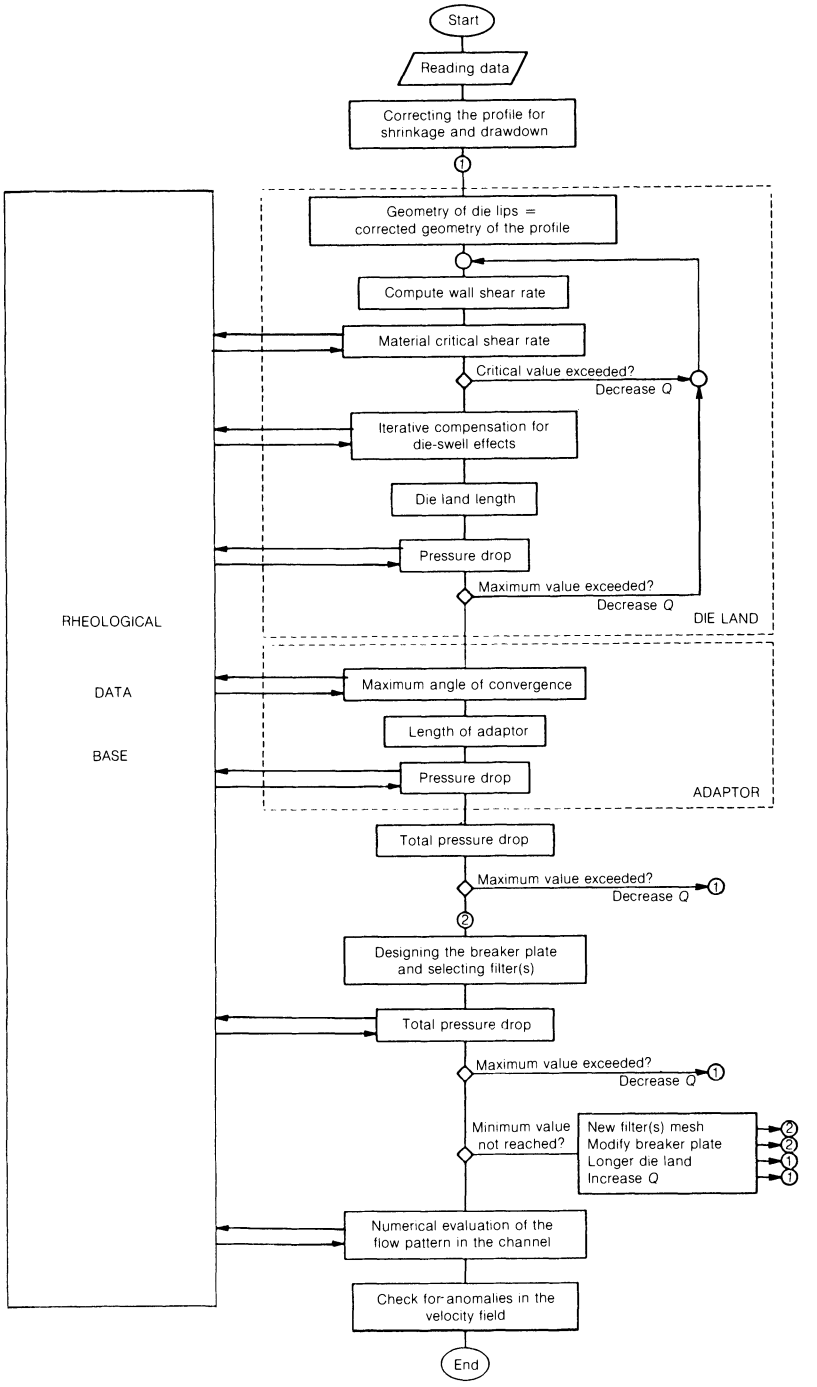


Figure 5.18 Defining the flow channel of a simple profile die.

design purposes. For example, Schenkel (1981) studied the flow through narrow rectangular channels, introducing an aspect ratio factor (W/H), which quantifies the retarding effect of the lateral walls. The methodology is similar to that generally used to simulate the flow in the pumping section of an extruder. Lahti (1963), Kozicki, Chou and Tiu (1966) and Miller (1972) adopted a similar philosophy, defining a general flow equation affected by a shape factor. Figure 5.19 displays the general equation and the 'flow coefficients' calculated by Lahti for different aspect ratios. Weeks (1958) and Lenk and Frankel (1981) proposed formulae for many different shapes, including linearly tapering slits. White and Huang (1981) studied the flow through rectangular and trapezoidal dies. Shenoy and Saini (1984) adopted the method also suggested by Lenk and Frankel (1981) to compute the pressure losses in various differently shaped ducts in terms of the polymer's melt flow index.

At this stage, the initial definition of the flow path is completed. The next step involves evaluating its adequacy numerically. This provides more accurate information on the extrudate swell, on the viscous heat dissipation, on the velocity field and on the mean residence time and residence time distribution. Here, the calculations are carried out in the die exit direction. The procedure may involve several numerical/analytical iterations, since any necessary modifications in the geometry, or in the processing conditions, will trigger a new analytical optimization cycle.

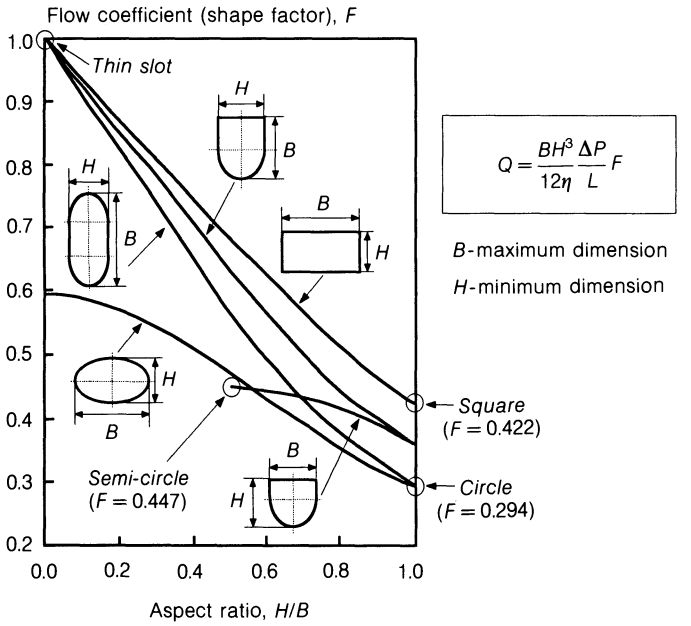


Figure 5.19 Shape factors, at different aspect ratios, according to Lahti (1963).

3. **Filters and breaker plate**. Since the size of the breaker plate holes determines the maximum pressure that can be supported by the filters without breaking due to bending stresses, the mechanical resistance of these accessories should be verified. Thus, designing the breaker plate and the filters encompasses rheological and mechanical aspects (which can be dealt with using the sequence depicted in Fig. 5.20) (Masberg, 1981; Covas, Carneiro and Brito, 1991). The pressure drop created by each filter pack can approximately be given by (Bauer, Ehrmann and Schneider, 1981):

$$\Delta P = \frac{8dk}{w}\left\{\frac{2m[(3n+1)/n](w+d)^2}{\rho F w^3}\right\}^n \tag{5.12}$$

where m is mass throughput, ρ melt density, w mesh width, d wire diameter, F effective flow area; and k and n are power-law constants.

Other approximate methods have been proposed in the literature (Carley and Smith,1978; Kaplan, Morland and Hsu, 1979). Since the filters are bent in areas adjacent to the breaker plate holes, the size of the latter should induce deflections lower than the wire's limit value (Masberg, 1981):

$$f_{\max} = \frac{R\Delta P}{64N}\cdot\frac{5+\nu}{1+\nu} \tag{5.13}$$

The corresponding maximum stress is:

$$\sigma = \frac{SE}{2}(f_{\max}/R)^2 \tag{5.14}$$

In these equations ΔP is the total pressure drop, computed from equation (5.12); R the radius of the breaker plate holes; ν the Poisson coefficient; N the rigidity of the filter (from the theory of plates), given by:

$$N = \frac{0.01Eh_s^3}{12(1-\nu^2)F^{(0.75)}} \tag{5.15}$$

S is the safety factor; E the Young modulus of the wire; and h_s the total thickness of the filter, given by $d(1+d/w)$.

The breaker plate consists of a number of short parallel holes, hence entrance effects play a major role. Their influence can be ascertained by artificially increasing the channel length, to generate the same equivalent pressure drop:

$$L^* = (L/R+6)R \tag{5.16}$$

where L is the real length. The breaker plate thickness can be obtained (Masberg, 1981) from:

$$H = BD(\Delta P S/\sigma_{\text{adm}}\alpha)^{0.5} \tag{5.17}$$

where B is a factor taking into account the effect of the breaker plate clamping conditions, which usually varies between 0.3 and 0.45; D the breaker plate

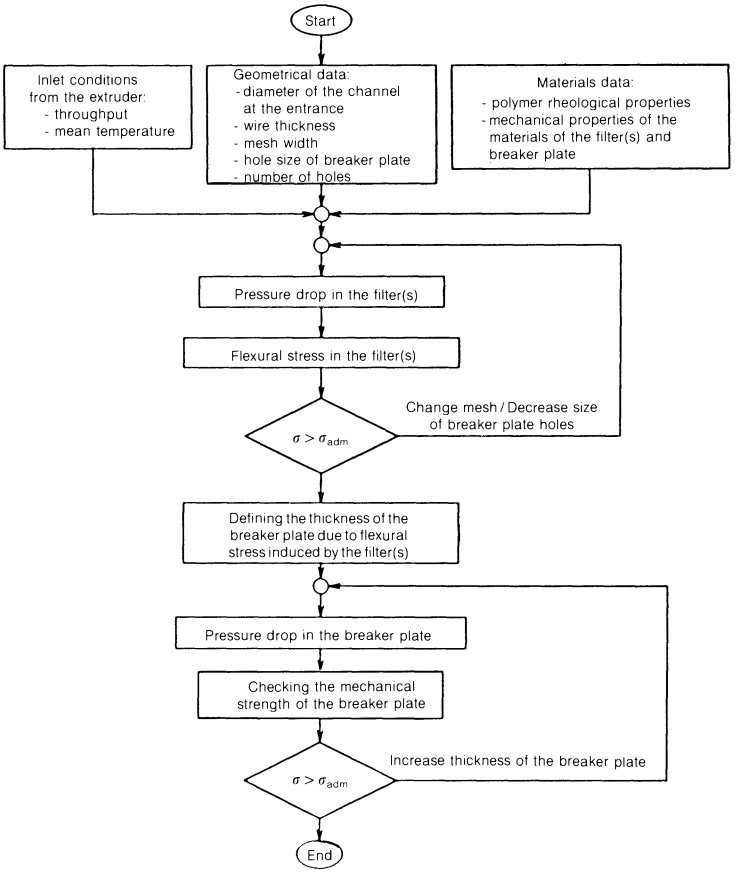


Figure 5.20 Mechanical and rheological dimensioning of the filters and breaker plate (Covas, Carneiro and Brito, 1991).

diameter; ΔP the total pressure drop (the value computed due to the pressure flow along the individual holes should be doubled or even trebled, to anticipate the consequences of the partial blockage of the filters, or of pressure peaks upon starting the extrusion process); σ_{adm} the material's limit stress; and α the stress concentration caused by the existence of holes in the plate, which is given by $(1 - 2R/t)$, where t denotes the distance between the centre of the holes with radius R. In practice, the number of holes may be defined by $A_c/0.866t^2$ (Masberg, 1981), where A_c is the surface area of the breaker plate.

4. The **mechanical design of the die** embraces some of the calculations described above, but generally considers all the forces acting on the entire die during operation, and the resulting deformations. Generally, they include wall shear forces, pressures and compressive forces. The mechanical design of dies has two objectives. The first is to design the die in terms of the resistance of its components to external forces. Michaeli (1992) has devoted attention to this

subject, establishing some general design rules and considering as case studies a spider-supported mandrel die and a flat film/sheet die. The second objective is to determine the deformations of the flow channel and compensate for their effect.

5. **Post-extrusion phenomena** should now be analysed in greater detail. Heat transfer calculations determine the period of time (or axial distance) during which the most relevant shape distortions occur. If a thermomechanical model for stretching, cooling and morphology development is available, the axial extrudate contour can be determined, hence providing the required information to establish the configuration of the die lips. Recently, Duffo, Monasse and Haudin (1991) studied the cast film extrusion of polypropylene and developed a thermomechanical model for stretching in air and a purely thermal model for cooling on the roll, accounting for the polymer crystallization. The 'neck-in' and edge 'bead' (uniform thickening along the periphery of the film) phenomena have also been predicted (d'Halewyu, Agassant and Demay, 1990).

6. **Thermal design of the die**. The total power of the heating system can be estimated through an energy balance of the die (Michaeli, 1992). The location and power of each individual heater can also be determined, but this involves knowing the temperature field both in the flow channel and in the die body. The various heat flows involved in the process are:

- $\dot{Q}_{me}$: heat flow entering the die with the melt;
- $\dot{Q}_{ma}$: heat flow exiting the die with the melt;
- $\dot{Q}_{kl}$: heat losses by convection to the surroundings;
- $\dot{Q}_{rad}$: heat losses by radiation;
- $\dot{Q}_{diss}$: energy dissipated in the die;
- $\dot{Q}_{H}$: energy supplied to the die by the heaters (this is the value to be determined).

According to the energy balance:

$$\dot{Q}_H = \dot{Q}_{kl} + \dot{Q}_{rad} - \dot{Q}_{diss} - (\dot{Q}_{me} - \dot{Q}_{ma}) \tag{5.18}$$

where

$$\dot{Q}_{kl} = A\alpha_{kl}(T_c - T_a) \tag{5.19}$$

$$\dot{Q}_{rad} = A\varepsilon\sigma(T_c^4 - T_a^4) \tag{5.20}$$

$$\dot{Q}_{diss} = m\Delta P/\rho \tag{5.21}$$

$$\dot{Q}_{me} - \dot{Q}_{ma} = mC_p(T_e - T_s) \tag{5.22}$$

in which A is the die surface area; α_{kl} the natural convection heat transfer coefficient; ε emissivity; σ the Stefan–Boltzmann constant; m mass throughput; ΔP the pressure drop in the die; ρ the polymer density; C_p the polymer specific heat; T_c die surface temperature; T_a room temperature; T_e melt temperature at the die entrance; and T_s melt temperature at the die exit.

5.5 SPECIFIC ASPECTS OF DIE DESIGN

5.5.1 Blown film

As seen in section 5.3.2, the best means of avoiding the weld line problem in blown film extrusion is provided by the spiral mandrel die configuration, where the incoming flow that is initially directed to the helical channels machined in the mandrel is progressively changed into an axial annular stream. This transformation is caused by the gradual decrease in the depth of the helical channels and the simultaneous increase in the clearance between the mandrel and the die body. This type of die was initially studied by Procter (1972), who established its general functional principles. Later analyses have essentially gradually abandoned some of the simplifications initially adopted (Kurzbuch, 1974; Ast, 1976; Helmy and Worth, 1980; Wortberg and Schmitz, 1982; Saillard and Agassant, 1984; Vlcek, Kral and Kouba, 1984; Perdikoulias, Vlcek and Vlachopoulos, 1987; Rauwendaal, 1987; Vlcek, Vlachopoulos and Perdikoulias, 1988; Benkoucha and Sebastian, 1989). A mass balance in an elementary volume of the die will yield (see Fig. 5.21):

$$Q_1 - Q_2 = Q_3 - Q_4 \tag{5.23}$$

where Q_1 and Q_2 represent the helical presssure flows at the entrance and exit of the element, respectively, and Q_3 and Q_4 the incoming and exiting axial flows in the same element, respectively. Assuming isothermal flow and a power-law fluid, the helical flow is given by (Rauwendaal, 1987):

$$Q_{\text{hel}} = \frac{FWH^2}{2[(2n+1)/n]} \left(\frac{H}{2k}\frac{\mathrm{d}P}{\mathrm{d}z}\right)^{1/n} \tag{5.24}$$

where k and n are the power-law constants, W and H are the local channel dimensions, F is the channel shape factor and $\mathrm{d}P/\mathrm{d}z$ is the pressure drop in the

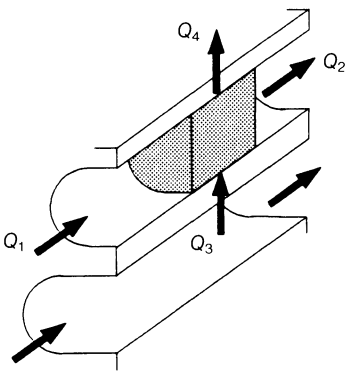


Figure 5.21 Mass balance in an element of the spiral mandrel.

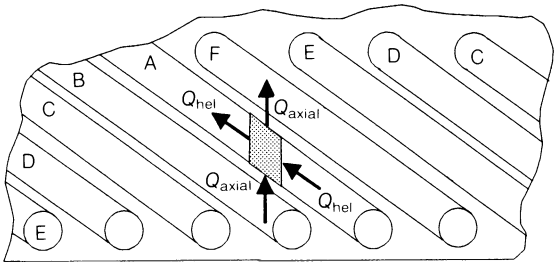


Figure 5.22 Unrolled spiral mandrel, showing the various helical channels, and the relevant flows.

downchannel direction. The axial flow is (Rauwendaal, 1987):

$$Q_{axial} = \frac{\delta^2}{2[(2n+1)/n]} \left(\frac{\delta}{2k}\frac{dP}{dy}\right)^{1/n} \tag{5.25}$$

where δ is the gap between the mandrel and the die body and dP/dy is the pressure drop in the axial direction. Now a stepwise procedure, following the flow between adjacent helical elements until the end of the spiral, can be envisaged. This is illustrated schematically in Fig. 5.22, where the mandrel was unrolled. Equation (5.23) is successively applied, with the values of each flow (as given by equations (5.24) and (5.25)) being locally updated. The first and last flow elements of the spiral have specific boundary conditions.

Unlike Procter (1972), Rauwendaal (1987) did not assume a linear pressure drop from the start to the end of the spiral. Instead, the pressure drop in the spiral direction is related to that across the channel via the helix angle (i.e. the pitch of the spiral). Saillard and Agassant (1984) and Vleck, Kral and Kouba (1984) adopted similar approaches, but relaxed some of the previous assumptions. Perdikoulias, Vlcek and Vlachopoulos (1987) compared these three models, and concluded that they produced significantly different results in terms of the total pressure drop, pressure profile along the spiral, and final flow distribution along the circumference of the die lips. Nevertheless, the predicted general trend was consistent and all the models showed that the flow uniformity increases with the power-law index, n. As expected, the more elaborate models produced the more accurate results, but this advantage was offset by the significantly longer computing times.

Several other one-dimensional analyses, assuming isothermal flow conditions, were published, namely by Kurzbuch (1974), Ast (1976), Helmy and Worth (1980) and Wortberg and Schmitz (1982). More sophisticated techniques have also been applied to the study of spiral mandrel dies. For example, Vlcek, Vlachopoulos and Perdikoulias (1988) used a lumped parameter method applied over a finite number of control volumes, for a power-law fluid, whereas Benkhoucha and Sebastian (1989) applied a flow analysis network to simulate the two-dimensional isothermal flow inside the die. All

these models provide the designer with a powerful, progressively more accurate tool for analysing the flow distribution system in this type of die. As a matter of fact, a poorly designed spiral mandrel die will cause non-uniform flow around the circumference of the gap, and a periodic flow variation (usually equal to the number of spirals in the die (Vlcek, Vlachopoulos and Perdikoulias, 1988)).

The above analyses can also be used to assess the effect of operational and geometrical parameters on the die performance. In addition to the role of the polymer rheology (e.g. temperature field), there are six important geometric factors: the number of helical channels; the helix angle; the width of the spirals; the initial depth of the spirals; the initial gap between the mandrel and the die body; and the final gap between the mandrel and the die body. The number of helical channels, the initial annular gap and the helix angle are often regarded as the three prime variables (Coyle,1991; Rauwendaal, 1991b). Generally, the flow uniformity improves dramatically with increasing number of channels. The value of the initial annular gap can also be optimized. Upon augmenting the gap the flow variations decrease, reach a minimum and beyond that increase again. In fact, at sufficiently large gaps, an annular flow in the axial direction, never participating in the helical flow (and, consequently, inducing weld lines), develops immediately. Reducing the helix angle generally improves the flow uniformity. However, since the corresponding pressure drop increases, a compromise should be sought (Rauwendaal, 1991b). The die land, where annular flow develops, contributes significantly to the total pressure drop. Therefore, its design should take into account the rheology of the polymer to be processed.

5.5.2 Flat film/sheet

The design of dies for flat film or sheet predictably focuses on the definition of the manifold, or distribution channel, that ensures the production of an extrudate with uniform thickness and velocity across the width. As seen previously, this is equivalent to guaranteeing the same total flow resistance regardless of the flow path considered, and the same residence time for each flow path. Another important design factor is the mechanical deformation of the die due to the pressures developed, usually known as **clamshelling**. Since the die is clamped together at the edges, the largest deflection occurs at the centre, resulting in an unbalanced incremented flow in this region. However, it must be borne in mind that adjusting the die lips to compensate for clamshelling affects the overall pressure drop and, consequently, the throughput. In practice, flat film/sheet dies differ in their design in terms of the manifold profile, the construction of the lip-adjustment system, the eventual existence of restrictor bars, the type of heaters employed (usually plate elements or cartridges) and the overall dimensions.

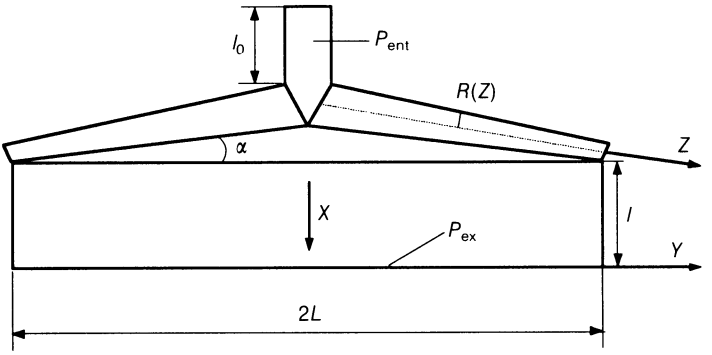


Figure 5.23 Dimensions of a linear tapered manifold (Vergnes, Saillard and Plantamura, 1980).

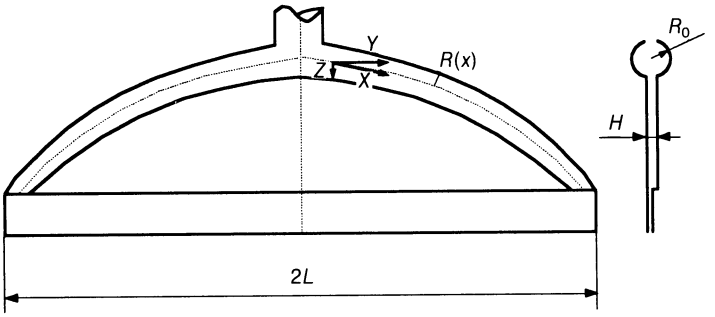


Figure 5.24 Dimensions of a curvilinear tapered manifold (Rauwendaal, 1991a).

Charbonneaux (1991) and Rauwendaal (1991a) reviewed some of the flow analyses proposed in the literature for the T-type, fishtail and coathanger dies. In particular, Charbonneaux (1991) presented for each case the assumptions and the corresponding design equations. For example, in order that a linear manifold die, geometrically characterized in Fig. 5.23, ensures uniform flow rate across the width, the manifold circular cross-section, $R(z)$, should follow the equation (Vergnes, Saillard and Plantamura 1980):

$$R(z) = \left[\frac{(1+3n)}{2\pi(1+2n)}(L - z\cos\alpha)\right]^{n/(1+3n)} \left(\frac{H^{1+2n}}{\sin\alpha}\right)^{1/(1+3n)} \tag{5.26}$$

The corresponding flow rate is:

$$Q = \frac{n}{2n+1} L h^{(1+2n)/n} \left[\frac{P_{ent} - P_{ex}}{2k}\right]^{1/n} \frac{1}{(1 + L\tan\alpha + 2^n l_0 \sin\alpha)^{1/n}} \tag{5.27}$$

where k, n are the power-law constants and P_{ent} and P_{ex} the die inlet and exit pressures, respectively. Equation (5.26) shows that the smaller the coefficient n,

as well as the manifold angle α, the larger the manifold section.The consistency index, k, does not affect the geometry. These equations, which were derived for ideal linearly tapered dies, can be adapted to the geometry of real dies with some approximations (Vergnes, Saillard and Plantamura, 1980). In the case of a curvilinear tapered coathanger die having a circular manifold $R(y)$ (see Fig. 5.24), and a slit channel length $Z(y)$ (Matsubara, 1980; Charbonneaux, 1991):

$$R(y) = \frac{m^{1/[3(n+1)]}}{\pi^{1/3}} \left[\frac{1+3n}{2(1+2n)}\right]^{n/[3(n+1)]} H^{2/3}(L-y)^{1/3} \tag{5.28}$$

$$Z(y) = \frac{3\sqrt{k}}{2}\left[(L-y)^{1/3}\sqrt{(L-y)^{2/3}-k} + k\log\left\{(L-y)^{1/3} + \sqrt{(L-y)^{2/3}-k}\right\}\right] \tag{5.29}$$

with:

$$k = \left[\frac{\pi H}{m^{(1+3n)/(1+n)}}\left(\frac{1+3n}{2(1+2n)}\right)^{2n/(1+n)}\right]^{2/3} \tag{5.30}$$

where m is the ratio of the average residence time in the manifold to that in the slit. Lower coathanger gaps can be obtained if m is chosen above unity. The above relationships assist the design of tools for specific applications. For existing extrusion heads, Dooley (1990), Wang (1991) and Pittman and Sander (1993) simulated the incompressible, isothermal flow of polymers (assuming various simple constitutive equations) by finite-element methods.

The above expressions incorporate, as expected, the material's power-law index, again demonstrating how the optimization of these dies is intrinsically related to a particular rheology and set of operating conditions. In practice, occasional changes in the value of n (due to the development of a non-predicted temperature field in the die), and the mechanical deformation caused by the pressure drop, will justify the poor performance of a geometry which in theory has been correctly designed. As seen previously, adjustment capability should consequently be incorporated. Winter and Fritz (1986) developed a coat-hanger design which is largely independent of the flow rate or of the polymer viscosity. It uses a rectangular manifold that induces a consistent shear rate. Two cases are considered, uniform width b, and constant aspect ratio b/h (see Fig. 5.25). For an invariable manifold width (and assuming $b/H \gg 1$):

$$h(y) = H\sqrt{\frac{L-y}{b}} \tag{5.31}$$

$$Z(y) = 2b\sqrt{(L-y)/(b-1)} \tag{5.32}$$

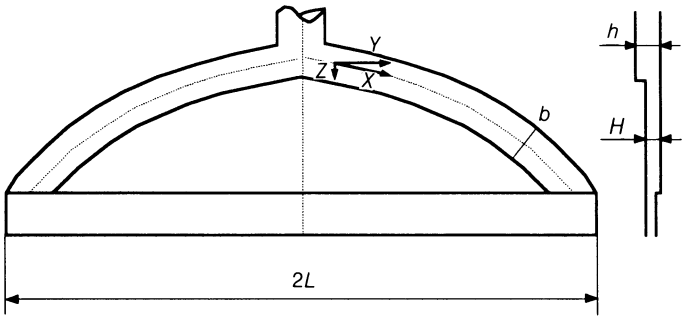


Figure 5.25 Dimensions of a curvilinear tapered manifold, with melt distribution characteristics independent of the polymer rheology (Winter and Fritz, 1986).

However, this solution is more susceptible to clamshelling, as the land length is particularly large at the centre. Also, these expressions were obtained with an isothermal analysis. In reality, changes in the local temperatures will have an effect on the average exit velocity across the width. Generally, the dimensions found to be determinant in terms of clamshelling are: the distance between the manifold and the die lips; the coathanger angle; the die land length; and the die land gap (Helmy, 1987). Based upon some illustrative case studies, Helmy (1987) showed that modifying the die geometry slightly can reduce clamshelling by 55%, whereas Michaeli (1992) found that a reduction in the die land of 33% reduced the total deflection by a factor of 4. Other design parameters include the manifold and the die body sizes (increasing the overall die thickness by 2.5 cm can result in a 7% decrease in clamshelling (Helmy, 1987)). The correct prediction of clamshelling requires the use of numerical techniques (very often finite-element methods), which are able to determine the deformations at any point in the die. Michaeli (1992) developed a much simpler approach. The deflection of the die lips is calculated by considering two overall die cross-sections in the longitudinal and transversal directions. The first is compared to a cantilever beam tightly clamped on one side and subjected to an uniform load distribution (given by the maximum pressure drop value). The transversal section is assumed to be held together without screws, and is considered to be equivalent to a cantilever beam, which is rigidly clamped at one end and guided on the other.

5.5.3 Profiles

The design of dies for manufacturing profiles is simplified if the extrudate to be produced is, whenever possible, defined according to the following general rules. First, the cross-section should be as simple as possible. Second, it is advantageous to fabricate a symmetrical profile. Third, material accumulation in any zone of the profile should be avoided. Fourth, the wall thickness should be kept uniform. Fifth, the interior walls must be 20–30% thinner than the

exterior walls (because they are not directly cooled). Sixth, the definition of the cavities of hollow profiles should consider the need to fasten the necessary metallic inserts in the die. Seventh, corner radii must be at least a quarter of the profile wall thickness to avoid stress concentration. Finally, the profile should be able to retain its shape for some time after exiting the die (Schiedrum, 1975; Rauwendaal, 1991c; Michaeli, 1992).

The problems associated with the design of some specific profiles have been addressed in the literature. For example, Krein (1983) discussed the design of corrugated tubing, Sirlereaux and Loewen (1983) considered the resistance requirements of window profiles, and Stokes (1987) studied the mechanical design of coextruded pipes. The complexities of the design are directly associated with the shape and size of the extrudate. Nevertheless, the following guidance can be provided. First, the adaptor, or transition zone, should be streamlined to avoid hang-up of material and the occurrence of flow instabilities. The flow should accelerate constantly, and reach the uniform maximum speed at the beginning of the die land. Second, the die land, or parallel zone, must guarantee uniform average velocity at all points of the extrudate cross-section. This may involve deliberate changes in the channel length across the width. Then, the undesirable twisting of the extrudate is avoided and the final product is largely free from residual stresses. In the case of hollow profiles, the die land generally accommodates the inserts that will create the cavities. Finally, the flow path design should promote one-dimensional flow conditions. However, as transversal flow may develop during production, some streamlining in this direction should be guaranteed.

Sors (1974) proposed the use of trumpet-shaped adaptors to maintain a constantly accelerating flow. However, the technique *per se* does not ensure the required geometrical continuity between the die entrance zone and the die land. Michaeli (1992) reported several empirical techniques for establishing the adaptor geometry, among them the possibility of gradually establishing the cross-section of the profile over a cone encompassing the transition zone (this is illustrated in Fig. 5.9). Chan and Hon (1990) proposed a geometrical method for the automatic generation of this flow channel, given the definition of the profile. The technique combines the proportional spacing of points on one section to determine the points on the second section, together with the shifting and the alignment of the centroids of each section. The philosophy appears promising, but it is still in its infancy. In practice, the adaptor is made as simple and streamlined as possible, its performance still relying upon the expertise and experience of the designer.

The definition of the die land geometry is currently based upon semi-empirical techniques. The flow uniformity at the die exit is generally pursued by two approaches. In the most widespread technique, the lengths of the individual parallel channels are differentiated. If two volumetric flows Q_1 and Q_2 must emerge from the individual parallel channels (as shown in Fig. 5.26), having lengths L_1 and L_2 and cross-sectional areas A_1 and A_2, with

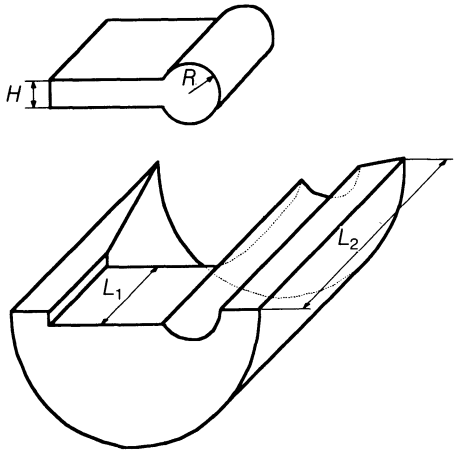


Figure 5.26 Die for the production of a simple profile, showing the relative die land lengths (adapted from Schenkel and Kühnle, 1983).

the same average flow speed, then:

$$\bar{V}_1 = \bar{V}_2 = \frac{Q_1}{A_1} = \frac{Q_2}{A_2} \rightarrow \frac{Q_1}{Q_2} = \frac{A_1}{A_2} \tag{5.33}$$

Considering a power-law fluid and the output versus pressure relationship:

$$\frac{Q_1}{Q_2} = F(n)\left(\frac{L_2}{L_1}\right)^{1/n} \tag{5.34}$$

or, in terms of the relative lengths:

$$\lambda = \frac{L_1}{L_2} = \sqrt[1/n]{F(n)A_2/A_1} \tag{5.35}$$

For the geometry considered in Fig. 5.26 (rectangle/circle) (Schenkel and Kühnle, 1983):

$$\lambda = \left(\frac{H}{R}\right)^{n+1}\left(\frac{1}{2}\frac{3n+1}{2n+1}F\right)^{n} \tag{5.36}$$

where H is the height of the rectangular subsection, R the radius of the circle and F is the rectangular shape factor. Other geometrical arrangements have been treated identically. For example, for two adjacent rectangles:

$$\lambda = \left(\frac{H_1}{H_2}\right)^{n+1}\left(\frac{F_1}{F_2}\right) \tag{5.37}$$

where the indices 1 and 2 refer, obviously, to each rectangle. One of the simplifications associated with this methodology is to ignore the transverse flow between adjacent parallel channels, caused by differences in the local

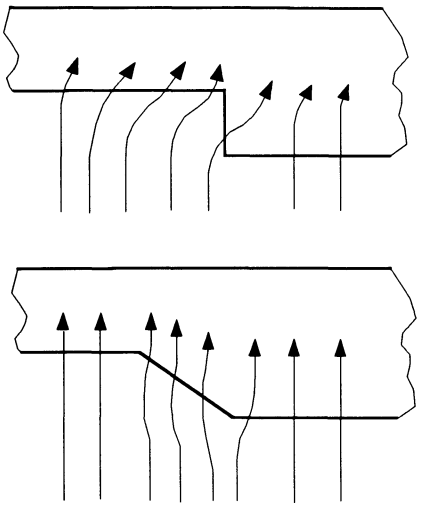


Figure 5.27 Avoiding premature polymer degradation due to transversal flow across the die land.

pressures. As shown in Fig. 5.27, one practical way of minimizing possible detrimental effects involves cutting a gradual transition from the thin to the wide land section. In this way, short-cutting of material from the lower gap, resulting in excess material on the edges of the wider gap, is avoided. A 45° angle dam is often built. Huneault, Lafleur and Carreau (1992) developed a more precise approach to the problem. The method follows the following sequence:

1. The flow geometry is subdivided into simpler sections, to form a flow network.
2. The relevant flow resistances ($\Delta P/Q$) in the longitudinal and transversal directions are calculated, assuming an initial guess on the flow rate distibution.
3. Pressure and flow rate are evaluated for each section by solving the flow network equations.
4. Steps 2 and 3 are repeated until convergence.

In the example given in Fig. 5.28 the two adjacent rectangular channels are subdivided into six elementary flow paths. The total flow rate is considered fixed by upstream conditions. The relevant flow equations are:

$$Q_i = \frac{P_i^{\text{up}} - P_i}{R_i} \tag{5.38}$$

$$Q_{ij} = (P_j^{\text{up}} + P_j - P_i^{\text{up}} - P_i)/2R_{ij}^{\text{t}} \tag{5.39}$$

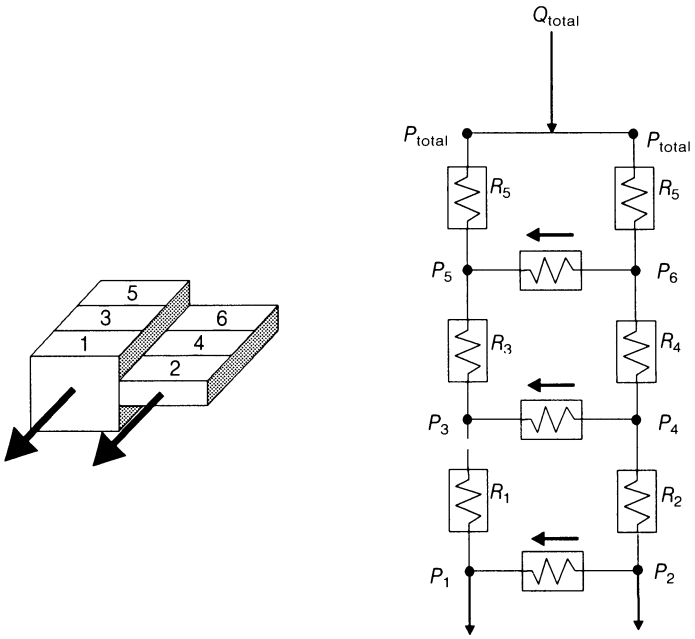


Figure 5.28 Flow geometry (left) and corresponding flow network (right) (Huneault, Lafleur and Carreau, 1992).

where Q_i and Q_{ij} refer to the flow in the main and in the transverse directions, respectively, P_i^{up} and P_i are the pressures upstream and downstream of section i, respectively, R_i is the resistance of section i, and R_{ij}^t is the resistance in the transverse direction between the adjacent sections i and j. For rectangular channels, the resistance to flow is given by:

$$R = 2kL[2(1/n + 2)]^n W^{-n} H^{-(2n+1)} Q^{n-1} \tag{5.40}$$

where k, n are the power-law constants and H, W and L are the thickness, width, and channel length, respectively. The transverse resistance from section i to section j is the sum of the transverse resistances in the two connecting half-sections, plus the resistance due to entrance effects. For each half-section, one may write approximately:

$$R_i^t = \frac{R_i}{2}\left(\frac{W_i}{L_i}\right)^{1+n} \tag{5.41}$$

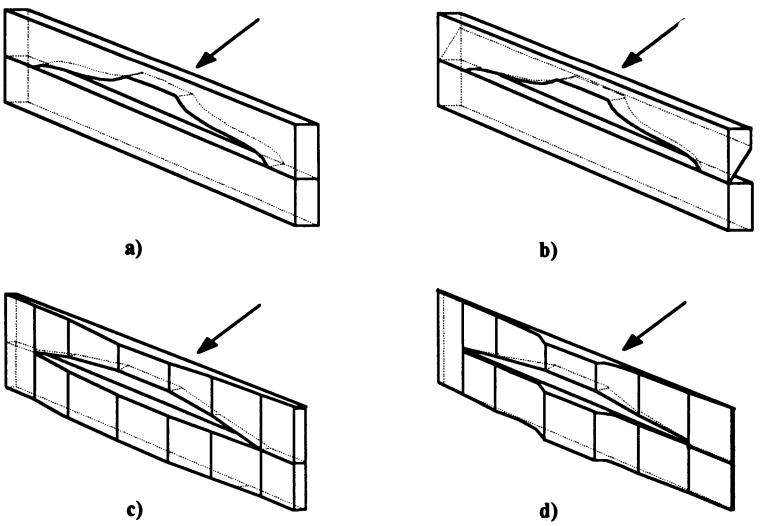


Figure 5.29 Die face-relief strategy: (a) straight-cut die; (b) back linearly relieved die; (c) linear face-relieved die; and (d) quadratic face-relieved die (adapted from Lee and Stevenson, 1992).

Entrance effects can be estimated on the basis of Bagley corrections, or by artificially augmenting the length of each channel (this technique was used for computing pressure drops in breaker plates – see equation (5.16)). It is possible to envisage the adaptation of this model to solving the inverse problem, i.e. given the specified outputs in each section of the die lips (computed from the uniform exit average speed requirement), calculate the appropriate length of each parallel channel.

The flow at the die exit can also be balanced through a face-relief strategy (Lee and Stevenson, 1992). Figure 5.29(a) shows a conventional straight-cut die, with a typical constant die land. Figure 5.29(b) shows the back-relieved die version, where metal was cut diagonally from the back of the upper plate. The cutting angle is such that where the die opening is thickest it also has the longest unrelieved land. Figures 5.29(c) and 5.29(d) show linear and quadratic face-relieved dies, respectively. These were designed according to the empirical rule:

$$L/L_{\max} = (H/H_{\max})^p \tag{5.42}$$

where H and L are the local gap and die land, respectively, and p takes the value 1 for the linear die and 2 for the quadratic die. The values of H and L are related in terms of constant average velocity at the die exit.

5.5.4 Case study: pipe production

This section considers the most relevant aspects of the design of a pipe extrusion die, following the general principles presented above (see the methodology presented in Fig. 5.18).

The rheological characteristics of the polymer (a typical HDPE extrusion grade was selected for this example) were defined according to the procedure presented in section 5.2.2. The dependence of the shear viscosity on the shear rate was described by a Munstedt-type polynomial (Munstedt, 1978). The effect of the temperature was considered through the introduction of a shift factor, a_T, computed at constant shear stress:

$$\log \tau = a_0 + a_1 \log(a_T \dot{\gamma}) + a_2 [\log(a_T \dot{\gamma})]^2 \tag{5.43}$$

where a_0, a_1 and a_2 are the coefficients of the second-order polynomial and

$$a_T = \left(\frac{\dot{\gamma}_{\text{ref}}}{\dot{\gamma}} \right)_\tau \tag{5.44}$$

where $\dot{\gamma}_{\text{ref}}$ represents the shear rate – at the reference temperature chosen – corresponding to the shear stress τ, while $\dot{\gamma}$ denotes the same shear rate, corresponding to the same shear stress, but now at the required temperature T. The extensional characteristics were computed from equations (5.2) and (5.3), using the same temperature dependence behaviour. This information is mainly used for design purposes (i.e. to define maximum convergences and mass flow rates), as the corresponding pressure drops assume values that are some 50–100 times lower than those due to shear flow (Covas, 1985) and can, therefore, be ignored.

The onset of flow defects was determined via the direct observation of the extrudates produced during capillary rheometry experiments. Although their characterization criterion is generally established in terms of a critical stress (section 5.2.2), it is more convenient to express the onset of the rheological anomalies in terms of critical shear rates. The effect of temperature can be included using again the concept of a shift factor, as defined in equation (5.44) – the shear rates will now correspond to critical values. The critical shear rate at a specific temperature, $\dot{\gamma}_c$, is computed from the knowledge of $\dot{\gamma}_{c,\text{ref}}$ at the reference temperature:

$$\log \dot{\gamma}_c = (\log \dot{\gamma}_{c,\text{ref}} - b) - m/T \tag{5.45}$$

with

$$\log a_T = b + m/T \tag{5.46}$$

i.e. an Arrhenius type of temperature dependence is assumed.

The entire configuration of the extrusion tool is defined as a series of simple flow channels. A conventional mandrel extrusion head, supported by six spider legs, and satisfactorily described by 11 geometrically distinct blocks, will be studied. Both the arrangement and the relevant *initial tentative dimensions* are

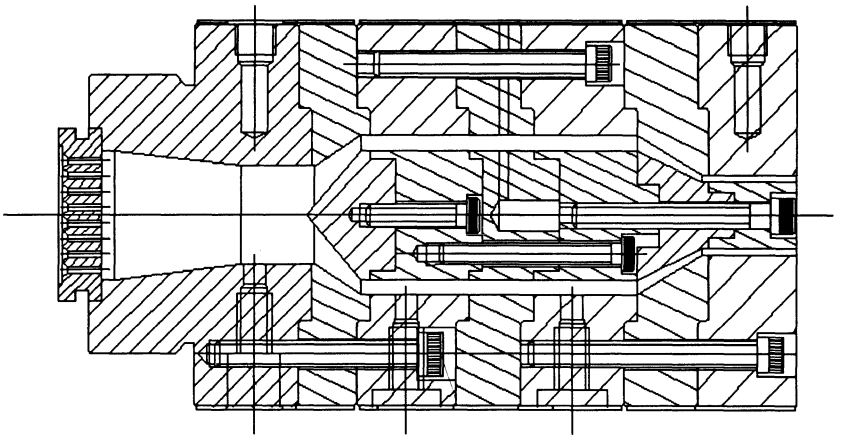


Figure 5.30 Tentative geometry of mandrel pipe die.

presented in Fig. 5.30. The die lips were made identical to the pipe cross-section (1 in pipe, 2 mm thick).

After specifying the mass throughput and the total pressure drop limit, the simulation can be initiated. A notoriously excessive output was defined, as a way of testing the ability of the algorithm to proceed with the necessary corrections. As seen in Fig. 5.31 (left), the initial value of 100 kg h^{-1} is progressively reduced to about 25 kg h^{-1}, to avoid the occurrence of flow deffects. This is a two-step process. Firstly, the output is fixed, taking the cross-section of the die lips equal to that of the pipe (the output decreases to about 72 kg h^{-1}). This result would be the same regardless of the value input, since it only depends on a material property. In the subsequent iterations the output is further decremented, because the initial size of the die lips will be modified to compensate for the combined effects of the extrudate swell (the cross-section should be reduced), shrinkage upon cooling (with the reverse consequences), and caterpillar drawdown (with an effect similar to that of the die swell). As shown in Fig. 5.31 (right), the initial external and internal radii (12.70 and 10.70 mm, respectively) will be decreased to 10.40 and 8.76 mm, respectively. The extrudate-swell effect is compensated according to the following iterative procedure:

1. The die lips are made equal to the pipe cross-section.
2. The shear rate is computed.
3. The extrudate swell is determined.
4. The dimensions of the die lips are corrected.
5. Step 2 and 3 are repeated for the new dimensions.
6. The resulting extrudate dimensions are established.
7. The size of the die lips is incremented/decremented.
8. Step 5–7 are repeated until step 6 produces the required extrudate dimensions.

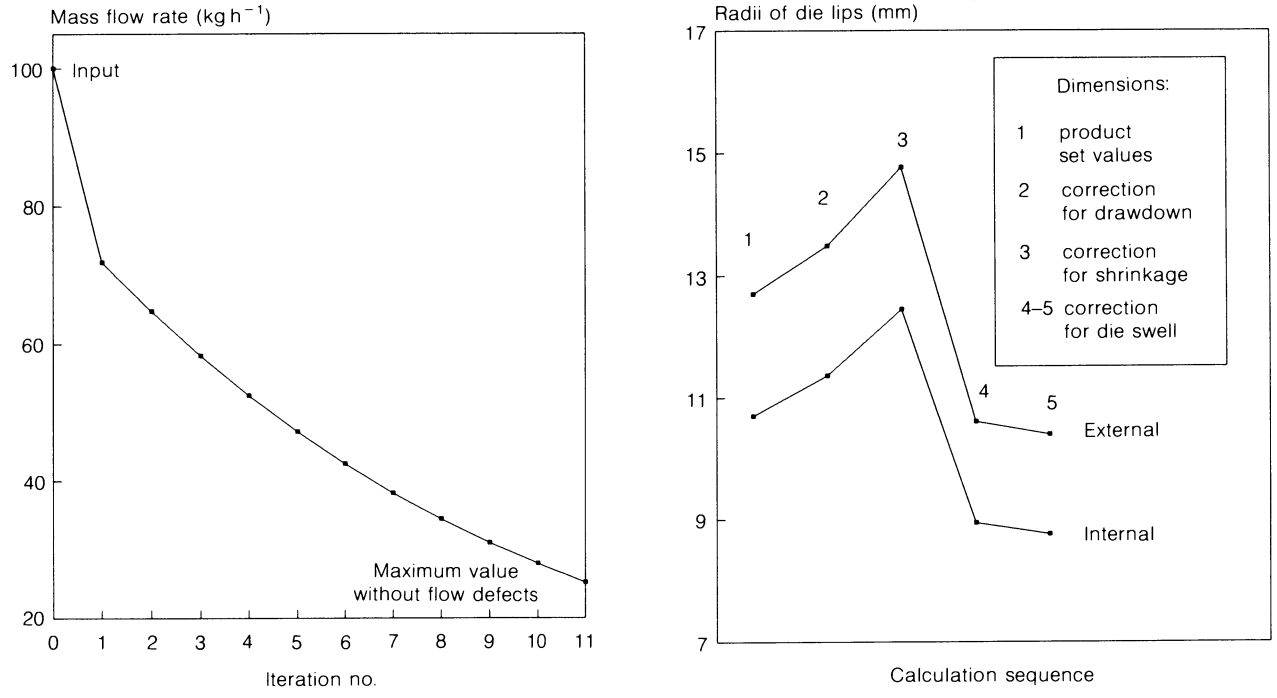


Figure 5.31 Defining the die geometry. Left: correcting the throughput to avoid flow defects. Right: defining the cross-section of the die lips.

As seen previously, extrudate swell and drawdown occur simultaneously. Whereas the former changes the shape (of non-axisymmetric profiles) and the size of the extrudate, the drawdown affects essentially the dimensions (Brown, Kim and Summers, 1979, Griffith and Tsai, 1980). Since die swell depends on the time available for relaxation, operating conditions that would induce the same equilibrium value (i.e. equal throughput, temperature and die geometry), once conjugated with different caterpillar velocities, will induce distinct cross-section profiles along the extrusion line. This is demonstrated in Fig. 5.32, where the cross-section of a simple circular extrudate was measured at different locations along the line, at several constant drawdown ratios (Huneault, Lafleur and Carreau, 1990). One would anticipate that when processing materials with low relaxation times, such as HDPE, the effect of the drawdown can be determined from a mass balance (equation (5.9)), assuming

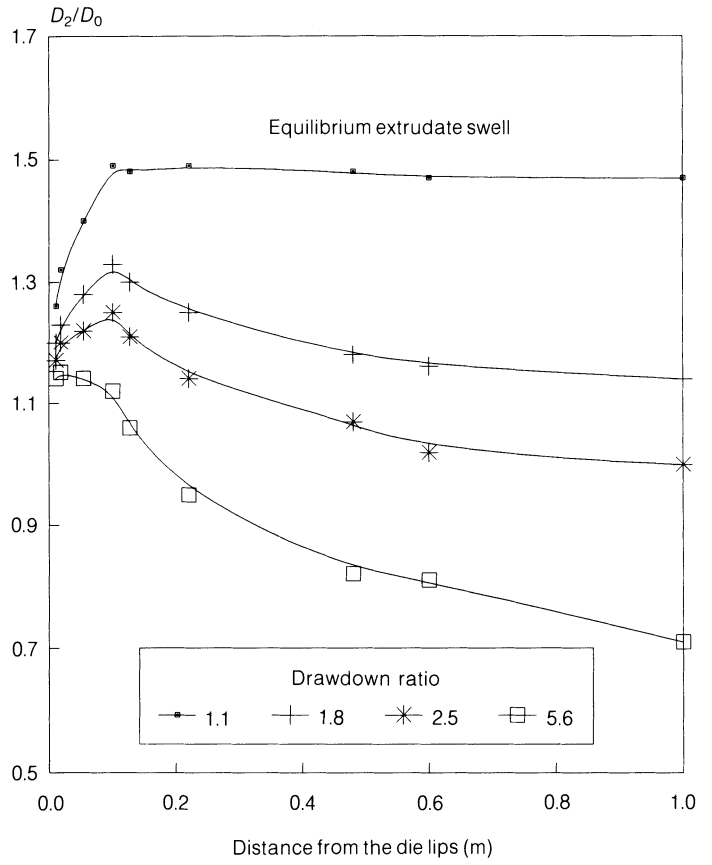


Figure 5.32 Changes in the cross-section of a PVC extrudate along an extrusion line, at different drawdown ratios (Huneault, Lafleur and Carreau, 1990).

that the die swell has reached the equilibrium. If the drawdown is isotropic:

$$\frac{D_2}{D_0} = DS_{\text{equi}}\left(\frac{1}{DR}\right)^{1/2} \tag{5.47}$$

where D_2 refers to the circular extrudate after stretching, D_0 is the die diameter and DS_{equi} is computed from equation (5.6). When DR was less than or equal to 2, the predictions were generally quite close (within 3% error) to the experimental values. As the typical draw ratios for HDPE extrusion are usually below 1.3, equation (5.47) can be adopted for practical purposes. Unfortunately, this procedure would produce important errors if applied to materials with long relaxation times (such as PVC), as extrudate swell may never attain its equilibrium. For an annular channel, three distinct die-swell ratios can be defined, namely DS_{ed}, DS_{id} and DS_{e}, referring to the external diameter, internal diameter and thickness, respectively. However, DS_{ed} and DS_{e} are identical if the extrudate orientation is uniaxial and uniform (Garcia-Rejon, 1982). This is generally valid for pipe dies with die land ratios in the range 10–25.

The computations will now proceed towards the first adaptor zone, which corresponds to an annular convergent channel including a certain degree of compression (promoting the welding of the individual melt streams exiting the spider legs). Since the flow accelerates, melt fracture may eventually occur. The criterion for its onset is given by a relation similar to equation (5.45), where $\dot{\varepsilon}_{\text{c, ref}}$ is calculated from equation (5.4). In principle, equation (5.46) will also hold. This limit should obviously be compared with the maximum local value of the extensional rate, $\dot{\varepsilon}_{\max}$. The location and value of the latter depend upon the geometry of the section (the annular convergent section can generate compression by varying the gap and the external radius differently). Carneiro (1994) has quantified $\dot{\varepsilon}_{\max}$ for various geometries (circular, rectangular and annular convergent channels) assuming isothermal flow, incompressible fluid and average flow speed in any cross-section of the channel. For example, for a rectangular convergent channel (this geometry is relevant for studying the flow of the individual melt fronts between the spider legs):

$$\dot{\varepsilon}_{\max} = \frac{nH\dot{\gamma}_{\max}\tan\alpha}{W(2n+1)} \tag{5.48}$$

where H is the gap, α the convergence angle, W the width at the end of the convergence and n denotes the power-law index. If $\dot{\varepsilon}_{\text{c, ref}} > \dot{\varepsilon}_{\max}$, the length of the block must be incremented, in order to decrease the convergence. However, one should notice that the corresponding pressure drop will increase accordingly.

The above procedure is progressively applied to the various die zones in the extruder direction, considering the eventual occurrence of flow anomalies whenever relevant, and computing the total pressure drop (which is compared with the total limit pressure drop initially defined by the operator). Figure 5.33

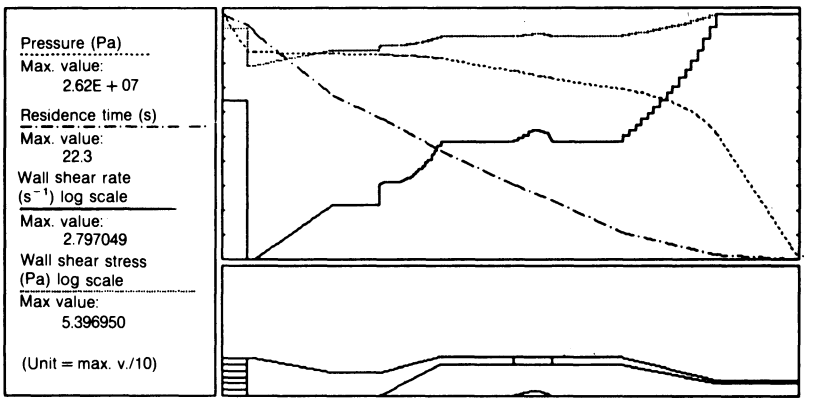


Figure 5.33 Results of the analytical flow computation inside the optimized die (Carneiro, 1994).

shows the results obtained after completing the analytical algorithm. The geometry of the die, together with the axial pressure, residence time, wall shear rate and wall shear stress, are represented graphically. When the analytical predictions of the pipe dimensions are compared with the values obtained experimentally for the same processing conditions, small errors (2–3% for the external diameter and about 5–6% for the internal diameter) are observed. These differences include the combined effects of all the post-extrusion phenomena considered. However, since previous studies showed that the errors associated with the extrudate-swell predictions reached 10%, the effects of shrinkage, drawdown and calibration seem to be negative and to compensate for that overdimensioning (Carneiro, 1994).

The numerical simulation of the flow through the optimized die (Fig. 5.16) provides more accurate information on the pressure drop, mainly due to the more adequate simulation of the flow between the spider legs. The practical relevance of the viscous dissipation can also be evaluated. This is important, because the development of a significant transversal temperature gradient in the die land will alter the predicted die swell, and hence the final dimensions of the extrudate.

5.6 OPERATIONAL STRATEGIES FOR PROBLEM-SOLVING

The purpose of this section is not to provide a general review of how to operate extrusion lines, as this is certainly beyond the scope of this book. Instead, it aims at providing the processor with some general guidance on possible practical action to accommodate changes in size, shape, or surface texture of the extrudate, in polymer properties, in output rate, etc., detected upon operating a particular extrusion line.

As emphasized throughout this chapter, there is a unique correlation between the compound characteristics, the set temperatures, the flow rate (or pressure), the mechanical/physical performance and shape of the extrudate, and the extrusion head geometry. Nevertheless, deliberate adjustments in the die geometry or in the processing conditions may increase the manufacturing flexibility of the line, albeit with some eventual decrease in the extrudate performance. Consequently, the engineer must be capable of setting efficiently an extrusion line producing a particular profile, and of overcoming performance difficulties, caused by either improper die design or equipment wear due to extensive use. The engineer is also expected to be able to extend the usefulness of the die in terms of materials processed, shapes produced and outputs reached. In each situation several possible actions, initially in operating conditions, and subsequently in the die dimensions or geometry, may be required. Each of these actions will produce various effects and interactions, which may be beneficial or detrimental to the expected goal, and of greater or lesser extent than the primary response.

Solving extrusion-related problems involves manipulating working parameters both upstream and downstream of the shaping tool. Anomalies such as erratic melt quality and surging are usually caused by the use of an unsuitable or worn screw, by some electrical fault, or by feeding difficulties. Film wrinkles and optical defects are very common and can be produced by non-uniform cooling, or by winder problems. However, given the nature of this chapter, only questions related to the performance and operation of the die will be considered here. Therefore, it seems appropriate to review some of the concepts previously introduced or discussed, as they are particularly relevant for practical operation purposes.

As stated in very simple mathematical terms in equation (5.1), there is a relationship between output, pressure drop, flow channel geometry and melt rheology. In other words, changing the extruder screw speed, the barrel/head set temperatures and the head geometry (via choker bars, centring bolts, or die lands) will affect the flow conditions. This is either pernicious or helpful, depending on whether it creates instabilities in the process, or whether it is used with advantage for corrective actions, respectively.

For practical purposes, one can assume uniform pressure at the extrusion head inlet cross-section, and atmospheric (or zero) pressure at the die exit. In the case of mandrel-type and profile dies, the corresponding flow created by this pressure drop is predominantly one-dimensional. In the remaining geometries flow is mainly two-dimensional. If the global die flow channel is hypothetically divided into various parallel geometries with simpler flow, and if equation (5.1) is again considered, the local velocity field depends on the polymer rheology and on the elementary geometry (local cross-section, and channel length). Changes in the temperature field (either unexpected or deliberate) will certainly change the various local resistances. The same effect can be achieved by modifying the elementary geometry. Choker bars and

centring screws allow local adjustment of the channel cross-section. Length differences across the die land width produce similar results. Thus, the first two parameters can be readily used in operating situations, whereas the latter must be applied during the die design stage.

Despite some inherent instabilities, single- and twin-screw plasticating extrusion can be assumed as steady processes, with constant die inlet and outlet conditions. This means that in mandrel-type and profile dies most of the transversal flow will occur at the early stages of the process. In fact, most of these dies are designed and operated considering only longitudinal flow. However, non-isothermal effects can develop differently in each subsection of the die, due to distinct flow conditions (temperatures, velocity profile). In this case, the local axial pressure drop profiles are affected, creating a transversal pressure drop component (whose importance varies along the die length) and, consequently, a transversal component of the flow. This will change the relative exit velocities and residence times, and may cause flow degradation (especially when the flow channel in the transverse direction exhibits step or abrupt tapers, which are usually avoided in the axial direction). This problem is particularly relevant when producing profiles with non-uniform wall thickness across the width.

Regardless of the contour and of the relative thicknesses of the composing extrudate subsections, the average exit flow velocity across the width of the die lips should be kept uniform, in order to prevent curling and twisting of the extrudate or, instead, non-uniform drawdown (including residual stresses and subsequent distortion during service). In fact this is not strictly correct, as constant exit average velocities may be obtained with varying local shear rates, or residence times, which will produce locally different extrudate swells and, consequently, will result in slightly different average extrudate velocities. Therefore, the required uniform average velocity across the width boundary condition must be implemented away from the die exit, when the extrudate swell has approached its maximum value and the effects of drawdown become critical. However, as it is very difficult to compensate for the changes in extrudate shape and for the corresponding changes in the longitudinal velocity, the initial condition can be taken as a good first approximation.

The above two concepts demonstrate the potential usefulness of axial flow dividers. These walls obviously prevent the development of transversal flow, thus facilitating the balance of the average exit velocities at the die. However, there is also an increase in the resistance to flow due to local changes in the velocity distribution, particularly at the interface between any two adjacent flow cross-sections. Other flow dividers, such as spiders and perforated rings, must be carefully designed in terms of their axial profile, and the temperature set accordingly, to minimize the possibility of flow stagnation and polymer degradation. As discussed previously, welding of the various individual flow fronts should be promoted to avoid rippling and wavy lines on the extrudate surface.

Table 5.2 Effect of operational and geometrical variables on flow conditions in the die

Parameter	*Effect*
Non-uniform exit velocity across the width	• Extrudate curling, twisting, rippling • Non-uniform drawdown, resulting in residual stresses in the extrudate
Non-uniform exit flow thickness across the width	• Non-uniform tranversal extrudate thickness before and after swelling • Non-uniform exit velocity across the width (see above)
Flow thickness varying longitudinally (tapers, steps, choker bars)	• Significant extensional effects, with possible melt fracture, and contribution to extrudate swell • Flow acceleration along the taper, with velocity instabilities at the entrance and exit of the taper • Possibility of stagnation points and corresponding material degradation • Relatively large pressure drop
Flow thickness of length varying transversely	• Pressure drop or flow rate varying transversely (thus extrudate curling, twisting and rippling) • Non-uniform residence time and relaxation (affecting degradation and extrudate swell) • Differences in shear heating, promoting transverse flow
Set (and melt) temperature varying transversely	• Transverse components of flow • Non-uniform extrudate swell and surface finish • Non-uniform shear heating effects • Possibility of material degradation • Pressure drop or flow rate varying transversely (thus, extrudate curling, twisting and rippling)
Transverse flow	• Non-axial exit velocities • Changes in the relative exit velocities and swelling • Distortion of the extrudate section • Possibility of stagnation points and corresponding material degradation

Each polymer, blend, or compound, features a typical practical operating window, and a specific energy consumption, which are a function of the type and relative size of the processing equipment, and of the profile being manufactured. The processing temperatures suggested by the polymer manufacturers are usually a compromise between adequate rheology, expected output, power consumption and thermal stability. Rheological defects (namely sharkskin and melt fracture) are unavoidable at certain shear stresses (or at the corresponding apparent shear rates), and can only be avoided through adjustments in the screw speed, die gap, or melt temperature. However, the possibilities are limited, given the secondary effects of these variables. The total pressure drop in the die is a relative measure of the processing intensity. Low values may signify low melt homogeneity or worryingly low outputs, whereas high pressure drops are related to a significant contribution of viscous dissipation. In this case, not only does controlling the melt temperature become problematic, but also premature polymer degradation may be obtained.

The study of the operational efficiency of a particular extrusion line should be accomplished by assessing sequentially: the flow conditions at the die inlet (pressure, temperature, melt quality and their stability); the flow conditions at the die lips (exit velocity across the width, melt temperature, extrudate surface quality and extrudate dimensions); and the extrudate characteristics at the end of the line.

Table 5.2 summarizes the effects of some operational and geometrical parameters on the flow conditions inside the die, and on subsequent extrudate features, as discussed above. This provides general guidance as to the consequences of both fortuitous and deliberate adjustments on the die operating conditions. Despite the general nature of the table, it has particular relevance for the extrusion of pipes and profiles. In practice, each type of extrusion process faces typical problems that processors try to solve, sometimes on a daily basis. For example, gauge variations are probably the biggest production problem in blown and cast film production. Although these difficulties are related to the effects of the parameters identified in Table 5.2, a more practical troubleshooting guide to some of the most common extrusion processes (blown film extrusion, cast film, pipes and profiles extrusion) is presented in Table 5.3. The most common problems (which might be related to die performance), their probable causes and possible actions to be taken are indicated for each process.

Table 5.3 Troubleshooting blown film, cast film, pipe and profile extrusion die related problems

Problem	*Causes*	*Solution*
Blown film extrusion		
Thickness variations across the extrudate circumference	Erratic melt quality	• Check screw design and/or wear • Check set temperatures • Check heaters and thermocouples
	Surging or feeding inconsistency	• Check screw wear • Check material in hopper • Check regrind percentage
	Dirty die	• Clean die (check for obstructions at the die lips)
	Inadequate die-bolts adjustment	• Readjust
	Misaligned die/air ring	• Centre die to nip rolls • Centre air ring to die
	Leaky die	• Check seals
	Temperature fluctuations at the die lips	• Check heaters and thermocouples • Check set temperatures
	Poor air flow distribution in the air ring	• Check and clean air ring
Lines, streaks and foreign specks	Dirty die	• Clean die (check for obstructions at the die lips)
	Scratched die lips	• Repair, or replace die lips
	Inadequate die-bolts adjustment	• Readjust
	Contaminated melt flow	• Check compound • Change filters
	Melt flow too hot	• Reduce set temperatures
	Welding lines	• Increase melt temperatures • Use spiral mandrel die
Sharkskin, melt fracture	Melt temperature too low	• Increase the die lips' temperature
	Friction at the die lips	• Repair die lips' coating • Modify formulation
	Die gap too narrow	• Increase
Bubble instability/ irregular frost line	Erratic melt quality	• Check screw design and/or wear • Check set temperatures • Check heaters and thermocouples
	Dirty die	• Clean die (check for obstruction at the die lips)
	Excessive air ring velocity	• Reduce
	Insufficient blow-up ratio	• Increase
	Excessive melt temperature	• Reduce set temperatures

(*Continued*)

Table 5.3 (*Continued*)

Problem	*Causes*	*Solution*
Wrinkles	Misaligned die/nip rolls	• Align die to nip rolls
	Non-uniform cooling and winding	• Check winder
Cast film extrusion		
Thickness variations across the width	Erratic melt quality	• Check screw design and/or wear • Check set temperatures • Check heaters and thermocouples
	Surging or feed inconsistency	• Check screw wear • Check material in hopper • Check regrind percentage
	Inadequate die-bolts adjustment	• Readjust
	Dirty die	• Clean die lips
Insufficient extrudate width	Insufficient die slot	• Adjust die deckles
	Inadequate polymer rheology	• Check melt temperatures at the die
Lines, streaks and foreign specks	Dirty die	• Clean die
	Scratched die lips	• Repair or replace die lips
	Contaminated melt flow	• Check compound • Change filters
	Melt flow too hot	• Reduce set temperatures
Sharkskin, melt fracture	Melt temperature too low	• Increase the die lips' temperature
	Die gap too narrow	• Increase
Wrinkles	Flow fluctuations at die exit	• Adjust set temperatures • Adjust die gap
	Excessive winding tension	• Adjust line speeds (increase tension gradually to winder)
	Non-uniform cooling	• Adjust casting unit operation
	Misaligned casting unit	• Verify rolls alignment
Web tear-off	Flow fluctuations at die exit	• Check material in hopper • Adjust set temperature • Adjust die gap
	Dirty die	• Clean die lips
	Melt temperature too low	• Increase set temperatures

(*Continued*)

Table 5.3 (*Continued*)

Problem	*Causes*	*Solution*
Pipe and profile extrusion		
Wavy inside surface	Melt temperature too low	• Increase set temperatures
	Low lubricant level	• Correct formulation
	Pulsating drawdown	• Check caterpillar
Excessive extrudate thickness	Inadequate die gap adjustment	• Adjust or replace die
	Inadequate operating conditions	• Adjust set temperatures, and/or drawdown ratio
	Profile slippage at the caterpiller	• Check pulling force • Dry profile before reaching the caterpillar
Line, streaks and foreign specks	Dirty die	• Clean die (check mandrel)
	Scratched die lips	• Repair die
	Drag plug (pressure calibration) too close to die	• Correct drag-plug location
	Excessive melt temperature	• Reduce set temperatures
	Contaminated melt flow	• Check compound • Change filters
Sharkskin, melt fracture	Melt temperature too low	• Increase the die lips' temperature
	Friction at the die lips	• Repair die lips' coating • Modify formulation
	Die gap too narrow	• Increase
Extrudate velocity with a transversal component	Unbalanced exit flow	• Modify die land geometry
	Temperature fluctuations in die	• Check heaters and thermocouples • Check set temperatures
	Dirty die	• Clean die

Principles of melt flow in single-screw extruders

6

In this chapter, a simplified analysis leads to equations relating output, pressure and screw speed for the melt pumping section for several typical screw types. The flow patterns within the screw and pressure profiles along it are discussed, together with an examination of leakage flow. Graphical presentations are used to analyse the output/pressure characteristics of the screw/die combination, for simple and some more complex situations, including venting. Corrections to the simplified equations are discussed, leading to those due to pseudoplastic and non-isothermal conditions. The mechanisms of solids conveying and melting are covered in Chapter 7.

6.1 FUNCTIONS OF THE EXTRUDER

As discussed in Chapter 3, the mass flow through the die is related to the pressure drop, the die dimensions and the viscosity, the last being mainly a function of temperature. Since the outlet conditions from the die are only slightly affected by the haul-off, the function of the extruder is to deliver to the die the required mass flow at the corresponding pressure and temperature, with minimum fluctuations of these three quantities in space and time (section 11.1) and correct composition, e.g. shear history (section 11.3) and dispersion of additives (section 4.4). The output of a given extruder screw is mainly dependent on rotational speed, so the relation between mass flow output, screw speed and back pressure will be considered in this chapter, together with the influences of screw dimensions and viscosity, and the interactions with the die pressure.

A principal function of the extruder for plastics and rubbers – which it shares with those for clays, bitumen, paste explosives, pastas and even the domestic

meat mincer – is thus to pump material in a fluid state against the back pressure created by the resistance of the die. This is the function which is susceptible to hydrodynamic analysis and is the main subject of this chapter. Because this flow is complex a certain amount of both distributive and dispersive mixing occurs (section 4.4), and energy is transformed into heat (section 8.1) by shearing, leading to temperature changes and distributions (section 11.1). Coincidentally, the single-screw extruder, which is an Archimedean screw or 'drag' pump, will also convey solid particles and generate pressure in the solid; this causes shearing and, together with heat conducted from the barrel, generates heat to melt the solid polymer (Chapter 7). The extruder may also be used for removing air, volatiles, water, etc., at the feed section and gases or vapours from the melt (section 6.5). The mixing action may be used for incorporating (compounding) solids or liquids, e.g. pigments or foaming agents, and solids, e.g. dirt may be removed from the melt by mechanical filtering. The mixing action of the screw enables it to be used as a 'scraped' heat exchanger, though cooling is limited by shear heating, and this is also utilized for chemical reaction, e.g. continuous polymerization when the extruder becomes effectively a stirred reaction vessel. The single-screw extruder thus has many possible functions including melting, conveying, mixing, compounding, pumping, separating and heat exchange, and several of these may have to be optimized in a specific case. However, some are difficult to analyse in theory or control in practice, so mass flow in the melt pumping region, often called the 'metering' section, is usually made the controlled (minimum) factor such that uncertainties in the others are of less significance.

The single-screw extruder for plastics usually consists of a single-start screw of constant pitch and rectangular thread section running in a barrel or cylinder of constant diameter. The following analysis can be adapted to multistart screws by substituting 'lead' for 'pitch' and multiplying the output by 'number of starts'. For rubbers, screws of varying diameter are sometimes used, e.g. in 'slabbers', and frequently of varying depth, with or without constant pitch. In the first case it may be necessary to use mean (McKelvey, 1962, p. 234) rather than maximum channel diameter in calculating velocities, and in the second case the 'wide channel' assumption may be invalid, so that shape factors (McKelvey, 1962, p. 236) must be included.

Note 1: This analysis concerns the screw only, giving $Q = f(N, P)$, i.e. assuming that Q or P can be varied independently of the die, e.g. by altering the die dimensions. But in section 3.2 it was shown that for the die $Q = f'(P)$; thus in the normal case of an extruder feeding directly to a die, *both* relations must be satisfied and at a given screw speed and temperature only one pair of real values of Q and P will hold (section 6.5).

Note 2: The equation $Q = f(N, P)$ seems to imply that mass flow (output) can always be raised by increasing screw speed. However, in practice,

energy considerations (Chapter 8), product quality (section 11.1) or stability (section 11.2) more often limit satisfactory operation. Many texts ignore these factors in analysing performance.

In this book the terms **front** and **back** refer to the die end and feed end, respectively; applied to the flight they are synonomous with **leading** or **pushing** and **trailing** edges. The terms **top** and **bottom** of the channel refer to the outer (barrel surface) and inner (thread root) diameters, respectively. Flight **clearance** refers to the radial gap necessary for free running, which is assumed constant round the circumference, which is consistent with observation in moderate-size machines containing polymer – but see Klein (1973) and Worth and Lai-Fook (1978) for very large machines. Wear, especially with glass-filled or other abrasive compounds, may lead to excessive clearance (section 6.3) or axial variation in clearance.

6.2 DERIVATION OF FLOW EQUATION

6.2.1 Introduction

The geometry of a simple screw is shown in Fig. 6.1 with the nomenclature used in this chapter. Note that the pitch p and flight width t are measured axially, whereas the channel width b is measured normal to the helix. (Weeks and Allen (1962) use t for the helical flight width, i.e. as measured in the workshop, leading to minor differences in equations (6.2) and (6.11).) The helix angle ϕ is the true angle, although for convenience the flight is often shown as a straight line in side view. Unless stated otherwise, all diagrams show a left-hand helix with the side nearest to the reader moving down the page, causing a flow from left to right. Evidently a right-hand screw must rotate in the opposite direction to cause the same flow, but the equations are equally valid. The rotational speed is given in revolutions per second (rps) and output in $m^3\,s^{-1}$ or $kg\,s^{-1}$ for dimensional consistency; more theoretical texts may use speed in radians per second where the numerical value will be greater by a factor of 2π. The components of output Q (equation (6.15)) are derived in *volume* terms and should be multiplied by the density at the mean temperature and pressure in the melt section of the screw to give the theoretical mass output (assumption 8 below). The rectangular coordinate system in the channel is given in Fig. 6.2; the length coordinates are x, y and z in the directions of (normal) channel width, (radial) channel depth and (helical) channel length, respectively. The limiting values are b, h and Z, respectively, where by development it can be seen that:

$$Z = L/\sin\phi \tag{6.1}$$

$$b = (p - t)\cos\phi \tag{6.2}$$

$$p = \pi D \tan\phi \tag{6.3}$$

for a screw having n_s turns and L is the corresponding axial length. The corresponding velocity components are u, v and w, with limiting values U at the barrel surface ($y = h$), V at the channel edge ($x = b$) and W at the barrel surface ($y = h$), respectively.

Note: The popular belief that the geometric sections of the screw correspond to the functions of solids conveying, melting and melt pumping, respectively, is not necessarily true (see section 6.4 and Chapter 7), and mention in this book of 'melting region' refers to those parts where this mechanism dominates rather than to a tapered portion as such.

6.2.2 Assumptions

The assumptions in the simplified flow analysis are:

1. Steady-state operation. Section 11.2 considers instability.

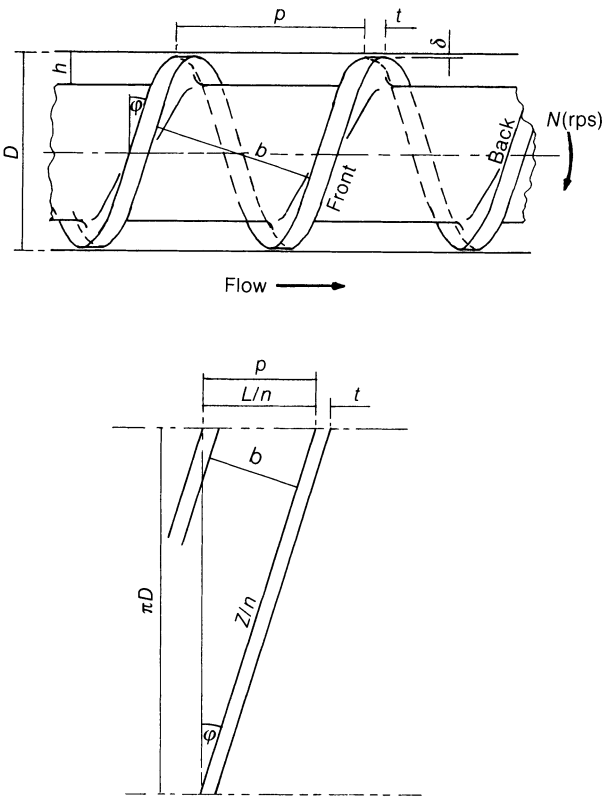


Figure 6.1 Screw dimensions.

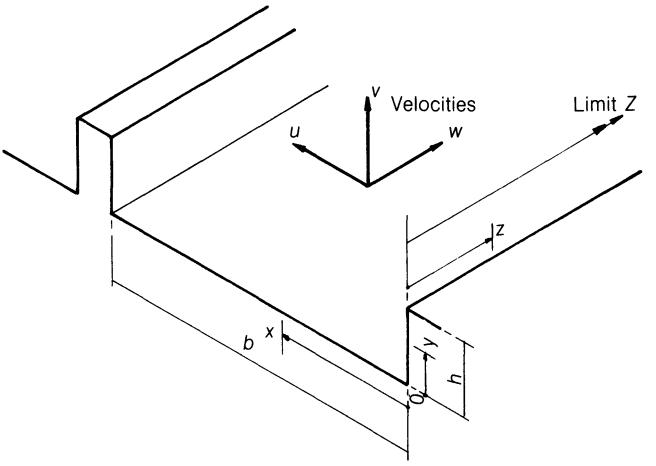


Figure 6.2 Co-ordinate system for screw channel.

2. The polymer is a homogeneous fluid, i.e. 'melt pumping' section only.
3. The polymer adheres to the barrel and screw root surfaces, but not to the flight front and back (channel sides).
4. Curvature is neglected, i.e. the helical channel is approximated by a straight channel of the same dimensions.
5. The channel depth is small compared with the internal barrel diameter.
6. Zero leakage flow. This is discussed in section 6.3.
7. The melt is Newtonian, i.e. viscosity is a function of temperature, but not of shear rate or time.
8. The flow is isothermal.
9. Gravity is neglected.
10. Initially the screw is treated as of constant depth. In differential form, the flow equation (6.15) may be applied to an elemental length of a screw of varying depth.

Fenner (1970) has published an excellent study of the differences produced by several of these assumptions and has shown that, while they are important for exact design, in most usual cases they can be approximated by correction factors, and thus the effects on *trends* caused by changes of operating conditions are negligible. It is those trends in operation which are the chief concern of the present book, so that useful conclusions may still be drawn from a very simplified mathematical treatment. However, the validity of these assumptions will be reviewed wherever necessary (e.g. sections 6.6, 8.3 and 9.2).

The author is greatly indebted to Weeks and Allen (1962) for the following analysis and that for power consumption in Chapter 8; however, he takes full responsibility for the deductions therefrom.

6.2.3 Drag flow

Assumptions 3, 4, 5 and 6 mean that flow in a straight channel may be further approximated as that between two parallel flat plates moving at an angle ϕ to each other (Fig. 6.3); for convenience the lower plate (screw) will be taken as stationary, so that velocities will be relative to the screw, not the barrel – this is obviously immaterial as far as axial components giving gross flow are concerned. Because viscosity is constant (assumptions 7 and 8) superposition of flows is valid and that due to relative motion of the plates is first considered in the absence of a pressure gradient. The velocity of the barrel relative to the screw is its circumference πD times the speed N; barrel velocity equals πDN and is at an angle ϕ to the screw channel. Since the polymer is assumed to adhere to the barrel and screw (assumption 3), its velocity at each limit will be the same as that of the adjacent solid surface, i.e. πDN at the barrel and 0 at the screw. Resolving the barrel velocity along and across the screw channel:

$$W = \pi DN \cos \phi \tag{6.4}$$

$$U = \pi DN \sin \phi \tag{6.5}$$

W and U being defined as in Fig. 6.2.

Evidently only the along-channel component W can cause a net flow from the extruder, although U is important in creating a transverse circulation (equation (6.26)). This is a case of isothermal simple shear, and from equation

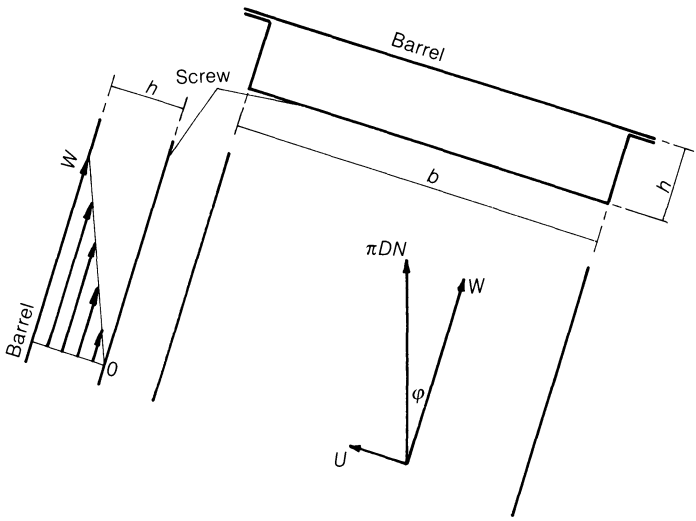


Figure 6.3 Velocities in drag flow.

(3.11) the shear rate $\dot{\gamma}$ will be uniform i.e.

$$\dot{\gamma} = \frac{w}{y} = \frac{W}{h} \tag{6.6}$$

giving the velocity distribution shown in Fig. 6.3. The along-channel flow dQ_D in a layer b wide and dy thick is:

$$dQ_D = wb \cdot dy \tag{6.7}$$

and the total flow:

$$Q_D = \int_0^h wb\,dy = \int_0^h b\frac{W}{h}y\,dy = \left[\frac{Wby^2}{2h}\right]_0^h \tag{6.8}$$

Since b is constant, $\int_0^h w\,dy$ is the area $Wh/2$ under the plot of velocity against depth and:

$$Q_D = \frac{W}{2}bh \tag{6.9}$$

where Q_D is the volumetric flow due to relative motion of barrel and screw, called **drag flow**, and $W/2$ is the mean downchannel velocity. Substituting for W gives:

$$Q_D = \frac{\pi}{2}DNbh\cos\phi \tag{6.10}$$

and substituting for b from equation (6.2):

$$Q_D = \frac{\pi}{2}DNh(p - t)\cos^2\phi^* \tag{6.11}$$

6.2.4 Pressure flow

To separate the effect of pressure, the screw is considered stationary, so that no drag flow takes place. Suppose a pressure is generated at the end of the screw by a separate pump (Fig. 6.4). At the same temperature (and viscosity) the flow through the die will remain the same as though the pressure were generated by the extruder. However, this pressure will also cause a flow *backwards*, i.e.

*As mentioned in section 6.2.1, Weeks and Allen (1962) define t as helical flight width, such that equation (6.2) becomes

$$b = p\cos\phi - t$$

Several authors, including Fisher (1976), neglect the flight width t so that $b = \pi D\sin\phi$ leads to a modification of equation (6.11).

$$Q_D = \frac{\pi^2}{2}D^2Nh\,\sin\phi\,\cos\phi$$

The present book expresses equations for flow and power primarily in terms of channel width b as being more appropriate to performance considerations; any of the above definitions may therefore be used.

towards the feed section, in the screw, which behaves as a long die of rectangular cross-section ($b \gg h$, assumption 3). In Chapter 3 the pressure gradient in an 'infinite' slit die T wide by H deep was given by:

$$\frac{dP}{dL} = \frac{12\eta Q}{TH^3} \tag{3.34}$$

Substituting the screw dimensions and putting $Q = Q_P$ for pressure flow:

$$\frac{dP}{dz} = \frac{12\eta Q_P}{bh^3} \tag{6.12}$$

or rearranging:

$$Q_P = \frac{bh^3}{12\eta} \cdot \frac{dP}{dz} \tag{6.13}$$

Note that for a positive pressure gradient (pressure rising from feed section to die) the pressure flow is in the reverse direction, i.e. subtracts from the drag flow. The velocity distribution is parabolic (Fig. 3.8) as shown in Fig. 6.5.

As mentioned on p.132 the assumption of Newtonian viscosity permits superposition of flows, i.e. the total volumetric flow Q_{Tot} is given by:

$$Q_{Tot} = Q_D - Q_P - Q_L \tag{6.14}$$

but by assumption 6, leakage flow Q_L is negligible (section 6.3) so substituting

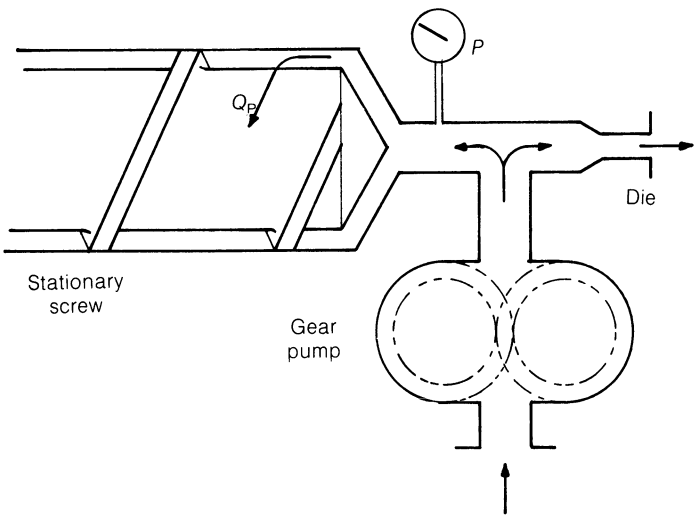


Figure 6.4 Analogy for pressure (back) flow.

equation (6.9) and (6.13):

$$Q_{\text{Tot}} = Q_{\text{D}} - Q_{\text{P}} = \frac{Wbh}{2} - \frac{bh^3}{12\eta} \cdot \frac{\mathrm{d}P}{\mathrm{d}z} \tag{6.15}$$

The same result may be obtained by the more rigorous mathematical method given in appendix B.1 based on the Navier–Stokes equation of one-dimensional flow. This may also be written in dimensionless form:

$$\frac{Q_{\text{Tot}}}{Wbh} = \frac{1}{2} - \frac{h^2}{12\eta W} \cdot \frac{\mathrm{d}P}{\mathrm{d}z} \tag{6.16}$$

This dimensionless output, abbreviated to Q/Wbh, is of great value both theoretically and practically in characterizing the operating condition of single-screw extruders and will be referred to in the following chapters.

Some authors have used the ratio (minus) pressure flow/drag flow, which has the following relation to Q/Wbh:

$$\frac{Q_{\text{P}}}{Q_{\text{D}}} = \frac{-(Q_{\text{Tot}} - Q_{\text{D}})}{Q_{\text{D}}} = 1 - \frac{2Q}{Wbh} \tag{6.17}$$

and

$$\frac{Q}{Wbh} = \frac{1}{2}\left(1 - \frac{Q_{\text{P}}}{Q_{\text{D}}}\right) \tag{6.18}$$

i.e.

$$0 < Q/Wbh < \tfrac{1}{2} \quad \text{as} \quad 1 > Q_{\text{P}}/Q_{\text{D}} > 0$$

and

$$\tfrac{1}{2} < Q/Wbh < 1 \quad \text{as} \quad 0 > Q_{\text{P}}/Q_{\text{D}} > -1$$

Referring to equation (6.15), by continuity Q_{Tot} must be approximately constant along the extruder, and therefore for a screw of constant channel width b and depth h:

$$\frac{\mathrm{d}P}{\mathrm{d}z} = \text{constant} = \frac{P}{Z} \tag{6.19}$$

i.e. the pressure rises uniformly along a constant depth screw and equation (6.15) may be rewritten:

$$Q_{\text{Tot}} = \frac{Wbh}{2} - \frac{bh^3}{12\eta} \cdot \frac{P}{Z} \tag{6.20}$$

where Z is the helical length of the melt pumping section and P is the pressure rise over that length. Note that this is not valid for a screw of varying depth, whereas equations (6.15) and (6.16) are valid for an incremental length of such a screw.

The velocity at any point in the channel is given in appendix B.1 as:

$$w = \frac{Wy}{h} + \frac{y^2 - yh}{2\eta} \cdot \frac{\mathrm{d}P}{\mathrm{d}z} \tag{B.8}$$

and is the algebraic sum of the velocities due to drag and pressure flows. The net flow will be proportional to the algebraic sum of the areas under the velocity profiles. When $dP/dz = 0$, there is no change of pressure along the screw and no pressure flow (this is quite possible in a parallel 'metering' section if pressure is generated in the preceding tapered portion). Then the velocity profile will be as in Figs 6.3 and 6.6(d), all the flow will be positive and $Q/Wbh = 1/2$. If a small back pressure is now introduced, dP/dz will be small and positive, causing a small (virtual) back flow represented by $-bh^3\, dP/12\eta\, dz$, reducing the total flow, and hence Q/Wbh is now less than 1/2; this is shown in Fig. 6.6(c). Note that the resultant velocity profile is no longer linear and its slope at the barrel $dw/dy_{(y=h)} = \dot{\gamma}_{wall}$, the shear rate at the barrel wall is greater than in the corresponding drag flow (see also p.168). If P and dP/dz are further increased, output and Q/Wbh are further reduced and over part of the channel depth the resultant flow will be reversed, as in Fig. 6.6(b), partially offsetting the positive flow nearer the barrel wall. At some value of pressure, the positive and negative flows will be equal (Fig. 6.6(a)) giving zero net flow and $Q/Wbh = 0$. This corresponds to a completely closed die and the pressure is the theoretical maximum achievable with the screw; in practice, shear heating due to 'churning' will modify this and the mechanism of melting will also be disturbed. If the pressure falls through this section of the screw, e.g. due to high pressure generation in an earlier portion of the screw, dP/dz will be negative and the pressure flow will be towards the die, giving a total flow greater than that due to drag flow alone, and $Q/Wbh > 1/2$ as in Fig. 6.6(e). Note that the shear rate at the barrel wall is now reduced.

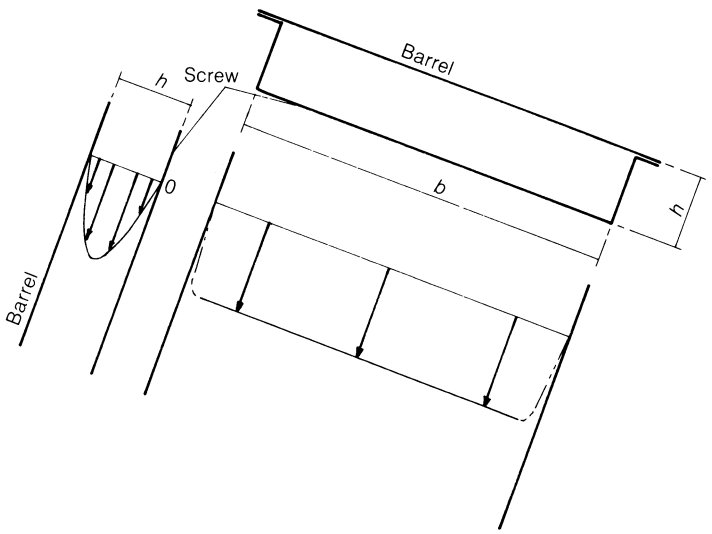


Figure 6.5 Velocities in pressure flow.

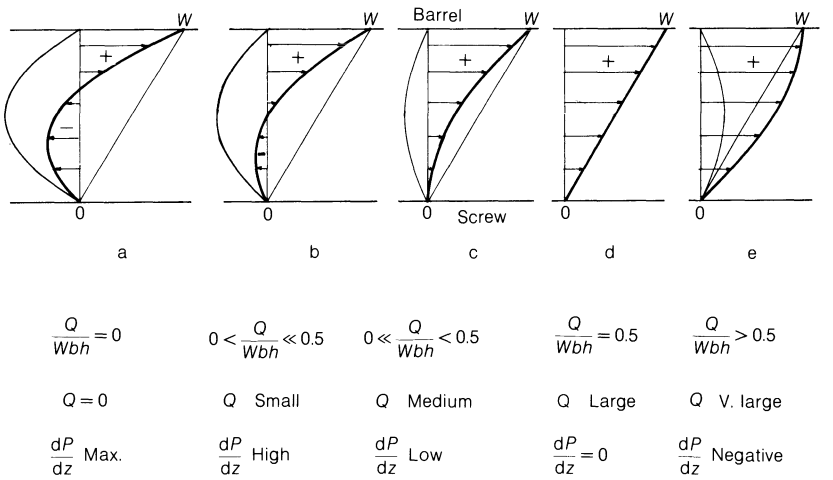


Figure 6.6 Velocity profiles for several outputs and pressure gradients.

The expression Q/Wbh is the ratio of the actual flow to that theoretically possible if the polymer moved as a plug with the barrel at velocity W and slipped on the screw – like a solid nut prevented from rotating with the screw. It is therefore a kind of 'volumetric efficiency' and compared to the value 1/2 for drag flow gives an impression how much less (or greater) the actual flow is than at drag flow. More importantly, it indicates whether the pressure gradient in the screw is small (Q/Wbh slightly less than 1/2) or large (Q/Wbh tending to zero) or even negative ($Q/Wbh > 1/2$).

In practice it is difficult to envisage what is occurring within the screw, and even if a pressure gauge is fitted before the die, it does not indicate whether the pressure is seriously affecting the performance of the screw. The expression Q/Wbh can be determined in a particular operating condition if the screw dimensions are known. It is only necessary to measure accurately the screw speed (giving W) and the output, e.g. by weighing and dividing by the density at the melt temperature to give the volumetric output Q. The magnitude of Q/Wbh is therefore valuable as a first step in shop-floor troubleshooting – see example on p. 150.

6.2.5 Transverse flow

So far, only the longitudinal or downchannel component of velocity has been considered. The flow transverse to the channel has been analysed by Mohr, Saxton and Jepson (1957), starting from the Navier–Stokes equation (see appendix B.1):

$$\eta \frac{\partial^2 u}{\partial y^2} + \eta \frac{\partial^2 u}{\partial z^2} - \frac{\partial P}{\partial x} = 0 \qquad \text{(B.10)}$$

and ignoring stagnation at the channel sides. In a channel of constant dimensions, the cross-channel component:

$$U = \pi DN \sin \phi \tag{6.5}$$

is independent of z, and since the along-channel velocity distribution (Fig. 6.6) is also independent of z, it is reasonable to assume that $\partial u/\partial z = 0$ throughout and hence $\partial^2 u/\partial z^2 = 0$. Eliminating this term and rearranging:

$$\eta \frac{\partial^2 u}{\partial y^2} = \frac{\partial P}{\partial x} \tag{6.21}$$

Since viscosity η is Newtonian and isothermal, integration gives:

$$u = \frac{1}{2\eta} \cdot \frac{\partial P}{\partial x} (y^2) + Cy + D \tag{6.22}$$

But $u = 0$ at $y = 0$, and $u = U$ at $y = h$, therefore $D = 0$ and

$$C = \frac{U}{h} - \frac{1}{2\eta} \cdot \frac{\partial P}{\partial x} \cdot h$$

leading to:

$$u = \frac{Uy}{h} + \frac{1}{2\eta} \cdot \frac{\partial P}{\partial x} (y^2 - yh) \tag{6.23}$$

Note that this is of the same form as the along-channel velocity distribution, i.e. a 'drag flow' term due to the relative motion of the two surfaces and proportional to distance from the screw, followed by a parabolic term with the pressure gradient. This is shown diagrammatically in Fig. 6.7, which is similar to Fig. 6.6(a), the positive and negative areas being equal.

The total transverse flow is given by:

$$Q = \int_0^h uz \, dy = \left[\frac{U}{h} \frac{zy^2}{2} + \frac{z}{2\eta} \cdot \frac{\partial P}{\partial x} \left(\frac{y^3}{3} - \frac{y^2 h}{2} \right) \right]_0^h$$

$$= \frac{Uzh}{2} - \frac{zh^3}{12\eta} \cdot \frac{\partial P}{\partial x} \tag{B13}$$

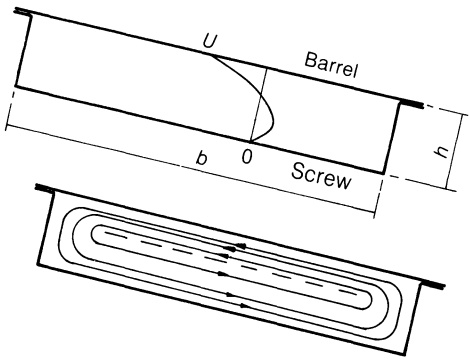


Figure 6.7 Transverse velocity profile.

But since leakage is assumed negligible, the transverse flow Q must be zero. Then:

$$\frac{Uzh}{2} - \frac{zh^3}{12\eta} \cdot \frac{\partial P}{\partial x} = 0$$

rearranging:

$$\frac{\partial P}{\partial x} = \frac{6\eta U}{h^2} \tag{6.24}$$

or:

$$\frac{1}{2\eta} \cdot \frac{\partial P}{\partial x} = \frac{3U}{h^2} \tag{6.25}$$

Substituting equation (6.24) in (6.23):

$$u = \frac{Uy}{h}\left(\frac{3y}{h} - 2\right) \tag{6.26}$$

giving the velocity at any point independent of the transverse pressure gradient.

In practice the flow near the barrel wall, leftwards in Fig. 6.7, must go down the front of the flight (inwards) to return, rightwards in Fig. 6.7, nearer the screw. The circulation is completed by a flow upwards at the back of the next flight (outwards). The foregoing analysis refers to the central portion of the channel where the radial component is negligible, in accord with assumption 3 that the channel is wide relative to its depth. The implications of this transverse flow for leakage, power and mixing will be discussed in sections 6.3, 8.2 and 9.1, respectively.

The longitudinal and transverse velocities in the channel combine to form a complex flow pattern which may perhaps best be described as an oblique helix, which itself is centred on the helix described by the channel – a sort of 'coiled coil'.

When the die is closed and there is zero net flow $Q = 0$, and substituting in equation (6.15) gives:

$$\frac{\mathrm{d}P}{\mathrm{d}z} = \frac{6\eta W}{h^2} \tag{6.27}$$

When this is substituted in equation (B.8), the latter gives the downstream velocity:

$$w = \frac{Wy}{h}\left(\frac{3y}{h} - 2\right) \qquad (Q = 0 \text{ only}) \tag{6.28}$$

which is of identical form to equation (6.26), U being replaced by W. But by equations (6.4) and (6.5) these are, respectively, $\pi DN \sin\phi$ and $\pi DN \cos\phi$, so these vectors may be combined to give:

$$\text{total velocity} = \pi DN \frac{y}{h}\left(\frac{3y}{h} - 2\right) \qquad (Q = 0 \text{ only}) \tag{6.29}$$

in a plane normal to the screw axis, as shown diagrammatically in Fig. 6.8(a).

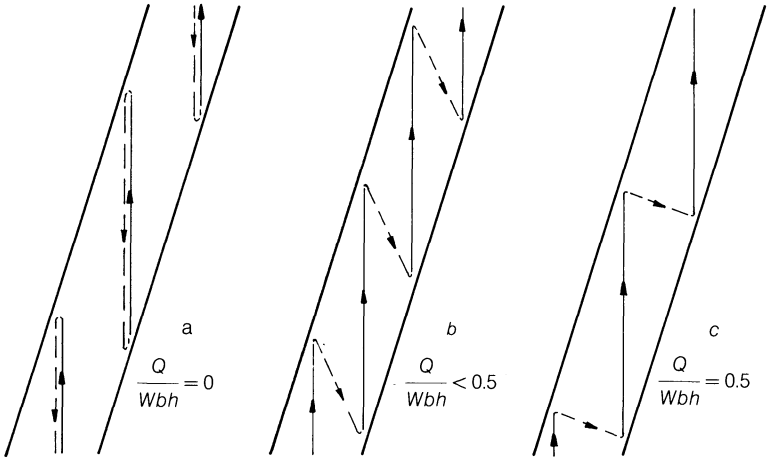


Figure 6.8 Flow patterns in screw channel (only extreme elements shown).

When the die is opened and flow commences, the transverse circulation remains but the longitudinal profile changes as shown in Figs 6.6(b)–6.6(d), giving a resultant as in Figs 6.8(b) and 6.8(c). These flow patterns have been experimentally confirmed by Eccher and Valentinotti (1958) and Kennaway (1957), the latter producing a ciné film of a transparent model with solid tracer particles in the fluid. Bernhardt (1959) gives more a precise representation by means of a 'flagpole' diagram showing the changing magnitude and directions of the total velocity vector. For pseudoplastic or other non-Newtonian fluids, where viscosity is dependent on the total shear in all directions, the longitudinal and transverse flows are interdependent through their effects on viscosity, and superposition of the components is no longer valid. In the same way drag and pressure flows cannot be superimposed, but this will be reconsidered in section 6.7.

6.3 LEAKAGE FLOW

This treatment is not exhaustive and is included in order to show the order of magnitude of leakage and the factors on which it depends. Approximate equations for the leakage flows are derived in appendix B.2 and expressed as fractions of the corresponding channel flows. Due to differences in the assumptions made, the expressions in appendix B.2 differ somewhat from those of other authors (Fisher, 1976; McKelvey, 1962; Bernhardt, 1959); these differences are of less importance than the conclusion that in most practical cases neglect of leakage flow is of less consequence than approximations inherent in the calculation of channel flow. Note that, as shown in section 8.4, it cannot be ignored in power consumption.

Leakage flow in the melt pumping section arises from two causes: the relative motion of screw flight and barrel; and the pressure difference (if any) between the two faces of the flight due to pressure gradients along and across the screw channel. The first is of the form of a drag flow, the polymer being sheared between two parallel faces so that part is carried along with the screw and part retained on the barrel surface.

As an example, using the results of appendix B.2, consider the following typical values:

Pitch p = Diameter D hence $\phi = 17° 40'$
Flight width $t = 0.1D$ hence $b = 0.858D$
Channel depth $h = 0.05D$ (low value taken to maximize proportionate leakage)
Flight clearance $= 0.0015D$ (high value taken to maximize leakage)

Substituting in equation (B.20) gives:

$$Q_{DL}/Q_D = 0.0367 \text{ or } 3\tfrac{2}{3}\% \text{ per turn}$$

and in equations (B.25) and (6.13) gives:

$$Q_{PL}/Q_P = 0.003\,26 \text{ or } \tfrac{1}{3}\% \text{ per turn}$$

To estimate the effect of transverse pressure gradient, further assumptions are necessary, e.g.

Diameter $D = 0.1$ m (100 mm or 4 in screw)
Viscosity $= 10^3\,\text{N s m}^{-2}$ (10^4 poise)
Pressure gradient $dP/dz = 20\,\text{MN m}^{-2}$ per metre (73.6 lb/in^2 per inch)
Speed $N = 1$ rps

Then from equations (B.29) and (6.13):

$$Q'_{PL}/Q_P = 0.001\,07 \text{ or } 0.1\% \text{ per turn}$$

and from equation (B.30):

$$\frac{Q_{PL} + Q'_{PL}}{Q_P} = 0.004\,33 \text{ or } 0.43\% \text{ per turn}$$

This pressure term of course only approximates that for a real machine, since local increases in shear rate and temperature will increase the leakage flow as a proportion of channel pressure flow, whereas the drag term (equation (B.20)) is scarcely affected. Note that the leakages are expressed 'per turn' since the leakage in successive turns is primarily in series and only to a limited extent in parallel, i.e. the output of a ten-turn screw would not be reduced by 35% due to drag flow leakage.

Since for a positive output $Q_P \not> Q_D$, the above example shows that in the usual case the drag flow element of leakage is the dominant factor. Analysing the effect of variables on leakage flow, equation (B.19) shows that the leakage

drag flow is proportional to the flight clearance δ, the screw speed N and the square of the screw diameter D. Further, equation (B.20) shows that for a screw of constant helix angle ϕ (so that $(p - t)/D$ is constant), as a proportion of the channel drag flow, the leakage drag flow is proportional to δ, inversely proportional to the channel depth h, and independent of screw speed and diameter. Thus, as a screw wears in service, the leakage increases approximately linearly in proportion to the clearance, but will be proportionately larger for a shallow screw. As with channel drag flow (equation (6.11) and discussion on p. 143), the leakage drag flow given by this analysis is independent of fluid viscosity, and hence of increased shear rate over the flight and consequent local shear heating. Equations (B.25) and (B.29) show that for a screw of constant helix angle ϕ ($t \propto D$) the (minor) leakage flows due to pressure differences are proportional to the diameter D and to δ^3. Equation (B.30) shows that, as a proportion of the channel pressure flow, the term which is due to the longitudinal pressure gradient is dependent only on $(\delta/h)^3$, whereas that due to the transverse gradient is more complex as there is no simple relation between longitudinal and transverse pressure gradients – however, it is still proportional to δ^3. The overall implication for operation is that the effect of leakage on output at low back pressures is small and broadly independent of speed and diameter, is proportional to flight clearance and proportionately greater for shallow screws (equation (B.20)); however, as back pressure is increased, the effect of clearance (wear) on the pressure terms dominates. In other words, at high back pressures, a severely worn screw will rapidly lose output, or have to turn faster to generate high pressures at the same output. The implications of leakage for energy consumption and heat generation will be discussed in section 8.2.

6.4 OUTPUT EQUATIONS AND LONGITUDINAL PRESSURE PROFILES FOR COMMON SCREW TYPES

6.4.1 Analysis of variables

First the variables in the equation for parallel (constant-depth) screws will be analysed. The volumetric flow equation (6.15) consists of two terms representing the drag and pressure flows, respectively. The first is given by equation (6.9) or (6.11); for geometric similarity, helix angle is constant and p, t and b (equation (6.2)) are all proportional to D, so:

$$Q_D \propto D^2 N h \tag{6.30}$$

i.e. drag flow is proportional to speed N and channel depth h, and to the square of diameter D. Drag flow can be increased by increasing screw speed and/or using a deeper screw. The effect of changing screw diameter will be considered

in section 11.5. Volumetric drag flow is also independent of the fluid properties, including viscosity, of the polymer melt; the mass drag flow will therefore be proportional to the polymer melt density and decrease only slightly due to thermal expansion with increase in temperature.

Note that since the dimensionless output Q/Wbh represents the ratio of actual output to (twice) the drag flow, for a constant value of Q/Wbh, the actual output Q_{Tot} will follow the same relationships as drag flow. The second term, representing the (negative) pressure flow, is given by equation (6.13). For geometric similarity ($b \propto D$), the pressure flow is proportional to screw diameter and pressure gradient and the cube of channel depth, but inversely proportional to melt viscosity. Thus the loss of output is proportional to the pressure gradient, but increases very rapidly with increase in channel depth, resulting in a relatively low output from deep screws at high back pressures (see Fig. 6.16). The effect of viscosity is that the loss of output with increasing back pressure will be greater for low-viscosity melts, e.g. due to high melt temperature or low intrinsic viscosity such as with nylons or low molecular weight polymers. The effect of shear rate, e.g. due to high screw speeds, must also be considered for pseudoplastic melts (section 6.7).

Longitudinal pressure gradients for various screw geometries will be considered later in this section, but the complicated effects of variables can be simplified by use of the dimensionless output Q/Wbh. It is therefore worth examining the relationship between Q/Wbh and the other variables in equation (6.13). It has already been seen (p. 136) that an increase in (positive) pressure gradient leads to a decrease in Q/Wbh from 1/2 towards zero, while a negative pressure gradient corresponds to $Q/Wbh > 1/2$. Equation (6.16) shows that if other factors are constant, a constant value of Q/Wbh corresponds to a constant pressure gradient. However, substituting equation (6.4) for W gives:

$$\frac{Q_{Tot}}{Wbh} = \frac{1}{2} - \frac{h^2}{12\eta\pi DN\cos\phi} \cdot \frac{dP}{dz} \tag{6.31}$$

or for constant Q/Wbh:

$$\frac{dP}{dz} \propto \frac{\eta DN\cos\phi}{h^2} \tag{6.32}$$

Thus for constant Q/Wbh and helix angle ϕ, dP/dz will increase linearly with viscosity η, screw diameter D and speed N but decrease as the square of channel depth h. In other words, a constant value of Q/Wbh implies an increase of pressure gradient for a high-viscosity polymer and a large or fast-running screw, but a substantial reduction for a deep screw. Thus an increase in temperature, reducing viscosity, implies a reduction in pressure gradient, while an increase in shear rate (W/h in equation (6.16)) implies an increase in pressure gradient. Alternatively, for a constant pressure gradient, Q/Wbh can only be held constant by adjusting the factors on the right-hand side of equation (6.32), e.g. if it is required to compare the performance of the same

screw at the same pressure gradient, this can be done at constant Q/Wbh if a reduction in viscosity (due to temperature increase) is compensated by a proportional increase in screw speed. This, and other, operating characteristics of a melt pumping section will be discussed in section 6.5 and Chapter 9. The foregoing analysis is in terms of pressure gradient; the relationships to pressure at the end of the screw are covered in section 6.5.1.

6.4.2 Constant-depth screw

The longitudinal pressure profiles for a constant-depth screw will now be derived. In the usual case, mass flow must be constant at all points along the length of the screw. Exceptions occur with additive injection, extraction and some multiscrew arrangements. Thus, except for variations in density due to pressure, temperature or chemical reaction, the volumetric flow will also be constant along the melt pumping section. Equation (6.15) shows that for an isothermal Newtonian fluid in a screw of constant speed N and dimensions D and b, the channel depth h and pressure gradient $\mathrm{d}P/\mathrm{d}z$ are uniquely related. Thus in a parallel screw (constant h) $\mathrm{d}P/\mathrm{d}z$ will be constant along the length of the melt pumping section and equal to P/Z (equation (6.19)), where P is the total pressure increase and Z the helical length of the melt pumping section; $Z = L/\sin\phi$ (equation (6.1)), where L is the axial length. Equation (6.20) applies and may be rearranged in the form:

$$P = \frac{12\eta WZ}{h^2}\left(\frac{1}{2} - \frac{Q}{Wbh}\right) \tag{6.33}$$

or:

$$P = K_1\left(\frac{1}{2} - \frac{Q}{Wbh}\right) \tag{6.34}$$

where:

$$K_1 = \frac{12\eta WZ}{h^2} \tag{6.35}$$

The pressure profile is therefore a straight line as shown in terms of axial length in Fig. 6.9. It is assumed in Fig. 6.9 that the 'gel point' is fixed – see section 6.6 for corrections. As the die pressure is increased, $\mathrm{d}P/\mathrm{d}z$ must increase and equation (6.15) and (6.16) show Q and Q/Wbh must decrease. In the limit, the output Q and Q/Wbh are zero, and rearranging equation

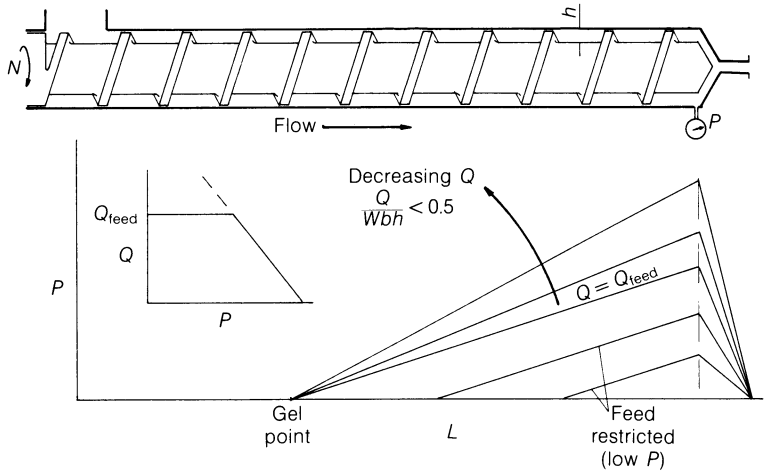


Figure 6.9 Pressure profiles: parallel screw.

(6.16) gives:

$$\frac{dP}{dz} = \frac{6\eta W}{h^2} \tag{6.36}$$

or:

$$P = \frac{6\eta WL}{h^2 \sin\phi} \tag{6.37}$$

which represents the maximum gradient and pressure this screw can deliver – but see p. 136 for practical limitations. If the pressure is reduced, e.g. by opening the die, dP/dz will decrease and output Q will increase. In practice, before the die pressure falls to zero, other factors are likely to limit output. The most obvious is the solids feeding and conveying capacity of the feed hopper and screw, which is largely independent of die pressure, and will limit further increase in output rate. Then, as die pressure is further decreased, output remains constant and equation (6.20) can only be satisfied by decreasing Z; thus dP/dz remains constant but pressure commences to rise further along the screw, implying that up to this point the screw is only partially filled – see p. 166. At low back pressures, melting will be mainly by conduction and the screw is likely to deliver largely unmolten polymer. The condition of zero pressure gradient, when $Q/Wbh = 1/2$, is thus unlikely to be achieved by a constant-depth solid-fed screw. It is, however, perfectly possible for a melt-fed screw (in which the effective length is from the front face of the feed opening, where pressure can commence to rise) to operate with either a uniformly increasing pressure along its length or a zero change of pressure. If fed under pressure, a melt-fed screw may also suffer a uniform decrease of pressure, when $Q/Wbh > 1/2$. The same possibilities exist with a constant-depth section within a compound screw; the result that there is no change of pressure along

that section when $Q/Wbh = 1/2$ is extremely important, especially for a compound screw with a parallel (constant-depth) 'metering' section. Limitations on practical output will be discussed in section 6.6.

6.4.3 Double-parallel (stepped) screw

The merits of a double-parallel or stepped screw (often called a 'nylon' screw) are discussed in section 9.4. Assuming D, p, t, ϕ, b, etc., are similar in the two sections, equation (6.20) may be applied separately to the each section:

$$Q_1 = \frac{Wbh_1}{2} - \frac{bh_1^3}{12\eta} \cdot \frac{P_1}{Z_1} \tag{6.38}$$

and

$$Q_2 = \frac{Wbh_2}{2} - \frac{bh_2^3}{12\eta} \cdot \frac{P_2}{Z_2} \tag{6.39}$$

But by continuity,

$$Q_1 = Q_2 \tag{6.40}$$

and

$$P_1 + P_2 = P \tag{6.41}$$

An alternative equation, eliminating P_1 and P_2, is given in appendix B.3. As for the parallel screw, the pressure gradient within each section will be constant, but generally different in the two sections. Starting from the die pressure at which $Q/Wbh_2 = 1/2$, P_2 will be zero and $P_1 = P$, i.e. the total pressure is raised in the first section. If, as is usual, $h_1 > h_2$, then $Q/Wbh_1 < 1/2$, indicating a positive pressure gradient in the first section; this is illustrated in Fig. 6.10. If the die pressure is now increased, output Q will decrease (equation (B.31)) and both Q/Wbh_2 and Q/Wbh_1 will be less than 1/2; however, it is always the case that $Q/Wbh_1 < Q/Wbh_2$ ($Q \neq 0$). Thus pressure will rise throughout the melt pumping section, with a step change in gradient (but not pressure) at the change of channel depth. Ultimately, a die pressure will be reached at which output is zero, so that Q/Wbh_2 and Q/Wbh_1 are also zero, representing the maximum pressure achievable with the screw. It will be noted that for the usual ratios of depths h_1/h_2, Q/Wbh_1 will be much less than Q/Wbh_2; however, the cubic term in equations (B.31) and (B.33) dominates, and except at values of Q/Wbh_2 only slightly less than 1/2, dP_2/dz_2 is greater than dP_1/dz_1. The relative magnitudes of the pressure gradients are further

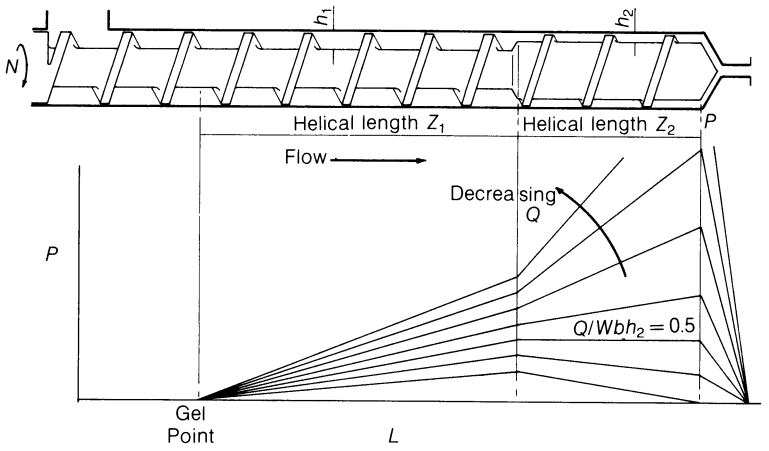


Figure 6.10 Pressure profiles: stepped screw.

examined in appendix B.4, which shows, e.g. for $h_1/h_2 = 3$, $dP_2/dz_2 > dP_1/dz_1$, for all values of $Q/Wbh_2 < 0.46$, when $Q/Wbh_1 \simeq 0.15$. At this condition dP_1/dz_1 is only 4% greater than at $Q/Wbh_2 = 0.5$. This means that unless the second section L_2 is very short, most of the pressure is raised in the second section of the screw; however, this is not the case when $Q/Wbh_2 > 1/2$. When die pressure is reduced below that at which $Q/Wbh_2 = 1/2$, output increases so that $Q/Wbh_2 > 1/2$ and dP_2/dz_2 is negative, i.e. pressure falls along the second section. However, Q/Wbh_1 remains less than 1/2 and pressure rises in the first section. The maximum output is achieved when pressure at the end of the screw is zero, i.e. the rise in pressure in the first section is exactly balanced by the fall in the second section. Since in this condition there is resistance to the forward movement through the melting section and output is to some extent limited by the melt pumping section, melting by mechanical shearing can take place. It is thus possible for a stepped screw to operate satisfactorily with low or zero die pressure, especially with a high compression ratio (large h_1/h_2) or large L_2/L_1; this can be of use where there is little or no die resistance as in thick tube and section extrusion, or in flow moulding. In effect the second screw section becomes a resistance equivalent to a die, in which melt is forced through it at a greater rate than its own natural pumping rate (when $Q/Wbh_2 = 1/2$). A further increase in output would imply a negative die pressure, where the pressure rise in the first section was insufficient to overcome the 'resistance' of the second section, and evidently Q/Wbh_1 cannot reach a value of 0.5. Screws having the second section deeper than the first ($h_1/h_2 < 1$) have been proposed; in this case the pressure profiles are transposed; at high die pressures, pressure will rise rapidly in the first section and more gradually in the second, whereas at low die pressures,

pressure in the first section may be constant zero or even negative, and rise in the second section to a zero or positive value.

6.4.4 Taper and taper-parallel screws

Similar features are to be found with screws having a gradual taper (continuous decrease in h), with or without a parallel section following without a step. In this case the channel depth is assumed to decrease uniformly from h_1 at the commencement of pressure rise over a helical length Z_1 to h_2 at the die or start of the parallel section of depth h_2 and helical length Z_2. Note that in this case, if the point at which pressure commences to rise changes in a real screw, both Z_1 and h_1 will also change, though the taper angle θ remains constant. Equation (6.15) may be applied to any small element of length dz of the first (tapered) section and rearranged as:

$$\frac{dP}{dz} = \frac{12\eta W}{h^2}\left(\frac{1}{2} - \frac{Q}{Wbh}\right) \tag{6.42}$$

and integrated between the limits $h = h_1$ at $z = 0$, and $h = h_2$ at $z = Z_1$, remembering that Q is constant and for a constant pitch screw W and b are also constant. The detailed derivation in appendix B.3 yields the pressure rise in the first section P_1 given by:

$$P_1 = \frac{6\eta W Z_1}{h_1 h_2}\left(1 - \frac{Q}{Wbh_2}\cdot\frac{h_1 + h_2}{h_1}\right) \tag{6.43}$$

Equation (6.20) may then be rearranged and applied to the parallel section (if any):

$$P_2 = \frac{6\eta W Z_2}{h_2^2}\left(1 - \frac{2Q}{Wbh_2}\right) \tag{6.44}$$

and combined with equation (6.43), remembering that $Q_1 = Q_2$ and $P = P_1 + P_2$:

$$P = \frac{6\eta W Z_1}{h_1 h_2}\left(1 - \frac{Q}{Wbh_2}\cdot\frac{h_1 + h_2}{h_1}\right) + \frac{6\eta W Z_2}{h_2^2}\left(1 - \frac{2Q}{Wbh_2}\right) \tag{6.45}$$

If $Q/Wbh_2 = 1/2$, then the second term in equation (6.45) is zero (no pressure rise in the parallel section) and since $h_2/h_1 < 1$ both equations (6.43) and (6.45) give P_1 positive. Since $h_1 > h > h_2$, the differential form of equation (6.42) shows that dP/dz at all points in the first section is positive, though tending to zero as $h \to h_2$. To complete the pressure profile it is necessary to examine the trend of the pressure gradient. Differentiating equation (6.42) gives:

$$\frac{d^2P}{dz^2} = -\left(\frac{-12\eta W}{h^3} + \frac{36\eta Q}{bh^4}\right)\left(\frac{h_1 - h_2}{Z_1}\right) \tag{6.46}$$

A point of inflexion occurs when $d^2P/dz^2 = 0$ or:

$$\frac{Q}{Wbh} = \frac{1}{3} \tag{6.47}$$

Thus the pressure profile for $Q/Wbh_2 = 1/2$ is as shown in Fig. 6.11, but note that the point of inflexion is independent of the value of Q/Wbh_2 and occurs at all values of the latter greater than 1/3. As die pressure is increased, the pressure gradient dP/dz increases at each point along the length of the screw, and output Q decreases, giving a corresponding decrease in Q/Wbh at each point. At high die pressures giving values of Q/Wbh_2 less than 1/3, the pressure gradient increases continuously along the taper section so that the major portion of the pressure rise is contributed by the later, shallower portion of the screw. Since there is no step change in h at the end of the taper, there is no change in Q/Wbh and dP/dz, so that at all die pressures the pressure profile in the parallel section (if any) is a straight line tangential at that point to the curve in the taper section. If there is a parallel section of substantial length then at high die pressures this section will contribute the major portion of the pressure rise, in which case the output/pressure relation will be similar to that of a simple parallel screw of the same depth and slightly greater length than the parallel 'metering' section, i.e. the first term in equation (6.45) can be neglected in favour of a small increase in Z_2 in the second term. If the die pressure is low so that Q/Wbh_2 is greater than 1/2, pressure will fall at the end of the taper section and in the parallel section, if present. Thus a maximum pressure will occur at some point within the taper at which $Q/Wbh = 1/2$. This point, and that at which the point of inflexion occurs ($Q/Wbh = 1/3$), will move back towards the feed end as die pressure is reduced and output increased; a greater

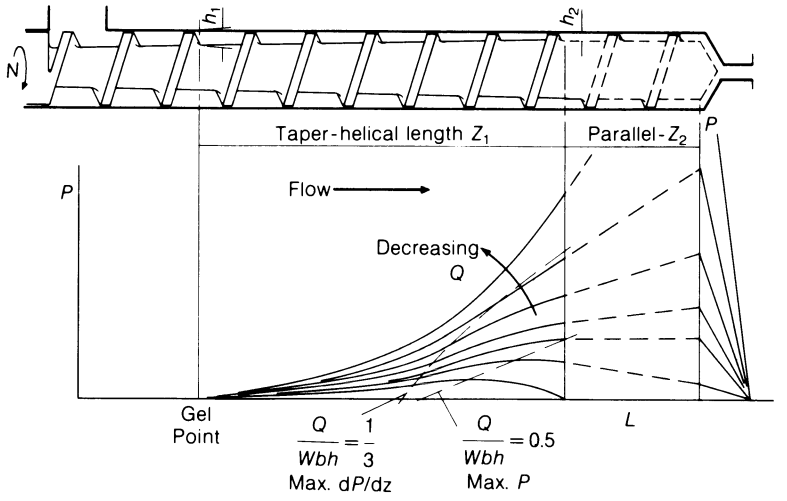


Figure 6.11 Pressure profiles: taper and taper-parallel screw.

proportion of the pressure is raised in the earlier portion of the taper, which becomes more significant in determining the output for a given die pressure. As with the stepped screw, maximum output occurs at zero die pressure, and since positive pressure is generated within the screw, this type also may operate satisfactorily with low or zero die pressure.

An industrial example illustrates the higher pressures possible within a screw than at the die and the significance of the ratio Q/Wbh in understanding the conditions within the screw. A 200 mm (8 in) diameter solid-fed extruder had a taper-parallel screw with pitch and diameter equal ($\phi = 17°36'$), total length 24 diameters and a metering section depth of 5.59 mm (0.22 in). At 60 rpm it gave an output of 1091 kg h^{-1}(2400 lb/h) of LD polyethylene with a die pressure of only 13.8 MN m^{-2} (2000 lb/in^2). Trouble was experienced with granulation due to the high melt temperature and the drive motor tended to be overloaded. With a melt density of approximately 760 kg m^{-3} (47.4 lb/ft^3), Q/Wbh_2 was calculated as 0.672 showing that pressure was falling in the parallel metering section; this only required knowledge of the screw dimensions, speed and output – see p. 137. When a pressure gauge was fitted half way along the metering section it registered 55.2 MN m^{-2} (8000 lb/in^2), indicating a pressure at the start of the metering section of 96.6 MN m^{-2} (14 000 lb/in^2). As shown by Fig. 6.11 the maximum pressure would be even greater. The immediate remedy was to reduce speed, reducing shear heating and pressures (equation (6.44) and die equation) and increase barrel temperatures to reduce power input and pressures through reduction in viscosity (equations (8.9) and (6.44), respectively). A lower output, of course, resulted, but it was judged preferable to continue making good product at low rate, rather than make scrap at high rate, until a screw of different profile could be obtained!

Some authors, e.g. Bernhardt (1959), have identified the value $Q/Wbh = 1/3$ with some form of optimum design. Figure 6.11 shows that for tapered screws it represents neither the maximum output nor maximum pressure, only the position of the point of inflexion in the pressure curve and the maximum value of the pressure gradient. For a constant-depth screw, rearranging equation (6.20) in the form of equation (6.33) and differentiating P with respect to h, treating Z and Q as constant, gives:

$$\frac{dP}{dh} = \frac{-12\eta WZ}{h^3} + \frac{36\eta ZQ}{bh^4} \tag{6.48}$$

and:

$$\frac{d^2P}{dh^2} = \frac{+36\eta WZ}{h^4} - \frac{144\eta ZQ}{bh^5} \tag{6.49}$$

but $dP/dh = 0$ when $Q/Wbh = 1/3$ and then d^2P/dh^2 is negative, indicating a maximum value of P. Thus the corresponding (constant) depth h of screw will give the maximum pressure for given values of output and speed; as shown by

comparing equations (B.32) and (B.39) with (6.33), this is approximately true for variable-depth screws at high back pressure. However, to the present author, this seems of doubtful value, since in practice the pressure required is determined by the type of die used and output is limited by considerations of energy, mixing and stability, as will be discussed later in Chapters 9 and 11.

The foregoing shows the pressure profiles along several common types of screw and their changes with output and back pressure. These can be extended to other screw types, but increasingly complex output/pressure equations can better be solved by use of graphical representations.

6.5 GRAPHICAL REPRESENTATION OF OUTPUT FOR SCREW/DIE COMBINATIONS, INCLUDING VENTING

6.5.1 Graphical representation

From equation (6.9) it is seen that the drag flow is proportional to W and hence to screw speed N (equation (6.11)). Equation (6.13) shows that the pressure gradient dP/dz, and hence pressure, is independent of screw speed for a Newtonian fluid. Thus at *constant pressure*, output Q is linear with N (equation (6.20)) being the proportional drag flow minus a constant pressure flow of the form:

$$Q_{\text{Tot}} = AN - \frac{BP}{\eta} \tag{6.50}$$

where:

$$A = \frac{\pi}{2} Dbh \cos\phi \tag{6.51}$$

(from equation (6.10)) and:

$$B = \frac{bh^3}{12Z} \tag{6.52}$$

(from equation (6.20)). Thus output versus speed is represented in Fig. 6.12 by a series of parallel straight lines for various back pressures. Equation (6.50) shows that as temperature increases, causing a decrease in viscosity η, the pressure flow Q_P will increase and the total output decrease for a given speed, as shown by the dashed lines for constant pressure and increasing temperature. Of more practical interest is the variation of output with speed for the combination of extruder and a fixed die. From equation (3.22), the Q/P relation for a die of fixed geometry is:

$$Q_{\text{Die}} = \frac{KP}{\eta} \tag{6.53}$$

where:

$$K = \frac{\pi R^4}{8L} \tag{6.54}$$

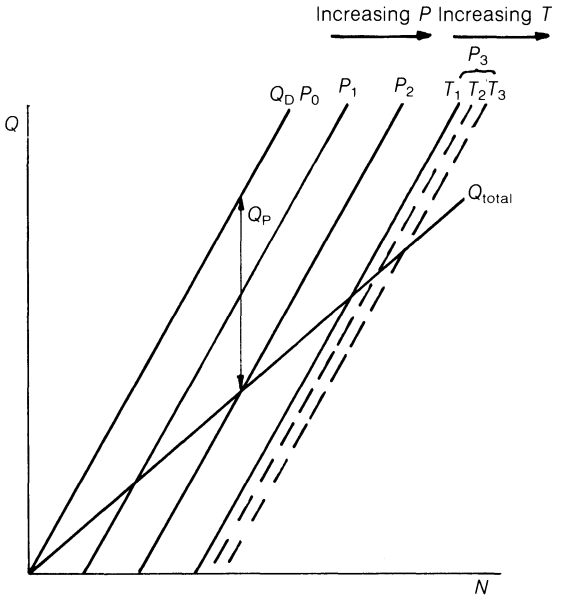


Figure 6.12 Total output vs speed.

for a capillary of radius R and length L, or:

$$K = \frac{TH^3}{12L} \tag{6.55}$$

for an 'infinite' slit of width T and depth H. But by continuity:

$$Q_{\text{Tot}} = Q_{\text{Die}} \tag{6.56}$$

Combining equations (6.53) and (6.56) and rearranging:

$$P = \frac{\eta Q_{\text{Tot}}}{K} \tag{6.57}$$

and substituting in equation (6.50) and rearranging:

$$Q_{\text{Tot}}\left(1 + \frac{B}{K}\right) = AN \tag{6.58}$$

that is, as shown in Fig. 6.12, the total output and pressure are proportional to speed N:

$$Q_{\text{Tot}} \propto P_{\text{Die}} \propto N \tag{6.59}$$

This is only approximate since in practice temperatures are also likely to change with speed (section 9.2). Pseudoplastic fluids are considered in section 6.7, but for convenience the effect on output versus speed is included here. Most important is that shear rates and hence viscosities in screw channel and

die will be different (equations (6.50) and (6.53)) and therefore the bracketed term in equation (6.58) becomes $(1 + B\eta_{Die}/K\eta_{Screw})$. The ratio of these viscosities will depend on the shear rates in screw and die and on the values of the pseudoplasticity index n at these shear rates. However, even if the separation of drag and pressure flows is still taken to be valid for a pseudoplastic fluid, equation (6.69), combined with equation (6.17), shows that shear rate in the screw, unlike that in the die, is not proportional to the pressure flow Q_P or pressure P, so that the ratio of these shear rates, and hence of viscosities η_{Die} and η_{Screw}, will change with screw speed. This would be expected to lead to a slightly more than proportional increase in output with speed. In practice, due to the increasing specific mechanical power E/Q (Fig. 8.13), temperatures tend to rise with increasing speed, which may reduce viscosity in the screw more than in the die if the temperature coefficient of viscosity is greater at shear rates in the screw than in the die. This is implied by the converging lines in Fig. 3.5, often found experimentally. It is frequently found that even with highly pseudoplastic polymers, output and speed are

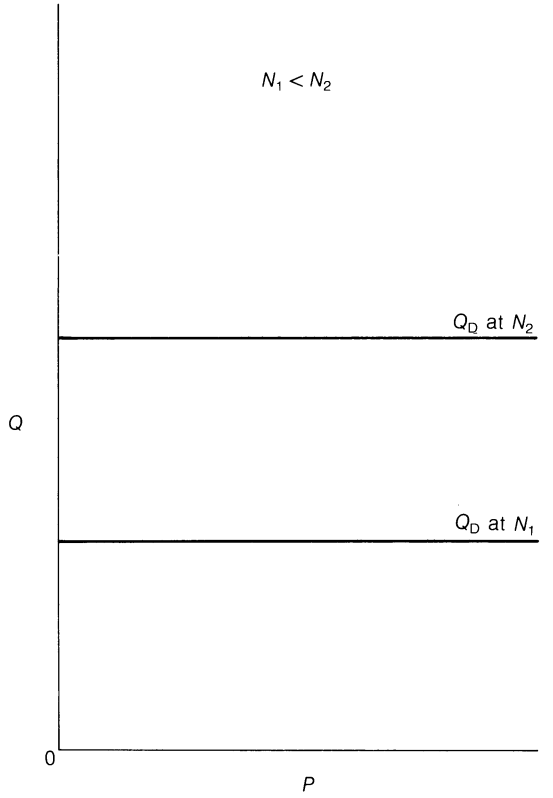


Figure 6.13 Drag flow vs speed.

nearly linear until feed or melting restrictions become apparent (Chapter 7). At high pressures or with large machines where temperature control is difficult, the output/speed curve may droop, probably due to temperature effects on viscosity.

Equations (6.20), (B.31), (B.37) and (B.38) indicate that for several common types of screw the drag flow is proportional to speed and independent of pressure. Thus in Fig. 6.13 the Q/P diagram shows Q_D as a series of horizontal lines at distances above the origin proportional to speed N. Figure 6.14 shows a similar effect of channel depth h, drag flow at constant speed being proportional to channel depth. According to equation (6.20), the (negative) pressure flow Q_P is proportional to pressure P and independent of speed N, so Fig. 6.15 consists of Fig. 6.13 with a superimposed series of parallel straight lines for different speeds commencing from drag flow Q_D at zero pressure and decreasing linearly with pressure P; then $Q_{Tot} = Q_D - Q_P$ (equation (6.15)) is represented by the ordinate. Equations (B.32), (B.39), and (B.42) show that for other types of screw output also varies linearly with

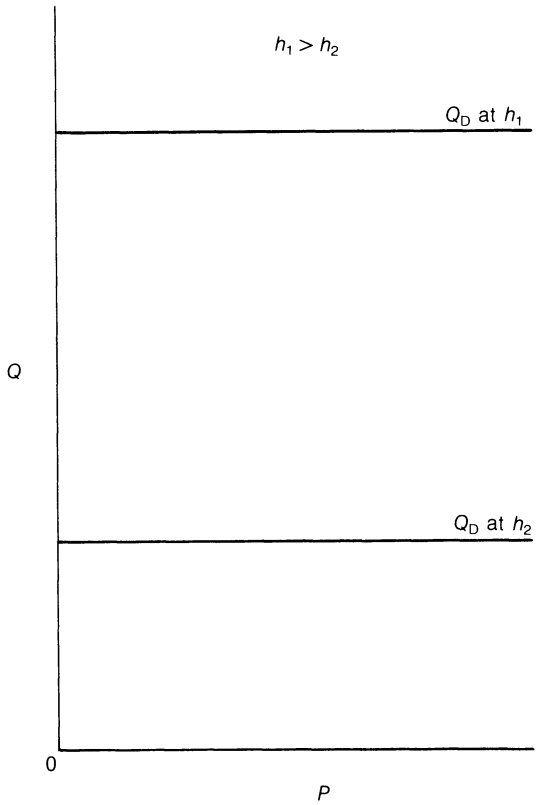


Figure 6.14 Drag flow vs channel depth.

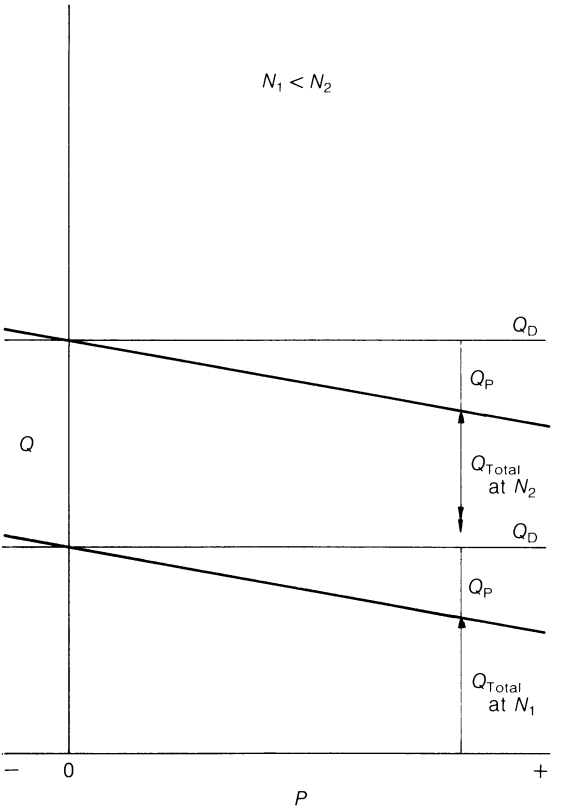


Figure 6.15 Pressure and total flows vs speed.

pressure (but see sections 6.7 and 6.8). In Fig. 6.16, pressure flow Q_P is similarly superimposed on Fig. 6.14 with Q_{Tot} as the resulting ordinate, but since Q_P is proportional to h^3, the slope of the Q/P line increases rapidly with increase of channel depth. This diagram immediately explains several operational features of screws of different depths – as explained on p. 149, final channel depth is of more significance than 'compression ratio' h_1/h_2 and use of the latter term will be avoided as a common but misleading colloquialism. Firstly, for a given increase in pressure, the output of a deep screw will decrease much more than that of a shallow screw – for this reason they are sometimes referred to as 'soft' and 'hard' screws, respectively. Secondly, although the output of a deep screw will be greater than that of a shallow one at low pressures, at high pressures the reverse will be true. The maximum pressure achievable (at zero output) will also be less than that of a shallow screw. The effects of decreasing melt pumping section length Z will be similar to those of increasing depth h, though less dramatic since Q_P varies only linearly with Z (equation (6.13)). Since Q/Wbh is proportional to Q_{Tot}, the vertical ordinate of Fig. 6.16 may

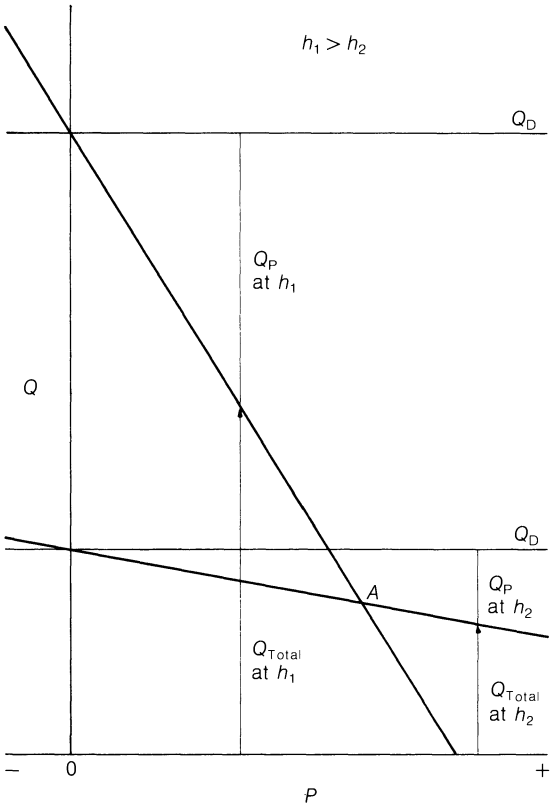


Figure 6.16 Pressure and total flows vs channel depth.

also represent a linear scale of Q/Wbh for a given speed and channel depth, with a value of 1/2 at zero pressure, corresponding to drag flow. Values of $1/2 < Q/Wbh < 1$ represent negative pressure changes by continuation of the output/pressure line to the left of the vertical axis – this will be used in considering two-stage screws, in appendix B.5. This output/pressure line is a graphical representation of equation (6.20) or (6.33) and must be satisfied for the screw in question; however, it gives no information on what values of output, and its corresponding pressure, will be experienced in combination with a die. The output/pressure relation for a die with a Newtonian isothermal fluid is given by equation (6.53), which is represented by a straight line through the origin. Equations (6.54) and (6.55) show that if the die is narrow and/or long, K will be small and the slope small; if wide and/or short, the slope will be large as shown in Fig. 6.17, the slope representing K/η. For a screw and die in steady operation, both the relations between output Q and pressure P must be satisfied, and the intersection of the screw and die lines represents the unique (real) solution of two simultaneous equations. Figure 6.18 shows that for a

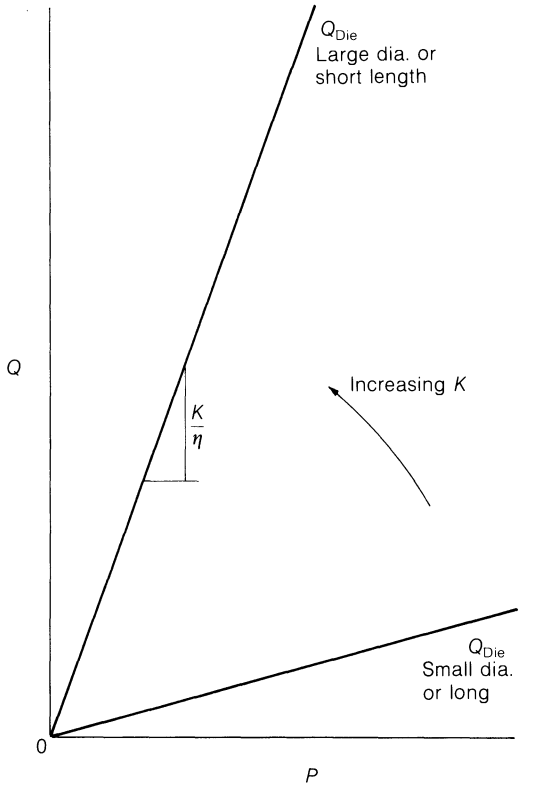


Figure 6.17 Die characteristics (Newtonian).

large die, a deep screw may give a substantially higher output and pressure (point *A*) than a shallow screw (point *B*). However, with a small die the shallow screw (point *D*) may give a higher output than a deep one (point *C*) at the same speed; this may be overcome by increasing the speed of the latter, and the choice between screw designs, like that of back pressure, then becomes a matter of energy, mixing and stability (see Chapters 9 and 11). Modification to this diagram due to non-Newtonian and non-isothermal operation will be considered in sections 6.7 and 6.8. For more complex problems, continuity requires that for sections in series:

$$Q_1 = Q_2 = Q_3, \quad \text{etc.} \tag{6.60}$$

and:

$$dP_1 + dP_2 + dP_3 + \cdots = 0 \tag{6.61}$$

(including pressure drop through the die) where dP_x is the pressure change in section x. In the case of operation in parallel:

$$Q_1 + Q_2 + Q_3 + \cdots = Q_{Tot} \tag{6.62}$$

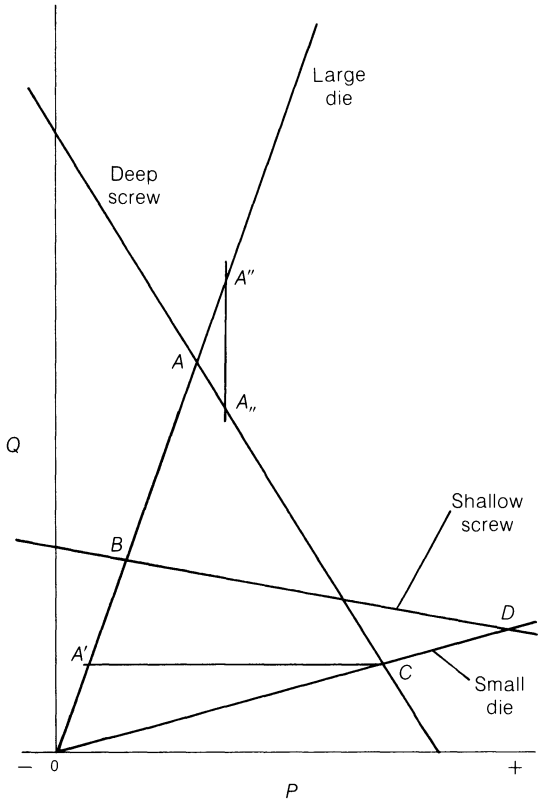


Figure 6.18 Operating points of screw/die combinations.

and:

$$dP_1 = dP_2 = dP_3, \quad \text{etc.} \tag{6.63}$$

Further, where screw sections are on a common shaft, speed N is the same for each section, and where diameter D and helix angle ϕ are also constant, downchannel velocity W and channel width b will be constant.

6.5.2 Venting or vacuum extraction

The use of this type of diagram is exemplified by considering venting or vacuum extraction, using the isothermal Newtonian approximation for simplicity. The purposes of venting are: (i) to remove air trapped in the feed section; (ii) to remove water vapour on or in solid feed material; (iii) to remove residual volatiles, e.g. monomer, diluent; and (iv) to remove degradation products produced during heating in the screw. This may assist in giving non-porous, steady, smooth-surfaced product and in reducing odour, die build-up and 'smoking', e.g. due to high temperatures used in paper-coating with LDPE.

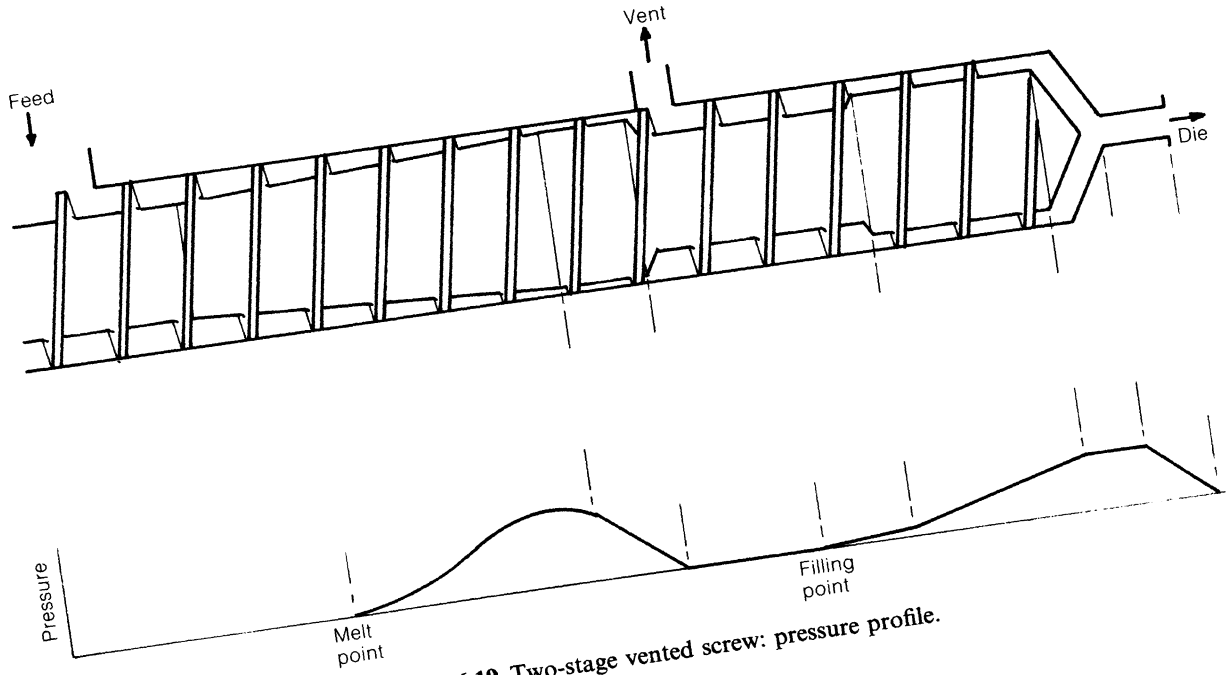


Figure 6.19 Two-stage vented screw: pressure profile.

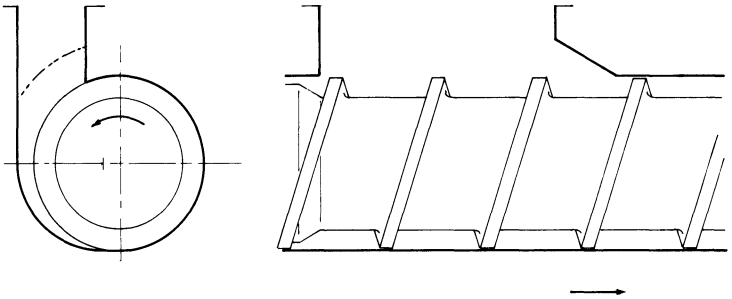


Figure 6.20 Vent for vacuum extraction.

Trapped air, and to a partial extent purposes (ii) and (iii), can also be achieved by vacuum feeding (Chapter 7); purpose (iv) can obviously only be achieved after melting.

Several methods are used of which the commonest is probably a decompression section in the screw with a vent in the barrel over it (Fig. 6.19). All the polymer melt passes over the vent, which is therefore liable to blockage; various shapes, including removable inserts, have been used to reduce blocking of the vent and assist in clearing material forced into the vent, such as that shown in Fig. 6.20 where the vent port is arranged tangentially

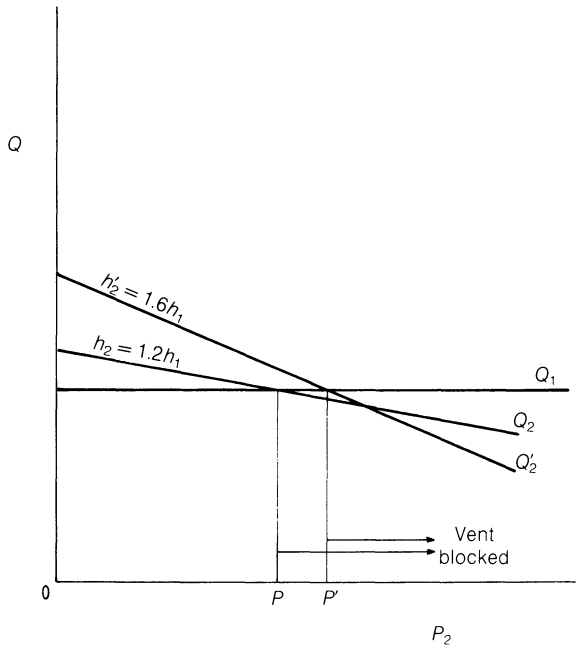


Figure 6.21 Effect of die pressure on venting.

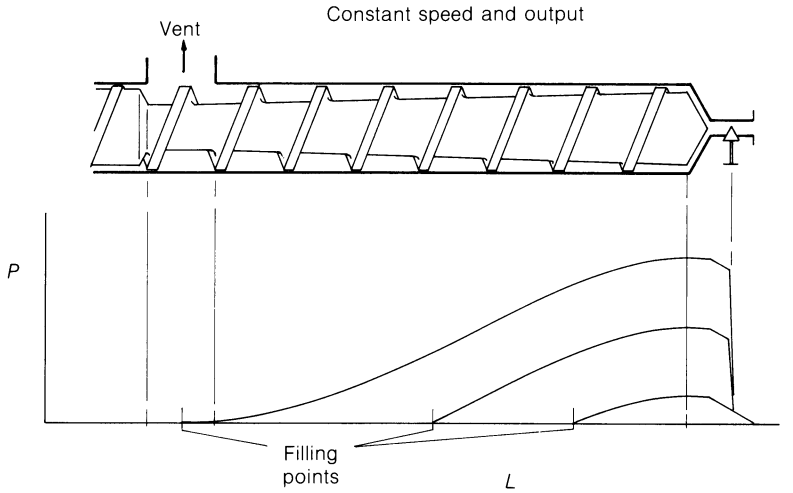


Figure 6.22 Effect of die pressure on filling position.

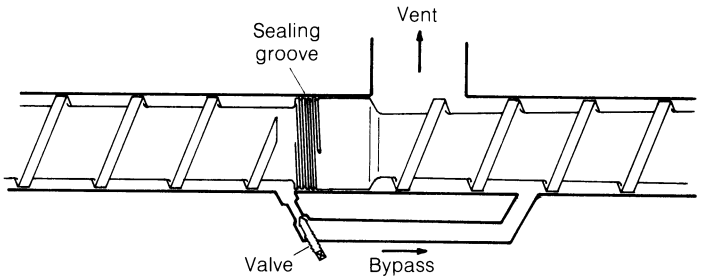


Figure 6.23 Valved bypass venting system (Bone–Cravens patent).

above the downgoing side of the screw, and elongated to increase the area for vapour release, and the trailing edge is well chamfered to assist in re-entrainment (Chapter 7). Since the principle is that after melting in the first section of the screw, the pressure is reduced to zero under the vent, a second shallow section is usually necessary to raise the requisite pressure before the die. This may be satisfactory for one set of operating conditions, though requiring careful prediction in the design of the screw, but is quite inflexible, since an increase in die pressure is liable to cause vent blockage. Analysing the output/pressure relations, speed is the same for both sections and while the vent is unblocked the first section is operating against zero back pressure so that its output is independent of die pressure. By continuity, if the vent is to remain unblocked, $Q_2 \geq Q_1$, so h_2 must be greater than h_1. As the die pressure P_2 is increased, Q_2 will decrease until at $P_2 > P$ (Fig. 6.21) it is less than Q_1, when the vent will block since the second section is not removing material from the vent region as fast as the first section is supplying it. To avoid this, h_2 is often

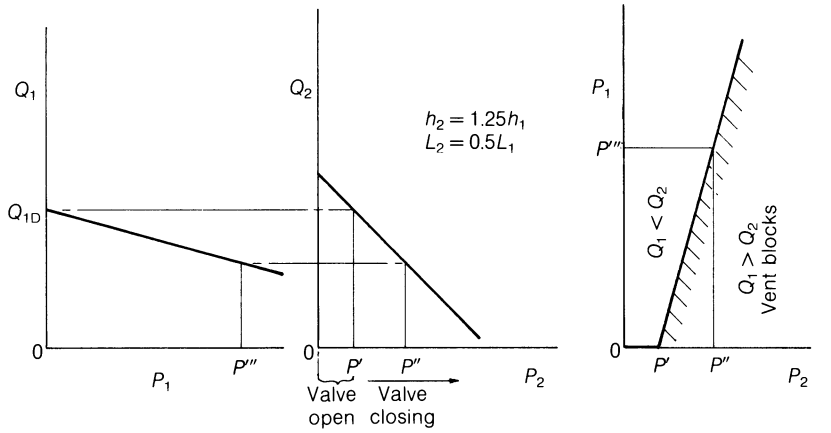


Figure 6.24 Valve closing vs die pressure P_2 to avoid vent blocking.

designed considerably greater than h_1, which may allow a slightly higher die pressure P' but, as Fig. 6.16 shows, leads to a steeper gradient of dQ/dP, i.e. output falls more for a given increase in pressure and therefore this design is even more sensitive to changes in die pressure. To permit vapour release, the screw channel at the vent must be only partially filled; if the second section is tapered, it will fill at some point depending on the die pressure. If the die pressure is increased, the same output can be maintained if the channel is filled further back (Fig. 6.22), increasing the effective length, until eventually it fills at the vent, causing blockage. However, as will be seen in section 6.6, the pumping rate of a partially filled screw is very sensitive to the degree of filling, and surging is likely to result in otherwise satisfactory conditions; this is aggravated by increasing the depth of the second section h_2 beyond the minimum.

Another method of venting with a similar screw is to make use of the partial filling to avoid the polymer melt passing directly over the vent by placing the latter in the screw itself just behind a flight (Bernhardt, 1956), where filling is normally last to occur. The vent is then taken out through a hollow screw to a rotary joint at the drive end. The output/pressure characteristics are similar to the preceding method, but the area of the vent is very restricted, it is difficult to incorporate with screw heating or cooling, and if it becomes blocked is inaccessible for manual clearing. Since the first section is operating against zero back pressure, the last part of this section is acting as a resistance to raise pressure and promote melting and mixing in the earlier parts; it has been proposed to replace this with a restriction in the form of a short annulus, e.g. a 'smearhead', permitting a deeper first section with probably a higher output and/or more complete mixing. However, the output of the first section is still independent of die pressure; limitation of the latter and/or surging are still probable.

If this restriction is carried to the limit, with a close clearance and reverse-pitch groove for sealing, the flow may be diverted through a bypass channel in the barrel and returned to the screw downstream of the vent position. In this way the melt does not pass over the vent and, in the event of accidental blockage, the second section of the screw will tend to pump the vent clear. A refinement of this system is to incorporate an adjustable valve in the bypass (Grant, 1961) so that the back pressure P_1 on the first screw section can be varied to compensate for changes in die pressure P_2 (Fig. 6.23). This, in general, will permit higher values of die pressure without vent blocking, but more importantly enables the depths of the first and second screw sections to be more nearly equal and so reduce the risk of surging. Operation with a given screw may be summarized by a diagram of P_1 against P_2 (Fig. 6.24); a pressure gauge upstream of the valve will assist the operator. The author has seen the vent blocked by increasing P_2 and subsequently cleared by increasing P_1 accordingly. This system has an additional advantage of a large melt surface for release of volatiles depending on the filling point of the second section. Actual experience has shown two limitations: (i) thermal degradation due to long residence time of polymer in the seal or vent regions may contaminate the product; (ii) although adjustment of the valve will avoid vent blocking, the increased back pressure on the first screw section will alter the work input and melt temperature. This is qualitatively the same as in a simple unvented screw but made more critical by the understandable tendency to try to accommodate venting within the length of a simple screw, thus reducing the effective length for melting and mixing, but expecting similar performance in terms of output, melt temperature, stability, etc. The present author believes it would be more correct to treat the vent and second screw section as an addition to the length of the simple screw and accept a compromise between output and the additional shear history imposed on the polymer by the extra length. Within-the-barrel systems may remove up to about 5% by mass of water vapour – multiple extract points have been used to remove approximately 15% of a volatile monomer down to much less than 1% residual content.

A more radical system (Fisher, 1976, p. 83) is the use of two distinct extruders with a venting vessel between the first solid-fed machine which melts and pumps the polymer to the vessel, and a second melt-fed machine pumping the devolatilized polymer to the die. The vessel must be heated and may have a stirrer and/or vacuum applied to assist in volatile removal. It can have a large polymer surface and long residence time for separation, and it is claimed that the second machine is surge-free, though this depends on satisfactory feeding of the melt to it. The two extruders may run at different speeds and even be of different diameters; control of relative outputs does not need to be refined because of the large capacity of the vessel. Although the equipment is cumbersome, and the long residence time may give degradation of heat-sensitive polymers, it appears suitable for removal of large proportions of water vapour and other volatiles.

In appendix B.5 further examples of the use of Q–P diagrams are given.

6.6 OUTPUT CORRECTIONS

The ten assumptions in section 6.2 permit derivation of flow rate and mechanical power input in terms of simple analytic equations, from which the trends caused by changes in operating conditions may clearly be seen. Further, numerical values can be obtained with the aid of a pocket calculator.

Of these assumptions, nos 1, 6, 7, 8 and 10 are treated in sections 11.2, 6.3, 6.7, 6.8, and 6.4 respectively, and gravity (assumption 9) is clearly negligible with high viscosity melts. Apart from external causes such as feed variations, inhomogeneities may arise within the extruder, for instance by selective feeding (p. 271) or selective melting (p. 282). Although partly-melted polymer may behave as a fluid and generate pressure, appropriate values of viscosity and heat content must be used.

If the polymer does not adhere to the barrel and screw surfaces, the flow becomes indeterminate. If low viscosity occurs near the barrel, e.g. due to excessive heating or separation of low molecular weight material (monomer, lubricant, etc.), the drag flow will be decreased. If conditions aproaching 'slip' occur at the screw surface, drag flow may actually be increased, but the pressure flow will also be distorted. Assumption 3 neglected the drag due to adherence of the polymer to the sides of the flight; the drag flow is not truly one-dimensional and the mean drag velocity is less than $W/2$ (equation (6.9)). Similarly, the pressure flow is not completely represented by flow through an 'infinite' slit. McKelvey (1962, p. 236) has presented graphs of correction factors for drag and pressure flow for various ratios b/h of channel width to depth. These show that for $b/h = 10$, which is typical for extruders for plastics, $K_D = 0.93$ and $K_P = 0.94$, and these vary only slowly with b/h so may be neglected in estimating changes due to operating conditions, though not in design. Neglect of these corrections will cause approximately 7% overestimate in the calculated flow rate and corresponding underestimate in the value of Q/Wbh based on observed flow rate, so they are significant in deductions made from the value of Q/Wbh. These corrections will be greater than the above in the deep channels often associated with screws for extruding rubbers.

The main effect of assuming a shallow channel and neglecting curvature, since inertia terms are negligible, is that the mean channel velocities are overestimated by equations (6.9) and (6.10)–the latter would better be represented by:

$$Q_D = \frac{\pi}{2}(D - h)Nbh\cos\phi \tag{6.64}$$

The error for a diameter/depth ratio $D/h = 10$ is +11%, but the approximation is convenient, especially for tapered screws, where $(D - h)$ would vary along the length. A smaller error arises because the areas, and therefore the stresses, at the barrel wall and the screw root are unequal, so that drag flow shear rate (velocity gradient) is not constant and the velocity distribution

shown in Fig. 6.3 should be similar to that in Fig. 6.6(e) – the parabolic velocity distribution (Fig. 6.5) due to pressure flow will similarly be distorted with a maximum nearer the screw root.

A major uncertainty which directly affects the output/pressure characteristic is the effective melt length Z. Experiments by Weeks and Allen (1962) have shown that the point of initial pressure rise in a solid-fed extruder can be determined quite reliably by plotting pressure measurements at a series of points along the melt pumping section and extrapolating to zero pressure. The same researchers measured melt temperature by allowing polymer to flow out of the barrel at various points and over thermocouples. This of course gave time-averaged readings, but in the region of the 'gel point' may have given high readings, since any solid particles in the flow could not pass through the relatively narrow passage surrounding the thermocouple. A recalculation by the present author from the measured final temperature and total output, together with the calculated power input in the length from the point of initial pressure rise, gave the enthalpy and mean temperature at this point. For the high-compression screw this indicated a temperature between 105°C and 110°C for LDPE in the conditions of the experiment, compared with the nominal crystalline melting point of approximately 117°C. This suggests that in this case the point of initial pressure rise was a good indication of the 'gel point' since partly-solid particles in suspension in a molten matrix might have an average temperature below the nominal melting temperature, but would behave as a fluid and be capable of generating hydrodynamic pressure. Experiments made with thermocouples attached to the screw and immersed in the channel flow have been reported by Marshall, Klein and Uhl (1965) and Barnett *et al.* (1966). Diagrams of temperature against position along the screw reproduced from these authors by Tadmor and Klein (1970) show: (i) the existence and nature of time-fluctuations of temperature at a point; (ii) the variation in temperature across the channel width; (iii) the tendency for fluctuations and variations to increase with screw speed; and (iv) the movement of the region of fluctuations towards the die with increase of speed. The implications for the melting process (Chapter 7) and homogeneity at the die (section 11.1) will be considered later, but they demonstrate that simple measurements of temperature are unreliable in determining the point at which pressure begins to rise. Practical experience confirms the findings of Weeks and Allen (1962) that this point moves back, i.e. towards the feed end, with increasing pressure. Calculations based on the Tadmor melting model reported in Chapter 7 (Figs 7.23 and 7.31(b)) predict substantial pressure rise within the melting section, giving a smaller pressure gradient dP/dz and greater output Q in the melt pumping section for a given die pressure. As discussed on p. 275, this effect is likely to be small, except with deep screws and high die pressures, so that output based on length Z from the point where the channel is effectively filled with melt should not be unduly conservative. The Tadmor melting model (Chapter 7) predicts the position at which melting of

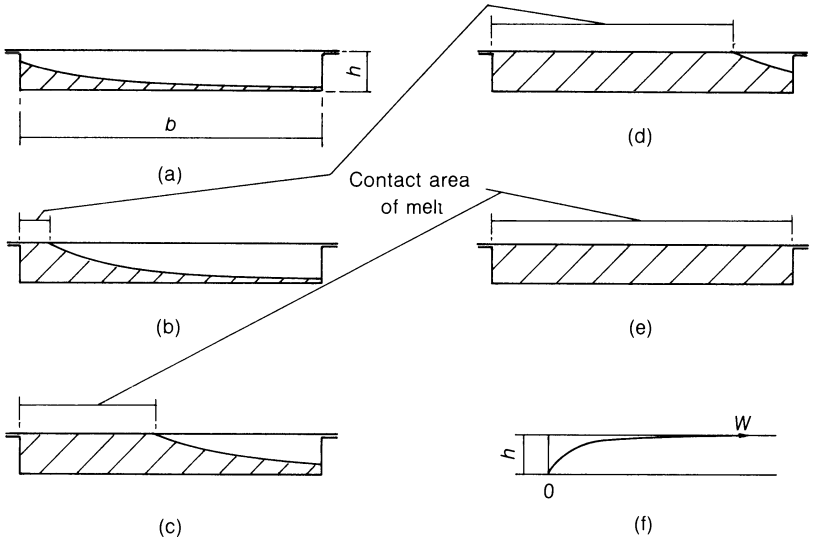


Figure 6.25 Melt cross-section of partially filled channels.

the solid bed should be complete, and this seems the best basis for effective melt length Z until theory or experiment can predict the point at which the solid bed will break up.

The pumping rate of partially filled screws has been mentioned in connection with pressure profiles (p. 145) and venting (p. 162); various situations are shown diagrammatically in Fig. 6.25. If the channel is filled to a very small extent as in Fig. 6.25(a), the melt will form a thin film over the screw surface and rotate without touching the barrel and thus without any forces tending to move it along the screw. Any material which adheres to the barrel or is trapped in the flight clearance will tend to be collected on the leading face of the screw flight (Fig. 6.25(b)) by the transverse movement represented by velocity component U (equation (6.5)). The material represented by the shaded area will be subjected to a shear force at the barrel, opposed by an equilibrium force on the much larger surface in contact with the screw; the shear stress and hence shear rate at the barrel will thus be much higher than at the screw, resulting in a velocity gradient as in Fig. 6.25(f). The drag flow will be given by a modification of equation (6.8):

$$Q_D = \int_0^h wx\,dy \tag{6.65}$$

but in this case both w and x are nonlinear functions of y, so $Q_D \ll Wbh/2$. As the degree of filling increases through the situation represented by Fig. 6.25(c), the area in contact with the barrel will increase faster than both the volume of melt, represented by the shaded area, and the area in contact with the screw, so that the shear stresses and shear rates tend to become more

nearly equal and the 'pumping efficiency' increases. When the channel is nearly filled, as in Fig. 6.25(d), the shear conditions and pumping efficiency will be similar to those of the filled channel, as in Fig. 6.25(e), and a nearly filled channel therefore may be expected to operate similarly to one completely filled, except that evidently the pressure must remain zero, otherwise the channel would fill. However, the nonlinear increase in pumping rate with the degree of channel filling brings the possibility that a slight increase in feed rate to the screw section may cause a disproportionate increase in its pumping rate, which then pumps the section empty, reducing the pumping rate until the feed again causes an increase in the degree of filling. This is believed to be the cause of the output instability known as **surging** (section 11.2) which is frequently encountered with the second section of conventional vented screws (section 6.5). It is analogous to the classical surging due to the stalling of the inlet stages of turbocompressors.

6.7 PSEUDOPLASTIC FLOW

On p. 143 it was mentioned that drag flow is independent of viscosity and therefore if screw speed is increased, this element of output will be unaffected by pseudoplastic behaviour. However, increased speed entails an increase in shear rates and reduction of viscosity of a pseudoplastic melt; this in turn will increase the back flow due to pressure represented by the last term of equation (6.15). Therefore, as speed increases, the slope of the output/pressure line will increase in contrast to the constant slope for a Newtonian fluid shown in Fig. 6.15. It has been shown in Fig. 6.6 that, except in the case of drag flow when $Q/Wbh = 1/2$, the velocity profile over the depth of the screw channel is nonlinear, and since $\dot{\gamma} = \mathrm{d}w/\mathrm{d}y$ (equation (3.4)) the shear rate varies with position, its value depending on the magnitudes of both drag and pressure flow. In appendix B.1, the downstream velocity w at a point y from the root of the screw channel is given as:

$$w = \frac{Wy}{h} + \frac{(y^2 - yh)}{2\eta} \cdot \frac{\mathrm{d}P}{\mathrm{d}z} \tag{B.8}$$

Then the shear rate at this point:

$$\dot{\gamma}_y = \frac{\mathrm{d}w}{\mathrm{d}y} = \frac{W}{h} + \frac{(2y - h)}{2\eta} \cdot \frac{\mathrm{d}P}{\mathrm{d}z} \tag{6.66}$$

But by rearrangement of equation (6.16):

$$\frac{\mathrm{d}P}{\mathrm{d}z} = \left(\frac{1}{2} - \frac{Q}{Wbh}\right) \frac{12\eta W}{h^2} \tag{6.42}$$

Substituting in equation (B.8):

$$w = \frac{Wy}{h} + \frac{6W}{h^2}\left(\frac{1}{2} - \frac{Q}{Wbh}\right)(y^2 - yh) \tag{6.67}$$

Substituting in equation (6.66) gives:

$$\dot{\gamma}_y = \frac{\mathrm{d}w}{\mathrm{d}y} = \frac{W}{h} + (2y - h)\left(\frac{1}{2} - \frac{Q}{Wbh}\right)\frac{6W}{h^2}$$

$$= \frac{W}{h} + \frac{W}{h}\left(\frac{12y}{h} - 6\right)\left(\frac{1}{2} - \frac{Q}{Wbh}\right) \tag{6.68}$$

At the barrel surface, when $y = h$:

$$\dot{\gamma}_h = \frac{\mathrm{d}W}{\mathrm{d}y} = \frac{W}{h}\left[1 + 6\left(\frac{1}{2} - \frac{Q}{Wbh}\right)\right]$$

$$= \frac{W}{h}\left(4 - \frac{6Q}{Wbh}\right) \tag{6.69}$$

This is valid for constant viscosity, i.e. isothermal Newtonian flow (assumptions 7 and 8 in section 6.2.2), but as shown in appendix B.1, for a non-Newtonian fluid, in which viscosity η is a function of shear rate, viscosity will vary across the channel depth and will be a function of Q/Wbh, i.e. a function of the ratio of pressure flow to drag flow (equation (6.68)). Thus the integration of the Navier–Stokes equation (B.1) becomes complex, precluding an analytical solution such as equation (6.15) which clearly indicates the effects of operational variables. However, an approximate method which takes account of the major effect on viscosity of shear rate (e.g due to changes in speed or channel depth) and the change in shear rate with increasing back pressure, uses equation (6.69) to determine the shear rate at which viscosity is taken for insertion in the flow equation. It does not include the effect of changes in viscosity on the shape of the velocity profile, i.e. the distortion of the curves in Fig. 6.6 (see also Fig. 4.1). The method is first to calculate the value of Q/Wbh for a known condition of either output or pressure, and hence the apparent wall shear rate given by equation (6.69). The intercept at this shear rate on the curve of viscosity against shear rate for the polymer in question at the appropriate melt temperature then gives the viscosity to be used in the flow equation (6.15) or (6.20). This enables $\mathrm{d}P/\mathrm{d}z$ or P to be calculated for the assumed Q or vice versa, with little more difficulty than for the Newtonian case, except that it must be repeated for each value of Q or P.

The implications of equation (6.69) for pressure profiles and output/pressure characteristics will now be examined briefly. When $Q/Wbh = 1/2$, equation (6.69) reduces to $\mathrm{d}W/\mathrm{d}y = W/h$, consistent with Fig. 6.6(d), and the second term of equation (6.15) disappears, giving an output independent of viscosity, as for the Newtonian case. For a constant-depth screw, consider first the condition at which the viscosity of two fluids, one Newtonian and the other

pseudoplastic, is equal at the drag flow shear rate, given by W/h. If back pressures are now applied, such that output Q and Q/Wbh are decreased by the same amount for each fluid, then by Fig. 6.6 and equation (6.69), wall shear rate $\dot{\gamma}_h$ will be increased and the viscosity η of the pseudoplastic will be decreased, whereas viscosity of the Newtonian fluid remains constant. Then, by equation (6.15) and compared with the Newtonian fluid at the same output Q and Q/Wbh, Q_P must be the same, but the pressure gradient dP/dz decreased in proportion to the viscosity. Since the channel depth h is constant, dP/dz remains constant along the length, so that Fig. 6.9 remains valid, but with smaller pressure gradient and final pressure P for a given value of Q/Wbh. On the output/pressure diagram a given value of output Q and Q/Wbh will occur at a lower pressure than for the Newtonian fluid, i.e. a horizontal shift towards the origin. If the comparison is made on the basis of equal back pressures, then equation (6.15) shows that the lower viscosity of the pseudoplastic fluid implies a lower output, i.e. a vertically downward shift on the diagram of Q against P. Thus in Fig. 6.26 the output line for the pseudoplastic lies below that for a Newtonian fluid. Note that since viscosity is nonlinear with shear rate and pressure gradient, the Q/P characteristic for a pseudoplastic fluid is no longer a straight line; the Newtonian line is tangential to this curve at $P = 0$ if viscosities of the two fluids are equal at shear rates near to that for drag flow, i.e. $\dot{\gamma}_h = W/h$.

For screws of varying depth, e.g. stepped or tapered screws, the above trends will also be observed, but also the variation of shear rate and viscosity along the screw will cause additional changes in pressure gradient to those shown in Figs 6.10 and 6.11. By differentiating equation (6.69) with respect to channel

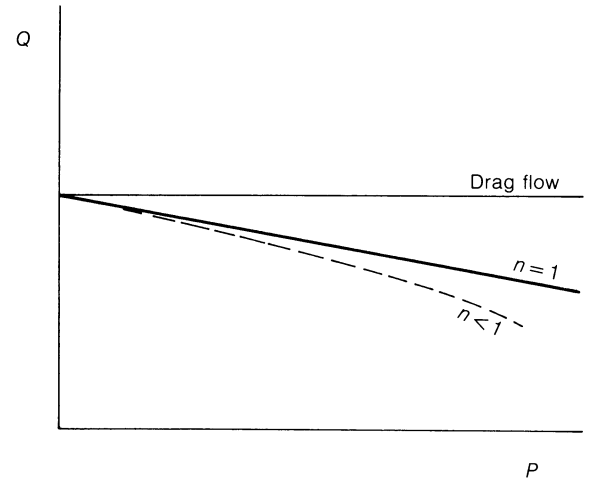


Figure 6.26 Effect of pseudoplasticity on output/pressure line. —— Newtonian; ---- pseudoplastic.

depth h:

$$\frac{d\dot{\gamma}_h}{dh} = \frac{W}{h^2}\left(\frac{12Q}{Wbh} - 4\right) \tag{6.70}$$

This shows that at constant output (as at various positions along the same screw), the wall shear rate increases as the depth h decreases when $Q/Wbh < 1/3$ i.e. the same condition as shown on p. 149 for the point of inflexion in the longitudinal pressure gradient. This is shown by the horizontal lines in Table 6.1; for instance in a 4:1 stepped screw ($h_1/h_2 = 4.0$) operating at drag flow in the metering section, the wall shear rate increases from 0.81 in the first section to 1.00 in the metering section. In a 5:1 tapered screw ($h_1/h_2 = 5.0$) operating at $Q/Wbh_2 = 0.2$, the wall shear rate increases progressively from 0.75 at the gel point to 2.80 at the end. As shown for the parallel screw, increasing shear rate gives decreasing viscosity and decreasing pressure gradient compared with a Newtonian fluid, therefore a horizontal line on Table 6.1 shows that the curvature of the upper pressure profiles in Figs 6.10 and 6.11 will be decreased and a smaller proportion of the total pressure will be generated in the shallower sections. At values of $Q/Wbh > 1/3$, i.e. to the right of the heavy line in Table 6.1, the wall shear rate decreases as depth h decreases, so that viscosity and pressure gradient will increase compared with the Newtonian fluid. These changes to the longitudinal pressure gradient are shown qualitatively in Fig. 6.27 for comparison with Fig. 6.11 for a tapered screw. The actual values of pressure P and gradient dP/dz at a point will depend on the value of shear rate at which Newtonian and pseudoplastic viscosities are assumed equal.

A vertical line on Table 6.1 shows the variation in shear rate with back pressure at a given point within the length of the screw, e.g. for a 3:1 screw, the wall shear rate at the gel point only varies from 1.33 to $0.93W/h_2$ over the whole useful range of back pressures and Q/Wbh. In fact, it is only at low values of

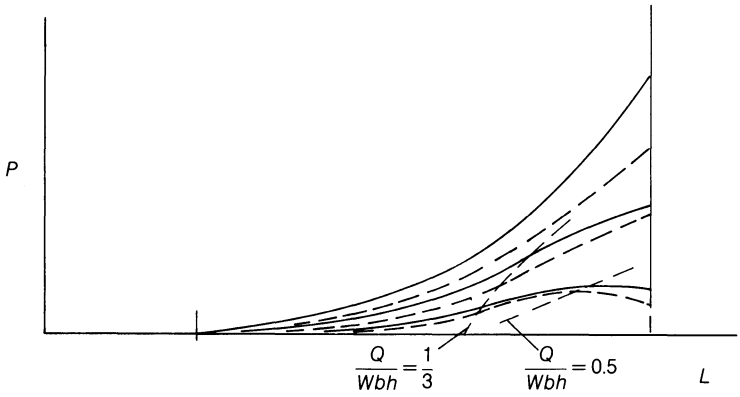


Figure 6.27 Pressure gradients in pseudoplastic flow.
—— $n = 1$; --- $n < 1$.

Table 6.1 Wall shear rate from equation (6.69) vs dimensionless output for screws of various tapers h_1/h_2, expressed as a ratio of the shear rate at the end of the screw in drag flow W/h_2

$\frac{Q}{Wbh_2}$	h_1/h_2 5.0	4.5	4.0	3.5	3.0	2.5	2.0	1.5	1.0
0	0.80	0.89	1.00	1.14	1.33	1.60	2.00	2.67	4.00
0.1	0.78	0.86	0.96	1.09	1.27	1.50	1.85	2.40	3.40
0.2	0.75	0.83	0.92	1.04	1.20	1.41	1.70	2.13	2.80
0.3	0.73	0.80	0.89	1.00	1.13	1.31	1.55	1.87	2.20
0.4	0.70	0.77	0.85	0.95	1.07	1.22	1.40	1.60	1.60
0.5	0.68	0.74	0.81	0.90	1.00	1.12	1.25	1.33	1.00
0.6	0.66	0.71	0.77	0.85	0.93	1.02	1.10	1.07	0.40

Decreasing back pressure

Distance along tapered screw

Q/Wbh_2 and near the end of the screw (when pressure gradients will be high) that the wall shear rates differ markedly from those in drag flow. These are Newtonian shear rates, but the modest departure from drag flow values implies that they will also not differ greatly from those in pseudoplastic flow, making the foregoing approximation for viscosity reasonable in most instances.

In estimating the performance of a varying-depth screw at a given speed and back pressure, a reasonable approximation is to take a viscosity which is an arithmetic average of those equivalent to the range of wall shear rates given by equation (6.69). However, at low back pressures, when $Q/Wbh_2 > 1/3$, the maximum shear rate is no longer at the end of the screw, and evidently it would be more correct to take a viscosity which is an average of those corresponding to the maximum and minimum shear rates rather than shear rates at the two ends of the screw. A more accurate method would be to treat the screw as composed of a number of separate sections, each of constant shear rate and viscosity, and combine them by use of equations (6.60) and (6.61). In the case of a stepped screw, this reduces to using equations (6.38), (6.39), (6.40) and (6.41) with different values of viscosity in the first two equations. The viscosity to be used in the die equation (6.53) must also be based on the shear rate in the die, e.g. equation (3.24).

When the screw is considered in combination with a die of fixed geometry, the Q–P relationship for the latter with a pseudoplastic fluid must be included. As shown in section 3.1, if the rheological equation is approximated by a power law:

$$\tau \propto \dot{\gamma}^n \tag{3.6}$$

$$\eta = \frac{\tau}{\dot{\gamma}} \propto \dot{\gamma}^{n-1} \tag{3.7}$$

But in the die:

$$\dot{\gamma}_w \propto Q$$

e.g. for a circular capillary (Table 3.1):

$$\dot{\gamma}_w = \frac{3n+1}{n} \cdot \frac{Q}{\pi R^3}$$

Then substituting in equation (3.7):

$$\eta \propto Q^{n-1} \tag{6.71}$$

Substituting equation (6.71) in (6.53) gives:

$$Q \propto \frac{KP}{Q^{n-1}} \tag{6.72}$$

or:

$$Q^n \propto KP \tag{6.73}$$

where $n < 1$. This is a concave upward curve compared with $Q \propto KP$ for a Newtonian fluid ($n = 1$) in Fig. 6.17. Then, the Newtonian screw and die characteristic equations (6.15) and (6.53) must be replaced by Fig. 6.26 and equation (6.73), respectively, and Fig. 6.18 is modified to Fig. 6.28 and the operating point moves from A to A'.

In short, the effects of a pseudoplastic polymer melt are threefold. First, the drop in output due to pressure tends to be greater than for a Newtonian fluid, especially at high screw speeds and/or back pressures. Second, the shapes of the longitudinal pressure profiles are modified. Third, in combination with a die, at a given screw speed the output will be little changed but the die pressure will be less and increase at a slower rate with output (screw speed) than for a Newtonian fluid.

The foregoing assumes isothermal conditions are maintained; the effects of changing temperatures, some of which are implicit in changing shear rates, are considered in the next section. The effects of both pseudoplastic and non-isothermal conditions on power consumption and heat generation are dealt with in Chapter 8.

This discussion has treated viscosity as a separate variable, dependent on Newtonian shear rate. Fenner (1970) has compared the Newtonian output/pressure characteristic with those for power-law pseudoplastic fluids. The latter show the expected increase in the pressure dependence, especially for high pseudoplasticity (low values of n) leading to reduced total output at a given pressure and lower maximum pressure (at zero output). In the one-dimensional case, the viscosity is taken as a function of the downstream shear rate only; in the two-dimensional case, the viscosity is dependent on the resultant shear rate including cross-channel velocities (Fig. 6.8). As Fenner points out, the differences in Q/Wbh for the two cases are generally small (less than 0.025) except near the drag flow condition (with $n = 0.25$, the difference in

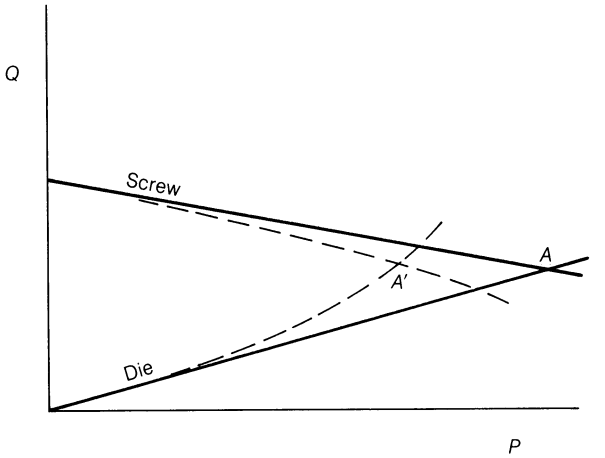


Figure 6.28 Operating point for pseudoplastic flow. — $n = 1$; - - - $n < 1$.

Q/Wbh is approximately 0.07). Comparison with his Fig. 4.1 shows that the viscosity corresponding to the Newtonian shear rate underestimates the departure from the Newtonian Q–P diagram at low pressures, but overestimates it at high pressures.

In addition to pseudoplasticity, real polymer melts may also be time-dependent, which may be evident as a delay in responses at start-up and speed changes, but in steady-state extrusion such effects are likely to masked by those due to heat capacities and mechanical inertia. In the steady state, viscoelastic effects will only be apparent in longitudinal retraction and lateral swelling from the die.

6.8 NON-ISOTHERMAL FLOW

Firstly, variations in melt density due to longitudinal changes of mean temperature will modify equation (6.60) such that mass flow, rather than volumetric flow, is constant; apart from this, the drag flow element is independent of material properties and hence of temperature. It must be remembered that, as discussed in section 8.2, the temperature of the polymer melt is not the same as the set temperatures on the heater controls, even when steady conditions have been attained; the melt will generally be at a lower temperature except when severe cooling is in operation. As will be seen in section 8.4, except at drag flow, the variations in shear rate through the channel depth will give rise to non-uniform shear heating. This, coupled with temperature variations 'inherited' from earlier in the screw, will lead to radial temperature variations in the channel–usually significantly higher temperature near the barrel wall. This will be exaggerated by intentional

heating from the barrel. The consequent changes in viscosity from the isothermal values will further modify the velocity distribution – see section 4.3 for these effects in a simple capillary. It is shown in section 8.4 that radial conduction in the polymer will only slowly reduce these temperature variations, but will be assisted by mass transfer through the transverse circulation (Fig. 6.7). The effect of both viscous heating and conduction from the barrel will thus be to reduce viscosity and hence further reduce output at a given pressure, and this effect will increase rapidly at lower values of Q/Wbh, i.e. the output/pressure diagram with heating a Newtonian fluid will resemble that in Fig. 6.26 for an isothermal pseudoplastic. With a pseudoplastic melt, heating will further lower the output line and accentuate its curvature.

However, the output is represented by the net area under the velocity distribution, and Fig. 6.6 shows that even at drag flow condition ($Q/Wbh = 1/2$) nearly half the output (44%) is accounted for by the 25% of channel depth nearest the barrel. Evidently when back pressure is applied this percentage is increased, and more so when pseudoplasticity and viscous heating are taken into account, so that the bulk average temperature will be higher than indicated by the radial temperature distribution. This will be returned to in considering heat flows in section 8.4. An extreme case of radial temperature gradients occurs with screw cooling (section 9.1) with an effect resembling a decrease of channel depth and which is not necessarily reversible.

Longitudinal temperature gradients will reduce the viscosity at regions of higher temperature (generally nearer the die) so further reducing the longitudinal pressure gradient in these regions (irrespective of the value of Q/Wbh, since temperature has a direct effect on viscosity). These changes in gradient will lead to changes in pressure profiles similar to the upper left-hand portion of Fig. 6.27.

The reduction of viscosity due to temperature increase in the flight clearance will only affect the pressure term, so that the effect on leakage flow will only be significant with large clearances (worn screws).

The radial temperature gradients in the melt channel make reliable measurement difficult (see pp. 246 and 358) and the necessary instruments are not usually available to the industrial operator. The best approximation for output/pressure estimation is therefore the barrel temperature close to the inner surface, as for power estimation (p. 232). An average viscosity for use in the isothermal flow equation must be estimated from these temperatures, corresponding to the longitudinal temperature variation, and in the case of tapered screws may need to be weighted to take account of the variation of channel depth. As with pseudoplastic behaviour, a closer approximation can be sought by assuming a series of sections, each at uniform temperature, and summing the pressure changes; the validity of this depends on the accuracy of available data on the actual melt temperatures.

Solids conveying and melting in single-screw extruders

7

J. A. Covas

7.1 THE RELEVANCE OF SOLIDS CONVEYING AND MELTING

An extruder is not merely a melt pumping device, with the characteristics and capacity discussed in Chapter 6. Optimizing the pumping capacity of an extruder may be useless if the extrudate becomes incompletely melted or unsteady. Thus, the solids conveying and melting performance is crucial in determining the global behaviour of the machine.

The flow of powdery and granular solids is affected by the geometry of the particles, by the friction between particles and between the particles and the metal surfaces, and by additional parameters such as moisture. There are three processes of solids conveying which are directly relevant to the performance of the extruder. These are: gravity flow through the hopper, filling of the screw channel from the feed throat; and transport along the screw.

During gravity flow a pressure profile develops in the bulk of the material contained in the hopper. Fluctuations of the pressure at the base of the hopper (caused by changes in the height of the column of solids or by difficulties in the flow) lead to variations in extrusion rate, power consumption and melt temperature. The most serious problem with hoppers is the partial or total interruption of flow due to the development of conditions of significant interparticle friction. This will be dealt with later in this chapter. To overcome these difficulties, mechanical solutions such as vibration of the hopper, gentle agitation of the feed and forced feed (use of a screw to convey the granules and generate pressure) have been used. The discharge capacity of the hopper also determines the maximum possible extruder throughput.

Filling of the screw may also affect the performance of the process. The feed throat must have good cooling capacity to avoid the granules sticking to the walls, which would affect the flow stability. If the feed pocket liner is not

suitable for the material being processed, this may be forced back into the feed throat, hindering the inflow of fresh material. Usually, the feed opening is offset or tangential to the screw. In the case of rubber extrusion, the presence of coarse agglomerates may block the feed throat. Consequently, the opening is frequently made tangential to the downgoing side of the screw, whereas on the upcoming side the screw cuts into the descending column of material. Experiments (Hayward, 1977) with conventional and modified feed pocket liners (Fig. 7.1 and Table 7.1) showed that there was little difference between

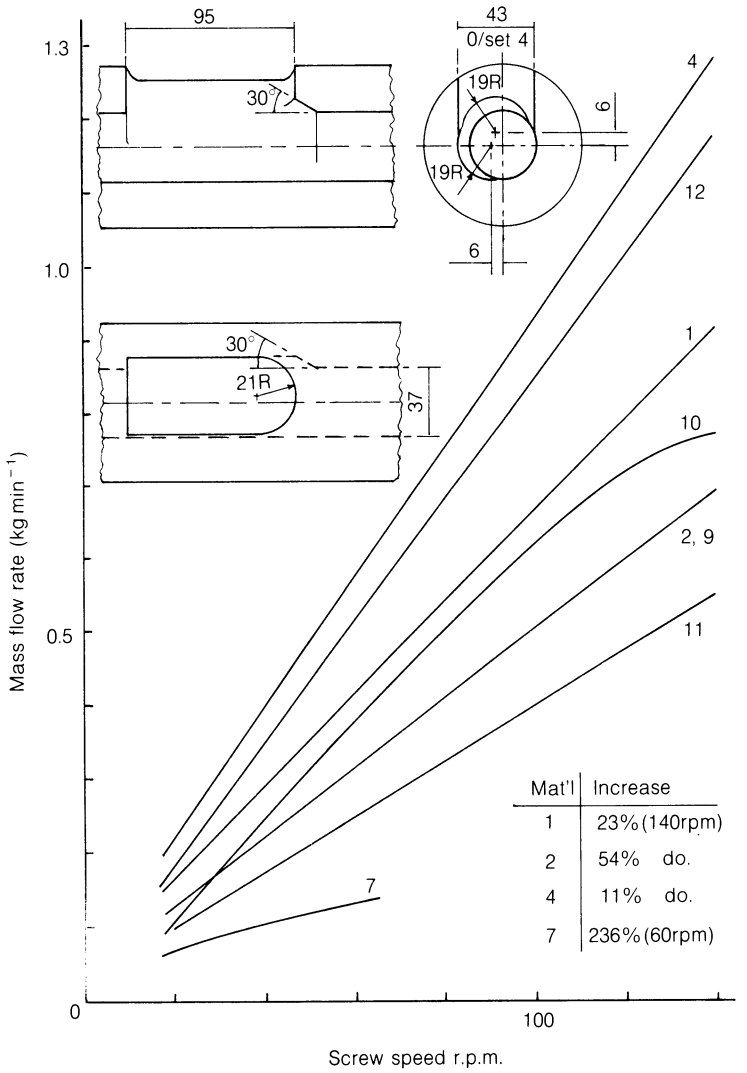


Figure 7.1 Performance of a modified feed pocket liner.

Table 7.1 Materials used in feeding trials

No.	*Material*	*Hardness*	*Shape*	*Size*	*Size distribution*
1	LDPE	Soft	Cylindrical	2 mm diameter × 3 mm long	Very even
2	LDPE regrind	Soft	Rough lumps and flakes	4 mm max. dimension	Very uneven
3	HDPE	Hard	Lenticular	4 mm diameter × 3 mm long	Very even
4	PS	Hard	Rhombic	1.5 mm × 2 mm × 3 mm	Very even
5	LDPE	Soft	Spherical-ended cylinders	5 mm diameter × 4 mm long	Very even
6	PS	Hard	Cylindrical	2 mm diameter approx. 4 mm long	Even diameter variable length
7	Synthetic rubber	Soft elastic	Large curled strips	Not specific 20 mm × 8 mm × 4 mm	Very uneven
8	Synthetic rubber	Soft elastic	Roughly tetrahedral chips	Not specific 4 mm height 9 mm × 9 mm base	Uneven
9	Synthetic rubber	Soft elastic	Roughly cubic/ cylindrical lumps	6 mm × 7 mm × 9 mm	Uneven
10	Rubber granules	Very soft elastic	Roughly tetrahedral lumps	5 mm height 9 mm × 9 mm base	Uneven
11	Rubber crumb	Soft	Very small particles, almost a powder	–	Variable sized particles
12	PVC powder	–	Powder	–	Even sized particles

the flow rates induced by the two designs when working with free-flowing solids. However, when working with materials with poor flow characteristics, the modified design showed appreciably higher and more consistent flow.

In the screw, the granules are soon compacted into a solid plug which is conveyed forward by the frictional forces developed at the inner barrel wall, whereas the friction on the screw is the retarding force. It is important to ensure that the friction coefficient at the barrel wall is sufficiently greater than that at the screw surfaces. Then, occasional variations in the friction characteristics of the material being processed should not significantly affect the stability of the system. One often-used method to obtain high barrel friction is to machine longitudinal or helicoidal grooves.

Generally, the importance of the solids conveying zone depends mostly on the operating conditions selected. When the operation is controlled by the melt conveying capacity, solids conveying is limited to the first few turns of the screw. This results in a small pressure rise. If the barrel is cooled efficiently, a long solids conveying zone will develop relatively large pressures, increasing the delivery capacity of the extruder (Broyer and Tadmor, 1972).

The melting mechanisms developed in single-screw extrusion may vary from one material to another and, for the same material, with different operating conditions. In all of them the solid bed, more or less surrounded by melted material, may break prematurely, originating fluctuations in pressure. Recognition of the relevance of this phenomenon has led to the development of barrier screws that separate the melt pool from the solid bed, thus ensuring the integrity of the latter. For a given screw geometry and specific operating conditions, the completion of the melting process requires a well-defined helicoidal length of the screw channel. If this is too long, no true melt conveying will take place (thus compromising both the pressure generation and the distributive mixing processes that occur simultaneously) and the screw is likely to deliver largely unmolten and poorly mixed polymer. Under these conditions, melting limits the throughput of the process and may require the adoption of specific operational strategies.

The importance of solids conveying and melting, and their interaction, in the performance and stability of the process has been demonstrated experimentally. One prerequisite for stability is the satisfaction of the condition:

$$Q_s \geq Q_m \geq Q_p \tag{7.1}$$

where Q_s, Q_m and Q_p are the capacities of the solids conveying, melting and pumping functional zones, respectively. The instabilities are usually distinguished according to the frequency with which they come about. They can be periodic or random, and may occur at frequencies higher than, equal to or lower than the screw rotation frequency. Instabilities with frequencies higher than that corresponding to the screw rotation, such as sharkskin or melt fracture, are associated with die flow conditions (Chapter 5). The major cause of instabilities at the screw frequency is attributed to the transversal pressure gradient in the screw pumping section. However, a small pressure change is additionally induced by the cyclic interruption of the polymer intake from the hopper, as the screw flight passes by the feed opening. According to Fenner, Cox and Isherwood (1979), the solid bed breaks up upon the acceleration of the bed, causing pressure surging at frequencies five to ten times lower than the frequency of screw rotation. Furthermore, solid bed break-up produces heterogeneous extrudates with large temperature distributions (Sakai, 1990). The escape of air entrapped in the solid bed, and the uneven solid bed surface are also important sources of unstable melt flow (Becker *et al.*, 1990; 1991). The latter changes the effective hydrodynamic dimensions of the space available to the melt flow. Instabilities are generated as well when the taper of the compression zone

causes the solid bed to reshape across the screw channel, disrupting the melting process (Bigg, 1987). Fluctuations in pressure or flow rate can likewise be caused by temperature fluctuations, which are associated with the performance of the temperature control system or, at very low frequencies, with changes in the ambient temperature. Gitschner and Lutterback (1984) correlated the variations in pressure, induced by the on and off phases of the barrel heating system, with throughput fluctuations. Finally, instabilities with a random character are usually associated with the irregular feeding conditions mentioned above. Similarly, any variation in the location at which melting is initiated affects the pressure build-up profile (Bigg, 1987).

Cheng (1990) studied the effect of the geometries of the granules on the extrusion rate and mixing quality. Since the shape of the pellets is determined both by the available pelletizing system and by the operating conditions, this is an important issue for compounders. Cold cutting systems, such as strand cutting, usually produce a more uniform geometry than hot face cutting systems, such as air/water pelletizers. The shapes can vary according to the type of cooling, cutting speed, die-hole geometry and type of material. It was found that the influence of the pellet size increased with the screw speed, the output rate varying up to 16%. PE pellets (having higher compressibility) were less dependent on particulate size than the more rigid PP pellets. Small particulates (relative to the depth of the screw channel) presented higher solids conveying and melting rates, but the effect on the output rate was also dependent on the screw design.

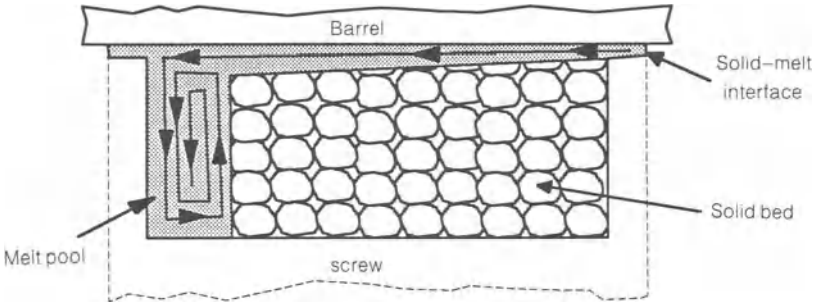
7.2 PHENOMENOLOGICAL DESCRIPTION OF SOLIDS CONVEYING AND MELTING

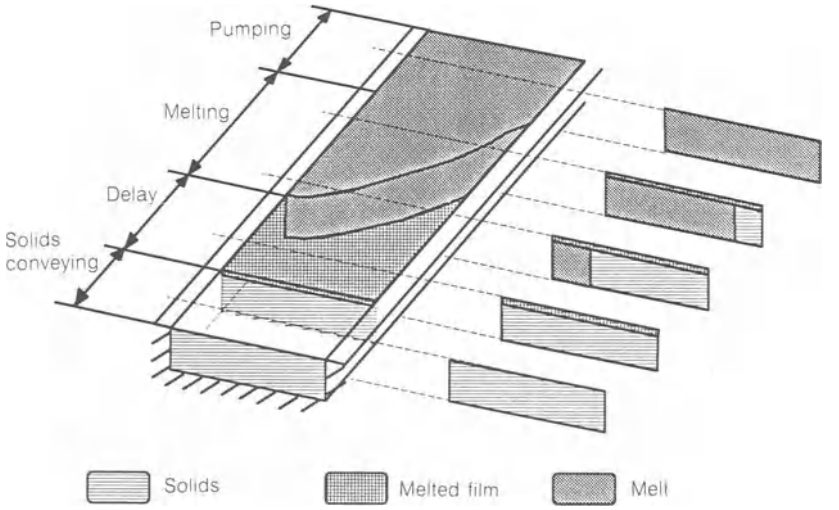
Since the 1960s extensive work has been carried out with the aim of thoroughly understanding polymer extrusion. Hundreds of papers and many books have been published, and several software packages for simulating the process are currently available. The initial attempts to describe the process theoretically were restricted to solids and melt conveying, as these can be studied starting from continuum mechanics considerations. However, understanding the melting mechanism, and thus being able to describe the plasticating process, required the development of specific experimental procedures. Maddock (1959) and Street (1961) devised a method of producing an 'instant picture' of the process, which instigated many more studies on extrusion. Upon reaching the steady state in the extrusion of a specific material, the rotation of the screw is interrupted, the system is chilled and the screw is extracted. Use of extruders with efficient cooling systems (barrels with circulating cooling media) is preferred. Some coloured pellets mixed with the granules produce, upon fusion, a notable pattern that corresponds to the movement of the material along the screw. The material helix is unwound or broken, depending on the

polymer rigidity, and cut transversally in several known locations along its length, in order to obtain a global view of the process.

The careful observation of many samples corresponding to the extrusion of several thermoplastics in different extruders, provided some general conclusions on the features of the process.

1. Three **functional zones**, corresponding to distinct material physical phases, can generally be identified. Initially, all the material remains solid; then the solid and melt phases coexist; finally, all the polymer appears to be melted. Usually, these zones occur in the feed, compression and metering zones of the screw, respectively. However, there is no direct correspondence between functional and geometrical zones, since the location of the first melt and the melting rate depend on the processing conditions, on the screw and die geometries, and on the thermophysical properties of the polymer.
2. While in the initial screw turns the polymer pellets are loose (and are lost during the screw extraction), they become compacted as they progress in the channel, resembling an elastic solid body. This zone can apparently be divided into two sub-zones. The first corresponds to a true **solids conveying** stage (i.e. only solid material can be detected), whereas the second develops a thin melt film in the interface at the top of the solids/inner barrel wall. It is known as the **delay zone** because, although a melt has already been created, the main fusion mechanism has not yet started (Kacir and Tadmor, 1972). Similar films of melted material can also appear near to the screw flights and root.
3. Figure 7.2 Represents a typical, although idealized, cross-section of the screw channel in the **melting zone**. The solid and the melted material are well segregated. The first accumulates in a well-compacted block, whereas the melt forms a pool encompassing the height of the channel. In the figure fusion is only taking place at the inner barrel wall, although in practice it may also occur (at a smaller rate) at the screw root and trailing flight. The film that separates the solids from the barrel has increasing thickness in the direction of the melt pool. This results from the relative velocity between the screw and the barrel, which forces back the melt towards the screw pushing flight. The traces created by the coloured pellets mixed with the original polymer show that the material in the melt pool follows a helicoidal path, similar to that represented in Figs 6.8(b) and 6.8(c).
4. As melting progresses, the melt pool width increases and that of the solid bed decreases. The solids fill the channel gap, except for the melted polymer film at the interface(s) with the metal wall(s). The solid granules are increasingly distorted and compacted. Often, the solid bed breaks prematurely, the fragments being surrounded by melted material.
5. Eventually, all the material melts. In the **melt conveying zone** the elements of fluid are propelled with the helicoidal pattern previously identified for the melt pool.


Barrel
Solid–melt interface
Solid bed
Melt pool
screw


Pumping
Melting
Delay
Solids conveying
Solids
Melted film
Melt

forces developed between the solids and the surrounding metal surfaces, they become compacted and warmer, due to the increasingly efficient heat transfer from the inner barrel wall. After a few screw turns the solids behave like a plug, which means that the velocity at any point of the channel varies only in the downchannel direction, z. Eventually, the material near the barrel wall reaches its melting point, thus initiating the delay zone. The exact location of this point depends on the relative magnitude of the mechanisms of heat conduction (linked to the temperature of the barrel) and of dissipation of mechanical energy into heat (which is a function of the friction forces). A thin melt film forms at the interface at the top of the solids/inner barrel wall. As this film is subjected to high shear rates, its thickness increases dramatically, due to the contribution of viscous dissipation. However, the corresponding gradual decrease of the shear rate will diminish the pace of the process. Subsequently, films of melted polymer may also develop near the three surfaces of the screw channel. Now, the role of friction is entirely replaced by a mechanism based upon viscous drag. The relative velocity between the solids and the barrel pushes the interfacial film towards the active screw flight. If the film thickness is smaller than the mechanical gap between the screw tip and the inner barrel wall, the film flows through the gap without creating a melt pool. The fusion mechanism depicted in Fig. 7.2 can only be initiated when the majority of the melt cannot cross the gap and has to accumulate near the pushing flight of the screw. This means that the film thickness must at least equal the value of the mechanical gap. In practice, it has been observed that the melting zone initiates when the film is five to seven times thicker than the gap.

During melting, the screw pushing flight scrapes off part of the melted film, which is deposited in a pool. Each fluid element will initiate a regular and well-defined helicoidal pattern, whose characteristics depend on the coordinates of the element in the channel when the movement started, as seen previously when studying melt conveying. The melt pool pushes the solid bed against the screw trailing flight. Melting takes place at the melt film/solid bed interface. Thus, as the film is dragged by the barrel surface to the melt pool, which forces the solids into a continuous rearrangement, the plug acquires a velocity component upwards, in the y direction, V_{py}, exposing more material for fusion. This fresh melt is immediately removed back, exposing more solid and continuing the mechanism. Therefore, V_{py} is a measure of the melting rate. This mechanism was evidenced experimentally (Covas and Gilbert, 1992) by taking advantage of the fact that degraded PVC, when exposed to ultraviolet radiation, fluoresces in the visible region, the fluorescence intensity (FI) being proportional to the degree of degradation. Figure 7.4 shows the variation of the FI of the solid bed, melt pool and their interface along the channel, for two operating conditions. Globally, the FI increases with increasing residence time. The solid bed exhibits the highest FI because, in the absence of relative movement between the solid particles, the stabilizer present in the formulation has limited efficiency. The smallest FI values were observed at the interface. Here, the

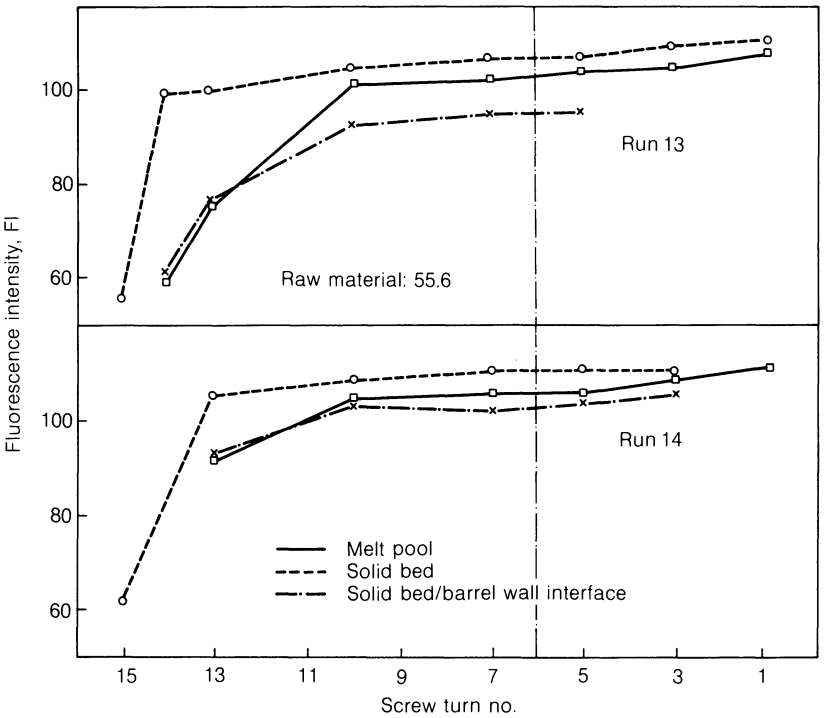


Figure 7.4 Fluorescence intensity (FI) of PVC along the length of an extruder, for two operating conditions (Covas and Gilbert, 1992).

material has just melted and the additives are quickly dispersed. The two curves are almost parallel. The FI of the melt pool is higher than that at the interface, as the material is continuously subjected to heat and shear.

The mechanism described will last, with the melt pool progressively occupying a larger percentage of the channel width, until the polymer has completely fused. However, as mentioned above, the local pressures and the shear forces acting on the solid bed may induce stresses that cause its premature rupture. The resulting fragments are soon suspended in the melt, influencing the melting and the pressure development. Also, unmelted fragments can accumulate in the screw channel, causing instabilities in the throughput of the extruder, one cause of *surging*. This problem can be minimized by creating the conditions to strengthen the solid bed, such as cooling the screw or reducing the melt pool velocity, thus decreasing the shear forces acting on the solid bed (Klein, 1972). However, the extruder output will be reduced. Melting in the compression zone is complicated by the rate of channel depth change. In a tapered channel the melting rate increases, as the relative surface area of the solid bed exposed to heat increases. However, since the decrease in cross-section forces the solid to reshape and grow in width, the solid bed width

generally decreases at a slower rate than in a constant depth channel, and an increase in the solid bed width may even be observed. Meanwhile, since the melt is confined to the smaller pool dimensions, it accelerates, causing more heat generation, i.e. higher melt temperatures. This phenomenon is particularly relevant to heat-sensitive polymers that require the use of screws with small compression ratios. If the compression zone is short and the variation of depth is too rapid, the rate of solids exposure for melting may be higher than the melting rate. The solids will fill most of the channel cross-section, preventing the melt pool flow in the downchannel direction. A cyclic process is then initiated: the resulting lower output at constant screw speed increases the rate of melting and, consequently, promotes the unplugging of the channel. The output recovers its previous value, but soon the channel will be plugged again. This severe surging affects product uniformity and quality (Klein, 1972). Rauwendaal (1990) quantified the maximum compression ratio and taper that avoid plugging in terms of the operating variables and material properties, and concluded that the use of large compression ratios and short compression zones is particularly dangerous.

As seen in the previous chapter, during melt conveying the melt continues the pattern initiated in the melt pool. The pitch and amplitude of the helicoidal movement are determined by the frequency of the screw rotation, by the resistance to flow created by the die and by the initial location of the element of fluid in the channel. Figure 7.5 depicts the path of a typical material element along the screw channel, as it cruises through successive functional zones. The initial straight line parallel to the sides of the channel acquires a vertical

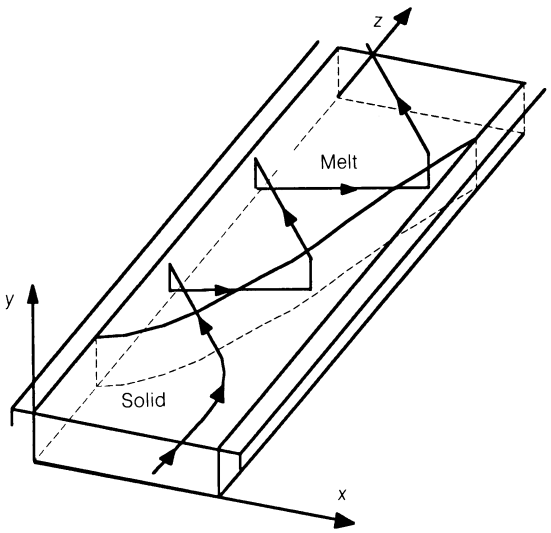


Figure 7.5 Flow pattern of a polymer fluid element along the screw channel.

component during transport in the melting zone. When the element reaches the solids/melt film interface it melts and moves towards the screw pushing flight. Upon incorporation in the melt pool, the material will go forward in the top portion of the channel and backward near the screw root, in accordance with the helicoidal pattern already referred to. The distance between each element of fluid and the side walls will be determined by the transverse streamlines (Fig. 6.7). The motion induces distributive mixing, but the process is not uniform, as the strain rates vary within each cross-section. The shear rates involved may cause significant viscous dissipation, especially when working with highly viscous materials. For example, it has been observed that the temperature of UPVC extrudates produced under a wide variety of processing conditions is always higher than the values set and, for the same temperature settings, the values attained are sensitive to changes in screw speed and die resistance (Covas and Gilbert, 1992).

Plasticating single-screw extrusion produces distinct processing histories in the various polymer elements, from the moment they are deposited in different screw channel coordinates in the solids conveying zone. Any pellet positioned near the inner barrel wall will soon melt and incorporate into the melt pool, where the flow pattern, together with an appreciable residence time, may favour acceptable distributive mixing. However, one pellet resting close to the screw root will be subjected to progressive heat and pressure, deforming significantly as it approaches the solids/melt film interface. When the granule finally melts, the global melting mechanism may be almost complete, and this new melt may not have sufficient residence time in the screw to ensure proper mixing with the adjacent material. This process characteristic is particularly adverse when processing heat-sensitive polymers. As discussed above for PVC compounds and as illustrated in Fig. 7.4, while the material remains solid relevant additives, such as heat stabilizers, are unable to penetrate the grains and to retard the degradation pace. As a result, not only does the average material degradation level increase along the screw length, but also the final solid bed may degrade significantly. Conversely, in counterrotating intermeshing twin-screw extruders, characterized by an average low shear level and a practically simultaneous fusion of the solids, there is no increase in the degradation level along the screws, once the material melts (Covas and Gilbert, 1988).

The melting sequence described is usually known as the **Maddock** or **Tadmor mechanism** (because the latter author developed the first – and still relevant – theoretical description of the process (Tadmor and Klein, 1970)). However, it is not unique. When studying the extrusion of polypropylene in large-diameter extruders (90 mm), Dekker (1976) observed a different melting mechanism, where the solid bed is entirely surrounded by melt (Fig. 7.6). As fusion progresses, the solid bed reduces both in width and thickness. Substantial axial pressure profiles were measured (about 3 MPa per screw turn). A third melting mechanism was initially reported by Menges and Klenk (1967) and later observed by several authors working with PVC compounds (see Covas and

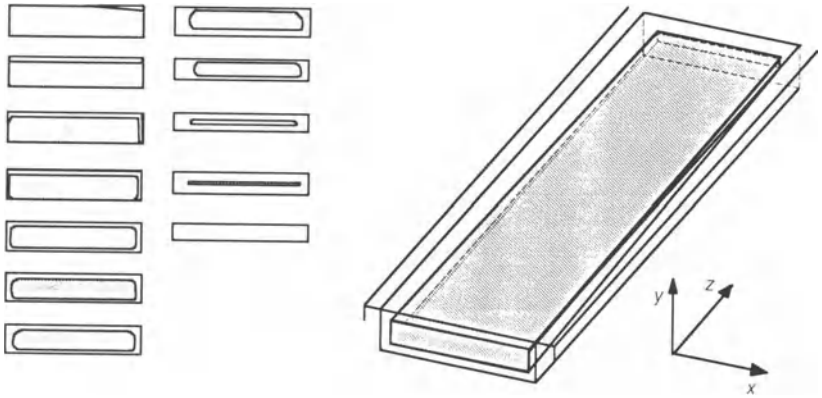


Figure 7.6 Melting mechanism observed by Dekker (1976).

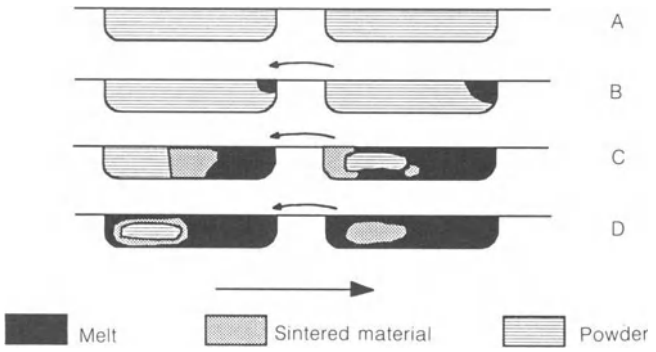


Figure 7.7 Melting sequence, with the melt pool developing near the screw trailing flight (Covas and Gilbert, 1992).

Gilbert, 1992). These materials are characterized by high viscosity and wall slippage. Pressures of 8 MPa per screw turn may be generated. As illustrated in Fig. 7.7, the melt pool accumulates near to the screw trailing flight. The process is preceded by a delay zone (A). The film flows backwards through the mechanical gap, pushing the solid bed against the active screw flight and accumulating as a pool (B). The plug flow originated by the wall slippage increases the effective gap flow capacity. Hence, despite the progressive increase of the film thickness, the melted material is able to flow backwards and feed the melt pool, which grows in width. The high pressures also promote an efficient heat transfer within the solid bed. As a consequence, some of the solid material is sintered (C). Under most operating conditions, the material near the screw tip is mostly melted (D). This mechanism is generally regarded as inefficient, requiring a significant portion of the screw to be completed, and inducing poor mixing. Figure 7.8 shows the melt pool and pressure

development along the screw for different screw speeds, during the extrusion of a dry-blend UPVC compound (Covas and Gilbert, 1992). The material is only fully melted near the screw tip, which means that there is little opportunity for distributive mixing. The rate of melting progression is apparently smaller in the compression zone, which is probably due to intraparticular fusion, along with interparticular fusion. The high shear levels present in the metering zone may account for the dramatic increase of the melting rate. Since slip depends mainly on the formulation and processing temperature, one can speculate whether it is possible to switch from this to the Tadmor mechanism, by changing the formulation or increasing the melt temperature. At high levels of temperature, Covas (1985) observed the presence of an additional melt pool formed near the screw pushing flight, the melting process being completed in the beginning of the metering zone. As a matter of fact, the processing history within the extruder is critical when extruding PVC compounds. The morphology of this polymer, consisting of a hierarchy of aggregates of small entities inside each grain, is progressively destroyed upon processing, giving rise to the so-called **gelation** mechanism. Since the degree of gelation is directly related to the physical and mechanical extrudate properties, it is important to understand the sequence of gelation and to determine the influence of the operating conditions on that mechanism. The gelation sequence is a consequence of the high shear rates in the melt film on the top of the solid bed and of the high local pressures generated. The first grains to melt, having their inner structure surviving the conducted heat, break open due to effects of shear and form a melt with the primary particles as the flow units. The material in the solid bed is

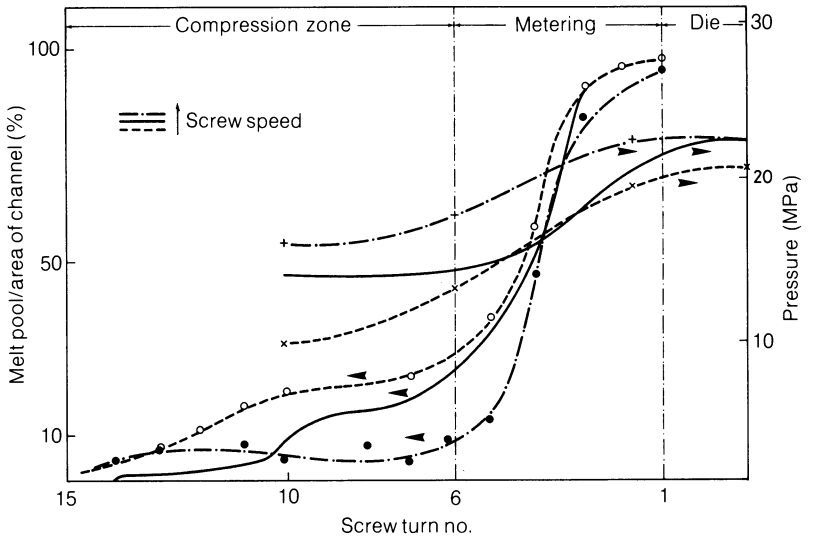


Figure 7.8 Development of pressure and fusion along the screw (melting sequence as depicted in Fig. 7.7) (Covas and Gilbert, 1992).

progressively compacted and deformed, its inner structure gradually melting. Upon arriving at the solid/film interface, the grains are initially elongated in the direction of flow, then their contours disappear and the material integrates into the film. In the melt pool the granular structure is progressively destroyed due to shear and heat but, within the usual processing conditions, the flow remains supermolecular, as some initial crystallinity of the material survives (Covas and Gilbert, 1992). This supermolecular flow accounts for some of the peculiar rheological characteristics of PVC compounds.

Lindt (1981) attributed the occurrence of the above mechanisms to the conditions that promote the melt flow in the channel's transversal direction. This flow depends on the interaction between the transversal circulation of polymer and the leakage flow through the gap. As the Tadmor, Dekker and Menges–Klenk mechanisms are sequentially considered, the effect of the pressure component of the flow through the gap influences the circulation pattern more decisively. While in the Tadmor mechanism closed circulation of flow around the solid bed predominates, the Menges–Klenk mechanism is determined by flow through the mechanical gap. Lindt (1976) also showed that the transversal force pushing the solid bed against the screw pushing flight decreases with increasing downchannel pressure gradient. Thus, for high-viscosity materials, which generate considerable pressure gradients, the transversal force may reverse its direction, promoting the occurrence of the Menges–Klenk mechanism.

Recent work has questioned the established ideas concerning fusion. Using extruders provided with transparent windows, Zhu and Chen (1991) were able to study the process on-line. The authors concluded that the melting process can be divided into various stages, where some of the conventional melting mechanisms can develop along the screw. Operating conditions such as screw speed, temperature profile, or the possibility of cooling the screw, were found to be significant. The work has yet to be extended to different polymers and equipment geometries.

The development of a particular melting mechanism influences the performance of the process, since it affects the length of the screw required for fusion, the residence time and strain distributions (thus mixing), the amplitude of surging and, eventually, the degree of polymer degradation. Wolf and White (1976) obtained experimental data of the residence time distribution (RTD) for liquid conveying, solids conveying and plasticating extrusion of polyethylene. The RTD function is a measure of the distribution of the residence time of particles within the system, providing some information on the degree of mixing in the direction of flow, and is influenced by the flow characteristics of the extruder. In the case of liquid conveying, they found that the results were in good agreement with the RTD functions derived by Pinto and Tadmor (1970), who assumed Newtonian isothermal flow on a unwound screw channel. The solids conveying process was close to plug flow. The RTD in the plasticating process was better represented by the Pinto–Tadmor model

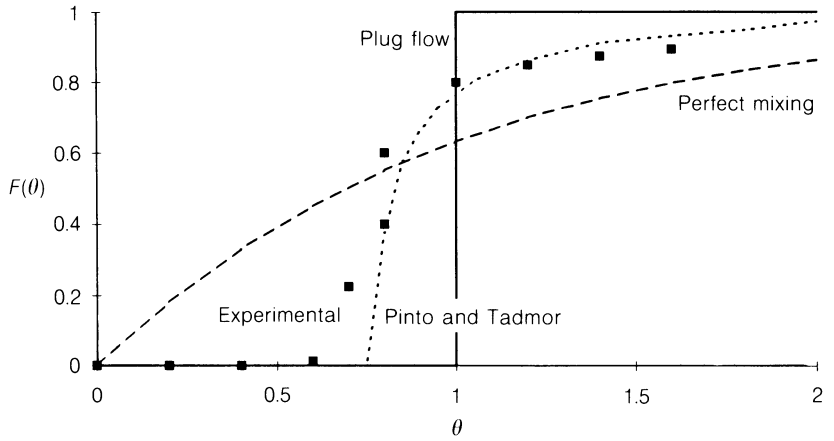


Figure 7.9 RTD curves of various mixing systems.

than by the usual perfect mixing and plug flow combinations. Thus, one may infer that melting influences the distribution function. The theoretical curves computed by Lidor and Tadmor (1976) for the plasticating process (adopting the Tadmor mechanism) are also in good qualitative agreement with the results of Wolf and White. Zemblowski and Sek (1981) studied the RTD for a wide range of operating conditions and concluded that, although the results of Wolf and White were valid, the RTD function could vary over a broad range between plug flow and perfect mixing. The above authors were probably working in conditions favourable to the occurrence of the Tadmor melting mechanism. Benkreira, Shales and Edwards (1992) observed experimentally that most of the mixing occurs while the Tadmor mechanism is developing, with little subsequent improvement. Increasing screw speed and lower barrel temperatures were found to improve the process. Covas (1991) obtained RTD data in the presence of the Menges–Klenk mechanism for a range of processing conditions. Increasing die resistance, temperature or screw rotation broadens the distribution, thus reflecting better axial dispersion. Curves with short tails were frequently obtained, probably due to high viscosities and extreme non-Newtonian behaviour, together with wall slippage, thus favouring plug flow and poor mixing. As shown in Fig. 7.9, which illustrates RTD curves for plug flow, perfect mixing, the Pinto–Tadmor model, and PVC extrusion, the distribution curves of PVC may exhibit an inflection point, which is usually associated with highly non-Newtonian flow and considerable values of back pressure.

7.3 THEORETICAL ANALYSIS

Little attention has been paid to solids conveying in comparison with the other functional zones. Solids conveying is usually a minor part of the plasticating

process, evolving in the first few screw turns and rarely controlling the machine output. Most analyses still follow the main assumption of Darnell and Mol (1953), pioneers of the solids conveying theory, who assumed that the solid pellets are compacted into a solid plug subjected to frictional forces at the barrel and screw surfaces. The model has been progressively improved – see reviews by Fenner (1977) and Amellal, Lafleur and Arpin (1990) – but its framework remains virtually unchanged. Recently, Fang, Chen, and Zhu (1991) computed three-dimensional velocity and stress profiles of the pellets in the first screw turns, before the generation of the solid plug. The loose pellets have little shear resistance and flow under the influence of small applied forces. Chung (1970) adopted a different approach to the problem, assuming that the elastic solid bed is conveyed forward by a viscous drag mechanism developed in the polymer melt films generated by friction on the surfaces of the plug.

The quantitative melting theory developed by Tadmor (Tadmor and Klein, 1970) was the foundation for subsequent adjustments and improvements. Initially, it was assumed that a film of constant thickness across the channel formed on top of a rigid solid bed moving at constant downchannel velocity. Later, the presence of a molten film near the screw surface was considered together with rigid or deformable solid beds (i.e. beds containing either freely deformable particles, or an agglomeration of solids without cohesion). In the most sophisticated models, the channel cross-section is divided into up to five independent zones, the behaviour of the solids or melt being described by the continuum balance equations. A number of reviews on the modelling of the melting process have been published (Fenner, 1977; Lindt, 1985; Amellal, Lafleur and Arpin, 1990). Lindt (1985) concluded that all the models give a reasonable estimate of the progression of fusion along the screw length. However, pressure development in the melting zone is much more sensitive to the assumptions of each model. While deformable bed models seriously underestimate the pressure, rigid bed models produce better results. Thus, Lindt suggested the application of a non-Newtonian analysis of the melt flow pattern, particularly cross-channel circulation, coupled to a rigid solid bed concept. This requires that, in addition to the melt pool and upper molten film, the lower film, in contact with the screw surface, is included in the model. The subject is still capturing the attention of researchers. Vincelette *et al.* (1989) modified the Tadmor model and computed the melting rate, considering changes in the solid bed velocity as a function of a solid bed acceleration parameter (SBAP), previously defined by Donovan (1971). Lee and Han (1990) modified the non-isothermal, non-Newtonian, five-zones model developed by Lindt and colleagues (Elbirli *et al.* 1984; Lindt and Elbirli, 1985), and introduced a concept of solid bed deformation based on force balances at the surfaces of the solid bed, and on the use of the solid bed modulus in bulk state. Later, the model was assessed experimentally (Han, Lee and Wheeler, 1990). Attempts have also been made to find analytical solutions to the problem (see Potente, 1991). For example, Rauwendaal (1991–92) derived

the exact analytical solution for the melting of a power-law fluid. Apparently, no available theory is yet able to predict the premature bed break-up and its subsequent effects. Improving the available melting models, by incorporating the viscoelastic nature of polymers, or a more comprehensive study of the solid bed mechanics (which would allow the prediction of premature bed break-up) is certainly desirable. However, consideration should also be given to the requirements and cost of the computations, in terms of the resulting practical benefits in the precision of the predictions.

7.3.1 Solids conveying

Conveying mechanism

This section adopts the analysis of Tadmor and Klein (1970), based on the framework provided by Darnell and Mol (1953). Despite its simplicitly, the model provides a convenient tool for understanding and optimizing the process. Some of the refinements made by Tadmor and co-workers (Broyer and Tadmor, 1972; Kacir and Tadmor, 1972; Tadmor and Broyer, 1972) are also considered.

The solid bed is dragged in the downchannel direction by the tangential friction force between the barrel surface and the top of the solid bed. The movement is retarded by the friction forces acting on the root and flights of the screw. Therefore, the solid bed acquires a velocity in the downchannel direction, V_{pz}. The pressure in the solid increases along the channel, but this pressure gradient opposes the motion of the material. The following assumptions are made:

1. The solid behaves as an elastic continuum; there is no internal deformation inside the solid, which has a plug type flow with constant velocity.
2. The channel runs full of polymer. This condition is required to ensure plug flow and material compaction, leading to pressure generation. In practice, this assumption is unfounded during metered starve feed operating mode, or when disruptions of flow occur, either through the hopper or in the feed port of the extruder.
3. The depth of the channel is uniform. However, if computations are performed for small downchannel increments, changes in depth can be accounted for.
4. There is no backward flow through the mechanical gap between the barrel and the screw.
5. The polymer density and friction coefficients are independent of the pressure and temperature. This is certainly questionable, but can be avoided by adopting the procedure described above.
6. The stress distribution is isotropic, thus pressure varies only along the downchannel distance.

7. The material is at constant and uniform temperature. Again, small Δz increments can be used to account for changes in the barrel temperature.

Some of these assumptions have been relaxed by various authors. A rectangular coordinate system is used for the channel. This means that the channel is unwound from the screw and considered as a perfectly linear duct with rectangular cross-section. The lower the ratio of h (channel depth) to D (screw external diameter), the smaller the error introduced by this simplification. It is also easier to consider the screw as stationary and the barrel as an infinite plate sliding on the top of the channel, moving at constant velocity V_b in a direction making an angle ϕ (helix angle) with the downchannel direction. This simplification alters the effect of the inertia forces acting on the polymer, but this produces a small error.

Figure 7.10 shows the velocity components of the solid plug, when a longitudinal cut to the system is considered. The solids move along the channel at a velocity V_{pz}, with tangential and axial components $V_{p\phi}$ and V_{pa}, respectively. Since the solids output is the product of their velocity and the effective cross-section, one may write:

$$Q_p = V_{pa}[\pi(D^2 - D_i^2)/4 - ith/\sin\bar{\phi}] \tag{7.2}$$

where D_i is the internal diameter of the screw, i the number of flights of the thread and t is the screw flight width. The subscripts s and b will refer to values measured at the root of the screw and at the inner barrel wall, respectively. The term $ith/\sin\bar{\phi}$ represents the thread area projected on to a plane perpendicular to the screw axis. As seen above, the solids conveying mechanism results from the difference between the friction forces developed at the metal contact

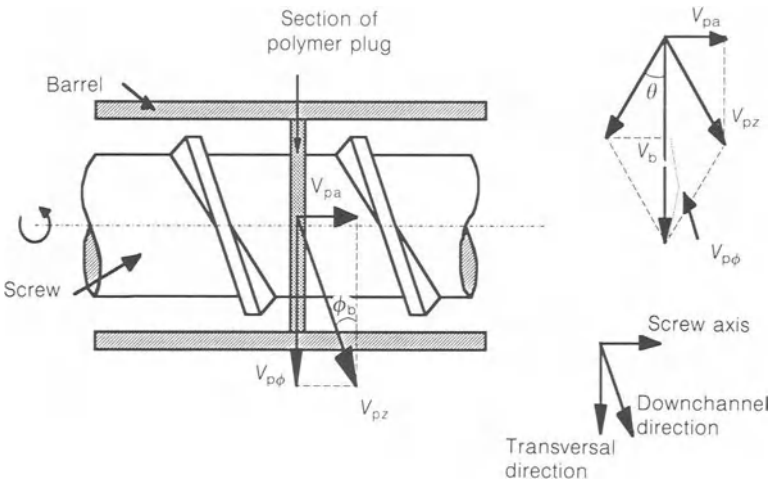


Figure 7.10 Section of the solids conveying zone.

surfaces. Thus, the tangential solids velocity, $V_{p\phi}$, is smaller than the corresponding barrel velocity, V_b (πND, where N is the frequency of screw rotation). Figure 7.10 also represents the vectorial difference between the barrel surface velocity and the downchannel solid plug velocity, which makes an angle θ with V_b. The solids conveying angle, θ, is inversely proportional to that velocity difference. When $\theta = 0$, $V_{pa} = 0$, and the throughput is zero. If $V_{bz} = V_{pz}$, the output reaches its maximum and $\theta = 90 - \phi°$. Theoretically, it is possible to have $V_{p\phi} = V_c(\theta = 90°)$, which would mean that the plug would slide down the channel. From Fig. 7.10 one may conclude that:

$$\tan\theta = \frac{V_{pa}}{V_b - V_{p\phi}} = \frac{V_{pa}}{V_b - V_{pa}/\tan\phi_b} \tag{7.3}$$

thus,

$$V_{pa} = V_b \frac{\tan\theta\tan\phi_b}{\tan\theta + \tan\phi_b} \tag{7.4}$$

Substituting in (7.2):

$$Q_p = \pi ND \frac{\tan\theta\tan\phi_b}{\tan\theta + \tan\phi_b}\left\{\frac{\pi}{4}(D^2 - D_i^2) - \frac{ith}{\sin\bar{\phi}}\right\}. \tag{7.5}$$

Rearranging:

$$Q_p = \pi^2 NhD(D-h)\frac{\tan\theta\tan\phi_b}{\tan\theta + \tan\phi_b}\left[1 - \frac{it}{\pi(D-h)\sin\bar{\phi}}\right] \tag{7.6}$$

This expression has no practical use, since θ is unknown. Also, the influence of the friction coefficients is not apparent, despite their importance to the conveying mechanism. A second relationship can be obtained by considering the forces acting on an segment of solids, as represented in Fig. 7.11. Among these forces are the friction force (F_1 in Fig.7.11) between the barrel and the solids, acting in a direction making an angle $(\theta + \phi)$ with the downchannel direction; friction forces (F_3, F_4, F_5) developed due to the contact of the solids with the screw; normal forces (F_7, F_8) exerted by the two sides of the channel on

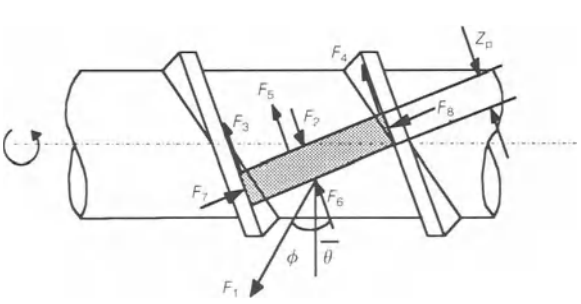


Figure 7.11 Force balance on the solid plug.

the plug; and forces (F_6, F_2) resulting from the pressure drop in the downchannel direction:

$$F_1 = f_b P b_b \, dz \tag{7.7}$$

$$F_3 = f_s F_7 \tag{7.8}$$

$$F_4 = f_s F_8 \tag{7.9}$$

$$F_5 = f_s P b_s \, dz \tag{7.10}$$

where f_s and f_b are the dynamic friction coefficients between the solid polymer particles and the barrel and screw surfaces, respectively; b is the channel width; P is the local pressure; and

$$F_7 = Ph \, dz + F^* \tag{7.11}$$

$$F_8 = Ph \, dz \tag{7.12}$$

$$F_6 - F_2 = h\bar{b} \, dp \tag{7.13}$$

in which F^* is an unknown force required for the system to be in equilibrium. Executing force and momentum balances ($\Sigma F = 0, \Sigma M = 0$), F^* is eliminated and an expression relating θ with P is obtained. Upon integration from a distance $z = 0$, where $P = P_1$, to $z = Z_b$, where $P = P_2$, the result is:

$$\cos\theta = K \sin\theta + M, \tag{7.14}$$

where K is a constant depending on the geometry of the system:

$$K = \frac{\bar{D}}{D}\left(\frac{\sin\bar{\phi} + f_s \cos\bar{\phi}}{\cos\bar{\phi} - f_s \sin\bar{\phi}}\right) \tag{7.15}$$

and M is the following expression:

$$M = 2\frac{hf_s}{b_b f_b}\sin\phi_b\left(K + \frac{\bar{D}}{D}\cot\bar{\phi}\right) + \frac{b_s f_s}{b_b f_b}\sin\phi_b\left(K + \frac{D_i}{D}\cot\phi_s\right)$$
$$+ \frac{\bar{b}h}{b_b Z_b f_b}\sin\bar{\phi}\left(K + \frac{\bar{D}}{D}\cot\bar{\phi}\right)\ln(P_2/P_1) \tag{7.16}$$

Equation (7.14) can be rearranged and presented in another form:

$$P_2 = P_1 \exp\left(\frac{B_1 - A_1 K}{A_2 K + B_2} Z_b\right) \tag{7.17}$$

where A_2 and B_2 are constants depending on the geometry, and A_1 and B_1 parameters depending on the geometry, on the coefficients of friction and on the solids conveying angle, θ. P_1 and P_2 are the pressures at the beginning and end of the solids zone, which has a helicoidal length Z_b. The drag mechanism should be capable of conveying solids at a higher rate than the adjacent melting zone, to ensure a stable process. It must be also a good pressure generator, to contribute significantly to the extruder pumping capacity. Since high throughputs require high θ, K and M in equation (7.14) should be small.

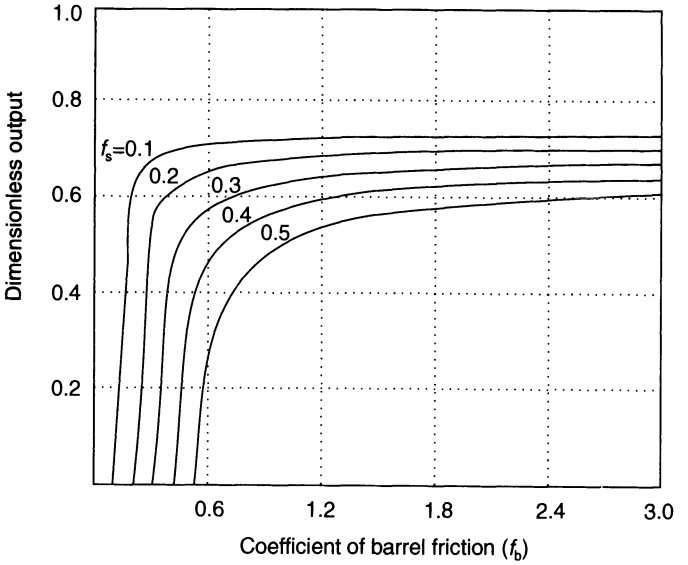


Figure 7.12 Influence of the relative magnitude of the friction coefficients on the solids conveying capacity.

From equations (7.15) and (7.16) three conclusions may be drawn. First, the ratio f_s/f_b should be small. This justifies the practical concern in polishing or coating the screw and allowing an appreciable roughness in the inner barrel wall. A low-friction screw surface can also be obtained using PTFE-impregnated nickel plating. As Fig. 7.12 clearly demonstrates – using the methodology adopted by Rauwendaal (1990) – the output varies significantly with the relative magnitude of the friction coefficients. The example shows that, for a particular geometry and screw rotation frequency, increasing friction at the barrel surface, f_b, may dramatically influence the performance of the screw. If $f_b \approx f_s$ the output is small, but a little increment in f_b induces a significant increase in the conveying capacity. Thus, if the machine is operating in this region, small variations between different batches of polymer may cause considerable instabilities in the process. When $f_b \gg f_s$ the output increases, and the stability of the operation upon changes in the physical properties of the material is guaranteed. At this point, it is worth mentioning that the current unavailability of accurate and complete data for the friction coefficients of polymers in granulate form, measured under conditions similar to those found in industrial extrusion, limits the practical usefulness of the theory and its potential to diagnose and solve extrusion problems, or optimize the processing conditions.

Second, the ratio P_2/P_1 should be small. It may be concluded that the output and the pressure generated in the solids conveying zone (see equation (7.17)) depend on the initial pressure in the channel, P_1. Later we will present a

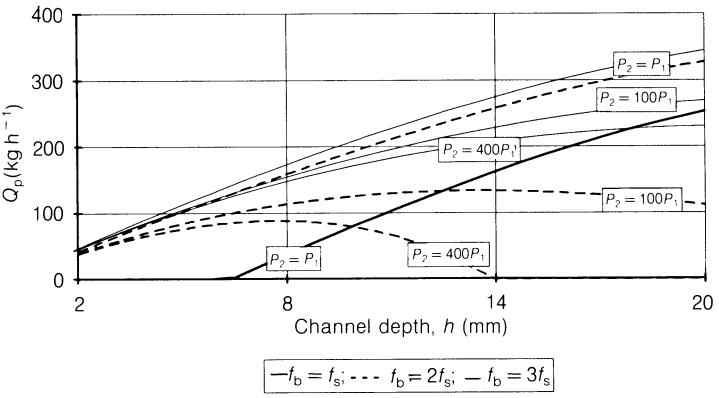


Figure 7.13 Influence of the channel depth, downchannel pressure gradient and relative magnitude of the friction coefficients, on the solids conveying screw capacity.

technique for estimating P_1. The maximum output will be attained when $P_2 = P_1$. This indicates that the conveying capacity of the screw is affected by the need to generate pressure. Pressure increases exponentially along the screw, lowering the output because it raises M. The effect of the downchannel length, Z_b, is determined by the relative magnitude of the quantity $(h/Z_b)(\ln(P_2/P_1))$.

Third, D_i/D or $\bar{D}/D$ should be small, i.e. the channel depth should be maximized. This is shown in Fig. 7.13 at zero pressure gradient ($P_2 = P_1$) for different ratios of f_b/f_s. As expected, the higher the difference between the friction coefficients, the higher the output. If the channel depth increased considerably (which is obviously limited by the mechanical resistance of the screw), the output would eventually reach a maximum and subsequently decrease. This would result from the conflicting effects of increasing the cross-sectional flow area (equation (7.6)) and incrementing the retarding friction forces on the screw flights (F_3, F_4, computed in equations (7.8), (7.9), (7.11) and (7.12)), and due to the downchannel pressure gradient (F_2, F_6 – see equation (7.13)). The effect of the latter is clearly confirmed in Fig. 7.13, which shows that, at constant channel depth and friction properties, the output decreases with increasing pressure development. As the increase in pressure becomes more important, the maximum throughput shifts to lower channel depths.

Additionally, equation (7.6) shows that the output is proportional to the quantity $(\tan\theta \tan\phi)/(\tan\theta + \tan\phi)$. In the graph shown in Fig. 7.14 the value of this term was plotted against the helix angle ϕ, for two values of the ratio f_b/f_s. Furthermore, different values of f_s were considered. Conditions of maximum throughput were assumed, i.e. there is no downchannel pressure gradient. As expected, higher friction coefficients at the inner barrel wall/solids interface promote higher conveying rates. The figure shows that, for each operating condition, there is an optimum helix angle for maximum flow rate. As Tadmor and Klein (1970) have previously shown, when the two friction

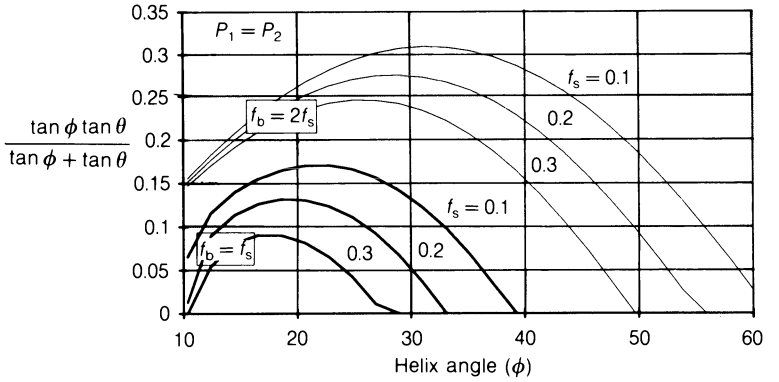


Figure 7.14 Effect of the helix angle on the solids conveying rate ($P_1 = P_2$).

coefficients are identical and have values of 0.3 or higher (which is common for most polymers), the largest throughput is attained for helix angles in the range 15–20°. This explains the classical choice of $\phi = 17.56°$ (square-pitched screw) for machining the majority of the screws. However, Fig. 7.14 also shows that, when the relative magnitude of the friction coefficients rises, the optimum helix angle increases. Fortunately, when the effect of the downchannel pressure gradient is included in the analysis (see Fig. 7.15), it may be observed that the optimum helix angle shifts back to lower values. In the example considered in Fig. 7.14, when $f_b = 2f_s$ and $f_s = 0.3$, the optimum angle $\phi \approx 26°$. If the pressure increases 100 times along the channel (which is normal), the value reduces to about 15°. A square-pitched screw should therefore display good conveying capabilities.

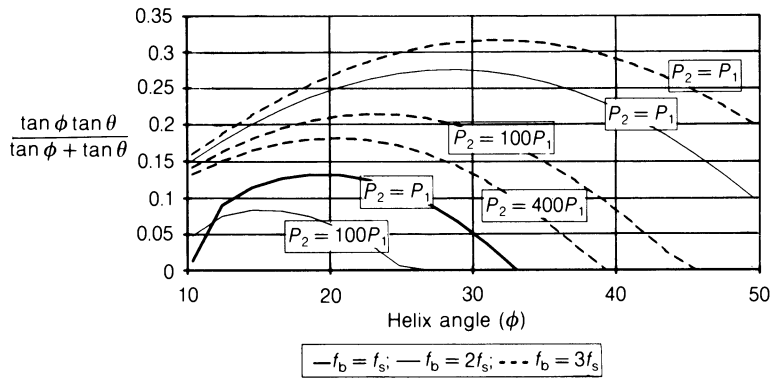


Figure 7.15 Effect of the helix angle on the solids conveying rate, when the downchannel presssure gradient is considered.

Equation (7.6) also shows that the throughput is proportional to the screw speed, and that single flighted threads are preferable for solids conveying.

The contribution of solids conveying to the total process power consumption is given by the product of the friction force acting on the top of the solid plug, F_1, and the barrel velocity in the direction of the force ($\pi ND\cos\theta$):

$$dE_w = \pi ND(\cos\theta) f_b b_b P\, dz_b \tag{7.18}$$

Inserting equation (7.17) and integrating:

$$E_w = \pi ND(\cos\theta) f_b b_b Z_b (P_2 - P_1)/\ln(P_2/P_1) \tag{7.19}$$

One particularly questionable assumption is that of constant temperature in the downchannel direction. Not only does the barrel temperature generally increase in the axial direction, but there is also a relevant contribution of friction to the development of the temperature near the polymer/metal interfaces. Therefore, part of the mechanical power input through the shaft is converted into heat at all contact surfaces. For example, the rate of heat generated by friction on the barrel surface (per unit barrel surface area) is given by the product of the tangential force between barrel and plug and their relative velocity (Broyer and Tadmor, 1972):

$$q_b = \pi NDPf_b b_b \sin\phi_b/\sin(\phi_b + \theta) \tag{7.20}$$

Considering that most of the heat is generated near the inner barrel wall, the mechanical power transformed into heat along the solids conveying zone is:

$$E_{wh} = \pi NDb_b Z_b f_b \frac{\sin\phi_b}{\sin(\phi_b + \theta)} \frac{P_2 - P_1}{\ln(P_2/P_1)} \tag{7.21}$$

As shown in equation (7.17), the pressure rises exponentially in this zone. According to relation (7.20), the rate of heat generation is directly proportional to the local pressure. Thus, during conveying of solids large pressures can develop (that is, before the surface temperature reaches the melting point), if the barrel is efficiently cooled (this fact is usually explored in grooved extruders), or if the material has a high melting point.

Assuming that conduction in the downchannel direction can be neglected compared with that in the radial direction, and that the heat fluxes on the flights and root of the screw are insignificant, the equation of energy reduces to equation (4.7). The heat generated at the barrel surface (equation (7.20)) is partially dissipated through the barrel, and the remaining is conducted to the solids. Thus, a temperature profile in the yy direction develops:

$$q_b = -k_p \left(\frac{\partial T_p}{\partial y}\right)_{y=0} + k_b \left(\frac{\partial T_b}{\partial y}\right)_{y=0} \tag{7.22}$$

In this equation k_p and k_b are the polymer and barrel thermal conductivities, and T_p and T_b the temperatures of the solids and barrel, respectively. Tadmor

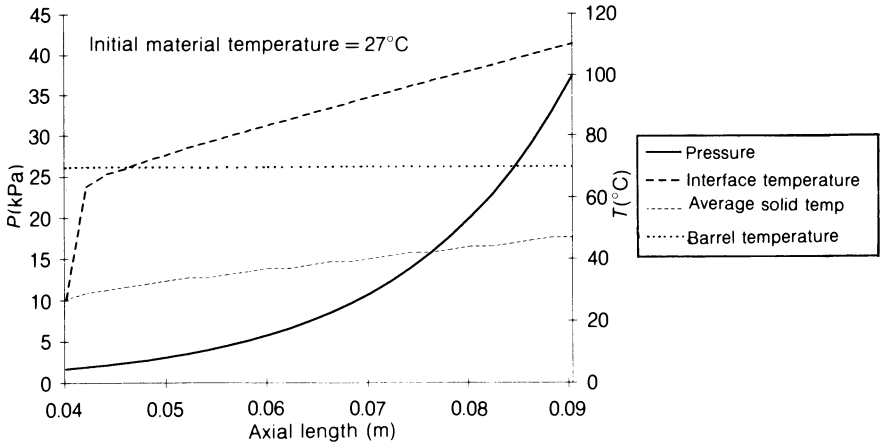


Figure 7.16 Pressure and temperature axial profiles for a given set of operating conditions.

and Broyer (1972) executed a differential heat balance on the solid bed surface and solved the heat transfer equations numerically. They computed the variation of the plug temperature profile in the downchannel direction, having concluded that the interfacial surface temperature increases exponentially. Consequently, they could infer that the first polymer generally melts before the barrel average temperature reaches its melt temperature, and that the maximum pressure developed during solids conveying is determined by the temperature rise of the solid plug surface. This is illustrated in Fig. 7.16, which shows the results of simulations produced for a 60 mm extruder (Covas and Cunha, 1993). The machine characteristics, which will be used in other examples throughout this chapter, are shown in Table 7.2. A set of operating conditions (barrel kept at 70°C and screw rotating at 60 rpm) was chosen. The expected exponential temperature and pressure increase is confirmed. The growth in temperature is slightly more complex in the initial screw turns, due to the difference in the solids and barrel temperatures. The interfacial temperature rapidly approaches the value set for the barrel, as a result of the combined effect of heat conduction and friction dissipation. Then, a second exponential growth, entirely caused by frictional effects, commences. The interface temperature reaches the polymer melting temperature (about 110°C for the LDPE considered in the example) well before the average solid or barrel temperature.

Table 7.2 Geometry of the screw used for computations

	Length	*Channel depth* (mm)
Feed zone	8*D*	10
Compression zone	9*D*	10–5
Pumping zone	8*D*	5

Square pitch; $t = 5$ mm; mechanical gap = 0.5 mm

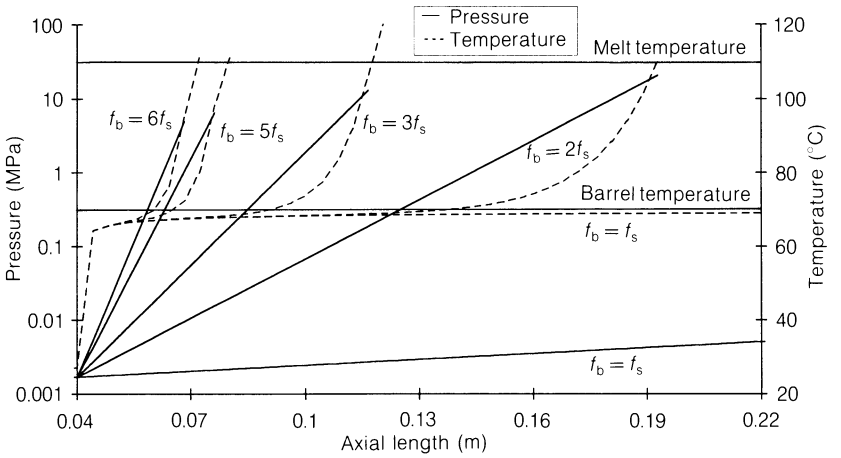


Figure 7.17 Effect of the relative magnitude of the friction coefficients on the pressure and temperature axial profiles in the solids conveying zone.

Figure 7.17 shows the effect of the relative magnitudes of the friction coefficients on the pressure and bed-top surface temperature axial development in the solids conveying zone. As expected, the two parameters have an exponential growth, following the pattern already pictured in Fig. 7.16, which depends mainly on the value of the friction at the barrel wall. If $f_b = f_s$, little pressure generation is achieved and solids conveying will extend for a considerable length of the screw. The situation changes as the friction factors increase. For the set of operation conditions input, the illustration clearly shows that incrementing the coefficient f_b from two to six times the value of f_s shortens the length of screw occupied in conveying solids from 0.19 to 0.07 m. However, the premature polymer fusion caused by mechanical heat dissipation does not necessarily induce higher maximum pressures. This is also apparent in Fig. 7.17, where it may be observed that while for $f_b = f_s$ the maximum pressure is only 0.01 MPa, the high increase produced when $f_b = 2f_s$ (when the maximum pressure reaches 20.6 MPa) is not continued with increasing barrel friction. In fact, higher f_b will actually produce progressively lower pressure growths (13.0, 6.5 and 5.0 MPa, respectively). As Tadmor and Broyer (1972) have pointed out, the single-screw extruder has an innate protection mechanism against excessive pressure rises, because the plug surface temperature may only reach the material's melting point. Beyond this location the delay zone develops, with the pressure increasing at a lower pace.

The curves depicted in Fig. 7.17 were computed imposing constant throughput, whereas in practice, and as seen above, higher friction at the barrel wall encourages the conveying mechanism. The example presented in Fig. 7.18 considers the processing of a typical LDPE extrusion grade through the 60 mm extruder already selected, coupled to a simple head, consisting of a

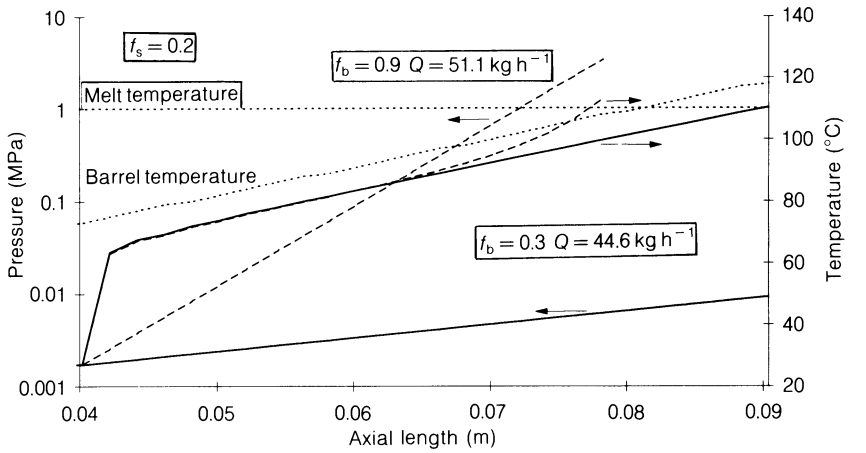


Figure 7.18 Pressure and temperature profiles in the solids conveying zone during plasticating extrusion. Two different friction coefficients at the inner barrel wall were considered.

conical adapter and die (producing a 6 mm rod). Conventional operating conditions (barrel temperature profile and screw speed) were input. Using the mathematical description of the plasticating process presented in this book, the computer package developed determined the throughput (and related functional parameters, such as pressure and temperature profiles) that ensured an approximately zero pressure drop at the die exit (Covas and Cunha, 1993). The figure presents the axial growth of both pressure and temperature in the solids conveying zone, for two different friction coefficients at the barrel. Since the differences in output of the two situations affect both the heat transfer and dissipation mechanisms, the safeguard mechanism discussed above now allows differences in pressure rise of more than one order of magnitude. Increasing the barrel wall friction coefficient from 0.3 to 0.9 increases the effective mass output from 44.6 to 51.1 kg h^{-1}, while decreasing the length of the solids conveying zone from 0.09 to less than 0.08 m. The barrel reaches the polymer melting temperature slightly after 0.08 m. The maximum pressure developed increases from 0.009 to 3.36 MPa.

Flow in hoppers

As seen above, evaluating the efficiency of solids conveying requires information on P_1, i.e. on the initial pressure at the beginning of the process. Usually, one assumes that this pressure equals that at the bottom of the hopper, which can be computed using bulk solids analysis. However, this approach ignores the complex transition from the gravitational flow of particulate solids in the hopper to the drag induced flow in the screw channel. The situation is further complicated during the changeover from static storage

to flow mode, as an overpressure propagates rapidly upwards through the material (Shamlou, 1988). Nevertheless, the method provides a link between the performances of the hopper and of the extruder, thus reflecting the practical experience of such a dependence. It is also possible to ignore the hopper, assuming instead that P_1 results from the effect of local gravitational and centrifugal forces (Lovegrove and Williams, 1973). This approach accounts for the possibility of the channel working partially full of material before the development of plug flow. However, it fails to consider the already mentioned connection between the hopper and the extruder. As Tadmor and Gogos (1979) have pointed out, there is a clear need for a model which includes the hopper, the inlet region of the extruder and the first screw turns (where the Darnell–Mol model cannot be applied).

Under these circumstances, the purpose of modelling the flow of material in the hopper is: to ensure an adequate throughput, i.e. that the productivity of the process is not limited by the hopper; to provide a link between the hopper and the extruder (via the parameter P_1); and to establish the loading/operating conditions that minimize pressure fluctuations at the bottom of the vessel.

The geometry of the hopper dictates the flow pattern and the resulting pressure profile developed within the solids during discharge. Hoppers can be conical, where an axisymmetric flow develops, or wedge-shaped, in which plane flow occurs. The half-angle is approximately 8–10° larger in this case, providing more effective storage capacity, but this is offset by the eventual build-up that is likely to take place in the sharp corners (Roberts, 1991). Two distinct flow patterns may develop. During **mass flow** there is a bulk flow of granules towards the exit, with only a small velocity gradient, guaranteeing the complete discharge of the vessel. In **funnel flow** the movement is confined to a vertical region in the centre of the vessel. A stable pipe is formed, with the stagnant material acting as a support. Flow is erratic and may cause segregation. Combinations of the two situations are also possible. Mass discharge is preferable, since flow usually initiates as soon as the outlet is opened, there is little tendency for flow disruptions (such as arching), and dead zones do not appear, with the first material going in being the first going out.

Currently, there are no theories capable of correlating the influence of the discharge rate upon the vertical pressure profile. Only situations of static loading or open discharge are usually considered. The derivation of equations quantifying the flow rate is complicated by the complex, and still little understood, rheology of solids in granular or powder form. Consequently, most authors fit correlations to their empirical data, or adopt dimensional analyses. Equations such as the one proposed by Beverloo, Leniger and de Velde (1961) quantify the gravity discharge of coarse particles through flat or converging vessels. For central conical apertures, the rate of mass discharge is given by:

$$Q = 0.58\rho g^{0.5}(D - kd_p)^{2.5} \tag{7.23}$$

where D is the aperture diameter, d_p is the diameter of the grains and k is a particle shape constant, with an average value of 1.4. Considering a conical hopper with a 6 cm opening, containing pellets approximately 3 mm in diameter and a material with a bulk density of 600 kg m^{-3}, the mass flow rate is predicted to reach 3000 kg h^{-1}. This is more than one order of magnitude above the expected throughput of a conventional extruder having the same feed port geometry. Thus, the pressure profile of the solids in the hopper of an extruder is probably more adequately described assuming static conditions, whereas for designing purposes discharge conditions should be considered (in order to account for the significant overpressures developed). There is now a more significant dependence of the base pressure on the loading conditions.

A century ago, Janssen (1895) considered the equilibrium forces acting on a small material slice contained in a vertical cylindrical column of solids, and predicted the vertical pressure profile:

$$P_v = \rho g D\{1 - \exp[-(KfD/4)h]\}/4fK \tag{7.24}$$

where ρ represents the material bulk density, g acceleration due to gravity, f the coefficient of wall friction, D the hopper diameter, h the depth from the top surface and K the ratio of lateral to normal pressure in the vessel. The weight of the solids is largely sustained by the lateral walls. Whereas at the top of the solids ($h = 0$) P_v matches the hydrostatic pressure, $h \to \infty$ produces a maximum value:

$$P_v(\max) = \rho g D/4f \tag{7.25}$$

Thus, unlike a column of liquids where the hydrostatic pressure at the bottom increases linearly with the height, in a column of solids the bulk pressure increases exponentially until an asymptotic value is reached. The location of this *critical height* depends both on the geometry and on the material properties. For practical purposes, the critical height corresponds to the minimum level of solids to be preserved in the hopper, if variations in the pressure in the initial turns of the screw are to be avoided. For the convergent region (static conditions), Walker (1966) postulated the inexistence of shear stresses on vertical planes and assumed that the vertical pressure at any level is equivalent to the hydrostatic pressure due to the amount of material above it. The resulting linear vertical pressure distribution is computed from:

$$P_v = \rho g[(P_{vo}/\rho g) + h] \tag{7.26}$$

P_{vo} expresses the pressure at the top of the convergence and h the height considered. As seen in Fig. 7.19, which shows the influence of the loading level on the vertical pressure profile in a conicylindrical hopper, there is now a significant dependence of the base pressure on the height of solids. The figure also compares the static and dynamic vertical pressure profiles for three loading levels. While during open discharge the dynamic analyses predict a

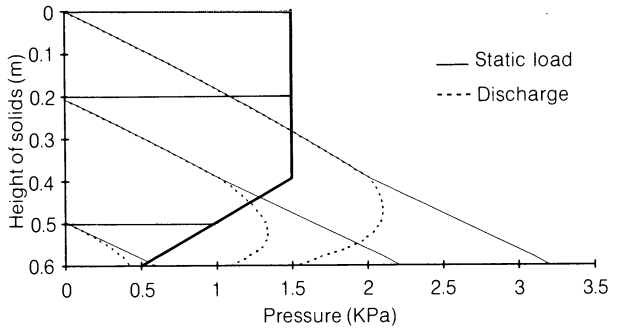


Figure 7.19 Computed vertical pressure profiles during loading and open discharge of a conicylindrical hopper.

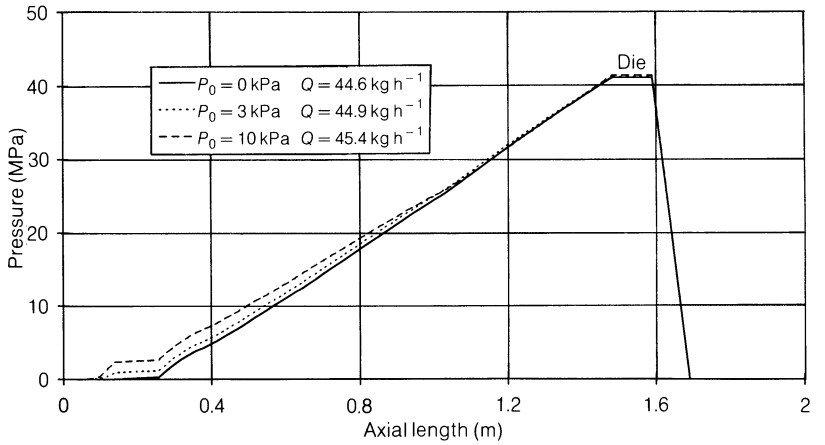


Figure 7.20 Effect of the pressure at the bottom of the hopper on the development of the axial pressure profile in an extruder coupled to a die.

variation in the base pressure between 0.4 and 1.5 kPa, when static conditions are assumed, the predicted pressures will vary in the range 0.6–3.2 kPa. Figure 7.20 exhibits the predicted influence of the hopper loading level on the performance of the extruder and die already taken as a case history. Three axial pressure profiles, corresponding to three different pressures at the bottom of the hopper, are represented, together with the mass throughput. Since pressures rise to megapascals, while the differences in loading levels amount to kilopascals, the deviation between the curves is hardly noticeable, and has a tendency to attenuate towards the die exit. Nevertheless, when the initial pressure (P_1) varies from 0 to 10 kPa, the output increases around 1.8%. This effect is comparable to that of the mechanical gap during melt conveying, which was discussed in the previous chapter.

The delay zone

When, due to the combined effects of the heat conducted and generated, the solid near the barrel wall reaches its melting point, a thin melt film is formed. From this location onwards, the solids conveying mechanism, based on the differences in friction forces acting at the solid interfaces, is replaced by another using drag flow, the role of friction now being played by the polymer viscosity. The delay zone evolves until the conditions for initiating the fusion mechanism are created. In principle, it would be anticipated that it progresses until the melted film thickness equals the mechanical gap between the flight of the screw and the inner barrel wall. Then, as the throughput capacity of the gap became lower than the amount of leakage flow of melted material, a melt pool would form near the pushing flight of the screw. In practice, however, it has been observed that the melt pool only grows when the film thickness reaches 5–7 times the value of the gap. This behaviour can result from several possible causes (Agassant, Avenas and Sergent, 1986):

1. The backward film flow drags the solid plug against the pushing flight of the screw, thus making the process initiation difficult.
2. The melt pool can only appear when the solid bed deforms, i.e. when the local pressure is larger than the bed yield stress. The maximum pressure drop in the gap, in the cross-channel direction, occurs when the film thickness reaches three times the mechanical gap. It has been shown (Kacir and Tadmor, 1972; Agassant, Avenas and Sergent, 1986) that, for an isothermal Newtonian melt, the cross-channel pressure is given by:

$$\Delta P = \frac{6\eta V_b}{\sin \phi_b} \frac{\delta_f - \delta}{\frac{\delta^3}{t} + \frac{\delta_f^3}{b}} \tag{7.27}$$

   where η is the polymer viscosity, and δ_f and δ the thicknesses of the film and of the gap, respectively. The pressure increases with increasing difference between δ_f and δ, passing through a maximum when the film thickness equals 1.5 times the flight clearance. If non-Newtonian and non-isothermal effects are taken into account, the maximum is now attained when δ_f is about 2.5–3 times the flight clearance, as mentioned above. If the gap is sufficiently high, the stresses created will be lower than the material's yield stress. In this case the Tadmor melting mechanism will not occur, or will develop very slowly. Instead, a mechanism similar to Dekker's may evolve.
3. The melted material can eventually penetrate within the intergranular spaces, the film growing in thickness at a lower pace.

The growth in the film thickness is directly dependent upon the relative contribution of heat conducted and generated. While the heat transfer mechanism is similar to that taking place in the melting zone, in the delay zone any newly melted material accumulates in the film, increasing its

thickness, instead of being scraped by the screw and deposited in the melt pool. However, the model does not hold for the initial stages of film formation, where the problem of melting solid polymer particles has to be solved. Several authors have studied the melting of a granular solid bed (Pearson, 1976; Kuo and Chung, 1989), albeit assuming the initial presence of a thin melt film. Kacir and Tadmor (1972) tackled the problem assuming spherical polymer particles and melt penetration in the gaps no deeper than half the particle diameter. The results showed that only 5% of the delay zone should be treated by this model.

It is not easy to predict the location of the transition from the delay to the adjacent melting zone. The two most popular criteria for determining the length of the delay zone are: to compute the length of the channel needed to develop a film of material with about 5.6 times the thickness of the mechanical gap, which was found experimentally to be the average film thickness at the end of the delay zone (Kacir and Tadmor, 1972); and to adopt empirical correlations based upon the results of visualization experiments using different thermoplastics. Figure 7.21 shows a relationship between the length of the delay zone and the rate of fusion, expressed by a dimensionless melt parameter ψ (Tadmor and Klein, 1970).

In this zone, pressure initially develops due to viscous drag on the barrel and friction on the screw. Thus, not only does equation (7.6) remain valid, but also in the force balance on the solid plug shown in Fig. 7.11 one simply has to replace the frictional force F_1 (equation (7.7) with a viscous drag force given by:

$$F_1 = \tau b_b \, dz_b, \tag{7.28}$$

where τ is the shear stress. The average shear rate in the film is:

$$\dot{\gamma} = \frac{V_b \sin \phi_b}{\delta_f \sin(\phi_b + \theta)} \tag{7.29}$$

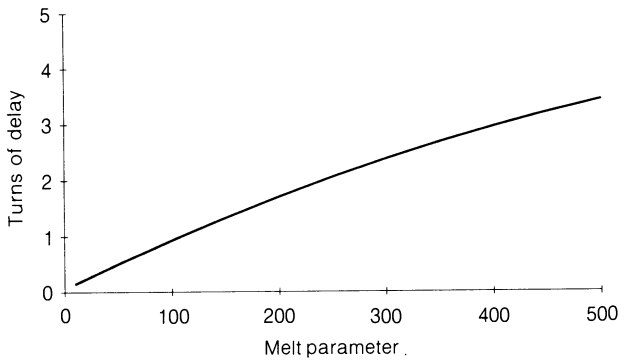


Figure 7.21 Length of the delay zone, in terms of a melting parameter ψ (adapted from Tadmor and Klein, 1970).

The resulting pressure rise is (Kacir and Tadmor, 1972):

$$P_3 = \frac{\tau b_b(\cos\theta - K\sin\theta)}{A_3K - B_3}\left[1 - \exp\left(\frac{B_3 - A_3K}{A_2K + B_2}Z_b\right)\right] + P_2\exp\left(\frac{B_3 - A_3K}{A_2K + B_2}Z_b\right) \tag{7.30}$$

where A and B are, as before (see equation (7.17)), constants depending on the system geometry, on the friction coefficients and on the solids conveying angle. The driving force F_1 is high in the preliminary stages of the process, because significant shear stresses are generated by the small film thicknesses (see equation (7.29)). As the film grows in thickness, the shear rate decreases and F_1 declines. Thus, it is possible to observe a pressure rise at the beginning of the delay zone, followed by a drop. The situation may be more complicated because, although the majority of melting occurs near the inner barrel wall, the friction coefficients at the other solid bed surfaces may also induce the melting of the material. This condition is analogous to that assumed by Chung (1970) who studied the conveying mechanism of the solid plug surrounded by a film of melted material. Although equation (7.6) still holds, when the thickness of the various interfacial films is identical and the material follows the power law, a linear pressure rise along the channel is predicted.

Grooved feed bushes

As shown previously (and illustrated in Fig. 7.12), the efficiency and stability of solids conveying increases with an increasing difference between the coefficients of friction between polymer and barrel and between polymer and screw. Figure 7.18 extended this concept to plasticating extrusion, demonstrating, for a case study, that the effective process throughput improves as the ratio f_b/f_s increases. One practical way of ensuring this mode of operation consists in a dramatic increase in the inner barrel wall surface roughness via the machining of either axial or helicoidal grooves. This solution was initially proposed and tested in Germany in the early 1970s, for processing high molecular weight HDPE, and has become popular throughout Europe. Machines with a grooved feed bush are often claimed to be positive pumping devices, with the output directly proportional to the material density and screw speed, and independent of the die resistance (however, despite this positive feeding and early good pressure generation, the screw still has to melt and adequately homogenize the material which, in itself, often limits the rate of material that can be fed).

Practical experience has proved that the number and geometry of the grooves depends on the screw diameter, on the nature of the polymer being processed and on the type of feedstock. Usually, the number of grooves increases with the screw diameter and upon processing softer plastics. The total

number of grooves is usually between $D/10$ and $D/5$. Frequently, the grooves have a rectangular cross-section, their depth decreasing linearly, from a maximum below the hopper opening, through a length of $2D$ to $4D$. Lower angles of taper compress the material less, thus inducing lower shear stresses. Although the main purpose of the grooves is to increase the equivalent frictional coefficient, their considerable dimensions relative to the channel depth and pellet size often modify the conventional flow of solids. Grünschloss (1990) observed the flow of powders in a tapered feed bush using a video technique, and concluded that in axial grooves there is a considerable velocity of solids both along and across the slots, whereas in the helicoidal solution the material moves along the small channels, thus improving self-cleaning. The velocity fields affect the pressure generation mechanism and make the mathematical treatment of this zone quite complex. Also, they probably justify the relatively modest increase in the performance of grooved feed extruders when processing powders.

Machining grooves in the barrel significantly alters the characteristics of an extruder and requires several modifications to its design and construction.

- A capacity for cooling the grooved bush, and existence of a thermal barrier in the remaining length of the barrel. It is necessary to avoid the premature melting of the material due to the intense heat created by the high friction forces (the rate of heat generation at the barrel wall is given in equation (7.20), and is proportional to the pressure generated and to f_b). The energy lost through the cooling channels may reach 15–40% of the mechanical power input, depending on the materials being processed. However, the 'specific power consumption' (i.e. the energy consumption per unit of extruded product) may be lower than in conventional machines, as the increase in energy required is more than compensated by the increased transport capability (Rauwendaal, 1990). Based on the fact that the friction coefficients of plastics generally increase with increasing temperature, Menges, Feistkorn and Fischbach (1984) postulated that the grooved bush must not cool the solids too fast, but should only prevent the formation of a melt film. Using a temperature-controlled grooved bush (with the water kept at 70°C), they observed higher melt throughputs and claimed an increase in the efficiency from 45% to 80%. Figure 7.22 complements the information presented in Fig. 7.18 and illustrates how controlling the temperature of the initial barrel section influences the plasticating process. The overall effect of the grooves was simulated by considering a relatively high value of f_b, which was taken as 4.5 times higher than friction at the screw surfaces. When a conventional barrel temperature profile is selected (see the barrel temperature profile in Fig. 7.18), increasing friction at the barrel wall augments the mass throughput from 44.6 to 51.1 $kg\,h^{-1}$. If the barrel temperature is kept at 70°C for 0.18 m (equivalent to $3D$), the corresponding lengthening of the

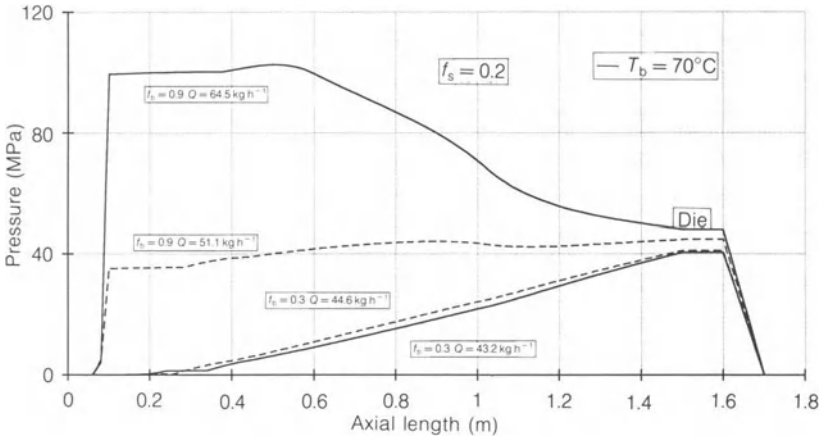


Figure 7.22 How controlling the temperature of the initial barrel section influences the axial pressure profile and mass throughput of the process. Two different friction coefficients at the inner barrel wall were selected.

solids conveying zone (from 0.090 to 0.096 m), and the simultaneous exponential growth in pressure, promotes the output. In particular, for high-friction barrel walls, the output rises from 51.1 to 64.5 kg h^{-1}. Pressures reaching 100 MPa are predicted, and are often observed in practice.

- Use of stronger materials for screws and barrels. Increasing friction near the barrel wall promotes wear and produces a significant early pressure development that can reach 100–300 MPa. Thus, not only does the length of the grooves have to be kept short (usually less than 5*D*), but also the materials used for construction have to be strong and wear resistant.
- Motor with increased power. As equation (7.21) indicates, increasing f_b requires a bigger torque at the same screw speed.
- Screws with lower compression ratios. With the aim of maintaining the pressures within reasonable limits, screws with a low compression ratio are usually adopted. But, since higher throughputs imply smaller residence times in the extruder, greater melting efficiency is required. This has resulted in the development of complex screw profiles, fitted with shearing and mixing sections or rings.

The loss of versatility of the extruder caused by the need to modify the screw, the enhanced wear possibilities, the increase in machine cost and greater quality concerns (there is a possibility of melting being overrun by the additional output of solids), have led some authors to conclude that the use of a grooved feed section is not usually justifiable, as good characteristics are usually obtainable with a properly sized extruder, working with a good screw (Steward, 1989). However, continued improvements in the theoretical

understanding and in the technology of grooved feed extruders have resulted in their extensive use in blow moulding, film blowing and pipe and profile extrusion. The higher machine costs and other disadvantages are felt to be of secondary importance compared with the benefits exhibited upon processing.

As seen above, the mathematical treatment of the effect of the grooves is complex (for a list of references on previous theoretical work, see Potente, 1985). Potente (1985) introduced simple approximate solutions to calculate the **equivalent coefficient of friction**, f_{bg}, the friction coefficient at the barrel wall resulting from the effect of the geometry of the grooves. The following equation provided good agreement with the experimental data:

$$f_{bg} = f_b + (f^* - f_b)\frac{b_g N_g}{\pi D}\left\{1 - \exp\left[-5\left(\frac{h_g N_g}{b_g}\right)^{0.9}\right]\right\} \tag{7.31}$$

where f^* is the internal friction coefficient, b_g groove width, N_g the number of grooves and h_g the maximum groove depth.

It is also possible to take into account the differences in the groove base and barrel surface roughnesses. The advantages of helicoidal grooves have been quantitatively explained by Rauwendaal (1990). The optimum helix angle increases with increasing screw helix angle and decreasing groove depth.

7.3.2 Melting

The model developed by Tadmor and Klein (1970) provides the means to understand and describe the Maddock melting mechanism developed in single-screw extruders with reasonable mathematical complexity. The resulting analytical equations can readily be used to study the effect of the system geometry, of the operating conditions, or of the thermophysical properties of the polymer on the melting rate. The model is quite popular in the literature and is frequently used in extrusion software packages. It will also be adopted in this section, providing coherent physical boundary conditions with the adjacent functional zones.

Consider Fig. 7.23, which represents a section of the screw channel during the development of the Tadmor melting mechanism (the figure corresponds essentially to one of the cuts considered in Fig. 7.3 and is a schematization of the cross-section depicted in Fig. 7.2). As before, a rectangular coordinate system was adopted, and the barrel was taken as an infinite plate sliding at constant velocity V_b in a direction making an angle ϕ with the downchannel direction, z. Both the solid bed and the melt pool have rectangular cross-sections, the melt pool encompassing the height of the channel, whereas a thin melt film, with thickness δ_f, separates the solid bed from the inner barrel wall. While the barrel is kept at T_b, the solid bed/melt film interface is at the polymer melt temperature, T_m. At any particular location, the solid occupies a width X, which is obviously smaller than the channel width, b. The plug moves at

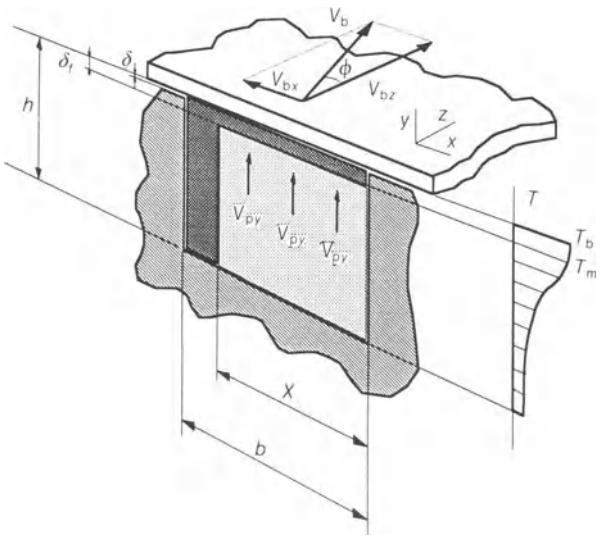


Figure 7.23 Idealized cross-section of the channel during melting.

constant downchannel velocity V_{pz} and has also a component in the yy direction, V_{py}, which, as seen in section 7.2, corresponds to the process melting rate. Thus, fusion of the solids takes place at the top surface of the plug, the resulting film of freshly melted material being dragged in the xx direction towards the melt pool. The melting mechanism is initiated when $X = b$ and will be completed when $X = 0$. It is important to know the progression of melting along the screw and to determine the length of the channel, usually denoted by z_t, occupied in melting the material, since it establishes the remaining portion of the screw available for the subsequent melt pumping and mixing stages.

The following conditions are assumed:

- The channel is rectangular, with width b and depth h, and runs full of polymer. The influence of the gap in terms of the melting progression and output is considered to be negligible.
- The solid bed behaves as a homogeneous elastic continuum.
- A steady state exists. At any location of the channel in the melting zone the barrel is at temperature T_b and the melt film/solid bed interface is at T_m. The solid occupies the width X, whose value decreases in the downchannel direction.
- The solid bed has infinite depth in terms of heat transfer. Heat transfer from or to the screw is neglected. This simplification ignores the progressive heating of the solid bed as it moves along the screw and precludes the model predicting the usual acceleration of melting during the later stages of the process. Thus, the predictions are frequently conservative.

- Melting occurs only at the interface defined by the outer surface of the solid bed and the film near the inner barrel wall. Since conduction from the melt pool is ignored, the problem is reduced to one-dimensional heat transfer. Although most of the melting occurs in the interface considered, the predictions will again become conservative. Nevertheless, avoiding this simplification would complicate the computations considerably, as a four- or a five-zone model would have to be adopted to take into account the presence of the films surrounding the solids.
- The melted film moves between parallel plates. The solid bed/melt film interface is assumed to be sharp and flat, thus simplifying the more realistic geometry shown in Fig. 7.2. The flow develops between two parallel plates moving at unequal speeds, V_b and V_{pz}, and in different directions. As seen in Fig. 7.24, it is easier to assume a lower stationary plate (top surface of the solids) kept at temperature T_m, and an upper plate, at temperature T_b, moving at a velocity V_j, which makes an angle α_j with the downchannel direction. From Fig. 7.24:

$$\vec{V}_j = \vec{V}_b - \vec{V}_{pz} \tag{7.32}$$

$$V_j = [(V_{bz} - V_{pz})^2 + V_{bx}^2]^{1/2} \tag{7.33}$$

$$\tan \alpha_j = \frac{V_{bx}}{V_{bz} - V_{pz}} = \frac{V_b \sin \phi_b}{V_b \cos \phi_b - V_{pz}} \tag{7.34}$$

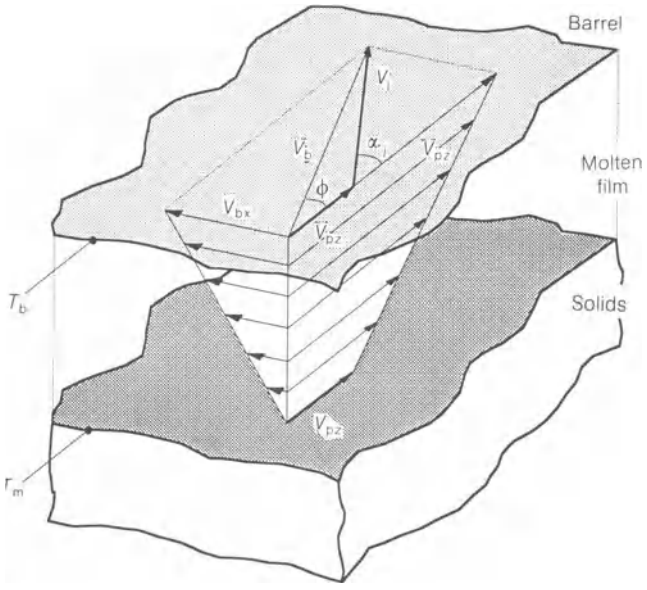


Figure 7.24 Velocity difference between the barrel and the solid bed.

- The melt is Newtonian, hence the velocity profile of the film is linear; the corresponding shear rate is V_j/δ_f. The melt is mainly removed in the cross-channel direction, the rate being primarily determined by the velocity component V_{bx}. Thus, the film thickness variation in the zz direction is small.
- The thermophysical properties of the polymer are constant. As in solids conveying, if computations are performed for small downchannel increments, the influence of local changes in pressure, temperature and shear rate on those properties can be considered.

The width of solids X, at any channel location can be determined through a mass balance in the solids. Considering a small plug increment in the downchannel direction, the rate of solids entering the element in the location Δz equals the sum of the rate of solids leaving the element at a location $(z + \Delta z)$ and through the solids/melt film interface, due to fusion:

$$\rho_p V_{pz} h X|_z = \rho_p V_{pz} h X|_{z+\Delta z} + V_{py} \rho_p \bar{X} \Delta z \tag{7.35}$$

In this equation V_{py}, X and V_{pz} are unknown. Since the latter was assumed to be constant throughout the process, immediately before melting is initiated one may write:

$$G = \rho_p V_{pz} h_0 b \tag{7.36}$$

where G is the mass flow rate of the plasticating process (which is assumed to be known) and h_0 is the channel depth at the onset of the melting mechanism. Thus, there are still two unknowns in equation (7.35). A heat balance at the solids/melt film interface may provide the required second correlation. In this case, the rate of heat conducted to the interface by the melted film is partially removed from the interface to the solids by conduction, and partially used to melt the material. Mathematically:

$$k_m \left(\frac{\partial T}{\partial y}\right)_{y=0} - k_p \left(\frac{\partial T}{\partial y}\right)_{y=0} = V_{py} \rho_p \lambda \tag{7.37}$$

where k_m and k_p are the thermal conductivities of the melted and solid polymer respectively, and λ is the polymer heat of fusion. This equation requires knowledge of the temperature profile in the melt and in the solids. Thus, the energy equation must be solved, and the film thickness, δ_f computed. This results in a relatively complex sequence of calculations to determine X:

1. Temperature profiles of the melted film and of the solids plug. The momentum and energy equations must be solved.
2. Heat transfer rates at the solids/melt film interface.
3. Heat balance in the interface (equation (7.37)).
4. Mass balance in the film. This is done to compute δ_f. Consider a small

film length in the downchannel direction. One may write,

[Rate of previously melted material entering the element at z] +
[Rate of newly melted polymer entering the element via the interface] =
[Rate of material leaving the increment at $z + \Delta z$] +
[Rate of material leaving the increment to feed the melt pool]

or, mathematically:

$$\rho \bar{V}_z X \delta_f|_z + V_{py} \rho_p \bar{X} \Delta z = \rho \bar{V}_z X \delta_f|_{z+\Delta z} + (V_{bx}/2) \rho \bar{\delta}_f \Delta z \tag{7.38}$$

where $\bar{V}_z$ and $V_{bx}/2$ are the film average flow speeds in the downchannel and cross-channel directions, respectively, and $\bar{X}$ and $\bar{\delta}_f$ are the average values along the increment.

5. Mass balance in the solid bed (equation (7.35)).
6. Solving the resulting differential equation for the geometry of the system. The function $X(z)$ will then be known, as well as z_t.

The relevant equations obtained throughout the above sequence will be presented in the following paragraphs.

1. **Temperature profile in the melted film**. From the momentum equation (one-dimensional flow, with $x = j$ and $v_j(0) = 0$ and $v_j(\delta_f) = V_j$ as boundary conditions), one obtains the linear film velocity profile. Inserting this profile in the energy equation ($x = j$) and integrating (with boundary conditions $T(0) = T_m$ and $T(\delta_f) = T_b$), one finally obtains:

$$\frac{T - T_m}{T_b - T_m} = \frac{\eta V_j^2 y}{2k_m \delta_f (T_b - T_m)} \left(1 - \frac{y}{\delta_f}\right) + \frac{y}{\delta_f} \tag{7.39}$$

The dimensionless term $\eta V_j^2 / 2k_m (T_b - T_m)$ is usually known as the **Brinkman number**, B_r, and quantifies the importance of viscous heat generation relative to the heat supplied by conduction. As seen in Fig. 7.25, which represents several possible temperature profiles across the melted film, when $B_r < 2$ the viscous dissipation is limited, hence the film temperature is always smaller than that in the barrel. However, if $B_r > 2$ the viscous dissipation becomes important, and the melt temperature may locally exceed the barrel set values. This has obvious practical consequences, especially when working with temperature-sensitive polymers, since it means that the polymer may degrade,

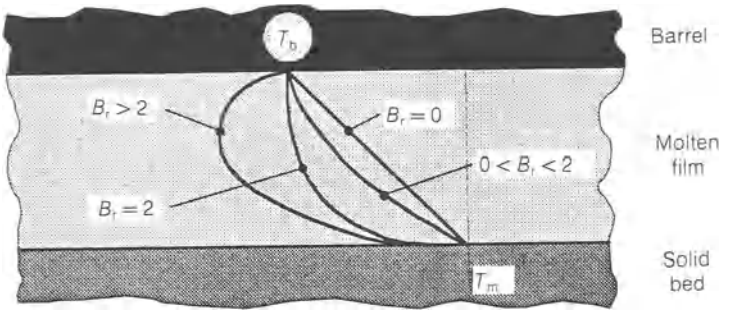


Figure 7.25 Temperature profiles in the melt film and corresponding Brinkman numbers.

even at moderate melt temperatures in the die. It also implies that increasing barrel temperatures, T_b, will decrease η and, consequently, the viscous dissipation, which may result in lower melt film temperatures. The maximum value of V_b that ensures $B_r \leq 2$ can be determined, i.e. for a certain barrel temperature, the maximum advisable screw frequency avoiding the premature polymer degradation can be computed.

2. **Temperature profile in the solids**. Integrating the energy equation with $T(0) = T_m$ and $T(-\infty) = T_p$ produces:

$$\frac{T - T_p}{T_m - T_p} = \exp\left(\frac{V_{py}}{\alpha_p} y\right), \tag{7.40}$$

where α_p is the thermal diffusivity of the solid polymer.

3. **The heat fluxes per unit area** from the melt film to the interface, and from the interface to the solids are, respectively:

$$-[q]_{y=0} = \frac{k_m}{\delta_f}(T_b - T_m) + \frac{\eta V_j^2}{2\delta_f} \tag{7.41}$$

$$-[q]_{y=0} = \rho_p C_p V_{py}(T_m - T_p) \tag{7.42}$$

where C_p is the specific heat of the solid polymer.

4. **Heat balance in the interface and mass balance in the film**. Combining the equations describing the two balances, the resulting expression reduces to:

$$\omega = V_{py}\rho_p X = \frac{V_{bx}}{2}\rho_p \delta_f = \Omega\sqrt{X} \tag{7.43}$$

with

$$\delta_f = \left\{\frac{[2k_m(T_b - T_m) + \eta V_j^2]X}{V_{bx}\rho_p[C_p(T_m - T_p) + \lambda]}\right\}^2 \tag{7.44}$$

$$\Omega = \sqrt{\left\{\frac{V_{bx}\rho_m[k_m(T_b - T_m) + \eta V_j^2/2]}{2[C_p(T_m - T_p) + \lambda]}\right\}} \tag{7.45}$$

The parameter Ω is a measure of the melting rate. The numerator is proportional to the rate of heat being supplied for melting, both from conduction (first term) and from viscous dissipation (second term). The denominator represents the heat required for converting the solid at temperature T_p into a melt at T_m. The relevant polymer properties are the heat capacity, C_p, and the heat of fusion, λ. The melting rate increases with increasing barrel temperature, T_b, and screw speed (contained in V_{bx}), but this is obviously limited by the eventual polymer degradation, as expressed by the Brinkman number, B_r. The melting rate also increases by preheating the solid polymer, T_p, since it decreases the heat required for melting. However, this solution must be considered with caution, as the polymer pellets may stick to the feed opening walls, hindering the flow of solids to the first screw turns.

5. **Mass balance in the solid bed**. The following differential equation describes the melting process:

$$-\frac{d(hX)}{dz} = \frac{\omega}{\rho_p V_{pz}} \tag{7.46}$$

6. **Influence of the system geometry**. For a **constant-depth channel**, inserting equation (7.43) in (7.46) and integrating, taking as initial condition $X(z_1) = X_1$ (where z_1 is an arbitrary helical distance), and using equation (7.36):

$$\frac{X}{b} = \frac{X_1}{b}\left[1 - \frac{\Omega b h_0}{2Gh\sqrt{X_1}}(z - z_1)\right]^2 \tag{7.47}$$

If $X(0) = b$,

$$\frac{X}{b} = \left(1 - \frac{\Omega\sqrt{b}h_0}{2Gh}z\right)^2 \tag{7.48}$$

The total helical length required for melting, z_t, can be determined from equation (7.48), with $X = 0$ (completion of melting):

$$z_t = \frac{2Gh}{\Omega\sqrt{b}h_0}. \tag{7.49}$$

If melting is completed in the geometrical section in which it started, $h \simeq h_0$. As seen in section 7.3.1, and illustrated in Fig. 7.21, the delay zone downchannel length may be correlated with a dimensionless melting parameter, ψ. This parameter represents the ratio of the melting rate per unit downchannel solid/melt interface (ω/X) to the solids rate ($V_{pz}\rho_p$):

$$\psi = \frac{\Omega}{V_{pz}\rho_p\sqrt{X_1}} = \frac{\Omega\sqrt{b}}{G/h_0} \tag{7.50}$$

Equations (7.47)–(7.49) can be rewritten, respectively, as:

$$\frac{X}{b} = \frac{X_1}{b}\left[1 - \frac{\psi}{2h}(z - z_1)\right]^2 \tag{7.51}$$

$$\frac{X}{b} = \left(1 - \frac{\psi}{2h}z\right)^2 \tag{7.52}$$

$$z_t = \frac{2h}{\psi} \tag{7.53}$$

For a **tapered channel** with a linearly decreasing channel depth:

$$h = h_1 - Az \tag{7.54}$$

where $h_1 = h(z = 0)$, and A is the degree of tapering (given by $(h_1 - h_2)/Z_{comp}$), equations (7.51)–(7.53) become, respectively:

$$\frac{X}{b} = \frac{X_1}{b}\left[\frac{\psi}{A} - \left(\frac{\psi}{A} - 1\right)\sqrt{\left(\frac{h_1}{h_1 - Az}\right)}\right]^2 \tag{7.55}$$

$$\frac{X}{b} = \left[\frac{\psi}{A} - \left(\frac{\psi}{A} - 1\right)\sqrt{\left(\frac{h_1}{h_1 - Az}\right)}\right]^2 \tag{7.56}$$

$$z_t = \frac{h_1}{\psi}\left(2 - \frac{A}{\psi}\right) \tag{7.57}$$

Tadmor and Gogos (1979) included the effect of convection on the temperature profile in the melt film and concluded that the above equations overestimate the melting rate. They also derived relations equivalent to those presented here, but for a power-law fluid.

If the progression of melting along the screw or the channel length required for melting is to be calculated, data on the thermophysical properties of the polymer, on the system geometry and on the mass throughput must be available. The melting rate (equation (7.45)) should first be computed and its value inserted in either equations (7.51)–(7.53) or (7.55)–(7.57), depending on the geometry of the system. However, to determine Ω, V_j (computed from equation (7.32) with (7.36)) and η must be known. Thus, the average film temperature and the shear rate must be estimated. The former may be taken, as a first approximation, and neglecting viscous dissipation, as $(T_b + T_m)/2$. The second is given by the ratio V_j/δ_f. The average film thickness may be estimated as half of its maximum value, which is reached at the beginning of the melting process, as expressed in equation (7.44). Considering the influence of the viscous dissipation, the average film temperature is:

$$\bar{T} = \frac{1}{\delta_f}\int_0^{\delta_f} T\,dy = \frac{T + T_m}{2} + \frac{\eta V_j^2}{12k_m} \tag{7.58}$$

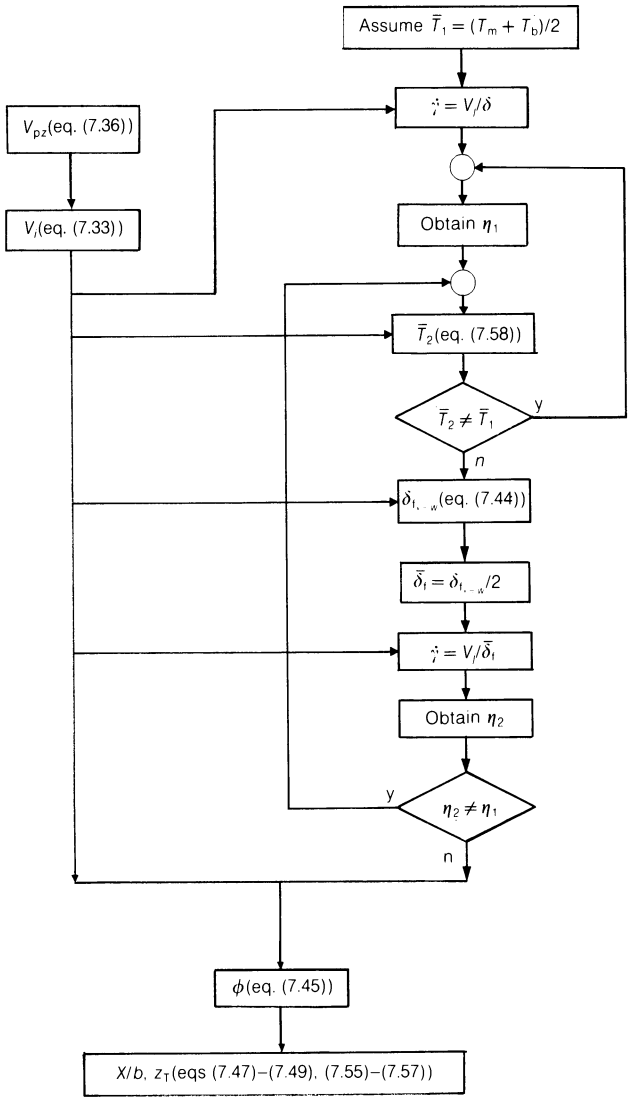


Figure 7.26 Use of Tadmor's melting model to compute the reduced solid bed width, or the length required for melting.

If an iterative procedure is adopted, the initial estimates of the average film temperature and thickness may be corrected. The flowchart depicted in Fig. 7.26 shows how to evaluate V_j and η before computing the melting rate, Ω. One should also be aware of the importance of the screw geometry upon the development of melting. If, for example, melting starts in the feeding zone of the screw, it may well continue along the compression zone. In this case,

equation 7.49 may be used to confirm whether melting will be completed in the geometric zone where it started. If not, through the application of equation (7.48), it is possible to determine X at location z corresponding to the transition from the feeding to the compression zone. Equation (7.55) should then become applicable. Eventually, if melting has not been completed during compression, the same reasoning will be adopted, and equation (7.47) will now be used to describe melting along the screw pumping zone.

For a constant-depth channel, the melting length is proportional to the mass flow rate and inversely proportional to the melting rate, Ω (equation (7.49)). Since the effect of the operating conditions is contained in this parameter (see equation (7.45)), one can easily arrive at three conclusions. First, an increase in the screw speed (contained in V_j) promotes viscous dissipation, and hence induces higher melting rates. Unfortunately, the conduction term becomes smaller, as the average material residence time inside the extruder diminishes. The overall effect will certainly depend upon the levels of polymer viscosity. Figure 7.27 simulates the effect of increasing screw speeds on the reduced solid bed width X/b, i.e. on the axial length required for replacing solids ($X = b$) by a melt flow ($X = 0$) in the screw channel (taking the extruder and polymer considered in the previous section as an example). The onset of the melting mechanism depends on the conditions developed during the previous solids (and delay) zone. The figure clearly shows that a bigger portion of the screw is dedicated to melting when operating at higher screw frequencies, although the differences between the various curves become smaller as the screw speed increases. This behaviour is obviously caused by the progressive importance of viscous dissipation as the screw speed increases. The plot also shows that high screw speeds may be encouraging from an output point of view, but questionable in terms of product quality. In fact, little or no screw length remains available for melt mixing and pumping purposes, when operating at

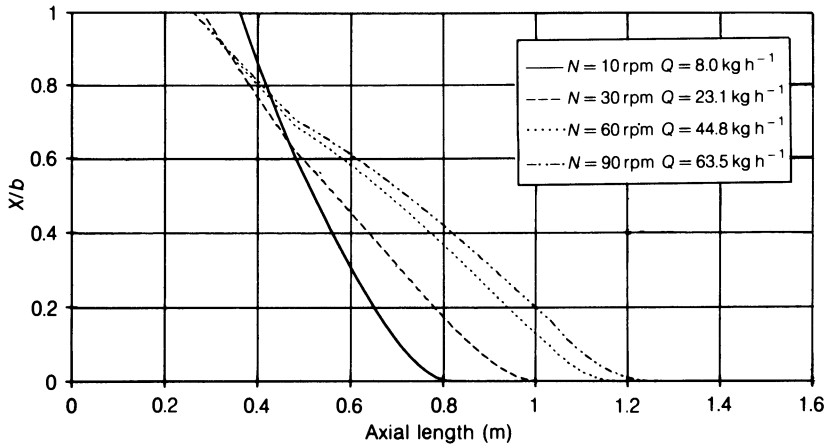


Figure 7.27 Influence of screw rotation on the solid bed profile.

elevated screw frequencies. Tadmor and Klein (1970) showed clearly that a good compromise between output and extrudate quality may be reached when running the machine at higher screw speeds than necessary for a particular output, together with high back pressures in the die (this can be achieved, for example, by fitting the die with a pressure value). The effect of this strategy can be easily understood with the assistance of plots of Q (output) against P (pressure), as presented in the previous chapter. The operating point is shifted to higher pressures, due to a decrease in the slope of the die curve, and to a vertical displacement of the extruder characteristic. Attention should be paid to the eventual vital role of viscous dissipation under these conditions.

Second, increasing barrel temperatures raises the melting rate, because the contribution of conduction increases. The barrel set temperatures are obviously limited by the possibility of the thermal degradation of the polymer. Simultaneously, the viscous dissipation component will drop, due to the progressive reduction of the melt viscosity. According to correlation (7.45), the heat necessary for melting is $[C_p(T_m - T_p) + \lambda]$. In fact, heat is required not only to melt the material, but also to bring it to the average temperature of the film, $\bar{T}$ (equation (7.58)). Thus, the total heat to be input is:

$$q_b = C_m(\bar{T} - T_m) + C_p(T_m - T_p) + \lambda \tag{7.59}$$

From the above considerations, it follows that for a specific screw speed, material, and extruder geometry, there may be an optimum barrel temperature maximizing the joint influence of heat conduction and viscous dissipation. Figure 7.28 shows the results of simulations performed for the case study referred to throughout this chapter. As expected, both the onset of the Tadmor melting process and the reduced solid bed width axial profile depend on the barrel set temperatures (Fig. 7.28(a)). The variation of the former can easily be identified in Fig. 7.28(b), which plots the axial pressure profiles for the various operating conditions. After an exponential growth during solids conveying, the rate of pressure increase is reduced in the delay zone, but recovers upon melting and melt conveying. The helicoidal length, z_t, decreases as the barrel temperature increases up to 190°C, where a minimum seems to be attained (Fig. 7.28(c)). Thus, in this example, the joint effect of the lower heat generation and of the additional heat needed to raise the temperature of the freshly formed melt is more intense than the effect of the strengthened heat conduction.

Third, as seen above, an increase in the inlet temperature, T_p, of the solids increases the melting rate. Using the equations presented here in small downchannel increments, it is possible to update the value of T_p (see equation (7.40)) and to account for the progressive heating of solids along the channel. The predictions will then accompany the observed acceleration of the melting process in its closing stages.

The melting length in a tapered channel is always shorter than in a constant channel (compare equation (7.57) with (7.53)). The effect of compression can

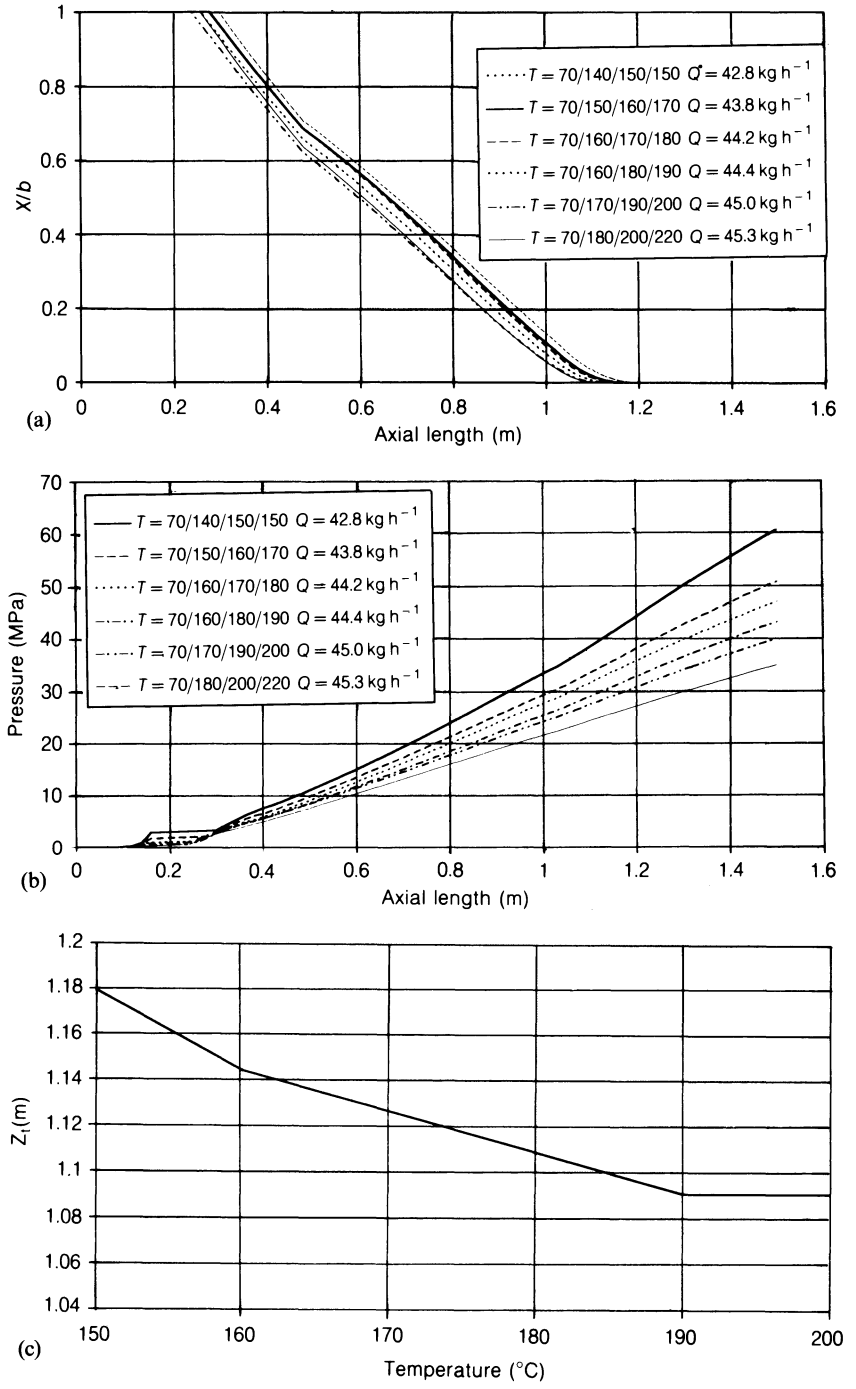


Figure 7.28 Simulation of the effect of barrel temperature on melting: (a) influence on the solid bed profile; (b) influence on the axial pressure profile; (c) effect on the length of channel required for melting.

be viewed as a relative increase in the width of the solids exposed to heat and shear, while the depth h decreases. This behaviour is illustrated in Fig. 7.29 for our case study (the performance of three screws having different channel depths in the pumping zone, the other parameters remaining unchanged, is compared – see also Table 7.2). When $A = 0$, equations (7.56) and (7.57) reduce to equations (7.52) and (7.53), respectively. In this case, the reduced solid bed width profile exhibits a parabolic regression. As the taper increases that decline becomes progressively less concave, then convex, while simultaneously z_t shortens. The higher the taper A, the shorter z_t. When $A/\psi = 1$ a limit is reached, and the length required for melting is at its minimum:

$$z_{t,\min} = \frac{h_1}{\psi} \tag{7.60}$$

In this case, the solid bed width remains constant throughout the melting process, then X reduces to zero over an infinitely small distance. Figure 7.30 presents four predicted reduced solid bed profiles for different values of the taper A. As seen above, the melting process is slower in a constant-depth channel, while maximum efficiency can be obtained if $A = \psi$. The other two intermediate situations will induce either concave ($A/\psi \ll 0.5$), or convex ($A/\psi \gg 0.5$) melting profiles. In a real situation, the melting rate may not be able to match the rate of compression, resulting in an observable increase in the solid bed width along the channel. This phenomenon has already been discussed in section 7.2, and may lead to severe extrusion instabilities, as a result of channel plugging. Rauwendaal (1990) has shown that plugging can be avoided when the length of the compression zone, L_c, is:

$$L_c \geq \frac{V_{pz}\sqrt{X_1}h_1\rho_p(C_R - 1)\sin\phi}{\Omega C_R}, \tag{7.61}$$

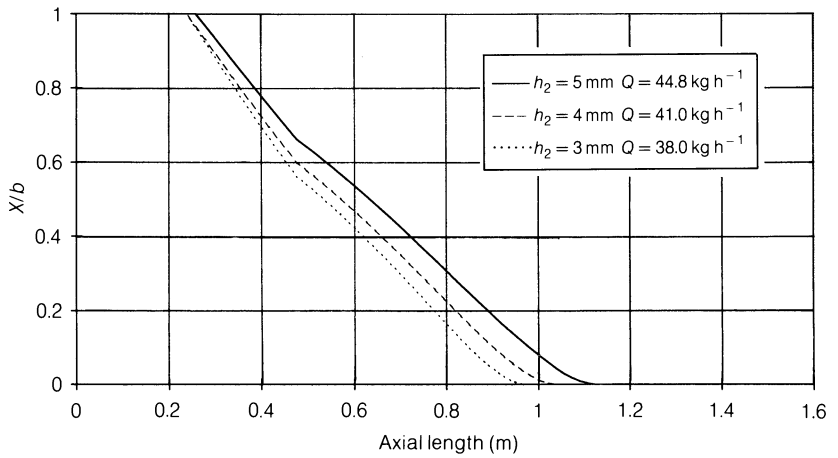


Figure 7.29 Influence of the channel depth on the solid bed profile.

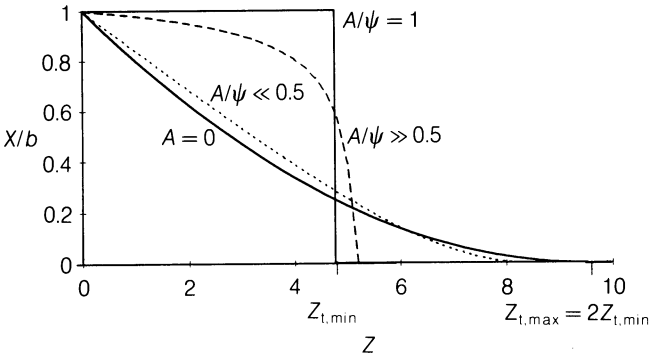


Figure 7.30 Effect of the taper, A, on the solid bed profile.

where C_R is the compression ratio (h_1/h_2), h_1 and X_1 are the channel depth and the width of solids at the beginning of the taper, respectively. A significant compression ratio requires a relatively long compression zone.

The mechanical power supplied by the screw drive during melting may be calculated as the rate of working at the interface between the polymer and the inner barrel wall (in the melting zone). Therefore, the total power consumption results from the contribution of the power used up in the melt film, E_f, in the melt pool, E_m, and in the mechanical gap, E_g:

$$E_w = E_f + E_m + E_g \tag{7.62}$$

Each component may be computed by integrating the product of the velocity and force (shear stress) over the relevant barrel surface. For the Newtonian isothermal case, which has been assumed in this section, the power consumption in the melt pool, in a length dz of the channel, can be calculated from equation (8.7) (melt pumping), replacing the channel width, b, by the local melt pool width, $b - X$. Similarly, the power consumption in the clearance is given by equation (8.8), which was obtained assuming that the local pressure flow was small compared to drag flow. Rauwendaal (1990) computed E_f for a power-law fluid. Tadmor and Klein (1970) adopted a different approach, and determined the power introduced in a film down-channel increment as the rate of energy introduced by viscous dissipation. This is given by:

E_f = [Rate of energy introduced by viscous dissipation in the increment dz]
= {[Heat required for melting]
− [Heat conducted at the barrel surface]}
× [Mass rate of melting]

The heat conducted at the barrel interface is obtained by differentiating equation (7.39):

$$-X[q]_{y=\delta_f} = \frac{Xk_m(T_b - T_m)}{\delta_f} \tag{7.63}$$

The mass rate of melting is $Q_x \rho_m \, dz$, where $Q_x = \delta_f V_{bx}/2$. Therefore,

$$dE_f = \frac{\delta_f V_{bx} \rho_m}{2} \left[C_m(\bar{T} - T_m) + C_p(T_m - T_p) + \Omega - \frac{Xk_m}{\delta_f}(T_b - T_m) \right] dz \tag{7.64}$$

Principles of energy balance

8

8.1 ENERGY BALANCE AND EFFICIENCY

The two preceding chapters have dealt with the mass output of the extruder and its relation to screw speed and back pressure, but it has been mentioned that energy considerations impose additional restrictions on the useful output in commercial operations. The purpose of the present chapter is to formulate the energy balance of the single-screw extruder, examine the components of this balance and the factors on which they depend, and deduce the overall effects on the energy balance of deliberate changes in operating conditions. These aspects have been largely neglected in the literature, so their inclusion gives greater relevance of theory to practical experience and permits further rational development of operating strategies.

If the extrusion process is considered as a total system, it takes in raw polymer, usually at room temperature, and by energy-consuming processes converts the polymer into semi-finished or saleable products, again usually at room temperature. The specific energy content of the polymer is only slightly changed by virtue of chemical degradation, changes in crystallinity, residual pressure or stresses, changes of shape, etc., and such changes in energy content can rarely be exploited in the final use of the product. Thus the consumption of energy is seen as an inevitable concomitant of the fabrication process and efficiency is defined in terms of specific energy input in joules per kilogram of useful product. This will depend at least as much on the characteristics of the polymer and the product as on the process, and thus bears only slight relationship to the efficiency of the latter. It also reveals little of the consequences for unit output or product quality, for which a closer study of the process and its interactions is necessary. The major energy input is to heat the polymer, either intentionally to the temperature required for shaping or incidentally in random processes such as mixing, and to supply the consequential losses to the surroundings. Rapid production requires that after shaping, the temperature and heat content of the product are reduced by large masses of low-temperature coolant (section 4.3), leading to small temperature rises and low-grade heat in ambient air or cooling water. Proposals have been

made for reclaiming this waste heat, which in any case contributes to space heating, thus reducing the overall energy consumption. However, it only affects the process itself if applied, for example, to preheating the raw polymer feed (section 9.1). Thus the main opportunity for improving the efficiency in energy terms lies in reducing the energy input required by the process; the following analysis therefore concentrates on the energy balance and utilization within the extruder itself, to give a supply of polymer at the correct temperature and degree of mixing for the shaping process.

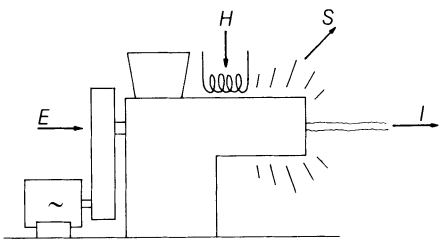
The block diagram in Fig. 8.1 shows the energy input to the extruder from three sources: (i) enthalpy of feed material I_1; (ii) mechanical energy to turn the screw E: and (iii) energy from heaters H. The energy output is in the enthalpy of the product I_2 and losses from the extruder S. Since by continuity of mass, the input and output masses are identical, it is convenient to consider only the increase in enthalpy of the product I where:

$$I = I_2 - I_1 \tag{8.1}$$

In steady state, the energy balance is then:

$$E + H = I + S \tag{8.2}$$

Considering each item in turn, the mechanical power applied to the screw shaft E is available for heating the polymer; if some is converted into frictional heat at the barrel surface or in the feed pocket seal, this is available for heating the polymer or contributes to the losses to feed pocket cooling or in radiation, and so is included in the balancing terms I and S. If E is measured at the drive motor output, then the losses in transmission belts or gears and in the bearings must be included in the total losses S to balance; if E is measured by electrical or hydraulic input to the drive then motor losses must also be included in S, since they cannot contribute to heating the polymer. The energy from the heaters H is conveniently measured as the electrical or fluid heat input to the heaters, since it is difficult to separate heat losses from the heater surfaces and from



E	+	H	=	I	+	S
Mech. work		Heater input		Heat in polymer		Heat losses

Figure 8.1 Extruder energy balance.

exposed areas of the extruder itself; if an electric heater were removed, then there would be appreciable heat losses from the additional barrel surface exposed, so it would be unreasonable to attribute this loss separately to the heater. When cooling is applied to barrel, screw or feed pocket, the heat removed must be included either as a negative input in calculating H or as a component of the losses S. Since barrel cooling is normally only applied when the heaters are switched off, the author prefers to count this as a negative input H, whereas cooling to the feed pocket (and screw) are applied for other purposes than controlling polymer output temperature, with either barrel heating or cooling, and are thus included in the losses S. The term H thus represents the energy in heating (or cooling) which must be intentionally applied to maintain steady operating conditions.

In the absence of chemical reactions within the extruder, such as polymerization, cross-linking, degradation, hydrolysis or reaction with additives, the energy input to the constant mass of polymer is the increase in enthalpy plus the pressure energy:

$$I = m \int_{T_1}^{T_2} C_p \, dT + p(V + dV) \tag{8.3}$$

If gas or vapour is removed in venting, this represents both a decrease of mass and an additional energy loss. The feed material is normally at or near atmospheric temperature and pressure; if preheating or melt-feeding, especially under pressure, is used I_1 becomes significant and must be deducted to give the increase of enthalpy I-(equation (8.1)). Otherwise the increase of enthalpy is sufficiently represented by the mass flow in kilograms per second times the specific enthalpy (heat content*) in joules per kilogram at the end of the machine, reckoned from room temperature. At the end of the screw, the polymer is also at elevated pressure and the corresponding pressure energy (the second-right-hand term in equation (8.3)) must be added to the increase in enthalpy to give the total energy input to the polymer. This may account for up to around 15% of the energy input and many writers (Bernhardt, 1959; Fisher, 1976) include it as a separate term. The screw does work in the polymer equivalent to that to 'compress and deliver' in a compressor; however, this is used to force the polymer through the die, where the work is converted to frictional heat, raising the temperature of the polymer and/or die. Since at the die exit the pressure is normally atmospheric, the pressure term may be excluded by taking the energy input I as mass flow times the enthalpy of the polymer at the die exit temperature; in any case this is usually the critical temperature for processing;

$$I = \rho Q \int_{T_1}^{T_2} C_p \, dT \tag{8.4}$$

*An average specific heat is valid for small changes in melt temperature, but not for total energy balance (section 4.1)

Since the adapter and die are rigidly connected to the barrel, heat flow between them is difficult to determine, so it is convenient for the energy balance to treat barrel and die together. Then the heater input H should include heat to the die and the losses S include the heat losses from the die – in the case of large sheet or tube dies, these may be substantial proportions of the totals, but not necessarily equal to each other.

The losses S (Fig. 8.2) include convection and radiation to the surroundings from the barrel, die and heaters, conduction to barrel and die supports and longitudinally to the feed pocket at one end and any die attachments, e.g. sizing plates, at the other. Conduction to the feed pocket reappears in feed-pocket cooling and heat to the bearing assembly. Cooling of the screw by air or fluid also removes heat from the system – estimation of these losses is considered in appendix C.1, but the foregoing emphasizes the importance of including all factors, for example by measurement under conditions as near as possible to those of actual operation.

The energy balance represented by equation (8.2) must be satisfied at all steady-state conditions, and the consequences of changes in operating conditions on the separate energy items will be considered later in this chapter (section 8.5) and in section 9.2. As discussed above, the magnitude of certain terms will depend on the definitions used, as also will the efficiency of the process, whether this is defined as the useful output per unit energy input ($\mathrm{kg\,MJ^{-1}}$), or as the ratio of useful energy to total energy. The former definition depends largely on the maximum temperature, which in turn depends on the polymer and requirements of downstream stages of the process. For the present purpose it is more instructive to take the second definition, where process efficiency is given by:

$$\Phi = \frac{I}{E+H} = \frac{I}{I+S} \tag{8.5}$$

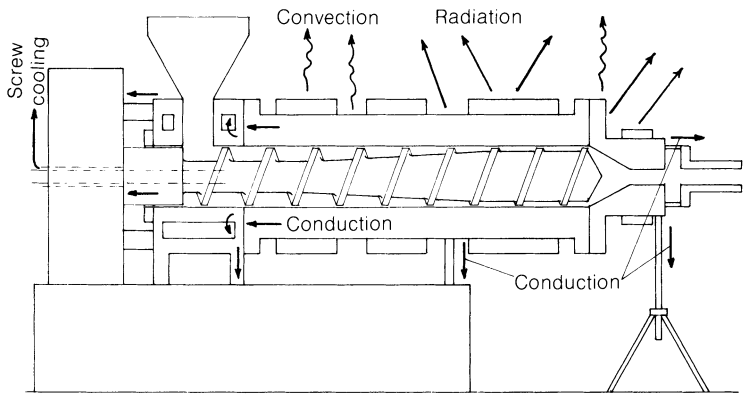


Figure 8.2 Heat losses.

which in the absence of preheating reduces to:

$$\Phi = \frac{I_2}{E+H} = \frac{I_2}{I_2+S} \tag{8.6}$$

It is evident that this value of efficiency will depend on the values of E, H and S and hence on how the latter are defined; if the power input is measured at drive motor input or output, E and S will be correspondingly greater and the efficiency Φ less than if power is measured at the screw. The effects on efficiency of *small* changes in operating conditions will be similar, but it must be remembered that the efficiency of certain drives such as Schrage and AC commutator motors and magnetic slip couplings varies widely with load and/or speed. Thus changes in efficiency based on electrical input may reflect the efficiency of the drive more than that of the extruder, and comparisons between different machines may be misleading.

As the energy balance and its effects on the performance of the extrusion process have not been widely discussed in quantitative terms, some comments are given in appendix C.1 on experimental measurement of the former in respect of semi-technical and production machinery; the special equipment and techniques applicable to research units are outside the scope of this work.

8.2 POWER CONSUMPTION IN THE SCREW: NEWTONIAN ISOTHERMAL CASE

Mechanical power is absorbed by turning the screw within the polymer mass in the channel and also by shearing between the screw flight and barrel. The former causes internal shearing of the polymer, but only by virtue of a circumferential component of shear stress between the polymer and the barrel wall; it is thus sufficient for total power to consider the screw and polymer as rotating together relative to the barrel exerting the same component of stress with the relative velocity of the screw to the barrel. Since the shear rate over the flight will be much greater than that over the channel, the shear stresses will differ and the two regions are conveniently considered separately. Components of shear stress which are parallel to the screw axis will cause a thrust on the barrel and equal reaction on the screw and thrust bearing; however, since no motion takes place in this direction, no work is done, and the circumferential or tangential components represent the consumption of power.

Newtonian behaviour implies that the viscosity of a given polymer is a function of temperature only, and not of shear rate; this also implies that the effective viscosity (ratio of shear stress to shear rate) in one direction will not be influenced by shear components in other directions and so the components may be treated independently – this is not the case with pseudoplastic fluids. The isothermal restriction implies that the effective temperature and hence viscosity is the same in both directions and also over the screw flight. Further, it

implies that viscous heating both due to shear at the surface and within the polymer mass is instantaneously dissipated (e.g. to the barrel and screw) so that temperature and viscosity are not functions of time and do not react on the velocity profile (section 4.3).

In order to derive expressions for velocity and shear rate in Chapter 6 the total velocity of the barrel relative to the screw πDN was resolved into components along and across the screw channel (equations (6.4) and (6.5)). The method followed here, for which grateful acknowledgement is made to Weeks and Allen (1962), is to derive the shear stresses corresponding to the velocity components and recombine them to give the total shear stress in the tangential direction. The shear rates at a depth y from the screw surface are given by equations (B.7) and (B.11). Putting $y = h$, these equations give the shear rates at the barrel surface, and substituting for the pressure gradients dP/dz and dP/dx from equations (6.16) and (6.24) respectively gives the wall shear rates in terms of Q/Wbh and the velocity components. When multiplied by the (Newtonian) viscosity, these give the corresponding shear stresses from which the tangential components are obtained. These are summed and multiplied by the area of barrel surface and tangential velocity to give the power absorbed. A similar method is used for the power absorbed over the flight. Detailed derivations are given in appendix C.2. Thus the power absorbed in a length dz of the channel is:

$$E_{Ch} = \frac{\eta W^2 b\, dz}{h}\left[4(1 + \tan^2\phi) - \frac{6Q}{Wbh}\right] \qquad \text{(C.14) (8.7)}$$

The power absorbed in the flight clearance is:

$$E_{Fl} = \frac{\eta W^2 t\, dz}{\delta \cos\phi} \qquad \text{(C.18) (8.8)}$$

The total power absorbed in length dz of the melt pumping section is:

$$E_{dz} = \frac{\eta W^2 b\, dz}{h}\left[4(1 + \tan^2\phi) - \frac{6Q}{Wbh}\right] + \frac{\eta W^2 t\, dz}{\delta \cos\phi} \qquad \text{(C.19) (8.9)}$$

For a screw of constant pitch p and depth h in the melt pumping section the total power in a channel of helical length Z is given by equations (8.9) with dz replaced by Z, where:

$$Z = \frac{L}{\sin\phi} \qquad (6.1)$$

and L is the corresponding axial melt length.

For a screw of constant diameter D but varying depth h, equations (8.9) may be integrated, or more simply approximated by summing the power absorbed in a number of elements, each of constant depth and to each of which equation (8.9) applies with the appropriate value of h. Note that for constant pitch, W, b, ϕ and t are constant, and the flight clearance δ is also normally constant;

the volumetric flow Q is constant by continuity, so a changing value of h implies also a changing value of Q/Wbh. Horizontal lines in Table 6.1, which is based on equation (6.69), show qualitatively the variation of power along the length of a tapered screw, neglecting the transverse component represented by the term $\tan^2 \phi$. These show that at deep portions of the screw the power is hardly affected by back pressure, that the power input generally increases towards the shallow parts of the screw and this is most marked at high back pressures. The right-hand term of equation (8.9) is independent of h and so may be calculated directly from the value of Z as for a constant-depth screw.

The power absorbed in the melt section is that likely to be affected most by changes in operating conditions, including the consequent change in effective melt length. In the usual single-screw extruder without force feeding, the power absorbed in conveying the solid polymer is likely to be a small proportion of the total, and little affected by operating changes except to screw speed, to which it would be expected to be approximately proportional. The several possible mechanisms of melting are extremely complex, as has been discussed in Chapter 7, and the temperature and shear rate will vary with position in the channel as well as from turn to turn. The power consumed in melting is inherent in estimation of the position where melting is complete, and in the adiabatic condition it is approximately equal to the mass flow multiplied by the polymer heat content (enthalpy) at the melting temperature (Fig. A.2). This may be taken as the crystalline melting point (Table A.1) for semi-crystalline polymers or the softening point (say, 30°C above T_g) for amorphous polymers. If it is necessary, for example, to determine the maximum output with the existing drive motor, it is suggested that the power absorbed in melting is added to that in the melt pumping section (equation (8.9)). The total power thus obtained will be an overestimate for small machines and low speeds, where considerable energy for melting is received from the heaters, but with larger machines or higher speeds it will become progressively more accurate as the adiabatic point is approached.

As suggested on p. 166, the position at which melting is complete, for estimating the effective melt length Z, may be computed theoretically from the Tadmor melting model; it is difficult to measure experimentally, but is not likely to be less than the length of any constant-depth 'metering' section (especially with stepped screws) or greater than the length over which pressure is generated.

In the present work it will be assumed that the specific enthalpy ($J\,kg^{-1}$) of the polymer at the beginning of the melt pumping section is constant, irrespective of the relative contributions from heaters and mechanical power to the screw up to that point. Thus the changes in power input in the melt pumping section, and hence changes in melt temperature, due to changes in operating conditions will be given by equation (8.9), although it is appreciated that the total power input and the energy balance will also be affected by associated changes in the mechanism of melting. Before analysing equation (8.9) in terms

of the effects of the independent variables (speed, back pressure, screw diameter, length, depth and flight clearance), the appropriate value of temperature for determining viscosity must be discussed. Since equation (8.9) is based on the shear stress at the barrel wall, the temperature and viscosity at this position are relevant, not the 'mean mixed' temperature for the whole channel; the latter is difficult to measure reliably, even by sophisticated sampling or integrated multiple-measuring methods. In practice, the temperature near the barrel will be influenced to some extent by cross-channel circulation (section 6.2), especially in conditions of severe heating or cooling, and by the distribution of shear heating within the channel (section 8.4). It will also be strongly affected by shear heating in the flight clearance (section 8.4) so the best compromise using the isothermal equation is to take the time-averaged temperature of the barrel wall *close* to the inner surface.* The necessity for measurement of temperature close to the inner surface of the barrel arises largely from the effects of heat transfer from/to the barrel heating/cooling system. For reasons of fast response, accurate control and reduction of temperature overshoot, the thermocouples providing the control signal for heaters and barrel cooling are situated near the heating or cooling elements or at least close to the outer surface of the barrel. As shown by equation (4.1), heat flow by conduction is in the direction of, and directly proportional to, the (falling) temperature gradient. Thus, for the same 'set' value on the temperature control, the temperature near the polymer will be lower or higher according to whether the heat is being supplied or withdrawn from the polymer (Fig. 8.3). Further, this difference will be greater for severe heating or cooling than for near-autogenous conditions when radial heat flow will be small. The implications of these temperature changes for operation and control will be considered in section 9.1, but here it must be noted that they will affect viscosity and power input and correct estimation of the latter must depend on choice of the appropriate temperature.

The longitudinal variation of temperature experienced in practice is best allowed for by applying equation (8.9) to successive length elements in a similar way to that suggested for varying-depth screws. The effects of shear rate and temperature variations on viscosity and power will be considered in sections 8.3 and 8.4; the purpose here is to determine what experimental values are most appropriate for use with the Newtonian isothermal approximation represented by equation (8.9). It may be noted that the form of the equation keeps separate the power absorbed in channel and flight clearance so that it is possible simply to insert different values of viscosity in the two terms of the equation to give a closer approach to the practical situation without impairing the simplicity of the equation and its implications for operation.

*Appropriate thermocouple tappings at several points along the barrel should be provided during initial manufacture, as these temperatures provide a simple but important signal for operational control.

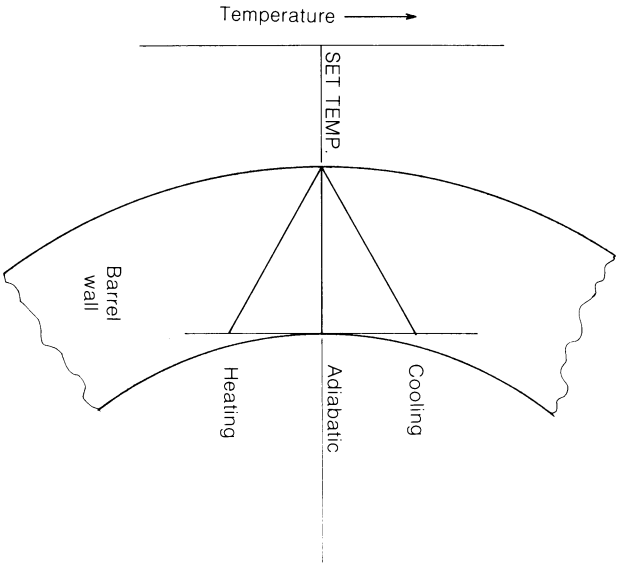


Figure 8.3 Temperature gradients in barrel.

8.2.1 Analysis of variables: power equation

The previous section emphasises experimental measurement because of the problems of theoretical calculation of certain items in the energy balance. In particular, as discussed in section 6.6 and p. 231, melt length Z changes in a complex way, especially with speed and back pressure. For simplicity, the following discussion will ignore this interaction and deductions in this and the following chapters regarding power input, energy balance, etc., must be modified by a correction to allow for the accompanying changes in melt length Z, especially with large changes of speed or pressure.

The increase in heat content I (enthalpy) of the polymer is directly proportional to the mass flow and change in specific enthalpy, but the latter requires laboratory data and in semi-crystalline polymers is dependent on the (usually unknown) degree of crystallinity of the feed material. However, for small changes of operating temperature, a constant (melt) specific heat may be an adequate approximation. The heat losses S are almost impossible to calculate with accuracy, but require a preliminary experiment (see appendix C.1) with the appropriate physical arrangement (barrel length, die and adaptor assembly, heater rating and location, feed pocket and screw cooling flows and temperatures) and *external* temperatures. The heater inputs H are difficult to

predict (except for the maximum available) and may be uncertain in measurement – this is perhaps best treated as the dependent variable or balancing factor in equation (8.2).

In contradistinction, the analysis leading to equation (8.9) gives a basis for estimating the mechanical power input E to the screw, and the effects upon it of changes in the independent variables η, D, N, Z, h, δ and pressure P. Both channel and flight terms in equation (8.9) are directly proportional to viscosity; thus power input increases with polymer molecular weight (decrease of Melt Flow Rate) and decreases with increase of temperature. By equation (6.4), for a constant helix angle ϕ:

$$W \propto DN \tag{8.10}$$

Thus both terms of the power equation increase in proportion to N^2. For constant helix angle ϕ and flight proportions, the channel width b and flight width t are proportional to diameter D, so that both terms are proportional to D^3 and directly proportional to melt length Z and L (equation (6.1)). The channel and flight power terms are inversely proportional to depth h and clearance δ, respectively. Although in the first term the helix angle ϕ only appears explicitly within the brackets, equations (6.1)–(6.4) show it to be implicit in W, b, t and Z (for constant L), so the effect of varying helix angle ϕ on power is complex–for small values of ϕ, when $\tan^2 \phi \ll 1$, and constant flight proportions (t/p constant), $b \propto \sin \phi$ (equations (6.2) and (6.3)) and power E is approximately proportional to $\cos^2 \phi$ for constant D, N, h and L, predicting a small decrease of power with increase of helix angle.* Since only the drag element of leakage flow is considered, the second term of equation (8.9) is independent of pressure; the latter is represented in the first term by the dimensionless group Q/Wbh, and as discussed on p. 136 (Fig. 6.6) a decrease in the latter corresponds to an increase in back pressure. Thus equation (8.9) indicates that the channel power increases as back pressure increases, notwithstanding the decrease in output Q given by equations (6.15), (B.9), etc. Thus for a given screw design and speed, Q/Wbh is a convenient way of including the effect of back pressure on power, and for a constant helix angle ϕ and pressure P, the terms in square brackets in equations (8.9) are constant. However, in other cases, equation (6.32) represents the effect of independent variables on pressure at constant Q/Wbh. This reinforces the assertion following equation (6.16) that the magnitude of Q/Wbh is valuable in characterizing operating conditions. Then for constant helix angle ϕ and constant dimensionless output Q/Wbh, equation (8.9) may be simplified to:

$$E_{Ch} \propto \frac{\eta D^3 N^2 L}{h} \tag{8.11}$$

*Compare McKelvey (1962, Fig. 10.11, p. 255). Q increases with $\theta(\phi)$ up to $\theta = 30°$. Efficiency Q/E decreases therefore power must increase.

and:

$$E_{Fl} \propto \frac{\eta D^3 N^2 L}{\delta} \tag{8.12}$$

These relations are tabulated in Table 8.3 and will be considered in conjuction with output in section 8.5 in the effects on the energy balance and in section 11.5 in the discussion of scale-up.

8.3 PSEUDOPLASTIC ISOTHERMAL APPROXIMATION

The numerical example given on p. 141 for leakage flow indicates that the flight clearance δ is usually one or two orders of magnitude smaller than the channel depth h; therefore the shear rate over the flight will be much greater than in the channel (equations (B.16)) and (6.69)). Since the two terms of equation (8.9) are independent, a crude approximation to pseudoplastic behaviour is to insert different values of viscosity into each term, corresponding to the respective shear rates (see p. 232). As the example in section 8.5 shows, the strict Newtonian isothermal application of equation (8.9) indicates that a high proportion of total power is absorbed over the flights; use of viscosities appropriate to the shear rates in channel and flight substantially reduces the contribution of the latter. This procedure also allows the inclusion of the effect of screw speed on viscosity, which decreases with increase of speed, offsetting to some extent the effect of the latter on power. For example, if the power-law approximation given in equation (3.7) is used:

$$\eta \propto \dot{\gamma}^{n-1} \propto N^{n-1} \tag{8.13}$$

and equation (8.9) becomes:

$$E \propto N^{n-1} \cdot N^2 = N^{n+1} \tag{8.14}$$

Since $n < 1$, the Newtonian relation of equation (8.9)

$$E \propto N^2 \tag{8.15}$$

is replaced by

$$E \propto N^{n+1} \tag{8.16}$$

where $1 < (n+1) < 2$, i.e. the power increases less rapidly with speed for the pseudoplastic than the Newtonian case.

Figure 6.6 shows that for a given speed N, as Q/Wbh decreases from 1/2 and pressure increases, the downchannel wall shear rate increases in accordance with equation (6.69). This expression is a factor of equation (C.9) and can be identified as part of equations (8.7) and (8.9), i.e. the effect of changes in shear rate due to back pressure is linear in the power equation. A further

approximation allowing for the effect of pressure is thus to take for the channel a viscosity η evaluated at the wall shear rate given by:

$$\dot{\gamma}_h = \frac{W}{h}\left(4 - \frac{6Q}{Wbh}\right) \tag{6.69}$$

This expression is strictly only applicable to Newtonian flow and, as shown in Fig. 4.1, underestimates the wall shear rate and overestimates the viscosity in pseudoplastic flow at the same flow rate; however, it is qualitatively correct, partially offsetting the increase in the bracketed term of equation (8.9) and giving a closer overall assessment of the effect of pressure on power input.

8.4 POWER IN NON-ISOTHERMAL FLOW

8.4.1 Estimation of heat flows in the melt pumping section

The isothermal assumption has been used to permit analytic equations for flow and power, from which the effects of dimensional and operational variables could be deduced. It also forms a convenient basis for local behaviour, which can be summed for an assumed longitudinal temperature profile. However, it provides only an approximate representation, based on an 'average' condition, of the overall performance of the actual extruder, in which the melt temperature usually increases in the downstream direction as the combined result of internal shear heating and external heating or cooling. On p. 232 it was suggested that the power consumption at a given axial position should be evaluated at the local temperature of the barrel wall close to its inner surface; the effect of the longitudinal temperature profile may then be estimated by summing over a number of axial sections, along with any changes in dimensions, e.g. channel depth. It is of course still necessary to know the effective melt length.

The flow of heated polymer along the screw represents an axial heat flux, due to mass transfer, which progressively increases with increase of average melt temperature; in the adiabatic case this is due to shear heating in the channel and flight clearance. However, radial temperature gradients will arise due to non-uniformity of shear heating and heat transfer to or from the barrel wall. These will be mitigated to some extent by transverse circulation (Fig. 6.7) and other lesser internal heat flows. Thus the surface temperature for evaluation of power consumption will generally differ from the local average temperature. In addition, radial temperature variations will lead to a nonlinear velocity distribution for drag flow and a further departure from equation (6.69) for wall shear rate where pressure flow is included (Fig. 4.1). In general, for a given screw speed, the shear rate near the wall will increase and viscosity decrease with increase of temperature near the wall above the bulk average. This will lead to a change (probably increase) in power input from that predicted from

the bulk temperature and also to a reduction in output due to distortion of the velocity profiles illustrated in Fig.6.6. In addition to causing radial temperature variations in the polymer, strong external heating or cooling will give radial temperature gradients within the barrel wall, so that the temperatures set on the heater controllers are only indirectly related to those at the inner surface, so that direct measurement of the latter remains the most reliable method for power estimation. With screws of varying depth, even if a linear variation of barrel temperature may be assumed, an axial average temperature will be incorrect because of the interaction with variation of local wall shear rate (horizontally in Table 6.1). On p. 232 a time-averaged temperature was recommended mainly because of the effect, local to the barrel wall, of shear heating resulting from power consumption in the flight clearance.

The example in section 8.5 (p. 260), calculated on isothermal Newtonian assumptions (equation (8.9)), shows that in the usual case, the power consumption over the screw flight is appreciable compared with that in the screw channel, despite the much smaller area over which it acts (proportional to flight width $t \cos \phi$ rather than channel width b). In extreme cases, the flight power may actually exceed the channel power. If the much higher shear rate in the flight clearance is taken into account (equation (C.15)), for a pseudoplastic fluid the contribution from the flight to total power is reduced, but still significant (see Table 8.4). This power consumption in the very small mass of polymer in the flight clearance will tend to cause a large local temperature rise; some heat will be conducted away in all directions in the barrel intermittently during the short time the flight passes a fixed point, some will be continuously conducted radially in the screw flight and some will be carried into the channel by polymer not adhering to the screw flight. In order to set the boundary conditions for estimating these temperature rises and heat flows in the region of the flight clearance, it is necessary to consider all the various possible heat flows in the melt pumping section of screw and barrel. Figure 8.4 shows these diagrammatically, where they are lettered for reference as follows:

A Radial heat transfer at outer barrel diameter, e.g. from heaters or to coolant.
B Radial heat conduction within barrel thickness.
C Radial heat transfer at inner barrel diameter to or from polymer in the screw channel.
D Axial conduction in the barrel wall.
E Radial heat transfer at screw root to or from polymer in screw channel.
F Radial heat conduction in screw flight.
G Local axial conduction in screw between flight and channel root.
H Overall axial conduction in screw root.
J Axial conduction within flight thickness.

Table 8.1 Heat flows in melt pumping section

	Specific conditions			*Operating conditions*		
Heat flow	*Temperature or gradient*	*Area/turn (m^2)*	*Flux (W/turn)*	*Temperature or gradient*		*Flux (W/turn)*
A	1 °C	0.0628 200 mm o.d.	Dependent on source	–		1880 (3 W cm^{-2}) 8160 (13 W cm^{-2}) (outside)
B	1 °C/mm average	0.0471 average	2273	3.06 °C	in 0.05 m	139 total
C	1 °C	0.0283 channel only	8.5	10 °C		85
D	1 °C/mm	0.0236 200 mm o.d.	1180	125 °C/m 50 °C	per 4*D* zone	147 W
E	1 °C	0.0226 80 mm root dia.	6.8	10 °C		68
F	1 °C/mm (10 °C over flight height)	0.003 14	157	0.89 °C 1.53 °C 2.65 °C	mean excess temp. – see **P** below	14 (1 rps) 24 (2 rps) 42 (4 rps)
				0.89 °C	including flight-tip resistance	3.6 (1 rps)

G	1 °C over 0.0314 m see appendix C.3	0.0024	3.8	0.89 °C 1.53 °C 2.65 °C	mean excess temp. – see **P** below	3.4 (1 rps) 5.8 (2 rps) 10.1 (4 rps)	
				0.89 °C	including surface resistances	1.4 (1 rps)	
H	1 °C/mm	0.005 03	251	125 °C/m 50 °C	per 4*D* zone	31.4 W	
J	1 °C	0.003 14	15.7	125 °C/m 1.25 °C 0.03 °C	polymer/polymer in metal	0.57	
K	1 °C/mm	0.0283	14.1	0.42–3.8 °C	in 5 mm	1.2–10.7	No circulation
				0.05–0.30 °C	in 5 mm	0.14–0.85	With circulation
L	1 °C/mm	0.000 86	0.43	37.9 °C/m		0.016	
M	–	0.0283	21.9–33.4 kW m^{-2} @ 1 rps	–		620–946	W/turn @ 1 rps
N	–	0.0283	–	–		41.6–392	W/turn @ 1 rps Net
P	–	0.003 14		see appendix C.5			
R	1 °C/mm	0.95×10^{-4}	4.8	37.9 °C/m		0.18	
S	1 °C/mm	0.0033	1.65	10.2 °C		0.20	

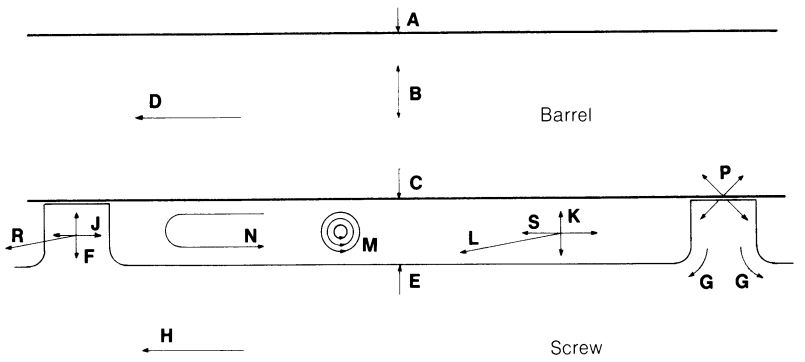


Figure 8.4 Local heat flows in melt pumping section.

K Radial conduction in polymer in channel.
L Longitudinal (helical) conduction in polymer in channel.
M Shear heating within polymer in channel.
N Radial mixing due to transverse circulation.
P Shear heating in flight clearance and local dissipation.
R Conduction along flight helix.
S Conduction in polymer across channel.

These are studied separately in appendices C.3, C.4 and C.5 for dimensions and material properties given in appendix C.3 and evaluated for a temperature difference of 1°C or a temperature gradient of 1°C mm^{-1} as appropriate. The results are tabulated in Table 8.1 to indicate the relative orders of magnitude, together with estimates of the values to be expected in operating conditions.

Considering first the screw, heat **H** will be conducted axially towards the feed end, and except for the change in cross-section due to varying channel depth, this will be proportional to the axial temperature gradient. The heat flux will be constant along the length for a uniform gradient with zero radial heat gain or loss. Evidently at the screw tip this axial heat flux must be supplied from the polymer, which must also be at a higher temperature. An increasing gradient towards the feed end at some axial position must similarly be compensated by a radial heat flow (**E** & **F** below) at that position. Screw cooling will increase both axial and radial heat flows, depending on the direction of flow of coolant which contacts the screw (i.e. whether supplied from the feed end or to the tip through the 'wand'). A temperature difference of only 1°C between screw and coolant could remove 15 W per turn (equation (C.56)), so that accurate screw temperature control is essential for steady operation and to avoid polymer freezing to the screw root. For the chosen example, the axial heat flow **H** is a moderate 31 W (equation (C.41)) for an axial gradient of 125°C m^{-1} or 50°C for a 4*D* zone.

A radial heat flux **E** from the channel root could supply the above axial flux **H** in one pitch of the screw (say at the delivery end) for an estimated 4.6°C polymer-to-metal temperature difference (equation (C.33)). Alternatively, if this heat were conducted radially in the screw flight **F**, a temperature difference between polymer in the flight clearance and the flight root of approximately 7.8°C (equation (C.37)) could be required, i.e. a polymer temperature more than 3°C higher than at the channel root; the calculation of shear heating **P** shows this to be unlikely, even at high screw speeds, so this contribution will be small and polymer-to-screw temperature differences are likely to be less than 5°C in most conditions. An estimate of local heat conduction between screw flight tip and channel root **G** shows a heat flux of 3.8 W for a 1°C temperature difference in the metal (equation (C.38)). This is reduced to 1.4 W for an average increase of polymer temperature in the flight clearance (at 1 rps) of 0.89°C, when surface heat transfer coefficients are included (equation (C.39)). These are very small compared with shear heat in the flight clearance **P** which will hardly be affected by conduction in the screw flight. Although the actual temperature difference across the flight thickness is difficult to define, it seems that surface heat transfer coefficients from/to the polymer will keep axial conduction in the flight **J** small, e.g. less than 1 W (equation (C.44)) so that the transfer of heat between polymer in adjacent turns of the screw channel will also be small. It will however tend to short-circuit the effect of transverse circulation **N** and maintain radial temperature differences in the channel. Comparison with radial heat flow in the flight **F** shows that the latter will dominate, though still small. Conduction along the screw flight **R** is shown to be very small, though still an order of magnitude greater than conduction in the polymer **L**, e.g. at standstill or very high back pressures, despite the much smaller cross-section. The conclusion is that in usual conditions the heat flows **E**, **F**, **G** and **J** within the screw will be small, so that the assumption that the screw is insulated is reasonable. The exceptions will be: (i) near the tip of the screw, (ii) where a substantial change exists in the longitudinal temperature gradient; and (iii) with screw cooling. In each case the radial heat flow is likely to be mainly from the screw root **E** with a smaller contribution from the flight **F**. As this flow increases, e.g. with severe screw cooling, the temperature of the screw will fall appreciably below that of the polymer (equation (C.56)) and due to the latter's small conductivity and low velocity near the screw surface the possibility will increase of polymer freezing to the screw, with the consequences referred to in section 9.1.

In the barrel, the energy **A** available from the heaters clearly exceeds that which can be transferred to the polymer **C** (equation (C.22)). Its main purpose is to ensure rapid warm-up and to supply heat losses, especially at high operating temperatures, when induction heating may be justified on these grounds (appendix C.1). Comparison of radial heat conduction in the barrel **B** with practical heater ratings in **A** shows that during warm-up the temperature gradient may exceed $1°C\,mm^{-1}$ or 50°C over the barrel thickness. However,

the surface heat transfer to the polymer **C** is likely to limit the temperature drop through the barrel (equation (C.20)) to about one-third of that between barrel and polymer. This heat transfer coefficient (Table C.3) is difficult to determine reliably, either from theory or experiment, as is that over the flight tip **P**, though the latter is likely to be several times greater: conclusions must be treated with caution. Theory predicts that the coefficient will increase by about one-third (Table C.3) as back pressure increases from $Q/Wbh = 0.5$ to $Q/Wbh = 0$ and by about one-quarter as screw speed is doubled. The former is unlikely to compensate for the increased power at high back pressure (Fig. 8.14) while the latter confirms practical experience that control of melt temperature becomes increasingly difficult at high screw speeds (Fig. 8.12). Heat conducted axially in the barrel **D** (equation (C.23)) may be of the same order as that transferred radially to the polymer **C** (equation (C.22)), but is less than 10% of the heater power **A** so is unlikely to affect heating or cooling of the polymer **C**. With a uniform axial temperature gradient, axial heat flux **D** will be equal into and out of a barrel zone, but at the delivery end it must be supplied by the heaters, which may also contribute to maintaining die and adaptor temperatures (appendix C.1). The main effect of axial conduction **D** will therefore be to couple the temperature control systems for adjacent barrel zones, so that interactions experienced in practice must be allowed for in the overall control, whether manual or automatic, especially if the longitudinal temperature profile is to be modified.

Within the polymer in the channel, estimates show that longitudinal **L** (equation (C.50)) and transverse **S** (equation (C.53)) heat flows are negligible. Radial conduction **K** is small – say, 14 W per turn (equation (C.46)) for a 10°C difference over the channel depth, especially when compared with heat transferred radially by mass transfer **N** (appendix C.4), caused by the transverse circulation (Fig. 6.7); it does, however, play a part in reducing radial temperature differences due to external heating **C** or internal shearing **M**. Before considering shear heating **M** and circulation **N** in section 8.4.2, this study may be summarized by: (i) a largely insulated screw; and (ii) severely restricted heat transfer between the barrel and polymer in the screw channel, especially at high screw speeds. During warm-up it is impossible to predict heat transfer resistances at interfaces; if these are neglected it appears that up to 80% of heat will reach the screw root through the flight (equation (C.54)) or that the polymer will be heated almost equally from the barrel and screw. For the machine considered in this section, it seems likely that the temperature difference between barrel and screw towards the end of the warm-up will be halved approximately every five minutes (equation (C.55)).

8.4.2 Distribution of shear heating

The mechanical power applied to the screw is partly absorbed in conveying the solid polymer and supplying some or all of the energy required to raise the

polymer temperature to the melting or softening point. The remainder, estimated approximately by equation (8.9), is absorbed in the melt pumping section in shear heating (**M** in Fig. 8.4) and raising pressure in the fluid polymer. Together with external heating/cooling, this raises the polymer temperature to that required at the die. However, since the shear rate is not uniform across the channel depth, (Figs 6.6 and 6.7), the shear heating will lead to non-uniform temperature increases, which are a source of non-uniform temperatures at the die and thus detrimental to product quality and uniformity. Because of the low thermal conductivity of the polymer (**K** in Fig. 8.4), external heating or cooling will also cause radial temperature differences. These temperature differences will be modified by mass transfer (**N** in Fig. 8.4) due to the transverse circulation shown in Fig. 6.7. However, it is important to note that, except at zero output, this is accompanied by a downstream flow, the polymer moving in an oblique spiral, so that the upper and lower radial layers are not merely exchanged. In moving radially from upper to lower position and vice versa, polymer elements are also moved downstream and by different distances, where the bulk mixed temperatures in the absence of circulation may also be different. Thus a simple calculation of the effect of circulation can only be related indirectly to the distribution of polymer temperature at the end of the screw.

It has been mentioned previously (p. 139) that the longitudinal and transverse velocities in the screw channel combine to form a complex flow pattern, and various approximations have been used to determine the resulting shear rates. In equation (6.69) the downchannel shear rate at the wall is expressed in terms of the back pressure (Q/Wbh) and used in equation (8.9) to give an approximate effect of back pressure on viscosity and power input. In appendix C.3 the differences in downchannel and transverse velocities over a thin lamina close to the wall are summed vectorially and divided by the lamina thickness to give the total shear rate for estimation of surface heat transfer coefficient to the barrel. A more approximate method in which the downchannel and transverse shear rates are summed vectorially is used to show that the coefficients are similar at the screw root. For the present purpose a more accurate estimation is required, though still for isothermal Newtonian conditions in order to preserve the simplicity of algebraic relations.

Using the equations ((6.26) and (6.67)) for the cross- and downchannel components of velocity, an algebraic expression (equation (C.59)) is developed in terms of W, h, y/h and Q/Wbh for the resultant velocity at a radial position given non-dimensionally by y/h.* This expression is differentiated with respect to y to give the total shear rate (equation (C.61)) with the approximation that the change of direction of the total velocity vector with y/h is neglected. Since

*In the 1st edition of this book this was approximated by $u\sin\phi + w\cos\phi$, i.e. assuming the resultant is normal to the screw axis. Figure 6.8 shows this is only true at $y/h = 1$ or at zero output ($Q/Wbh = 0$).

this involves the square root of the sum of several non-homogeneous terms, it cannot be expressed more simply. The shear heating per unit volume is then calculated by equation (3.57) as $\eta\dot{\gamma}^2$ W m^{-3}. For brevity, the symbols T and q are used, where:

$$q = \frac{1}{2} - \frac{Q}{Wbh} \tag{8.17}$$

$$T = \tan\phi \tag{8.18}$$

The expression then becomes:

Shear heat per unit volume (W m^{-3})

$$= \eta \frac{W^2}{h^2} \cdot \frac{\left[1 + 4T^2 - 12q + 36q^2 - 18T^2\left(\frac{y}{h}\right) + 18q\left(\frac{y}{h}\right) - 108q^2\left(\frac{y}{h}\right) + 18T^2\left(\frac{y}{h}\right)^2 + 72q^2\left(\frac{y}{h}\right)^2\right]^2}{\left[1 + 4T^2 - 12q + 36q^2 - 12T^2\left(\frac{y}{h}\right) + 12q\left(\frac{y}{h}\right) - 72q^2\left(\frac{y}{h}\right) + 9T^2\left(\frac{y}{h}\right)^2 + 36q^2\left(\frac{y}{h}\right)^2\right]} \tag{C.62) (8.19}$$

The results for pitch equal to diameter and $T = 1/\pi$ are plotted against y/h for several values of Q/Wbh in Fig. 8.5.

For $Q/Wbh = \frac{1}{2}$, $q = 0$ and equation (8.19) reduces to:

$$\text{Shear heat (W m}^{-3}) = \eta \frac{W^2}{h^2} \cdot \frac{\left[1 + 4T^2 - 18T^2\left(\frac{y}{h}\right) + 18T^2\left(\frac{y}{h}\right)^2\right]^2}{\left[1 + 4T^2 - 12T^2\left(\frac{y}{h}\right) + 9T^2\left(\frac{y}{h}\right)^2\right]} \tag{8.20}$$

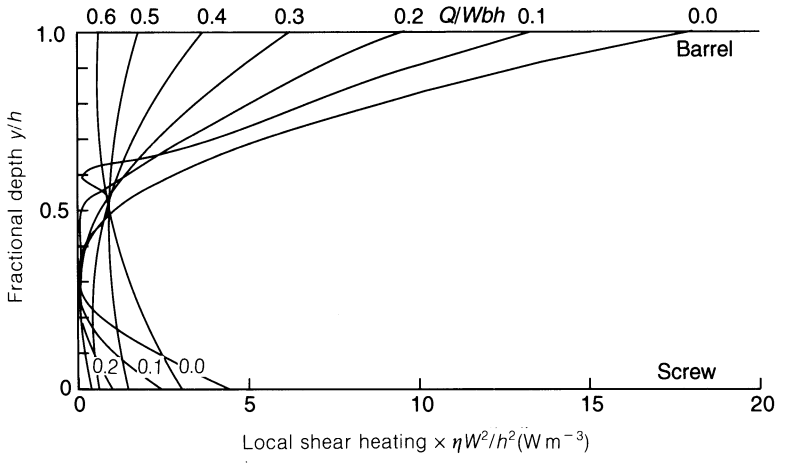


Figure 8.5 Radial distribution of local shear heating in combined flow.

For the usual case of pitch equal to diameter, $T = 1/\pi$ and equation (8.20) further reduces to:

$$\text{Shear heat } (\text{W m}^{-3}) = \eta \frac{W^2}{h^2} \cdot \frac{\left[1.4053 - 1.8238\left(\frac{y}{h}\right) + 1.8238\left(\frac{y}{h}\right)^2\right]^2}{\left[1.4053 - 1.2159\left(\frac{y}{h}\right) + 0.9119\left(\frac{y}{h}\right)^2\right]} \tag{8.21}$$

The shear heating in a lamina between y and $y + \mathrm{d}y$ is $\eta\dot{\gamma}^2\,\mathrm{d}y\,\text{W m}^{-2}$ and the cumulative shear heating from 0 to y is:

$$\text{Cumulative shear heat} = \eta \int_0^y \dot{\gamma}^2\,\mathrm{d}y \tag{8.22}$$

Since the fraction in equation (8.19) is cumbersome to integrate, a numerical approximation is achieved by summing $\eta\dot{\gamma}^2\,\mathrm{d}y$ for successive laminae between 0 and y. The result, in terms of $\eta W^2/h$, is plotted in Fig. 8.6. It should be noted that the foregoing expressions are based on Newtonian velocity distributions and no allowance is made for the change of viscosity with shear rate across the channel depth (y/h) or consequent modification of the velocity and shear rate profiles. The numerical example uses the viscosity at the downstream wall shear rate, given by equation (6.69), for comparison with the calculation of total power in Table C.11. In that example, neglect of the transverse velocity distribution, where:

$$\left(\frac{\partial u}{\partial y}\right)_{y=h} = \frac{4U}{h} \tag{B.15}$$

leads to an underestimate of the wall shear rate (compare Tables C.3 and C.11) and overestimate of the viscosity, shear heating and power in the melt pumping section. This approximation is justified by the complexity of an analytic solution to the total wall shear rate for the present purpose of studying the variations in shear heating. Evidently any suitable value for viscosity may be used here, since it is a separate factor. Pseudoplasticity is only allowed for in this calculation to avoid the extreme effect of back pressure (Q/Wbh) predicted for a Newtonian fluid (Fig. 8.15). However, the transverse component of wall shear rate (equation (B.15)) is independent of back pressure, so the true variation of total shear rate, viscosity and shear heating will be even less than predicted by equation (6.69).

The effect of radial temperature variations on viscosity, and hence velocity distribution, is neglected since Table C.12 in appendix C.5 shows a small effect even for moderate changes in average temperature. These radial variations will also be further reduced by transverse circulation (see below).

Shear heating **M** is evidently the dominant energy source compared with heat flows within the melt pumping section; it also increases rapidly as pressure

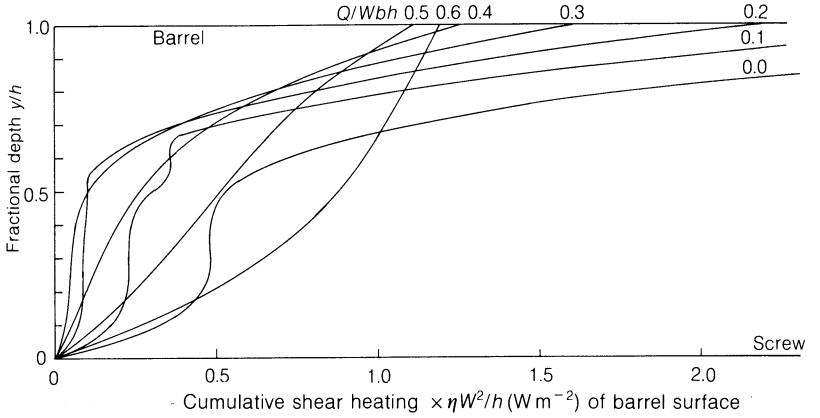


Figure 8.6 Radial distribution of cumulative shear heating in combined flow.

gradient increases. Figures 8.5 and 8.6 show it to be highly non-uniform across the channel depth, leading to the development of temperature non-uniformities, which, if allowed to persist to the die, will cause problems of flow distribution and uneven shrinkage in the product. The simultaneous reduction of these non-uniformities due to transverse circulation **N** is discussed below. Even at modest pressure gradients ($Q/Wbh = 0.4$), over 50% of the total heating occurs in the 25% of depth nearest the barrel and nearly 15% in the outermost 5% of depth. At higher pressure gradients (lower Q/Wbh) the non-uniformity is even greater, with very little heating in the inner half of the channel depth. Even at very high back pressure and low output, the shear heating near the screw root, although significant, remains a small fraction of the total (Table C.6). As expected from the velocity diagram Fig. 6.6(e), with negative pressure gradients the shear heating is greatest near the channel root, and although $Q/Wbh = 0.6$ represents a large gradient (approximately 5 MN m^{-2} per turn for the example used) both the total and its distribution are not greatly different from those with zero gradient ($Q/Wbh = 0.5$). While high back pressures, giving appreciable longitudinal mixing (Fig. 6.6(b)) are often advocated to give uniformity of composition, it may be argued that low or even slightly negative pressure gradients towards the end of the screw will promote temperature uniformity at the die. Even though the following study suggests that the non-uniform temperatures resulting from shear heating may be much reduced by transverse circulation **N**, the residual temperature differences are also likely to increase with back pressure.

Although this study strictly only applies to isothermal Newtonian behaviour, it is evident that shear heating and temperature variations are likely to be emphasized by the increase of shear rate near the wall (Fig. 4.1) with external heating or pseudoplastic fluids.

8.4.3 Mixing by transverse circulation

The closed flow transverse to the downstream direction of the screw channel necessarily involves radial flow near the flight flanks (Fig. 6.7). This is neglected in the flow equations which assume an infinitely wide channel relative to its depth. However, the mass transfer represented by this radial flow produces a circulation (**N** in Fig. 8.4) which exchanges heat between the upper and lower layers of polymer in the channel and tends to reduce the radial temperature differences due to shear heating and heating/cooling from the barrel. In appendix C.4 the transverse velocities and flow rates are calculated for increments of y/h (Table C.7). These give the positions in the channel depth y/h between which the leftward and rightward flows are equal and which may be assumed to be exchanged in pure laminar mixing. These depths correspond to the streamlines in the lower part of Fig. 6.7; note that these are not isovels, since the velocities in the lower part of the channel are generally less than in the upper part. Consistent with the assumption of a shallow channel, the radial movement is assumed to be instantaneous. It is shown in appendix C.4 that the heat transferred radially is the shear heat in the source lamina divided by the mean time to traverse that lamina. Thus the heat transferred inward at the leading flight flank and the heat transferred outward at the trailing flank are calculated; each is summed to give the respective totals and the difference of these gives the net heat transferred inward (Table C.9). This difference is subtracted from the upper layer and added to the lower layer, respectively, to give an estimate of the effect of circulation. Since the volumes of material in the upper and lower layers are different, the equivalent temperature rises are calculated, with and without circulation. The reduction in these differences due to circulation is then taken as a measure of the latter's effect (Table C.10).

The effect of increased back pressure (reduced Q/Wbh) is thus to increase the total shear heating (Tables 8.4 and C.10) and radial temperature differences (Table C.10). However, transverse circulation reduces these very substantially and by an almost constant proportion. This is a consequence of the transverse circulation being independent of back pressure and the deduction in appendix C.4 that the radial heat transfer is inversely proportional to the transverse transit time at each fraction of channel depth. Note that this is only an average reduction of temperature difference between the leftward and rightward portions of transverse flow; a trial calculation shows that it is in the surface regions, where the temperature differences are greatest, that the percentage reduction is also greatest. The smaller reduction in the centre layers is due to the slower circulation and is accompanied by (usually) smaller downstream movement, which, however, is also dependent on the value of Q/Wbh (Fig. 6.6). This is of limited significance for temperature uniformity, which is also assisted by local thermal conduction **K**; mixing for composition is dependent only on relative velocity (between upper and lower regions) and shear rate (between adjacent laminae) so that a poorly mixed zone may be expected near

$y/h = 2/3$ where transverse velocity is zero, especially at low back pressures (high Q/Wbh) where the downstream velocity at this position is relatively high.

The foregoing calculations are for a screw speed of 1 rps. As screw speed is increased, mechanical power in the melt pumping section increases as the $(n+1)$th power of screw speed N (equation (8.14)), increasing radial temperature differences. The transverse velocity u at position y/h is proportional to that at the barrel, U (equation (6.26)), which is proportional to speed (equation (6.5)). Thus the transit time across the channel will be inversely proportional to speed N. Thus the radial heat flow:

$$Q_x \rho C_p \, dT \propto \frac{N^{n+1}}{N^{-1}} = N^{n+2} \tag{8.23}$$

The radial heat flow thus increases with speed as a proportion of the shear heat generated (equation (8.14)), which will tend to reduce the (greater) temperature differences more rapidly. However, the downchannel velocities also increase, so that this reduction may well take place over a greater length, giving greater temperature non-uniformity at the die, as is commonly experienced with increasing speed.

This effect of transverse circulation should similarly reduce radial temperature differences due to moderate barrel heating or cooling, since it is dependent on the relative temperature rises at different points in the channel depth. However, severe cooling of either barrel or screw will distort the velocity profiles or even cause local freezing, inhibiting the reduction of temperature difference.

8.4.4 Heat generation and dissipation in flight clearance

If the polymer in the channel is assumed to be in thermal equilibrium with the surroundings, then the shear heating **M** is absorbed in maintaining the temperature of the melt in the channel; the greater shear heating over the flight clearance must produce an imbalance and consequent local temperature rise. Any polymer which adheres to the screw flight and rotates with it will be subjected continuously to this heating, whereas the remainder will be sheared and heated while in the clearance and then will return to the lower shear rate in the channel, where sensible heat may be lost again by conduction and convection in the surrounding channel flow. In the extreme, polymer adhering to the barrel will be heated during approximately 10% of each revolution by the passing flight tip and relax during the remaining 90% to a quasi-steady state, which is likely to be above the average temperature in the channel. The metal of the screw flight will be heated continuously and reach a steady-state temperature dependent on heat flows within the screw **F**, **G**, **H**, **J**. In appendix C.3 it is shown that in the absence of intentional cooling, the screw is largely insulated with small local heat flows **F**, **G**, **J**, through the flight, unless large temperature differences

exist in the polymer. Because of its very small volume, the polymer in the clearance has negligible heat capacity, and because of its small thickness cannot maintain substantial temperature differences; it therefore represents a negligible heat sink and its temperature will follow closely that of the surroundings. The barrel is subjected to a cyclic heating, and during passage of the flight and the channel, the barrel will conduct heat away from points on its inner surface in all directions.

If the barrel (assumed to be initially at the temperature of the polymer in the channel) constituted negligible thermal resistance, the heat generated over the flight would be conducted away and the isothermal pseudoplastic calculation (see example on p. 260) would remain valid. However, a finite thermal resistance (conductivity) would cause a transient temperature increase in the flight clearance and consequently a reduction in viscosity, heat generated and power absorbed. It is believed that this problem has not been studied previously in the literature and the purpose here is limited to a preliminary study to assess the order of magnitude of the effect and how it may be influenced by operating conditions. In appendix C.5 an example is taken, based on the data given at the head of appendix C.3.

The heat generated in shearing the polymer in the flight clearance is calculated for several mean temperatures and shear rates. It is shown that the flow of this energy into the barrel may reasonably be represented by radial one-dimensional transient heat conduction. Standard methods (McAdams, 1954, pp. 33ff.) for this case give the distribution of temperature as a function of time and position. They also give the heat absorbed as a function of time, showing that it is directly proportional to the excess of surface temperature above the original (uniform) temperature of the barrel. Equating this heat for the transit time of the flight to the shear heat generated in the polymer determines the excess surface temperature T of the barrel as the trailing edge of the flight passes, e.g. 1.54°C at 1 rps. When the flight has passed, the heat source is removed but heat will continue to diffuse within the barrel. The very low thermal conductivity of the polymer and low heat transfer coefficient **C** gives a resistance ratio (m in McAdams, 1954) for heat flow from barrel to polymer in excess of 10, so that, as shown by McAdams (1954, Figs 3.2 and 3.4), this surface may now be treated as insulated, and the heat stored in the barrel will diffuse further into the barrel thickness. This continues for the 'rest' period of 0.9 s (at 1 rps) and gives a residual excess temperature at the start of the next revolution, e.g. 0.32°C at 1 rps, when the flight again passes. In the conditions of the example, this residual excess is small, as is the reduction of flight power (the second term of equation (8.9)). However, this excess temperature will be cumulative during successive revolutions of the screw, which in the absence of other heat transfer mechanisms would lead to considerable increase of barrel temperature above that of the polymer. This in turn must affect the effective viscosity within the screw channel near the barrel and thus reduce the power represented by the first term of equation (8.9).

From Table C.12 it is seen that the above conditions correspond to a melt viscosity in the flight clearance of the order of $100\,N\,s\,m^{-2}$ and evidently the effects would be similar for a Newtonian fluid of this viscosity, which approximates to typical values at processing temperatures for nylon 66 and PETP. However, a Newtonian fluid of similar viscosity to that of polyethylene at low shear rate – say, $2000\,N\,s\,m^{-2}$ – would lead to a temperature rise of approximately 20°C and a reduction of some 20% in flight power; the reduction in channel power must also be significant.

Increasing the mean temperature in the channel will reduce the viscosity and shear work in the flight clearance, e.g. by approximately one-half from 150°C to 200°C with this polymer ($n = 0.315$). These will in turn reduce the temperature rises in the barrel at the end of flight transit and at the end of 'rest' period in approximately the same proportion. The cyclic temperature fluctuations will thus be minimized at high average melt temperatures. The flight power will also be decreased, but may well become an increased proportion of the (now smaller) total power.

Calculations in appendix C.5 on the same assumptions show (Table 8.2) the temperature rise increasing to 2.68°C and 4.61°C at 2 and 4 rps respectively, while the residual increase before the next revolution is 0.55°C and 0.94°C respectively, i.e. the temperature increases at end of shearing and end of the 'rest' period rise with speed and proportionately to each other. For this case, with a polymer having a pseudoplasticity index $n = 0.315$, the initial and residual increases are respectively approximately proportional to screw speed raised to the power 0.8. The temperature increases of the barrel when surface resistance is included are smaller, but still significant. However, the rise in polymer temperature predicted in appendix C.5 is now approximately 30°C at 1 rps, which though it will quickly dissipate in the channel may disturb the flow in the channel by promoting surface slip. This increase in polymer temperature will also increase the heat flow between the screw flight and the channel root **G** to 40–50 W per turn (Table 8.1), giving further reduction in the heat to the barrel.

These temperature rises will certainly give an important reduction of total power, and a reduction in the proportion contributed by the flight clearance at high rotational speeds and high melt viscosities.

Table 8.2 Shear heating and temperature rises in flight clearance, negligible surface resistance

Screw speed (rps)	*Temperature at end of shearing* (°C)	*Shear work* (J/turn)	*Residual temperature at end 'rest'* (°C)
1	1.54	24.45	0.32
2	2.68	30.05	0.55
4	4.61	36.63	0.94

Superimposing on Fig. C.4 the radial temperature gradient **B** in the barrel due to external heating shows that this is similar in magnitude, but opposite in direction, to that near the barrel surface during all but the first moments of the 'rest' period. Thus this degree of external heating would severely reduce the diffusion of heat from the flight, increase the local temperature rise and reduce the power consumption. In contrast, severe barrel cooling will produce a temperature gradient in the same direction as diffusion from the flight, leading to a decrease in local polymer temperature and increase in flight power consumption. This preliminary study shows how sensitive flight power will be to barrel heating or cooling; indeed the observed effects on total power may well be due primarily to this (second term of equation (8.9)), with important consequences for stable operation and final melt temperature uniformity. Especially with viscous polymers, low melt temperatures and high rotational speeds, substantial effects on performance may be expected, and the subject deserves further study.

8.5 EFFECT OF VARIABLES ON ENERGY BALANCE

The direct effects of dimensions and operating variables on power consumption with a Newtonian fluid ($n = 1$) have been discussed on pp. 233–4, and the modifications for a pseudoplastic fluid ($n < 1$) on p. 235. In Chapter 6 (equation (6.30)) the drag flow was expressed in terms of dimensions D, h and N, and for a constant value of dimensionless output Q/Wbh, the total flow followed the same relation to diameter D, channel depth h and speed N:

$$Q \propto D^2 Nh \tag{8.24}$$

For some purposes it is convenient to express energy per unit volumetric output E/Q; then, combining equations (8.11) and (8.12) with equation (8.24):

$$\frac{E_{\mathrm{Ch}}}{Q} \propto \frac{\eta DNL}{h^2} \tag{8.25}$$

and:

$$\frac{E_{\mathrm{Fl}}}{Q} \propto \frac{\eta DNL}{h\delta} \tag{8.26}$$

For other purposes it is useful to group independent variables such that the effect of varying shear rate is revealed. From equation (6.69) wall shear rate is given by:

$$\dot{\gamma}_h = \frac{W}{h}\left(4 - \frac{6Q}{Wbh}\right) \tag{6.69}$$

Table 8.3 Output and power input as functions of dimensions (constant Q/Wbh), from equations (8.11), (8.12) and (8.24)–(8.27)

Independent variable	Q	E		E/Q	
		Proportional to:			
D	D^2	D^3		D	
L	Constant	L		L	
		channel	flight	channel	flight
h	h	$\frac{1}{h}$	$\frac{1}{\delta}$	$\frac{1}{h^2}$	$\frac{1}{h\delta}$
η (e.g. changing temperature T)	Constant	η		η	
N	N	N^2	N^2	N	N
ηN Newtonian $(n = 1)$	N	ηN^2		ηN	
ηN Pseudoplastic $(n < 1)$	N	N^{n+1}		N^n	
Q/Wbh[a] (e.g. changing pressure)	$\frac{Q}{Wbh}$	$4(1+\tan^2\phi) - \frac{(6Q)}{(Wbh)}$	Const.	$\frac{4(1+\tan^2\phi)}{Q/Wbh} - 6$[b]	$\frac{1}{Q/Wbh}$[b]

[a] See Fig. 8.15.
[b] Equations (8.29) and (8.30).

and for constant Q/Wbh and substituting equation (6.4):

$$\dot{\gamma}_h \propto \frac{W}{h} \propto \frac{DN}{h} \tag{8.27}$$

The results are summarized in Table 8.3, the lines for ηN representing the total effect of speed changes, as equations (8.25) and (8.26).

The important deduction at this stage from Table 8.3 is that every change of dimension or operating conditions causes different changes in power input E from those in output Q. Consequently, the specific power input E/Q changes, resulting in changes in energy balance. The implications for scale-up (changes of D), for example from laboratory semi-technical machine to large-scale production, will be studied in section 11.5. Increase of melt length L produces no direct change in output Q but a proportional increase in both total power input E and specific power E/Q. Thus, other things being equal, a long machine will tend to run hotter than a short one, which may be an advantage for processes like paper-coating which require high melt temperatures but a disadvantage for blow moulding or for high-viscosity melts such as high molecular weight UPVC and HDPE and certain rubbers. If melt temperature (and I) is controlled to be constant (Fig. 8.7), lengthening the melt section will

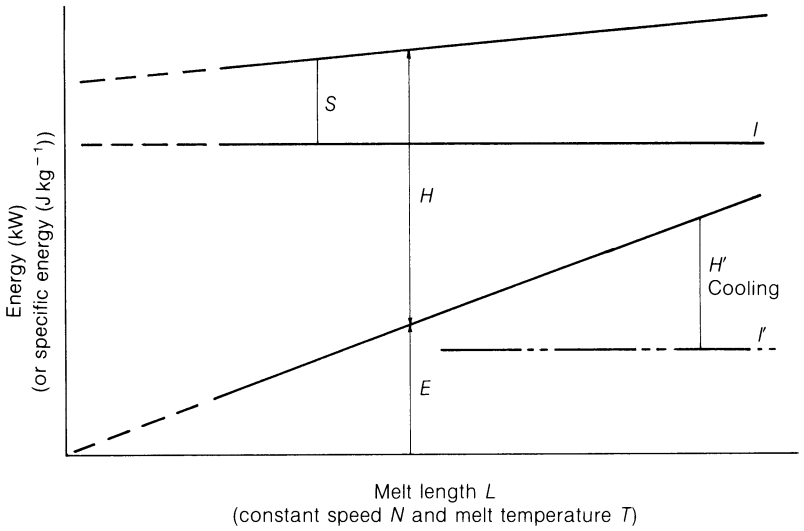


Figure 8.7 Effect of melt length on heat requirements.

decrease the heater input to the polymer, although losses S will increase. In most cases the increased surface area will permit a decrease in the heater rating ($W\,cm^{-2}$). If power input is high or melt temperature low such that barrel cooling is required, then, as shown in Fig. 8.7, increasing length will increase the cooling required. As mentioned on p. 219, increasing screw speed tends to decrease melt length, and this interaction modifies, as above, the effects of screw speed as such.

Increasing the channel depth h increases the drag flow Q_D in proportion, and also the total output Q if Q/Wbh is held constant. Note that the latter condition implies a pressure gradient dP/dz varying inversely as the square of the channel depth h (equation (6.32)). However, because of the decrease of shear rate with increasing channel depth h or flight clearance δ, the power input in channel and flight clearance is inversely proportional to h and δ, respectively. Thus with increase of channel depth h, the specific power input E/Q in channel and flight clearance decreases (inversely) as $1/h^2$ and $1/h\delta$, respectively. If, for mechanical reasons, flight clearance δ is constant, the corresponding specific power E_{Fl}/Q varies as $1/h$ and the total specific power inversely by a factor between $1/h^2$ and $1/h$. Equation (8.4) shows that at constant temperature the enthalpy increase I is proportional to output Q and therefore:

$$\frac{I}{Q} = \rho \int_{T_1}^{T_2} C_p \, dT - (\text{a constant for given } dT) \tag{8.28}$$

In Fig. 8.8, output Q and enthalpy I are represented by straight lines, proportional to channel depth h. However, $E_{Ch} \propto 1/h$. At constant

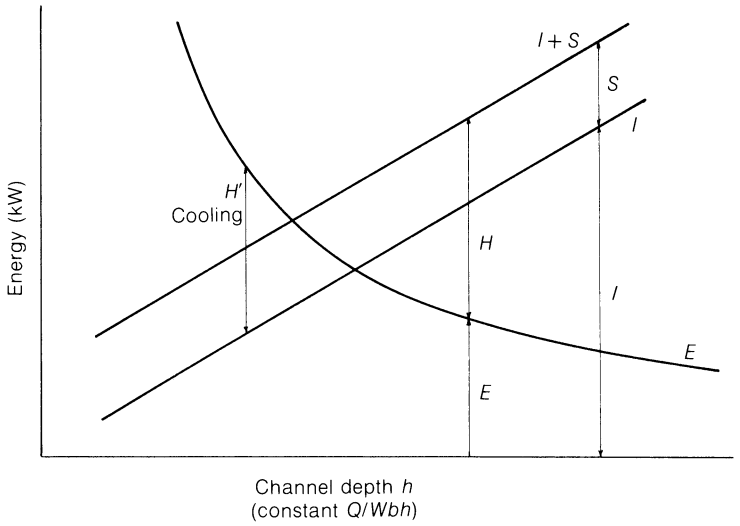


Figure 8.8 Effect of channel depth on heat requirements.

temperature the losses S will be constant, so as channel depth is increased, barrel heating H must be rapidly increased (or cooling decreased) to maintain temperature. Figure 8.9 represents the same situation in terms of energy per unit output and demonstrates not only that the total heater power increases with channel depth, but also the proportion of energy from the heaters increases and from the mechanical drive decreases. This means that low melt temperatures will be easier and high melt temperatures may be more difficult to achieve, that steady conditions will be more dependent on the performance of the temperature controllers and less on a consistent viscosity (molecular weight, composition, etc.) of feed material, but that greater radial temperature differences may occur in the channel due to greater heat flow across a deeper channel.

An increase of polymer molecular weight or decrease of melt temperature implies an increase of viscosity; at constant Q/Wbh this has no effect on output Q, though equation (6.32) shows it implies an increased pressure gradient $\mathrm{d}P/\mathrm{d}z$. However, both terms of the power equation (8.9) are increased in direct proportion, hence also is the specific power E/Q. Thus in Fig. 8.10, the power E decreases with increase of melt temperature T. However, increased temperature involves increased enthalpy I in the polymer, and also increased heat losses S from the machine, so heater power H increases rapidly with temperature, owing both to the increased heat requirements I and S and to the reduction in mechanical power input E. Since output is constant, it is only necessary to change the vertical scale for Fig. 8.10 to represent the specific power input E/Q and the balancing factors I/Q (equation (8.28)), losses S/Q and heater input H/Q ($\mathrm{J\,m^{-3}}$).

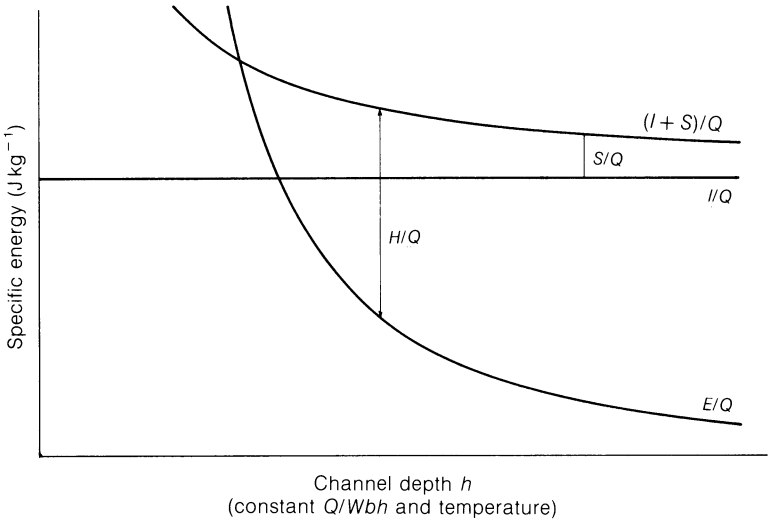


Figure 8.9 Channel depth vs specific energy.

This shows that, as with increasing channel depth h, heater input not only increases but also becomes a greater proportion of the total energy; also it is difficult to operate at high temperatures, especially with large machines where the heater surface generally increases more slowly than output (section 11.5). It will be noted that, at T_A, the drive motor supplies all the required increase in polymer enthalpy, leaving the heaters to supply only the heat losses; this is sometimes referred to as the 'adiabatic' temperature, since the polymer is neither giving heat energy nor receiving it from the surroundings. The actual value of T_A in a given case will depend on the output and the power input, which itself depends on screw dimensions, pressure (Q/Wbh), speed, and polymer type and molecular weight. At a somewhat lower temperature T_B, the drive motor also supplies the losses, so that the heaters may be switched off. This temperature T_B is also sometimes referred to as the adiabatic temperature, but the present authors believe is more correctly called 'autothermal' or 'autogenous', since mechanical work is converted into heat in the polymer, some of which is then transferred to the barrel, etc., to supply the heat losses. It has been held that this temperature is highly desirable for stable operation; it is true that temperature gradients due to external heat flows will be minimized, but other factors, e.g. shear rates, may not be optimized and, as discussed in section 11.4, control problems may result. If a melt temperature below T_B is required, then barrel cooling must be applied, and Fig. 8.10 shows that this must increase rapidly as temperature is further reduced. However, barrel cooling necessarily affects most the polymer nearest the barrel surface, where, as shown in section 8.4, shear rate and shear heating are generally a maximum, and the latter will be disproportionately increased by local increase of viscosity

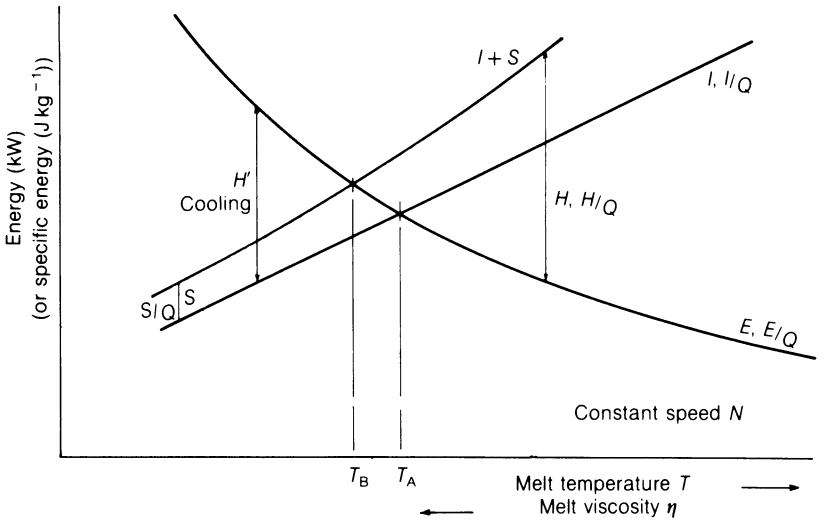


Figure 8.10 Change of energy balance with melt temperature.

due to external cooling. Similarly, barrel cooling has a profound effect on the energy dissipated in the flight clearance. Practical experience shows that these effects cause a disproportionate increase in mechanical power and a corresponding increase in cooling requirement (Fig. 8.11) which may be beyond the possibilities of heat transfer to the barrel, especially with large machines. The author has experience of 200 mm and 250 mm diameter extruders in which barrel cooling caused overload of the drive motor without significantly reducing the polymer melt temperature; the additional power only increased the losses to the cooling water, giving very inefficient operation. In such cases, lower melt temperature may only be possible by reducing speed and output, a deeper screw and/or a larger machine. Screw cooling generally has a quite different effect and is discussed in section 9.1. It will be noted that in Figs 8.10 and 8.11, the arrows relating to H (cooling) extend to the enthalpy line I rather than to that for $I + S$, as in heating. This is approximately correct because when the heaters are shut off and cooling applied, the external surface temperature of the barrel (but not the die) drops to near the coolant temperature and most of the natural cooling due to heat loss from the heaters disappears. This effect is minimized with induction heaters where most of the heat is generated by eddy currents within the barrel itself or with externally heat-insulated heaters where the losses are in any case much reduced.

At constant Q/Wbh, the effect of screw speed is simply that output Q is increased in direct proportion (equation (8.24)), whereas both terms of the power equation (8.9) increase as the square of the speed (equations (8.11) and (8.12)). Thus the specific power input E/Q (per unit output) increases in

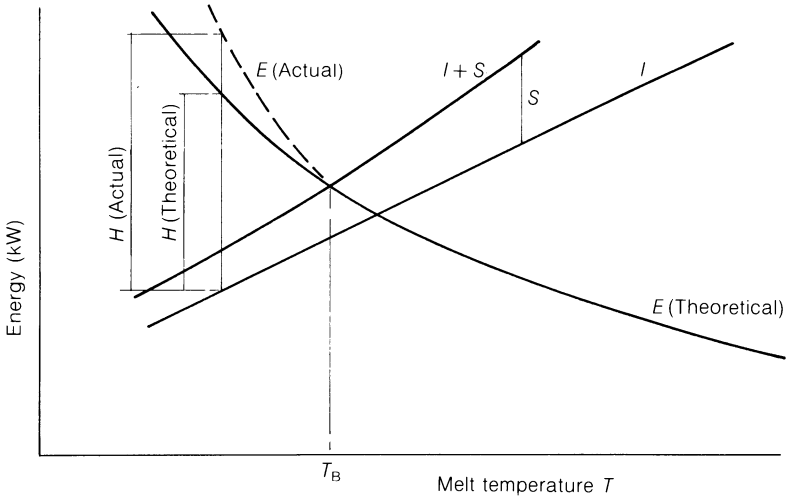


Figure 8.11 Interaction between barrel cooling and mechanical power.

proportion to speed. At constant melt temperature, the total enthalpy increase I is proportional to output Q, while the losses S are constant. Thus Fig. 8.12 represents the total energy balance and Fig. 8.13 the energy per unit output. Figure 8.12 shows that at standstill the heaters supply only the losses, but at low speeds must also supply an increasing deficiency from the drive motor. Due to the upward curve of the latter's contribution, a speed is reached at which the heater power is again reduced, until at N_A the motor supplies all the enthalpy

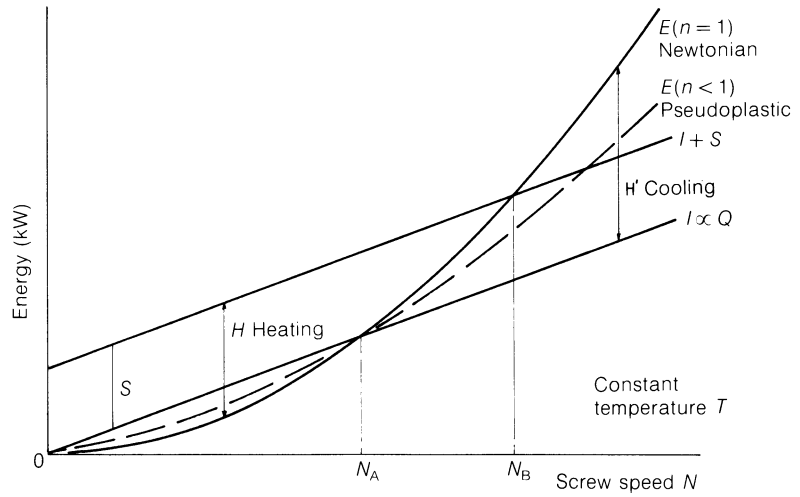


Figure 8.12 Change of energy balance with screw speed.

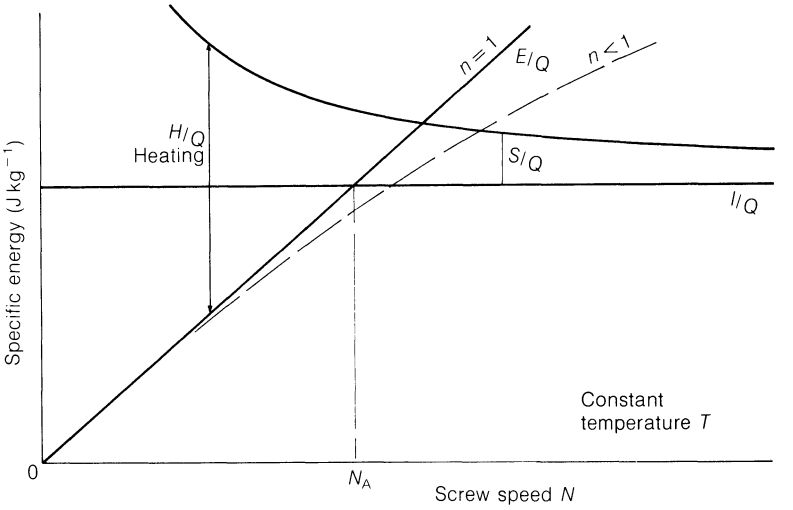


Figure 8.13 Specific energy vs screw speed.

increase I in the polymer and the heaters again supply only the losses. As speed is further increased to N_B, the autogenous speed, the heaters are shut off and the drive motor supplies energy to meet both enthalpy increase in the polymer I and losses S. This point corresponds to the autogenous temperature T_B, where N and T_B in Fig. 8.10 are, respectively, equal to N_B and T in Fig. 8.12. As speed is further increased at melt temperature T, the drive motor power increases more rapidly than the polymer enthalpy and cooling is required to maintain temperature T. As in Fig. 8.10, barrel cooling reduces the natural cooling represented by S and the heat to be removed by intentional cooling approximates to $E - I$ rather than $E - (I + S)$. As given by equations (8.11) and (8.12), in the Newtonian case $E \propto N^2$; the numerical value of E at any speed, and hence the position of the intersections N_A and N_B, will depend on the dimensions of the screw and viscosity of the polymer, including in the latter the effect of temperature. For a given screw and polymer, Figs 8.10 and 8.12 may be regarded as mutual sections of three-dimensional surfaces of E, I, S and H representing together the energy balance.

In Fig. 8.13 the energy values are plotted per unit flow rate, when I/Q is constant at constant melt temperature and S/Q decreases with speed due to the increase of Q. Then E/Q, as given by equations (8.25) and (8.26), is proportional to speed N. This again shows heater input H/Q decreasing with increase of speed, both in absolute value and as a proportion of total energy. This again shows that severe cooling, with its attendant problems, is necessary to avoid melt temperature rising with speed above N_B, just as Fig. 8.10 shows cooling necessary if it is required to reduce melt temperature below T_B at fixed speed N. The author recalls operating a 50 mm (2 in) diameter laboratory extruder with a 2:1 compression ratio screw on a K65 UPVC at a melt temperature of

approximately 200°C; the autogenous speed was reached at 40 rpm. With the same screw at similar temperatures, LDPE of MFR 2.0 still required heating at 200 rpm. Since the enthalpies of the two polymers are not grossly different at this temperature, the difference in autogenous speed N_B was a reflection of the very different melt viscosities and hence drive power required.

In the Newtonian case, viscosity is a function of temperature and not of speed, so that the effects of temperature and speed can be separated. As shown by equation (8.16), in the pseudoplastic case, the combined effect of speed N on shear rate and viscosity gives:

$$E \propto N^{n+1} \tag{8.16}$$

where the index $(n + 1)$ is between 1 and 2. The dashed line (Fig. 8.12) shows this function compared with the full line for a Newtonian fluid ($n = 1$). It will be noted that as a result the required heater power H changes more slowly with speed and less cooling will be required at speeds above the autogenous speed N_B. Note also that for purposes of comparison, this curve is shown for a pseudoplastic material having the same viscosity as the Newtonian material at temperature T and shear rate corresponding to screw speed N_A, so that at this speed the drive power is the same for both materials. The lines for ηN in Table 8.3 show that the increase in enthalpy (or temperature) equivalent to the drive motor power increases as the nth power of speed ($n < 1$) for a pseudoplastic material compared with direct proportionality ($n = 1$) for the Newtonian. Hence the achievable melt temperature will be less dependent on speed in the former case than in the latter. Although the effect of shear rate will be discussed further in section 11.5, the effect of maintaining constant shear rate on heat balance (e.g. when varying more than one dimension) is mentioned briefly here. Dividing equation (8.24) by equation (8.27) gives output Q varying with Dh^2 at constant shear rate. Then for a Newtonian polymer, drive power in the screw channel varies as $\eta D^2 NL$, and over the flight the same with the addition of the ratio h/δ. The specific drive power E/Q, representing the temperature increase due to shearing, increases as $\eta DNL/h^2$ and $\eta DNL/h\delta$, respectively. For a pseudoplastic polymer, the relations are similar, with ηN replaced by N^n The implications of this are that: (i) an increase of viscosity, speed or dimensions will tend to increase the autogenous temperature, i.e. the temperature below which cooling is required; (ii) a decrease in channel depth will cause a greater increase in specific power (proportional to $1/h^2$); and (iii) pseudoplastic rather than Newtonian behaviour of the polymer only reduces somewhat the effect of screw speed. These serve to emphasize that altering dimensions or operating conditions almost inevitably leads to changes in energy balance and the 'window' of satisfactory operation, which must be considered in adapting processing techniques and experience from one polymer, machine, output or scale to another. This will be a major aspect of operation included in Chapters 9 and 11.

Table 8.4 Variation in mechanical power with back pressure (kW/turn)

		Q/Wbh						
		0	0.1	0.2	0.3	0.4	0.5	0.6
Channel								
$n = 1$	E	2.233	1.928	1.624	1.320	1.016	0.7122	0.4081
	E/Q_{rel}	∞	13.54	5.701	3.089	1.783	1.000	0.477
$n = 0.5$	E	1.116	1.045	0.9712	0.8897	0.8037	0.7122	0.6452
	E/Q_{rel}	∞	7.336	3.409	2.082	1.411	1.000	0.755
$n = 0.3$	E	0.846	0.819	0.7893	0.7603	0.7315	0.7122	0.7750
	E/Q_{rel}	∞	5.750	2.771	1.779	1.284	1.000	0.907
Flight								
$n = 1$	E	←			3.100			→
	E/Q_{rel}	∞	15.5	7.75	5.17	3.875	3.100	2.583
$n = 0.5$	E	←			0.428			→
	E/Q_{rel}	∞	2.14	1.07	0.713	0.535	0.428	0.357
$n = 0.3$	E	←			0.194			→
	E/Q_{rel}	∞	0.97	0.485	0.323	0.242	0.194	0.162

So far comparisons from Table 8.3 have been made at constant Q/Wbh, i.e. with longitudinal pressure gradient as given by equation (6.32). If this dimensionless output is now considered as a variable, then for given dimensions and speed, output Q is proportional to Q/Wbh. Drive power in the channel is proportional to $4(1 + \tan^2 \phi) - 6Q/Wbh$, while that in the flight clearance is unchanged. Dividing out:

$$\frac{E_{Ch}}{Q} \propto \frac{4(1 + \tan^2 \phi)}{\dfrac{Q}{Wbh}} - 6 \tag{8.29}$$

and:

$$\frac{E_{Fl}}{Q} \propto \frac{1}{\dfrac{Q}{Wbh}} \tag{8.30}$$

Thus, as pressure gradient is increased, Q and Q/Wbh decrease, but channel power increases. The result, mainly due to decreasing output, is that specific power E/Q increases, tending to higher melt temperatures (compare Fig. 8.10).

The following example illustrates the variations of total and specific power (representing temperature rise due to shear heating) as functions of back pressure. The results for several values of Q/Wbh are given in Table 8.4 and plotted in Figs 8.14 and 8.15. These show that in the Newtonian case the channel power increases rapidly with increase of back pressure, but that the constant flight power is also large. With more highly pseudoplastic melts, the variation of channel power with back pressure becomes much smaller, as does

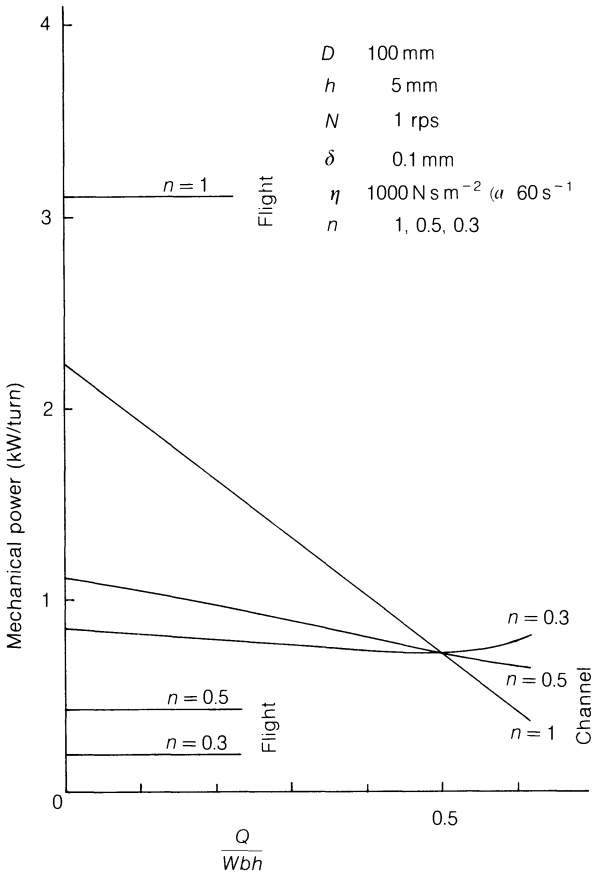


Figure 8.14 Variation of mechanical power with pressure.

the proportion of total power contributed from the flight clearance. Due to the decrease of output Q with increase of back pressure, the specific power E/Q (plotted relative to a value of unity at $Q/Wbh = 1/2$ for the channel) increases even more rapidly, indicating severe problems of temperature rise at high back pressures and low outputs.

Diameter	D	100 mm
Channel depth	h	5 mm
Pitch	p	100 mm
Flight width	t	10 mm
Speed	N	1 rps
Viscosity (channel)	η	1000 N s m^{-2} at shear rate 59.87 s^{-1}
Pseudoplasticity index	n	1, 0.5, 0.3
Flight clearance	δ	0.1 mm

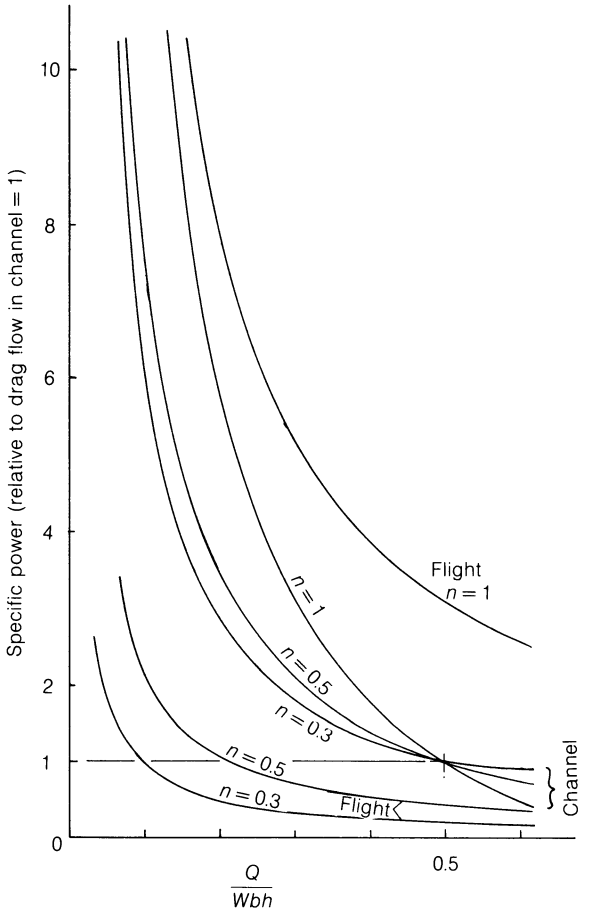


Figure 8.15 Specific power vs back pressure.

Then

Channel width	$b = (p - t)\cos\phi = 0.085\,76\,\text{m}$
Helix angle	$\phi = 17.657°$
Helical length	$\mathrm{d}z = 0.1\pi/\cos\phi = 0.3297\,\text{m}$ (one turn)
Peripheral speed	$\pi DN = \pi 0.1 \times 1 = 0.3142\,\text{m s}^{-1}$
Longitudinal velocity	$W = 0.2994\,\text{m s}^{-1}$
Transverse velocity	$U = 0.0953\,\text{m s}^{-1}$
Drag flow	$Q_\text{D} = 0.2994 \times 0.085\,76 \times 0.005/2$ $= 0.642 \times 10^{-4}\,\text{m}^3\,\text{s}^{-1}$
Mass drag flow	$\rho Q_\text{D} = 0.0505\,\text{kg s}^{-1}$ if density is $786\,\text{kg m}^{-3}$

Drag flow shear rate $\dot{\gamma}_D = W/h = 0.2994/0.005 = 59.87\,s^{-1}$

Factor $4(1 + \tan^2\phi) = 4.4053$

Newtonian channel power

$$dE = \frac{1000 \times (0.2994)^2 \times 0.08576 \times 0.3297}{0.005}\left(4.4 - \frac{6Q}{Wbh}\right)$$

$$= 506.8\left(4.4 - \frac{6Q}{Wbh}\right) \text{ W/turn}$$

Flight power

$$= \frac{\eta \times (0.2994)^2 \times 0.01 \times 0.3297}{0.0001 \times \cos\phi}$$

$$= 3.10\eta \text{ W/turn}$$

The above example may be extended to illustrate the effect of back pressure on heat balance. Further assumptions are required:

Melt temperature	T	157.6°C (for consistency with following example on effects of N and T)
Melt density	ρ	$786\,kg\,m^{-3}$ from Fig. A.1
Specific heat	C_p	$2300\,J\,kg^{-1}\,K^{-1}$ from Table 4.1 for LDPE
Energy to melt at 115°C.		$3.3 \times 10^5\,J\,kg^{-1}$ from Fig. A.2 (ref. 70)
Melt length		8 turns
Pseudoplasticity index	n	0.3436

The internal energy at the crystalline melting point, 115°C, is $3.3 \times 10^5\,J\,kg^{-1}$. The internal energy at 157.6°C is then:

$$3.3 \times 10^5 + 2300(157.6 - 115) = 4.28 \times 10^5\,J\,kg^{-1}$$

The mass flow at $Q/Wbh = 0.5$ is:

$$0.642 \times 10^{-4} \times 786 = 0.0505\,kg\,s^{-1}$$

and at other values in direct proportion to Q/Wbh, from which the total internal energy in watts is obtained by multiplying by $4.28 \times 10^5\,J\,kg^{-1}$. The losses S are calculated from the data in Table C.1 for a barrel 1.7 m ($20L/D$ less $3L/D$ for feed) in length and 150 mm in outside diameter, by simple proportion from that used in the trials tabulated in appendix C.1, i.e. 600 mm long $\times$127 mm OD, with the same losses assumed from the die and adaptor. Then from settings 1,3 and 5 of Table C.1, the total losses for the 100 mm diameter machine are predicted as:

Melt temp. (°C)	*Total losses* (W)
150	6374
200	8970
250	13061
157.6	6769 by interpolation

Table 8.5 Change in energy balance with back pressure

Q/Wbh		0	0.1	0.2	0.3	0.4	0.5
Flow rate $\times 10^{-4}$	$m^3 s^{-1}$	0	0.128	0.257	0.385	0.514	0.642
Mass flow	$kg s^{-1}$	0	0.0101	0.0202	0.0303	0.0404	0.0505
Internal energy I	W	0	4320	8640	12961	17281	21601
Wall shear rate	s^{-1}	239.5	203.6	167.6	131.7	95.79	59.87
Channel viscosity	$N s m^{-2}$	402.5	447.9	508.7	596.0	734.5	1000
Channel power	W/turn	897.7	862.8	825.1	785.5	744.6	709.3
Flight power	W/turn	230.3	230.3	230.3	230.3	230.3	230.3
$E_{Ch} + E_{Fl}$	W/turn	1128.0	1093.1	1055.4	1015.8	975.4	939.6
Power (8 turns)	W	9024	8745	8443	8126	7803	7517
Power to melt	W	0	3331	6662	9993	13324	16655
Total power E	W	9024	12076	15105	18119	21127	24172
Heat losses S	W	6769	6769	6769	6769	6769	6769
Heater power H $H = I + S - E$	W	−2255	−987	304	1611	2923	4198

The mechanical power in the channel E_{Ch} is calculated from equation (8.7) for each value of Q/Wbh, using a viscosity calculated from the wall shear rate from equation (6.69), taking viscosity as $1000 N s m^{-2}$ at a drag flow shear rate of $59.87 s^{-1}$ and the pseudoplasticity index n as 0.3436. The flight power E_{Fl} is similarly calculated from equation (8.8), using the shear rate of $\pi DN/\delta = 3142 s^{-1}$, giving a viscosity of $74.3 N s m^{-2}$ and flight power per turn of 230.3 W. The sum of the channel and flight powers is multiplied by 8 turns (assumed constant) and added to the energy to melt (equals the internal energy at 115°C) i.e. 3.3×10^5 times the mass flow rate. The calculated values are given in Table 8.5 and plotted in Fig. 8.16. This shows that as back pressure is increased, the total mechanical power E does not decrease as quickly as the internal energy I (or $I + S$ since losses S are constant), so that whereas heating is required to maintain the chosen melt temperature (157.6°C) at drag flow ($Q/Wbh = 0.5$), at high back pressures and low relative flow rate cooling will be required. This example is roughly equivalent to the curve for $n = 0.3$ in Figs 8.14 and 8.15, though less dramatic, since the latter refer to power in the melt section only. However, the melt point tends to move back with increasing pressure, giving longer melt length, higher mechanical power, and more rapid change than shown in Fig. 8.16 from heating to cooling as pressure is increased.

In practice this means that it may be difficult to maintain low melt temperatures, e.g. for blow moulding, with high back pressures, whereas the latter may be beneficial in reducing external heating requirements, and accompanying radial temperature gradients, where high melt temperatures are desirable, e.g. for paper-coating, where die resistances are in any case likely to be high.

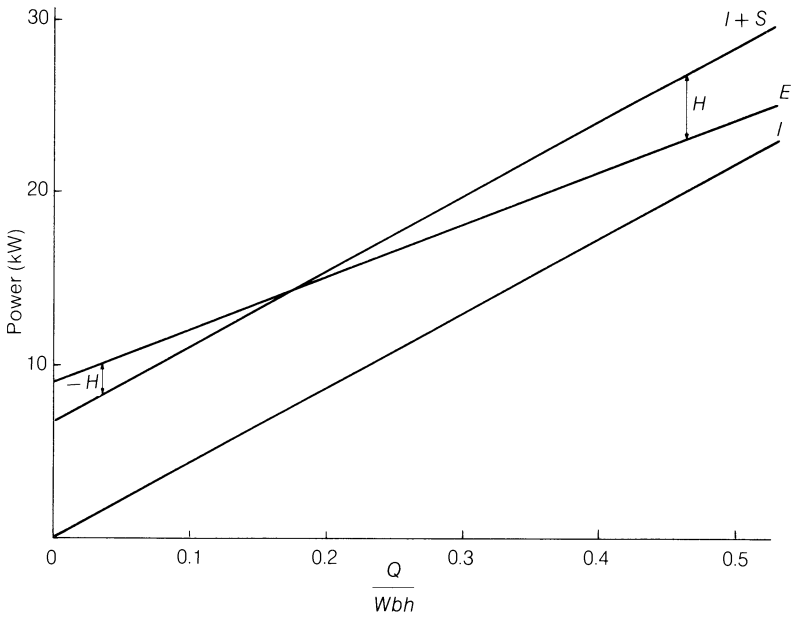


Figure 8.16 Change in energy balance with back pressure.

By changing dimensions and material properties, the position, slope and shape of the curve can be changed, e.g. so that heating is always required, so Fig. 8.16 should be taken as typical rather than universal.

A further example, using the same dimensions, shows the variations in heat balance with melt temperature T and screw speed N at a fixed value of Q/Wbh. The latter is taken arbitrarily as 0.3, representing a moderate back pressure. As with Fig. 8.16, the purpose is to show trends, rather than absolute values.

To emphasize the changes, but without altering the values of autogenous temperature T_B and speed N_B, only the internal energy I above the melting point and the mechanical power E in the melt section are considered, i.e. the energy to melt the polymer is deducted from I and E respectively, maintaining the balance; this cannot of course be neglected in estimating the drive motor power required or the torsional strength of the screw.

The polymer chosen (also used in appendix C.5) is a typical MFR 2.0 LDPE having viscosities at a shear rate of $30\,s^{-1}$ (typical of the screw channel) of $2200\,N\,s\,m^{-2}$ at 150°C and $730\,N\,s\,m^{-2}$ at 200°C. At a shear rate of $2000\,s^{-1}$ (typical of the flight clearance), the viscosities are $124\,N\,s\,m^{-2}$ at 150°C and $61\,N\,s\,m^{-2}$ at 200°C. To extend the example to 250°C, equation (3.8) is used to cover the wide temperature range, but since viscosity is effectively infinite at the crystalline melting point (taken as 115°C), T in that equation is taken as the temperature difference above 115°C. Then from the above experimental

viscosities:

$E/R = 65.639$ at $30\,s^{-1}$
$E/R = 42.210$ at $2000\,s^{-1}$
$n = 0.3152$ at 150°C
$n = 0.4090$ at 200°C
$n = 0.4333$ at 250°C
$\eta = 548.4\,N\,s\,m^{-2}$ at $30\,s^{-1}$ and 250°C
$\eta = 50.75\,N\,s\,m^{-2}$ at $2000\,s^{-1}$ and 250°C
$\eta = 1000\,N\,s\,m^{-2}$ at $60\,s^{-1}$ and 157.6°C, as in the previous example

For $Q/Wbh = 0.3$, the wall shear rate given by equation (6.69) is

$$\dot{\gamma}_h = \frac{W}{h}(4 - 6 \times 0.3) = 2.2\frac{W}{h}$$

and the channel power given by equation (8.7) is

$$E_{Ch} = \frac{\eta W^2 b\,dz}{h}[4(1 + \tan^2\phi) - 6 \times 0.3] = \frac{2.6\eta W^2 b\,dz}{h}$$

The melt length is again assumed constant at 8 turns. The values for melt temperatures of 150, 200 and 250°C and screw speeds of 1, 2 and 4 rps are given in Table 8.6. The heat balance is plotted in Figs 8.17 and 8.18 against melt temperature and screw speed, respectively.

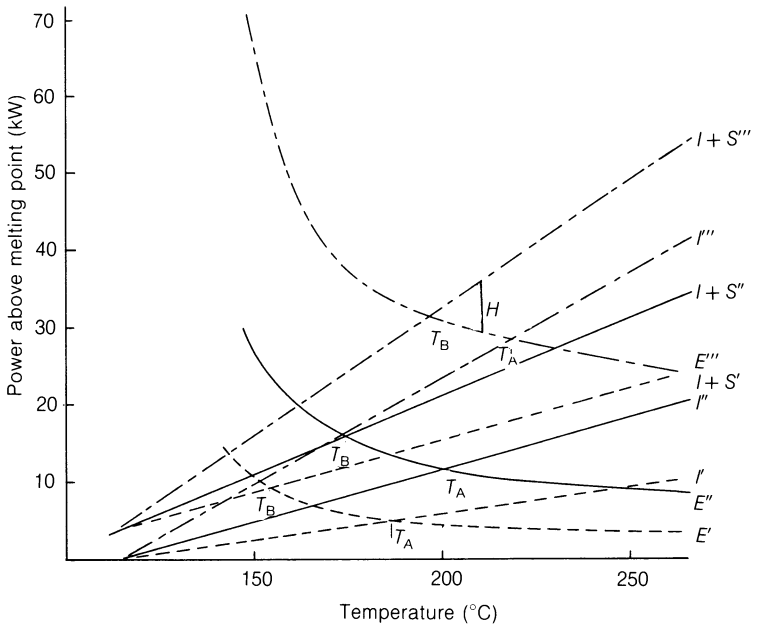


Figure 8.17 Change in energy balance with melt temperature.

Table 8.6 Changes in energy balance with melt temperature and screw speed

Melt temperature	°C	150	200	250
1 rps				
Wall shear rate	s^{-1}	131.7	131.7	131.7
Viscosity η_{Ch}	$N s m^{-2}$	798.8	304.5	237.2
Channel power	W/turn	1 052.8	401.3	312.6
Flight power	W/turn	282	145	122
Total power (melt)	W	10 678	4 370	3 477
Int. energy I_{115-T}	W	2 439	5 830	9 110
Losses S	W	6 374	8 970	13 061
Heat energy H	W	−1 865	10 430	18 694
2 rps				
Wall shear rate	s^{-1}	263.4	263.4	263.4
Viscosity η_{Ch}	$N s m^{-2}$	497.0	202.2	160.1
Channel power	W/turn	2 620.1	1 065.9	844.0
Flight power	W/turn	702	384	329
Total power (melt)	W	26 577	11 599	9 384
Int. energy I_{115-T}	W	4 883	11 660	18 202
Losses S	W	6 374	8 970	13 061
Heat energy H	W	−15 320	9 031	21 879
4 rps				
Wall shear rate	s^{-1}	526.9	526.9	526.9!
Viscosity η_{Ch}	$N s m^{-2}$	309.1	134.2	108.1
Channel power	W/turn	6 518	2 830	2 279
Flight power	W/turn	1 746	1 021	888
Total power (melt)	W	66 112	30 807	25 340
Int. energy I_{115-T}	W	9 761	23 319	36 403
Losses S	W	6 374	8 970	13 061
Heat energy H	W	−49 977	1 482	24 124

The rapid rise of mechanical power E at melt temperatures below about 150°C shown in Fig. 8.17 is partly a consequence of the equation (3.8) used, as is the almost horizontal line above 200°C. However, it emphasizes that low melt temperatures are difficult to achieve, especially at high screw speeds, requiring severe cooling, with the consequences mentioned on p. 256. This calculation makes no attempt to include the additional effect of barrel cooling indicated in Fig. 8.11. At high melt temperatures, the mechanical power may vary little, but increased heater input H is required to raise melt temperature due to the increased internal energy I required in the polymer, and to a lesser extent to the increased heat losses S. The set of curves for each speed is qualitatively similar to the diagrammatic representation in Fig. 8.10, showing in each case an adiabatic temperature T_A and a somewhat lower autogenous temperature T_B; the difference $T_A - T_B$ is comparatively large in this example due to the relatively large heat losses assumed. As expected, both T_A and T_B increase with screw speed N, but T_B increases more rapidly than T_A and the difference $T_A - T_B$ becomes less, due to the smaller proportion of the total

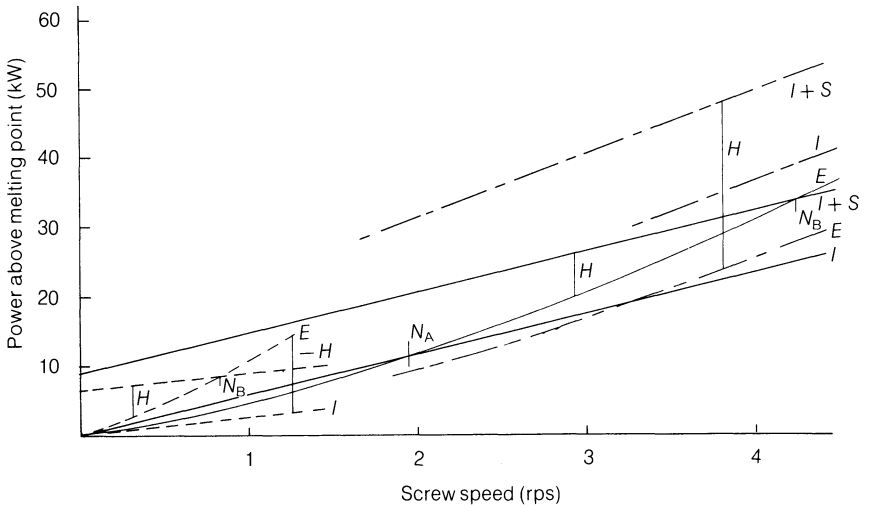


Figure 8.18 Change in energy balance with screw speed.

energy represented by the losses S at high screw speeds. With the same screw, a higher-viscosity polymer, e.g. a less plasticized PVC or a higher molecular weight, would develop more mechanical power E at a given melt temperature and speed, but with little change in internal energy. Thus the adiabatic and autogenous temperatures would be higher, placing further restrictions on minimum melt temperature or maximum speed; evidently the screw design would require reconsideration if either of these were critical. Conversely, if very high melt temperatures are required with a low-viscosity polymer, a shallower screw running faster might be desirable, or a longer screw would give increased mechanical power input E and a greater surface area for external heating H – in any case the greater residence time would minimize radial temperature differences at the end of the screw.

At first sight, the sets of curves in Fig. 8.18 appear rather different from those in Fig. 8.12. This is partly because the LDPE used for the example is highly non-Newtonian ($0.3 < n < 0.45$), giving flatter curves (proportional to the $(n + 1)$th power of speed N) than a Newtonian fluid, as indicated by the dashed line in Fig. 8.12. Thus only the extreme left-hand portion of Fig. 8.12 represents this example at 250°C, extending up to about the point of maximum heat input H and not approaching the adiabatic speed N_A, which at this temperature would be very high. At 200°C the adiabatic point N_A is reached at about 2 rps and the autogenous speed at about 4.2 rps – the large difference between these values is partly due to the flat curve of E (highly non-Newtonian) and partly to the large heat losses S assumed, as mentioned above. However, it is noteworthy that in these conditions the change from heating to cooling is also slow, so that the autogenous speed N_B can be exceeded without severe cooling or with only

modest increase of melt temperature, and the temperature control should be stable. This is borne out in practice with LDPE, where extruders have been operated over wide ranges of screw speeds with little difficulty in maintaining moderate melt temperatures, e.g. for hot melt granulation; also by 90 mm production units running at 4 rps and a melt-fed machine* at 6–7 rps without excessive melt temperatures or cooling. In contrast, at 150°C the whole of Fig. 8.12 represents the example up to only about 1 rps, and clearly it would be difficult to operate above this speed at 150°C. If the polymer were more nearly Newtonian, the change from heating to cooling as speed is increased would be more rapid, as indicated in Fig. 8.12, which assumes equal viscosities at T_A, N_A.

This example assumes that the position of the melt point remains constant, despite changes in melt temperature and speed. Melt temperature *per se* would be expected to have little influence on melt point, though this might move back as a consequence of increased barrel set temperatures. This would tend further to flatten the right-hand, high-temperature portion of the mechanical power E curves in Fig. 8.17, leading to small reductions in the external heat H required. Increase of speed is likely to cause the melt point to move forward, decreasing the length of the remaining melt section and the mechanical power dissipated in it. This would further flatten the power curves E in Fig. 8.18, permitting greater screw speeds before the autogenous speed N_B was reached and cooling was required, provided that melt temperature variations at the end of the screw were acceptable.

This emphasizes the importance of experimental determination of melt point position and its changes with polymer viscosity, screw design, temperature and screw speed for reliable estimation of the energy balance. This presentation and the example only purport to illustrate the trends and offer explanations for observed changes in, for example, melt temperature or energy inputs. More exact quantitative predictions would require not only accurate knowledge of polymer viscosity over a wide range of shear rate (including flight clearance) and temperature and changes in the position of the melt point, but also inclusion of the effects of barrel cooling (Fig. 8.11), local heating in the flight clearance (appendix C.5) and heat loss data (including dies). Such predictions are also unlikely to indicate temperature variations at the end of the screw and other factors influencing product quality. These will be further discussed in Chapters 9 and 11.

*The author has used a diphenyl jacketed hopper of simple 'V' form with an opening approximately 280 mm (11 in) square immediately above the screw. A melt of high molecular weight LDPE was fed to a 90 mm (3.5 in) 16:1 L/D extruder running at 400 rpm at rates up to 1090 kg h^{-1} (2400 lb/h). The extrudate was successfully granulated by an underwater die face cutter at these rates with no problems of excessive melt temperature.

9 Operation of single-screw extruders

9.1 OVERALL PERFORMANCE OF THE SCREW

The preceding chapters have dealt separately with mass and heat flows within the various functional sections of the screw channel and the flight clearance. Even in steady-state operation, these interact with each other and with pressure and temperature gradients to produce a complex pattern of simultaneous velocity, shear and temperature variations. Any attempt at a total representation of these in mathematical terms would lead either to a very generalized formulation or to an extremely complex one, neither of which would readily lead to an understanding of the mechanisms or the consequences of changes imposed on the operating conditions. An understanding of the latter, which is the chief concern of this book, is essential for rational and effective operation. The alternative approach taken here is to use a qualitative description to modify and extend the approximate solutions of the simplified theories in Chapters 6–8. Practical experience suggests that these solutions are useful guides to operating strategies and the consequences of *changes* in conditions, as distinct from design for a specified performance. The following description refers to steady-state operation of a solid-fed single-screw extruder with fixed die, but without optional attachments or functions.

In considering the performance of the extruder as a whole, requirements of continuity impose restrictions on the physical parameters of mass flow, pressure, temperature, energy and mixing such that a change to a parameter in one section requires complementary changes in the remaining sections as well as in the overall characteristics of the process. For clarity, each parameter is considered in turn, though interaction with the other parameters is inevitable and forms part of the overall response.

9.1.1 Material flow

The steady state requires that the net mass flow rate of material must be constant with time and the same at all points within the extruder and die, despite differing densities (due to temperature and change of state) and mechanisms of flow.

Variation of flow in the hopper may arise intermittently due to bridging. This may coexist with segregation due to funnelling or differing particle densities or shapes, e.g. with regrind, giving non-uniform composition. Flow may also be interrupted with fine powders and high hopper levels due to trapped air. If this cannot escape through the shaft seal, a lateral division near the rear of the feed opening will allow air to escape behind it. Mechanical stirrers or vibrators have been used to reduce bridging and air entrapment. Insufficient cooling of the feed throat may lead to particles of low melting polymers adhering, especially to the front face, and restricting flow.

Filling of the screw is usually by gravity, with a relatively close clearance of a hardened feed pocket liner around most of the circumference of the screw to prevent the feed material falling out again and provide some resistance so that it is conveyed into the barrel instead of merely being carried round by the screw. With a purely radial inlet to the screw, the latter can force material back into the feed throat and hinder the in-flow of fresh material, especially if the particles are elastic or large relative to the dimensions of the screw channel. For this reason the opening is frequently made tangential to the downgoing side of the screw, although some designers argue that at high speeds the screw will 'run away' from the feed, whereas on the upcoming side the screw cuts into the descending column of material. Experience shows that a substantial chamfer (Fig. 7.1) is helpful, both on the downgoing side and at the end leading into the

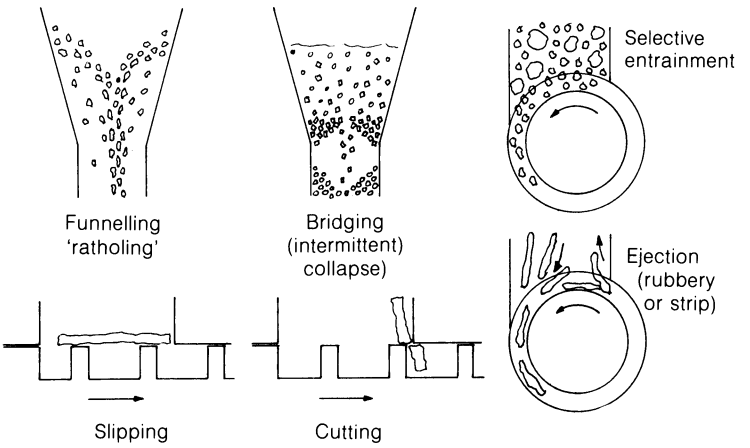


Figure 9.1 Causes of feed segregation.

barrel, in leading material which is outside the path of the screw flight into the channel rather than ejecting it by hitting a near-radial surface. Especially with large particles or elongated strips it can be seen that a wedging action occurs not only between the screw root and the feed pocket liner, but also between the flight tip and the liner – in the absence of a chamfer, the flight tends to cut and/or eject the particles (Fig. 9.1). A feed opening of length three times the screw diameter is usually adequate for complete filling of the screw. Note that the screw length is usually reckoned from the rear of the feed opening though compaction to form a plug of material commences from the front face. Any restriction of output caused by these mechanisms is more likely to occur at high screw speeds.

Rapid compaction of feed particles to a solid plug is accompanied by rearward displacement of entrained air; if this is unduly delayed, e.g. by low first-zone barrel temperature, some air may be carried forward and appear in the extruded product. The conditions for forward conveying of this solid plug have been dealt with in Chapter 7. For continuity of mass flow with the melt pumping section (equation (6.15)), the downchannel velocity V_{pz} of the plug will be given by:

$$\rho_p b h_1 V_{pz} = \rho_m \left[\frac{W b h_2}{2} - \frac{b h_2^3}{12\eta} \cdot \frac{dP}{dz} \right]$$

or

$$V_{pz} = \frac{\rho_m}{\rho_p} \cdot \frac{h_2}{h_1} \left[\frac{W}{2} - \frac{h_2^2}{12\eta} \cdot \frac{dP}{dz} \right] \tag{9.1}$$

From Fig. A.1 it is seen that for several common polymers the ratio ρ_m/ρ_p of melt and solid densities, which depends only on the respective temperatures, lies between 0.7 and 0.9. Then for a 3:1 compression ratio screw operating at $Q/Wbh = 0.5$, $V_{pz} \approx 0.13\,W$. For a constant-depth screw with the high back pressure necessary for melting, say $Q/Wbh = 0.2$, $V_{pz} = 0.16\,W$. Thus in most cases the velocity of the solid plug is a small fraction of the peripheral velocity of the screw flight ($\pi DN = W/\cos\phi$) and there is no difficulty in matching the conveying rate of solids to the melt pumping rate. In some cases of very positive solids conveying, not only may very high pressures be generated, but also excessive torque on the screw. This has been discussed in Chapter 7 in relation to grooved feed sections; the author has experienced overload of the drive motor when feeding simultaneously a number of strips of film for reclaim, e.g. unblown LDPE tubular film 50–100 mm wide by 2×0.25 mm thick and PETP edge trim film 25 mm wide by 0.025 mm thick. If two dissimilar materials, which each separately feed satisfactorily, are fed as a mixture, it is possible for selective conveying to occur, e.g. from a mixture of rubber crumb and polypropylene powder, the rubber was conveyed, largely displacing the PP powder and substantially altering the composition of the extruded product.

Some writers have proposed controlling the extruder output by 'starve' feeding using some form of continuous weigh feeder; the author's experience is that the solids feeding becomes less regular and possibly affects the melting process, the delivery pressure tends to fluctuate, but the power input decreases only slightly, leading to higher final temperature. Other workers have employed a robust screw and drive in the feed hopper, referred to as a 'force-feeder', in conjunction with an improved shaft seal, which not only prevents bridging in the hopper but also imposes pressure in the feed section. The author witnessed trials of a 150 mm (6 in) extruder densifying polypropylene powder for granulation; the output at a given screw speed was increased some 25–30% and melt temperature and degradation of the polymer were decreased significantly. The load on the main drive motor was increased considerably and when feeder speed was increased, the 82 kW (110 hp) main motor stalled before the 2.2 kW (3 hp) feeder motor reached full load, so that careful control was necessary.

The concurrent flow of compacted solid and melt in the melting section has been analysed in Chapter 7; in steady operation the sum of these must evidently equal that in the melt pumping section. The mechanism and flow pattern in the melt pool will resemble that in the melt pumping section (section 6.2), being driven primarily by the relative motion of screw and barrel. Unless pressure is generated earlier, e.g. in the solids conveying section, this drag flow represents the maximum flow rate in the melt pool and is given approximately by $\rho_m F_D W(b - X)h/2$, where F_D is the drag-flow shape factor (Mckelvey, 1962) for a channel $(b - X)$ wide by h deep. This will be a slight underestimate due to the forward velocity of the solid bed forming one side of the 'channel'. The mass flow in the solid bed is $\rho_p V_{pz} Xh$. In a constant-depth screw operating with no pressure rise:

$$\frac{\rho_m F_D W(b - X)h}{2} + \rho_p V_{pz} Xh = \frac{\rho_m F'_D Wbh}{2}$$

or

$$V_{pz} = \frac{\rho_m}{\rho_p} \cdot \frac{W}{2}\left[F_D + (F'_D - F_D)\frac{b}{X}\right] \tag{9.2}$$

As above, $0.7 < \rho_m/\rho_p < 0.9$, $b/X > 1$ and $F'_D - F_D$ is positive, though small except near the start of melting when $b/X \to 1$, while F_D is somewhat less than unity; thus continuity would require $V_{pz} \approx 0.4\,W$. Practical experience that a constant-depth screw requires appreciable back pressure in order to achieve moderately satisfactory melting may then be interpreted as restricting the mean velocity in the melt pumping section to give continuity with achievable downchannel velocities of the solid bed. If back pressure is applied, reducing Q/Wbh to 0.2 (say) then $V_{pz} = 0.16\,W$ (as above). The Tadmor theory assumes V_{pz} is constant through the melting zone and gives an almost linear reduction in solid bed width X. This requires $Q/W(b - X)h$ in the melt pool to

vary only as $1/F_D$ from Q/Wbh in the melt pumping section. This will predict a longitudinal pressure gradient only slightly increasing as melting proceeds and continuous with that in the melt pumping section.

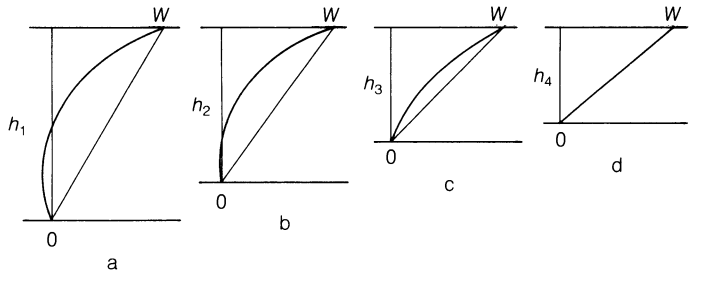
If the same assumptions are applied to the previous example, i.e. a 3:1 compression-ratio screw with $Q/Wbh_2 = 0.5$ in the melt pumping section, then $V_{pz} \approx 0.13\,W$. If melting is assumed to occupy the compression section of the screw and the solid bed velocity is assumed constant throughout the melting zone, then its width X will decrease almost linearly, as in Fig. 7.28(a). Continuity will then predict $Q/W(b - X)h$ in the melt pool increasing from approximately $0.3/F_D$ at the start of melting to $0.5/F_D$ at the end of melting. This corresponds to a decreasing pressure gradient through the melting zone, as for a tapered melt pumping zone (lower right portion of Fig. 6.11). If pressure is increased through the melt pumping zone ($Q/Wbh_2 < 0.5$) then the pressure gradients in the melt pool will progressively approach those in the upper left of Fig. 6.11 and as predicted in Fig. 7.28(b). If the solid bed velocity decreases from its initial value or its width decreases more slowly than predicted, then continuity will require a greater flow rate in the melt pool, especially near the start of melting, and pressure generated in the melting zone will be much reduced. Similar effects would be expected if melting continues beyond the tapered section of the screw into a constant-depth 'metering' section. Conversely, if melting commences before the start of the tapered section, pressures may still be generated even if melting is slower than predicted by the Tadmor model.

Isothermal flow in the channel of the melt pumping zone is adequately described by equations (6.67) and (6.26) for the downchannel and transverse velocities, respectively:

$$w = \frac{Wy}{h} + \frac{6W}{h^2}\left(\frac{1}{2} - \frac{Q}{Wbh}\right)(y^2 - yh) \tag{6.67}$$

$$u = \frac{Uy}{h}\left(\frac{3y}{h} - 2\right) \tag{6.26}$$

The former gives a net flow rate as in equation (6.15) and the latter (neglecting leakage) gives zero flow rate represented by equation (6.24). The resulting flow pattern is discussed in section 6.2 (Fig. 6.8), producing both end-to-end and transverse mixing, the former (only) being influenced by longitudinal pressure gradient. The effect on pressure gradient of a screw of varying depth is discussed in section (6.4) (Fig. 6.11), where it is seen that, Q being constant by continuity, decreasing h implies an increase in the local value of Q/Wbh. If the position in the channel y is represented by extracting the fractional depth y/h from equation (6.67), it is seen that the drag flow term changes only by the vertical (radial) scale of h, whereas the pressure flow term also decreases in magnitude as $Q/Wbh \rightarrow 1/2$. Thus in a tapered screw, the downchannel



$$\frac{Q}{Wbh_1} < \frac{Q}{Wbh_2} < \frac{Q}{Wbh_3} < \frac{Q}{Wbh_4}$$

$$Q_1 = Q_2 = Q_3 = Q_4$$

Figure 9.2 Changing velocity profiles in a tapered screw.

velocity distribution changes from Fig.6.6(b) to 6.6(c) and eventually to Fig. 6.6(d) or 6.6(e), though with a changing scale of h (Fig. 9.2). Equation (6.26) shows that the transverse velocity distribution changes only with the scale of h. Thus the flow pattern along the length of a varying depth screw is continually changing even on an isothermal basis. The qualitative effects of non-Newtonian and non-isothermal flow have been discussed in sections 6.7 and 6.8, respectively. Leakage, although small (section 6.3), reduces net flow as given by equation (6.15), re-entraining into the flow in the previous turn of the screw close to the barrel surface, where it is rapidly dispersed.

9.1.2 Pressure

The effects of pressure are inseparable from those of flow. The pressure increase (or drop) in successive sections of the screw must be additive, as indicated for the melt pumping section by equation (6.61), and equal to the total resistance of the die, breaker plate, etc. In Chapter 7 it has been shown that in the absence of force-feeding or grooved feed section liners, pressure is modest in the solids conveying zone. However, this pressure or its associated velocity appears to be the principal mechanism for forward movement of solid material along the screw in the melting zone (Stevens, 1970). As discussed above, the melting theory predicts substantial pressure rise in the melt pool. Weeks and Allen (1962) found evidence of such pressure rises with high die pressures and relatively deep melt pumping sections, which would require considerable length to generate such pressures. The point of initial pressure rise appeared to move towards the feed end as die pressures was increased. In contrast, a screw with a shallow melt pumping section showed an almost constant position within the tapered portion of initial pressure rise for die pressures between 5 and 45 MPa and screw speeds between 0.3 and 1.3 rps. The

melt temperature in this case was close to that of the inner surface of the barrel and at least 15°C above the crystalline melting point, suggesting that the melting process was essentially complete at this point of initial pressure rise. The sensitivity of pressure rise in the melting zone to the rate of melting makes prediction of the former difficult; at high die pressures it appears to make a significant contribution to the total pressure increase, whereas at low die pressures for the type of screw under consideration, it appears to make little contribution. Thus the effective length for generation of pressure is uncertain, but on the other hand the point of initial pressure rise is unreliable as a guide to the 'gel point', e.g. in determining appropriate barrel temperature profiles.

The longitudinal pressure gradients in the melt pumping section, including the effects of back pressure and channel depth, have been dealt with in section 6.4. These, combined with the transverse pressure gradient (rising from the trailing to leading flight edge, right to left in Fig. 6.7), give rise to a periodically fluctuating pressure at a fixed point on the barrel, as indicated in practice by a pressure gauge. This fluctuation is normally damped out a short distance beyond the end of the screw. Pressure falls progressively through the adaptor and die, with the major drops through the die lands and any restrictor bar/ring, which thereby control the flow. The possibility of lateral pressure difference in the die is indicated in section 5.3.3 while time fluctuations of pressure will be discussed in section 11.2.

9.1.3 Temperature

The primary effect of an increase in the polymer temperature within the extruder is a reduction of viscosity (equation (3.8)) and, to a lesser extent, of melt elasticity. The former results in a decrease in mechanical work and consequent shear heating (equation (3.57)) and also a reduction of pressure drop at fixed flow rate (equation (3.23)). The low thermal conductivity of most polymers (Appendix A) limits the heat flow and the increase in polymer temperature due to increased barrel temperatures, which also tend to reduce shear heating, so the resultant change is ambiguous. Longitudinal conduction in the metal barrel and screw also limits the longitudinal temperature gradients in the polymer (Table 8.1).

Solid feed to the extruder is usually at room temperature;* water cooling of the feed pocket is commonly used to maintain the feed in a free-flowing state until it is beyond the feed opening – whether this also contributes to conveying along the screw is uncertain. Heat conducted from the first barrel heater may cause sticking in the feed, which sets an upper limit to the first zone

*The author has used air at up to 105°C in a partly fluidized bed to preheat LDPE granules, which fed satisfactorily by gravity. Drive motor power was considerably reduced. Preheating would be expected to reduce the length of the melting zone, but the effect on uniformity of melting could not be verified.

temperature. The feed section of the screw also receives heat by longitudinal conduction, but its temperature is usually unknown and uncontrolled – an exception is referred to on p. 20. Within the barrel the polymer is heated by conduction from the barrel and possibly from the screw, leading to temperature gradients within the compacted plug; shear heating will also occur, mainly at the metal surfaces. Since the solid bed retains its general form, these temperature differences within it will tend to persist until it breaks up at the end of the melting zone. As soon as an axial position is reached at which the barrel temperature is above the softening/melting point of the polymer, a film of molten polymer will form due to a combination of conducted and local shear heating. Initially this film will improve contact between the barrel and solid polymer particles and thus improve conducted heating, but possibly reduce frictional heating. When the film thickness exceeds the flight clearance, it will tend to be collected by the flight, forming a 'melt pool', usually on the leading flight face, as described in Chapter 7. Viscous heating in the molten film may tend to raise its temperature above that of the barrel, reducing thermal conduction from the barrel and raising the mean temperature in the melt pool. Here, less intense viscous heating will also occur, but will tend to be dissipated by conduction to the exposed barrel and screw surfaces and also through the interface to the solid bed. Temperature differences within the melt pool will be minimized by transverse circulation (Fig. 6.7) but at the point of solid bed break-up the mean temperature of the melt may be appreciably above that of the freshly-melted material and of the remaining solid particles. When the melting process reaches this state of solid bed break-up, softened particles become suspended in the melt. It is a matter of common experience that uniform melting of powder in a single-screw extruder is often more difficult than with the same polymer in granule form; the author has found at high screw speeds a stream of unmolten powder particles sheathed with a coating of molten polypropylene in conditions in which the same polymer in granule form gave a satisfactorily melted output. For this reason the melting section of powder-fed extruders is often extended by four to eight diameters to allow for slower melting. The mechanism giving rather slow elimination of these heat-softened but still comparatively rigid particles is mainly conduction from the melt; this will occupy considerable time and may be incomplete when the polymer reaches the die, especially when high screw speeds extend the melting length and reduce the length for melt pumping. Even in the absence of such particles, the polymer leaving the melting zone is likely to be non-uniform in temperature.

A relatively low barrel temperature in the melting section may be expected to suppress formation of the molten film near the barrel surface and enforce shearing within the solid bed, increasing mechanical work input and reducing heater input. The latter is confirmed by experience, which also shows output is not necessarily affected and final melt temperature may increase. In some cases it appears to improve temperature uniformity in the final melt and increase the

limiting speed at which unmolten particles appear at the die. This emphasizes the importance of correct setting and accurate control of barrel temperatures in the melting section.

The effect of screw temperature in the melting section has not been determined, but would be expected to affect the forward velocity of the solid bed and possibly the position at which the bed breaks up; especially with low barrel temperatures, screw cooling in this section only (to avoid disturbing the melt pumping section) might be expected to improve melting by delaying both solid bed movement and break-up.

Within the melt pumping zone, internal shear heating will be non-uniform, as shown in section 8.4, and heat conducted from the barrel will tend to produce higher temperatures in the melt near the barrel surface. As shown in section 8.4, transverse circulation tends to reduce these temperature differences, though downchannel velocity differences (Fig. 6.6) ensure that this does not occur in a transverse plane and thus does not give lateral temperature uniformity. This circulation is a laminar flow (Fig. 6.7) so there is a tendency to form an unmixed central core which has a significant down-channel velocity (Figs 6.6(c) and 6.6(d)) but a different temperature from the outer layers at the end of the screw. The experiments of Barnett *et al.* (1966) show these temperature differences decreasing from a maximum towards the die, but also that at high screw speeds significant temperature variations may persist at the die – these will be discussed further in section 11.1 – and it has been suggested that elimination of these is a main function of the 'metering' section of the screw. Generally such temperature differences are undesirable in their direct effect on flow in the die and in differential cooling of the product and indirectly through melt elasticity and recovery on post-extrusion operations involving die swell, drawdown, film blowing, parison sag, etc. It may be argued that the effect of non-uniform shear heating and barrel conduction will be minimized by small pressure gradients (Figs 6.6(c) or 6.6(d)) and small axial temperature differences in the barrel near the end of the melt pumping section; the former implies a tapered screw at modest die pressure (Fig. 6.11) and the latter a stepped set temperature profile (3 in Fig. 9.6).

9.1.4 Energy transfer

Generation and transfer of energy are closely related to temperature changes; imbalance in the former appears as a change in sensible heat (internal energy) and temperature, while the latter affects viscosity and energy generated by shearing.

The primary energy sources are the drive motor and the barrel heaters which provide useful internal energy and pressure energy to the polymer fed to the die and incidentally heat losses to the surroundings. The balance between these and the effects on it of changes in operating conditions have been discussed in section 8.5. The balance between mechanical work and thermal energy within

each section of the extruder depends primarily on local conditions of shear rate and temperature. Little energy is absorbed in conveying the uncompacted polymer from the feed opening, but significant mechanical energy is utilized in compacting the polymer, conveying the solid plug against shear forces on the barrel and screw surfaces and raising pressure within the plug. The low thermal conductivity of the polymer will ensure that heating due to these shear forces will be concentrated near the surfaces, reducing local stresses and energy input, and will be critically dependent on the temperatures of the metal surfaces. When the surface temperature reaches the polymer melting point and the delay zone commences, the film of melt and solid plug will be subjected to a common shear stress, but the much lower viscosity of the film will result in a higher shear rate, so that shear heating (equation (3.57)) will be concentrated in the film, assisted by heat conducted from the metal surface. For the same reason energy dissipation in the melting zone proper will be concentrated at the barrel surface and possibly the screw surfaces, with the solid bed being heated mainly by conduction. Shear heating will also occur in the melt pool, though at a lower rate than in the melt film. In both cases barrel temperature will play an ambiguous role in overall energy transfer in that an increase in temperature will increase conducted heat but decrease shear heating. Because of this, the temperature set on the barrel heater controllers may be regarded more as an adjustment of energy input to the polymer, since the former bears only an indirect relation to the polymer temperature.

As mentioned in section 9.1.3, in the melt pumping section barrel heating will tend to raise the polymer temperature, but non-uniformly. However, it will reduce shear energy, especially over the flight tip. The gross mechanical power input will be reduced by increase of temperature through barrel heating, while increased back pressure (equation (8.7)) increases the specific power input, mainly by decreasing output, and hence forms a second means of control of final melt temperature and the balance between mechanical and heater energy inputs.

Barrel cooling is considered separately from heating since its effects are not simply negative; it produces a reversed temperature gradient through the channel depth, but the lowest temperature and highest viscosity now occur in the region of highest shear rate, tending to modify the latter. In pressure (capillary) flow, boundary cooling decreases wall shear rate (Fig. 4.1), and accentuates the velocity profile, which here occurs asymmetrically (Fig. 9.3(a)), regarding the screw as thermally neutral. The drag flow will also be distorted by cooling (Fig. 9.3(b)), so although superposition of flows is no longer strictly valid, the resultant profile (Fig. 9.3(c)) will be distorted from the isothermal condition. Since velocity at the barrel remains constant and viscosity increases, the power dissipated in the channel (equation (8.7)) must increase, as commonly observed. The effect of barrel cooling on power absorbed in the flight clearance (equation (8.8)) will be much greater, so that both total power and the proportion from the flight clearance will increase,

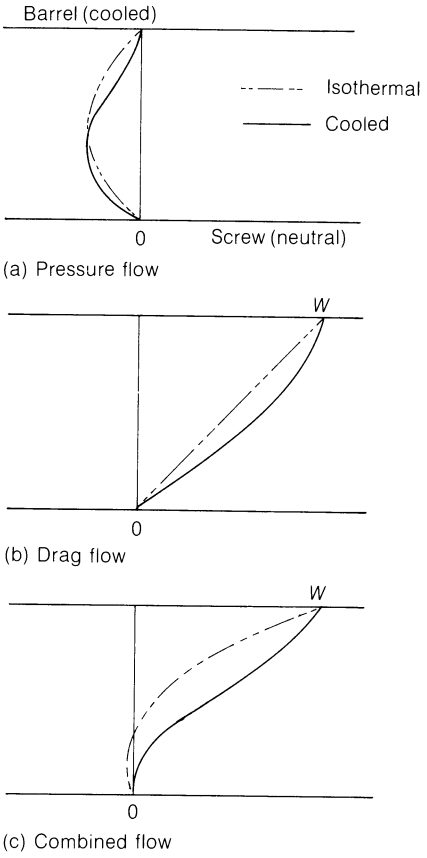


Figure 9.3 Velocity profile with cooled barrel.

tending to increase the melt temperature. In the limit, barrel cooling will freeze a layer of polymer and stall the motor, but if heat removal is inadequate, cooling will increase mechanical power but also increase bulk mean temperature and probably increase spatial variation of temperature. In large machines, the greater channel depth permits greater temperature differences and also the surface area for cooling is limited in comparison with the heat and mass flows. The author recalls a large hot-fed extruder in which barrel cooling dramatically increased the mechanical power input, but the final melt temperature tended to rise rather than fall.

Screw cooling depends on quite different factors from barrel cooling. Its possible use in feeding and melting sections has been mentioned on pp.20 and 278. Due to low thermal conductivity of the melt and low relative velocities near the screw root (Figs 6.6 and 6.7), screw cooling in the melt pumping section has little direct effect on conditions near the barrel wall and so on power

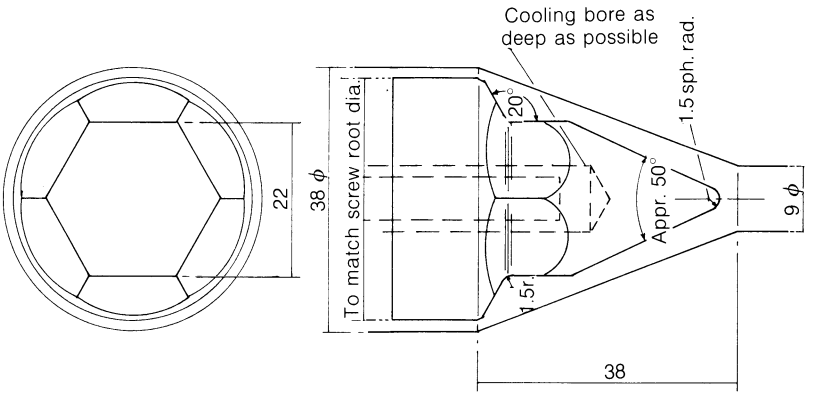


Figure 9.4 Experimental screw nose.

input. A small degree of screw cooling, preferably directed to the extreme tip of the screw, is frequently used with heat-sensitive polymers such as UPVC to reduce the temperature of the screw tip and hence the build-up of degraded polymer at this point.* Larger flows of air or water or lower inlet temperatures produce significant reductions in output with frequently some increase in mechanical power input and melt temperature – similar effects to those of reducing channel depth at constant screw speed (Fig. 8.8). The effect in the melt pumping section of screw cooling indeed appears to be mainly that of reducing channel depth and is conventionally used for this purpose when the available screw is too deep. However, this is not always immediately reversible; the author made a momentary application of water cooling to the screw of a 50 mm extruder running on UPVC, but 8 h after removing cooling, output and power had not returned to the values before applying cooling. For this reason, and because of the sensitivity of operation to changes in channel depth (pp. 143, 253 and Fig. 8.8), screw cooling must be gradually applied and accurately controlled for flow rate and temperature.

9.1.5 Mixing

Mixing is associated with the mechanisms of flow and energy transfer and has been included under these headings. Here it is only necessary to summarize the main features. Little mixing occurs while the polymer is solid; indeed the avoidance of segregation is probably the chief concern. The mechanism of melting leads to a degree of end-to-end mixing as well as transverse mixing in the molten portion. The unmolten material is only mixed as it is incorporated in the melt, and thus the last portion, which eventually breaks up into

*The author has found in extended running a tendency to form a discoloured 'pipe' down the centre of the extrusion; in addition to cooling the screw tip, a pointed screw nose (Fig. 9.4) with radiused spanner flats minimized the fault.

semi-molten particles, undergoes least mixing in this section and has least time for subsequent mixing. Until these semi-molten particles melt, they cannot mix into the bulk and remain a source of thermal inhomogeneity; however, despite mixing in the melt due to both transverse circulation and longitudinal back mixing due to pressure, non-uniform temperature is frequently encountered at the end of the screw. At least four sources of inhomogeneity can be listed, though their relative importance is difficult to quantify and will change with operating conditions. These include:

(i) lack of radial mixing in the channel – the transverse circulation in Fig. 6.7 tends to be laminar, with an almost static 'core', although the latter has a longitudinal velocity (except at $Q = 0$);
(ii) non-uniform shear heating in the channel, as discussed in sections 9.1.4 and 8.4, leading to non-uniform temperature increases;
(iii) barrel heating or cooling, producing temperature gradients between barrel and screw root;
(iv) incomplete mixing in the channel of polymer undergoing drastic shearing and heating in the flight clearance.

Mixing in the melting section will assist uniformity of composition (additives, etc.), and distributive mixing continues in the screw channel in the melt pumping section, though with the limitation in (i) above. Shear stresses high enough for significant dispersive mixing occur only in the flight clearance, they apply only to a small proportion of the total flow, and non-uniformly within that proportion. Back pressure improves distributive mixing both by changing the longitudinal velocity distribution (Fig. 6.6) and by increasing mean residence time through reduced output.

The scale of longitudinal mixing is necessarily limited by the volume of material present in the screw. Within this limit, it might be argued that the highest degree of mixing would occur when one portion moved downchannel with velocity W while another remained stationary in both x and z directions. However, the latter would then have an infinite residence time, detrimental to polymers of limited thermal stability, so a compromise is necessary, especially to ensure that the layer with zero transverse velocity (Fig. 6.7) has a finite downchannel velocity (Fig. 6.6(b) or 6.6(c)), which coincides with useful output.

9.2 EFFECTS OF CONTROLLED VARIABLES

The foregoing description of the simultaneous mechanisms in the extruder gives the qualitative background against which operating strategies and decisions must be made. The extruder operator is usually faced with the problem of operating an existing set-up, including extruder, screw, drive motor and gearing, heating/cooling system, control systems and die to make a

saleable product or intermediate of sufficient quality and uniformity at maximum output and efficiency. Only when this is impossible, or only possible at uneconomic output, can changes in the machine be considered, though since the latter are expensive in terms of cash and loss of production, it is as well to know what changes are required and what they can achieve. Frequently, the set-up, or some part of it, was designed for a different polymer, product or output rate and compromises must be made, at least until new equipment can be obtained or justified by the market.

The machine variables under the operator's control are usually screw speed, back pressure, heater temperature and temperature profile. The general effects of these will first be summarized, together with those of melt temperature, polymer properties and screw profile, which are important, though not usually under direct control. In making any such summary, it is important to define the conditions, and in this case it will be that generally independent variables other than that under consideration are held constant. Here the die geometry will be regarded as fixed, so that back pressure (except where stated otherwise) becomes a variable dependent on output and melt temperature, and with a constant controlled (heater) temperature profile, energy balance and melt temperature become dependent variables.

9.2.1 Screw speed

It is shown in section 6.5 that for a fixed die, the output of an isothermal. Newtonian fluid is directly proportional to screw speed (equation (6.59)) and that for a pseudoplastic polymer it is approximately proportional (p. 153). Thus at any point in the screw the dimensionless flow rate Q/Wbh is approximately constant. Equation (8.9) shows that for a Newtonian fluid at constant Q/Wbh, mechanical power in both channel and flight clearance increases in proportion to the square of speed (equation (8.15)), whereas for a pseudoplastic it increases in proportion to an index of speed between 1 and 2 ($n + 1$ for a power-law fluid, where $0 < n < 1$; see equation (8.16)). Consequently, the mechanical power input per unit volume output, which equals the shear heating per unit volume, is proportional to speed N for Newtonian and N^n for pseudoplastic fluids (Table 8.3). At constant temperature, Fig. 8.12 shows that as a consequence the energy required from the heaters first increases and then decreases with increasing speed, before ultimately going negative (cooling). If at any point heating or cooling is inadequate to maintain set temperature, then final melt temperature will fall or rise accordingly. As screw speed increases, the melting section will occupy a greater length of the screw so that the effective melt point and start of pressure rise will move forward. This reduces melt length, Z so that B in equation (6.52) must increase, Q_{Tot} in equation (6.58) will decrease and P must decrease (equation (6.53)) compared with these factors for the original melt length, i.e. the previous statement (equation (6.59)) must be modified so that output and pressure increase, but

somewhat less than the increase in speed. In practice, this effect is usually small and depends on the screw profile and on where the melt point occurs – Fig. 6.11 shows that in a tapered screw, the first portion of the melt length usually contributes a comparatively small proportion of the total pressure. A more important effect is that the distance is reduced for melting the particles remaining after the solid bed breaks up. This, together with a shorter residence time in the melt pumping section for mixing (for composition and temperature) results in greater temperature variations and poorer mixing at the die. The more common limits on speed increase are: (i) restriction of solid feed – in the hopper or conveying section of screw: (ii) unmolten polymer at the die; (iii) excessive temperature variation at the die; (iv) inadequate mixing for composition at the die; (v) inadequate cooling to maintain melt temperature or excessive rise of melt temperature; and (vi) inadequate motor power.

9.2.2 Back pressure

This may be increased by increasing the land length of the die lips, partially closing a restrictor bar or ring before the die lips or inserting additional screens or breaker plate. Here the conditions are assumed to be constant speed and set temperatures. Equations (6.15), (6.20), (B.31), (B.37) and (B.38) show that for all common types of screw, increasing pressure will decrease output. This is also shown from A to C in Fig. 6.18, but note that the pressure drop through the die decreases from A to A', so that the pressure restriction must raise the pressure on the screw from A' to C. The mechanical power absorbed in the channel increases with increase of pressure (decrease in Q/Wbh) according to equation (8.7), though the effect seems small in practice, but the decrease in output means that the specific power E/Q increases significantly and temperatures tend to rise (equation (8.29)). The power consumed in the flight clearance is nominally unchanged (equation (8.8)). The wall shear rate increases (equation (6.69)) and longitudinal mixing is increased (Figs 6.6(b) and 6.6(c)), but transverse flow is nominally unchanged (equation (6.24)). There is more time for melting because of the reduced output; and experience shows melting to be more complete, although temperature variations at the die may increase, possibly due to increasing non-uniformity in the radial distribution of shear heating (section 8.4). Incidentally, increase of back pressure increases the load on the thrust bearing ($\pi D^2 P/4$).

9.2.3 Heater temperature

Raising the set temperatures on the barrel heaters will of course tend to increase the heater energy to the polymer and also the heat losses. By reducing the viscosity near the barrel, it will also decrease the mechanical power input in the channel, and to a greater extent in the flight clearance. This leads to a change in the energy balance in the melt pumping section (to the right in

Fig. 8.10) and a higher final melt temperature. The higher temperatures in screw and die will give lower pressures, but assuming the temperature coefficients of viscosity are similar at the different shear rates in screw and die, the output will be little changed since, if suffixes 1 and 2 refer to screw and die, for the die

$$Q_{\text{Tot}} = \frac{KP}{\eta_2} \tag{6.53}$$

and for pressure flow

$$Q_{\text{P}} = \frac{BP}{\eta_1} \tag{6.50}$$

and

$$B = \frac{bh^3}{12Z} \tag{6.52}$$

At higher temperature (Q', P', η', etc.)

$$\eta_2' = C\eta_2 \tag{9.3}$$

and

$$\eta_1' = C\eta_1 \tag{9.4}$$

Then

$$Q'_{\text{Tot}} = \frac{KP'}{\eta_2'} = \frac{KP'}{C\eta_2} \tag{9.5}$$

and

$$Q'_{\text{P}} = \frac{BP'}{\eta_1'} = \frac{BP'}{C\eta_1} \tag{9.6}$$

By rearrangement of equation (6.15):

$$Q_{\text{D}} = Q_{\text{Tot}} + Q_{\text{P}} \tag{9.7}$$

$$Q'_{\text{D}} = Q'_{\text{Tot}} + Q'_{\text{P}} \tag{9.8}$$

Substituting equations (6.53) and (6.50) in (9.7) and equations (9.5) and (9.6) in (9.8):

$$Q_{\text{D}} = \frac{KP}{\eta_2} + \frac{BP}{\eta_1} \tag{9.9}$$

$$Q'_{\text{D}} = \frac{1}{C}\left(\frac{KP'}{\eta_2} + \frac{BP'}{\eta_1}\right) \tag{9.10}$$

But from equation (6.9), and independent of temperature:

$$Q'_{\text{D}} = \frac{Wbh}{2} = Q_{\text{D}} \tag{9.11}$$

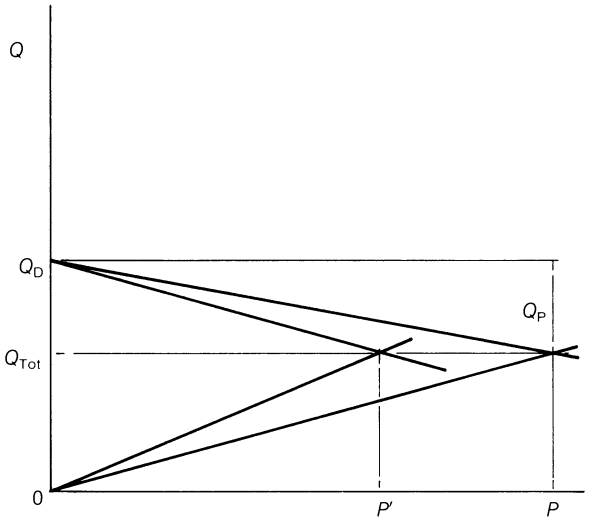


Figure 9.5 Output and pressure vs temperature.

therefore

$$\frac{P'}{C}\left(\frac{K}{\eta_2}+\frac{B}{\eta_1}\right)=P\left(\frac{K}{\eta_2}+\frac{B}{\eta_1}\right)$$

or

$$\frac{P'}{C}=P \tag{9.12}$$

Then from equations (9.5) and (9.6):

$$Q'_{\mathrm{Tot}}=\frac{KP}{\eta_2}=Q_{\mathrm{Tot}} \tag{9.13}$$

$$Q'_{\mathrm{P}}=\frac{BP}{\eta_1}=Q_{\mathrm{P}} \tag{9.14}$$

This is represented graphically in Fig. 9.5. From equation (9.13):

$$\frac{Q'_{\mathrm{Tot}}}{Wbh}=\frac{Q_{\mathrm{Tot}}}{Wbh} \tag{9.15}$$

and since Q/Wbh is constant, the bracketed term in equation (8.7) is constant, and the channel power is also decreased only by the change in viscosity, i.e. by the factor C in equation (9.4). If the viscosity in the flight clearance changes by the same factor C, i.e. the temperature coefficient of viscosity is independent of shear rate, the total power given by equation (8.9) also changes by factor C. Constant Q/Wbh (equation (9.15)) also implies that the longitudinal velocity profile (Fig. 6.6) is constant, giving similar mixing, but the increase in the proportion of the total energy which comes from the heaters is likely to create

additional radial temperature gradients, leading to greater variations in final melt temperature.

Additional heating in the melting section may promote faster melting, but may also lead to earlier break-up of the solid bed and hence poorer temperature uniformity of the melt, so that, as discussed on p.278, temperature control in this section is of great importance. Barrel and screw cooling have been discussed previously on pp. 279–81.

9.2.4 Temperature profile

This refers to the intentional variation of set temperatures along the barrel, for which it is difficult to give general rules since it depends on the screw profile and polymer, and on the rate of melting relative to the length of screw and especially to the level and uniformity required of final melt temperature. If the first heating zone temperature is too high, it may cause slippage in the solids feeding section; if it is too low it will delay melting and may cause problems due to entrained air in the feed. However, the latter is sometimes used to reduce the effective length of the screw and limit power input. As remarked earlier, this set temperature is more closely related to the heater power input than to the polymer temperature in this zone. One policy (profile 1 in Fig. 9.6) is to set the temperature as high as possible without affecting feeding; this will tend to promote rapid melting and heating of the polymer before the melt pumping section and will minimize the mechanical power input for a given screw design and speed. However, this leads to conductive rather than internal shear heating and may tend to give early break-up of the solid bed and large temperature fluctuations at that point. This profile is thus possibly worthwhile with high melting point polymers such as nylon 66 and PETP which are difficult to shear in solid form and which usually use screws with a long parallel or slightly tapered section, said to allow for adequate heating. It is also a possible strategy where motor power is limited or maximum melting rate is required, but melt temperature variation is not critical, or where screw length is barely sufficient for the required output.

A common strategy is to use a uniform gradient of *set* temperatures in the melting section (profile 2); this is likely to lead to a slower initial melting rate but raise the temperature of the polymer at the end near to that required in the melt pumping section. However, it may also lead to early break-up of the solid bed.

A third policy (profile 3) is to maintain as low a temperature as motor power, screw strength, etc., allow, but sufficient to allow melting, which may now require an undesirably large part of the screw length, but delay solid bed break-up and give more uniform heating of the polymer in this section, so that when break-up occurs the temperature is fairly low but uniform, and less time is required for melting the remaining solid particles. This may be the ideal for low and uniform final melt temperature, but impractical for higher temperatures in view of limited length of screw.

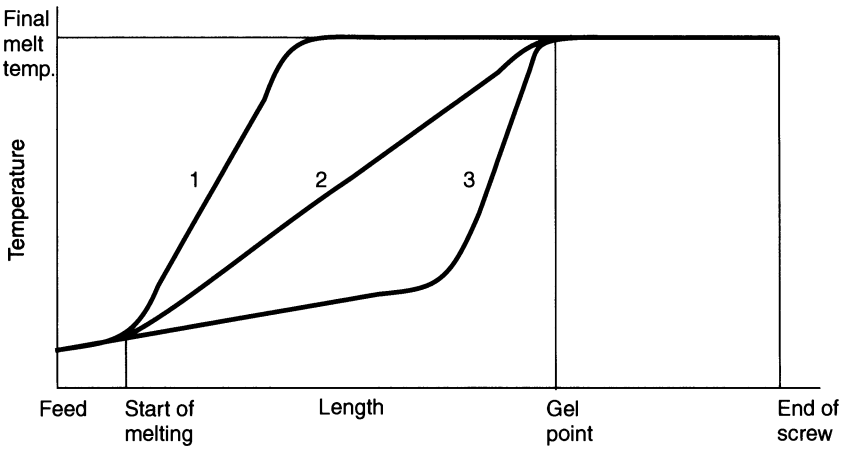


Figure 9.6 Idealized barrel set temperature profiles.

It is generally agreed that in the melt pumping section the melt temperature should be raised as quickly as possible to the final value required and then be held constant to enable variations in temperature to be minimized or eliminated, so a constant set temperature profile is usually employed in this section. This may seem to favour the 'ramp' profile 2 in the melting section since a step change in barrel temperature is impractical; a compromise between profiles 2 and 3 is probably preferable, bearing in mind that the position of the melt point is usually unknown and changes with screw speed.

9.2.5 Melt temperature

Although this is strictly a dependent variable, largely determined physically by heating and temperature profile, its value must be correct for the polymer and downstream processes of shaping, drawing, quenching, etc., so it is often a matter of adjusting temperature profile to give the desired melt temperature. The effects of an increase in melt temperature on other factors are similar, e.g. lower pressure in screw and die with similar output, lower mechanical power input but greater heater input (Fig. 8.10), and possibly less mixing and poorer temperature uniformity; this assumes a constant screw design and speed.

9.3 POLYMER PROPERTIES

The most important property in the context of extrusion is the melt viscosity, which depends on polymer type and molecular weight, as well as on temperature and shear rate. Operating temperatures are usually adjusted to give melt viscosities in a range of about 100–1000 N s m^{-2} at low shear rates;

however, limits for thermal degradation give viscosities near the upper value for UPVC, while extrusion grades of nylon 66 have viscosities nearer the lower value. The temperature, and hence viscosity, will also depend on the fabrication and downstream processes as indicated in Chapter 2, and which may be determined more by other properties such as melt elasticity. For a given polymer and temperature, viscosity increases with molecular weight and is approximately inversely proportional to Melt Flow Rate (BS2782 (1970), Method 720A), since the latter represents mass flow rate at a given pressure drop (compare equation (6.53)). Melt viscosity decreases with increase of temperature, as characterized by a temperature coefficient of viscosity (equations (3.8)–(3.10)), though in practice this varies with temperature and shear rate.

The general level of viscosity, whether resulting from polymer molecular weight or working temperature, is shown in Fig. 9.5 to have little effect on flow rate, but an increase in viscosity causes a proportionate increase in pressure. Equations (8.11) and (8.12) show that it also gives a proportionate increase in both channel and flight power, which Fig. 8.10 shows results in a change in the energy balance, reducing the external heating required. In extreme cases this may require an increase in channel depth and/or reduction in screw speed to maintain control of melt temperature or avoid overload of the drive motor, with other consequent effects. High melt viscosity at low shear rates will make vapour and volatile removal more difficult (section 6.5).

The variation of viscosity with shear rate, characterized by the pseudo-plasticity index n (equation (3.7)), is important both in giving the relation between viscosity in the screw channel (low shear rate) and die (high shear rate) (p. 153) and that in the flight clearance (equations (8.11)) and (8.12)). The former relation affects the depth and length of melt pumping section necessary to generate pressure before the die corresponding to the chosen flow rate and the latter influences the proportion of the total power which is absorbed over the flight clearance. The temperature determining the effective viscosity in the flight clearance is discussed in sections 8.4 and C.5. Pseudoplastic behaviour of the polymer melt also influences the effect of screw speed – flow is discussed in section 6.7 and power and energy balance in sections 8.3 and 8.5 (especially Fig. 8.12). The main influences are twofold. First, output will remain approximately proportional to screw speed but pressure will increase less rapidly with speed than for a Newtonian fluid with the same screw/die combination. Second, mechanical power input will be more nearly linear with speed (proportional to N^2 for Newtonian) and so the change in external heating/cooling will be more gradual, making control of melt temperature more certain. Polymers including the nylons and PETP have values of $0.8 < n < 0.9$, i.e. they are nearly Newtonian, predicting a rapid change of energy balance with screw speed. However, low melt viscosities at working temperatures mean that power input in the melt pumping section is in any case low, so the effect of screw speed may not be evident. Polyacetal and unplasticized PVC have values

of $0.4 < n < 0.5$ while polyolefines and polystyrene have values of $0.2 < n < 0.5$. It is commonly observed with these latter polymers that while output increases approximately in proportion to screw speed, increase of pressure is noticeably slower. It is also possible to operate over a wide range of speeds with little change of energy balance, as predicted in Fig. 8.18 for certain melt temperatures, although, as mentioned above, the high viscosity of UPVC results in that range being at low absolute values of speed. Non-Newtonian behaviour is also a function of molecular weight distribution, a broader distribution generally giving a lower value of n, but a smaller dependence on temperature (Brydson, 1981). A less obvious effect is that highly non-Newtonian flow in the die will tend towards plug flow (Fig. 4.1) while the velocity distribution in the screw at low values of Q/Wbh will be more severe than in Fig. 6.6(b), with higher shear rates at the barrel wall. Thus flow in die and screw, and mechanical power input in the latter, may be expected to be even more sensitive to barrel temperature and heat flows (section 8.4).

The softening or crystalline melting temperature is mainly dependent on the polymer type, differing little with molecular weight in the commercial range (Table A.1). A high melting point tends to require a long length of melting section in the screw and a high heater power, but in the case of nylon 66 and PETP melt viscosities are fairly low at temperatures little above the melting point, so substantial heating after melting is rarely required. Another factor is the high rigidity of these two polymers in their solid form, which means that they are less easily heated by internal shearing before melting; this is given as a reason for the common use of stepped screws with long first sections of constant or near-constant depth rather than because of their high melting points. The low viscosities then require rather shallow melt pumping sections in the screw if substantial die pressures are required, e.g. for film or fibre extrusion. A low melting or softening temperature restricts both the amount of, and need for, preheating (see p. 276) which may be carried out for other purposes such as polymer drying. At the downstream end of the process it requires lower coolant temperatures to ensure sufficient rigidity of the product to avoid distortion of the section or post-drawing or to suppress crystallization, e.g. when orientation is to follow. Especially when the viscosity changes fairly slowly with temperature, a low melting temperature may allow the use of a wide range of final melt temperature, according to process, and consequent wide range of temperature rise required in the melt pumping section, with its implications for energy balance and temperature uniformity. On the other hand, a rapid change of viscosity with temperature, i.e. a high temperature coefficient as with PMMA, entails rapid changes of mechanical power input and energy balance and hence the need for more accurate temperature control and possibly a restriction on the range of other variables such as screw speed and screw design.

The differences in specific heat of various polymers lead to differences in energy requirements for a given increase in working temperature and also for

heat removal in product cooling. Specific heats vary little with temperature in the melt and within a given type of polymer (Fig. A.3), so effects are only likely to be apparent at high melt temperatures, where viscosity is low and external heating dominates.

Reliable data on thermal conductivity in the melt are scarce, and Figs A.4 and A.5 show the variation in published figures. The values at room temperature (Table A.1) are little guide to the melt. A low themal conductivity would be expected to lead to large transverse variations in melt temperature and their slow elimination along the length of the melt pumping section.

Elastic effects, especially die swell (recoverable strain) and melt fracture have been discussed in Chapter 5 and are vital to product quality (pp. 353 and 354). They are dependent on temperature and shear (or extensional) stress as well as polymer type. However, within the screw they are only likely to be apparent in unsteady conditions, e.g. during rapid speed changes or in the flow into and out of the flight clearance (p. 248).

9.4 SCREW DESIGN

Other factors being constant, residence time in the screw is proportional to its effective length and inversely proportional to speed (output). Thus factors dependent on residence time such as melting, heating between melting and final temperatures, distributive mixing and reduction of solid particles and temperature variations in the melt pumping section will all be similarly influenced, and a longer screw will tend to offset limitations occurring with increased speed. A longer melt pumping section permits higher pressures at the same output or a deeper screw (and higher output) with similar response to pressure and pressure changes. A short screw will show limitations in situations requiring high output, high temperature, high pressure, but small change in output, etc., with pressure, also for uniform mixing or uniform melt temperature; operating changes tending to improve one factor will probably cause deterioration in at least one other (see Tables 9.2–9.9).

The author would regard a total length of 15 diameters as a minimum for thermoplastics, although $12D$ is used for cold-fed rubbers, and $20D$ is normal. If high speeds, high pressures or high melt temperatures or very stable output and uniform temperature are required, then $24D$ or even $28D$ would be recommended. If venting is required, an additional $6D$ or preferably $8D$ should be provided; a vented screw of less than $28D$ total length would almost certainly be limited in one of the foregoing aspects, especially if the first section is working against zero back pressure. These lengths are only rules of thumb regarding the limits within which it is suggested the operator should work with an existing machine; for design it would be preferable to determine the total length by summing the lengths required for feeding, melting and pumping/mixing. It must be remembered that a longer screw will generally absorb more

power, so a limit is placed by torsional strength at the feed end. Where low melt temperatures are required, these also set limits to practicable length, which are likely to be different for various polymer types. For example, UPVC at low outputs may require a screw of $15D$ or even less, whereas nylon 66 at high output may require a minimum of $24D$ screw length. A screw $24D$ in length would almost certainly entail high mechanical power input and excessive melt temperatures with highly viscous melts such as UPVC and raw natural rubber; reducing the effective length by using low temperatures at the feed end to delay melting may cause air entrapment (see p. 272).

Compression ratio is a term commonly used and may be significant in the melting process – see Chapter 7. For this discussion a better basis of comparison is channel depth in the melt pumping section. As shown by equation (6.9), a shallow screw will have a low drag flow rate, but equation (6.13) shows that the pressure flow is also small, being proportional to h^3, and, as shown in Fig. 6.16, at high die pressures may have a greater output than a deeper screw at the same speed. Figure 6.16 also shows that the output changes much less with a change in pressure than in a deeper screw, and in this sense the shallow screw will tend to be more stable. Appendix B.4 compares pressure gradients in the two sections of a stepped screw, i.e. where speed and output are equal. On this basis (point A in Fig. 6.16) it is shown that, except when Q/Wbh_2 is close to 0.5, i.e. the pressures are low, the pressure gradient in a shallow screw is always greater than in a deep screw, so that a given die pressure may be reached in a shorter melt pumping section. However, at a given output, when h is reduced, Q/Wbh is increased so that the velocity distribution resembles Fig. 6.6(c) rather than Fig. 6.6(b), indicating a reduction in longitudinal mixing; on the other hand, the smaller depth will give smaller temperature differences due to a given external heat input but might be expected to give increase variations due to different rates of internal shear heating (section 8.4). The wall shear rate and mechanical power absorbed in the channel will increase due to a reduction in depth. This may be seen from Table 6.1 by comparing, at constant speed W and output Q, a screw of depth h_2 at say $Q/Wbh = 0.4$, when the wall shear rate is 1.60 times that at drag flow, with deeper screws of depths $h_1 = 2h_2$ $(Q/Wbh_1 = 0.2)$ and $h_1 = 4h_2$ $(Q/Wbh_1 = 0.1)$, when the Newtonian wall shear rates are 1.40 and 0.85, respectively. From equation (8.7) the power absorbed in the channel will change from $2\eta W^2bd\,z/h_2$ to 1.6 and 0.95 times the same factor, respectively. As a result, a shallower screw will give higher temperatures with a given heater input, or at fixed temperature the heater input will become smaller. As mentioned on p. 281, similar effects may often be obtained by screw cooling, which appears to reduce the effective depth of the melt pumping section. In the melting section, a reduction in depth will reduce the residence time and may well lead to a deficiency in melting rate; of course a reduction in feed section depth may lead to reduction in feed rate (Fig. 6.9). However, reduction in output rate from either of these causes is of less importance than the unstable operation which is likely because both the

mechanisms of solid feeding and of melting are more subject to random disturbance than melt pumping. So far the comparison has been made on the basis of identical output and pressure from shallow and deep screws. More frequently a shallow screw gives a lower output at the same screw speed (e.g. *A* and *B* in Fig. 6.18), or a higher speed is used to give the same output. In the case of a lower output, mechanical power input will be somewhat lower but will be absorbed in a smaller flow of polymer so that specific power input and temperature rise will be greater, less dependent on external heating, and mixing will be improved. The lower output will also tend to result in a more uniform final melt temperature. If output is restored by increasing screw speed, then the effects will combine to give a higher temperature or less heat input (i.e. approach the autogenous point in Figs 8.10 and 8.12). However, increase of speed will tend to increase temperature inhomogeneity and melting limitations may occur; the product uniformity may be either better or worse than with a deeper screw at lower speed.

The screw profile, i.e. the variation in depth along the length, is the subject of strongly held views, especially in respect to certain polymers and product types. It is often stated, for instance, that certain nylons will hardly extrude at all through taper or taper-parallel screws, while these are almost universally used for UPVC. It seems logical that polymers of low melt viscosity such as nylons and PETP are usually extruded with screws having shallow and comparatively long final sections for melt pumping, in order to achieve useful pressure gradients (equation (6.15)) and stability against pressure fluctuations. Usual applications for these polymers, e.g. film and fibres, require high pressures and stable outputs, again leading to long, shallow 'metering' sections. Polymers of high melt viscosity such as natural rubber and UPVC tend to be extruded with deeper and shorter melt pumping sections, which achieve sufficient pressure without excessive power input (proportional to dz in equation (8.9)) and temperature rise; the latter is important since these polymers are usually processed at temperatures near to the limit of thermal degradation in order to reduce their viscosities. Other polymers of limited thermal stability such as polypropylene and polyacetal (POM) also tend to be processed with deeper screws, but often of considerable 'metering' length. Evidently a deep feed section is desirable to avoid limitations from solid feeding, but, except with very large machines, feed depth is limited by torsional strength of the screw. To assist in feeding, many screws have a parallel section of 4 to 6 diameters (including the feed opening). The controversy therefore centres around a uniform taper or a parallel followed by a step, in the melting section. As stated earlier, the argument for the latter seems to be that as rigid solids, the polymers used with stepped screws are not readily sheared to assist melting and require a long time to reach their high melting points by conducted heat, leading to long parallel or near-parallel sections which are usually continuations of the feed section. It is claimed that the rapid decrease of channel depth ('step') in one turn or less acts as a barrier to forward flow of unmolten polymer and thereby 'fixes'

the gel point. As shown in Fig. 6.10, most of the pressure will be raised in the shallow section and considerable movement of the gel point (point of initial pressure rise) rearward will give little change in pressure (or output), tending to stable operation. The case for a uniform taper is less clearly stated though it arguably maintains the downchannel velocity of the unmolten portion of the melting bed (p. 184) and reduces stagnation which might form a hold-up point for degradation. It also means that matching of the screw profile to the actual point of pressure rise is less critical, so might be expected to perform more flexibly, in respect of both an initial mismatch and the changes which take place in operation, especially with increasing screw speed.

It is impossible to generalize further on screw dimensions, leaving aside special types for venting, compounding, etc. It may be useful to give some examples (Table 9.1) which have operated successfully; they are given in relation to a 90 mm diameter screw with a 15 mm deep feed section, though, as discussed in section 11.5, channel depths usually vary somewhat less than in direct proportion to screw diameter. The terms used refer to the geometric portions of the screws, not the functional sections for feed, melting and melt pumping used in the remainder of this book to describe regions of particular mechanisms.

Table 9.1 Examples of screw types (90 mm diameter, single start, pitch equal to diameter (helix angle 17.6°))

		Depth (mm)			*Length (diameters)*				
Purpose	*Polymer*	*Feed*	*Transition*[a]	*Meter*	*Feed*	*Transition*	*Meter*	*Total*	*Compression ratio*[b]
High-output compounding	LDPE	15	15–6.5T	6.5	6	12	6	24	2.1:1
General purpose	LDPE, HDPE, PS	15	15–5.5T	5.5	4	10	6	20	2.4:1
Film	LDPE	15	15–3.0S	3.0	10	11	9	20	4.3:1
High-output compounding	PP powder	–	15–7.9T	7.9	–	18	2	20	1.8:1
General purpose	PP	–	15–6.0T	6.0	–	16	–	16	2.2:1
General purpose	PP	–	12.7–5.6T	5.6	–	10.9	9.1	20	2.1:1
General purpose	POM	15	15–5.0T	5.0	4	12	4	20	2.7:1
General purpose	PMMA	15	15–4.0S	4.0	14	1	5	20	3.3:1
Compounding	Nylon 66	–	11.1–9.6T/S	2.8	–	$12+\frac{1}{2}$	7.5	20	3.6:1
Film	PET	15	15–3.0S	3.0	14	1	9	24	4.3:1
Film	UPVC	15	15–7.0T	7.0	4	12	4	20	1.9:1
Low-output compounding	UPVC	15	15–9.0T	9.0	4	7	4	15	1.5:1

[a] T = tapered; S = stepped.

[b] Cross-section basis.

Note: The screw lengths recommended on p.291 are generally greater than listed here, due to development in design and requirements since these screws were commissioned

Many special forms of screw, with barriers, double, interrupted or reversed flights or intermediate mixing sections, some of which are described in Chapter 7, are used either to improve the melting process or prevent flow of unmolten particles into the melt pumping section. Other special types aim to reduce the time or space variations of melt temperature at the end of the screw. The mechanisms are too varied, and in some cases undefined, to detail here; the following section may not be applicable, as it is intended as a guide to operation of conventional designs, for which the mechanisms are reasonably understood.

9.5 OPERATIONAL STRATEGIES

Section 9.1 has described the overall performance of the extruder in respect of flow, pressure, temperature, energy transfer and mixing; section (9.2) has examined the effects of changes in controlled variables of screw speed, back pressure, heater temperature, temperature profile and melt temperature. Sections 9.3 and 9.4 have considered the effects of polymer properties and screw design, respectively. This section takes the opposite view, in showing what operational changes may be made to achieve a desired objective, and what other consequences may follow, so that the operator may choose which alternative to apply, depending on other constraints of the individual situation. For clarity, this is given in tabular form (Tables 9.2–9.9). To avoid unnecessary reference back, the basic equations for flow and energy are reproduced here; Figs 6.18 and 8.10 are also relevant.

Flow in a channel of constant depth:

$$Q_{\text{Tot}} = \frac{Wbh}{2} - \frac{bh^3}{12\eta} \cdot \frac{P}{Z} \tag{6.20}$$

Mechanical power in channel only:

$$E_{\text{Ch}} = \frac{\eta W^2 b\, \mathrm{d}z}{h} \left[4(1 + \tan^2 \phi) - \frac{6Q}{Wbh}\right] \tag{8.7}$$

Mechanical power in channel and flight clearance:

$$E_{\text{dz}} = \frac{\eta W^2 b\, \mathrm{d}z}{h} \left[4(1 + \tan^2 \phi) - \frac{6Q}{Wbh}\right] + \frac{\eta W^2 t\, \mathrm{d}z}{\delta \cos \phi} \tag{8.9}$$

In Tables 9.2–9.9, some of the statements, especially on the effects of reduction in screw channel depth, may appear contradictory. At constant output and appreciable back pressure, the velocity distribution in the channel will change from Fig. 6.6(b) with a deep screw to Fig. 6.6(c) with a shallow screw, but with the vertical scale reduced so that wall shear rate and stress are increased (unless the situation of Fig. 6.6(e) obtains); however, the reverse-flow component

Table 9.2 Operational strategies: increased output required

Action	*Response*	*Reference*	*Limitations*
Increases speed (fixed die)	Output Q and pressure P increase approx. proportional to speed N	eqn. (6.59)	Feed restriction Maximum haul-off and cooling speeds
	Mechanical power increases approx. proportional to $N^{1.5}/N^2$	Fig. 8.12	Maximum motor power Maximum heater/cooling power
	Heater power increases/decreases	Fig. 8.12	Thermal degradation
	Melt temperature T_m rises (heaters constant)	p. 258	Unsatisfactory flow from die (e.g. drawing, blowing, quenching)
	Gel point moves towards die	pp. 219, 283 Fig. 7.27	
	Temperature variations increase	p. 284	Incomplete melting and surging
	Residence time (mixing) decreases	p. 283	Unstable flow and poor distribution in die Non-uniform composition and product properties
Increase 'metering' depth (fixed speed and die)	Q increases at low P only	Fig. 6.16	Feed restriction
	Greater fluctuation in Q if P changes	Fig. B.7	Product breaks in haul-off, especially with drawdown
	Mechanical power E decreases slightly	eqn. (8.11)	
	Melt temperature T_m may fall	Fig. 8.8	
	Gel point moves towards die	Fig. 7.29	Incomplete melting and surging
	Temperature variations may increase	p. 292	Unstable flow in die
	Residence time (mixing) increases but mixing uniformity may decrease	p. 293	Non-uniform product properties Non-uniform composition

Table 9.3 Operational strategies: increased pressure required

Action	*Response*	*Reference*	*Limitations*
Add screens to breaker plate (fixed die)	At constant speed, output Q from screw decreases, requiring higher speed N (as above) to restore Q and P in die.	Fig. 6.15	Output may be restored by increasing screw depth (Fig. 6.16)
	Mechanical power E increases	eqn. (8.9)	Maximum motor power
		Fig. 8.14	Maximum torsional strength of screw
		p. 235	
	Heater power H decreases	Analogous to Fig. 8.10	Heaters off (no cooling) Maximum cooling (if cooled)
	Melt temperature T_m rises (heaters constant)	eqn. (8.29)	Thermal degradation
		p. 284	Unsatisfactory flow from die
	More complete melting	p. 284	
	Temperature variations may increase	p. 284	
	Residence time (mixing) increases	p. 284	
	Mixing uniformity increases		

Table 9.4 Operational strategies: increased melt temperature required

Action	*Response*	*Reference*	*Limitations*
Increase barrel set temperatures	Output Q approx. constant	eqn. (9.13)	
	Pressure reduced (fixed speed and die)	Fig. 9.5	
	Mechanical power E decreased considerably	eqn. (8.9) p. 279 p. 284	
	Heater power H increased	Fig. 8.10	Maximum heater power
	Melt temperature T_m rises if E was previously small, e.g. deep, short screw	Fig. 8.10	As required – degradation, etc., will be anticipated
	Melt temperature falls if E was previously large, e.g. shallow screw, high pressure	p. 277 p. 287	*Contrary to requirement*
	Melting may be more complete, if output Q and mechanical power E are low	p. 287 p. 355	
	Melting may be less complete, if output Q and mechanical power E are high	p. 277 p. 287	Incomplete melting
	Temperature variations may increase/decrease, depending on melting	p. 287 p. 288 p. 354	If 'increase', unstable flow in die Non-uniform product properties
	Mixing decreases, especially dispersive, due to lower shear stresses and power	p. 288 p. 353	Non-uniform composition and product properties
Decrease set temperature in melting section *only*	Output Q and pressure P approx. constant (fixed die)	Fig. 7.28(a) p. 277	
	Mechanical power E increased considerably	p. 279 p. 287	Maximum motor power Maximum torsional strength of screw
	Heater power H decreased	p. 287	

(*Continued*)

	Melt temperature T_m rises if mechanical power E was previously high	p. 279	As required – may give shear degradation, e.g. dulling of pigments
	Melt temperature T_m falls if mechanical power E was previously low or if considerable heating took place after melting	p. 287	*Contrary to requirement*
	More complete melting – gel point may move towards feed	p. 287	
	Break-up of solid bed may be delayed	p. 287	
	Temperature variations may decrease	p. 277	
	due to more uniform temperature at	p. 287	
	start of melt pumping section, giving improved flow in die	p. 288	
	Mixing may increase due to longer time after melting, giving improved uniformity in product	p. 282	
Commence or increase screw cooling	Effective channel depth in pumping section is reduced	p. 281 p. 292	
	If pressure is low, output Q and pressure P will be decreased	A to B in Fig. 6.18	Uneconomic output
	If pressure is high, output Q and pressure P will increase slightly	C to D in Fig. 6.18	
	Mechanical power E increases slightly	p. 280 p. 281	
	Melt temperature T_m increases due to smaller Q	Fig. 8.9 p. 281 p. 293	As required
	Reduced effective depth may give more complete melting	Fig. 7.29	But see the equivalent case (p. 292)

(*Continued*)

Table 9.4 (*Continued*)

Action	*Response*	*Reference*	*Limitations*
	Temperature variations may increase due to greater difference in screw and barrel temperatures and shorter residence time	p. 292	But see equivalent case (p. 293) Unstable flow in die Non-uniform product properties
	Mixing may decrease due to longitudinal shear gradient, though radial mixing distance reduced	Fig. 9.2(c)	Compare with Fig. 9.2(a) and p. 292 Possible non-uniform composition
Increase screw length	Pressure gradient decreased, so output Q and pressure P increase (fixed die)	Fig. 6.18 p. 291	
	Mechanical power E in pumping section increased	eqn. (8.9)	Maximum motor power
	Losses S increased. Heater power may increase	Fig. 8.7	Maximum heater power
	Melt temperature T_m increased, especially if previously close to melting point	Fig. 8.7	As required – degradation, etc., will be anticipated
	Melting more complete if reduced pressure gradient allows length for melting to increase, despite greater output Q	p. 291	
	Melt temperature variations decrease due to more complete melting and greater pumping length for mixing	p. 291 p. 354	
	Mixing increases due to greater pumping length	p. 291	

Table 9.5 Operational strategies: reduced melt temperature required

Action	*Response*	*Reference*	*Limitations*
Reduce barrel set temperatures	Output Q approx. constant	eqn. (9.13)	
	Pressure P increased (fixed speed and die)	Fig. 9.5	Safe working pressure of barrel and die
	Mechanical power E increased considerably	eqn. (8.9) p. 279	Maximum motor power Torsional strength of screw
	Heater power H reduced	Fig. 8.10	
	Melt temperature T_m falls if E was previously small, e.g. deep, short screw	Fig. 8.10 p. 369	As required
	Melt temperature T_m *rises* if E was previously large, e.g. shallow screw, high pressure	p. 277 p. 369	*Contrary to requirement*
	Melting may be less complete if output Q and power E were previously low (mainly conducted heating)	p. 220 p. 220 p. 287	Incomplete melting
	Melting may be more complete if output Q and power E were previously high (mainly shear heating)	p. 287	
	Temperature variations may increase or decrease, depending on melting	p. 287 p. 287 p. 354	If increase, unstable flow in die Non-uniform product properties
	Mixing increases, especially dispersive, due to higher shear stresses and power	p. 288 p. 353	
Increase set temperatures in melting section *only*	Output Q and pressure P approx. constant (fixed die)	Fig. 9.5 p. 277	
	Mechanical power E decreased considerably	p. 277 p. 287	
	Heater power H increased	p. 277 p. 287	Maximum heater power

(*Continued*)

Table 9.5 (*Continued*)

Action	*Response*	*Reference*	*Limitations*
	Melt temperature T_m falls if mechanical power E was previously high	Fig. 8.10 p. 277 p. 369	As required
	Melt temperature T_m *rises* if mechanical power E was previously low	p. 369	*Contrary to requirement*
	Less complete melting – gel point may move towards die	p. 287	Incomplete melting
	Break-up of solid bed may be accelerated	p. 287	
	Temperature variations may increase due to less complete melting	p. 287	Unstable or non-uniform flow in die Non-uniform product properties
	Mixing may decrease due to shorter time after melting	p. 282	Non-uniform composition and product properties
Decrease screw length (melt pumping section)	Pressure gradient increased so output Q and pressure P decrease (fixed die)	Fig. 6.18 p. 291	Uneconomic output
	Mechanical power E (in pumping) decreased	eqn. (8.9)	
	Losses S decreased. Heater power H may decrease	Fig. 8.7	
	Melt temperature T_m decreased, especially if considerably above melting point	Fig. 8.7	As required Minimum processing temperature will be anticipated
	Melting less complete if higher pressure gradient tends to reduce length for melting, despite lower output Q	p. 291	Incomplete melting
	Melt temperature variations increase due to poorer melting and shorter pumping length	p. 291 p. 354	Unstable or non-uniform flow in die Non-uniform product properties

(*Continued*)

	Mixing decreases due to shorter pumping length	p. 291	Non-uniform composition and product properties
Increase channel depth in melt pumping section	At low pressures, output Q and pressure P will increase	B to A in Fig. 6.18	
	Mechanical power E in channel will decrease	eqn. (8.7)	
	Constant flight power becomes greater proportion of total power E	eqn. (8.9)	
	Melt temperature T_m decreases due to lower specific power E/Q	Fig. 8.8	As required Minimum processing temperature will be anticipated
	Melting may be less complete due to deeper channel and higher output	p. 292	Incomplete melting
	Temperature variations may increase due to greater output Q and greater channel depth h	p. 292	Unstable flow in die
	Mixing may increase or decrease depending on melting and effect of higher output	p. 293	Non-uniform composition

Table 9.6 Operational strategies: reduced mechanical power input required

Action	*Response*	*Reference*	*Limitations*
Reduce screw speed	Output Q and pressure P decrease approx. in proportion to speed N	eqn. (6.59)	Uneconomic output Minimum haul-off and drawdown speeds
	Mechanical power E decreases *more* than in proportion to speed, so also reduces torque, where this is limited by the drive	Fig. 8.12 eqn. (8.16)	As required
	Almost instantaneous effect		
	Melt temperature T_m decreases	p. 258 p. 283 p. 284	
	Melting more complete – longer residence time	p. 283	
	Mixing more complete – longer residence time	p. 284	
Increase set temperatures in melting section *only*	Output Q and pressure P approx. constant (fixed die)	Fig. 9.5 p. 277	
	Mechanical power E decreased considerably	p. 276 p. 277 p. 287	As required
	Heater power H increased	p. 284 p. 287	Maximum heater power
	Melt temperature falls if mechanical power E was previously high	p. 277 p. 369	Softening/melting point reached
	Melt temperature rises if mechanical power E was previously low	p. 369	Thermal degradation
	Less complete melting – gel point moves towards die	p. 287	Incomplete melting
	Break-up of solid bed may be accelerated	p. 287	
	Temperature variations may increase due to lower temperature at start of melt pumping section	p. 287 p. 287	Unstable or non-uniform flow in die Non-uniform product properties

(*Continued*)

	Mixing may decrease due to shorter time after melting	p. 282	Non-uniform composition and product properties
Increase *all* set temperatures	As above, but further decrease in power E and increase in melt temperature T_m due to melt pumping section	eqn. (8.9) Fig. 8.10	Thermal degradation
	Further heating in melt pumping section may lead to greater temperature variations	p. 287 p. 288	Non-uniform flow and product properties
Decrease screw length (melt pumping section)	Pressure gradient increased so output Q and pressure P decreased (fixed die)	Fig. 6.18 p. 291	Uneconomic output
	Mechanical power E (in pumping section) decreased	eqn. (8.9)	As required
	Losses S decreased. Heater power may decrease	Fig. 8.7	
	Melt temperature T_m decreased, especially if considerably above melting point	Fig. 8.7 p. 291	Softening/melting point of polymer reached
	Melting less complete if higher pressure gradient tends to reduce length for melting, despite lower output Q	p. 291	Incomplete melting
	Melt temperature variations increase due to poorer melting and shorter pumping length	p. 291 p. 354	Unstable or non-uniform flow in die Non-uniform product properties
	Mixing decreases due to shorter pumping length	p. 291	Non-uniform composition and product properties
Increase channel depth in melt pumping section	At low pressures, output Q and pressure P will increase	B to A in Fig. 6.18	
	Mechanical power E in channel will decrease	eqn. (8.7)	As required
	Constant flight power becomes greater proportion of total E	eqn. (8.9)	
	Heater power H increases	Fig. 8.8	Maximum heater power

(*Continued*)

Table 9.6 (*Continued*)

Action	*Response*	*Reference*	*Limitations*
	Melt temperature T_m decreases due to lower specific power E/Q	Fig. 8.9	Softening/melting point reached
	Melting may be less complete due to deeper channel and higher output Q	Fig. 7.29	Incomplete melting
	Temperature variations may increase due to greater output Q and greater channel depth h	p. 292 p. 292 p. 293	Unstable flow in die
	Mixing may increase or decrease depending on melting and effect of higher output	p. 293	If decrease, non-uniform composition
Reduce die restriction or remove screens	At constant speed, output Q increases with decrease in (total) back pressure	C to A in Fig. 6.18	Maximum haul-off and cooling speeds
	Mechanical power in channel E decreases with decrease of pressure (increase of (Q/Wbh) (melt pumping section only)	p. 284 eqn. (8.7) Fig. 8.14	As required. *NB*: Small effect in practice, perhaps due to reduction in T_m See also Table 8.5 (channel power) Total power may increase due to greater Q – *contrary to requirement*
	Heater power H increases	Table 8.5 Fig. 8.16	Table 8.5 assumes constant T_m Maximum heater power
	Melt temperature T_m reduced due to lower specific power E/Q	p. 284 eqn. (8.29) Fig. 8.15	Softening/melting point reached Viscosity rises, partially offsetting power reduction
	Melting may be less complete due to higher output Q	p. 284	Incomplete melting
	Temperature variations may increase due to greater output Q	p. 284	Unstable flow in die
	Mixing may increase or decrease depending on melting and effect of higher output	p. 284	Non-uniform composition

Table 9.7 Operational strategies: reduced melt temperature variations required

Action	*Response*	*Reference*	*Limitations*
Reduce screw speed N (fixed die)	Output Q and pressure P reduced approx. in proportion to speed N	eqn. (6.59)	Uneconomic output
	Mechanical power E reduces approx. proportional to $N^{1.5}/N^2$	Fig. 8.12 eqn. (8.16)	
	Heater power H increases/decreases depending on high/low speed	Fig. 8.12	Maximum heater power Maximum cooling or heaters off
	Melt temperature T_m falls (heaters constant)	p. 258	Softening/melting point reached
	Gel point moves towards feed	Fig. 7.27 p. 283	
	Melting more complete – longer time	p. 284	
	Temperature variations decrease	p. 284	As required
	Residence time for mixing increases	p. 284	
Reduce barrel set temperatures	Output Q approx. constant	eqn. (9.13)	
	Pressure P increased (fixed speed and die)	Fig. 9.5	Safe working pressure of barrel and die
	Mechanical power E increased considerably	eqn. (8.9)	Maximum motor power Torsional strength of screw
	Heater power H reduced	Fig. 8,10	
	Melt temperature T_m falls if E was previously small	Fig. 8.10 p. 277 p. 369	Softening/melting point reached
	Melt temperature T_m rises if E was previously large	p. 369	Effect on temperature variations (see below)
	Melting may be less complete if output Q and power E were previously low (mainly conducted heating)	p. 287	Incomplete melting
	Melting may be more complete if output Q and power E were previously high (mainly shear heating)	p. 277 p. 287 p. 287	

(*Continued*)

Table 9.7 (*Continued*)

Action	*Response*	*Reference*	*Limitations*
	Temperature variations may decrease if melting improves, and longer time in pumping section if temperature rise in latter is small, i.e. T_m low	p. 287 p. 354	As required
	Temperature variations may increase if melting deteriorates, and/or temperature rise in pumping section is large, i.e. T_m is high		*Contrary to requirement*
	Mixing may improve if T_m decreases, due to longer residence time and higher shear stress in pumping section	p. 282 p. 288 p. 353	
Increase back pressure by die restriction or adding screens (constant speed)	Output Q decreases and total pressure P increases	A to C in Fig. 6.18	Uneconomic output Safe working pressure of barrel
	Mechanical power in channel E increases	eqn. (8.7) Fig. 8.14	Maximum motor power
	Heater power H decreases	Analogous to Table 8.5	Table 8.5 assumes constant T_m
	Melt temperature T_m rises due to increased specific power E/Q (heaters constant)	eqn. (8.29) p. 284	Thermal degradation Unsatisfactory flow from die Effect on temperature variations (see below)
	More complete melting due to longer residence time and increased specific power	p. 284	
	Temperature variations may decrease due to improved melting and longer time in pumping section, if temperature rise in pumping section is small, i.e. T_m is low	p. 284	As required

(*Continued*)

	Temperature variations may increase if temperature rise in pumping section is large, i.e. T_m is large/increases		*Contrary to requirement*
	Mixing improves due to longer residence time in melt pumping section	Fig. 6.6 p. 284	
Increase screw length (melt pumping section)	Pressure gradient decreased so output Q and pressure P increase (fixed die)	Fig. 6.18 p. 291	
	Mechanical power E (in pumping) increased	eqn. (8.9)	Maximum motor power
	Losses S increased. Heater power H may increase	Fig. 8.7	Maximum heater power
	Melt temperature T_m increased especially if previously close to melting point	Fig. 8.7	Thermal degradation increased Effect on temperature variations (see below)
	Melting more complete if reduced pressure gradient allows length for melting to increase, despite greater output Q	p. 291	
	Melt temperature variations decrease due to more complete melting and greater pumping length for mixing, despite greater output Q	p. 291 p. 354	As required
	Mixing increases due to greater pumping length	p. 291	
Change depth of melt pumping section	At constant screw speed, output will usually increase with screw depth	Fig. 6.16 p. 292	
	Theoretically mechanical power E will decrease with increase of screw depth, but in practice changes appear small	eqn. (8.7) eqn. (6.69) Table 6.1	

(*Continued*)

Table 9.7 (*Continued*)

Action	*Response*	*Reference*	*Limitations*
	Melt temperature will decrease with increasing screw depth due to smaller specific power E/Q	Fig. 8.8 p. 292	Softening/melting point reached
	Melting may be less complete with deeper screw and higher output Q	p. 292	Incomplete melting
	Temperature variations – experiment suggests medium-depth screws give more uniform temperature than very shallow or deep screws.	p. 292 p. 293 p. 358	Complex, depending on previous N, dP/dz, E, h, melting length Depends on comparison at constant N or constant Q

Table 9.8 Operational strategies: improved melting required

Action	*Response*	*Reference*	*Limitations*
Reduce screw speed N	Output Q and pressure P reduce approx. in proportion to speed N	eqn (6.59)	Uneconomic output
	Mechanical power E reduces approx. in proportion to $N^{1.5}/N^2$	Fig. 8.12 eqn. (8.16)	
	Melt temperature T_m falls due to reduced specific power (heaters constant)	Fig. 8.13 p. 258	Softening/melting point reached
	Gel point moves towards feed	Fig. 7.27	
	Melting more complete – longer residence time for conducted heat	p. 284	As required
	Temperature variations decrease due to more complete melting and longer time/greater length in pumping section	p. 284	
	Residence time for mixing increases	p. 284	
Increase back pressure (constant speed)	Output Q decreases and total pressure P increases	A to C in Fig. 6.18	Uneconomic output
	Mechanical power E increases	eqn. (8.7) Fig. 8.14	Maximum motor power
	Heater power H decreases	Table 8.5	
	Melt temperature T_m rises due to greater specific power E/Q (heaters constant)	eqn. (8.29) p. 284	Thermal degradation
	More complete melting	p. 284	As required
	Temperature variations may increase or decrease	p. 284	
	Mixing improves due to longer residence time and greater longitudinal mixing	p. 284	

(*Continued*)

Table 9.8 (*Continued*)

Action	*Response*	*Reference*	*Limitations*
Reduce barrel set temperatures in melting section *only*	Output Q and pressure P approx. constant (fixed die)	Fig. 7.28(a)	
	Mechanical power E increased considerably	p. 279 p. 287	Maximum motor power Maximum torsional strength
	Heater power H decreased	p. 287	
	Melt temperature T_m rises if mechanical power E was previously high	p. 279	Thermal degradation
	More complete melting due to greater shear stresses, smaller temperature differences between solid and molten portions, possible delay of solid bed break-up	p. 287	As required
	Temperature variations (at die) may increase due to lower average temperature at start of melt pumping section	p. 277 p. 288	Unstable flow in die Non-uniform product properties
	Mixing may increase due to longer time after melting, and greater shear stresses at lower temperatures	p. 282	
Increase screw length	As previously, lower pressure gradient tends to increase length for melting	p. 291	
	Greater length also allows more gradual temperature gradients in melting section	p. 288	
	Greater length also allows greater time in melting section for elimination of solid particles and temperature variations	p. 291 p. 354	

Table 9.9 Operational strategies: improved mixing required

Action	*Response*	*Reference*	*Limitations*
Increase back pressure (constant speed)	Output Q decreases and total pressure P increases	A to C in Fig. 6.18	Uneconomic output
	Mechanical power E increases	eqn. (8.7) Fig. 8.14	
	Heater power H decreases	Table 8.5	
	Melt temperature T_m rises due to greater specific power E/Q (heaters constant)	eqn. (8.29) Fig. 8.15 p. 284	
	More complete melting	p. 284	
	Temperature variations may increase or decrease	p. 284	
	Mixing improves due to longer residence time and greater longitudinal mixing	p. 284 Fig. 6.6	As required
Reduce screw speed (fixed die)	Output Q and pressure P reduced approx. in proportion to speed N	eqn. (6.59)	Uneconomic output
	Mechanical power E reduces approx. proportional to $N^{1.5}/N^2$	Fig. 8.12 eqn. (8.16)	
	Melt temperature T_m falls (heaters constant)	p. 258 p. 283	
	More complete melting	p. 284	
	Temperature variations decrease	p. 284	
	Mixing improves due to longer residence time, lower temperatures and more complete melting	p. 284	As required

(*Continued*)

Table 9.9 (*Continued*)

Action	*Response*	*Reference*	*Limitations*
Reduce barrel set temperatures	Output Q approx. constant	eqn (9.13)	
	Pressure P increased (fixed speed and die)	Fig. 9.5	
	Mechanical power E increased considerably	eqn. (8.9) Fig. 8.10	Maximum motor power Torsional strength of screw
	Melt temperature falls if E was previously small	Fig. 8.10 p. 369	Softening/melting point reached
	Melt temperature T_m rises if E was previously large	p. 277 p. 369	Thermal degradation Effects on temperature variations
	Melting may be more/less complete if mechanical power was previously high/low	p. 287	
	Break-up of solid bed may be delayed	p. 287	
	Temperature variations may increase/ decrease depending on changes in melting, in melt temperature T_m, and whether latter is much above melting point	p. 287 p. 287 p. 354	
	Mixing will probably improve due to more complete and uniform melting, and higher shear stresses in pumping section, but may be offset if melt temperature is raised appreciably in pumping section	p. 288 p. 353	As required
Increase screw length	As previously, lower pressure gradient tends to increase length for melting	p. 291	
	Greater length in pumping section allows more time for mixing	p. 291 p. 354	As required
Surging	See section 11.2		

giving longitudinal mixing is reduced or eliminated. Reference to Fig. 6.16 shows that for two screws of different depths, running at the same speed to give the same output with the same die, the operating point must be at A, and the die line of Fig. 6.17 must also pass through this point; this is the basis of comparisons made at constant output. Any other depth of screw will require some adjustment of speed to give the same operating point, as discussed on p. 293. In other cases the comparison is made on a basis of a fixed die characteristic K (as in Fig. 6.18) and constant speed, where decreasing the screw channel depth decreases output and pressure, though increasing the value of Q/Wbh (from A to B in Fig. 6.18). Then if the operational requirement is for a constant output (as at A in Fig. 6.18), the speed of the shallower screw must be raised until the operating point B coincides with A. As shown in Table 9.2, the consequences of increasing speed will frequently be contrary to those of other changes, especially reducing channel depth, and the total effect may be improvement or deterioration depending on the relative magnitudes of the changes and their effects in a particular situation.

10 Twin-screw extruders

The twin-screw extruder differs from the single screw-machine in geometry, in the mechanism of melting, mixing and pumping, and hence to a large degree also in suitable applications and method of operation. Further comparison must await a more detailed study of the principles of the twin-screw extruder and the many variations possible within the basic type. The author is indebted to Martelli (1983) for his excellent analysis of the mechanisms of twin-screw extrusion, resulting from extensive practical experience. The purpose here is to concentrate on the aspects influencing operation, and the present author accepts full responsibility for the selection and presentation of the following material. The twin-screw extruder has features resembling the gear pump, certain multiscrew pumps designed for non-polymer fluids and even the two-roll mill, but its complex geometry requires several definitions and additional nomenclature, though these have been kept consistent with those of the single-screw machine (Chapters 6–9) as far as possible.

We begin with some notation and definitions:

- I interaxis distance
- D' primitive (outer) diameter
- D actual outer diameter
- D_i root diameter
- D_e equivalent diameter
- h' primitive channel depth
- h actual channel depth
- e_m maximum flight-tip width
- e actual flight-tip width (equivalent to t in single screw)
- p pitch
- N screw speed
- N_f number of filled flights
- N_e speed of equivalent screw
- Q output
- Q_c output capacity (swept volume per turn $\times N$)

Q_p back flow
C_e equivalent channel length
t_r residence time
E power
β semi-angle of intermeshing (circumferential)
γ shear strain – hence $\dot{\gamma}$ = shear rate
δ clearance between flight and barrel
ε clearance between tip and channel root (do not confuse with 'direct strain' in Chapter 3)
η viscosity
θ flank angle of ideal flight
ρ density (of melt, etc.)
ϕ pitch angle (measured at D)

Counterrotating	Screws rotating in opposite directions when viewed from the same end.
Corotating	Screws rotating in the same direction when viewed from the same end.
Non-intermeshing	Screws adjacent to each other without engaging threads – implies some barrel opening for communication between material in the two screws. Usually the screw flights are tangential to each other except for mechanical clearance.
Intermeshing	Screws in which the flights of each screw interpenetrate the channels of the other screw.
Fully intermeshing	Screws in which the tip of each flight penetrates the other channel to its full depth, except only for mechanical clearance.
Conjugated	Screws in which, apart from mechanical clearance, each flight completely fills the channel of the other screw, at least at one point.
Non-conjugated	Screws in which at no point does each flight completely fill the channel of the other screw – in fully intermeshing screws this may be by gaps at one or both flanks. In partially intermeshing screws, non-conjugation is by gaps at flight tip and root, with or without gaps at the flight flank(s).
Axis plane	The plane in which the axes of the two screws lie and in which the interaxis distance is measured. The two screw profiles most nearly approach each other in this plane, and generally if conjugation occurs, it occurs in this plane. The screws and barrel are geometrically symmetrical about this plane, except for the longitudinal displacement due to the flight helix.

Mid-plane	The plane perpendicular to the axis plane and mid-way between the screw axes. By symmetry, this is the common tangent plane to two non-intermeshing screws. In this plane lie the cusps of the figure-'8'-shaped barrel and the limiting circumferential positions of intermeshing, when this occurs. It also represents the plane across which material may or may not move from the channel of one screw to that of the other. The mid-plane is also a plane of geometrical symmetry, except for the axial displacement between the flights of the two screws. In the counterrotating case, the mid-plane is also a plane of symmetry for velocity.
Calender nip	Flow through a small clearance between two converging surfaces moving in the same direction with the same or similar velocities, with or without an independently generated pressure difference.

The intersection of the axis plane and the mid-plane is a line, which for fully intermeshing screws is at mid-depth of each channel and therefore for all flight shapes will generally divide equally the flights and channels of the two screws. The foregoing definitions apply equally to tapered screws.

This chapter will exclude multiscrew machines; those with two screws of different length will be regarded as a series combination of single and twin screws. Generally, the screws will also be of the same diameter D, pitch p, channel depth h, and shape; with their axes lying in a common plane. The pitch and channel shape, especially flight tip width, may vary along the screw length. However, tapered screws in which interaxis distance I, diameter D and/or pitch vary along the length are often used; the following analysis may be applied to a short section of such screws, but the effects of varying peripheral velocity, output capacity, pressure gradient, etc., will often be nonlinear and complex in considering the overall performance. Any comparison between twin- and single-screw machines will depend firstly on the degree of intermeshing of the twin-screw machine.

10.1 NON-INTERMESHING SCREWS

Where the intermeshing is small or non-existent, the screw profile is largely free of geometrical constraints, and the mechanisms of melting, mixing and pumping depend primarily on the viscous drag on the polymer between the screw and barrel surfaces in relative motion. This is also the basic principle of the single-screw extruder, and to this extent the performance and operation of single- and non-intermeshing twin-screw extruders will be similar. Unless a

barrier is deliberately introduced between the screws where they adjoin, there will be the possibility of transfer of some polymer in this region from the channel of one screw to that of the other (but see below). There will also be some drag on the material in one channel due to the presence of the flight of the other screw. The degree of shearing will depend on the geometry.

10.1.1 Counterrotating

If one screw is a right-hand helix and the other left-hand, they must rotate in opposite directions (counterrotation) in order that both pump in the same axial direction, i.e. towards the die. (Otherwise the net output would be small, being the difference in flow in the two screws, but with enhanced mixing due to recirculation.) In that case, the adjacent parts of the two flights lie at the same angle to the axis plane and move in the same direction, e.g. from front to back of this plane. Since there is zero relative circumferential velocity between the two screws, the flight will exert no additional drag on the material in the channel of the other screw. (It is also immaterial for local velocities whether the flights of the two screws are staggered or opposite each other, except that in the latter there will be a 'calender' flow in the nip formed by the two flights.) There is also no relative axial movement of the flights of the two screws so that no transverse circulation is induced within the channel by the flight of the other screw. There is no mechanism resulting directly from the screw motion to induce movement of material between the screws and so little mixing between them.

10.1.2 Corotating

If both screws have a helix of the same hand, they must rotate in the same direction, though where they are adjacent, the movement of one will be from front to back of the axis plane and the other will be from back to front, and the relative circumferential velocity will be twice the absolute velocity of each screw. This will cause considerable drag of the flight tip on the material in the other channel. However, at this point the two flights make mutually opposite angles with the screw axes, so that each flight appears to move across the opposite channel, creating a transverse drag and resulting in an oblique circulation and a degree of mixing within the channel. There will also be a local, intermittent, but intense shear of a small volume of material when the two flights cross each other. This circulation and shear are additional to those caused in the remainder of the screw circumference, as in the single-screw machine, by the drag of the stationary barrel. There is again no direct mechanism causing movement of material from one screw to the other and hence little large-scale mixing. White (1990), in reviewing commercial twin-screw machines, appears to make no reference to applications of this type of machine.

10.2 PARTIAL INTERMESHING

Even a slight degree of intermeshing imposes limitations on the geometry of the screw channels and flights in certain cases. It also introduces the possibility of a direct thrust from the flight flank of one screw on material in the channel of the other screw, in addition to viscous drag at the flight tip. Thus each flight will tend to 'scoop' material into its neighbouring channel(s) with a degree of mixing between screws. It will also tend to divide the material in the channel of the other screw into at least two flows, with further consequences for mixing.

10.2.1 Counterrotating

Since adjacent parts of the flights of the two screws lie at the same angle to the axis plane, it is possible for the two flights to intermesh to any degree up to the full channel depth without interference, provided only that each flight is narrower than the channel of the other screw. As the degree of intermeshing is increased, e.g. by bringing the screw axes closer together, the flight forms a local restriction in the other channel, tending to limit rotation of material with the screw. Also, due to the smaller radius, the velocity $(\pi dN \cos \phi)/2$ of the adjacent points on the sides of the channel becomes less than that of the meshing flight tip $(\pi DN \cos \phi)/2$, so that a degree of relative motion, and hence shear rate, will occur laterally in the channel. This will increase with the degree of intermeshing, i.e. as $d \rightarrow D_i$, as will the shear between the flight tip and the channel root. The former will also increase if the flight width is increased close to that of the channel. Additionally, any material tending to move from the channel of one screw will be displaced and divided by the meshing flight tip into its two adjacent channels, producing a degree of mixing, although there will be a similar tendency in the other screw, but in the reverse direction.

In order to estimate the effect of the restriction due to the intermeshing flight, assume that its width equals that of the channel, so that a gap exists only at the flight tip and channel root. Then in the absence of an overall longitudinal pressure gradient, the drag flow Q'_D through one tip–root gap will be the mean velocity multiplied by the cross-section:

$$\begin{aligned} Q'_D &= \frac{\pi N(D + D_i)}{2} \cdot \frac{p}{2} \left(I - \frac{D + D_i}{2} \right) \\ &= \frac{\pi N p}{4} (D + D_i) \left(I - \frac{D + D_i}{2} \right) \end{aligned} \tag{10.1}$$

The drag flow along the screw channel due to drag on the barrel surface will be approximately (McKelvey, 1962, p. 236, Fig. 10.6):

$$\begin{aligned} Q_D &= \frac{\pi D_i N}{2} \cdot \frac{p}{2} \left(\frac{D - D_i}{2} \right) \\ &= \frac{\pi N p}{4} D_i \left(\frac{D - D_i}{2} \right) \end{aligned} \tag{10.2}$$

With little or no intermeshing ($I \rightarrow D$), the drag flow in the tip–root gap will clearly always be greater than that in the channel, so the former will present no flow restriction. With full intermeshing ($I = (D + D_i)/2$) the drag flow in the tip–root restriction is zero, forming a total flow restriction, apart from leakage. Taking an example similar to Martelli (1983, p. 25), if $D = 100$ mm and $D_i = 50$ mm, giving a channel depth of 25 mm, the two flows will be equal when the tip–root gap is about 8.3 mm, i.e. one-third of channel depth. At smaller interaxis distances I, giving smaller tip–root gaps, $Q'_D < Q_D$, giving a flow restriction. If the root diameter is increased to 75 mm, giving a channel depth of 12.5 mm, the two flows will be equal when the tip–root gap is about 5.4 mm or 43% of the channel depth. Thus the tip–root gap forms a restriction when the degree of intermeshing is greater than 65% for the deeper screw and 57% for the shallower screw. This restriction increases rapidly as the degree of intermeshing increases beyond these limits, creating high pressures at the start of the intermeshing region. Evidently, by continuity, the total flow in channel and gap must be equal, so that:

$$Q_D - Q_P \text{ (channel)} = Q'_D + Q'_P \text{ (gap)} \tag{10.3}$$

i.e. the pressure must rise in the remainder of the channel (Q_P negative) and fall in the restriction (Q'_P positive). Equations (10.1) and (10.2) show that at small degrees of intermeshing the ratio Q'_D/Q_D of the drag flows is greater than unity, so that in these cases the pressure will tend to rise in the restriction and fall in the remainder of the channel. Assuming that the circumferential pressure

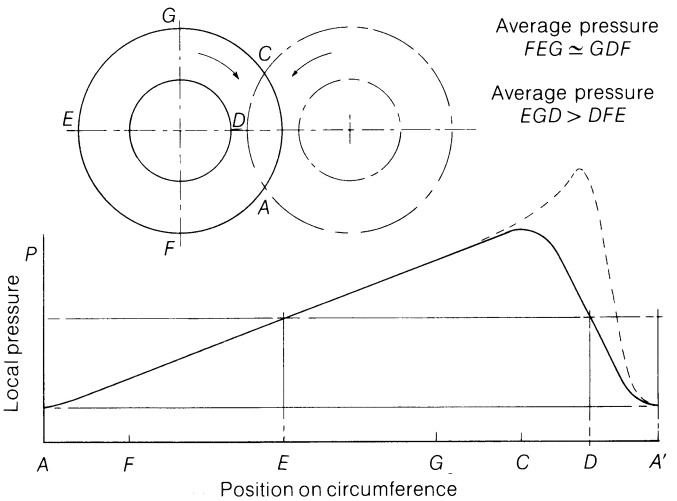


Figure 10.1 Local pressure variations round counterrotating screw channels.

gradients in the channel and restriction are linear (the latter is only approximate, due to the converging/diverging gap, as are the points of maximum and minimum pressure) the pressure variation round the circumference will be as in Fig. 10.1. Thus there is a net force on each screw across the axis plane, but any force tending to separate the screws, as is usually claimed, can only be due to local pressure generated by the calender nip.

10.2.2 Corotating

Due to the opposing angles of the adjacent flights, in order to avoid mechanical interference there must be geometrical limitations on the degree of intermeshing possible, depending on the pitch angle and the flight width relative to the width of the opposite channel. This will be examined for the fully intermeshing case in section 10.4. As in the counterrotating case, the flight will provide a restriction in the other channel, which increases with the degree of intermeshing, as does the shear (now more intense due to the opposite directions of movement) between the flight tip and the channel root. However, like the flight tips, the flight flanks appear to move across the channel with which they mesh, so forcing part of the material out of this channel and into *one* channel adjacent the flight, creating a positive flow from one screw to the other, but without dividing it.

In the corotating case, any pressure rise in the channels of the two screws will be diagonally symmetrical, but the opposite directions of motion will cause minimal flow through the restriction and such circumferential pressure rise will tend to force material into the channel of the other screw, at a point where the pressure is low. As with the counterrotating machine, to a first approximation there will be little force separating the screws due to channel pressures and in this case little local pressure rise at the gap in the absence of a 'nip'. For the same reason, there will be little flow through the gap, and the flow in the channels will be mainly a figure '8' round both screws, with little local variation in pressure; thus the pressure forces across the axis plane will be small, and in opposite directions. This absence of major lateral forces on the screws permits the use of close clearances and minimizes wear on the flight tips (see p. 344).

With both kinds of rotation, both partial and non-intermeshing types are lengthwise open, according to Erdmenger's classification (Martelli, 1983, p. 9), which means that there is a continuous channel between the screws for back flow due to die pressure, so that although pumping may be by mechanical action rather than solely by viscous drag, the pumping is not positive in the sense of a gear pump. The counterrotating type is crosswise closed in that though there are spaces through which material can move from the channel of one screw to two different channels of the other screw, they recombine at the next intermeshing, limiting the mixing action; however, there is little driving force for this movement to take place. In contrast, the corotating machine with

a degree of intermeshing has a positive action transferring material between the screws, but may or may not divide the flow to give large-scale mixing.

Because of the number of variables (direction of rotation, degree of intermeshing, ratio of flight to channel width, as well as dimensions, speed, pressure, degree of filling) it is difficult to generalize further on the performance of partially intermeshing designs. It has been stated that such designs have some advantages, but mostly disadvantages of both single- and conjugated twin-screw types (Martelli, 1983, p. 12). These, together with non-intermeshing types, may perhaps best be considered from the point of view of performance, as variants of the single-screw machine.

10.3 FULL INTERMESHING: COUNTERROTATION

If the degree of intermeshing is increased until the flight tips of each screw reach the root of the channel of the other screw, excepting only for the necessary mechanical clearance, the screws are said to be fully intermeshing. In this case the restriction, mentioned above, in one channel due to the presence of the flight of the other screw, further limits the tendency of the material to rotate with the screw and thus increases the propelling action axially towards the die.

The differences already noted due to the two types of counter- and corotation are enhanced by full intermeshing. The following discussion will therefore treat them separately.

10.3.1 Counterrotation

If at no point do the flights of one screw completely fill the channels of the other screw, e.g. a rectangular section in which the flight is narrower than the channel, then the performance will be similar to that for partially intermeshing screws. The axial gaps between adjacent screw flanks, moving in the same direction, will replace the gap between the flight tip and channel root. The restriction formed by these gaps will again cause an increase in pressure on the 'ingoing' side and corresponding decrease on the 'outgoing' side, depending on the extent of the restriction. Because of the similarity to partial intermeshing, this geometry will not be considered further.

If in the axis plane, the flights of each screw match and completely fill the channels of the other screw, i.e. they are'conjugated', the material is completely prevented from rotating with the screw and thus positively moved in the axial direction, independent of material viscosity, its adherence to metal surfaces and the effects of back pressure and temperature. The screw length will then, in the absence of leakage, be independent of the back pressure required by the die. If the screw has a square thread, i.e the flanks are perpendicular to the screw

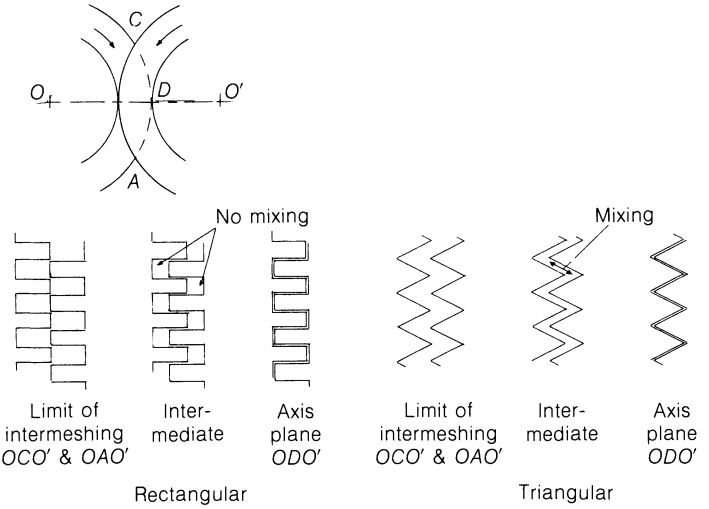


Figure 10.2 Counterrotating conjugated screws: effect of channel profile on mixing between screws.

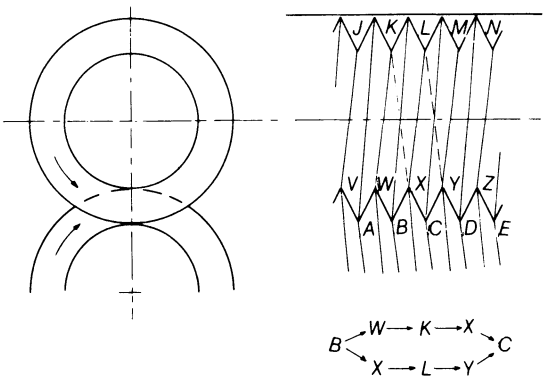


Figure 10.3 Counterrotating conjugated screws: flow division and recombination.

axis, then although either side of the axis plane the flight only partially penetrates the channel, there will be no path connecting the channels of the two screws and no mixing between them. If the flight flanks are inclined, e.g. a triangular thread, then on either side of the axis plane there will be paths between the channels of the two screws (Fig. 10.2). However, since on one side both channels are approaching, and on the other side both are receding, there is no positive force to create a transfer of material between the channels of the two screws. Although the flight, as it begins to mesh with the channel of the other screw tends to displace material into both its adjacent channels, these recombine at the next turn, giving little longitudinal mixing (Fig. 10.3).

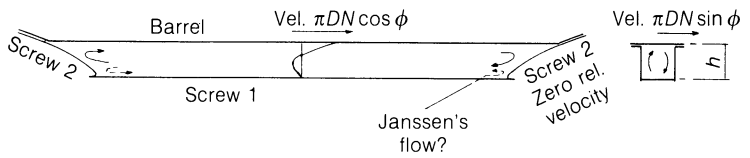


Figure 10.4 Developed screw channel showing local longitudial and transverse velocities.

Aside from the gaps between the channels (see above) each turn of the channel will have a closed 'C' shape, with concave ends defined by the opposite flight tip. Due to the relative movement of screw and barrel, the flow within the channel will resemble that in a deep single screw against a closed die (Figs 6.6(a) and 6.7 refer to shallow channels), giving a degree of local distributive mixing and the maximum pressure rise per turn. Figure 10.4 represents the flow in a channel approximated by 'unwrapping' the helix into a linear shape; with the deep channels usual in twin-screw machines the area of barrel in contact with the polymer will frequently be larger than that of the screw root. For the same reason, the longitudinal flow will be three-dimensional and the transverse flow also cannot be regarded as one-dimensional, though the usual small pitch and pitch angle will make this component small. Janssen (1978) reports that with small calender gaps he has found a closed and stable flow at the bottom of the channel which mixes very poorly with the remainder. A trapezoidal flight and channel shape will have features similar to those of a triangular flight, but with the addition of 'calender gaps' at flight tip and channel root.

To match the screws' performance to the various functions discussed below, counterrotating machines are frequently made in two or three sections or with continuous variation of screw profile. These may be of varying flight width (with some loss of conjugation) and/or varying pitch, in which the volume displaced per turn changes, as does the degree or filling with a uniform (metered) feed rate.

10.3.2 Feeding

In some instances this type of machine may be flood-fed, in which case the feed section is usually non-conjugated with large clearances to allow compression of the solid polymer and release of trapped air. The second section would then follow with smaller, conjugated channels, e.g. rectangular flights, to ensure good forward propulsion of the compressed material. However, it is more usual for such screws to be starve-fed by a separate metering mechanism, which determines average output independent of screw speed. Output and screw speed thus become variables independent of each other and available for control of mixing, shear heating etc. If the metered feed rate is to be less than the natural flood feed rate of this section, then a large volumetric capacity is

required when feeding material of low bulk density such as reclaimed film or foam. Especially with such materials, there is a tendency to convey forward air trapped in the solid feed so that venting is often necessary. To eliminate time fluctuations due to the metering device, it is often desirable to introduce a degree of mixing, e.g. by reducing flight width. The screws usually run inwards at the top, so that the feed falls at the sides into the upcoming channels to ensure adequate filling.

10.3.3 Melting

Melting of the polymer occurs from the combined effects of heat conducted from the barrel and internal shearing of the polymer. With metered feed, the filling ratio of the channel before melting is less than unity, so that little shearing occurs and heating is mainly by conduction. The maximum heat required to melt the polymer may be estimated as:

$$H_{\text{melting}} = \rho Q_c \int_{T_0}^{T_m} C_p \, dT \tag{10.4}$$

which is similar to equation (8.4); Q_c is the output capacity and T_m the crystalline melting point of the polymer. For amorphous polymers this may be approximated by replacing T_m by $T_g + 50°C$. If the permissible heater rating ($W\,m^{-2}$) is known, or a surface heat transfer coefficient, these may be used to estimate the length of the barrel required for melting. Further heating, by conduction or shear, will be required to bring the melt to the temperature required for extruding at the die.

10.3.4 Mixing

The shear and temperature history to be achieved by mixing is ideally the same for all the polymer particles. Distributive mixing is primarily dependent on the units of shear, i.e. the product of shear rate and residence time. The latter is discussed below while the former may be approximated by:

$$\dot{\gamma} = \frac{\pi DN}{h} \tag{10.5}$$

This is identical to the drag flow shear rate in a single screw (equations (6.4) and (6.6)) neglecting the pitch angle. More accurate equations are obtained by differentiating the vector sum of the velocities represented by equations (6.26) and (6.28). Dispersive mixing is a function of shear stress and time, the former being a function of shear rate and temperature. Thus mixing in the screws is determined by combinations of shear rate, temperature and residence time. Movement within the closed channels gives only small-scale mixing, so that partial movement between channels is necessary for effecting distributive mixing. This must be achieved in a reasonably short barrel length without

excessive shear rate which, together with shear heating, might cause degradation of the polymer. These conditions will also cause in fibre-reinforced polymers shortening of the fibres and impairment of product properties. The high shear stresses near the calender nip will aid dispersion, e.g. of pigments, but with no guarantee that the whole body of material will be treated.

Movement between channels for mixing may be enhanced by reducing flight width, though this entails non-conjugation and a loss of positive self-cleaning. However, high velocities in the gaps connecting screw channels will tend to keep them clear of stagnant material. Conjugation ensures that any material adhering to the screw flight will be displaced in the intermeshing region, though since the relative velocities are small (due to different centres of rotation and to the different radii, e.g. of flight tip and adjacent channel root) there will be little wiping action. However, such screws will be largely self-cleaning. Changing the screw pitch and/or number of thread starts along the screw maintains conjugation but changes the degree of filling. It is not clear how this provides adequate distribution, since division of the flow only occurs at the points where the pitch changes. Distributive mixing may also be increased by interrupting the flights in otherwise conjugated sections so that pressure gradients, e.g. within the closed 'C'-shaped channels, will cause flow of material through the cuts into another channel.

Mixing is very dependent on the screw geometry but is said to be largely independent of operating conditions. The extent of mixing is not readily estimated since the various flows are not accurately known.

10.3.5 Venting

The virtually closed 'C'-shaped chambers of the conjugated counterrotating type give little opportunity for escape of air trapped with the feed or volatiles generated on heating. If this is so, a section with a vent and with a large channel volume, giving a low degree of filling and low pressure, may follow a pumping section. Mixing is required in this section to expose the maximum surface to vacuum, and this may be by non-conjugation and/or interrupted flights; however, little flow will occur as the channels are incompletely filled.

Such a venting section must be followed by a second pumping section to ensure forward flow of material and to raise pressure before the die.

10.3.6 Pumping

The closed chambers of conjugated screws lead to a negligible overall backflow due to die pressure and hence output is not a function of pressure. However, leakage flow Q_L at the axis plane (calender nip) reduces the pumping capacity of the machine, since the flow is into a different channel (chamber) of the screw.

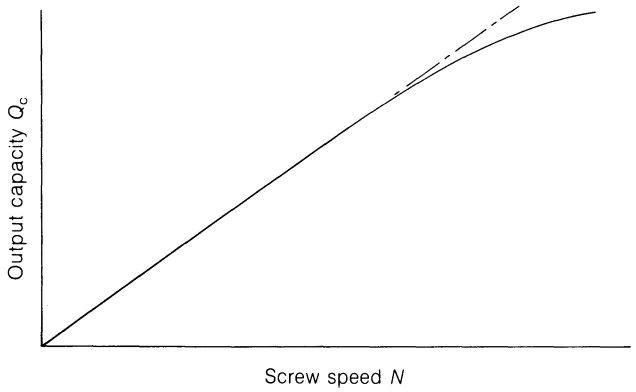


Figure 10.5 Influence of leakage on output capacity of counterrotating screws.

The resistance R to this flow may be likened to that of a narrow slit (equation (3.34)):

$$R = \frac{1}{K} = \frac{12L}{TH^3} \tag{10.6}$$

(compare equation (6.55)) where

$$Q_L = \frac{PK}{\eta} \tag{6.53}$$

Here the viscosity will be low due to the local high shear. The effect of increasing screw speed N will be to increase the output capacity Q_c, but by increasing shear rate will also reduce the viscosity. In addition, the increased drag flow in the channel will increase the pressure rise round the channel, i.e. the pressure difference across the calender gap; this and the reduction of viscosity will both increase the leakage flow Q_L and in extreme cases may affect the increase in output capacity, leading to a curve of actual output versus speed similar to Fig. 10.5. The increase in shear rate near the calender nip will increase the local temperature rise and may lead to polymer degradation.

Usually only two or three turns of conjugated screws are required to raise the necessary die pressure, whereas loss of conjugation drastically reduces the pumping ability. Because of the high local pressures generated where the two counterrotating screws converge, these machines usually run at say, one-third of the speed of corotating types, giving correspondingly smaller outputs for a given size of machine; this makes useful comparisons between the two types difficult.

10.3.7 Residence time

If the screws are conjugated, the material in the closed chambers advances one pitch per revolution of the screws. Then if V_e is the axial velocity corresponding

to this, the residence time (Martelli, 1983):

$$t_r = \frac{N_f p}{V_e} = \frac{N_f \pi D \tan\phi}{N \pi D \tan\phi} = \frac{N_f}{N} \tag{10.7}$$

However, if the whole screw were designed for pumping, the residence time t_r would be too short for adequate heating, melting and mixing. Thus part of the screw will be non-conjugated or slotted (section 10.3.4) allowing material movement between channels to increase the mixing in this section and extend the residence time. The pumping action will be reduced, although it is claimed that the channels will still be completely filled. Equation (10.7) shows that at high screw speed N, the residence time will be reduced, also reducing the heat conducted from the barrel, but the increase of shear rate will increase the contribution from shear heating. Low screw speed N increases the residence time and thus the proportion of heat conducted from the barrel, while the shear heating is reduced. As mentioned above, the latter is the usual case with counterrotating screws.

10.3.8 Power

The power consumption in filled channels of volume V is approximately:

$$E = \eta \dot{\gamma}^2 V \tag{10.8}$$

(compare equation (3.57)). In the absence of reliable determination of the flow in the channel, the shear rate is taken from the approximation in equation (10.5); however, section 8.4 shows that for zero net flow ($Q/Wbh = 0$) the total shear heating is greater than for drag flow ($Q/Wbh = 0.5$), represented by equation (10.5). The volume of one channel of each screw equals the cross-sectional area multiplied by the combined circumference minus the intermeshing region. An equivalent screw may be defined (Martelli, 1983, p. 56) such that $C_e = \pi D_e/\cos\phi$ equals this combined channel length. Then:

$$\begin{aligned} V = AC_e &= \tfrac{1}{2}\pi Dh \sin\phi \cdot \frac{\pi D_e}{\cos\phi} \\ &= \frac{\pi^2 D D_e h \tan\phi}{2} \end{aligned} \tag{10.9}$$

Then the power absorbed in N_f filled flights is:

$$\begin{aligned} E &= \bar{\eta}\left(\frac{\pi DN}{h}\right)^2 \cdot \frac{\pi^2 D D_e h \tan\phi}{2} \cdot N_f \\ &= \frac{\bar{\eta}\pi^4 D^3 D_e \tan\phi}{2h} N^2 N_f \end{aligned} \tag{10.10}$$

where $\bar{\eta}$ is an average viscosity. In counterrotating screws, N_f is usually reckoned as the total turns less those which are interrupted or in a venting section.

The reader is referred to Martelli (1983, pp. 57–59) for details of power calculation for the various clearances and through the die. As explained on p. 227, the die term may be excluded if the final energy content of the polymer is taken at the die exit. It is noteworthy that all the remaining terms differ from equation (10.10) only in the geometrical quantities – all are proportional to the prevailing viscosity, the number of filled flights (effective length) and the square of the screw speed, as in the single-screw machine (equations (8.11) and (8.12)). Each is inversely proportional to the local clearance and approximately proportional to D^3 or D^4. These equations, however, make no allowance for non-Newtonian behaviour (shear thinning) due either to increased speed or decreased clearances; but it is claimed that the combined effects of increased shear rate and shear heating largely offset the effect of increased screw speed (cf. equations (8.16) and (8.19)).

10.3.9 Energy balance

The energy balance will be qualitatively similar to that for corotating screws (section 10.4) except that here in the pumping section the number of filled flights N_f is likely to vary much less with back pressure and viscosity. Also the mechanical power may be dominated by that in the intermeshing region.

10.4 FULL INTERMESHING: COROTATION

As with counterrotation, non-conjugation will lead to performance similar to that of partially intermeshing screws. Compared with conjugated screws, the leakage flows and flows between channels will be increased, reducing the

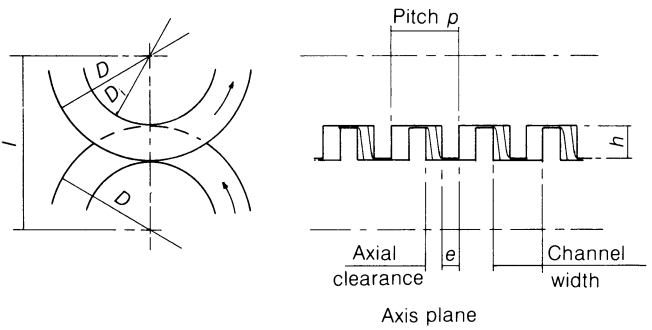


Figure 10.6 Non-conjugation by reduced flight width: corotating screws.

pumping ability e.g. by increasing the number of filled turns N_f for a given die pressure, probably increase the power consumption (due to lower pumping efficiency), increase the large-scale mixing and increase the spread of residence times. If non-conjugation is due to increased tip clearances, the maximum shear stress and local shear heating near the axis plane may be reduced, giving more uniform treatment to the material. Non-conjugation due to reduced flight width (Fig. 10.6), giving increased axial clearance, reduces shear stress and energy consumption over the flank area of intermeshing, but also profoundly affects flow between channels and mixing. Since the adjacent portions of flights of the two screws are at opposite angles to the axis plane and move in opposite circumferential directions, rectangular flights which are fully intermeshing cannot be conjugated, i.e. the flight width must be less than the channel width (Fig. 10.7) to avoid mechanical interference. Clearly there is a relation between the maximum flight width e_m and the axial displacements during intermeshing of the two screws, which are proportional to the pitch and the angles $AOC = AO'C = 2\beta$ of intermeshing.

If a triangular flight is now considered in which the outer diameter:

$$D' = 2I$$

(Fig. 10.8) then

$$h' = I, \quad D'_i = 0$$

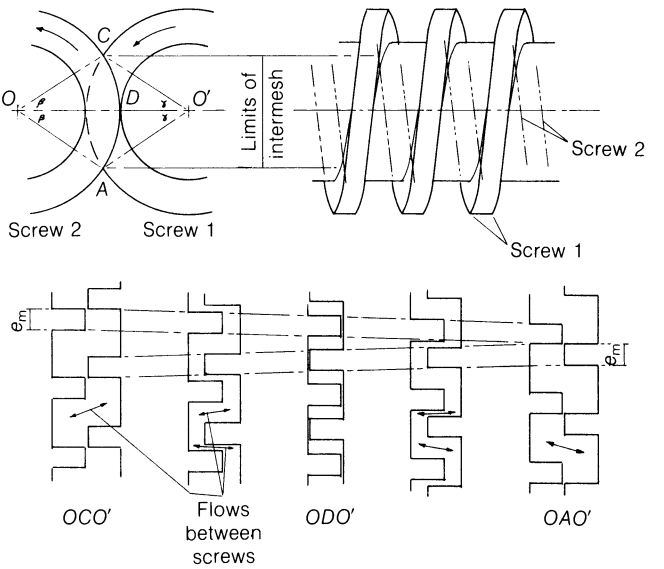


Figure 10.7 Limiting flight width to avoid interference: rectangular flight, showing flows between screws.

and the flank angle is given by:

$$\theta = \tan^{-1}\left(\frac{p}{D'}\right) \tag{10.11}$$

Then the flight tips intermesh at A and C, where angle $AOO' = COO' = \beta = 60°$ and angle $AO'O = CO'O = \gamma = 60°$. Then, by definition of a helical thread, the axial displacement of each flight tip from the axis plane OBO' will be $p \times 60/360 = p/6$ at the limits of intermeshing A and C, or the relative displacement between the screws is $p/3$ (Fig. 10.9). Thus the total relative displacement between A and C will be $2p/3$, and this is clearly the maximum possible for any triangular thread. (Some authors have suggested that during intermeshing the relative displacement is p, i.e. the flight of one screw moves from a position opposite one flight to opposite the next flight of the other screw. This would imply an angle 2β of intermeshing of 180°.) This configuration would apparently give conjugation without mechanical interference. However, the thread profile is the same at all

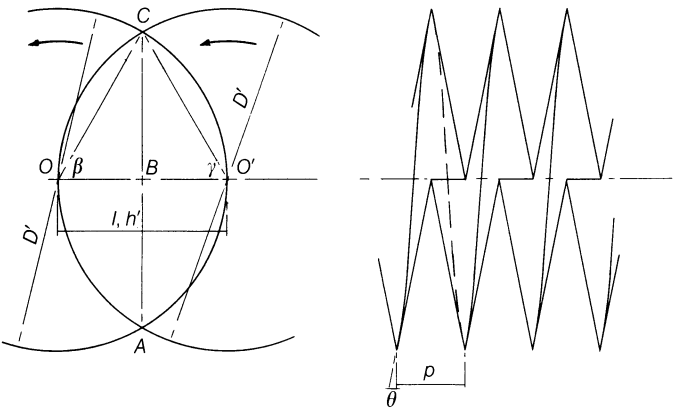


Figure 10.8 Theoretical triangular flight with $D' = 2l$ and zero root diameter.

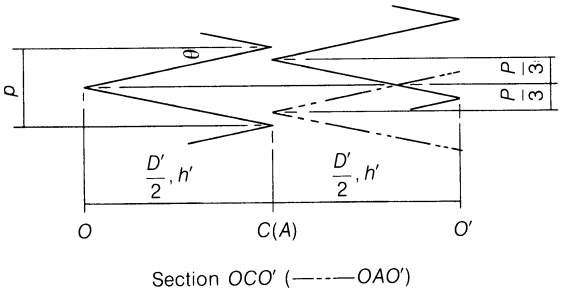


Figure 10.9 Relative axial flight displacements during intermeshing: triangular flight as Fig. 10.8.

points along its length, in axial section if turned with a fixed tool, or in section normal to the helix angle if thread-milled, according to the method of manufacture. Therefore for equal angles of rotation of the solid screw, the axial displacement must be the same at all points on the thread profile. The helix angle changes with radius, e.g. a 100 mm diameter screw with 10 mm deep channel and 50 mm pitch has a tip helix angle of $\phi = \tan^{-1}(50/100\pi) = 9.04°$ and a root angle of 11.25°. When $D_i' = 0$, $\phi_{root} = 90°$. Thus, near the axis plane OBO', the root of one screw will move axially while the engaged tip of the other screw will move at a lesser angle in the opposite axial sense, both with little or no radial movement. Thus, apart from being impractical in having no torsional strength, this configuration inevitably gives mechanical interference.

Note that in general, while equal increments from the axis plane give equal axial displacements, the radial displacement on screw 2 of a given point on screw 1 (e.g. the flight tip) is small near the axis plane, but increases more rapidly at larger angles. (Note that at large angles from the axis plane (i.e. $\beta > 45°$), as angle β for screw 1 increases towards points A or C, the angle γ and axial displacement of the opposing point on the flight of screw 2 may decrease slightly, though the total relative displacement increases monotonically.) Thus the trace of such a point at successive angular increments cannot be a straight line. (The concept of a 'sliding angle', fixed for a given geometry, thus seems misleading.) The present author believes, contrary to some authorities, that in a corotating, fully intermeshing machine, a triangular thread must lead to mechanical interference, especially near the axis plane (cf. Fig. 10.2 for counterrotating). To avoid interference, identical fully intermeshing screws must have a profile which at least approximates to the appropriate 'interference curves' (Fig. 10.11), and since these are concave, this author believes conjugation is also not achievable.

10.4.1 Trapezoidal flights

It has been stated by others that the triangular thread may be used as a basis for practical designs in which this is truncated to a trapezoidal section by a cylindrical 'flat' or 'land' at tip and root (Fig. 10.10). This reduces the channel depth from h' to h and reduces the outer diameter from the 'primitive' diameter D' to the actual diameter D, at the same time increasing the root diameter D_i' to a finite value of D_i. This design has the practical merits of a real torsional strength, increased wearing surface of the screw against the barrel wall and increased resistance to turn-to-turn leakage over the flight tips for a given mechanical clearance. Note that the transverse geometry on the upper left-hand side of Fig. 10.10 depends only on the ratio $D/2I$ or h/D and is independent of pitch p.

Avoidance of mechanical interference remains a determining factor in the shape of the flight flank. The trace of the flight tip of screw 1 has been calculated for two channel depths h of 25 mm and 16.7 mm, a primitive diameter D' of

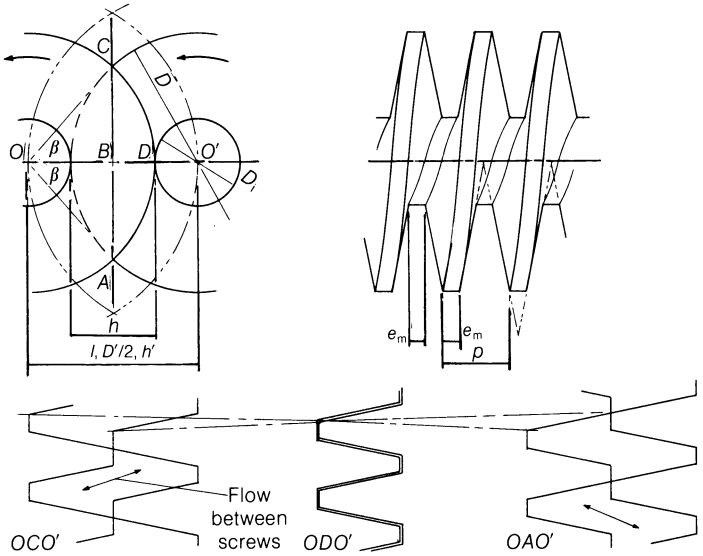


Figure 10.10 Trapezoidal flight based on triangular flight in Fig. 10.8, showing flows between screws.

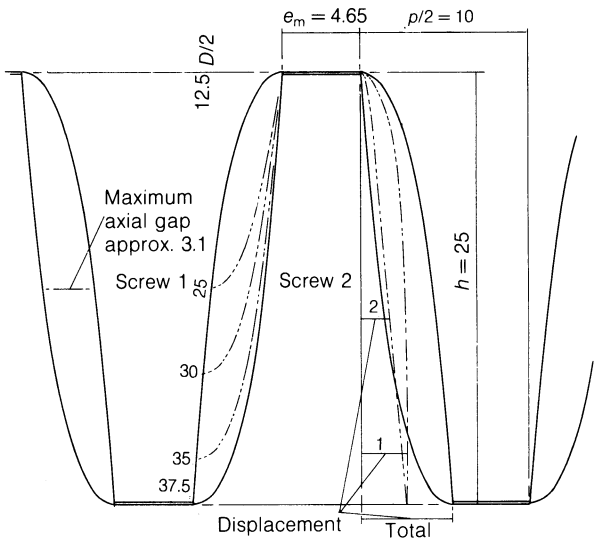


Figure 10.11 Relative axial displacements during intermeshing ('interference curves'), requiring concave flight flanks and maximum land width $e_m(h = 25\,\text{mm})$.

100 mm and pitch of 20 mm. The axial displacement of the opposing points on screw 2 has been calculated separately. The sum of these gives the total relative axial displacement of the flights of the two screws, with maxima of 5.35 mm and 4.60 mm respectively for the two channel depths, and the profile of each screw must accommodate this total displacement (Figs 10.11 and 10.12). Since the land width is half the pitch minus the 'taper' of the flight flank, the maximum land width e_m will be $20/2 - 5.35 = 4.65$ mm in the first case. This is only slightly less than the dimension of 5 mm for the corresponding trapezoidal profile. However, for the shallower channel of 16.7 mm, the maximum land width $e_m = 20/2 - 4.60 = 5.40$ mm compared with 6.67 mm for the corresponding trapezoidal profile, showing that land width cannot be increased proportionately as channel depth is decreased. These proportions correspond to $p/4 < e_m < p/3$ for the trapezoid, said to be the usual range. Having established a tentative flank profile, which avoids interference at the flight tip, the relative displacements of intermediate points on the flank of screw 1 are calculated and superimposed on its flank profile in Fig. 10.11. This shows that these points also will not interfere with the same profile for screw 2, lending support to the assertion of Janssen (1978, p. 28) that if interference of the tip is avoided, it will not occur at any intermediate position. It will be noted that even at mid-depth, the relative axial displacement is larger near the axis plane (point *B* in Fig. 10.10) so that the axial gap cannot be reduced substantially by modifying the profile. The areas of the gap each side of the flight are approximately 62.6 and 32.9 mm^2 or 20% and 16.5% of the channel cross-section. This indicates significant loss of conjugation and consequent loss of

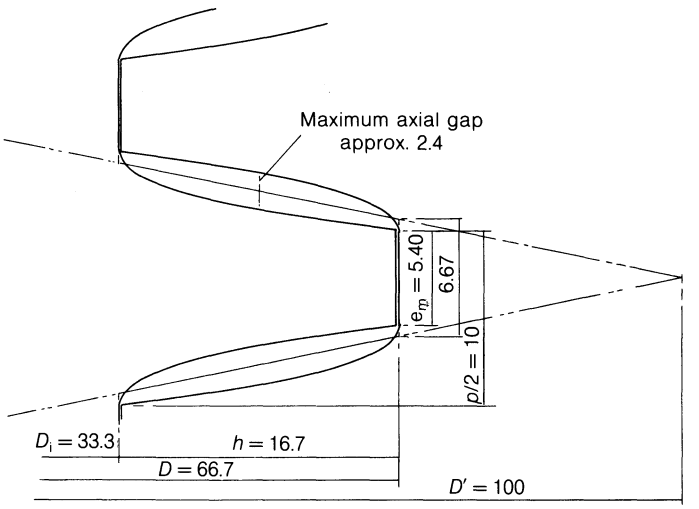


Figure 10.12 'Interference curves' as Fig. 10.11, but $h = 16.7$ mm.

positive pumping. Reduction of channel depth, with the associated increase of land width, appears to give a small reduction in the gap area as a fraction of channel area, leading to somewhat more positive pumping, but with reduction of output capacity. For the corresponding 25 mm deep rectangular and trapezoidal flights avoiding interference, the gap areas are approximately 35% and 24% of the channel areas, respectively.

As mentioned on p. 333, the transverse geometry, including the angles 2β of intermeshing, are independent of pitch, while the axial displacements for a given angle of rotation are proportional to the pitch. Therefore the axial scale of the interference curves (Figs 10.11 and 10.12) is also proportional to pitch. However, the channel cross-section is approximately the gap area plus $ph/2$, so the gaps will be an approximately constant fraction of channel cross-section, independent of pitch, and the examples in Figs 10.11 and 10.12 are typical for $D' = 2I$ at all values of pitch.

If the primitive diameter D' is reduced, so that $D' < 2I$, then the primitive root diameter D'_i becomes positive, h' is reduced and the flank angle of the triangular flight is increased (Fig. 10.13). This may also be truncated to the same diameters D, D_i and depth h, as in the previous example (Fig. 10.10 – flanks shown straight for clarity), but with smaller land width e. Evidently, the angles of intermeshing, etc., depend not on the primitive dimensions D', D'_i and h', but only on the actual dimensions D, D_i and h, so that the axial displacements will be as before, but superimposed on a theoretical profile inclined at a smaller angle to the screw axes. The gap area is the average axial displacement multiplied by the (same) channel depth and the channel cross-section remains approximately the gap area plus $ph/2$, so change in the inclination of the flight flanks does not of itself alter the proportion of gap to channel area or the loss of conjugation. The interference curves are shown on the modified flank profile in Fig. 10.14, from which it is seen that appreciable clearances would exist except at flight tip and root. The intervening profile may then be modified (by approximately half the disparity between the envelope of

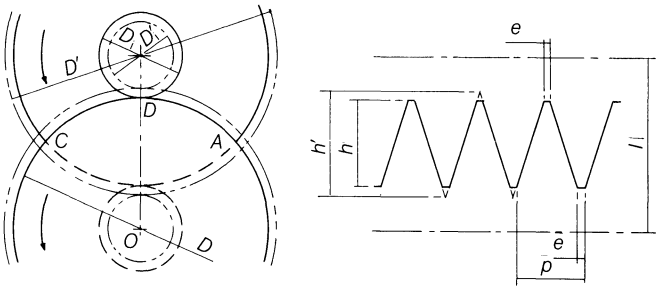


Figure 10.13 Trapezoidal flight based on triangular flight with $D' < 2I$. Actual diameters D and D_i and depth h as in Fig. 10.10.

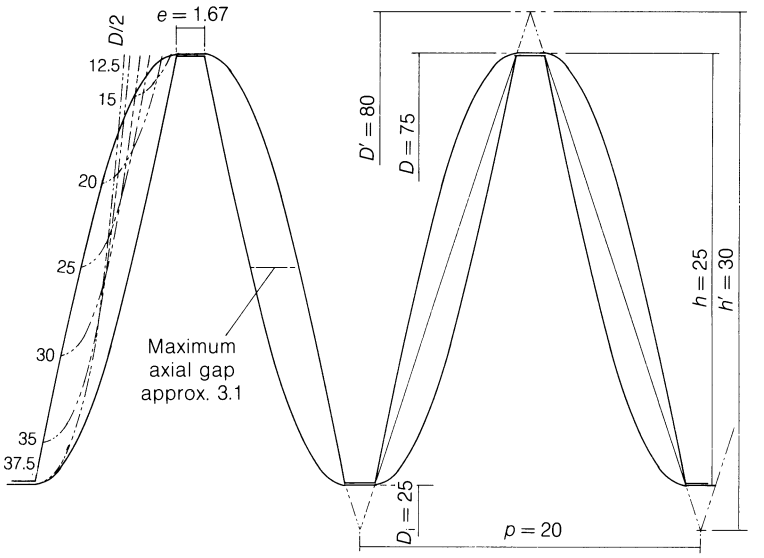


Figure 10.14 Relative axial displacement ('interference curves') for inclined profile based on Fig. 10.13, and reduced land width.

the interference curves and the opposing flight) to a convex curve. For these dimensions it is estimated that the ratio of gap area to channel cross-section could be reduced from 20% to approximately 14%, giving more positive pumping.

The remaining useful variant of flight profile is to reduce the land width e to less than the maximum value e_m already determined. This will increase the gap areas with further loss of conjugation and positive pumping, but may be useful to increase mixing. It will also relax to some extent restrictions on the flank profile and indeed the relative axial positions of the two screws, provided that in no case are the interference curves transgressed. If the flank profile of Fig. 10.11 is maintained, but the land width e is reduced to that of Fig. 10.14, i.e. 1.67 mm, the ratio of gap area to channel cross-section increases to approximately 38%, giving reduced pumping but improved mixing. Figure 10.15 shows diagrammatically at the axis plane three profiles avoiding interference and also the axial gaps at the limits of intermeshing. With maximum land width e_m, mixing is primarily with one channel of the other screw on one side of the axis plane, and with the next channel on the other side of the axis plane. Figure 10.15 also shows that with either method of reducing land width e, mixing is between the channel of one screw simultaneously with two adjacent channels of the other screw, though in varying proportions, giving effective turn-to-turn mixing.

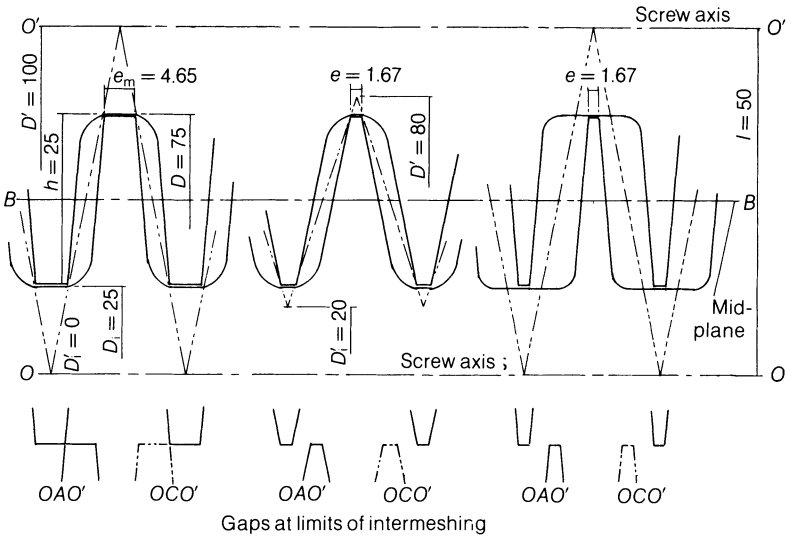


Figure 10.15 Practical flight profiles avoiding interference, with equal channel depths but varying land width.

So far, only the gaps between the two screw flights in the axis plane have been considered, as a departure from conjugation, affecting positive pumping. If the channel were completely closed, the flow within the channel would be similar to that in a closed counterrotating screw channel, except that the opposite motion of the intermeshing flight would create a circulation between flight and channel root surfaces in the gap near the axis plane, instead of the symmetrical calender 'nip' (Fig. 10.4). However, since mechanical interference precludes rectangular flights in corotation, the channels are not closed and gaps connecting the channels of the two screws occur on the mid-plane *ABC* in the intermeshing region, permitting flow from the channel of one screw to the channel(s) of the other screw. Because of the gaps necessary to avoid interference, the areas of these gaps cannot readily be expressed analytically. Although the direction of flow changes in moving from one screw to the other, the ratio of this gap area to the area of the channel gives an indication of the extent of the restriction to flow at this position. Thus with small land width and large channel depth there is little restriction to flow between the channels of the two screws; as depth decreases, giving increased maximum land width e_m, there is increased restriction. In Fig. 10.16 are plotted calculated dimensions of these gaps for the example of Fig. 10.11 and land widths of $e_m = 4.65$ mm and $e = 1.67$ mm (symmetrical). The approximate percentages of channel cross-section of the gaps are given in Table 10.1.

Although avoidance of interference requires appreciable gaps at the axis plane (Fig. 10.15 and *BB* in Fig. 10.16), Fig. 10.16 shows that with maximum land width, in the mid-plane this diminishes rapidly towards the limits of

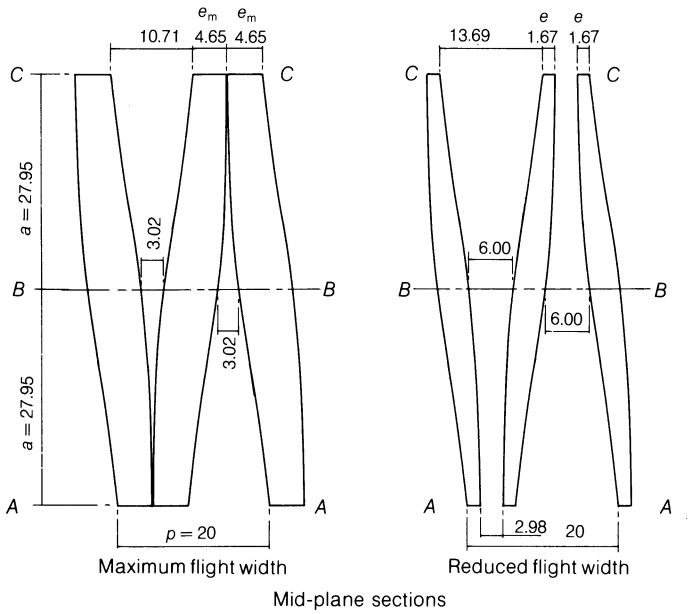


Figure 10.16 Mid-plane gap areas, which limit flow between screws.

intermeshing AA and CC, where the opposing flights approach each other. This gives a small area (e.g. 7.9%) and considerable restriction to flow between screws. Thus the flow will be mainly through the other gap area (e.g. 62.7%) to only one channel of the other screw. If land width is reduced, both areas are increased substantially, but they become more nearly equal, so that flow is more equally divided into two adjacent channels of the other screw. The motion of both screws will encourage, on one side of the axis plane, transfer of material from the channel of one screw to the other, and on the other side of the plane it will be transferred back to the next channel of the first screw, in what Martelli (1983, p. 29) describes as a 'twisted figure-8'. The length of the figure '8' normal to the screw axis is $2(\pi D - \sqrt{2Dh})$ (Fig. 10.8), which is the circumference of an equivalent screw having a diameter:

$$\begin{aligned} D_e &= \frac{2}{\pi}(\pi D - \sqrt{2Dh}) \\ &= 2D - 0.9003\sqrt{Dh} \end{aligned} \tag{10.12}$$

Thus, although it is not the purpose here to examine dimensional design, the consequences for operation appear to the present author to be that a spiral figure '8' flow round the combined channels of both screws will predominate with good mixing between them and with an open path from inlet to outlet, in this respect resembling a single screw. The subdivision of flow into two adjacent channels of the other screw will assist end-to-end mixing, especially

with reduced land width, along with that due to pressure (back) flow along the combined channel. It also appears that with corotating screws conjugation is not possible, preventing positive pumping, so that for both these reasons back pressure from the die will cause appreciable back flow along the combined channel and through the gaps at the axis plane. Thus the output will be to some extent dependent on back pressure.

10.4.2 Output

From equation (10.12), equivalent screw channel length C_e is given by

$$C_e = \pi(2D - 0.9\sqrt{Dh})/\cos\phi$$

Equivalent screw with the same circumferential velocity $\pi DN = \pi D_e N_e$:

$$N_e = N \frac{D}{2D - 0.9\sqrt{Dh}} \tag{10.13}$$

where for $0 < h < D/2$, $0.5N < N_e < 0.733N$. Then output capacity:

$$\begin{aligned} Q_c &= AC_eN_e \\ &= \frac{1}{2}\pi Dh \sin\phi \cdot \frac{\pi}{\cos\phi}(2D - 0.9\sqrt{Dh}) \cdot N \frac{D}{2D - 0.9\sqrt{Dh}} \\ &= \frac{\pi^2 D^2 Nh}{2} \tan\phi \end{aligned} \tag{10.14}$$

Putting $p = \pi D \tan\phi$,

$$Q_c = \frac{\pi DpNh}{2} \tag{10.15}$$

If the actual maximum output $Q_{max} = KQ_c$, Martelli (1983) gives average values of K in the range 0.85–0.90. Increasing screw speed N increases Q_c though K tends to fall, so the increase is not proportional.

To meet the different functions of the screws, the values of I and D are usually constant, giving constant thread depth, with variation of pitch p and/or flight tip width e; the former gives variation in the filling ratio whereas the latter alters the flow between the screws and thus the degree of mixing, though all sections have some conveying action. Where it is required to increase the residence time in a section, this will have little or no conveying action and take the form of interrupted flights, non-flighted lengths, kneading discs or counterflighted portions. The sections are usually 3–4 diameters in length but sometimes as much as 6–7 diameters – the total length/diameter ratio is non-significant but solely the sum of the parts required for the various functions. In practice the length is usually 8–15 diameters, with a modern tendency to 20–25 diameters, representing 30–50 flights. Alternatively, the diameter may decrease in steps from the feed to die end, so that the barrel could be removed from the screws towards the die end. With a constant interaxis

Table 10.1 Gap areas beween screws at axis plane and mid-plane

Land width	mm	4.65	1.67
Axis gap area (two per pitch)	mm^2	62.6	137.1
Channel cross-section $ph/2$ + gap area	mm^2	312.6	387.1
$\frac{\text{Axis gap area}}{\text{Channel area}}$	%	20.0	35.4
Smaller mid-plane gap	mm^2	24.6	107.8
	%	7.9	27.9
Larger mid-plane gap	mm^2	196	279
	%	62.7	72.2
$\frac{\text{Smaller gap area}}{\text{Larger gap area}}$	%	12.5	38.6

distance, this implies that the channel depth also decreases stepwise along the length; the pitch p and flight-tip width e then remain as variables to be chosen for each section, generally decreasing to accommodate the reduction in material volume and increase the pumping action.

10.4.3 Feeding

The usual nearly conjugated feed section gives good conveying of the solid material and good compaction of low-density feed. A large pitch and depth with small tip width gives a large volume of channel, while the existence of gaps between the screws gives good mixing and thorough air escape. The feed opening will usually be tangential on the downgoing side, to drag the solids into the circulation round the screws. As starve-feeding is usual, the output is not a function of screw speed and the filling ratio Q/Q_c in the feed section is appreciably less than unity; this possibly also assists in equalizing the feed rate fluctuations e.g. due to a batch feeder. The positive pumping associated with conjugation permits the handling of lubricants and very free-flowing particles.

10.4.4 Melting

The melting section requires a smaller volumetric capacity than the feed to provide for compaction of the solid material and maintain positive conveying when the polymer melts; this is usually achieved with a slightly smaller diameter and/or smaller pitch, which increase the filling ratio and give more positive propulsion. However, the filling ratio is likely still to be less than unity, so that little shear heating is experienced, and due to incomplete contact with

the barrel, heat conduction from it will be limited. Melting will only occur when the flights are filled and pressure can be built up. In order to promote early melting, pressure is raised within the section by means of unflighted portions, with small radial clearance, giving high back pressures and high shear. If only small pressures are required for easily melted polymers such as LDPE and plasticized PVC, the unflighted portion may be replaced by gashed flights. Another method is to use counterflighted portions with radial slots in the flights. The number of filled flights in the melting section will be proportional to the back pressure created, given by $P \propto \eta Q_{slot}/TH^3$, where T is the radial length and H the width of the slot. Then taking flows as positive in the downstream direction, in the first flighted portion:

$$Q = Q_{max} - Q_p \tag{10.16}$$

for the counterflight:

$$Q_{cf} = Q_{Pcf} - Q_{Dcf} \tag{10.17}$$

and for the combination of counterflight and slots:

$$Q = Q_{slot} + Q_{cf} \tag{10.18}$$

giving:

$$Q + Q_{Dcf} = Q_{slot} + Q_{Pcf} \tag{10.19}$$

Thus an increase in the rearward drag flow due to the counterflight Q_{Dcf} will increase the pressure before it and the pressure flows Q_{slot} and Q_{Pcf} through slots and counterflight, respectively. An increase in the slot width increases the flow Q_{slot} through the slots (proportional to the cube of the width) or decreases the upstream pressure and hence the number of filled flights. Therefore a larger number of filled flights for effective heat transfer requires narrow slots, which can be predetermined. A high degree of mixing in the slots and the counterflighted portion is desirable to achieve uniformity in the newly melted polymer.

10.4.5 Mixing

Since at the axis plane the two flights are moving in opposite directions, there will be only a small driving force for flow through these gaps, unlike the counterrotating type. As with maximum flight width e_m there is only one major gap from the channel of one screw to that of the other, there is little division of flow, and so little large-scale mixing. If a smaller flight tip width e is used with the same channel depth h, then two gaps are formed between the two screws and the material in one screw will be divided into two different channels of the other screw, where it will be mixed with material from adjoining channels of the first screw. Thus the maximum mixing is achieved with near-triangular flights (small e), and by choosing the value of the flight-tip width, a screw section may

be designed primarily for pumping or for mixing. Martelli (1983) states that the total gap area is usually 55–70% of the cross-sectional area of the channels in feed and mixing zones and 25–45% in pumping sections – the values in Table 10.1 are approximately half these as only one gap is attributed to each screw. In addition to the circulation at channel root and flight tip, mentioned on p. 338, in the intermeshing region there will be considerable shear and mixing between adjacent portions of the flank of flights of the two screws, the shear rate being a function of the sum of the two velocities, rather than the difference as in counterrotation. Aside from the angularity due to the separate centres of rotation, this sum will be constant over the channel depth, and act over the whole area of intermeshing, giving small-scale mixing additional to the large-scale mixing discussed above. When a fresh material, e.g. a different colour, is fed, these mixing actions will result in a rapid reduction in the old material left in the screws, and the self-wiping action of near-conjugated screws prevents material sticking in the channels and being overtaken by following material, giving rapid and complete cleaning and colour changing. Where kneading discs are used to increase mixing, these do not necessarily self-clean; they produce some back pressure on the preceding screw section, but their power consumption is not readily calculable since it is very dependent on the degree of filling.

10.4.6 Venting

If a section in which pressure is raised is followed by one of much greater volumetric capacity, the latter channel will not be filled and pressure will drop to zero, so that venting is possible. Since the diameter D and channel depth h are fixed, the volume can only be increased, while maintaining near-conjugation, by increasing pitch p. To promote mixing and vapour release from every part of the material, the flight-tip width e is small, as in the other mixing sections. Although the channel is not filled, near-conjugation ensures that material hold-up cannot occur.

10.4.7 Pumping

The head pressure required to give a flow rate Q through the die is given by:

$$P = \frac{\eta Q}{K_{\text{Die}}} \tag{6.57}$$

This pressure will be raised in a number of filled flights in which the positive displacement of the screw is reduced by back flows along the channel and leakage between the flight tips and the barrel. The flank and tip–root gaps are largely irrelevant for flow, since they only short-circuit *within* a turn, and, due

to the opposite screw velocities, should be very small. For one equivalent turn of the combined screws, the barrel/flight-tip leakage may be represented (Martelli, 1983) by:

$$K_L = \frac{2(\pi D - \sqrt{2Dh})\delta^3}{12e_m} \tag{10.20}$$

The pressure flow along the figure '8' channel is largely determined by the restriction of the gaps between channels, rather than the channels themselves. For the ideal trapezoidal flight the gap may be approximated as:

$$\text{width } AB = \frac{1}{2}\sqrt{D^2 - I^2} \quad \text{(Fig. 10.8)}$$

$$\text{height} = 0 \text{ to } (p - 2e_m);\ \text{average } \frac{1}{2}(p - 2e_m)$$

$$\text{average length} = h/2$$

represented by:

$$K_G \simeq \frac{\frac{1}{2}\sqrt{D^2 - I^2}\,[\frac{1}{2}(p - 2e_m)]^3}{12h/2} \tag{10.21}$$

As there are two gaps per equivalent turn, the conductance per turn will be $K_G/2$. These may be combined in a total conductance $K_s = K_L + K_G/2$. If the pressure rise per equivalent turn is dP, then the displacement flow Q_c will be reduced by $K_s\,dP/\eta$. The total head pressure $P = \Sigma\,dP \simeq N_f\,dP$ and the net flow $Q_c = K_s\,dP/\eta = Q_{Die}$.

From these it is theoretically possible to determine the number of filled flights; in practice, it is sufficient that this is always less than the actual number of flights in the section, as represented by the lower part of Fig. 6.9. However, it is evident that increasing the channel gap, e.g. by decreasing flight-tip width e, will increase K_G and reduce the pressure rise per turn at a given net flow rate. Similarly, an increase in barrel clearance, e.g. due to wear, will greatly increase the leakage flow conductance K_L. Both will lead to an increase in the number of filled flights required to raise the necessary die pressure and the latter especially will reduce local shear heating. The number of filled flights will also increase with increased feed rate, corresponding to higher die pressure, but decrease with increased screw speed which increases the displacement flow. Although increased temperature will first reduce viscosity in the screws and hence increase the number of filled flights, this will largely be compensated when the low-viscosity material reaches the die, lowering the die pressure. Martelli (1983) quotes the Colombo Model RC9 as having a radial clearance of 0.6 mm on a diameter of 82 mm, i.e. 0.7%. The usual figure for single-screw machines is 0.1–0.15%, so the clearances and leakage flows in the twin-screw machine may be relatively large.

10.4.8 Residence time

The residence time in the machine depends on the screw speed, screw design and filling ratio Q/Q_c. At the unmelted stage, especially if the filling ratio is small, the material tends to remain at the bottom of the channel and move forward one pitch per revolution; here the time must be sufficient for conduction from the barrel to heat the polymer to its melting point. As for counterrotating screws, $t_r = N_f/N$ (equation (10.7)). Practical tests confirm this approximately, giving an average 3.5 s per turn. Since the channels are usually deep, it is assumed that the melt flows approximately as a plug, with a circumferential velocity of $V = \pi DN \cos\phi$. The length of the total channel is N_f times the equivalent spiral, giving:

$$\begin{aligned} t_r &= \frac{L}{V_e} = \frac{N_f C_e}{V} \\ &= \frac{\pi(2D - 0.9\sqrt{Dh})N_f}{(\cos\phi)\pi DN\cos\phi} = \frac{2D - 0.9\sqrt{Dh}}{D\cos^2\phi} \cdot \frac{N_f}{N} \end{aligned} \tag{10.22}$$

Again, practical experience confirms $t_r \simeq 1.63N_f/N$ or an average time of 5.8 s per turn. The longest time in the melt state is important for degradation, but unlike the single-screw machine, in this case is not very different from the average. Modern machines with many sections are said to have residence times before melting of 70–100 s and in the melt of 90–150 s. In fact the time for flow through the adaptor and die may be many times these figures.

10.4.9 Power

In incompletely filled channels, there is little contact with the barrel or internal shearing and no rise in pressure; the material is carried along by the motion of the screws and little power is consumed. In filled channels, the equation for counterrotating screws (equation (10.10)) is valid with the same reservations, and is claimed to be valid also for non-intermeshing portions of the screws. The power absorbed in the clearance between the flight tip and the barrel would also be expected to be similar. The flow near the axis plane between flight tip and channel root will be circulatory rather than a 'nip' and little pressure will be raised, so power consumption would be expected to be small. On the other hand, the opposite directions of motion of the adjacent flight flanks, previously referred to, would be expected to consume power and generate heat, especially with the closer clearances associated with large flight-tip widths, i.e. pumping sections. As with the counterrotating machine, each of these additional constituents of the total power is proportional to the average viscosity and number of filled flights and the square of screw speed (neglecting pseudoplastic behaviour) and varies inversely as the local clearance. They also vary approximately as diameter cubed for geometrical similarity. Thus equation (10.10) may be used with a geometrical factor for considering operational methods.

10.4.10 Energy balance

The energy balance differs from that for single-screw machines, primarily because the customary metered feeding makes output independent of screw speed, so that these factors must be considered separately. For the same reason the specific power E/Q has only the same significance as power E when Q is predetermined by the operator.

The variation of energy balance with temperature at constant screw speed and output resembles Fig. 8.10 for the single screw, except that generally the power input from the screw E will be smaller, so that a greater proportion of the energy comes from barrel heating H. The lower output from a given size of machine may well mean that heat losses S become proportionately greater. This is indicated in Fig. 10.17, which suggests that low melt temperatures may be readily achievable, while high temperatures may be limited by heater power or heat conduction through the barrel.

At constant output and temperature the internal energy I and losses S will be independent of screw speed. Provided the speed is sufficient to give an output capacity Q_c greater than the actual output Q, an increase in speed N will reduce the number of filled flights N_f so that:

$$\begin{aligned} E &\propto \eta N^2 N_f \\ &\propto \eta N^2 \cdot \frac{1}{N} = \eta N \end{aligned} \tag{10.23}$$

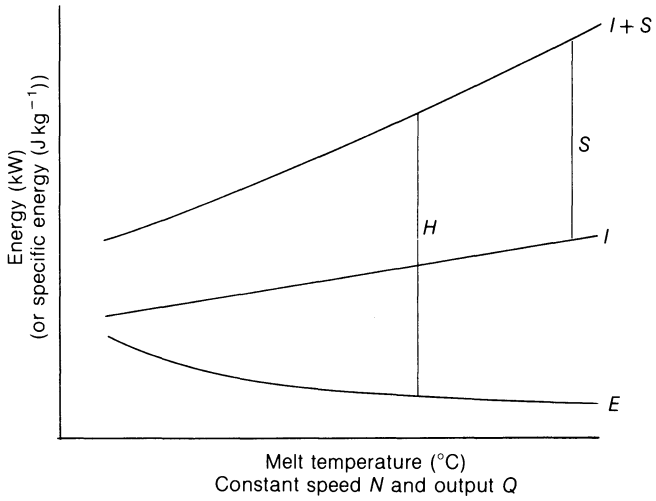


Figure 10.17 Change of energy balance with melt temperature: twin screw.

since $Q/Q_c \propto N_f \propto 1/N$. Then for a Newtonian fluid, power E is proportional to N, and for a power-law fluid $\eta \propto N^{n-1}$ and $E \propto N^n$. Figure 10.18 shows that as speed increases, motor power progressively increases and the heat required from the barrel decreases, though the adiabatic point is unlikely to be reached in practical operation; even then heat energy will still be needed to supply the losses.

If the feed rate is increased at constant screw speed and temperature, the internal energy I increases in proportion. The die pressure will also rise, as will

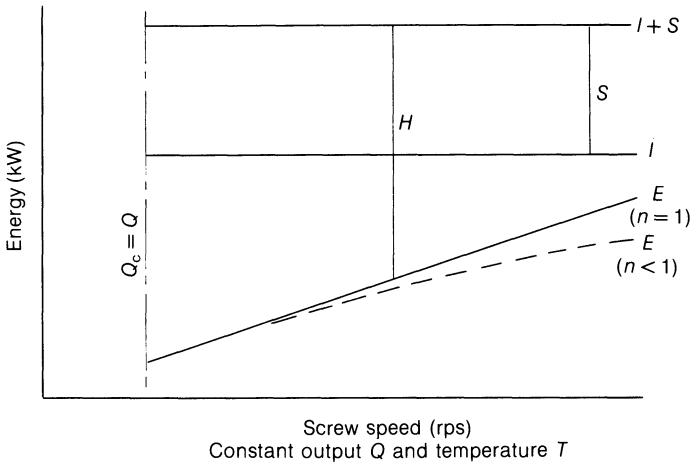


Figure 10.18 Change of energy balance with screw speed: metered feed.

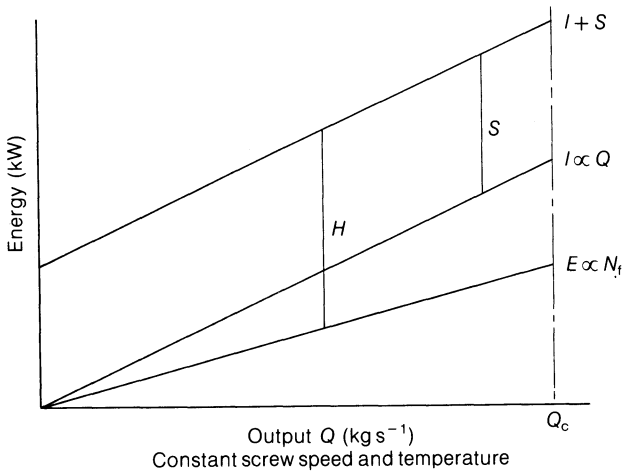


Figure 10.19 Change of energy balance with output: metered feed.

the number of filled flights N_f and the mechanical power E to the screws, until the whole of the pumping section is running full ($Q = Q_c$), when further increase becomes impractical. The power E will be less than the internal energy I because the melting process depends primarily on conducted heating, and otherwise the melt temperature would tend to rise above the stipulated value. Thus as feed rate is increased, the power E will rise, but so also will the heating H. This is represented in Fig. 10.19. Of the other variables, increasing die pressure by changing the die will result in a greater filled length and consequent increase of power E. This will be represented on Fig. 10.17 as a general raising of the power line E, and on Figs 10.18 and 10.19 by an increase in the slope, reducing the external heating required. If the viscosity of the polymer is increased, e.g. by changing grade, this will increase the die pressure, but also the screws' capacity to raise pressure, so that there should be little change in the filled length. The power equation shows that increased viscosity will increase power E in proportion, with similar effect on the energy balance to that of changing the die.

The decoupling of output and screw speed by metered feeding gives more operational variables than in the single screw, just as there are more dimensional variables in the screw design, e.g. pitch, depth, tip width, conjugation. However, the author's impression is that the range of satisfactory operation is more restricted, supporting the claims that twin screw machines are best designed for a specific process and set of conditions, with which they perform very adequately. This is facilitated by the common use of segmented screws, which can readily be changed for a different polymer, process or operating condition, though entailing high initial cost. The operator's task is then to run the machine as nearly as possible to those conditions predetermined by the design of screws, etc.

10.5 COMPARISON OF MACHINE TYPES

A comparison of machines is not the main objective of this book, but a summary of the principal differences may be useful where a choice of machine is possible for a specific purpose. The following comments should be read in conjunction with Table 2.2, which outlines the requirements of several processes. In Table 10.2 the main features of single- and twin-screw extruders are compared. The performance of the former is detailed in Chapters 6–8, while the latter is described in sections 10.3 and 10.4. Although mechanical design is outside the scope of this book, the complicated screw geometry and critical clearances of the twin-screw machine require precise and costly manufacture, the bilobed barrel is more liable to distortion from pressure and thermal stresses than the cylindrical barrel of the single-screw extruder and limited distance between screw axes causes problems in achieving robust screw drives and thrust bearings. It would be wrong to imply that the twin-screw

Table 10.2 Comparison of single- and twin-screw extruders

	Single-screw	*Twin-screw*
Flow type	Drag	Near positive
Residence time and distribution	Medium/wide	Low/narrow (useful for reaction)
Effect of back pressure on output	Reduces output	Slight/moderate effect on output
Shear in channel	High (useful for stable polymers)	Low (useful for PVC)
Overall mixing	Poor/medium	Good (useful for compounding)
Power absorption and heat generation	High (may be adiabatic)	Low (mainly conductive heating)
Maximum screw speed	High (output limited by melting, stability, etc.)	Medium (limits output)
Thrust capacity	High	Low (limits pressure)
Mechanical construction	Robust, simple	Complicated
First cost	Moderate	High

extruder is unreliable, but the foregoing entail high manufacturing cost and greater care in operation and these must be considered in any comparison such as Table 10.2, along with performance features.

The internal melt mixer (e.g. the Farrel-Bridge 'Banbury'* and Shaw 'Intermix'†) is essentially a batch mixer not intended for direct shaping operations and requiring very different ancillary equipment and method of operation. It is very robustly constructed and capable of very high power inputs, usually controlled by rotor speed and external pressure confining the polymer, leading to high shear stresses and rapid temperature rise. Batch operation permits accurate feeding and proportioning of additives by batch weighing, and automatic weigh/feed systems are eliminating errors due to manual feeding as well as providing a reliable record for quality control. However, the batch output is not often in quantities appropriate to downstream batch processes and storage, on roll mills or heated hoppers, is necessary to give a continuous output in other cases; indeed special hot-fed single-screw extruders (slabbers) have been used for continuous granulation or strip extrusion, but not usually for shaping the finished product. The kneading action in the space between the rotors is much more predetermined, largely by initial rotor design, than the flow in the single-screw channel, and this probably also makes the shear over the rotor tips less random than in the extruder; in any case, the mixing time is independently controllable to give a high probability that the whole batch has been subjected to the higher shear stress. The latter is effective in dispersing pigment agglomerates and takes place at the barrel surface so that energy removal and temperature control are facilitated, where

*The Farrel Corporation, Ansonia, Connecticut, USA.
†Francis Shaw and Co. Ltd., Manchester, UK.

heating/cooling may be programmed throughout the cycle. One of the benefits of batch operation is that severe shear may be imposed without excessive temperatures by a combination of heat build-up from the cold polymer and the heat capacity of the machine scantlings; power may be applied for, say, 2 min in each cycle, whereas cooling can be maintained for the complete cycle time of, say, 5 min. The internal melt mixer is thus very effective for dispersing pigments as well as melt blending and intentional degradation, e.g. raw natural rubber mastication; the single-screw extruder requires a preceding high-speed 'intensive' powder mixer or granular masterbatch for the former, while heat and temperature control are problems for the latter. The twin-screw extruder is an effective mixer, but both types have comparatively short residence times which limit the scale of mixing and depend on the feeding device for large-scale uniformity.

Various patented designs of continuous mixer have been developed to give the advantages of the internal mixer coupled with a continuous output. They usually consist of a pair of rotors in a jacketed chamber similar to the internal mixer, with a screw feeder, e.g. on one end of the rotors, which determines the throughput rate. Feeding may then be by gravity, requiring continuous or semi-continuous metering of additives. In this case, rotor speed is no longer available for power control since it is not independent of output, and back pressure by means of a valve is used. However, this would affect flow to a die, making problems for direct shaping. At high outputs, the surface area for cooling is limited, so restricting the level of energy input; the possibility of differing times for energy input and removal no longer obtains. Such machines are no doubt efficient mixers, but in the author's opinion do not constitute a complete compounding-shaping process or compete with the screw extruder for those shaping processes which require a modest amount of distributive mixing.

The ram extruder is mechanically simple and robust and is appropriate where very high pressures are required as in hydrostatic extrusion, extrusion of PTFE, and injection moulding. For the first two, the operation can be made continuous at the expense of complication by using two extruders alternately with a changeover valve. Since little flow takes place in the cylinder, heating is by conduction, and therefore is slow and involves temperature differences in the polymer, especially since diameters tend to be large to extend run length. As mentioned on p. 24 in connection with injection moulding, the sequence of flow from the cylinder is complex, so that initial temperature differences will be redistributed in passage through the die. High shear stresses and shear strain are unlikely to occur before the die entrance, so little mixing for temperature or composition will occur. If the usual direct extrusion is employed (force applied to a piston at the rear of the polymer charge) then the pressure at the die will tend to rise as the wall friction decreases due to the diminishing length of the charge, and there will be losses due to mechanical inertia and friction and stored elastic energy in the slightly compressible polymer. The ram extruder is thus an efficient but intermittent pump, but fulfils none of the other functions of the screw extruder, e.g. feeding, melting, mixing, venting and temperature

control, which are exemplified in the injection moulding machine, where the screw carries out all except the final pumping function.

In an unusual design, instead of running as a helix on a thin cylinder, the long narrow channel is wrapped as a spiral on a disc, running against a smooth disc, the flow taking place radially inwards or outwards. The functions of solids feeding, shear melting and melt pumping with a degree of mixing as in the single-screw extruder may be expected to take place. Unless the spiral contains as many turns as the conventional screw, the pressure difference across the flights between two turns will be greater, so leakage flow will be greater. The axial thrust between the discs will be large, especially if flow is outward, being the integral of pressure over the whole disc area, as compared with the conventional, in which it is the die pressure times the barrel cross-section; any lack of mechanical rigidity will increase the flight clearance and leakage. Note that for a constant drag flow along the length of the channel (equation (6.9)), the velocity W increases proportionally with radius, so width b or depth h must decrease. In the former case, where shear rate increases with radius, the wide-channel assumption may be invalidated and manufacture will be difficult; in the latter case, shear rate increases as the radius squared and shear heating as the fourth power of the radius. Perhaps the greatest practical disadvantage is the small physical distance (radially) between inlet and outlet, making the maintenance of substantial temperature differences difficult, and reducing operational flexibility.

A variation of the conventional single screw forms the channel on a cylinder of large diameter and shorter length.* This gives a lower rotational speed for the same shear rate, a smaller helix angle and higher shape factors F_D and F_P (McKelvey, 1962, p. 236) and a torsionally stronger screw. However, it involves a greater axial thrust at a given die pressure and the reduced length may give control problems in maintaining axial temperature differences. Other proprietory designs have been mentioned in the discussion of compounding (section 2.2.1), for which purpose they are often specifically intended.

A design apparently similar to the spiral disc extruder, but different in principle, is the smooth disc extruder, widely referred to in the literature under various titles including the Weissenberg extruder and the elastic melter. This is claimed to work on the elastic properties of the melt, typified by the 'climbing rod' phenomenon. It consists of a smooth disc rotating close to a similar stationary disc, which pumps material from the circumference towards the centre, where a die may be fixed. The author's experience is that this design did indeed melt polymer very rapidly, but that the final melt temperatures were highly non-uniform. Some assistance with solid feeding seemed necessary (possibly a force-feeder or a short spiral flight would assist) and the pressure generated was modest (less than $1\,MN\,m^{-2}$). To overcome the latter, a conventional screw extension has been proposed to generate pressure, but it is doubtful whether the temperature inhomogeneity would be sufficiently reduced. Separate control of the disc and screw speeds would further increase

*Frieseke u. Hoepfner GmbH, Erlangen-Bruck, Germany.

11 Extruder operation as part of a total process

In Chapter 2, the principles of several commercial extrusion processes have been described together with broad indications of the performance each requires from the extruder. In Chapters 9 and 10 the performance of single- and twin-screw extruders has been discussed together with the changes expected from intentional changes in the operating conditions. Since some form of die is always involved, this has been assumed to be fixed in dimensions by the remainder of the process. Note that if comparisons between machines or conditions are made on the basis of, say, constant pressure, very different conclusions will result. In Chapters 9 and 10, the discussion centres on steady-state conditions and parameters such as output, pressure, energy, temperatures and mixing; and small changes in these which may be brought about by altering the running conditions. In this chapter, an attempt will be made to see how these may be applied to meet the conditions and requirements of complete commercial processes, and this introduces additional factors such as stability and fluctuations, transients when conditions are altered, and methods of control. Scale-up is also considered in some detail, being an important step in establishing a new process.

11.1 QUALITY

Up to this point attention has been concentrated on physical quantities which can more or less readily be measured. For commercial products, however it is not sufficient to obtain a given mass flow rate at given conditions of temperature, pressure or energy input; the concept of 'quality' is rather intangible but very necessary in determining satisfactory operation. It cannot be overemphasized that one or other aspect of quality in the product is almost inevitably the limiting factor on output, rather than physical limits as such.

Many theoretical studies neglect quality and so are of limited value. Concepts of efficiency and optima which ignore the limits imposed by quality are also largely irrelevant. The theory presented in Chapters 6–8 and 10 is deliberately simplified to reveal changes in the overall performance until more exact mathematical models are interpreted in an equally comprehensive representation of the real situation.

So what is quality? In a finished product it involves uniform composition of polymer and additives on both microscopic and macroscopic scales; the required macromolecular structure, including crystalline form and extent, orientation in direction(s), distribution and extent, and residual strain; correct and uniform colour, appearance, surface texture and optical properties; the required combination of mechanical, electrical and chemical properties and their distribution, absence of visual and mechanical defects such as die lines, ripples, sinks, voids, cracks, crazing, warping, residual stress concentrations, dirt, gels, fisheyes, and pigment agglomerates. Even though not all of these may apply in a particular product, satisfactory quality represents a difficult target which may inadvertently be lost through process changes. Certain properties will depend largely on correct and consistent feed material, e.g. mean molecular weight, mean pigment and additive levels. Others, given correct feed material, depend heavily on post-extrusion operations such as drawing and cooling; these include crystallinity, orientation and surface texture. It is therefore desirable to define quality at the die, where it is largely a function of the extrusion process. These properties may be modified subsequently, but correct and uniform post-extrusion processes will depend on properties, e.g. uniform flow velocity and temperature, at the die. The following definition of quality of extrusion is proposed:

- Constant flow rate Q and pressure P
- Uniform and constant melt temperature, especially the absence of unmolten material
- Uniform and complete mixing of polymer constituents and additives
- Correct shear history, e.g. maximum for film-grade LDPE, medium for degradation of PP, minimum for compounding of PVC, and minimum for reducing elastic defects.

Mechanisms of mixing in the screw(s) have been discussed previously (sections 2.2, 9.1 and 10.4). In summary, the scale of mixing is limited by the rather small volume of the screw channel, and the scale will further decrease with the residence time as output is increased. A fair degree of distributive mixing, e.g. of masterbatch and base polymer having similar density and viscosity, is achieved in the single-screw channel, though not uniformly. Increased back pressure increases relative mixing velocities while reduced temperature increases the resultant shear stresses. Increasing speed reduces the time for mixing. High shear stresses necessary for dispersion of pigment agglomerates or mechanical chain scission only occur over the flight clearance,

involving randomly a small proportion of the flow and thus likely to be incomplete and energy-inefficient. In the twin-screw extruder, distributive mixing occurs within and between the channels. Dispersive mixing also occurs more uniformly where the flights of the two screws overlap.

11.1.1 Temperature variations

Temperature variations have been included in Tables 9.2–9.9, based largely on a qualitative understanding of changes in the melting process and the mixing effect in the melt pumping section. It is a matter of experience that as screw speed is increased, a point is reached beyond which the flow in the die becomes increasingly unstable, also that this is less likely to occur, or only at higher speed, with longer or shallower screws, other set conditions being equal. With increasing length the effect is likely to be small while with a shallower screw it is almost certainly at a lower output per revolution. The instability may be due to melt fracture or surface defects arising in the die or due to the onset of surging in the screw (section 11.2). In the limit, the outline of granules may be observed, or with powder feed a stream of opaque unmelted or partly melted powder may be encapsulated in a sheath of translucent melt. Such conditions will obviously give unsatisfactory drawdown and mechanical weakness, especially brittleness, in the product, but the unmolten material may exist along with molten polymer whose average temperature is well above the softening or crystalline melting point. As discussed in Chapter 7 and section 9.1, the solid material usually results from a gross break-up of the solid bed in the melting section and the subsequent mechanism of melting in the pumping section (which is almost pure conduction) is slow. However, the molten portion may simultaneously be heated both by conduction and internal shearing, giving considerable spatial difference in temperature of the polymer emerging from the die. Even at lower speeds or higher back pressures where unmolten material does not appear at the die, temperature variations may be sufficient to distort flow in the die and give unstable conditions in post-extrusion operations. Possible origins of these temperature variations include:

1. non-uniform temperature at end of melting section (break-up of solid bed) within melt and semi-molten solid;
2. conductive heating from/to the barrel wall;
3. internal shear heating within the melt pumping section;
4. heat transfer to the screw;
5. heat and mass transfer from polymer sheared in flight clearance.

The mechanisms tending to reduce temperature variations include:

1. transverse circulation in the channel (Fig. 6.7);
2. relative longitudinal velocities in the channel (Fig. 6.6);
3. thermal conduction within polymer in the melt pumping section (including remaining solid particles);

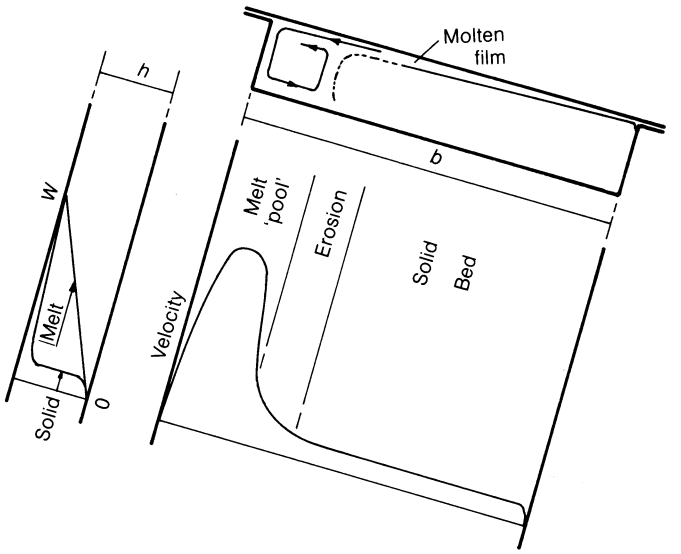


Figure 11.1 Velocities in melting section.

4. local multiaxial and overall longitudinal thermal diffusion in the barrel and screw metal;
5. preferential shear heating (see above) of a more viscous element where shear *rate* is defined.

Considering the possible origins first:

1. At the break-up of the solid bed this should occupy a relatively small proportion of the channel cross-section, leaving the melt in the remainder to follow flow patterns (Fig. 11.1) similar to Fig. 6.6(c), since usually little pressure is generated, and Fig. 6.7, and undergoing considerable mixing. In the melting region, the screw temperature is unlikely to be above the melting point or the solid bed would become detached, nor is it likely to be much below the melting point or the initial film of melt would refreeze when collected by the flight, and so fail to pump forward; hence little heat transfer is likely to the screw in the melting section. The barrel temperature is also unlikely to be below the melting point or a molten film would not form. Thus it would appear that any temperature differences within the molten portion will tend to be removed by mixing and that they will be minimized by keeping the barrel temperature in the melting section as low as possible without 'freezing' the polymer and causing excessive torque. In this case the mean temperature of the molten portion will also be as close as possible to that of the remaining solid portion. Low barrel temperatures will tend to minimize temperature differences due to conducted heat flow H_M, which

will also be small, giving slow melting; much of the energy for melting will come from internal shearing E_M, though this may also create temperature non-uniformities. The melting process is therefore likely to occupy a greater length of screw, giving a lower but more uniform temperature approximately equal to T_M at the end of the section and probably delay break-up of the bed, leaving smaller solid particles nearer to their melting point T_M.

2. The total conductive heating H_P from the barrel will be a function of the increase of polymer temperature from melting $\approx T_M$ to the end of the pumping section T_m and the radial temperature gradients in the polymer to achieve this will be inversely proportional to the length of the melt pumping section L, i.e. low final melt temperature and long pumping sections will favour temperature uniformity.
3. Internal shear heating and changes in its distribution with back pressure have been discussed in section 8.4 (Fig. 8.5). It will be noted that the maximum shear heating occurs near the barrel, where the downchannel velocity w is greatest, giving minimum residence time, but the transverse velocity u, giving mixing, is also greatest. Severe shear heating, e.g. with high back pressure, will therefore tend to increase temperature variations, though this will be minimized by low viscosities implied by high final melt temperatures.
4. Heat transfer from the polymer to the screw will tend to lower the polymer temperature near the screw, adding to the variations caused by shear heating. Note that the polymer velocities along and across the channel are small close to the screw, so little mixing will occur. (A similar effect has been noted experimentally in twin-screw machines – see p. 325.) If forced cooling of the screw is used, e.g. by circulating water, it will cause local cooling of polymer which cannot be dissipated by mixing. Further, unlike against the barrel, freezing can occur without direct effect on screw torque, and the indirect effects of this on output, velocity distribution, shear rates and energy input will be much greater than the direct effect on temperature variations.
5. As discussed in section 8.4, considerable energy is dissipated in shearing a small volume of polymer in the flight clearance; this will be affected by screw speed and shear rate/viscosity characteristics of the polymer. However, it will also be dramatically affected by barrel temperature; if the latter is high, the shear energy will be low but so will local heat diffusion into the barrel ((4) of reducing mechanisms). If barrel cooling is applied, local heating will diffuse within the barrel wall but also the local viscosity will be maintained which causes heat generation. Heat diffused within the barrel will raise the average wall temperature in the region and also be conducted longitudinally to cooler parts of the barrel (and possibly the die). Due to shearing in the flight clearance, this small proportion of the polymer will have a higher than average temperature which when mixed with the polymer in the channel will raise the latter's temperature, especially near the barrel where the leakage flow enters. As observed under (3) this will tend to increase temperature variations before the die.

Of the mechanisms tending to reduce temperature variations:

1. Transverse circulation (Fig. 6.7) will tend to reduce temperature variations by mass transfer, and since velocities are not uniform, by mixing, i.e. bringing closer elements which because of their initial position have different temperatures, and so promoting conduction between them. As mentioned earlier, note that there is a position in the channel depth where there is no lateral velocity, and Fig. 6.6(b) shows that at high back pressures this position has only a small downchannel velocity, and so will experience little mixing.
2. The relative longitudinal velocities, especially at high back pressure (Fig. 6.6), provide a degree of material mixing. In the absence of longitudinal temperature gradients this will not reduce lateral variations in temperature. In this respect it assists the transverse circulation in transmitting heat conducted from the barrel and generated by shear near the barrel throughout the channel cross-section, but as noted in section 6.2, the resultant velocity is never rearward in respect of the screw axis, and therefore does not convey heat in this direction, as does longitudinal conduction within the barrel wall.
3. Thermal conduction within the polymer is the most obvious mechanism for reducing temperature variations, but depends on these variations for its existence, so is self-extinguishing. Evidently the effect will increase with length of melt pumping section, with reduction in channel depth and with increase in residence time (reduction in output).
4. As discussed, local diffusion in the barrel will diminish extreme local temperature variations in space and fluctuations in time, e.g. due to movement of the screw flight. Overall longitudinal conduction will tend to reduce axial temperature gradients in the barrel, and to some extent in the polymer, compared with the set heater temperatures, so in a heating situation the polymer will tend to be heated earlier, with smaller temperature gradients towards the die.
5. In a system subject to constant shear stress, such as a suspension or a simple lateral temperature difference (equation (3.57)) the greater shear rate and hence shear heating occurs at the position of the lowest viscosity (e.g. highest temperature) tending to reinforce the temperature difference. However, where the shear *rate* is defined, as in the melting section (neglecting the molten film) where two streams of different viscosity are side by side, the greater shear stress in the stream of higher viscosity gives greater shear heating tending to reduce the temperature difference. This is unlikely to occur in the melt pumping section.

This it appears that conditions tending to minimize space variations in final temperature are long screws and low outputs and to some extent shallow channels; on balance, small longitudinal temperature gradients and low melt temperatures are probably beneficial, while the lowest feasible barrel

temperatures in the melting section will tend to minimize the temperature variations originating there. This suggests a set barrel temperature profile similar to 3 in Fig. 9.6, especially if final melt temperatures much above the softening/melting point are required. The step in temperature will be difficult to achieve, as would a form of construction which included longitudinal insulation to assist the temperature step; this emphasizes the importance of knowing the position at which the polymer effectively becomes a melt, and recognizing that this position changes with output, back pressure, etc.

Experiments carried out by the author to determine factors affecting temperature variations, admittedly not precisely controlled for operating conditions, used a 50 mm extruder with a 50 mm diameter barrel extension beyond the screw leading to an adjustable die. The first stage was to assess the reliability of temperature measurements; a 3 mm Pyrotenax* thermocouple was placed at the centre of the extension and a simple thermocouple was welded to the metal wall. The extruder was run in conditions expected to give considerable radial temperature variations and readings were taken with various levels of heating to the barrel extension. It was found that at 25 mm distance, the immersed thermcouple tended to follow the indications of the wall thermocouple, rather than the melt. When the barrel extension was unheated but lagged externally, relying on heat conducted axially from adjacent sections, its temperature appeared to be unrelated to that of the immersed thermocouple, either higher or lower depending on extrusion conditions; while not a proof of accurate absolute indication of temperature, the differences caused by changes in conditions should be at least approximately correct. An array of thermocouples 50 mm downstream of the screw tip was then arranged at various radii, together with a single couple adjustable over the full range (Fig. 11.2). The extruder was operated on LDPE at screw speeds from 20 to 100 rpm. Three screws of 16:1 L/D ratio were used: constant depth 6.3 mm ($\frac{1}{4}$ in); uniform taper over 16 diameters from 9.5 to 3.2 mm ($\frac{1}{8}$ in) – 2.6 : 1 compression ratio; 10 diameters' taper from 9.5 to 1.6 mm ($\frac{1}{16}$ in) plus 6 diameters at 1.6 mm ($\frac{1}{16}$ in) deep – 5.0 : 1 compression ratio. It was found that, when running, the adjustable thermocouple agreed at all times within 1 °C with the fixed couple at the same radius, including that at the wall. Each screw was found to give a characteristic profile of temperature, that for the first screw being hotter in the centre with a gradual fall to the wall, and for screw 3 being hotter at the wall and falling to the centre. Screw 2 showed a 'moustache' profile with higher temperatures at both wall and centre and a lower temperature at mid-radius. At 20 rpm the variations with screws 1 and 3 were about 5 °C and with screw 2 about 2 °C. As speed was increased, all three screws retained their characteristic profiles, but increasing in magnitude until at 100 rpm screws 1 and 3 showed overall variations of as much as 50 °C, with about 30 °C for screw 2. Because of the mass and response time of the

*BICC Pyrotenax Ltd, Hebburn on Tyne, UK.

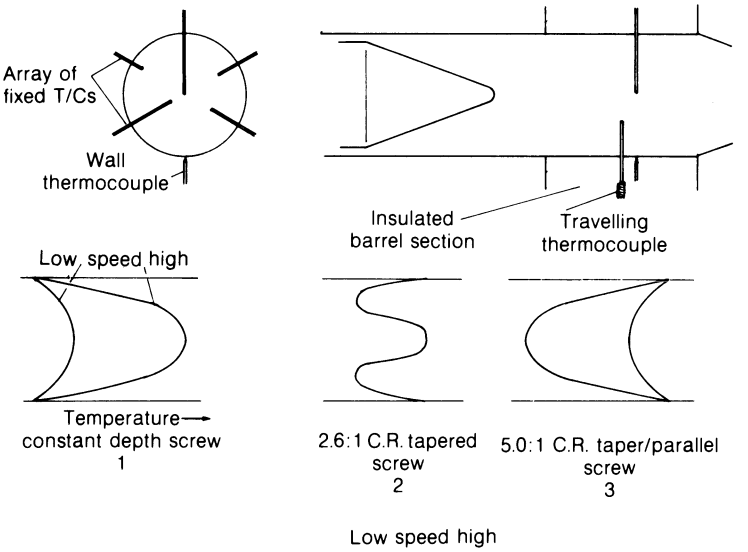


Figure 11.2 Radial temperature profiles at end of screw.

thermocouple, these readings represent time-averaged temperatures; a colleague obtained readings on a similar machine with fast-response couples and recorder and showed rapid time fluctuations of temperature of the same order of magnitude in apparently steady operation – see also Tadmor and Klein (1970) and p. 362. These results must be treated with caution; in some respects such as the effect of speed they agree with the foregoing theory but it is noticeable that variations with the shallowest screw (3) are greater than with screw 2, possibly due to excessive shear heating in the metering section.

Marshall, Klein and Uhl (1965) have also detected time variations of temperature, but show clearly that variations arise in the melting section and tend to be reduced in the melt pumping section. They also show that these variations increase considerably with screw speed and the subsequent reduction takes a greater distance, resulting in an increased residual variation at the end of the screw. These results do not of course separate the effects of the various mechanisms discussed in this chapter.

11.2 STABILITY

In addition to the limits set on the useful output by inadequate mixing and excessive temperature variations, a limit is frequently imposed by unsteady flow or 'surging' causing variations in product dimensions, drawdown, cooling and consequently in product properties. These usually occur, or only become

significant, at high screw speeds and outputs. Slow variations may arise outside the machine itself due to bridging in the feed hopper, erratic filling of the screw or switching of heater controls; the last occurring especially with time-proportioning controllers, characteristically over a period of 10–20 min. Modern proportional controllers avoid this, but inspection of the 'fast cycling' control suitable for resistive heating will often show a periodic variation in the power input over periods usually less than 1 min. This can be minimized by adjusting the 'power' limit until the load indicator light flashes at a constant frequency. Excessive deadband or overshoot in the control, or heat capacity in the barrel, can increase the temperature oscillations. Autogenous operation might be expected to improve temperature stability, since heat flows through the barrel are at a minimum. However, reversal of temperature gradients and the heat capacity of the barrel material, as well as the difficulty of controlling liquid cooling at low levels, must modify this. One approach is the energy-inefficient method of maintaining more or less constant air cooling and switching heaters to balance heat requirements. With correctly placed thermocouples and modern controllers a good compromise is to work slightly below the autogenous speed or above the autogenous temperature so that a small but continuous heat input is required.

It will be noted that the equations for flow and pressure (equations (6.15), (6.53) and (6.58)) are linear and thus their solution, represented by the operating point, e.g. A or B in Fig. 6.18, is single-valued. Equation (8.9) for mechanical power input E is linear in viscosity (temperature) and output Q, and thus single-valued (Fig. 8.10). Equation (8.29) shows that as back pressure is increased, the specific power input E/Q is a linear (reciprocal) function of Q/Wbh and therefore single-valued. It might appear from equation (8.9) that if Q is regarded as constant, two values of speed (proportional to W) will correspond to a given value of power E; however, Q and W are related (by the solution to equations (6.15) and (6.53)) and a single value appears if W and Q/Wbh are treated as independent variables, the latter being determined by pressure gradient $\mathrm{d}P/\mathrm{d}z$, or in a specific case by the die constant K. A double value of speed N occurs at which the heater input H has a given value (Fig. 8.12); it would appear that if the heater input was predetermined, an instability in speed N (and with it output Q and pressure P) could occur. In practice, the power/speed characteristic of the drive motor would inhibit this and the author has not observed this type of oscillation in experimental machines with constant heater loading. In the usual case in which heater input is controlled to give the required barrel temperatures there is thus no mechanism in the melt pumping section to cause instability. Thus the origin of surging is usually attributed to the melting section; in Chapter 7 this is due to periodic 'plugging' by the solid bed interrupting the melt pool. It has been observed previously that at given temperatures, the length required for melting increases with speed N (and output Q). A reasonable deduction from this is that, at a given speed and temperature, a shorter melting length will correspond to a lower rate of

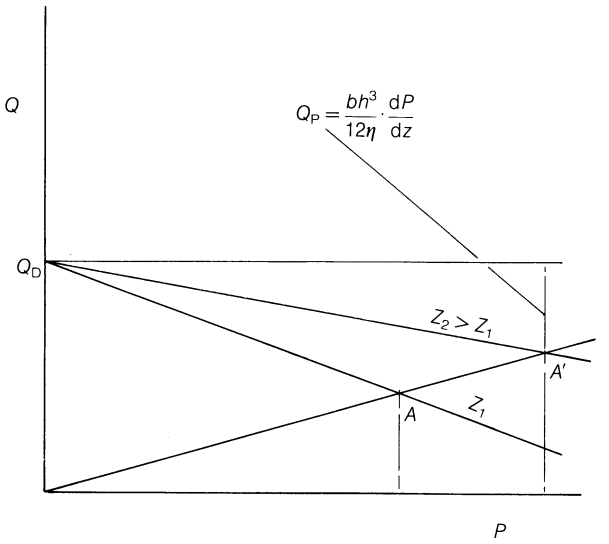


Figure 11.3 Effect of melt length on output.

melting. For the melt pumping section, Fig.11.3, which is derived from Fig. 6.18 and equation (6.15), shows that as pumping length Z increases, so do output Q and pressure P. In stable conditions, melting length plus pumping length is constant and $Q_{\text{melting}} = Q_{\text{pumping}}$. However, supposing for a short time the pumping rate exceeds the melting rate, the difference can only be supplied by partially emptying the screw channel at the start of the pumping section (section 6.6). Where the channel is no longer full, no pressure can be raised, and the start of the effective pumping section moves forward towards the die. As it does so, the pumping rate (and pressure) will fall, in some cases to zero, so that it is less than the melting rate. The excess melt now begins to refill the channel, and the greater length available increases the melting rate. As the channel is refilled with melt, the pumping length again increases, as do the output and pressure, so reducing the length for melting and hence the rate. When the pumping rate again exceeds the melting rate, emptying of the channel will recommence and the cycle be repeated indefinitely. Because of the melt capacity of the screw channel and the time required for additional melting to refill it, this cycling takes a finite time. It tends to increase in both frequency and severity with increasing screw speed and the author has found the period to be typically 5–15 revolutions of the screw, which corresponds roughly to a displacement equal to the volume of the melt pumping section; in extreme cases the output has temporarily ceased completely, but recommenced with apparently completely melted polymer. It is claimed that with stepped screws, the gel point is virtually predetermined by the rapid change of channel depth; it is true that if the pumping length exceeds the 'metering'

length, the excess will contribute little to the total pressure (Fig. 6.10 at low Q/Wbh) and therefore an approximate maximum output and pressure is fixed; however, this will reduce the length for the melting process and at the other extreme the effective length and output of the metering section can still be reduced by partial emptying. Surging can occur with stepped screws and this is colloquially explained as the metering section pumping itself empty and then waiting until the melting process (in this case said to be mainly by conduction) refills it so that pumping can recommence. Evidently in this case melting rate will be a positive function of the available length (barrel surface) and of the temperature difference between barrel and polymer, suggesting high temperatures in the melting section. Where melting is substantially by mechanical shearing, as is believed to be the case with the polymers for which tapered screws are suitable, low barrel temperatures and high mechanical power input should increase the rate of melting (see Table 9.8), delay break-up of the solid bed, and reduce the incidence of this type of surging.

Kirby (1962) has deduced an equation for the stability of the melt pumping section to an external disturbance, and Fisher (1976) concludes that an increase in die pressure or increase in melt pumping length will improve stability. While agreeing with these conclusions, Appendix D suggests Kirby's equation also indicates that a decrease in channel depth will improve stability; these changes do not of course remove the cause of instability. As mentioned in sections 6.5 and 6.6, the second portion of conventional vented screws is often subject to surging, due to the nonlinear change in pumping rate with degree of filling and also possibly due to intermittent flow of polymer in the section under the vent, and here also a decrease in final channel depth appears to reduce surging.

Tadmor and Klein (1970) quote interesting experimental results on time fluctuations of temperature and pressure and remark that

> a good correlation between pressure and temperature fluctuations implies that temperature fluctuation is the source of the problem and flow rate may be steady, while if a pressure fluctuation exists without a temperature fluctuation, it is almost certain that it will be accompanied by a flow rate fluctuation.

The suggestions under the heading 'Improve melting' in Table 9.8 may therefore help to minimize this source of surging, while the factors mentioned above should reduce the consequences; increasing length, in particular, will also help to reduce temperature fluctuations and variations at the end of the melt pumping section (see pp. 291 and 357).

Although strictly outside the extruder, the stability of the drive system will also affect the extruder performance. Figure 8.12 and equations (8.7) and (8.16) show that at constant temperature the power absorbed in the melt pumping section of the screw increases somewhat more than in proportion to its speed, depending on the shear rate/viscosity characteristics of the polymer.

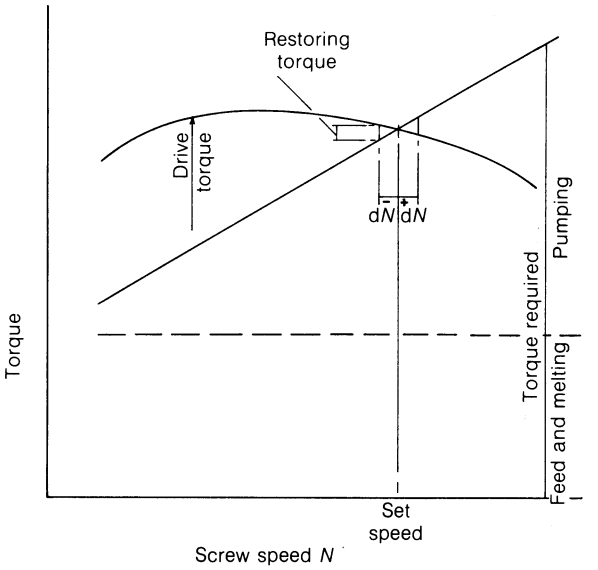


Figure 11.4 Speed stability of drive.

Thus torque on the screw from this source, proportional to E/N, will increase with speed, linearly for a Newtonian fluid. The total torque will therefore also increase with speed, since that due to feeding and melting will at least be constant (power proportional to speed). Except at low speeds (e.g. with an AC commutator motor), the torque/speed characteristic of electric motors usually droops, while the torque of hydrostatic motors is essentially constant. Thus if speed falls below the set value (Fig. 11.4), an excess torque is available to accelerate, while a speed increase due to, say, a temporary load reduction leads to torque deficiency tending to reduce speed, creating a stable system. With the usual high-speed motor driving through reduction gearing, there is appreciable rotational inertia tending to damp out such speed fluctuations. For applications requiring very stable speed, despite variations in extruder demand, thyristor controls for DC shunt motors with tachogenerator feedback are available up to several hundred kilowatts and increasing degrees of sophistication (and cost) for improved speed-holding down to 0.25% from zero to full load.

11.2.1 Start-up and condition changes

So far stability has been considered in nominally steady conditions. The speed-holding mentioned above would not be achieved instantaneously for such a large change in load. Thus at start-up or when deliberately changing speed, short-term transients may cause overload; provided they are of short duration

the motor will not be harmed and flexibility in couplings and belt drives will cushion the effects, but even momentary excess torque may damage the screw or drive shaft, for instance if solid material jams in the feed.

Gradual start-up and changing of conditions is discussed in section 12.3; here it is only necessary to mention that changes in pressure influence output almost instantaneously and power a little more slowly. Temperature equilibrium may be reached in 10–20 min on a small machine, but takes an hour or more on a larger or slow-running machine. Response to speed changes is only slightly slower than to changes of pressure, but the major changes in energy balance shown in Fig. 8.12 mean that temperature equilibrium may take longer than with change of pressure. Changes in set temperatures are usually the slowest to take effect and stabilize, partly because of thermal capacity of the extruder structure, partly due to changing ambient losses and partly due to changes in the mechanisms of melting. Limited heater power will slow temperature increases and temperature controllers must compromise between rapid warm-up and minimum overshoot. However, the slowest change is often in longitudinal temperature gradients, e.g. if the set point of one heating zone is changed in relation to neighbouring zones. With experience, such changes can be achieved quickly with minimum transients, but it must be realized that large changes will usually cause a temporary imbalance in the many mechanisms and interactions described in Chapter 9, and these will sometimes be in an opposite sense to that desired.

While modern temperature controllers respond quickly and smoothly to changes in requirement, they are limited by the system to which they are connected; the requirements for rapid start-up and stable running may be conflicting and, in particular, the maximum heater power used for heating up may be excessive for stable for control – it may be desirable to reduce power when running (e.g. by manual adjustment of the power limit on the controller) or consult the controller manufacturer for optimum settings of the differential term (for overshoot) and proportional band (for power limitation).

11.3 SHEAR HISTORY

The remaining criterion of quality at the die (p. 353) is the correct shear history. This may broadly be defined in terms of the units of shear strain experienced by the polymer although it has been remarked previously (pp. 19 and 64) for certain processes, such as dispersion of pigment agglomerates and polymer chain scission, that a threshold level of shear stress is required to produce any significant effect, regardless of the time of shearing. In such cases the definition might be modified to 'the units of shear strain at or above the threshold stress'. The shear strain is the integral of the product of shear rate and time:

$$\text{shear strain} = \int_{t_1}^{t_2} \dot{\gamma}\, \mathrm{d}t \tag{11.1}$$

Ideally this will be the same for each element of volume, so that even though the shear rate and the time for which it is experienced may both vary with position in the screw, all elements are subjected to the same pattern. This is evidently not true in the single-screw extruder; consider the longitudinal velocity w, which in the drag flow varies uniformly from zero at the screw to W at the barrel (Fig. 6.6) so that shear rate $\mathrm{d}w/\mathrm{d}y$ is constant. However, neglecting movement in the y direction (radially), the residence time in a given melt length will be Z/w_y, varying from Z/W to infinity. Thus at y from the screw root:

$$\begin{aligned} \text{shear strain} &= \dot{\gamma}_y \, \mathrm{d}t \\ &= \frac{\mathrm{d}w}{\mathrm{d}y} \cdot \frac{Z}{w_y} \end{aligned} \tag{11.2}$$

and this has the hyperbolic distribution:

$$\frac{Z}{h} < \frac{WZ}{hw_y} < \infty \tag{11.3}$$

Figure 6.7 shows that both transverse velocity and shear rate are nonlinear; at the position of maximum (rightward) velocity, the shear rate is zero so that at this position no transverse shearing is experienced, though presumably the same volume element undergoes considerable shear when moving leftward near the barrel. Thus the polymer in the channel is subjected to a wide spectrum of shear strain; if shear degradation is intentional, then some average is relevant, assuming that the final product is mixed to give acceptably homogeneous properties. Where degradation is to be minimized, then the maximum shear strain would be the correct criterion, but Figs 6.6 and 6.7 show that adjacent to the screw root the polymer theoretically has neither forward nor transverse velocity, indicating an infinite residence time; screw cooling will tend to increase the thickness of this stagnant layer. Traditionally, high back pressures are used to improve mixing, giving the maximum relative velocities in the longitudinal direction and greater residence time due to lower output; however, as pressure increases and $Q/Wbh \rightarrow 0$, the longitudinal velocity distribution of Fig. 6.6(a) is approached where a second point of zero velocity in both directions occurs. Thus, at high back pressures, a second layer experiences considerable shear rate in both directions, but a very long residence time. Further scatter of shear history is due to the small proportion of the flow subjected to very high shear rates for a short time in the flight clearance. This emphasizes that the single-screw extruder by itself is not very satisfactory for intentional shearing; the best conditions are evidently a long shallow metering section, low speed and fairly high back pressures giving low outputs. For heat- or shear-sensitive materials, such as rubbers and UPVC, short deep screws running at modest speed with low back pressures (which also minimize power input) are desirable and are in fact commonly used. The fact that the single-screw extruder performs reasonably well as a distributive mixer

suggests that there is some mechanism of mixing (not just circulation as at the flight faces, Fig. 6.7) in the y (radial) direction not revealed by the simplified flow analysis. If this mechanism is weak or does not exist, as suggested by striations found in microtome sections of extrudate (p. 20), there would be a case for radial mixing devices within the melt pumping section; otherwise it would be preferable to minimize shear strain in the screw and attach a mixing device, preferably giving uniform shear and residence time, and designed for the particular purpose and polymer in view.

Where severe shear is imposed by the extruder, this is dissipated in heat which increases the polymer temperature, reducing shear stresses and pressure gradients. If cooling is used to reduce temperature rises, this tends to increase power input and shear stresses and so be partly self-defeating. It also leads to distortion of temperature and velocity profiles (section 4.3 and Fig. 9.3) which militate against both cooling and homogeneity. If shear heating can be accommodated by temperature rise in the polymer, the extruder is a simple means of achieving it, but cooling of highly viscous materials is in any case difficult to achieve uniformly and the single-screw extruder is no exception. Where only a modest degree of shear is required, it must be accepted that this will not be uniformly distributed through the polymer mass and an acceptable level can only be achieved by trial. Tables 9.7 and 9.9 indicate how conditions favouring mixing and uniform temperatures can be obtained.

In the twin-screw extruder, residence time is more uniform and temperature is more dependent on external heating than on internal shear and so more readily controlled. Although shear rates and stresses will generally be higher in the clearances than in the channels of the screws, the relatively large size of these clearances (pp. 335 and 344) indicates that the disparity will be less than in the single-screw machine and that a larger proportion of the flow will be subjected to the higher shear, giving more uniform shear history. In particular, the mechanism of near-positive displacement will reduce the maximum residence time on which thermal degradation is dependent. Thus the twin-screw machine, especially if clearances are selected for the purpose, will give more uniform shear history and mixing than the single-screw extruder, while minimizing degradation. Effective dispersion, e.g. of pigment agglomerates, will depend critically on screw clearances, especially that between the flight flanks, through which a substantial proportion of the total flow should pass.

11.4 CONTROL

In the discussion on vented (two-stage) screws and combinations of screw extruder with gear pumps (section 6.5 and appendix B.5) it was pointed out that since an increase of pressure difference or pressure gradient reduces the output of the melt pumping section, it will automatically adjust to accommodate small changes in output or pressure. Referring to Fig. 6.18, if a disturbance increases

the output and pressure through the die from A to A'', the extruder output will decrease from A to $A_{//}$. Thus the supply of polymer to the die decreases and the die pressure tends to fall again. Similarly, if die output falls below A, the pressure will also fall, increasing the flow from the extruder, tending to restore output and pressure to point A. It will be noted that if the same screw was operating with a smaller die, as at C, the fluctuations in output corresponding to a given pressure variation would be larger than with a shallower screw. In this sense, the shallower screw can be said to be more stable, but for a given hold-up volume between screw and die, the greater output discrepancy between the die and the deeper screw could be expected to give more rapid restoration of the original conditions. The single-screw extruder running at constant speed and feeding a fixed die is thus a self-regulating system as regards output and pressure. Figure 8.10 shows that, at constant speed, a change in final melt temperature involves a substantial change in mechanical power input and even greater (absolute) change in heat supplied. Thus a temporary reduction in temperature will lead to an increase in mechanical power and a reduction in losses, tending to raise the temperature to the original level. If the reduction in temperature is sensed by the heater controllers, they also will tend to restore temperature by additional heat input, but, due to the thermal capacity of the machine, this will occur over a much longer time-scale. Thus the extruder tends to be self-regulating for temperature, irrespective of the heater controllers. It was shown in Fig. 11.4 that the usual 'regulation' curve of electric motors tends to make the drive self-stable in respect of speed and this inhibits a potential instability shown by Fig. 8.12. Therefore in many respects the single-screw extruder is self-stable against short time fluctuations in that these will be damped out more or less quickly, although transient effects cannot be avoided. This is provided that constant speed is assured. It is therefore unwise to impose any short-time external control on the extruder, apart from screw speed and barrel temperatures, which may react with the self-regulating system and even cause loss of control. For the same reason, any long-term adjustments should be made slowly and progressively.

The speed control provided by a thyristor drive is ideal in that the voltage output of the tachogenerator on the motor shaft responds virtually instantaneously and there is negligible lag in the thyristor control to provide the motor current necessary to maintain the speed. Provided that the speed regulation permitted by the control is small, the mechanical inertia of the motor and drive will also have negligible effect, giving a rapid and precise control of speed in response to load changes. However, when substantial changes in speed setting are imposed, mechanical inertia will cause a more delayed response and the possibility of slight overshoot. The speed regulation may be minimized by more sophisticated and expensive control circuits, which cannot always be readily adapted after initial installation; they are likely to be economically justified for products requiring minimum output fluctuations, such as film and fibre, and where drawdown is minimal, e.g. for large tube. It is

recommended that to assist in resetting conditions and for long-term stability, a digital setting should be provided for speed. Of the older types of drive, the AC commutator motor with induction regulator is probably the most satisfactory, having small regulation up to about 20% overload and a fairly constant efficiency around 85% between 50 and 120% load. However, the efficiency drops considerably at speed settings substantially above or below the synchronous speed with large circulating currents in the secondary circuit. The movable-brush AC Schrage motor is capable of sustaining considerable overload torque for long periods, but its speed-holding is poor, having characteristics similar to the series motor. The AC/DC Ward-Leonard drive is expensive and cumbersome, incorporating three rotating machines, which also limit the efficiency; the load/speed characteristics can largely be determined by design. The AC induction motor with magnetic slip coupling is subject near full load to the fairly large speed regulation of the induction motor and at low speeds to low efficiency due to losses in the coupling.

In production, output cannot be measured directly and often only remote from the extruder, e.g. by continuous measurement of product thickness at constant haul-off speed in wire covering, tube and sheet extrusion. As a result, there is a time delay and the possibility of errors due to 'storage' capacity in the system between the extruder and point of measurement, making output unsuitable as a signal for short-term control. Pressure can be measured on-line and at the end of the screw, with fast response and good accuracy. Unfortunately, aside from possible temperature errors, these instruments seem liable to damage in a production environment; the force-balance design originated by ICI Petrochemicals and Plastics Division (Lolley and Wykes, 1966) and marketed by Bowyer Engineering Ltd* was intended to minimize this problem and gives a 20–100 $kN\,m^{-2}$ (3–15 psi) pneumatic signal suitable for control. Pressure is therefore the most rapid and suitable indication of changes in the process; however, direct control of pressure by adjustable valves or restrictors is slow and mechanically unreliable in the environment of hot, highly viscous polymers. In addition, it has been shown earlier to be highly dependent on temperature and effective pumping length, as well as on output, so is not a good means of control, though as mentioned on p. 150 it is an essential indication of conditions in the extruder.

Final melt temperature is both an important indication of operating conditions and a vital factor to be controlled for subsequent processing and product properties. It can be measured roughly by a portable thermocouple inserted manually in the stream of polymer emerging from the die; the thermocouple must be robust and therefore slow in response, so cooling the polymer which tends to stick to it. Repeated insertion is usually necessary to obtain a reliable (maximum) indication, and so doing inevitably disturbs downstream operations. More reliable indication will be obtained from a

*Bowyer Engineering Ltd, Andover, UK.

thermocouple permanently installed just before the die, which like the pressure transducer requires careful handling during cleaning, especially if it is made small to give rapid response. It will not generally respond as rapidly as pressure gauges, and in view of the space variations and time fluctuations mentioned earlier (see p. 358) will not show a true average value; to minimize the former it should always be located in the same position, and preferably in a fairly narrow flow channel, though this will accentuate errors due to heat from the walls. Even so, the indication of a melt thermocouple forms an important and useful signal for long-term control of barrel temperatures, especially with changes in speed, output, etc. Melt temperature cannot of course be controlled directly, but, with a given screw design and speed, indirectly through barrel temperatures, and thus relatively slowly. Note from Tables 9.4 and 9.5 that increases in set temperature at different points along the screw length will have different (and even opposite) effects on the final melt temperature. In this connection the ammeter on the motor drive or other torque meter is a rapid indication, e.g. if the effect of an increase in a set temperature is a marked decrease in drive torque, the melt temperature is also likely to be increased. Thus the barrel temperature *profile* should be regarded as a control input distinct from the average or final set temperature.

Various temperature profiles were discussed in connection with Fig. 9.6 and in summary the author suggests the temperature of the first barrel zone determines the point at which melting commences; the set temperatures in the melting section determine the energy added by heat conduction, and by difference that from the mechanical drive; the set temperatures in the melt pumping section determine how far the final melt temperature is above the softening/melting point of the polymer.

Modern temperature controllers for plastics processing machines perform two main functions with a high degree of sophistication and reliability: to give rapid start-up and change of conditions with minimum overshoot; and accurate maintenance of set temperatures despite wide changes in heat demand by the process. The details of operation are beyond the scope of this book, but the instrument manufacturers are knowledgeable of the requirements of the plastics industry and very helpful in establishing the instrument settings (time constants, integral and derivative terms, power level, proportional band) to obtain the best performance in particular situations. For reasons of fast and unambiguous response, the control thermocouple should be close to the source of heating/cooling, and this is the temperature the controller attempts to maintain. As mentioned above, this is indirectly related to the desired polymer temperature, and subject to time delays, so the operator must establish the relation between set and melt temperatures and the appropriate strategy for control settings. Thermocouples close to the inner wall of the barrel (footnote p. 232 and Table C.2) are valuable in indicating the local melt temperature, which is more directly related to the set temperature than is the final melt temperature. In maintaining the set temperatures, the controllers will

automatically restore the energy balance (as represented by Figs 8.10 and 8.12) after a disturbance due to changes in polymer, speed, pressure or temperature, but due to interactions within the extruder this will take time, up to several hours, and this action must be recognized as accompanying any deliberate alteration in another set condition. During this stabilization time there is the probability of off-standard product with the attendant material, energy and labour costs and loss of production capacity. In extreme cases it may be more economical to stop the downstream processes and either stop the screw or reduce output to a minimum until temperatures reach approximately the required values. When speed is restored, the consequences of this on energy balance must take place, but acceptable product is likely to be achieved more quickly and with less waste of material, etc. With experience, it may be possible to reduce the time to reach equilibrium by judicious adjustment of speed, pressure or heater controls, but reaching correct temperatures is likely to remain the limiting factor on time and it must be remembered that any change of conditions will require time to stabilize, so inadvised adjustment is likely to extend the time to reach steady conditions.

Of the remaining parameters, a constant-torque control on the drive is undesirable, since it would lead to changes in speed and temperature, with consequent settling times; like pressure, motor amperes are useful for rapid indication but not control. Degree of mixing and melt temperature variations are difficult to measure on-line and are not directly controllable; the factors listed in Table 9.7 should be adjusted first, possibly with some sacrifice in output, and only then should changes in screw design be considered.

As discussed on p. 281, screw cooling requires very careful adjustment and reliable instantaneous indication of coolant flow and temperature; in practice it is usually under manual control as the operator's 'last resort'.

In the twin-screw extruder, barrel temperatures, especially in the melting zone, have a more direct effect on the polymer melt temperature than in the single-screw machine, and so should give improved control, although appreciable time delays will still occur. Barrel temperature, through viscosity, will still have considerable effect on mechanical power input, although this represents a smaller proportion of the total energy which raises melt temperature. With the usual metered feed, close control of feed rate is essential in determining output rate, pressure and number of filled flights, which in turn react on power input and melt temperature. Control of screw speed, however, is less important, since except when approaching flood feed, it has only an indirect effect on output, energy input, etc. Generally for a given polymer and/or product and design, e.g. L/D ratio and screw profile, the twin-screw will have a narrower range of satisfactory operating conditions than the single-screw; thus there is greater possibility of an overall control system to maintain 'design' conditions rather than to optimize performance by adjusting operating conditions such as screw speed, overall temperature level, temperature profile, back pressure, etc., as in the single-screw machine.

In considering overall control of an extrusion process, the task must be distinguished from that of, say, the injection moulding process. In the latter, consistent product dimensions and properties depend on repeatability of an inherently cyclic process. This in turn depends largely on the consistent performance of mechanical and hydraulic systems and even the semi-continuous melting process is subject to cyclic disturbance. In contrast, as detailed in section 11.2, the extrusion process is essentially continuous and has a considerable degree of self-stability. The first requirement, then, is direct closed-loop control of the external process parameters, e.g. temperatures and flow rate (feed rate in the twin; screw speed in the single) and then their relation to downstream factors such as haul-off speed, product cooling, and tubular film blowing pressure. If consistent rheological properties of the feed polymer can be assured, then a high degree of process stability should be achieved.

Any overall control system, e.g. by computer, should not modify the above controls in the short term and because of delays (mainly thermal) and interactions in the process, longer-term adjustments, e.g. of set points, should be gradual or in small steps well spaced in time; otherwise excessive transients may result, leading to out-of-specification product and even process interruption, e.g. broken thread-line, unstable film bubble, or motor overload. In the extreme, resonant oscillations may be caused, leading to loss of control.

It has been claimed that a mathematical model of the process, derived from regression analysis of experimental data, would permit overall computer control without the necessity for 'local' closed-loop control of separate variables such as screw speed and temperatures. Even with the approximations inherent in the simplified theories presented in this book it is unlikely that a completely general model could be established from a cost-effective experimental programme. A more practical approach would be an analysis of experiments, such as those outlined in Chapter 13, for a specific machine, screw design, die type, heater arrangement and polymer characteristics to produce a mathematical analogue of the processing of that polymer on that machine. This would need to include interactions such as those considered in sections 8.3 and 8.4; back pressure, shear rate, viscosity and shear heating; mechanical and heater energy in melting, pumping and flight clearance; heat flows and temperature gradients in channel and flight clearance; space and time variations of melt temperature, flow distribution in the die and downstream processes of drawing, blowing and cooling. An inadequate model would almost certainly lead to poor control of at least one parameter and probably introduce small fluctuations into inherently stable conditions, to say nothing of possible effects on product properties such as residual strain and orientation.

11.4.1 Control for specific processes

General conditions for control of the extrusion process have so far been discussed in this chapter. Because of the wide range of polymers, machines and

products involved, this has necessarily been qualitative. In Chapter 2 the principal extrusion processes were outlined, and their requirements in terms of process variables, e.g. output, pressure, melt temperature and mixing, were summarized, both as to magnitude and accuracy, in Table 2.2. Details of this are open to criticism, especially as each process category covers a wide range of polymers, sizes, linear speeds and product specifications, e.g. in relation to homogeneity and dimensional tolerance. However, it distinguishes the critical process factors and illustrates how these differ between processes. Table 11.1 suggests how these requirements might be met in terms of single-screw type and operating conditions. The table also indicates the accuracy of control which is desirable to achieve acceptable product quality and uniformity, as far as this is determined by the extruder itself. Naturally, control of the haul-off speed, especially in relation to screw speed, is vital in determining lateral dimensions in processes such as profile, tube and wire covering where drawdown is minimal, and important in sheet, film and fibre extrusion where substantial drawdown is common. Control of product coolant temperature and flow rate, including their relations to melt temperature and extruder output rate, is important in controlling distortion in shape and size, distribution and types of crystalline structure; these and similar control requirements are additional to those mentioned in Table 11.1.

One of the most common causes of fluctuations in extruder conditions and product properties arises from variations in properties of the polymer feed. This may arise from incorrect blending of constituents, especially refed scrap or deblending in storage or feeding; this is under the processor's control and must be monitored. Variations may arise from changes in size, shape or surface friction of solid feed particles; larger particles may be marginally poorer in packing and melting, but generally undue sensitivity to particle size, shape, etc., indicates poor design or conditions in the feed section so that potential solid feed rate is not sufficiently in excess of melt feed rate. A third source of fluctuations is due to changes in the melt viscosity and elasticity arising from changes in molecular weight, molecular weight distribution, chain branching, previous shear and heat history, etc. Polymer manufacturers are understandably reluctant to impose on themselves restrictions in terms of melt processing properties additional to those existing in respect of mechanical, electrical and environmental properties in the finished product. Such restrictions may impose undesirable economic limitations in respect of polymer intermediates, polymerization processes and operating conditions. The processor must therefore determine for himself the melt properties and permissible variations allowable for his particular process and product. He may be able to agree with the polymer supplier a more detailed purchase specification, but in any event must have equipment to monitor melt viscosity, swell ratio, and their variations with shear rate and temperature. A paper by Teh, Rudin and Schreiber (1984) describes equipment, methods and presentation of data, though the present author does not suggest that such

comprehensive work is necessary for day-to-day control. However, a model for on-line computer control of the process (see p. 371) must contain an analogue of these flow properties as well as an input based on previously determined characteristics of the actual feed material. In the absence of the latter, the control system must have means of distinguishing changes due to polymer properties from those due to operation, e.g. set temperatures (see next paragraph).

It would be tedious to detail all the effects of changes in melt properties, but from equation (6.53) it is seen that an increase in viscosity gives a proportional increase in pressure at the same output, while equation (6.15) shows that such proportional changes in pressure and viscosity cause no change in extruder output, so output is constant while pressure rises – the same effect as of a reduction in final melt temperature. Equation (8.9) shows that at constant output Q, the mechanical power input increases in proportion to viscosity and, according to Fig. 8.10, either melt temperature will increase or heat input will decrease or require cooling. On operational grounds it may be argued that temperature should be allowed to increase until viscosity and pressure are restored to their original values, but this requires a predetermined adjustment of heater set temperatures on the basis of either constant power or heater input; in any case the downstream cooling conditions will be disturbed and thermal stability of the polymer may be affected.

A change in the non-Newtonian response to shear rate represented by the pseudoplasticity index n would alter the relation between viscosity in the die (high shear rate) and in the screw channel (low shear rate). For instance, a narrowing of the molecular weight distribution causing an approach to Newtonian behaviour ($n \rightarrow 1$) would give, for a fixed viscosity in the screw, an increase in the viscosity in the die. By equation (6.53) this is equivalent to a decrease in the value of the die constant K, and Fig. 6.18 shows that the operating point will move, e.g. from A to C, or B to D, giving a lower output at higher pressure. This is also illustrated by equation (6.58), where a decrease in K gives an increase in the factor $(1 + B/K)$, or on p. 153 an increase in η_{Die} increases the factor $(1 + B\eta_{\text{Die}}/K\eta_{\text{Screw}})$ and hence reduction in output at a given speed. The effect on mechanical power is shown by equation (8.7), i.e. that a decrease in output causes an increase in power input, and since this is absorbed by a smaller flow of polymer, temperatures will tend to rise. This is analogous to the effects of increased back pressure discussed on p. 260. The increased viscosity at high shear rates will also increase the power absorbed in the flight clearance of the screw, and hence the total power and melt temperature. However, it also increases the *proportion* of total power contributed by the flight clearance and the resulting temperature effect on channel power (section 8.5). It is also likely to increase temperature variations at the die and consequently decrease product quality. Changes in melt elasticity will alter the swell ratio, modified by any accompanying changes in shear history in the extruder, leading to changes in the drawdown behaviour, or,

Table 11.1 Suggested conditions for individual processes

Process	*Screw diameter (relative)*	*Screw length L/D ratio*		*Screw type*	*Metering depth*	*Screw speed (relative)*	*Melt temperature*	*Degree of control*			*Comments*
								Speed	*Temperature*	*Mechanical power*	
Rod/section and profiles	High	20/24 15/20 20/24	PE, PP PVC Nylon	T T S	Shallow	Low	Medium	× ×	× ×	× × ×	Output relative to haul-off speed, for dimensions. Mimimum elastic memory. Medium temperature for rigidity while cooling. Add screens to promote mixing.
Tube	High	20/24 15/20 20/24	PE, PP PVC Nylon	T T S	Medium	Medium	Medium except die	× ×	× ×	× ×	Minimum elastic memory. High die temperature for gloss. Medium temperature for drawdown of small tubes.
Wire covering/ sheathing	Low	20/24 15/20 20/24	PE, PP PVC Nylon	T T S	Shallow	High	High	× ×	×	×	High temperature for good drawing and avoiding melt fracture. High pressure for thin insulation. Output relative to haul-off speed for thickness
Sheet/laminating (including continuous vacuum forming)	High	20/24 15/20 20/24	PE, PP PVC Nylon	T T S	Medium	Medium	Medium	× ×	× ×	× ×	Medium speed is compromise for high output and uniformity of Q and T. Steady output to avoid ripples. High output for thick sheet. Uniform temperature for die distribution. Medium temperature for drawdown.
Flat film	Medium	24/28 20	PE, PP PVC	T T	Shallow	Medium	High	× × ×	× × ×	× × ×	High temperature for drawdown. High pressure for die. Medium speed for uniform elastic memory. Uniform output for thickness.
Paper coating	Medium	24/28	PE,PP	T	Shallow	Medium	High	× × ×	× × ×	×	Output relative to drum/haul-off speed for thickness. Medium output for rapid cooling. Very high temperature for flow and surface finish.

(*Continued*)

Tapes	Medium	20/24	PE,PP	T	Medium	Medium	Medium	× × ×	× × ×	× ×	Medium temperature for crystallization and drawdown. Uniform output for dimensions and crystallization. Uniform temperature for dimensions.
Filament/fibres	Medium	20/24	PE,PP	T	Shallow	Medium	High	× × ×	× × ×	×	High temperature for drawing.
Tubular film	Medium	20/24	PE,PP	T	Shallow	Medium	Medium	× × ×	× × ×	× × ×	High pressure for die. Medium temperature for drawing and blowing. Medium speed for uniform elastic memory.
Foam	Medium	20/24		T	Medium	Low	Low	×	× ×	× ×	Temperature depends on blowing agent. Low shear heating for decomposition. Medium pressure and mixing for uniform distribution and pore size.
Compounding/ blending	Medium/ high	24/28	PE,PP	T	Deep	Medium	Low	×	× ×	× ×	Deep screw at high pressure for mixing. Large diameter and medium speed for high output. Low temperature for mixing and heat history.
		20	PVC	T							
		20/24	POM	T							
			PMMA	S							
			Nylon	S							
Degrading	Medium	24/28	PP	T	Shallow	High	High	×	× × ×	× ×	
Blow moulding	High	24/28	PE,PP	T	Medium	Medium	Low	× ×	× ×	× × ×	No haul-off. Melt temperature and swell ratio compromised with output by control, e.g. of speed and diameter.
Injection moulding	High	24/28	PE,PP	T	Medium/ shallow	Medium	Medium/ high	×	× ×	× ×	No haul-off. Melt temperature control important. Back pressures low in practice.
		20	PVC								
		20/24	PS								

Notes:The screw type and dimensions are largely dependent on the polymer and temperatures. Screw diameter and length are a compromise with capital cost. Screw speed is a compromise beween output and quality. The length/diameter ratio and channel depth depend largely on the polymer used. 'Temperature' under 'Control' refers to set temperatures in the melt pumping section. Mechanical power input is controlled mainly by temperatures in the melting zone. Screw cooling is excluded since it is always very sensitive, requiring precise control.

Suggested *running* limits are:

Speed:		Temperature:		Mechanical power:	
×	±1%	×	±2°C	×	±3%
× ×	± 0.3%	× ×	± 0.5°C	× ×	± 1%
× × ×	±0.1%	× × ×	± 0.1°C	× × ×	±0.4%

where drawdown is negligible, to changes in product dimensions. The foregoing illustrates the effects of changes in melt properties of the polymer, the necessity for prior knowledge of such changes by material testing, and the difficulties of incorporating the effects in the process algorithm necessary for on-line computer control. To add relevance to Table 11.1, suggested limits are included for the various degrees of control of speed, temperature and mechanical power input. It will be appreciated that these and other data given in Table 11.1 are in the nature of a general guide and will need to be modified in particular cases; the author trusts that it will not prove too far from processors' own experience and will be useful at least as a starting point.

11.5 SCALE-UP

Although scale-up borders on the province of the designer, it is included here because of operational factors which do not seem to have been fully considered in works on design. Also, these factors frequently become evident when the equipment has been manufactured and the operator is then expected to obtain the best performance from it. In particular, the author has on several occasions been faced with a demand for a changed screw design; this might take 6–12 months to manufacture, during which production would be less than optimum, and then costly losses in production time would be incurred while it is installed. In one instance, involving a number of very large identical machines, the author felt obliged to persuade management on theoretical grounds that such expense and delay was likely to leave the problem still unsolved; instead, the time and money were spent on gearing of a different ratio so that at full output the maximum motor power was available, as required.

The scale-up problem may occur in the progressive increase of production capacity, leading to larger machines; this may often be carried out successfully by empirical methods, and if the increments are modest any problems may be overcome by minor adjustments of machine dimensions or operating conditions. However, in the case of a new polymer, product or process, the initial development is necessarily done at small scale usually using extruders of 60 mm diameter or less. Economic production may require outputs more than ten times that of the laboratory scale so that the method of scale-up becomes important, not merely to achieve the output but to proportion correctly the drive motor, thrust bearing, heaters, screw, etc., and to obtain correct conditions of pressure, temperature, mixing, shear history, etc. A number of different strategies are possible, and several will be examined to show the likely results and where they might be employed.

The following analysis is based on the simplified Newtonian equations developed in Chapters 6 and 8 for output and mechanical power, modified where necessary for pseudoplastic flow. The deductions are thus not exact for design purposes, but enable the effects on a number of important operational

parameters clearly to be seen, and the correct general method of scaling to be selected.

In addition to output and mechanical power (giving the rating of the drive motor), the specific power input E/Q will be deduced, since this represents the adiabatic temperature, a key point on the energy balance. In order to operate at any other temperature, energy must be added by heaters or removed by cooling in proportion to the output, which if it increases faster than D^2, requires a higher heating density ($W\,cm^{-2}$) since the surface area increases as D^2 (for constant L/D ratio). If the adiabatic temperature represented by E/Q changes with scale-up, then, as shown by Fig. 8.10, the heat requirement per kilogram of output may change dramatically, even from heating to cooling or vice versa, and the total will be amplified by the increased output. However, of greater significance is that a change in the balance of energy input between mechanical E and heat H will alter the extruder performance in respect of melting, mixing, temperature variations at the die, stability, etc., so that the downstream processes may be affected and the quality of the product will almost certainly differ from that determined in the laboratory. The results are summarized in Table 11.2.

It has been seen earlier that the assumption of constant Q/Wbh simplifies comparison as well as ensuring similar velocity distributions in the screw channel. Equation (6.32) gives the implication for pressure gradient and this will be evaluated in each case. Mixing in the screw cannot be evaluated simply, but the maximum shear rate at a fixed Q/Wbh is given by equation (6.69) and is proportional to the drag flow shear rate W/h, proportional to DN/h. The mean residence time in the melt pumping section is given by volume/Q or:

$$\begin{aligned}\text{mean residence time} &= \frac{bhZ}{Q} \\ &= \frac{bhL}{\left(\dfrac{Q}{Wbh}\right)\pi DN\cos(\phi)bh\sin(\phi)} \\ &\propto \frac{L}{DN}\end{aligned} \tag{11.4}$$

for constant Q/Wbh and helix angle ϕ. Shear rate and residence time together give a semi-quantitative measure of total shear strain on which distributive mixing depends. Output is given by a modification of equation (6.30) for a fixed value of Q/Wbh:

$$Q \propto D^2Nh \tag{11.5}$$

Mechanical power in the channel is given by equation (8.7), which can be represented by:

$$E_{Ch} \propto \frac{\eta W^2 bZ}{h} \tag{11.6}$$

for constant Q/Wbh and helix angle ϕ.

Table 11.2 Scale-up of single-screw extruder: summary of effects of various scaling strategies with Q/Wbh as constant

	Volumetric output	*Mechanical power input*		*Specific mechanical power (adiabatic temperature)*		*Pressure gradient*	*Die pressure*	*Wall shear rate*	*Mean residence time*	*Shear strain (mixing)*	*Specific heating surface*
	Q	E		E/Q		$\mathrm{d}P/\mathrm{d}z$	P	$\dot{\gamma}$	t_{res}	$\dot{\gamma}t_{res}$	A/Q
		$n=1$	$n<1$	$n=1$	$n<1$	$n=1$	$n=1$	$n=1$			
Proportional to	D^2Nh	$\frac{D^3N^2L}{h}$	$\frac{D^{n+2}N^{n+1}L}{h^n}$	$\frac{DNL}{h^2}$	$\frac{D^nN^nL}{h^{n+1}}$	$\frac{DN}{h^2}$	$\frac{DNL}{h^2}$	$\frac{DN}{h}$	$\frac{L}{DN}$	$\frac{L}{h}$	$\frac{DL}{Q}$
Equation	(11.5)	(11.8)	(11.11)	(11.9)	(11.12)	(6.32)	(6.37)	(6.69), (6.4)	(11.4)	(11.4), (6.69)	–
Scale-up strategy											
Case 1: Constant depth h	D^2N	D^3N^2L	$D^{n+2}N^{n+1}L$	DNL	D^nN^nL	DN	DNL	DN	$\frac{L}{DN}$	L	$\frac{L}{DN}$
Case 2: Geometric similarity $D \propto L \propto h$	D^3N	D^3N^2	D^3N^{n+1}	N	N^n	$\frac{N}{D}$	N	N	$\frac{1}{N}$	Const.	$\frac{1}{DN}$
Case 2a: Constant speed N	D^3	D^3	D^3	Const.	Const.	$\frac{1}{D}$	Const.	Const.	Const.	Const.	$\frac{1}{D}$
Case 3: Constant peripheral speed $D \propto 1/N$	Dh	$\frac{DL}{h}$	$\frac{DL}{h^n}$	$\frac{L}{h^2}$	$\frac{L}{h^{n+1}}$	$\frac{1}{h^2}$	$\frac{L}{h^2}$	$\frac{1}{h}$	L	$\frac{L}{h}$	$\frac{L}{h}$

Case 4: Constant shear rate $N \propto h/D$	D^3N^2	D^2NL	D^2NL	$\frac{L}{DN}$	$\frac{L}{DN}$	$\frac{1}{h}$	$\frac{L}{h}$	Const.	$\frac{L}{DN}$	$\frac{L}{DN}$	$\frac{L}{D^2N^2}$
	Dh^2	DhL	DhL								
	$\frac{h^3}{N}$	$\frac{h^2L}{N}$	$\frac{h^2L}{N}$	$\frac{L}{h}$	$\frac{L}{h}$				$\frac{L}{h}$	$\frac{L}{h}$	$\frac{L}{h^2}$
Case 4a: $h \propto D$ N constant	D^3	D^2L	D^2L	$\frac{L}{D}$	$\frac{L}{D}$	$\frac{1}{D}$	$\frac{L}{D}$	Const.	$\frac{L}{D}$	$\frac{L}{D}$	$\frac{L}{D^2}$
Case 4b: $L \propto h$ $L/D \propto h/D \propto N$	Dh^2	Dh^2	Dh^2	Const.	Const.	$\frac{1}{h}$	Const.	Const.	Const.	Const.	$\frac{1}{h}$
	DL^2	DL^2	DL^2								$\frac{1}{L}$
Case 4b(i): $L \propto h \propto \sqrt{D}$ $N \propto 1/\sqrt{D}$	D^2	D^2	D^2	Const.	Const.	$\frac{1}{\sqrt{D}}$	Const.	Const.	Const.	Const.	$\frac{1}{\sqrt{D}}$
Case 4b(ii): $L \propto h \propto D^{1.5}$ $N \propto \sqrt{D}$	D^4	D^4	D^4	Const.	Const.	$\frac{1}{D^{1.5}}$	Const.	Const.	Const.	Const.	$\frac{1}{D^{1.5}}$
Case 5: $L \propto D$ $h \propto \sqrt{D}$	$D^{2.5}N$	$D^{3.5}N^2$	$D^{n/2+3}N^{n+1}$	DN	$D^{\frac{1}{2}(n+1)}N^n$	N	DN	$N\sqrt{D}$	$\frac{1}{N}$	$\sqrt{D}$	$\frac{1}{N\sqrt{D}}$
Case 5a: $h \propto \sqrt{D}$ $N \propto 1/\sqrt{D}$	D^2	$D^{2.5}$	$D^{2.5}$	$\sqrt{D}$	$\sqrt{D}$	$\frac{1}{\sqrt{D}}$	$\sqrt{D}$	Const.	$\sqrt{D}$	$\sqrt{D}$	Const.

For mechanical reasons, the flight clearance δ is approximately proportional to diameter D. Noting that h is usually increased as D increases, though not necessarily in proportion, if we take:

$$\delta \propto h \tag{11.7}$$

and take the ratio $\eta_{\text{flight}}/\eta_{\text{channel}}$ as constant (since shear rates are proportional to W/δ and W/h, respectively), then equation (11.6) also represents the total power given by equation (8.9). Substituting in equation (11.6) for W from equation (6.4), b from equations (6.2) and (6.3) and Z from equation (6.1) we can write:

$$E \propto \frac{D^3N^2L}{h} \tag{11.8}$$

in the Newtonian case. Dividing equation (11.8) by equation (11.5) gives:

$$\mathrm{d}T \propto \frac{E}{Q} \propto \frac{DNL}{h^2} \tag{11.9}$$

For a pseudoplastic fluid, from equation (3.7):

$$\begin{aligned} \eta &\propto \dot{\gamma}^{n-1} \\ &\propto \left(\frac{DN}{h}\right)^{n-1} \end{aligned} \tag{11.10}$$

Substituting in equation (11.6) gives:

$$E \propto \frac{D^{n+2}N^{n+1}L}{h^n} \tag{11.11}$$

and:

$$\mathrm{d}T \propto \frac{E}{Q} \propto \frac{D^nN^nL}{h^{n+1}} \tag{11.12}$$

Taking first the Newtonian case, if channel depth h is maintained constant, output only increases as D^2, i.e. a tenfold increase in output would require an extruder more than three times the diameter, with considerable increase in capital cost. However, the power input (and motor rating!) would increase as D^3 and the specific power would increase in proportion to diameter, speed and length, resulting in very much higher temperatures or dramatic changes in heating/cooling. In this case it is unnecessary to increase length to maintain mixing or die pressure, so L may be regarded as constant (decreasing the number of turns). However, if speed is decreased ($N \propto 1/D$) to maintain E/Q constant, the output and power increase only linearly with diameter D, which is evidently uneconomic. Scale-up at constant depth is thus extremely limited, either by excessive temperature rise or small increase in output.

A more common strategy is to increase all dimensions in the same proportion (geometric similarity); length L is proportional to diameter D and thus the number of pitches (turns) remains constant. Since channel depth h is also proportional to diameter, output Q increases as D^3N and mechanical power E increases as D^3N^2. The adiabatic temperature represented by E/Q is thus independent of D but increases with speed N as before (Fig. 8.13). Shear rate, residence time and mixing are independent of diameter, and mixing is also independent of speed. The pressure gradient decreases with increase of diameter, giving the same final pressure due to the greater length, both gradient and pressure being proportional to speed. At first this appears very satisfactory, requiring only just over twice the diameter to give a tenfold increase in output, with temperature, pressures and mixing remaining constant. However, the heat energy required to melt ten times the output must be transferred through only 4.5 times the barrel surface ($Q \propto D^3$, surface $\propto D^2$) so that some limitation in melting rate, at least at the same screw speed, may be encountered. The same situation applies in the melt pumping section if melt temperatures appreciably above or below the adiabatic value are required, and in addition this heat energy must be conducted through a greater mean distance due to the deeper channel; thus heating will be slower and probably give rise to additional variation in final melt temperature. The overall consequences at constant speed are likely to be less complete melting, less homogeneous product, and limitations on melt temperature above or below the adiabatic point. These in turn will set additional limits to the screw speed and output achievable before the output becomes too inhomogeneous or unstable for satisfactory production. The position can be improved by a reduction in speed, with consequent reduction in output and pressure; however, the accompanying reduction in adiabatic temperatures may exacerbate the problem if high melt temperatures are required. Another possibility is to increase the number of turns in the melt pumping section (L increases more than in proportion to D), giving higher power E and adiabatic temperature as well as higher pressure and mixing – see Fig. 8.7.

This case illustrates the ramifications of the scale-up problem and the difficulty of reproducing all aspects of small-scale performance; the disproportion between surface and volume is inherent.

Of case 3, where peripheral speed is constant, it is only necessary to point out that it implies that increased diameter is accompanied by decreased speed so that increases in output are very modest in relation to size and capital cost. By manipulation of length and channel depth it is, however, possible to hold adiabatic temperature, mixing and pressure approximately constant (but see case 5).

Since shear rate is significant in both power absorption and mixing, case 4 considers constant shear rate; this implies speed $N \propto h/D$, which, if h/D is constant, is similar to case 2a, geometric similarity at constant speed, but with the ratio L/D unspecified. If L/h is constant, adiabatic temperature, residence

time, mixing and pressure will remain constant. Other factors then depend very strongly on the choice of channel depth h; if $h \propto \sqrt{D}$, speed is reduced as $1/\sqrt{D}$ and output is proportional to D^2, but L is also proportional to $\sqrt{D}$ so that heat (proportional to D^2) is transferred through a barrel surface proportional to $D^{1.5}$, but still through an increased channel depth. If channel depth h is increased more than in proportion to D, say as $D^{1.5}$, speed increases as $\sqrt{D}$ and output as D^4. Length is also increased as $D^{1.5}$, giving barrel surface proportional to $D^{2.5}$, but with severe limitations on heating or cooling.

A compromise frequently followed in practice approximates to case 5, where the number of turns is constant ($L \propto D$), and $h \propto \sqrt{D}$. At constant speed, output increases as $D^{2.5}$ and E/Q, representing adiabatic temperature, is proportional to D. Mixing increases as $\sqrt{D}$ and pressure as D. Barrel surface increases as D^2, so that heat conduction problems will be slightly worse. If however, output is sacrificed by a modest reduction in screw speed (say, $N \propto 1/\sqrt{D}$), shear rate becomes constant and E/Q, residence time, mixing and pressure all increase as $\sqrt{D}$. Output is now proportional to D^2, as is barrel surface, so that the only factor in heat conduction is a slight (proportional to $\sqrt{D}$) increase in the mean radial distance for conduction through the polymer.

Since the shear rates at laboratory and production scales are the same in cases 2a, 4 and 5a, the same results will obtain for pseudoplastic polymers. In other cases equations (11.10), (11.11) and (11.12) apply with the general result that increases in pressure and adiabatic temperature will be less than for Newtonian behaviour, making these factors less critical. As observed on p. 259, the effect of speed on adiabatic temperature will also be less, so that the scale-up problem is less critical with highly pseudoplastic materials.

The conclusion from Table 11.2 is that a strategy for scale-up similar to cases 2a and 4b(i) represents a good compromise of all the factors considered. In specific cases the relative importance of these factors may be changed so that the strategy may be modified to suit the more important factors. It will be noted that increase of scale generally leads to higher specific power input and higher temperatures, as does increase of screw speed. Similar effects of diameter and speed are also anticipated in respect of difficulty in obtaining temperatures much above (or below) the adiabatic value, temperature uniformity and output stability. The last three, together with mixing, can be improved by increasing the length of the melt pumping section (compare case 5a with 4b(i)), though at the expense of greater power input, shear history and mean residence time (for polymers liable to degradation) and higher adiabatic temperatures (where processing temperatures are low). For reasons of heat transfer, melting may also be less complete in large machines, though the effect is likely to be less than that of increasing screw speed; this may be corrected by adjustments to channel depth, by increasing the melting length (e.g. by reducing appropriate barrel temperatures) or increasing the proportion of mechanical work input (again by reducing barrel temperatures).

In the twin-screw extruder, the metered feed rate is independent of screw speed so that comparisons of scale are more complex. However, if it is assumed that in order to maintain a constant number of filled flights, the ratio of actual output to output capacity Q/Q_c is maintained, then from equation (10.14):

$$\begin{aligned} Q &\propto Q_c \\ &\propto D^2Nh \end{aligned} \tag{11.13}$$

If the filled length D_eN_f is replaced by L, then from equation (10.10):

$$E \propto \frac{D^3N^2L}{h} \tag{11.14}$$

and specific power:

$$\frac{E}{Q} \propto \frac{DNL}{h^2} \tag{11.15}$$

These are equivalent to equations (11.5), (11.8) and (11.9), respectively, for the single-screw machine. With the above proviso on feed rate, the considerations on scale-up of twin-screw extruders should be generally similar to Table 11.2, although they may require modification to take account of consequential changes in flight geometry and clearances. As mentioned on p. 346, external heating represents a greater proportion of total energy input than in the single-screw machine, so the limitations imposed in larger machines on heating surface will be more restrictive in scaling up the twin-screw extruder.

12 Practical extruder operation

12.1 STEADY OPERATION

The principles of steady operation of single-screw extruders have been developed in Chapters 6 and 8 and their implications for operation discussed in Chapters 9 and 11. The principles and operation of twin-screw extruders have been covered in Chapter 10, where it is shown that the wide variety of designs entails operation largely guided by manufacturer's instructions. This is even more the case of dismantling and cleaning of twin-screw machines, which will therefore not be discussed in this chapter. However, an attempt is made to cover more practical aspects of operation to complement the theory of single-screw machines, including methods of achieving and maintaining safe and steady operation, starting-up and changing running conditions, shut-down and cleaning, and scrap recovery.

Unlike injection moulding, extrusion is fundamentally a continuous process and successful economic production depends on keeping steady conditions for long periods. Since both material and energy are used during start-up and changes due to material, operation or product, it is important that these are made economically and usually as quickly as possible. As discussed in section 11.2, the single-screw extruder combined with a die is to some extent a self-regulating system, though compensation for changes in pressure or temperature may produce undesired changes in mixing or stability. However, the downstream operations of sizing, drawdown and cutting directly affect the product, and equilibrium between these and the extruder itself must generally be controlled by the operator. Instrumentation, preferably automatically recording, is valuable as a guide to incipient changes in conditions, which are frequently due to changes in feed material properties. Instrumentation often does not include direct indication of melt pressure or temperature, and instruments provided may have a delayed response, for instance due to the

Table 12.1 Simple fault finding

Occurrence	*Condition*	*Cause*	*Action*
Heating interrupted	Temperature falling	(a) Control action to avoid overshoot, time-proportioning or interaction with adjacent zones	Observe if heating resumed in say 30 s, otherwise check (b), etc.
		(b) Fail-safe control, indicating broken thermocouple or connection	Check thermocouple continuity
Temperature continues to rise	Temperature above upper control limit	(a) Thermocouple slipped out or not in contact with heater/extruder	Replace, ensuring good thermal contact
		(b) Thermocouple incorrectly connected	Check connections and temperature indication, e.g. in hot water or body heat
Output suddenly falls	Steady screw speed	(a) Feed hopper empty	Refeed *gradually* (section 12.3). Investigate blocked feed line
		(b) Bridging in hopper or into screw	Stop screw and clear with non-metallic rod, e.g. strip of product. Check adequate feed pocket cooling. Check air entrapment esp. with powders
		(c) Polymer melting in feed section	Reduce first barrel zone temperature Increase feed pocket cooling Cool feed end (only) of screw
		(d) Surging	See section 11.2
Polymer leakage from joints or fittings	Excessive pressure	(a) Blocked die or screen	Immediately reduce screw speed. Check die and adaptor temperature Shut down and clear
		(b) Failed die heater or control	Immediately reduce screw speed Check thermocouple Shut down and replace heater
		(c) Incompletely melted polymer, esp. at start-up or after feed interruption	Stop screw Wait to heat up and restart *slowly*

(*Continued*)

Table 12.1 (*Continued*)

Occurrence	*Condition*	*Cause*	*Action*
Screw stops or speed drops	Excessive torque	(a) Low barrel temperature	Reduce speed setting and check heaters
		(b) Excessive pressure	As for 'Leakage' above
		(c) Excess feed, e.g. of strips	Stop or reduce speed setting
			Increase temperature of first barrel zones
		(d) Excessive speed	Reduce speed and/or increase barrel temperatures
Lumpy or unmelted polymer at die	Incomplete melting, esp. of powders	(a) Insufficient shearing/heating in barrel	Refer to Table 9.8
		(b) Excessive screw speed	Reduce screw speed *or* improve melting (Table 9.8)
		(c) Feed contamination, e.g. with hard-grade polymer	Reduce screw speed Check feed material If necessary, increase barrel temperatures
Foaming or bubbles at die (distinguish from later contraction bubbles due to rapid cooling), surface blisters	Steady running or start-up	(a) Moist polymer	Stop feed and restart with dried polymer
		(b) Excess temperature causing decomposition	Stop or reduce screw speed Refer to Table 9.5
		(c) Air entrapment in feed	Raise first barrel zone temperature (to reduce unmolten length)
			Fit vent at rear of feed opening

thermal mass of the machine part to which they are attached; hence the need for an understanding of the mechanism of extrusion to avoid over-hasty or inappropriate 'corrective' action. It is thus wise to be cautious about deliberate alterations to machine controls, and when the process is running steadily unnecessary stops or changes in speed or temperature should be avoided. It should also be appreciated that the reaction times of the process differ widely; a change in pressure will have an almost instantaneous effect on output and power input, but due to heat capacity of machine and polymer, temperature will respond more slowly, bringing consequent further changes to output, power, etc. Speed changes also produce rapid changes in output and power input, but more delayed changes in temperature, and, as seen in Chapter 8, profound changes in energy balance may occur. Changes in set temperature profile will usually affect melt temperatures quite slowly, but with complex

effects on energy balance, pressure and the melting mechanism. If changes in settings of pressure, speed, etc., must be made, they should generally be done one at a time and adequate time allowed for the system to come to near-equilibrium before further adjustments are attempted. Modern three-term temperature controllers are designed to respond automatically to wide changes of conditions, but the speed of their response must be a compromise with the avoidance of large overshoot or instability in the heat and flow mechanisms within the extruder. Sometimes repeated changes in output (surging) or temperature will take place over periods of several minutes – this is probably due to the temperature controllers being incorrectly adjusted, requiring expert attention.

With experience the operator may be able to anticipate the result of deliberate alterations and so save time and material, especially in setting temperatures, but it is always wise to watch for signs of overload or rapid fluctuations of the motor ammeter and pressure gauge (if fitted). The main requirement for steady operation of the extruder itself is a continuous feed of polymer – possible problems in the feeding mechanism have been dealt with in Chapter 7. A temporary reduction in output due to these will upset downstream operations, possibly requiring rethreading to restore stable conditions, but if the screw has substantially emptied, care must be exercised in recommencing feeding to avoid pressure or power surges (section 12.3). Some common operating problems and possible corrective action are given in Table 12.1.

12.2 COLOUR AND GRADE CHANGING

A frequent cause of disturbance of steady running and good product is a change in the feed material; this may be due to variations in the raw material as supplied, to variations in compounding or rework, or feeding incorrect material. This can only be corrected by empirical and wasteful changes in operating conditions unless rigid quality control of the feed enables the cause to be discovered quickly.

If it is required to change from a low-viscosity (high Melt Flow Rate (MFR)) to higher viscosity (low MFR) grade of the same polymer, this is readily achieved, since the higher viscosity usually ensures removal of the softer polymer. However, some mixing is likely to occur, giving off-standard product, and this may recur intermittently for some time due to material held up on the screw or in the die adaptor. To minimize wastage, screw speed and output may be reduced temporarily. If the change in viscosity is considerable, this opportunity can be taken to increase barrel and die temperatures, so that drive power is not excessive when output is restored to its original value.

Changing from high to low viscosity is much more difficult, since the fresh material will tend to bypass the harder polymer, which is liable to break away intermittently when steady conditions have apparently been re-established. If it is not practicable to stop and remove the screw for cleaning, probably the best strategy is to remove any screw cooling, reduce speed and temperature to the minimum practicable to produce maximum shearing action for melting and mixing, stop feeding and allow the machine to empty as far as possible. Then the machine should be kept running for several minutes to allow the screw to warm up and soften any remaining polymer. Then feeding should be recommenced with the softer grade, slowly as in start-up, and the mixed polymer allowed to run to waste for, say, 5 min before attempting to thread up the haul-off. It may be desirable to repeat this procedure rather than keep running steadily, then watch for contamination when returning to desired operating conditions. The change may be assisted, though at some cost in material, by first feeding a blend of the original hard grade with much softer material in an attempt to match the viscosity of the new grade to be introduced.

Changing colour may follow a similar procedure, bearing in mind that different pigments and other additives will give different viscosities to their compounds. If detailed information on viscosity versus temperature for each compound is available, it may be possible to program the changes from softer to harder compounds, though for reasons of colour matching it is more usual to move from light to dark colours, through greens and blues to greys, or through oranges and reds to browns, before dismantling and cleaning for a return to white or pastel colours. Alternatively, since the change of viscosity with temperature may vary, it may be possible to operate temporarily in a temperature range in which the colour change is also from lower to higher viscosity.

When changing from one class of polymer to another, either temperature or shear rate (output) may be used to ensure the change is from lower to higher viscosity, especially for groups such as polyolefines, within which different polymers mix readily with each other. In changing between different groups such as from polyethylene to PVC or vice versa, where little mixing occurs, factors such as adhesion to metal surfaces make generalizations impossible. Indeed, these two polymers are frequently used in special formulations specifically for purging each other from extruders and other processing machines. However, as explained under 'partially filled screws' in section 6.6, it is unlikely that the purging compound itself will be completely emptied and may cause contamination when production is resumed. Because of lack of mixing, such changes almost certainly lead to breaks in the haul-off line and scrap which cannot be reused. If raw material is valuable or freedom from contamination in the product vital, shut-down and cleaning of screw and die may be essential; loss of production can be minimized by a combination of good design and efficient dismantling procedure, as indicated in section 12.4.

12.3 START-UP AND SHUT-DOWN

All extrusion processes involve hazards, and the time to start safety precautions is *before* starting the machine, by observing safe working practices, by ensuring safety equipment is to hand and by familiarity with emergency procedures, e.g. where the stop buttons are, and which drives they control. The first essential is that plant instructions are rigidly followed in respect of protective clothing and gear, safe operating procedures, and the requirements for skill and training for specific tasks, especially in maintenance and repair. Table 12.2 is intended only to supplement these instructions and draw attention to the avoidance of common hazards. Special precautions for *trained personnel* during dismantling and cleaning are detailed in section 12.4.

Steady operation requires a satisfactory start-up, and this requires care and often time. The operator should first check that there is a screw in the extruder and that it is pushed right back – the start of the thread should be in line with the back edge of the feed opening. Then he should check that the die and head bolts or clamps are correctly fitted and tightened, and that the thermocouples are all in position and connected to the control panel. If there is plastic in the hopper, the feed valve should be closed, the motor switch in the OFF position and the speed set to the lowest position. The feed pocket cooling should be turned on and the screw cooling off. The heater controls should be set and switched on. Unless certain that they are functioning correctly, it is a good idea first to set them all to 40 or 50 °C; the controllers should then show they are supplying heat, the moving pointer should rise to the set point (40 or 50 °C) in a few minutes and then the heaters should shut off. This checks that the thermocouples are connected, and the right way round, the heaters are functioning (sometimes they have separate power switches which must be 'on') and that the controllers switch heat on and off as required; this only takes a few minutes but may save hours later and avoid damage due to overheating. It should then be safe to reset the controllers to the required temperatures and leave the machine to heat up. If temperatures near to the minimum for the polymer are required, it will reduce motor load at start-up if the controllers are first set 10 to 20 °C *higher*, and then reduced to the proper setting when the extruder is running. On the other hand, if high temperatures are needed, or the polymer is very sensitive to heat (especially PVC), it is wise to set the controllers 10 to 20 °C *lower*; when the temperatures have reached these settings, they may be raised to the proper temperatures until they are again steady before starting to run the extruder. When the temperatures have reached the correct point (which may take an hour or more for a large extruder) the moving and fixed (indicating and set) pointers on all the controllers should be very close to the same temperature position. As a final check, and on controllers without an indicating pointer, the indicator light showing that the controller is supplying heat should either be flashing or coming on and off periodically. When quite sure that the extruder is at the correct temperatures, the haul-off should be in position and connected to

Table 12.2 Safety of operators

Operation	*Hazard*	*Action*
Feeding, esp. from bags or drums	Fire risk Trip hazard	Avoid spillage on to heaters or floor Clean up with vacuum, not brush or compressed air
Feeding with powders	Fire/explosion risk	Avoid spillage Earthing against static electricity No smoking
	Possible toxicity	Wear dust mask
Clearing bridging or blockage in feed	Injury and machine damage if caught in revolving screw	Don't remove safety/magnetic grid Don't lean over hopper Use only long strip of polymer, never metal
Excess pressure giving leakage of molten polymer from joints	Fire if contacting heaters	Stop/reduce speed (see Table 12.1)
	Injury if bolts break	Wear goggles and gloves
	Burns from hot polymer from die[a]	Never lean or stand in front of die, even when screw stopped[a]
Accidental contact with metal parts or heaters[b]	Burns	Avoid contact Wear gloves and footwear Post warning notices 'HOT' or 'LIVE ELECTRICS' if leaving machine
Contact with molten polymer	Skin burns[c] Eye injury	Avoid contact Wear goggles, protective gloves and footwear *Isolate* motors when working on extruder, die or haul-off
Contact with live electrics, e.g. exposed terminals, wet cables	Electric shock Consequential injuries	Wear gloves Keep cables off floor *Isolate* heaters when covers removed
Mechanical movement or falling components	Trapping, esp. fingers	*Isolate* drive motors
	Crushing, esp. feet	Keep guards in place whenever possible Avoid in-running 'nips' and close clearances Wear protective gloves and footwear

[a]Molten polymer may be suddenly and violently ejected from the die after several minutes due to decomposition and gas formation at high temperature.
[b]May be much hotter than set temperatures (see A and C in Table C.2).
[c]Avoid instinct to pull off polymer, which will cause an open wound. Though very painful, plunge in cold water and shake about until cold; then get medical attention *immediately*.

power, water, air, etc., e.g. the wire threaded up in wire covering. With waterbaths, as in tube sizing, it is usually as well to move the bath several centimetres from the die to give space for handling and avoid splashing water on the hot die. A tin with some water may be placed under the die for start-up material, or the haul-off started running at minimum speed. While watching the motor ammeter for overload, and pressure gauge if fitted, the motor should be started at lowest speed without any polymer. If the motor amperes or pressure get near the safe limit, stop the motor immediately and wait for the machine to heat further or investigate the cause. If molten polymer comes from the die, this indicates that it is clear and it is safe to feed polymer, but *slowly*. If no polymer comes from the die, the machine is probably empty and care must be taken until certain that the die is clear. The operator should drop powder or granules by hand a little at a time into the feed hopper, but never enough to fill the screw; this is because the polymer will travel quickly down an empty screw, without time to melt properly, and if then forced into the die when the screw fills, it may block the die with unmolten particles, bursting the joints or damaging the die. This is especially important with very narrow dies, e.g. for film, or where there is a large space between the screw and the narrow part of the die, which may take several minutes to fill. When molten polymer is flowing steadily from the die, without excessive motor load, the feed may be gradually increased until the screw is full in the feed opening – it is then safe to fill the hopper or open the feed valve completely. To save waste, as soon as the polymer flows from the die, it can be fed through the haul-off – this is usually much easier when running slowly. Cooling water or air pumps and jets should then be started and the haul-off speed adjusted to give approximately the correct size of extrusion, waterbaths can be carefully moved closer to the die, and vacuum for tube sizing, air for tubular film blowing and cooling, etc., gradually supplied. When the whole line is running steadily, the extruder screw speed and the haul-off speeds should be increased slowly to the running speed, approximately in step, while watching the main ammeter for overload. The speeds should then be adjusted to give correct dimensions as far as possible, and only then final adjustments made to the die settings – it is a waste of time to do it earlier since swelling and drawdown depend on temperatures and speeds. It is impossible in this volume to cover all the different types of haul-off equipment and end product. The aims are first to achieve the right size and shape, then the right properties (opticals for film, wire adhesion for insulation, etc.), the right appearance and surface finish, and then to keep all these at the highest possible output.

To shut down the process in emergency only requires shutting off the feed and stopping the main motor. For a short break (say, up to 2 h), feed pocket cooling and barrel heating should be left on. For heat-sensitive materials such as PVC, company policy may be to reduce barrel temperatures while standing, or purge the barrel with a different polymer such as polyethylene. More usually, barrel and screw cooling, if used, should first be shut off and then

speeds lowered to reduce the load on the motor. Barrel temperatures may then be reduced (say, 20–50 °C) while checking on motor load, to delay decomposition of the polymer. Companies use different procedures and these should be followed carefully. Usual methods are: (i) feed through a purging compound, and stop the screw only when the compound has cleared all the working polymer from the die ; (ii) close the feed valve and let the extruder pump itself out as far as possible, then stop the screw; (iii) close the feed valve and stop the screw immediately, leaving the extruder full of working polymer, which must be melted before restarting – this keeps air and moisture from rusting the inside of the machine and accelerating decomposition of the still-hot polymer. It is obviously unsuitable for polymers which will decompose under heat alone during lengthy heating up before the next run. Once the screw is stopped, the heat to the barrel may be shut off, but not if the machine is to be restarted in the next couple of hours or if it is to be dismantled (section 12.4). If there is still polymer in the feed end of the screw, feed pocket cooling should be left on until zone 1 temperature has fallen below the melting/softening temperature.

Before leaving the machine, a prominent notice should be posted if electric supplies or the heaters are still on, or if parts of the machine are hot. Water supplies and pumps, and air supplies should be turned off. Always *isolate* the motors and pumps so that they cannot be started accidentally.

12.4 DISMANTLING AND CLEANING

Generally extruders are best dismantled hot; it will save a lot of time and hard work if dismantling, and cleaning if necessary, is done at the end of a run, and with less risk of damage. If the machine is cold, the start-up and shut-down procedures should first be followed through. For a conventional extruder and die, the following steps must be taken after shut-down:

- Close the feed valve.
- Shut off cooling (except feed pocket).
- Turn off and *isolate* drive motor.
- Check all heaters are on and temperatures appropriate for cleaning.*
- Check there are no exposed heater terminals or bare wires.
- Switch off and unplug die-lip heaters before working on or near them.
- Switch off heaters before removing their control thermocouples, to avoid overheating.
- Move waterbaths, etc., to leave space in front at least as long as extruder screw.

*Polymer should be quite soft, but not decomposed in air during time required for cleaning.

- Place conveniently safety gear, tools, cleaning materials and lifting gear, including a bucket of cold water, useful for cooling spanners, bolts and brushes. A rubber moulder's pad, or even a folded glove, is useful, in addition to heat-resisting gloves, when supporting or carrying hot die parts.
- Provide bench, stout boards or other non-scratch, non-inflammable supports ready for hot metal parts.
- Disconnect cooling pipes and other connections not part of the heating system.

Dismantling can now proceed, starting from the die exit:

- Aim to keep each part hot as long as possible, so disconnect heaters one at a time, as far as consistent with electrical safety.
- When each heater or group is disconnected, remove the corresponding control thermocouple(s) and tie it/them back away from damage by tools or hot polymer.
- Remove the heater cover and again check all exposed heaters for disconnection. **This is the most dangerous part of extruder operation so plant safety procedures must be rigidly followed.**
- Carefully remove the first (usually die-lip) heater, using heat-resisting gloves.

Heaters are easily damaged by tools so should, generally, be removed first, with minimum flexing, using heat-resisting gloves. A mica-insulated heater (about 3 mm thick) need only be loosened by slackening screws in the joint and then sliding off endwise; if it cannot be slid off, it should not be flexed more than 6–12 mm (depending on size), but separated completely into halves or left until a later stage. A ceramic-insulated heater (about 12 mm thick) must not be flexed and must usually be separated into halves. The segmental ceramic type made up of separate pieces of rigid insulator surrounded by metal bands must be handled even more carefully – they will flex slightly, but the coiled heating element running between the insulators can be stretched and damaged*. Cartridge heaters (rod type) should if possible be left in place.

- As soon as the heater is removed, dismantle the first part of the die.

Before the next part is taken off, the first should be cleaned and placed carefully on a clean smooth surface, avoiding joint faces or parts which contact the polymer.

Contact surfaces should be cleaned first and only with aluminium and brass tools, brass brushes or brass wool. Special care is needed with chromium-plated surfaces – if scratched they will spoil the product and be

*Heaters should be stowed off the floor and away from risk of damage; they should not be handled by the cable, but by the joint flange or terminal box and without tools.

more difficult to clean next time. Rigid polymers like polystyrene and acrylic tend to crack off cold metal surfaces (others, including polypropylene, will peel off); the purpose in these cases of cleaning hot is to remove as much as possible while soft so that the remainder can be removed cold with as little force as possible – with accompanying reduction in damage to the die. Polyproyplene sticks to hot metal while LDPE sticks to both hot and cold metal – so it is better cleaned hot, while it is still soft. Rigid (unplasticized) PVC peels away quite cleanly from both hot and cold metal, provided the PVC has not degraded (decomposed) too far, and the metal is smooth and not rusty, but like polypropylene it is very stiff when cold requiring more force and risk of damage. Plasticized PVC is similar, but being softer is probably better peeled off when cold. With most polymers, once cleaned and dry, the die only needs keeping dry or a light smear of grease. PVC is the exception – a clean, dry warm die smeared with grease will (unless chromium-plated) rust under the grease overnight – because acids from the PVC soak into the pores of the metal, and these acids then pick up moisture from the air. The best remedy is that for cleaning army rifles and for the same reason; several litres of boiling water poured through the die, which is then allowed to dry and lightly greased – the water 'sweats out' and dissolves the acids and the heat also ensures it dries quickly before being greased or otherwise protected from rusting.

The die should then be dismantled and cleaned, piece by piece, removing heaters as necessary. Tapered die entrances often hold a considerable amount of polymer; if this can be eased away from the metal at the wide end and then allowed to cool until it is slightly leathery, it can be gripped with a pair of pliers and *slowly* pulled out. Pulling makes it narrower, separating it gradually from the metal before it breaks off at the narrow end and releases a large piece; this is usually quicker and cleaner than poking or digging out the polymer. Any plug remaining at the narrow end can then be pushed through with a wooden, Tufnol or aluminium cleaning rod, preferably in the flow direction to avoid damage to the die lips. This should be done slowly so that the polymer does not swell and wedge in the die. The die can then be brushed with a fine brass bottle-brush, preferably wetted with a little cold water to prevent clogging. If still hot enough, the die may be polished with a clean, strong cloth wrapped round the cleaning rod – if the die is too cold, the cloth will stick.

If solvents are used, instructions should be followed, especially to avoid fire and breathing fumes. Solvent baths require special precautions, which should be followed carefully. On removal, die parts should be allowed to cool slowly out of draughts and supported away from cold metal to minimize distortion, but with fume removal. When cold, they should be kept dry and protected, e.g. with a film of grease, as the solvent leaves the surface very liable to corrosion.

With dies having a separate core or mandrel (as for tube and tubular film) this should be cleaned as soon as removed since it will cool quickly and is difficult to reheat out of the die. If the die's outer element has meanwhile cooled too much, it can be warmed on a laboratory hotplate, but quick work can often avoid this. Heating in an oven is not recommended; it is usually slow, produces fumes and drips of soft polymer in the oven, which may catch fire when the door is opened, and cleaning cannot continue while the die is heating up. Burning off in a furnace or with a gas torch should only be used as a last resort, e.g. if the polymer has already decomposed to a hard char – the burnt plastic residues are hard to remove, the metal surface will be roughened with 'scale' and the die parts may be distorted by uneven heating or cooling and rendered useless. When the die is fully dismantled and cleaned, it should whenever possible be left assembled mounted on the extruder or on a bench to minimize the possibility of accidental damage.

The screenpack, breaker plate and die adaptor may now be removed and cleaned in the same way, except that the screenpack will probably be replaced.

Ready-made packs with a soft metal binding are expensive, but much better than ones made from loose pieces – the soft edge makes a good seal, the finer gauzes cannot be displaced or trapped at one edge by the spigot, and correct combination of gauzes is ensured; they must still be replaced the right way round so that the fine gauzes are supported by the coarser ones from being pushed into the breaker-plate holes by the pressure from the extruder. If the screenpack is to be reused, do not forget that it may contain 'gels' of hard plastic which will cause 'fisheyes', etc., in the product, as well as dirt, fibres, burnt plastic, etc.

Next, clean out the polymer at the end of the screw and from the joint face ready for reassembly of the adaptor and die. If the screw is also to be cleaned or exchanged, then a screw or hydraulic jack designed for the job should be used – a hammer is ineffective and liable to damage the machine.

If the screw is to be pulled out, the screw nose will usually be removed first so that the puller can be inserted. If the screw is pushed from the back, the screw-cooling rotary union and 'wand' (inner tube) must be removed and possibly the outer tube. (This tube and the thread for it in the back of the main screw are much more easily damaged than the screw itself.)

Release any locking ring or screw on the drive shaft. Slacken the gland at the back of the feed pocket. Pull or push the screw forward, not more than to expose two turns. If the screw will not move or sticks at some point, ensure:

- it is not locked back, e.g. by the screw cooling tube;
- it is not fouling, e.g. on a register ring or pressure transducer at the front, a drive key hitting the back of the feed pocket or solid polymer jammed in the feed pocket;
- temperatures are high enough to melt the polymer;

- it can be pushed back to its running position; and
- it can be turned (by barring the motor by hand if still engaged with the drive shaft).

Strip exposed turns of the screw and clean thoroughly.

Except on chromium-plated screws, steel scrapers can be used; a wall-paper or paint scraper with rounded corners and width to fit easily within the screw channel is convenient, but not harder than spring-temper. This may be frequently dipped in cold water to reduce sticking to the polymer and a steel wire hand-brush similarly wetted will remove the remaining plastic without clogging. A strong clean cloth used like a strap may be used for a final polish, but first make sure that the corners of the channel are free from hard or decomposed plastic.

Push the screw forward another two or three turns and repeat the cleaning process before this portion cools. Repeat as necessary, ensuring the polymer is removed while still soft and that the portion of the screw being cleaned is well supported. This method is excellent for LDPE but for polymers such as polypropylene which do not stick to cold metal, it may be preferable to scrape off the bulk while hot, let the screw go quite cold and then peel off the thin film remaining. When the feed section is reached, the unmolten power or granules should just brush off. Pull the screw right out and place it either flat on a wooden bench or vertically in a rack to cool naturally to avoid warping.

Now switch off the barrel heaters and, while still hot, clean the barrel. A steel wire flue brush may be used, say, 3 mm larger than the barrel bore and welded to a handle at least 1 m longer than the barrel. It should be worked up and down with a screw action until the barrel is shiny throughout when viewed from the die end. Take care not to push the brush past the feed opening, where it may damage the rear seal. With a gentle blast of compressed air in the feed pocket, any loose particles or polymer or broken wire from the brush should be blown out. The barrel should be inspected again for cleanliness and finally the bore and face of the drive shaft checked for damage and that the drive key(s) is in position in the shaft or screw.

With twin-screw machines the barrel is usually withdrawn forward over the interlocking screws; maker's instructions must be followed carefully, especially to support the barrel weight correctly so that it does not deflect the screws.

When reassembling, check that keys are in position, that they are aligned with keyways in both shaft and screw, and that the screw is tight against the end of the shaft – this is important if mixing devices are fitted as otherwise the screw may foul or move back when the extruder is started. The correct position of the front of the screw relative to the barrel sealing face should also be checked. The feed pocket seal, if fitted, should be readjusted, the screw nose and then the

screenpack (right way around) and the breaker plate refitted. Before refitting the adaptor or die, it is as well to make sure there is a screw in the machine!

Rapid and effective cleaning can be aided by careful design. In one instance a production team required 32 h to strip, clean and reassemble a 114 mm (4.5 in) extruder with a hot-melt cutter. An alternative design of cutter, incorporating a hinged door in line with the screw and several other aids including mountings for screw-puller gear, hooks for the dismantled heaters, flexible hydraulic hoses and plug connectors for heaters, was demonstrated to the production management in which two men completed the operation, from shutting down the extruder and cutter, removing and cleaning the screw, to resuming operation at full output in 8.5 min, using procedures described in this chapter. This undoubtedly owed much to the experience and organization of Mr J. Whitenstall as a Naval Chief ERA, but would have been impossible without the practical understanding and careful design of Mr B. Tunnicliffe.

12.5 WASTE RECOVERY

Scrap always represents a cost, usually in several ways, and often results in a waste of expensive raw material. Even if the material can be fully recovered, this requires extra energy, labour and cost. It also represents a waste of energy in the main process and a loss of production capacity – production which otherwise could have been sold at a profit. Scrap is of several types:

1. Edge-trim, 'ends', etc., produced as part of the process.
2. Raw material spillage.
3. Clean, undecomposed product with wrong dimensions, breaks, incompletely melted or poor surface, etc. This results from wrongly compounded material, incorrect extrusion conditions (including running too fast – see section 9.5), unsteady operation, incorrect haul-off or cooling conditions.
4. Product containing slight contamination due to dirt, colour or grade changes, purge material, decomposition due to excessive temperatures, etc.
5. Material in strips or long lengths produced during start-up or output changes, clean but of incorrect dimensions and surface, and possibly incorrectly melted or compounded.
6. Lumps and irregular pieces produced during start-up, shut-down, or jams in the haul-off, clean or dirty.
7. Purgings, cleanings, machine leakage, spillage on heaters and other hot parts, pieces 'lost' in water system, cutters, etc. (often grease- or dirt-contaminated).

Scrap of type 1 should be totally recoverable for sale or reuse. Cleanliness is paramount, and it is better to waste a little more than risk spoiling a whole batch. Sacks, bins and granulators for reclaim must be scrupulously clean and it is better to run a trial first. If reused, check operating instructions for

permitted proportions of rework as even a different particle shape may affect feeding or product properties may be changed.

Scrap of type 2 should be avoided or minimized at all costs as it is a direct addition to raw material cost. In this state it is easily contaminated and impossible to clean – only recover what is certainly clean and sweep up the remainder immediately – it is a hazard for falls and possibly fire.

Scrap of type 3 should be recoverable as type 1 if quantities and shape justify the cost of granulators, storage, etc. As for type 1, check on proportions permitted for reuse.

Scrap of type 4 should be stored separately and protected from further contamination if quantities are likely to justify recovery. It should only be regranulated if the granulator can be cleaned afterwards for use on type 1, 3 or 5 scrap. If so, it may be useful for trials, purging, start-up, etc., but contamination of the extruder must always be watched.

Scrap of type 5 can be treated as type 3 scrap if of convenient shape and sufficient quantity.

Scrap of types 6 and 7 cannot easily be recovered, so should be kept separate from other scrap and disposed of as soon as possible, but not mixed with metal, paper, etc., because of risks of injury and fire.

Granulators are dangerous; watch should be kept for loose parts or insecure guards and instructions should be observed. If the machine jams and does not clear in 5–10 s, do not push in more scrap but switch off, wait for it to stop, and follow cleaning instructions. While cleaning or dismantled, pull the plug or make sure it cannot be switched on accidentally – do not rely on safety switches. Even without power, cutters are very sharp and have high momentum – they will cause severe injury even when turned by hand. The corners and crevices in the granulator are difficult to clean and some materials may smear on the blades or casing, only to break off later and spoil another batch. After cleaning, a trial run is always worthwhile to ensure correct working and clean product. Granulators produce dust and noise, so are often in a separate room. The dust attracts static electricity and so dirt, and is often highly inflammable – it also hinders refeeding to the extruder, so is best disposed of. Dust masks and/or ear muffs should be worn as instructed.

Compounding of either powdered polymers or colours, etc., into granules is also often dangerous, dusty and noisy, and wherever possible should be carried out in a separate room; safety procedures for cleaning are especially important. Contamination is at least as great a hazard as in the extrusion operation, especially if scrap is being recovered. This may arise from spillage, dirty containers, cross-contamination of one batch or colour by another, by water or moisture in the atmosphere.

Application to the individual machine

13

It would be easy to call for more data in every aspect of extruder operation; reliable data, especially on larger machines, are always valuable in verifying and extending generalized predictions. The trade processor, however, needs more immediate information to obtain the best quality product and then maximize the efficiency of production, usually by maximizing output without significant loss of product quality. The following ten items are proposed to form a basis for satisfactory operation; most of them use the processor's own equipment, and are to some extent specific to it. Some require instruments not commonly found on production machinery, but well worth installing for a limited period to obtain data important for product quality and uniformity.

1. **Screw dimensions**. As mentioned in Chapter 6, the basic screw dimensions of diameter, pitch, flight width, channel depth and length permit calculation of the volumetric drag flow at any speed by means of equation (6.11). Comparison of the actual flow rate with (twice) the drag flow gives the value of Q/Wbh and hence the sign and approximate magnitude of the pressure gradient, which coupled with the (helical) length gives an indication of the total pressure. This dimensionless flow rate also gives an indication of the relative specific power input and the proportion of energy contributed by internal shearing. Most important, it indicates the general position in the operating field and so the likely consequences of any deliberate change in operating conditions.

2. **Flow properties**. As suggested in section 11.4, unforeseen changes in flow properties of feed material are a common cause of unprogrammed changes in operation and in product quality; equipment for routine testing of Melt Flow Rate is therefore essential. This equipment can be used without modification to obtain the melt viscosity of the polymer at low shear rates and over a range of temperature, representing conditions within the screw channel. This permits estimation of the effects of melt temperature on mechanical power input E,

and, with the specific heat (see 3 below), estimation of the change in adiabatic temperature or heater power input H (Fig. 8.10).

The standard equipment for determination of Melt Flow Rate is restricted to a fairly narrow range of low shear rates, so gives little indication of viscosity at the high shear rates existing in the die and in the screw flight clearance. Capillary viscometers designed for these higher shear rates are more expensive, but can be used, with due precaution, to obtain Melt Flow Rates as well as a wide range of much more informative data. Values of viscosity in the die permit estimation of die pressure drops and hence the balance between screw and die characteristics represented by the factor $(1 + B\eta_{\text{Die}}/K\eta_{\text{Screw}})$ on p. 153. Viscosity in the flight clearance permits estimation of the balance between mechanical power in the screw channel (equation (8.7)), which varies with back pressure, and the power in the flight clearance (equation (8.8)), which is independent of pressure. The high shear viscometer also gives the variation of viscosity in the die with temperature – usually less than that at low shear rates applicable to the screw channel (p. 31). But the high shear viscometer not only gives the viscosities appropriate to different parts of the process, but also by calculation of the pseudoplasticity index n gives the correct shape of the (isothermal) non-Newtonian flow curves for screw and die (Fig. 6.28) and also the curve of mechanical power E against speed (Fig. 8.12). The former gives more accurate estimates of the effects of speed change on output and pressure, while the latter permits estimation of the effects of speed on mechanical power and energy balance or temperature change.

3. **Thermal properties**. Data on the specific volume of the polymer at processing temperature are essential to convert volumetric flow rates calculated in 1 above to mass flow rate and also in estimating energy requirements which are based on mass. The enthalpy content of the polymer at processing temperature I is a necessary factor in the energy balance (equation (8.2)). As a simple guide, enthalpy multiplied by desired mass flow rate gives the mechanical power required at the adiabatic temperature, and an over-estimate of that required at higher melt temperatures; this gives a rough guide to the maximum output achievable with a given drive motor, disregarding limitations of product quality. Enthalpy of the polymer is also an important factor in deducing the changes in mechanical power and heating/cooling requirements consequent on deliberate changes in temperature, screw speed or back pressure. However, for small changes from an established datum, the mean specific heat in the melt state is a sufficient approximation.

4. **Heat losses**. In appendix C.1 the measurement of heat losses from the machine is shown to be a simple, once-for-all test for each physical set-up of barrel length, adaptor and die type and heaters. It indicates the stand-by losses and, with the polymer enthalpy (3 above), the total energy input required and its variation with temperature (Fig. 8.10). These permit construction of the energy balance and determination of the maximum heater energy required to maintain a specified combination of output (speed) and temperature. Heat

losses are also significant in the temperature (or speed) difference between adiabatic and autogenous conditions; Figs 8.10 and 8.12 illustrate how these losses permit a lower melt temperature or higher screw speed than in the absence of losses, before intentional barrel cooling must be employed.

In addition to the physical set-up, the usual feed pocket cooling rate and inlet temperature should be set, the screw fitted (for heat conduction along the screw) and ideally the screw channel should be filled with polymer (for heat transfer to the screw). Screw cooling should not be used and ambient temperature will have a slight effect on the general level of losses. The main variables are the (set) temperature level (say, at the end of the barrel, approximating the desired final melt temperature) and the temperature profile along the barrel.

5. **Mechanical power input**. Measurement of output Q and mechanical power input E against speed N for fixed temperatures gives the basic performance of the screw with the polymer used. The output and screw dimensions (see 1 above) give the value of Q/Wbh and any changes with speed. The power input indicates whether operation is possible at the given temperature and, since power is nonlinear with speed, whether the rating of the drive motor limits the maximum screw speed. Power measurement will also indicate (by extrapolation if necessary) the adiabatic and autogenous speeds for the given temperature (Fig. 8.12). Since mechanical power E increases more than in direct proportion to speed N, the specific power E/Q will increase with speed. However, the *rate* of increase will indicate how closely the viscosity approaches Newtonian behaviour (Table 8.3 for ηN), including the effect of power absorbed in the flight clearance. The trial may be carried out either at fixed back pressure or with fixed die dimensions. The former is perhaps more useful for academic investigations, while the latter is closer to the usual industrial situation. As shown in section 6.5, in this case output is approximately proportional to screw speed and thus Q/Wbh is nearly constant. As suggested previously, this is a useful basis for comparing performance, both in respect of velocity and shear rate distribution in the channel, and hence of mixing and shear heating, and also of longitudinal pressure profiles (see Figs 6.9–6.11). Constant Q/Wbh also gives wall shear rate proportional to speed (equation (6.69)) and a constant value to the square bracket in equation (8.7).Thus the change in power is due only to the direct effects of speed and viscosity, and for a power-law approximation gives a constant proportion between the power in the channel and in the flight clearance (the two terms of equation (8.9)). The test at fixed die dimensions also avoids the use of a pressure transducer and manual adjustment of back pressure.

Practical methods of power measurement are discussed in appendix C.1.

6. **Power versus temperature**. The preceding test would naturally be carried out at the desired operating temperature and need only be of sufficient duration to allow steady-state temperatures to be re-established at a few speed settings. It may be that the desired final melt temperature is unknown or that a range of

temperatures or polymer viscosities may be used. This then requires the tests to be repeated at, say, three temperatures, though the changes are likely to be such as to permit linear interpolation for other temperatures within the range. This also gives an indication of the change in mechanical power input with temperature at a given speed, from which the heating/cooling power for other temperatures can be deduced (Fig. 8.10). It will also indicate the sensitivity of the system to small deviations in temperature and help fix the allowable tolerances for satisfactory process control (Table 11.1). Possibly even more important would be measurement of mechanical power at a fixed speed and final melt temperature, but varying the temperatures in the melting section only. As mentioned in Tables 9.4–9.8, the relative contributions of conducted and shear heating will affect the mechanism of melting and possibly the position and temperature variation at break-up of the solid bed, with the consequences for subsequent elimination of the remaining solid particles.

If direct measurement of power is impossible, ammeter readings will give qualitative indications and a basis for resetting conditions – with the provisos for older types of drive mentioned in appendix C.1.

7. **Limiting outputs**. In the preceding tests the product quality has largely been neglected. As a first step, the maximum screw speed and corresponding output should be found for each final melt temperature and for several practicable temperature profiles (see Fig. 9.6). This may be on the basis of visibly distorted or unmolten particles at the die or on an accepted criterion of satisfactory product dimensions or quality; in the latter case assessment may be confused by consequential changes in downstream processes, such as cooling and drawing. The effect of barrel temperature profile is particularly informative, since a profile giving a higher limiting output on any of the above criteria is also likely to permit higher output on any more severe criterion such as melt temperature variation, which cannot be so easily determined.

8. **Space variation of melt temperature**. This requires an array of melt thermocouples and/or a travelling thermocouple beyond the end of the screw and at various radial positions (section 11.1). Because of possible damage, it is suggested that these are only installed for the duration of these tests, but that they are of fairly robust construction (say, 3 mm in diameter) since a time-averaged temperature is required. As described in section 11.1, the profile appears to be characteristic of the screw type, but to amplify with screw speed. It is not clear to what extent it is dependent on the polymer used, or on the barrel temperature profile. The former may be of no consequence to a processor using a single polymer, but the latter would extend the information from 7 above. The two significant factors appear to be the average temperature in the melting section, and hence the subdivision between conducted and shear heating (see 6 above), and the temperature rise in the melt pumping section, i.e. the excess of the final melt temperature over the softening/crystalline melting point.

The data from this series of tests would give direct evidence of lack of uniformity in the melt at the die, give warning of incipient incomplete melting and contribute to understanding of non-uniform flow in the die, drawdown problems and non-uniform properties in the product. It is basic to maintenance of product quality and could be combined with 6 above.

9. **Movement of 'gel' point**. This requires initial provision of at least three tappings in the barrel for pressure transducers, the latter being fitted only for these tests. The movement of the position of initial pressure rise with speed would be useful in any calculations of performance requiring a value for melt length z, and especially in modifying the effects of screw speed discussed in section 8.5, where melt length was assumed constant. It will also indicate the melt length available for reducing temperature variations originating in the melting process and possibly the onset of incomplete melting.

Movement of the gel point with changes in temperatures in the melting section would help explain the effects on final temperature variation found in 8 above.

This test would be important in finding the correct temperature settings for the melting section, as well as its location, and might usefully be combined with 6 above.

10. **Effect of back pressure on melting**. This requires the same instrumentation as the preceding test, with the addition of an adjustable restrictor at the die. The aim would be to find the movement of the 'gel' point with increase of back pressure at constant speed and temperature. A movement towards the die might imply a delay in break-up of the solid bed, but also an increase in final melt temperature variations. The decrease in melt output rate should ease melting requirements and might permit a higher speed before surging or unacceptable temperature variations set a limit to output. Thus increased back pressure by means of screen packs might improve performance, or it might indicate improved performance from a shallower screw (see Table 9.8).

The last three of these tests require special equipment and may be considered as 'research' by industrial operators. They are included as giving direct indication of factors affecting product quality. The whole series of tests has been deliberately arranged in order of effort required, recognizing that many processors will not have the wish or opportunity to complete them all. However, the author believes that each will contribute valuable information and together they will form a sound basis for improved operation and control; indeed they will provide much of the process model necessary for the most sophisticated computer control. Much of the foregoing is specific to a particular machine, screw, polymer and die arrangement and lacks the generality for extension of the principles of operation and control. The author would select just five areas for more fundamental study as likely to make the greatest contribution to understanding these principles:

1. Factors affecting the melting process, including the position of break-up of the solid bed, and the resulting non-uniformity of temperature.

2. Actual comparative performance, including 'quality' factors, of different screw lengths, depths and profiles for several commercial polymers over a range of speeds, temperatures and back pressures.
3. Effects of barrel and screw cooling on energy balance, mixing and final temperature variations.
4. Factors affecting time fluctuations of final temperature as an indication of origins of instability and poor quality.
5. Development of a *general* process model for single-screw extrusion, including 'quality' factors, for use in improved overall process control.

Appendix A
Properties of polymers for heat and flow

The physical properties of polymers which are important in melt processing have been discussed in Chapters 3 and 4. They include density (or its reciprocal, specific volume), specific heat, thermal conductivity and melt viscosity. These are dependent to a greater or lesser extent on polymer type, molecular weight, distribution of molecular weight, pressure, temperature, and flow conditions. They may also be influenced by previous history of temperature or shear, causing changes in crystallinity, orientation or residual strain. These in turn may lead to anisotropy of particular properties: e.g. thermal conductivity increases (in all directions) with crystallinity; it is also increased (anisotropically) in the direction of orientation in both amorphous and semi-crystalline states, though probably not to the same extent in each state. There is also some evidence that thermal conductivity is anisotropic in strong shear flows, possibly due to melt orientation.

Some of these properties and interactions are extremely difficult to measure with accuracy and reliability; consequently there is a scarcity of data, especially in the melt state, and in some cases lack of agreement. For these reasons the thermal data given here (Table A.1), which are only intended as a guide, largely refer to the solid state and room temperature. These provide an approximate basis for comparisons between the processing behaviour of widely differing polymers; data for the melt state and a range of temperatures are given where possible (Figs A.1–A.5), but must not be assumed to be valid for other polymers or grades. As pointed out on p. 54, for the polymers given, specific volume will depend on the reference density (molecular weight) while changes in specific volume and enthalpy from room temperature also depend on the initial crystallinity.

Table A.1 Thermal properties in the solid state (room temperature)

Polymer (*Table* 2.1)	*Glass transition temperature* (°C)	*Crystalline melting point* (°C)	*Density* ($kg\,m^{-3}$)	*Specific heat* ($J\,kg^{-1}\,K^{-1}$)	*Thermal conductivity* ($W\,m^{-1}\,K^{-1}$)
ABS	–	–	990–1150	1380–1680	0.19–0.36
PMMA	105	–	1170–1200	1470	0.19–0.21
CAB	–	–	1150–1220	1260–1680	0.17–0.33
PC	160	–	1200	1260	0.19
PS	105	–	1040–1065	1340	0.10–0.14
PVAC	–	–	1350–1450	840–1170	0.13–0.29
SAN	105	–	1075–1100	1340–1420	0.12
UPVC	67–80	220	1350–1450	840–1170	0.15–0.17
PPVC	–	–	1160–1350	1260–2100	0.13–0.17
HIPS	–	–	980–1100	1340–1470	0.04–0.13
PPO[a]	195	–	1060	–	0.21
PES[b]	195	–	1240	1260	0.26
POM	−70	180	1410	1470	0.23[c]
EVAC	–	–	920–950	2300	–
PA 6–6	−25	250–267	1090–1140	2300–2350	0.21–0.25
PA 6	−30	215–225	1120–1140	–	0.24
PA 6–10	–	220	1090	–	0.21
PA 11	–	190	1040	2430	0.29
PETP	+70	260–267	1350	–	0.23–0.29
PBTP	–	–	–	–	–
LDPE	−60	110–117	910–925	2300	0.33–0.36
HDPE	−80	135–138	941–965	2300	0.46–0.52
PP	0	165–175	895–910	1930	0.12–0.14
TPX[d]	–	250	830	2180	0.17
PTFE	–	327	2100–2200	1050	0.25

[a]Polyphenylene oxide
[b]Polyethersulphone
[c]POM homopolymer. Copolymer $k = 0.07$ approx.
[d]Trade name of Imperial Chemical Industries PLC.
Data for density, specific heat and conductivity primarily from ref. A

For data on melt viscosity the reader is recommended to consult Cogswell (1981). This may be taken as respresentative of each class of polymer, though the variation with shear rate is strongly influenced by distribution of molecular weight. However, the absolute values are liable to considerable variation with molecular weight, manufacturing variables, and compounding additives; since viscosity enters directly into calculations of die pressure, mechanical energy, etc., an in-house measurement of viscosity at a minimum of one known temperature and two (widely spaced) shear rates is highly desirable.

For certain purposes, such as calculating heat transfer coefficients and transient conduction, combinations of properties are required, e.g. thermal diffusivity ($\alpha = k/\rho C_p$), Prandtl number ($Pr = C_p\eta/k$), Graetz number ($G_z = WC_p/kL$); these may be calculated from individual values, but in

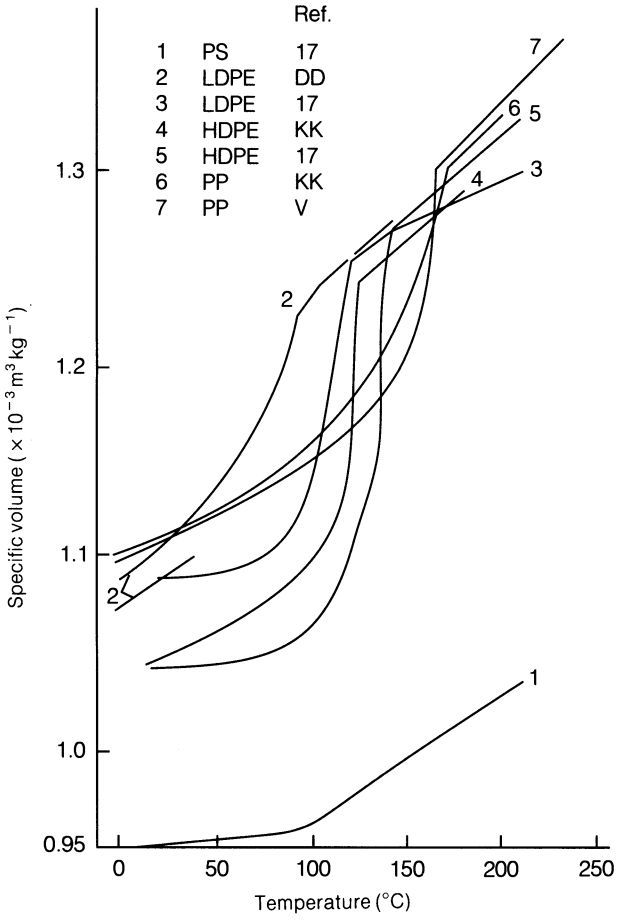


Figure A.1 Specific volume vs temperature.

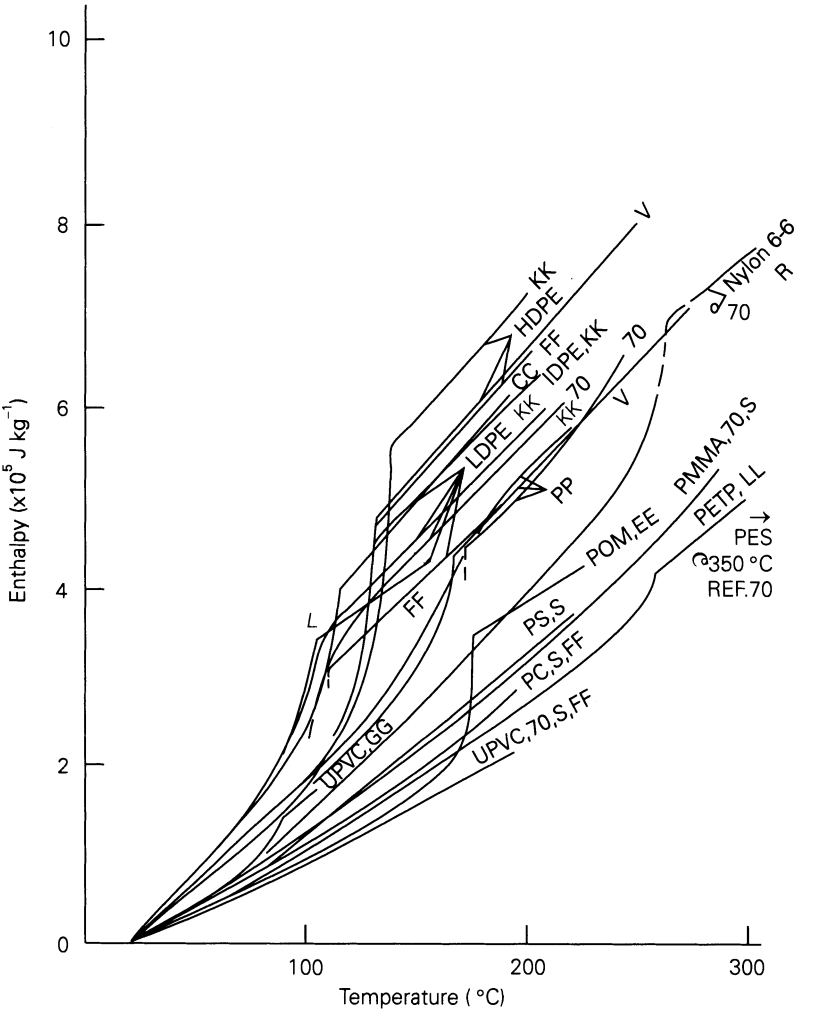


Figure A.2 Heat capacity: enthalpy above 20 °C.

some instances may be more reliably determined by other methods (e.g. thermal diffusivity from cooling experiments).

Some typical data for LDPE, air, water and steel are given in Table 4.1. An example of swell ratio (for polystyrene) is given in Figs 3.10 and 3.11.

The reference letters given in the following list are quoted against the appropriate data in Figs A.1–A.5. In some cases the same experimental data appear to have been published in more than one journal and under different

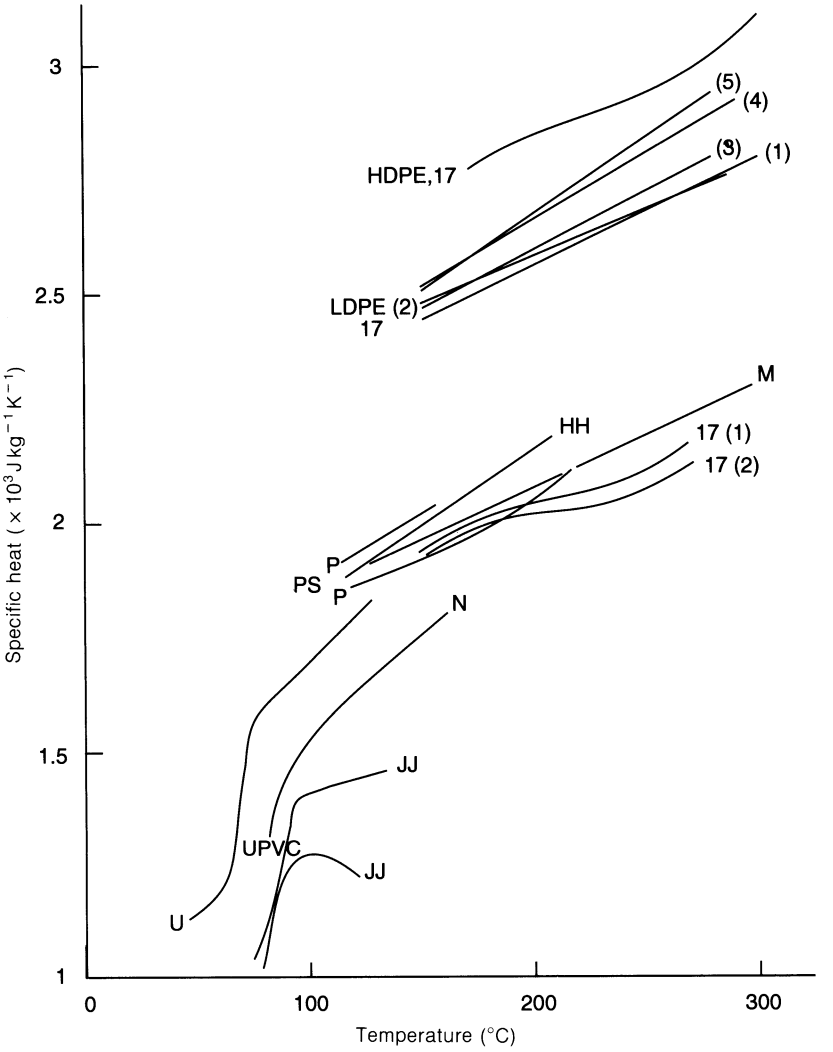


Figure A.3 Specific heats in the melt.

combinations of author's names; duplication has been avoided in this appendix where possible. The present author had endeavoured to reproduce the data as accurately as possible, but problems of scale and units may have led inadvertently to some averaging; the reader is directed to the original publications for exact values, individual data points and values outside

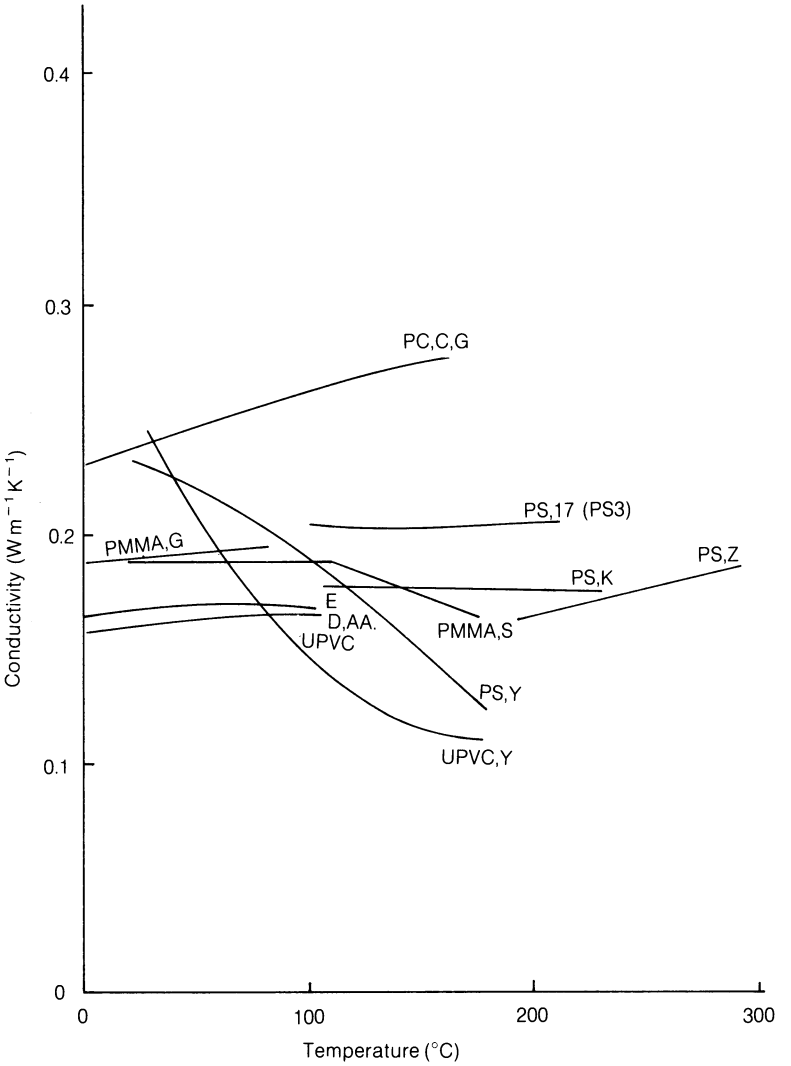


Figure A.4 Thermal conductivity: amorphous polymers.

the scope of this book. Reference back should also be made for precise materials and pretreatments used, which are here lumped under generic names for clarity. The materials tested in Adamski (1974) were supplied by the UK Science and Engineering Research Council's Polymer Supply and Characterisation Centre (PSCC) at the Rubber and Plastics Research Association and coded by them LDPE4, PS2, etc., as indicated in the figures.

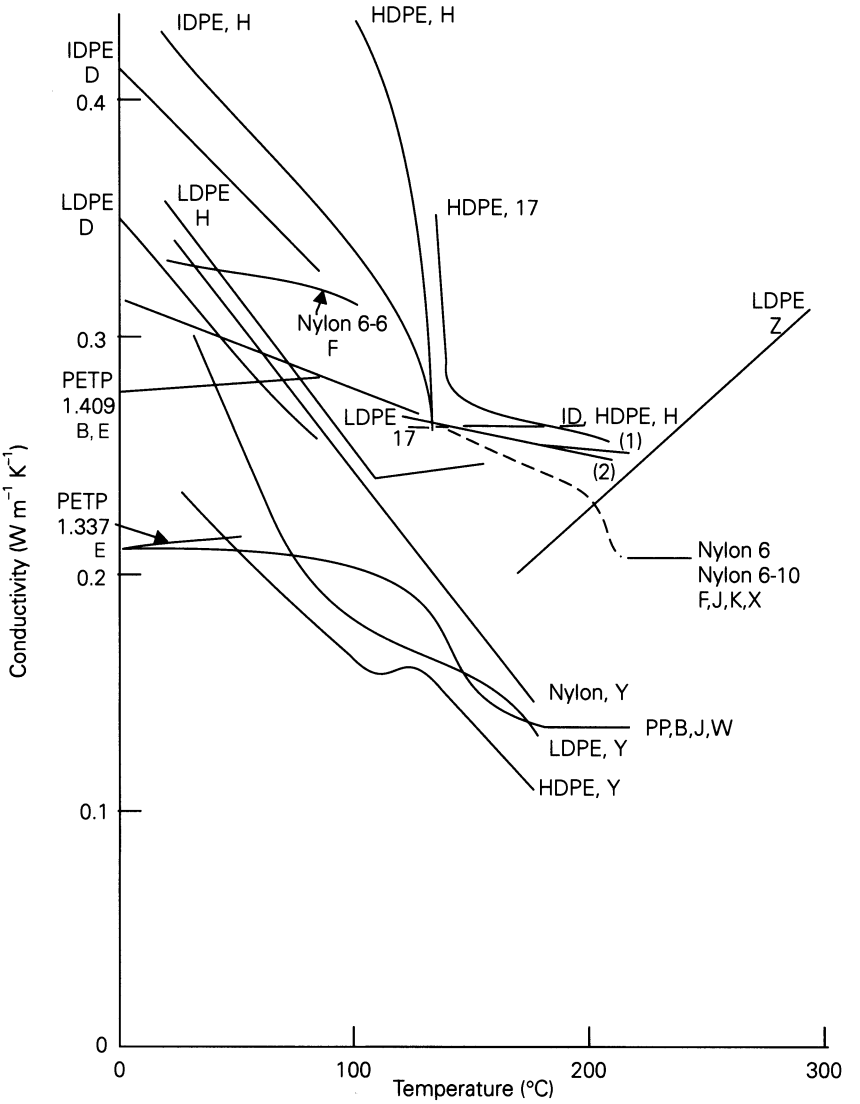


Figure A.5 Thermal conductivity: semi-crystalline polymers.

REFERENCES FOR FIGS A.1–A.5

A Anon. *Plastiques Modernes et Elastomères*, **18** (6) (1966), 128–149.
B. Eiermann, K., *Koll. Zeit.*, **201** (1965), 3–15.
C Eiermann, K., *Kunstst.*, **55** (1965), 335.
D Eiermann, K. and Hellwege, K.-H., *J. Poly. Sci.*, **57** (1962), 99–106.

E Eiermann, K., Hellwege, K.-H. and Knappe, W., *Koll. Zeit.*, **174** (2) (1961), 134–142.
F Hellwege, K.-H., Hoffmann, R. and Knappe, W., *Koll. Zeit.*, **226** (1968), 109–115.
G Hellwege, K.-H., Hennig, J. and Knappe, W., *Koll. Zeit.*, **188** (1963), 121–127.
H Hennig, J., Knappe, W. and Lohe, P., *Koll. Zeit.*, **189** (1963), 114–116.
J Knappe, W. *et al.*, *Kunstst.*, **51** (1961), 707.
K Lohe, P. *et al.*, *Koll. Zeit.*, **203** (1965), 115–119.
L Dole, M. *et al.*, *J. Chem. Phys.*, **20** (1952), 781–790.
M Abu-Isa, I. and Dole, M., *J. Phys. Chem.*, **69** (8) (1965), 2668–2675.
N Alford, S. and Dole, M., *J. Amer. Chem. Soc.*, **77** (1955), 4774.
P Currie, J.A. and Dole, M., *J. Phys. Chem.*, **73** (10) (1969), 3384–3389.
R Wilhoit, R.C. and Dole, M., *J. Phys. Chem.*, **57** (1953), 14–21.
S Wunderlich, B. and Baur, H., *Adv. Poly. Sci.*, **7** (1970), 151.
T Bares, V. and Wunderlich, B., *J. Poly. Sci. A2*, **11** (1973), 861–873.
U Wilski, H., *Koll. Zeit.*, **210** (1) (1966), 37–45.
V Wilski, H., *Kunststoffe*, **50** (6) (1960), 335–336.
W Tomlinson, J.N. and Kline, D.E., *J. Appl. Poly. Sci.*, **11** (1967), 1931–1940.
X Holzmüller, W. and Münx, M., *Koll. Zeit.*, **159** (1958), 26–28.
Y Holzmüller, W. and Lorenz, J., *Plaste u. Kautschuk*, **8** (1961), 351–352.
Z Fuller, T.R. and Fricke, A.L., *J. Appl. Poly. Sci.*, **15** (1971), 1729–1736.
AA Sheldon, R.P. and Lane, S.K., *Polymer*, **6** (1965), 77–83.
BB Shoulberg, R.H. and Shetter, J.A., *J. Appl. Poly. Sci.*, **6** (23) (1962), S32–33.
CC Raine, H.C., Richards, R.B. and Ryder, H., *Trans. Farad. Soc.*, **41** (1945), 56–64.
DD Hunter, E. and Oakes, W.G., *Trans. Farad. Soc.*, **41** (1945), 49–56.
EE Linton, W.H. and Goodman, H.H., *J. Appl. Poly. Sci.*, **1** (2) (1959), 179–184.
FF Cogswell, F.N. and Couzens, D.C., unpublished data.
GG Griskey, R.G. *et al.*, *Mod. Plast.*, **43** (11) (1966), 119–123.
HH Karasz, F.E., Bair, H.E. and O'Reilly, J.M., *J. Phys. Chem.*, **69** (8) (1965), 2657–2667.
JJ Dunlap, L.H., *J. Poly. Sci., A2*, **4** (1966), 673–684.
KK Hanna, R.D. and Lomax, J.Y., *Mod. Plast.*, **36** (6) (1959), 111–122.
LL Smith, C.W. and Dole, M., *J. Poly. Sci.*, **20** (1956), 37–56.
17 See Adamski (1974) in main References section.
70 See Cogswell (1981) in main References section.

Appendix B
Derivations of flow and pressure

B.1 ALTERNATIVE DERIVATION OF FLOW EQUATION

In a system of rectangular coordinates x, y, z, where the local velocities are respectively u, v, w, if there is a pressure gradient $\partial P/\partial z$ in the z direction only, the general flow equation for an incompressible fluid reduces to the Navier–Stokes equation:

$$\eta \frac{\partial^2 w}{\partial x^2} + \eta \frac{\partial^2 w}{\partial y^2} = \frac{\partial P}{\partial z} \tag{B.1}$$

where η is the local dynamic viscosity.

If the width b of the channel in the x direction is much greater than depth h in the y direction, the shear stress and shear rate $\partial w/\partial x$ in the x direction are constant and:

$$\frac{\partial^2 w}{\partial x^2} \approx 0 \tag{B.2}$$

Then approximately:

$$\eta \frac{\partial^2 w}{\partial y^2} - \frac{\partial P}{\partial z} = 0 \tag{B.3}$$

If viscosity η is independent of shear rate $\partial w/\partial y$ (as for a Newtonian fluid) and integrating with respect to y:

$$\eta \frac{\partial w}{\partial y} - y \frac{\partial P}{\partial z} = C \tag{B.4}$$

and integrating again:

$$\eta w - \frac{y^2}{2} \cdot \frac{\partial P}{\partial z} = Cy + D \tag{B.5}$$

Note that if viscosity is dependent on shear rate, this cannot be simply integrated.

In an extruder screw, taking velocities relative to the screw, the boundary conditions are: at $y = 0$, $w = 0$; and at $y = h$, $w = W$. Substituting in equation (B.5) gives $D = 0$ and:

$$C = \eta \frac{W}{h} - \frac{h^2}{2h} \cdot \frac{\partial P}{\partial z} \tag{B.6}$$

Putting this value of C in equation (B.4) gives:

$$\frac{\partial w}{\partial y} = \frac{W}{h} + \frac{(2y - h)}{2\eta} \frac{\partial P}{\partial z} \tag{B.7}$$

and equation (B.5) becomes:

$$\eta w - \frac{y^2}{2} \frac{\partial P}{\partial z} = \eta \frac{Wy}{h} - \frac{yh}{2} \frac{\partial P}{\partial z}$$

or:

$$w = \frac{Wy}{h} + \frac{y^2 - yh}{2\eta} \frac{\partial P}{\partial z} \tag{B.8}$$

The volumetric flow rate is given by:

$$\begin{aligned} Q_{\text{Tot}} &= \int_0^h wb \, \mathrm{d}y \\ &= \left[\frac{Wby^2}{2h} + \frac{b}{2\eta} \cdot \frac{\partial P}{\partial z} \left(\frac{y^3}{3} - \frac{y^2 h}{2} \right) \right]_0^h \\ &= \frac{Wbh}{2} - \frac{bh^3}{12\eta} \frac{\partial P}{\partial z} \end{aligned} \tag{B.9}$$

which is identical to equation (6.15).

If the pressure gradient $\partial P/\partial x$ in the x direction is considered, equation (B.1) is transformed by change of coordinates as:

$$\eta \frac{\partial^2 u}{\partial y^2} + \eta \frac{\partial^2 u}{\partial z^2} = \frac{\partial P}{\partial x} \tag{B.10}$$

Equation (B.7) becomes, for the transverse shear rate:

$$\frac{\partial u}{\partial y} = \frac{U}{h} + \frac{(2y - h)}{2\eta} \frac{\partial P}{\partial x} \tag{B.11}$$

Equation (B.8) becomes, for the transverse velocity:

$$u = \frac{Uy}{h} + \frac{y^2 - yh}{2\eta} \frac{\partial P}{\partial x} \tag{B.12}$$

Equation (B.9) becomes, for transverse volumetric flow rate:

$$Q_x = \frac{Uzh}{2} - \frac{zh^3}{12\eta} \cdot \frac{\partial P}{\partial x} \tag{B.13}$$

If equation (6.25) is substituted in eqn (B.11):

$$\frac{\partial u}{\partial y} = \frac{U}{h}\left(\frac{6y}{h} - 2\right) \tag{B.14}$$

At the barrel wall $u = U$ and

$$\left(\frac{\partial u}{\partial y}\right)_{y=h} = \frac{4U}{h} \tag{B.15}$$

The corresponding equations for downstream shear rate $\partial w/\partial y$ are equations (6.68) and (6.69). As discussed in section 8.4, this transverse shear rate will contribute to the total wall shear rate, which in the pseudoplastic case reduces the viscosity and power consumption from those based on the downstream shear rate, equation (6.69), alone.

B.2 ESTIMATION OF LEAKAGE FLOWS

For drag flow in the clearance δ the shear rate is:

$$\dot{\gamma}_{\text{clearance}} = \frac{\pi DN}{\delta} \tag{B.16}$$

Taking velocities relative to the screw, the velocity of the barrel perpendicular to the channel is $U = \pi DN \sin\phi$ so that the mean polymer velocity is:

$$\frac{U}{2} = \frac{\pi DN \sin\phi}{2} \tag{B.17}$$

(cf.equation (6.9)). The helical length of one turn (Fig. 6.1) is:

$$\frac{Z}{n} = \frac{\pi D}{\cos\phi} \tag{B.18}$$

Thus the leakage flow due to drag is:

$$Q_{\text{DL}} = \frac{U}{2}\,\delta\,\frac{\pi D}{\cos\phi}$$

$$= \frac{\pi^2 D^2 N \delta \tan\phi}{2} \text{ per turn.} \tag{B.19}$$

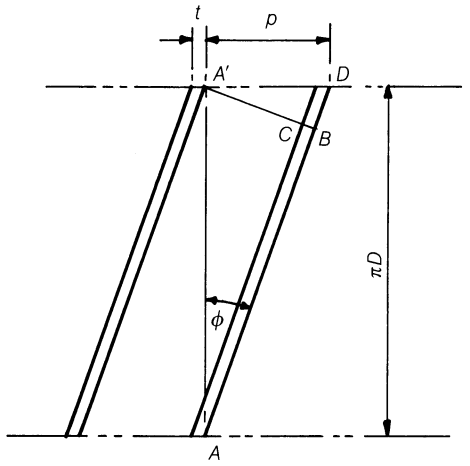


Figure B.1 Development of channel.

Expressed as a fraction of the drag flow in the channel, given by equation (6.11):

$$\frac{Q_{DL}}{Q_D} = \frac{\frac{1}{2}\pi^2 D^2 N \delta \tan\phi}{\frac{1}{2}\pi D N h(p-t)\cos^2\phi}$$

$$= \frac{\delta}{h\left(1-\frac{t}{p}\right)\cos^2\phi} \tag{B.20}$$

Typically $t/p = 0.1$ and $\cos\phi = 0.953$ ($\phi = 17.6°$, $p = D$) giving:

$$\frac{Q_{DL}}{Q_D} = 1.224\,\frac{\delta}{h} \tag{B.21}$$

If the flight width t is neglected, giving $b = \pi D \sin\phi$, equation (B.20) further reduces to:

$$\frac{Q_{DL}}{Q_D} = \frac{\delta}{h\cos^2\phi} \tag{B.22}$$

Consider now a longitudinal (downchannel) pressure gradient of dp/dz. Then in Fig. B.1 the distance $AB = \pi D\cos\phi$ and the pressure difference:

$$P_{BA} = (\pi D\cos\phi)\,\frac{dP}{dz} \tag{B.23}$$

Point A' represents the same position on the screw as A, and hence the pressure difference between B and C is also $P_{BC} = (\pi D\cos\phi)dP/dz$ due to longitudinal pressure gradient–positive if dP/dz is positive, i.e. pressure increasing towards the die.

Again applying equation (3.34) for flow through a slit die, and analogous to equation (6.13), the leakage flow Q_{PL} due to longitudinal pressure gradient will

be:

$$Q_{PL} = \frac{\pi D}{\cos\phi} \cdot \frac{\delta^3}{12\eta} \cdot \frac{P_{BC}}{t\cos\phi} \text{ per turn} \tag{B.24}$$

i.e. over a length A to D in Fig. B.1. Substituting equation (B.23):

$$Q_{PL} = \frac{\pi^2 D^2 \delta^3}{12\eta t \cos\phi} \cdot \frac{dP}{dz} \tag{B.25}$$

However, there is also a transverse pressure gradient between A and C in Fig. B.1 given by equation (6.24), i.e. $dP/dx = 6\eta U/h^2$ so that the pressure difference:

$$P_{AC} = b \cdot \frac{dP}{dx} \tag{B.26}$$

Substituting from equations (6.2), (6.5) and (6.24):

$$P_{AC} = \frac{6\pi\eta DN(p-t)\sin\phi\cos\phi}{h^2} \tag{B.27}$$

In Fig. 6.7 it is seen that the transverse pressure flow is left to right, i.e. from leading to trailing sides of the channel, and hence pressure must fall in this direction. Hence P_{AC} is always positive and the total pressure difference across the flight is given by:

$$P_{BC} = P_{BA} + P_{AC} \tag{B.28}$$

This may be substituted from equations (B.23) and (B.27), but since flow is proportional to pressure difference, the leakage flow due to transverse pressure gradient dP/dx may be calculated seperately as:

$$Q'_{PL} = \frac{\pi^2 D^2 \delta^3 N(p-t)\tan\phi}{2th^2} \tag{B.29}$$

The relative importance of drag and pressure leakage flows will evidently depend on the channel pressure gradient, i.e. on whether the screw is operating on a high or low value of Q/Wbh. Thus the leakage flow due to pressure difference is conveniently expressed as a fraction of the channel pressure flow, by analogy with equation (B.20). Adding equation (B.25) and (B.29) and dividing by equation (6.13) (substituting for b from equation (6.2)):

$$\begin{aligned}\frac{Q_{PL} + Q'_{PL}}{Q_P} &= \frac{\dfrac{\pi^2 D^2 \delta^3}{12\eta t\cos\phi} \cdot \dfrac{dP}{dz}}{\dfrac{(p-t)(\cos\phi)h^3}{12\eta} \cdot \dfrac{dP}{dz}} + \frac{\dfrac{\pi^2 D^2 \delta^3 N(p-t)\tan\phi}{2th^2}}{\dfrac{(p-t)(\cos\phi)h^3}{12\eta} \cdot \dfrac{dP}{dz}} \\ &= \frac{\pi^2 D^2}{(p-t)t}\left(\frac{\delta}{h}\right)^3 \cdot \frac{1}{\cos^2\phi} + \frac{6\eta\pi^2 D^2 \delta^3 N}{th^5} \cdot \frac{\sin\phi}{\cos^2\phi} \cdot \frac{1}{\dfrac{dP}{dz}}\end{aligned} \tag{B.30}$$

Equations (B.20) and (B.30) are used on p. 141 to estimate numerical values in a typical case and to examine the effects of the variables on leakage.

B.3 LONGITUDINAL PRESSURE PROFILES

B.3.1 Double-parallel (stepped) screw

Equations (6.38) and (6.39) are convenient for finding the pressure generated at a given speed N and output Q. If it is required to determine the output corresponding to a given total pressure rise P, then P_1 and P_2 must be eliminated. If the point at which pressure commences to rise is at, or forward of, the step, then the pressure profile will be as for the parallel screw and equation (6.20) will apply, substituting h_2 for h. If however, pressure commences to rise L_1 axially or Z_1 helically before the step, equation (6.20) must be modified to the equation due to Weeks and Allen (1962):

$$\frac{Q}{Wbh_2}\left(1+\frac{Z_1h_2^3}{Z_2h_1^3}\right)=\frac{1}{2}\left(1+\frac{Z_1h_2^2}{Z_2h_1^2}\right)-\frac{h_2^2P}{12\eta WZ_2} \tag{B.31}$$

This may be rearranged to give:

$$P=K_1\left(K_2-\frac{Q}{Wbh_2}\right) \tag{B.32}$$

where:

$$K_1=\frac{12\eta WZ_2}{h_2^2}\left(1+\frac{Z_1h_2^3}{Z_2h_1^3}\right) \tag{B.33}$$

(similar to equation (6.35)) and

$$K_2\approx\tfrac{1}{2} \tag{B.34}$$

Note that this is still a linear relation between P and Q. For pressure gradients in the stepped screw, see appendix B.4.

B.3.2 Taper and taper-parallel screws

For a uniform taper with half-angle θ (measured helically: see Fig. B.2), by similar triangles:

$$\begin{aligned}h&=h_2+(h_1-h_2)\left(\frac{Z_1-z}{Z_1}\right)\\&=h_1-\frac{z}{Z_1}(h_1-h_2)\end{aligned} \tag{B.35}$$

Thus:

$$\frac{\mathrm{d}h}{\mathrm{d}z}=-\left(\frac{h_1-h_2}{Z_1}\right)=-\tan\theta \tag{B.36}$$

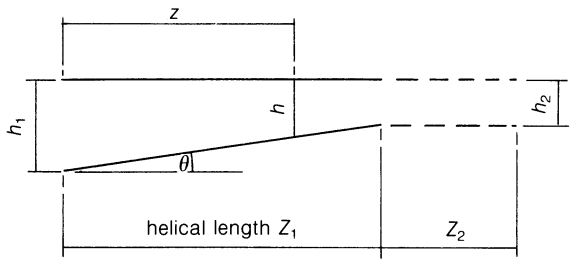


Figure B.2 Definition of half angle θ for tapered screw.

But:

$$\frac{dP}{dz} = \frac{12\eta W}{h^2}\left(\frac{1}{2} - \frac{Q}{Wbh}\right) \tag{6.42}$$

and since $P = 0$ at $z = 0$ by definition of z, the pressure rise in the first section P_1 is given by:

$$\begin{aligned} P_1 &= \int_0^{Z_1} \frac{dP}{dz}\, dz \\ &= -\frac{6\eta W Z_1}{h_1 - h_2}\int_{h_1}^{h_2}\left(\frac{1}{h^2} - \frac{2Q}{Wbh^3}\right) dh \\ &= -\frac{6\eta W Z_1}{h_1 - h_2}\left[-\frac{1}{h} + \frac{Q}{Wbh^2}\right]_{h_1}^{h_2} \\ &= \frac{6\eta W Z_1}{h_1 h_2}\left(1 - \frac{Q}{Wbh_2}\cdot\frac{h_1 + h_2}{h_1}\right) \end{aligned} \tag{6.43}$$

Alternative forms of equations (6.43) and (6.45) are given by Weeks and Allen (1962) as:

$$\frac{Q}{Wbh_2}\left(1 - \frac{h_2^2}{h_1^2}\right) = 1 - \frac{h_2}{h_1} - \frac{h_2 P \tan\theta}{6\eta W} \tag{B.37}$$

and:

$$\frac{Q}{Wbh_2}\left(1 + \frac{2Z_2 \tan\theta}{h_2} - \frac{h_2^2}{h_1^2}\right) = 1 + \frac{Z_2 \tan\theta}{h_2} - \frac{h_2}{h_1} - \frac{h_2 P \tan\theta}{6\eta W} \tag{B.38}$$

Equation (6.43) is of the form:

$$P = K_3\left(K_4 - \frac{Q}{Wbh_2}\right) \tag{B.39}$$

where:

$$K_3 = \frac{6\eta W Z_1 (h_1 + h_2)}{h_1^2 h_2} \tag{B.40}$$

and:

$$K_4 = \frac{h_1}{h_1 + h_2} \tag{B.41}$$

Also equation (6.45) may be rearranged to:

$$P = K_5\left(K_6 - \frac{Q}{Wbh_2}\right) \tag{B.42}$$

where:

$$K_5 = \frac{6\eta W}{h_2}\left(\frac{(h_1 + h_2)Z_1}{h_1^2} + \frac{2Z_2}{h_2}\right) \tag{B.43}$$

and:

$$K_6 = \left(\frac{Z_1}{h_1} + \frac{Z_2}{h_2}\right)\Big/\left(\frac{(h_1 + h_2)Z_1}{h_1^2} + \frac{2Z_2}{h_2}\right) \tag{B.44}$$

Thus for both the taper and taper-parallel screws P is linear with Q, which is utilized in Section 6.5.

B.4 PRESSURE GRADIENTS IN A STEPPED SCREW

In a stepped screw, having sections of channel depth h_1 and h_2, the pressure gradient dP/dz will generally be different in the two sections (p.146). Since the flow equation (equations (6.15) and (B.9)) is a cubic in h, it is not possible to state unambiguously which is the greater, dP_1/dz or dP_2/dz. The objective here is to determine the conditions in which dP_1/dz is greater or less than dP_2/dz. Since downstream velocity W and channel width b are commonly the same in both sections, and volumetric flow rate Q is the same by continuity, pressure gradients can be represented by the (local) dimensionless flow rates Q/Wbh_1 and Q/Wbh_2, which are inversely proportional to the channel depth. When $Q/Wbh_2 > 0.5$, the pressure gradient dP_2/dz is negative and when $Q/Wbh_2 = 0.5, dP_2/dz = 0$; in both cases the whole of the pressure is raised in the first section, where if $h_1/h_2 > 1$, $Q/Wbh_1 < 0.5$. The effective melt lengths z_1 and z_2 will differ in different screw designs, and the former also with the position of initial pressure rise (gel point). However, this study shows that, except over a very small range of flow rates ($Q/Wbh_2 \simeq 0.5$), the pressure gradient in the shallow second section is greater than in the deeper first section and thus unless the second section is very short, most of the pressure before the die will be generated in this section. In Table B.1 the values of Q/Wbh and dP/dz are calculated for three ratios of h_1/h_2, viz. 2,3 and 4, and in Fig. B.3 the ratio of dP_2/dz to dP_1/dz is plotted against the respective dimensionless flow

Table B.1 Pressure gradients in a stepped screw

$\frac{h_1}{h_2}$	$\frac{Q}{Wbh_1}$	$\frac{Q}{Wbh_2}$	$\frac{dP_1/dz}{\times \frac{12\eta W}{h_2^2}}$	$\frac{dP_1/dz}{dP_1/dz_{(P_2=0)}}$ (Fig. B.4)	$\frac{dP_2/dz}{\times \frac{12\eta W}{h_2^2}}$	$\frac{dP_2/dz}{dP_1/dz}$ (Fig. B.3)
2	0.25	0.50	0.0625	1.00	0	0
2	0.22	0.44	0.070	1.12	0.060	0.858
2	0.21	0.42	0.0725	1.16	0.080	1.103
2	0.20	0.40	0.075	1.20	0.100	1.333
2	0.15	0.30	0.0875	1.40	0.200	2.285
2	0.10	0.20	0.100	1.60	0.300	3.000
2	0.05	0.10	0.1125	1.80	0.400	3.56
2	0	0	0.125	2.00	0.500	4.00
3	0.167	0.50	0.0370	1.0	0	0
3	0.160	0.480	0.0378	1.02	0.020	0.530
3	0.155	0.465	0.0383	1.036	0.035	0.914
3	0.150	0.450	0.0389	1.050	0.050	1.286
3	0.120	0.360	0.0422	1.14	0.140	3.32
3	0.100	0.300	0.0444	1.20	0.200	4.50
3	0.050	0.150	0.050	1.35	0.350	7.00
3	0	0	0.0556	1.50	0.500	9.00
4	0.125	0.500	0.0234	1.0	0	0
4	0.120	0.480	0.0238	1.014	0.020	0.842
4	0.115	0.460	0.0241	1.027	0.040	1.661
4	0.110	0.440	0.0244	1.04	0.060	2.462
4	0.100	0.400	0.0250	1.068	0.100	4.00
4	0.070	0.280	0.0269	1.15	0.220	8.17
4	0	0	0.0312	1.33	0.50	16.0

rates. If equation (6.16) is rearranged, it gives:

$$\frac{1}{2} - \frac{Q}{Wbh} = \frac{h^2}{12\eta W} \cdot \frac{dP}{dz} \tag{B.45}$$

Thus:

$$\begin{aligned} \frac{dP_1}{dz} &= \left(\frac{1}{2} - \frac{Q}{Wbh_1}\right) \frac{12\eta W}{h_1^2} \\ &= \left(\frac{1}{2} - \frac{Q}{Wbh_1}\right) \cdot \frac{12\eta W}{h_2^2} \cdot \frac{h_2^2}{h_1^2} \end{aligned} \tag{B.46}$$

and:

$$\frac{dP_2}{dz} = \left(\frac{1}{2} - \frac{Q}{Wbh_2}\right) \frac{12\eta W}{h_2^2} \tag{B.47}$$

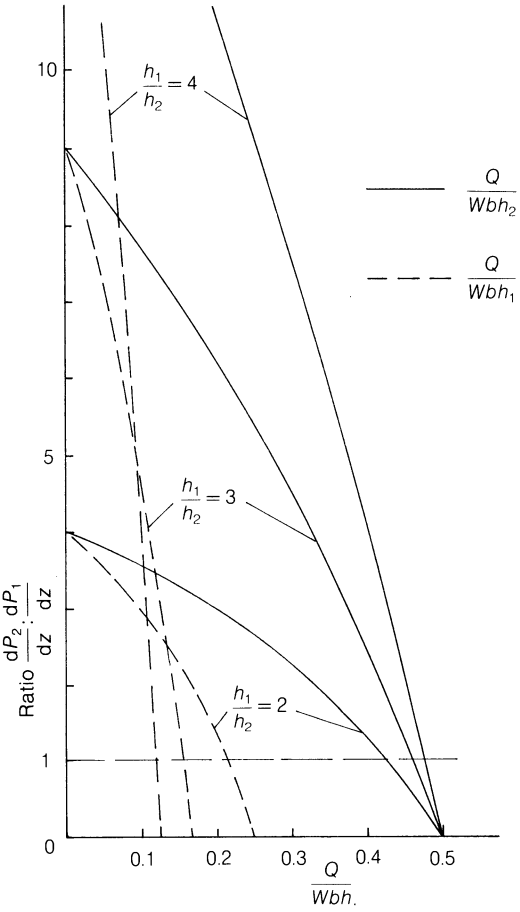


Figure B.3 Stepped screw: ratio of pressure gradients in the two sections.

The pressure gradients are calculated from equations (B.46) and (B.47) in terms of $12\eta W/h_2^2$.

Referring to Fig. 6.10, it is also interesting to see how the pressure gradient in the first section changes with flow rate (Q/Wbh_1) and die pressure; this is done in Fig. B.4 by comparing dP_1/dz with its value when it represents the total pressure rise, i.e. when $Q/Wbh_2 = 0.5$. This shows that even with a depth ratio h_1/h_2 of only 2:1, the maximum pressure gradient (at zero output) is only twice that when there is no pressure change in the shallow section, i.e. dP_1/dz is not only usually smaller than dP_2/dz, but also changes less with die pressure.

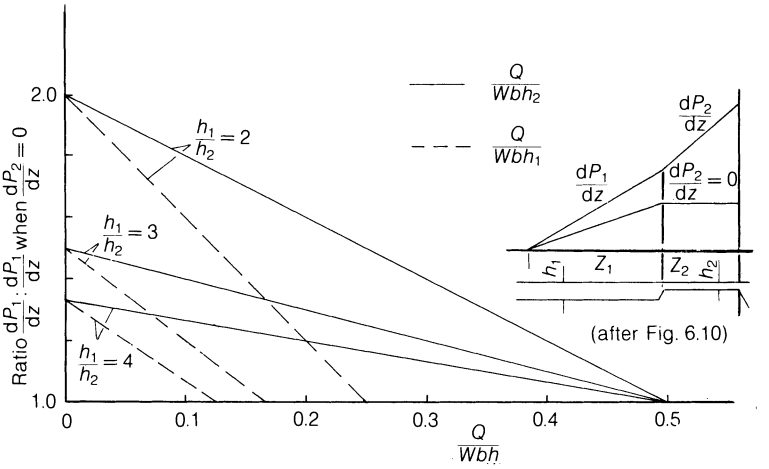


Figure B.4 Pressure gradient in first section dP_1/dz in terms of that when $dP_2/dz = 0$ ($Q/Wbh_2 = 0.5$).

B.5 FURTHER EXAMPLES OF *Q–P* DIAGRAMS

B.5.1 Double-parallel screw

Instead of the rather cumbersome equation (B.31), the performance of the double-parallel or stepped screw may be represented by graphical forms of equations (6.38) and (6.39). Consider a double-parallel screw of constant diameter and pitch, with channel depths h_1 and h_2, h_1 being greater than h_2. The corresponding drag and pressure flows will be Q_{1D}, Q_{2D} and Q_{1P}, Q_{2P}, respectively. Figure B.5 represents these flows and the resultant total flows Q_1 and Q_2 giving in steady state:

$$Q_1 = Q_2 = Q_{Die} \tag{B.48}$$

The pressure rises P_1 and P_2 are algebraically additive and together equal the die pressure:

$$P_1 + P_2 = P_{Die} \tag{B.49}$$

Then with a small die requiring high pressure at a low output, Q is determined by a horizontal line, satisfying equation (B.48) such that the intercepts P_1 and P_2 together equal P_{Die} to satisfy equation (B.49). If this is replaced by a larger die so that the output becomes Q'_{Die} which is larger than Q_{2D}, $Q/Wbh_2 > 1/2$ and pressure falls in the second section, as shown by a negative intercept of pressure on the Q_2 line. Then Q'_{Die} is given by a horizontal line such that the (arithmetic) difference of P'_1 and P'_2 equals the die pressure P'_{Die}. Note that the

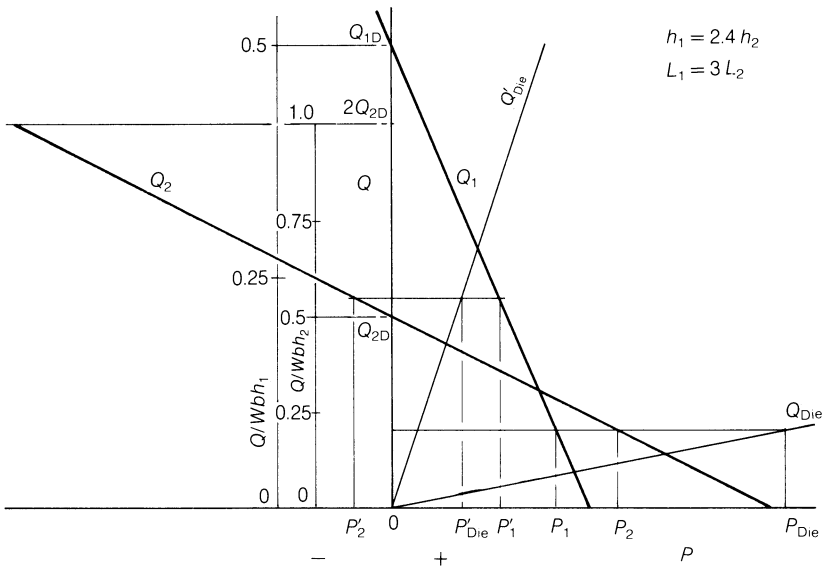


Figure B.5 Output vs pressure for a stepped screw.

vertical scales of Q/Wbh_1 and Q/Wbh_2 give an immediate clue to the pressure and flow conditions in each screw section, for any known value of Q. This method illustrates better than a single Q/P line what is happening in a multisection screw and can be used for more complicated forms of screw, providing the constraints corresponding to equation (B.48) and (B.49) are observed; for instance the venting system referred to on p.163 may be analysed, if due regard is paid to differences in diameter, pitch, speed, etc., in calculating values of Q/Wbh.

B.5.2 Screw extruder and gear pump

A system used for the melt spinning of fibres consists of a single-screw extruder melting solid polymer and feeding it to a gear pump used for metering the flow. The flow through the gear pump is proportional to its speed of rotation, but almost independent of pressure difference, so that as the filter pack becomes partially blocked by dirt and gels, the flow through the spinaret is maintained in balance with the drawdown system, and major adjustment of the latter is not required. In steady conditions the extruder automatically adjusts its output to equal that of the gear pump by raising or lowering the pressure between them. However, if the extruder is set at too low a speed, this pressure may fall below, say, 0.3 MN m^{-2} (50 lb/in^2) at which the gear pump begins to cavitate, giving erratic output and voids in the product. If speed is too high, the pressure

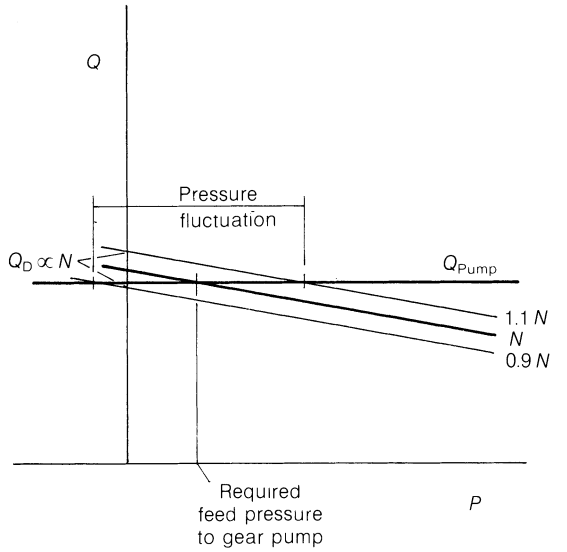


Figure B.6 Shallow screw feeding gear pump.

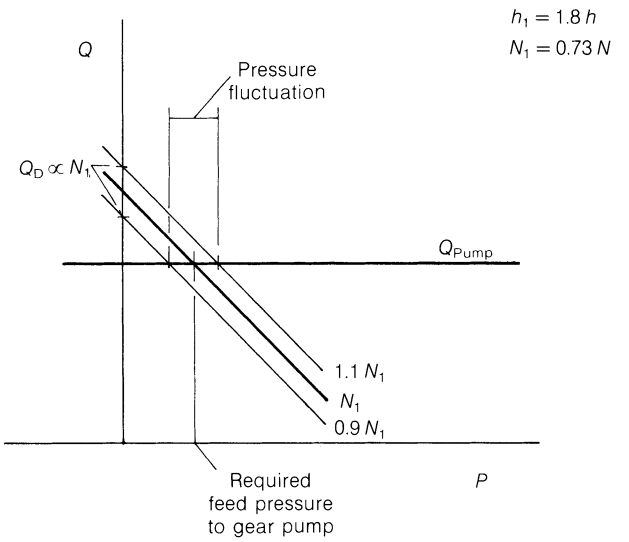


Figure B.7 Deep screw feeding gear pump.

between extruder and pump may rise unacceptably. Consider a system in which a pressure P is desired at the pump inlet at a constant flow rate of Q_{Pump}. A shallow screw, depth h gives this pressure and output at speed N. If extruder speed is now varied by $\pm 10\%$, the drag flow (the intercept on the vertical axis)

will vary by the same proportion. However, as shown by Fig. B.6, the small slope of the Q/P line for a shallow screw gives a large variation in pressure, including the possibility of insufficient pressure to prevent pump cavitation. Figure B.7 shows that a deeper screw, giving the same pressure P at a speed N_1, will give a larger absolute variation in drag flow Q_D, but a smaller variation in P due to $\pm 10\%$ speed variation.

Thus the shallow screw, which may be necessary for adequate melting and mixing, requires much closer control of speed, which could only be achieved automatically by a feedback signal from the inlet pressure to the pump. Even so, inherent delays in the response of the extruder might lead to undesirable transients. The author recalls an installation in which a 114 mm (4.5 in) extruder fed 12 gear pumps and spinarets in parallel, involving considerable high pressure heated pipework due to the space required for the drawdown and winding equipment. When one of the pumps was stopped for filter cleaning, a similar situation arose in that Q_{Pump} was effectively reduced by 8.3% while extruder speed was constant, leading to a temporary increase in pressure. It was then proposed to substitute a screw with vacuum extraction to remove volatiles; the performance of the second screw section would then be similar to Fig. B.7. However, the output of the first section depends only on screw speed and would not be influenced by the pressure between extruder and gear pump, and the extruder speed must be set to match exactly the flow through the gear pump to avoid pump cavitation or vent blocking. The pressure realized would then depend on the relative proportions of the two screw sections; the diagrams illustrate the replacement of a self-regulating system by one requiring very precise external control.

Appendix C
Energy consumption and energy balance

C.1 EXPERIMENTAL DETERMINATION OF ENERGY BALANCE

C.1.1 Mechanical power input

The most direct methods of measuring mechanical power input to the screw involve concurrent measurements of speed and torque. Speed may be measured by tachometer, but below about 1 rps it is more reliable to integrate over a fixed time period of 1 min or more by automatic or visual counting of revolutions, especially if speed variation with load is appreciable due to slip or regulation in the drive. This may also be valuable for calibrating tachometers at higher speeds. If tachometers are driven from an input shaft, due allowance must be made for slip in magnetic couplings, variable-speed gearboxes, belt drives, etc. A method of torque measurement applied to small machines (especially vertical shaft) which can be supported entirely from the feed end, consists in measuring the torque reaction on the supports, which must be of low friction. Unless the speed reduction exceeds, say 100:1, allowance must be made for the much smaller reaction on the drive motor stator, which must be added or subtracted according to the relative directions of rotation. Care must be taken to minimize the restraint of feed, pipe and cable connections and that due to the product or downstream equipment. Another method is to apply strain gauges to a short section of the drive shaft and conduct the output signal to fixed recorders by telemetering or slip rings. To maximize the signal, a more flexible section (often by reducing diameter) is introduced; this brings the possibility of changing calibration and even drive failure during overload, e.g. at starting. Sharp changes of shaft section usually result in the limited length available in production machines giving nonlinear

strain patterns, and compensation or corrections for temperature and bending stresses are also necessary. Torsional strains have also been measured by optical interference, using mirror systems to amplify the deflection; these have the possibility of incremental output leading to digital signals and long-term stability and can be statically calibrated, but are rather fragile for industrial use. For large machines, systems designed for ship propeller shafts and rolling mill drives have been adapted. One such is the ASEA* Torductor in which a section of shaft acts rather like the magnetic core of a transformer; two rings of radial windings surrounding the shaft and fed with alternating current produce a continuous pattern of magnetic fields at $\pm 45°$ to the shaft axis, the directions of the principal shear stresses due to torsion. Torque on the shaft produces a difference between these principal stresses and, due to the consequent changes in magnetic susceptibility of the shaft material, a proportional difference is produced in the mutual inductance between the primary windings and a third ring of secondary windings placed between the two primary rings. The voltage induced in the secondary winding is thus directly proportional to primary voltage and to torque on the shaft. It is claimed to be insensitive to temperature and adjacent changes of cross-section, and the effects of bending stresses and varying air-gap are cancelled by integration round 360°. It is claimed to be suitable for most magnetic steels, with appropriate calibration, which may be done statically and is very stable. Such a torquemeter was used by the author and others on a 90 mm (3.5 in) diameter 20:1 L/D solid-fed extruder driven by a 270 kW (360 hp) electric motor at speeds up to 400 rpm.

The author had considerable experience on several machines up to 26 kW of an indirect system designed by Allen and Hillman (1957). This essentially measured the difference in tension in the two sides of a drive belt, and could be statically calibrated; though allowance must be made for losses in any gearbox and bearings between the drive belt and the screw, it proved accurate and reliable in semi-technical work. With the same proviso, other indirect methods may be used, having the advantages of lower torque at higher speed and more freedom for physical arrangement than measurement directly on the screw shaft. Measurement of torque by reaction on the motor stator requires precautions both in respect to losses in the transmission system and physical restraint from cables. As mentioned on p. 226, if mechancial energy input to the screw is measured by electrical input to the motor, then in addition to the transmission losses, allowance must be made for electrical losses in the motor. These may be obtained from the manufacturer's efficiency data or by calibration against a mechanical brake – if the latter is mounted in place of the screw then it will also determine the transmission losses, which vary with both speed and torque. In the case of AC induction motors, speed and torque are related so that a single efficiency curve is sufficient. With DC shunt motors (as often used with thyristor drives), no-load speed is primarily dependent on

*ASEA Ltd, Earl Road, Cheadle Hulme, Cheshire SK8 6QP, UK.

applied voltage, and the *percentage* reduction in speed with torque is almost independent of voltage, so again a single efficiency curve is approximately correct. However, with variable-speed AC motors, including the Schrage (brush-shifting) and commutator (induction regulator) types, the efficiency is also substantially dependent on the nominal speed setting (i.e. no-load or full-load speed); in some conditions the latter suffers very large losses due to disproportionate circulating currents in the secondary windings. The electrical location of metering instruments must also take account of losses in auxiliaries, e.g. cooling fans.

The measurement of mechanical power is thus quite complex and, for reliable indication, needs to be considered when specifying initial equipment. However, with experience, a simple ammeter will give warning of overload and some appreciation of the *changes* in load with MFR, temperature, speed, pressure, etc.

C.1.2 Heater energy

The energy added to the system by heaters or removed by cooling is not susceptible to direct theoretical analysis; under the usual system of a closed-loop temperature control, this will automatically adjust the energy input or output to maintain the desired temperatures. This energy is determined as the balancing factor in equation (8.2), depending on the values of mechanical power E, increase of enthalpy in polymer I and losses S appropriate to these temperatures. It is of course possible to determine the maximum power available, e.g. from the wattage of electric heaters at the corresponding operating temperature or the sensible heat of heating/cooling fluid at the available flow rate and permissible temperature change. This can be used, in conjunction with the energy balance (Figs 8.10 and 8.12) to determine the approximate limiting operating temperature for a given output or vice versa. The reliability of experimental measurement of heat input is highly dependent on the type of control system; if power is applied to resistance heaters by direct connection to the mains supply or under manual control, e.g. through an autotransformer, then the electrical input is simply measured by root mean square (RMS) current and voltage, the power factor being nearly unity. The risk here is that a slight lack of energy balance will cause a slow drift of temperature and related factors including heat losses, the energy discrepancy being mainly absorbed in heating or cooling the barrel and other machine parts. This departure from the steady-state assumption will be significant for small machines or low outputs (as usually used for experimental work) since the heat capacity of the metal parts of the machine is high in comparison with that of the polymer product. With the older time-proportioning controls, a domestic-type integrating wattmeter in each circuit may be sufficiently accurate, though since these are not designed for suddenly changing

loads, it is probably more accurate to monitor the total heater load, where different switching times will reduce the proportional load changes. An alternative, described below, uses a multichannel event recorder to record the on and off periods of each heater and give an average percentage 'on' time for each zone – if taken over 10–20 min this allows for time fluctuations due to interaction between zones. This percentage 'on' time may then be multiplied either by the rated wattage of each heater and summed or by a separate measurement of the actual wattage at operating temerature. A source of error here is due to the change in heater resistance with temperature, for example:

Set control temperature 200°C.
Off period, winding temperature (say) 180°C, resistance 58 Ω.
On period, winding temperature (say) 500°C, resistance 61.7 Ω, if temperature coefficient of resistance is constant 0.0002 $\Omega\,°C^{-1}\,\Omega^{-1}$ from 180° to 500°C. Then the instantaneous power during the on period will decrease from 993 W to 933 W; if this is assumed to change linearly, a continuous rating of 933 W will underestimate the actual power by some 3%. This error is reduced if a steady temperature of the winding is reached before switching off.

Phase-angle firing thyristors give a non-sinusoidal waveform while fast-cycling thyristors may only give half-wave output – in either case a simple RMS measurement is inaccurate, though in the latter a long time-constant ammeter will give a qualitative indication. The controller manufacturer should be consulted if more accurate measurement is required, but usually it is sufficient to know how the balance between heater and mechanical power input is affected by changes in material, screw or operating conditions. With mains-frequency induction heaters it is necessary to take account of the power factor – usually below 0.8. For fluid heating or cooling the difficulties are mainly in maintaining steady flow rate and accurate measurement of small temperature changes.

It is hardly practicable to estimate heating/cooling energy from temperature gradients within the barrel walls since longitudinal gradients cause conduction from zone to zone within the wall (appendix C.1.4) and control action causes fluctuations in radial temperature gradient with time. In addition, because of longitudinal conduction and variations in outer temperature between heaters and exposed barrel parts, it is difficult to define the areas over which heat transfer occurs.

C.1.3 Heat content (enthalpy) of polymer

A first requirement for assessing the energy content of the polymer as it leaves the die is accurate knowledge of the mass flow rate. If the downsteam process can be interrupted, this is most simply measured by allowing the extrudate to fall into a weighed metal container and cutting the thread by sliding a knife quickly across the die face after a known period – which should be at least 60 s to

allow for short-term fluctuations. To avoid disrupting the process, the extrudate at the die may be marked with a wax pencil at the beginning and end of a timed period and then removed for weighing after the cooling process. Measurement of the dimensions near the die is unlikely to be satisfactory, both because of the difficulties of accurate measurement of cross-section and uncertainty of the relevant mean temperature and consequent density. Measurement of dimensions after cooling (and drawing) is unlikely by itself to be sufficiently accurate; if cut lengths are produced it would be better to time the production of a suitable number of lengths, which can then be weighed. With this, and other indirect methods including weighing the feed material, it is important to ensure that the mass of material 'stored' in the system between the die and the measuring position is the same at start and finish of the timed period.

The specific enthalpy (J kg^{-1}) at the die requires knowledge of the mean melt temperature; determination of the appropriate value is discussed in section 11.1. The corresponding enthalpy may be read from a chart (section 4.1) for the appropriate polymer. A difficulty which arises with semi-crystalline polymers is that though the melt state is amorphous and the energy content unambiguous, the energy content of the solid feed material processed may differ from that of the sample used for the chart, mainly due to differences of crystallinity, which in turn depend largely on the rate of cooling during granulation or compounding. As explained in section 4.1, this is not likely to be significant with HDPE, but more so with polypropylene and especially branched LDPE. However, if the feed material is consistent, this will involve a constant error, and thus comparisons between different operating conditions will be unaffected. The same applies to a constant degree of preheating of the feed material. Enthalpies are usually given on a mass rather than a volume basis, so measurement of volume output must be multiplied by the density corresponding to the temperature of measurement. It is important to note that calculation of heat content from specific heat data is generally inaccurate. First, published specific heat figures usually relate to ambient temperature, which may be a sufficient approximation up to the glass transition temperature T_g of amorphous polymers. The specific heat at higher temperatures is often higher, so that heat contents based on ambient values of specific heat will be low, both in absolute terms, and for small changes in operating conditions. If the specific heat at operating temperature is available, this may be adequate for the latter purpose, but will overestimate the former. With semi-crystalline polymers, changes in specific heat with temperature may occur, especially between the solid and melt states, but in addition the latent heat of crystallisation involves a further increase in the heat content in the melt state. Even integration of the area under a curve of specific heat against temperature is uncertain, since the precise shape of the melting peak is influenced by the speed of response of the measuring instrument (usually in the temperature-scanning mode). The increase of enthalpy is expressed in equation (8.4) in intergral terms purely for convenience.

C.1.4 Energy losses

If, because of their physical connection, the die and the extruder are considered as a single system, then the energy losses from the system (Fig. 8.2) are in conduction, convection and radiation to the ground and surrounding atmosphere, conduction to the drive bearings and gearbox, heat loss in feed pocket cooling water and screw cooling (if used). Barrel cooling, which is specific to certain processes and conditions, is treated as negative heating and included as such under appendix C.1.2. As discussed in appendix 4.2, conduction is proportional to temperature gradient, or temperature difference between two fixed points, and convection is proportional to temperature difference. Radiant heat loss increases at a greater rate, so that heat losses will increase considerably as operating temperature increases; if the external surface temperature of the extruder was precisely known, these might be calculated according to the equations given in Chapter 4. However, because of the control action, the temperature of the heater element, and hence of the outer surface, may rise considerably above the control temperature while heating, but fall slightly below the latter during off periods – see example on p. 430. This control action will cause consequential, but smaller, time variations in the temperature of other exposed surfaces, which will, since they are heated by conduction, be nearer the control temperature. Conduction along the barrel (and screw) to the feed pocket coolant will also increase with operating temperature, but will also depend on the set temperature profile along the barrel. An example of a calculation of this type, using measured temperatures, is given in Table C.1 for comparison with experimental values. The latter were determined by measuring the heater input necessary to maintain the preset temperature profile when the screw was stationary, giving zero output, i.e. $E = 0$ and $I = 0$, so equation (8.2) reduces to $H = S$. These results show, as expected, that losses rise with temperature and also the effects of altering temperature profile, e.g. from the usual slope to a uniform (set) value. For this machine it is clearly seen how in certain conditions the balance of energy from the various heater zones changes and how zones mutually interact by longitudinal conduction within the barrel wall. For instance, the large heater on the die adaptor contributes most of the heat to the rather small die used, while the die heater only modifies the temperature at the die exit. The experimental method is evidently more reliable than calculation and only needs to be done once for any physical configuration, e.g. barrel length and die type. It does require separate readings for different temperatures and temperature profiles, the main limitation being the time necessary to establish steady conditions. Normal variations in ambient temperature will have little effect, though it is important that feed pocket and screw cooling conditions remain as in normal operation. A further limitation of this method is that when the extruder is running, heat is conveyed towards the die by mass transfer of the polymer, and so large temperature gradients can be maintained, which in the static test would be reduced by longitudinal conduction.

C.1.5 Heat loss experiment

Extruder: 37 mm (1.5 in) diameter, 20:1 L/D
Barrel: 127 mm (5 in) outside diameter, approximately 600 mm (24 in) long
Barrel heaters: (3) 200 mm (8 in) outside diameter, 150 mm (6 in) long, each rated at 3 kW
Adaptor flange heater: 280 mm (11 in) outside diameter, 63 mm (2.5 in) long, rated at 2.3 kW
Die heater: 82 mm (3.25 in) diameter, 89 mm (3.5 in) long, rated at 0.6 kW
Control thermocouples close to heater elements, with three-term time-proportioning controllers and relays, having auxiliary contacts connected to separate pens of a multichannel event recorder.
Indicating thermocouples (L,M,N) between heaters, extending to within 3 mm of inner barrel surface.
Event recorder (Fig. C.1) gave on and off times over 15 min period; summed manually to give an average percentage on time and multiplied by the

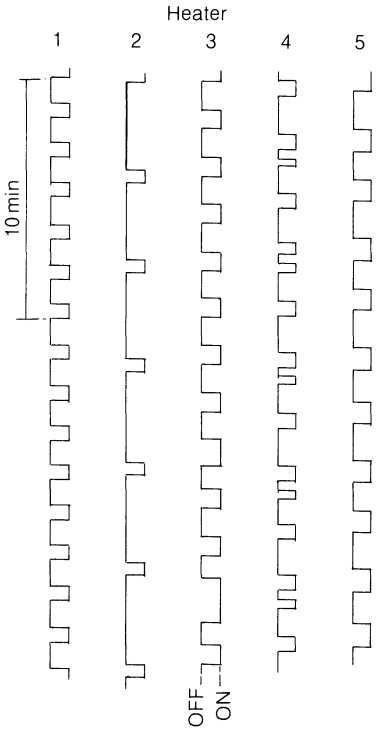


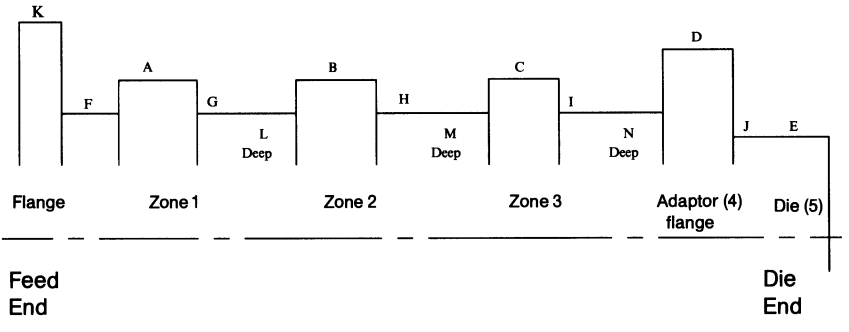
Figure C.1 Event recorder: heater switching.

Table C.1 Static heat losses

	Set temperatures (°C)					*Power comsumption* (W)					
	Barrel zone			*Flange*	*Die*	*Barrel zone*			*Flange*	*Die*	*Total*
Heater rating	1	2	3	4	5	1 3000	2 3000	3 3000	4 2200	5 600	8800
Setting											
1	100	125	150	150	150	276	289	789	342	105	1801
2	150	150	150	150	150	996	0	498	356	123	1973
3	150	175	200	200	200	619	182	1056	626	182	2665
4	200	200	200	200	200	1189	324	757	562	185	3017
5	200	225	250	250	250	990	339	1396	867	241	3833
6	250	250	250	250	250	2015	444	1074	821	246	4600
Calculated heat losses by radiation and convection											
2	150	150	150	150	150	352	171	235	295	48	1101
4	200	200	200	200	200	588	342	400	497	99	1926

Table C.2 Surface temperatures in heat loss tests (°C)

Setting	*Position*													
	K	F	A	G	L	B	H	M	C	I	N	D	J	E
1	57	74	125	105	110	105	134	145	203	154	145	137	–	130
2	65	90	240	131	145	128	144	155	175	150	155	150	146	150
3	74	111	210	152	160	157	183	190	250	193	190	210	173	216
4	100	137	322	188	200	221	201	210	248	207	215	207	200	233
5	104	137	286	205	210	212	240	250	231	262	250	255	250	265
6	115	172	390	240	245	242	255	255	315	260	255	252	250	285



continuous rating to give actual power input to each heater. Cold water continuously circulated through feed pocket jacket as in normal operation; flow rate and temperature rise not recorded.

Table C.1 tabulates six sets of control temperatures and corresponding heater power inputs, with calculated values (as above) for settings 2 and 4 for comparison. Table C.2 gives recorded surface temperatures used for this calculation.

The distribution of energy between heaters has some unexpected features. Zone 3 is high even with 'level' temperature profiles, when longitudinal conduction should be minimal. The high contribution from zone 1 is presumably due to conduction to the feed pocket, and since it is frequently on, may also conduct heat forward, reducing the demand on the zone 2 heater; this is supported by the surface temperatures in Table C.2. The substantial heat loss to the feed pocket suggests that a thermal barrier between feed pocket and barrel would be worthwhile in saving energy and permitting higher temperatures in the first barrel zone.

Calculation of longitudinal heat flow based on temperatures of the 'deep' thermocouples for settings 1, 3 and 5 suggests that within the barrel this may only be 100–150 W, which is small compared with the energy consumption of the heaters. However, it will limit temperature differences between adjacent zones as well as influencing the respective energy contributions from the heaters.

It will be noted that, especially at the higher set temperatures, the energy losses are a substantial proportion of the rated input of the heaters – 8.8 kW total. Since losses increase with temperature, this not only sets an upper limit to achievable barrel temperatures but will also limit the rate of temperature rise and extend the time to re-establish steady conditions after a change of temperature settings. A type of heater suitable for continuous operation at (element) temperatures around 350°C or for use with external insulation, e.g. a mains-frequency induction heater, could allow substantial reduction of these losses and improvement in energy utilization as well as more rapid response to intentional changes in set temperatures.

The data presented are strictly only applicable to the external temperatures given in Table C.2, which do not necessarily relate directly to temperatures at the internal surface of the barrel. The distribution of energy between heaters, which largely determines these external temperatures, is governed primarily by the profile of set temperatures, especially near the feed end. For most practical purposes the energy losses can therefore be regarded as dependent only on the set temperatures and the physical arrangement.

C.2 DERIVATION OF POWER ABSORBED IN SCREW

From appendix B.1 the downstream velocity at a distance y from the screw surface is:

$$w = \frac{Wy}{h} + \frac{(y^2 - yh)}{2\eta} \cdot \frac{dP}{dz} \tag{B.8}$$

and the shear rate at y is:

$$\dot{\gamma}_y = \frac{dw}{dy} = \frac{W}{h} + \frac{(2y-h)}{2\eta} \cdot \frac{dP}{dz} \qquad (6.66)\,(B.7)$$

giving the shear rate at the wall ($y = h$) as:

$$\dot{\gamma}_h = \left(\frac{dw}{dy}\right)_{y=h} = \frac{W}{h} + \frac{(2h-h)}{2\eta} \cdot \frac{dP}{dz}$$
$$= \frac{W}{h} + \frac{h}{2\eta} \cdot \frac{dP}{dz} \qquad (C.1)$$

To eliminate dP/dz, equation (6.16) may be rearranged as:

$$\frac{h}{2\eta} \cdot \frac{dP}{dz} = \frac{6W}{h}\left(\frac{1}{2} - \frac{Q}{Wbh}\right)$$

and substituting in equation (C.1) gives:

$$\dot{\gamma}_h = \frac{W}{h}\left(4 - \frac{6Q}{Wbh}\right) \qquad (6.69)\,(C.2)$$

The shear stress in the downchannel direction is thus:

$$\tau_h = \eta\dot{\gamma}_h = \frac{\eta W}{h}\left(4 - \frac{6Q}{Wbh}\right) \qquad (C.3)$$

and the tangential component of this stress is:

$$\tau_h \cos\phi = \frac{\eta W}{h}\left(4 - \frac{6Q}{Wbh}\right)\cos\phi \qquad (C.4)$$

Similarly, the transverse velocity is:

$$u = \frac{Uy}{h} + \frac{y^2 - yh}{2\eta} \cdot \frac{dP}{dx} \qquad (B.12)$$

and the shear rate at y is:

$$\frac{du}{dy} = \frac{U}{h} + \frac{2y-h}{2\eta} \cdot \frac{dP}{dx} \qquad (B.11)$$

giving the shear rate at the wall ($y = h$) as:

$$\left(\frac{du}{dy}\right)_{y=h} = \frac{U}{h} + \frac{h}{2\eta} \cdot \frac{dP}{dx} \qquad (C.5)$$

Substituting to eliminate dP/dx by:

$$\frac{1}{2\eta} \cdot \frac{dP}{dx} = \frac{3U}{h^2} \qquad (6.25)$$

gives:

$$\left(\frac{du}{dy}\right)_{y=h} = \frac{4U}{h} \tag{C.6}$$

The shear in the cross-channel direction is:

$$\eta\left(\frac{du}{dy}\right)_{y=h} = \frac{4\eta U}{h} \tag{C.7}$$

and the tangential component of this stress is:

$$\eta \frac{du}{dy} \sin\phi = \frac{4\eta U}{h} \sin\phi \tag{C.8}$$

The total tangential stress at the barrel surface is thus:

$$\eta \frac{W}{h}\left(4 - \frac{6Q}{Wbh}\right)\cos\phi + 4\eta \frac{U}{h}\sin\phi \tag{C.9}$$

Combining equations (6.4) and (6.5) gives:

$$U = W\tan\phi \tag{C.10}$$

and substituting for U in (C.9) gives:

$$\text{tangential stress} = \eta \frac{W}{h}\left[\left(4 - \frac{6Q}{Wbh}\right)\cos\phi + 4\sin\phi\tan\phi\right] \tag{C.11}$$

For an elemental length dz of the channel, this stress acts over an area $b\,dz$ giving:

$$\text{tangential shear force} = \frac{\eta W b\,dz}{h}\left[\left(4 - \frac{6Q}{Wbh}\right)\cos\phi + 4\sin\phi\tan\phi\right] \tag{C.12}$$

The power absorbed is force × distance/time or force × velocity and by rearrangement of equation (6.4), the tangential velocity is:

$$\pi DN = \frac{W}{\cos\phi} \tag{C.13}$$

Thus the power absorbed in a length dz of the channel is:

$$\text{channel power} = \frac{\eta W^2 b\,dz}{h}\left[4(1 + \tan^2\phi) - \frac{6Q}{Wbh}\right] \tag{8.7)(C.14}$$

As shown in section 6.3, the pressure flow through the flight clearance is usually small compared with the drag flow, and in view of other approximations (sections 8.3 and 8.4) it is sufficient to consider only the latter. Because this is simple shear flow, independent of pressure gradient in the channel, it is unnecessary to resolve it into downchannel and cross-channel components. As

for channel flow, the tangential velocity is given by:

$$\pi DN = \frac{W}{\cos\phi} \tag{C.13}$$

and the shear rate in the flight clearance δ is:

$$\dot{\gamma}_{fl} = \frac{W}{\delta\cos\phi} \tag{C.15}$$

The corresponding shear stress is:

$$\tau_{fl} = \frac{\eta W}{\delta\cos\phi} \tag{C.16}$$

and this acts over an area $t\cos\phi\,dz$ giving a shear force:

$$\text{flight shear force} = \frac{\eta W}{\delta\cos\phi}\, t\cos\phi\,dz \tag{C.17}$$

for a channel length dz.

The velocity is $W/\cos\phi$ as before, giving:

$$\text{Power absorbed over flights} = \frac{\eta W}{\delta\cos\phi}\, t\cos\phi\,dz\,\frac{W}{\cos\phi}$$

$$= \eta\,\frac{W^2 t\,dz}{\delta\cos\phi} \tag{8.8)(C.18}$$

The total power absorbed in length dz of the melt pumping section is:

$$E_{dz} = \frac{\eta W^2 b\,dz}{h}\left[4(1+\tan^2\phi) - \frac{6Q}{Wbh}\right] + \frac{\eta W^2\, t\,dz}{\delta\cos\phi} \tag{8.9) (C.19}$$

These power equations are analysed in section 8.2.

C.3 HEAT FLOWS IN MELT PUMPING SECTION

In Table 8.1 and Fig. 8.4 the several possible heat flows in the melt pumping section are indicated by alphabetical letters. These are examined in turn, an estimate made of the magnitude of each, and the effects deduced of operational variables, especially screw speed and back pressure.

To permit estimates of the relative numerical values in typical conditions, the dimensions and properties given below are used. These differ from those in the example on p. 260, mainly in increased channel depth and flight clearance (10 mm and 0.15 mm rather than 5 mm and 0.1 mm, respectively) and in the

viscosity data, typical of an MFR 2.0 LDPE, as follows:

Shear rate (s^{-1})	*Temperature* (°C)	*Viscosity* ($N\,s\,m^{-2}$)	*Temperature coefficient* ($°C^{-1}$)
30	150	2200	$\beta = 0.0134$
30	200	730	
2000	150	124	$\beta = 0.0102$
2000	200	61	

Then:

Pseudoplasticity index	n	0.3152 (150°C), 0.4090 (200°C)
Diameter	D	100 mm
Channel depth	h	10 mm
Pitch	p	100 mm
Flight width	t	10 mm
Speed	N	1 rps
Viscosity	η	see above
Flight clearance	δ	0.15 mm
Barrel outside diameter	D_0	200 mm

Then:

Channel width	$b = (p - t)\cos\phi = 0.085\,76\,\text{m}$
Helix angle	$\phi \quad 17.657°$
Helical length per turn	$dz = 0.1\pi/\cos\phi = 0.3297\,\text{m}$
Peripheral speed	$\pi DN = \pi \times 0.1 \times 1 = 0.3142\,\text{m s}^{-1}$
Longitudinal velocity	$W \quad 0.2994\,\text{m s}^{-1}$ at 1 rps
Transverse velocity	$U \quad 0.0953\,\text{m s}^{-1}$ at 1 rps
Drag flow	$Q_D = 0.2994 \times 0.08576 \times 0.01/2 = 1.284 \times 10^{-4}\,\text{m}^3\,\text{s}^{-1}$
Drag flow shear rate	$\dot{\gamma}_D = W/h = 0.2994/0.01 = 29.94\,\text{s}^{-1}$
Factor $4(1 + \tan^2\phi)$	4.4053
Channel power at 150°C	$dE = \dfrac{2200 \times 0.2994^2 \times 0.08576 \times 0.3297}{0.01} \times \left(4.4 - \dfrac{6Q}{Wbh}\right) = 557.6\left(4.4 - \dfrac{6Q}{Wbh}\right)\,\text{W/turn}$
Channel power at 200°C	$dE = 185.0\left(4.4 - \dfrac{6Q}{Wbh}\right)\,\text{W/turn}$

Thermal properties (from Table 4.1):

Density of steel	$7800\,kg\,m^{-3}$
Density of polyethylene at 150°C	$785\,kg\,m^{-3}$
Density of polyethylene at 200°C	$774\,kg\,m^{-3}$
Specific heat of steel	$503\,J\,kg^{-1}K^{-1}$
Specific heat of polyethylene	$2300\,J\,kg^{-1}K^{-1}$
Thermal conductivity of steel	$50\,W\,m^{-1}\,K^{-1}$
Thermal conductivity of polyethylene	$0.50\,W\,m^{-1}\,K^{-1}$
Thermal diffusivity of steel	$1.3\times10^{-5}\,m^2\,s^{-1}$
Thermal diffusivity of polyethylene	$1.5\times10^{-7}m^2\,s^{-1}$
Assumed longitudinal temperature gradient equivalent to 50°C per 4*D* zone and	$125°C\,m^{-1}$ axially $37.9°C\,m^{-1}$ helically

A Surface heat transfer: heaters to barrel

Typical heater ratings are:

- resistance 3–4 $W\,cm^{-2}$ equivalent to 7.5–10 kW per 4*D* zone
- induction 13 $W\,cm^{-2}$ equivalent to 33 kW per 4*D* zone.

If all the heat is transferred to the barrel, these correspond to a heat flux of 30–40 $kW\,m^{-2}$ and 130 $kW\,m^{-2}$, respectively, or 940–4080 W per turn.

B Radial conduction in barrel

For Radial conduction through a cyclinder, heat flux q is:

$$q = \frac{2\pi kL(T_2 - T_1)}{\log_e(R_2/R_1)} \tag{4.6}$$

inserting the given values,

$$\begin{aligned} T_2 - T_1 &= \frac{q \times \log_e(0.1/0.05)}{2\pi \times 50 \times 0.1} \\ &= 0.022q \\ &= 41.5°C \text{ for } 3\,W\,cm^{-2} \\ &\text{or } 180°C \text{ for } 13\,W\,cm^{-2} \\ &\text{or } 3.06°C \text{ for } 10°C \text{ difference} \\ &\quad \text{between barrel and polymer (see C below)} \end{aligned} \tag{C.20}$$

C Surface heat transfer between barrel and polymer

For a parabolic velocity distribution (e.g. pressure flow of a Newtonian fluid) the heat transfer coefficient h_a based on arithmetic mean temperature

difference is given by:

$$\frac{h_a D}{k} = 1.75 \left(\frac{wC_p}{kL}\right)^{1/3} \tag{4.14}$$

for values of Graetz number $w\,C_p/kL > 10$. For a wide rectangular slit $T \times H$, this equation may be used with $H = D/2$ and w, the mass flow rate through a width πH.

In the screw channel the velocity distribution is complex, so for the purpose of estimating heat transfer, a simple flow with parabolic velocity distribution is taken having the same shear rate at the wall. As shown in appendix C.4, the total shear rate at the wall is difficult to calculate, so a further approximation is to calculate the change in magnitude of the total velocity over a small distance from the wall and divide by that distance to give a wall shear rate. The downstream and transverse velocities are given in terms of fractions y/h of the channel depth (from the screw root) by equations (6.67), (6.26). The resultant at $y/h = 0.99$ is calculated as $(w_{0.99}^2 + u_{0.99}^2)^{1/2}$. The difference in magnitude (neglecting the change in direction) from that at the barrel surface πDN is divided by the distance $0.01h = 1 \times 10^{-4}$ m, to give the total shear rate. This is calculated for several values of back pressure (Q/Wbh). From Table 3.1 it is seen that the volume flow rate for a slit:

$$Q = \dot{\gamma}\frac{TH^2}{6} \tag{C.21}$$

which, when multiplied by the melt density, gives the mass flow rate through a slit H deep by $T = \pi H$ wide, for estimation of the Graetz number. Since the velocity (relative to the barrel) does not reach a maximum (corresponding to the centre of a pressure flow) until at least two-thirds of the channel depth (Figs 6.6(a) and 6.7) any lesser depth should be considered as equivalent to half the slit depth i.e. $H/2$ or $D/4$. For the present values, the Graetz number exceeds 10 for any depth $H/2$ greater than 1.57 mm, and since Q is proportional to D^3, the heat transfer coefficient is predicted as constant for any greater depth, so that choice of the latter is not significant. The length L before the velocity distribution is disturbed is the channel width normal to the screw axis, $b/\sin\phi$. Table C.3 shows the calculation of total shear rate, Graetz number and heat transfer coefficient for a screw speed of 1 rps. This shows that the increase of wall shear rate with back pressure will give a modest increase in heat transfer coefficient of about one-third. Since shear rate, and thus Graetz number, are proportional to velocity (equations (6.67) and (6.26)), a doubling of screw speed would be expected to multiply the heat transfer coefficient by $(2)^{1/3} = 1.26$.

For a typical heat transfer coefficient of 300 W m^{-2} K^{-1} and a polymer/metal temperature difference of 10°C.

$$\begin{aligned}\text{radial heat flux} &= 300 \times 0.085\,76 \times 0.3297 \times 10 \\ &= 84.8\ \text{W/turn}\end{aligned} \tag{C.22}$$

Table C.3 Surface heat transfer coeffecient: barrel to polymer

Q/Wbh		0	0.1	0.2	0.3	0.4	0.5	0.6
Downchannel velocity W at barrel $y = h$	$m\,s^{-1}$	----------			0.2994	----------		
Downchannel velocity w at $y = 0.99h$	$m\,s^{-1}$	0.2875	0.2893	0.2910	0.2928	0.2946	0.2964	0.2981
Velocity difference dw	$m\,s^{-1}$	0.0119	0.0101	0.0083	0.0066	0.0048	0.0030	0.0012
Crosschannel velocity U at barrel $y = h$	$m\,s^{-1}$	----------			0.0953	----------		
Crosschannel velocity u at $y = 0.99h$	$m\,s^{-1}$	----------			0.0915	----------		
Velocity difference du	$m\,s^{-1}$	----------			0.0038	----------		
Total velocity difference $\sqrt{dw^2 + du^2}$	$m\,s^{-1}$	0.0125	0.0108	0.0092	0.0076	0.0061	0.0048	0.0040
Total shear rate $\dot{\gamma} = \frac{dV}{0.0001}$	s^{-1}	124.7	107.9	91.5	75.6	60.9	48.2	39.7
Equivalent flow rate $\times 10^{-6}$ $Q = \dot{\gamma}TH^2/6$	$m^3\,s^{-1}$	2.02	1.75	1.48	1.22	0.987	0.781	0.644
Graetz number $Q\rho C_p/kL$		25.8	22.3	18.9	15.6	12.6	9.97	8.22
Nusselt number $1.75(Gz)^{1/3}$		5.17	4.93	4.66	4.37	4.07	3.77	3.53[a]
Heat transfer coefficient $h_a = 0.5Nu/4 \times 0.001\,57$	$W\,m^{-2}K^{-1}$	411.7	392.2	371.1	348.1	324.2	299.9	281.2[a]

[a]Slight overestimate, since curve falls below $1.75(Gz)^{1/3}$ below $Gz = 10$

D Axial conduction in barrel wall

The longitudinal temperature gradient of 50°C per $4D$ zone or $125°C\,m^{-1}$ is assumed for the melt. The limitation of radial heat transfer to the polymer **C** predicts small radial temperature differences **B** in the barrel wall. Thus, unless there are large polymer/metal temperature differences, the average axial gradient in the barrel wall will also be close to $125°C\,m^{-1}$. Note that because of possible large heat losses to the surroundings (appendix C.1), the gradient of heater set temperatures may be appreciably larger or smaller than that in the polymer.

For an outside diameter of 200 mm, the barrel cross-section is $0.023\,56\,m^2$, giving:

$$\begin{aligned} \text{axial heat flux} &= 50 \times 0.023\,56 \times 125 \\ &= 147\,\text{W/turn} \\ &\text{or } 1180\,\text{W for a gradient of } 1°C\,mm^{-1} \end{aligned} \tag{C.23}$$

If the barrel outside diameter is reduced to 150 mm, the cross-section is $0.009\,817\,m^2$ and:

$$\begin{aligned} \text{axial heat flux} &= 50 \times 0.009\,817 \times 125 \\ &= 61.4\,\text{W/turn} \end{aligned} \tag{C.24}$$

For a given heater type, the heater flux density will be approximately constant and heater power proportional to the square of the diameter. With an almost

constant heat transfer coefficient to the polymer (p. 442), the radial heat flux will also be proportional to the square of the diameter and thus a constant fraction of heater power. The radial thickness is approximately proportional to diameter so that the radial temperature difference in the barrel will also be proportional to diameter. The cross-sectional area of the barrel is proportional to the square of the diameter and for a constant temperature difference between zones, the axial gradient will be inversely proportional to diameter. Then:

$$\begin{aligned}\text{axial heat flux} &= kA \cdot \frac{dT}{dx} \\ &\propto k \cdot D^2 \cdot \frac{1}{D} \\ &\propto D \text{ (diameter)}\end{aligned} \tag{C.25}$$

Thus the axial heat flow becomes relatively smaller in larger machines.

E Radial heat transfer at screw root

Using the same assumptions and method as for heat transfer at the barrel surface (Table C.3), from equations (6.68) and (B.14), at $y/h = 0$:

$$\left(\frac{dw}{dy}\right)_{y=0} = \frac{W}{h}\left(\frac{6Q}{Wbh} - 2\right) \tag{C.26}$$

and

$$\begin{aligned}\left(\frac{du}{dy}\right)_{y=0} &= \frac{-2U}{h} \\ &= \frac{-2W}{h}\tan\phi\end{aligned} \tag{C.27}$$

At $Q/Wbh = 1/2$, equation (C.26) becomes:

$$\left(\frac{dw}{dy}\right)_{y=0} = \frac{W}{h} \tag{C.28}$$

and at $Q/Wbh = 0$,

$$\left(\frac{dw}{dy}\right)_{y=0} = -\frac{2W}{h} \tag{C.29}$$

As an approximation, if:

$$\text{total shear rate} = \sqrt{\left(\frac{dw}{dy}\right)^2 + \left(\frac{du}{dy}\right)^2} \tag{C.30}$$

at $Q/Wbh = 1/2$

$$\text{total shear rate} = \frac{W}{h}\sqrt{1 + 4\tan^2\phi} \tag{C.31}$$

Table C.4 Radial conduction in screw flight for several resistance ratios $m = k/hx$

Screw speed	rps	1	2	4
$m = 0$				
Temperature rise at end of transit	°C	1.54	2.68	4.61
Residual temperature rise at end of 'rest' and start of next transit	°C	0.32	0.55	0.94
Mean excess temperature	°C	0.93	1.61	2.77
$m = 2.909$ ($h = 1719\,\mathrm{W\,m^{-2}\,K^{-1}}$)				
Polymer temperature rise at end of transit	°C	15.2	21.9	28.4
Metal temperature rise at end of transit (uniform), $r_m = 0.01$ m	°C	0.068	0.049	0.032
$m = \infty$				
'Adiabatic' polymer temperature rise	°C	29.7	36.5	44.5

and at $Q/Wbh = 0$

$$\text{total shear rate} = \frac{2W}{h}\sqrt{1 + \tan^2\phi} \tag{C.32}$$

At 1 rps and $\tan\phi = 1/\pi$, equations (C.31) and (C.32) give total shear rates of $35.5\,\mathrm{s^{-1}}$ and $-62.8\,\mathrm{s^{-1}}$, respectively.

Since the transverse shear rate $\mathrm{d}u/\mathrm{d}y = 0$ at $y/h = 1/3$, H for the equivalent slit is taken as $0.01 \times 2 \times 1/3 = 0.006\,67$ m. By the method of Table C.3, the corresponding values of heat transfer coefficient are 271 and $328\,\mathrm{W\,m^{-2}\,K^{-1}}$ respectively, so that a uniform value of $300\,\mathrm{W\,m^{-2}\,K^{-1}}$, as for **C**, is reasonable. To supply in one turn the heat required by axial conduction in the screw, the temperature difference between polymer and screw root would be:

$$\mathrm{d}T = \frac{31.4\cos\phi}{300 \times 0.08576 \times \pi \times 0.08}$$
$$= 4.6°\mathrm{C} \tag{C.33}$$

F Radial conduction in screw flight

The flight area of one turn is $0.003\,14\,\mathrm{m^2}$. For a temperature gradient of $1°\mathrm{C\,mm^{-1}}$, equivalent to 10°C over the flight height:

$$\text{radial heat flux} = 50 \times 0.003\,14 \times 1000$$
$$= 157\,\mathrm{W/turn} \tag{C.34}$$

The excess of temperature in the flight clearance over that in the screw channel (150°C) is calculated in appendix C.5 as shown in Table C.4.

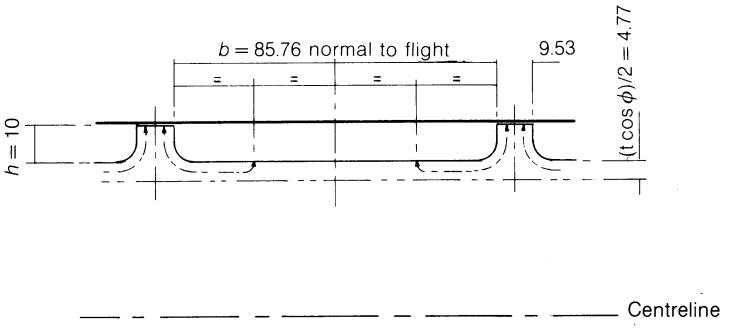


Figure C.2 Assumed heat path between flight tip and channel root.

If the heat transfer coefficient of 1719 $W m^{-2} K^{-1}$ (From **P**, p. 459) at the flight tip is included, the overall coefficient between polymer in the clearance and the screw root is:

$$U = \frac{1}{\frac{1}{1719} + \frac{0.01}{50}}$$

$$= 1279 \, W m^{-2} K^{-1} \qquad (C.35)$$

and

$$\text{radial heat flux at 1 rps} = 3.6 \, W \qquad (C.36)$$

To supply in one turn all the heat required by axial conduction in the screw root, the radial temperature difference would be:

$$dT = \frac{31.4}{1279 \times 0.003\,14}$$

$$= 7.8°C. \qquad (C.37)$$

G Local axial conduction in screw between flight and channel root

To estimate these heat flows (Fig. C.2), several approximating assumptions are necessary:

1. The thermal resistance of polymer at flight flank is infinite (see also **J**).
2. The relatively large surface of channel root ensures approximately uniform heat flux **E** across it.
3. Heat flows across the channel i.e. normal to the flight direction, although conduction in the screw root is primarily axial.
4. Heat flows to channels on each side of the flight.
5. The two effective heat paths are each half the flight width, i.e. $(t \cos \phi)/2 = 0.004\,76$ m from the channel root and the effective length is $h + b/4 = 0.031\,44$ m. The former corresponds to a cross-section $2\pi \times 0.08 \times 0.004\,76 = 0.002\,40 \, m^2$.

For a 1°C difference over 0.031 44 m,

$$\text{heat flux} = 50 \times 0.002\,40 \times \frac{1}{0.031\,44}$$
$$= 3.8\,\text{W} \tag{C.38}$$

If the surface heat transferer coefficients **E** and **P** are considered, the overall coefficient referred to an area of 0.002 40 m^2:

$$U = \frac{1}{\frac{1}{1279} + \frac{0.031\,44}{50} + \frac{0.002\,40}{300 \times 0.085\,76}}$$
$$= 665\,\text{W m}^{-2}\,\text{K}^{-1}$$

For an average temperature difference of 0.89°C (from **P**) between the polymer in the flight and in the channel, the heat via the screw will be:

$$\text{heat flux} = 665 \times 0.002\,40 \times 0.89$$
$$= 1.4\,\text{W} \tag{C.39}$$

H Overall axial conduction in the screw root

The cross-sectional area at the root of a screw with 10 mm deep channel is 0.005 03 m^2. For a longitudinal temperature gradient of 1°C/mm:

$$\text{heat flux} = 50 \times 0.005\,03 \times 1000$$
$$= 251\,\text{W} \tag{C.40}$$

For the assumed temperature gradient of 125°C m^{-1}:

$$\text{heat flux} = 31.4\,\text{W} \tag{C.41}$$

J Axial conduction within the flight thickness

The cross-sectional area of the flight normal to the screw axis is $0.01 \times \pi \times 0.1 = 0.003\,14\,m^2$. For a 1°C temperature difference:

$$\text{heat flux} = 50 \times 0.003\,14 \times \frac{1}{0.01}$$
$$= 15.7\,\text{W} \tag{C.42}$$

If surface heat transfer coefficients of 300 W m^{-2} K^{-1} are assumed, as for the channel root, the overall coefficient:

$$U = \frac{1}{\frac{1}{300} + \frac{1}{300} + \frac{0.01}{50}}$$
$$= 145\,\text{W m}^{-2}\text{K}^{-1} \tag{C.43}$$

then

$$\text{heat flux} = 145 \times 0.003\,14 \times 125 \times 0.01$$
$$= 0.57\,\text{W} \tag{C.44}$$

and temperature difference within the flight metal:

$$dT = \frac{0.57 \times 0.01}{0.003\,14 \times 50}$$
$$= 0.036°\text{C} \tag{C.45}$$

K Radial conduction in polymer in channel

For one turn of the channel,

$$\text{surface area} = 0.085\,76 \times 0.3297$$
$$= 0.0283\,\text{m}^2$$

For a temperature gradient of 1°C/mm,

$$\text{radial heat flux} = 0.5 \times 0.0283 \times 1000$$
$$= 14.1\,\text{W/turn} \tag{C.46}$$

In section C.4 it is shown that without circulation **N**, shear heating **M** will cause a radial temperature difference per turn ranging between about 0.42°C at $Q/Wbh = 1/2$ and 3.8°C at $Q/Wbh = 0$ over an average distance of about 5 mm or half the channel depth. Then due to pure conduction,

$$\text{radial heat flux} = 0.5 \times 0.0283 \times \frac{0.42}{0.005}$$
$$= 1.2\,\text{W to } 10.7\,\text{W} \tag{C.47}$$

Circulation **N** reduces the radial temperature differences to 0.05–0.30°C for which,

$$\text{radial conduction} = 0.14\text{–}0.85\,\text{W} \tag{C.49}$$

L Longitudinal (helical) conduction in polymer in channel

The channel cross-sectional area is $0.01 \times 0.085\,76 = 0.000\,86\,\text{m}^2$. For a temperature gradient along the helix of 1°C/mm,

$$\text{heat flux} = 0.5 \times 0.000\,86 \times 1000$$
$$= 0.43\,\text{W} \tag{C.49}$$

The assumed axial gradient of 125°C/m corresponds to a gradient along the helix of $125 \times 0.1/0.3297 = 37.9$°C/m, for which, conduction along channel helix,

$$\text{heat flux} = 0.5 \times 0.000\,86 \times 37.9$$
$$= 0.016\,\text{W} \tag{C.50}$$

M Shear heating in channel

See section C.4.

N Transverse circulation in channel

See section C.4.

P Shear heating and dissipation in flight clearance

See section C.5.

R Conduction along flight helix

The cross-sectional area of the screw flight is

$$0.01 \times 0.01 \cos\phi = 9.5 \times 10^{-5}\,\mathrm{m}^2$$

The temperature gradient along the helix (as for **L**) is 37.9°C/m, giving conducted

$$\begin{aligned}\text{heat flux} &= 50 \times 9.5 \times 10^{-5} \times 37.9 \\ &= 0.18\,\mathrm{W}\end{aligned} \tag{C.51}$$

S Conduction across channel

This is estimated in the absence of mass transfer due to polymer velocities. The cross-sectional area normal to screw axis is

$$0.01 \times \pi \times 0.1 = 0.003\,14\,\mathrm{m}^2$$

For an axial temperature gradient of 1°C/mm,

$$\begin{aligned}\text{axial heat flux} &= 0.5 \times 0.003\,14 \times 1000 \\ &= 1.57\,\mathrm{W}\end{aligned} \tag{C.52}$$

For the assumed temperature gradient of 125°C/m,

$$\begin{aligned}\text{axial heat flux} &= 0.5 \times 0.003\,14 \times 125 \\ &= 0.20\,\mathrm{W/turn}\end{aligned} \tag{C.53}$$

The heat conducted normal to the channel helix will be similar, the smaller temperature gradient being partially offset by a greater cross-sectional area.

This small heat flux may be significant at standstill, though in operation the polymer flow near to the barrel is normal to the screw axis so conveys no heat by mass transfer, and at other positions has a forward component, contrary to pure conduction.

Standstill – e.g. during warm-up

When the screw is stationary, it is not possible to determine heat transfer coefficients at the surfaces. If these are neglected, the screw may be regarded as heated by pure conduction through parallel paths in the screw channel and the screw flight. Evidently if the screw is empty of polymer, the latter will predominate. Otherwise, suppose there is 10°C overall temperature difference between barrel and screw. Then in the channel,

$$q = kA \cdot \frac{dT}{dx}$$
$$= 0.5 \times \frac{10}{0.01}$$
$$= 500\,W\,m^{-2}$$

or

$$500 \times 0.085\,76 \times 0.3297 = 14.14\,W/turn$$

For the flight,

$$U = \frac{1}{\frac{0.000\,15}{0.50} + \frac{0.01}{50}}$$
$$= 2000\,W\,m^{-2}\,K^{-1}$$

and

$$\text{heat flux} = 2000 \times 0.009\,53 \times 0.3297 \times 10$$
$$= 62.84\,W/turn$$

The proportion flowing through the flight is:

$$\frac{62.84}{62.84 + 14.14} = 0.816 \text{ or } 81.6\% \qquad \text{(C.54)}$$

so that heating through the flight still predominates with a full channel.

At the screw tip, suppose 31 W is conducted axially in the screw, leaving approximately 46 W for heating the screw. Then heating rate would be:

$$\frac{46}{0.005\,03 \times 0.1 \times 7800 \times 503} = 0.023°C\,s^{-1}$$

or

$$1.4°C\,min^{-1} \text{ for } 10°C \text{ radial difference} \qquad \text{(C.55)}$$

If, in view of the heater power, it may be assumed that the barrel temperature is constant, the screw heating rate would be $0.7°C\,min^{-1}$ for 5°C difference. Thus

it will take approximately 5 min to reduce the barrel/screw temperature difference by half.

Screw cooling

A heat transfer coefficient to water in turbulent flow may be taken as 1705 $W\,m^{-2}\,K^{-1}$ (300 BTU/hr · ft^2 · °F). Then if the cooling bore is 30 mm in diameter, the surface is $\pi \times 0.03 \times 0.1 = 0.0094\,m^2$ per turn.

For 1°C difference, heat flow = $1705 \times 0.0094 \times 1 = 16$ W per turn. If this came from the channel **E**, then

$$\text{polymer/metal difference} = 2.47°C \tag{C.56}$$

C.4 DISTRIBUTION OF SHEAR HEATING AND TRANSVERSE CIRCULATION

M Shear heating in screw channel

The longitudinal (downchannel) velocity at distance y from the screw root is given by:

$$w_y = \frac{Wy}{h} + \frac{6W}{h^2}\left(\frac{1}{2} - \frac{Q}{Wbh}\right)(y^2 - yh) \tag{6.67}$$

Putting

$$q = \frac{1}{2} - \frac{Q}{Wbh} \tag{8.17}$$

then

$$w_y = \frac{Wy}{h} + 6Wq\left[\left(\frac{y}{h}\right)^2 - \frac{y}{h}\right] \tag{C.57}$$

The transverse velocity at distance y from the screw root:

$$u_y = \frac{Uy}{h}\left(\frac{3y}{h} - 2\right) \tag{6.26}$$

Substituting $U = W \tan\phi$ from equations (6.4) and (6.5) and putting

$$T = \tan\phi \tag{8.18}$$

$$u_y = \frac{WTy}{h}\left(\frac{3y}{h} - 2\right) \tag{C.58}$$

Total velocity at distance y from the screw root:

$$\text{Velocity at } y = \sqrt{w_y^2 + u_y^2}$$

$$= \sqrt{\begin{aligned} &W^2\left(\frac{y}{h}\right)^2 + 12W^2q\left(\frac{y}{h}\right)^3 - 12W^2q\left(\frac{y}{h}\right)^2 - 72W^2q^2\left(\frac{y}{h}\right)^3 \\ &+ 36W^2q^2\left(\frac{y}{h}\right)^4 + 36W^2q^2\left(\frac{y}{h}\right)^2 \\ &+ 9W^2T^2\left(\frac{y}{h}\right)^4 + 4W^2T^2\left(\frac{y}{h}\right)^2 - 12W^2T^2\left(\frac{y}{h}\right)^3 \end{aligned}} \tag{C.59}$$

Differentiating, the shear rate at y is:

$$\dot{\gamma}_y = \frac{\mathrm{d}}{\mathrm{d}y}(\text{Velocity})$$

$$= \frac{W^2}{2} \cdot \frac{\left[\begin{aligned} &\frac{2}{h}\left(\frac{y}{h}\right) + \frac{36q}{h}\left(\frac{y}{h}\right)^2 - \frac{24q}{h}\left(\frac{y}{h}\right) - \frac{216q^2}{h}\left(\frac{y}{h}\right)^2 + \frac{144q^2}{h}\left(\frac{y}{h}\right)^3 \\ &+ \frac{72q^2}{h}\left(\frac{y}{h}\right) + \frac{36T^2}{h}\left(\frac{y}{h}\right)^3 + \frac{8T^2}{h}\left(\frac{y}{h}\right) - \frac{36T^2}{h}\left(\frac{y}{h}\right)^2 \end{aligned}\right]}{\sqrt{\begin{aligned} &W^2\left(\frac{y}{h}\right)^2 + 12W^2q\left(\frac{y}{h}\right)^3 - 12W^2q\left(\frac{y}{h}\right)^2 - 72W^2q^2\left(\frac{y}{h}\right)^3 + 36W^2q^2\left(\frac{y}{h}\right)^4 \\ &+ 36W^2q^2\left(\frac{y}{h}\right)^2 + 9W^2T^2\left(\frac{y}{h}\right)^4 + 4W^2T^2\left(\frac{y}{h}\right)^2 - 12W^2T^2\left(\frac{y}{h}\right)^3 \end{aligned}}} \tag{C.60}$$

Extracting $(2/h)(y/h)$ from the numerator and $[W^2(y/h)^2]^{1/2}$ from the denominator,

$$\dot{\gamma}_y = \frac{W}{h} \cdot \frac{\left[\begin{aligned} &1 + 18q\left(\frac{y}{h}\right) - 12q - 108q^2\left(\frac{y}{h}\right) + 72q^2\left(\frac{y}{h}\right)^2 + 36q^2 \\ &+ 18T^2\left(\frac{y}{h}\right)^2 + 4T^2 - 18T^2\left(\frac{y}{h}\right) \end{aligned}\right]}{\sqrt{\begin{aligned} &1 + 12q\left(\frac{y}{h}\right) - 12q - 72q^2\left(\frac{y}{h}\right) + 36q^2\left(\frac{y}{h}\right)^2 + 36q^2 \\ &+ 9T^2\left(\frac{y}{h}\right)^2 + 4T^2 - 12T^2\left(\frac{y}{h}\right) \end{aligned}}} \tag{C.61}$$

Shear heating per unit volume is

$$\eta\dot{\gamma}^2 \,\mathrm{W\,m^{-3}} \tag{3.57}$$

Then, rearranging terms, shear heating per unit volume ($\mathrm{W\,m^{-3}}$) is:

$$\frac{\eta W^2}{h^2} \cdot \frac{\left[\begin{aligned} &1 + 4T^2 - 12q + 36q^2 - 18T^2\left(\frac{y}{h}\right) + 18q\left(\frac{y}{h}\right) - 108q^2\left(\frac{y}{h}\right) \\ &+ 18T^2\left(\frac{y}{h}\right)^2 + 72q^2\left(\frac{y}{h}\right)^2 \end{aligned}\right]^2}{\left[\begin{aligned} &1 + 4T^2 - 12q + 36q^2 - 12T^2\left(\frac{y}{h}\right) + 12q\left(\frac{y}{h}\right) - 72q^2\left(\frac{y}{h}\right) \\ &+ 9T^2\left(\frac{y}{h}\right)^2 + 36q^2\left(\frac{y}{h}\right)^2 \end{aligned}\right]} \tag{C.62}$$

Table C.5 Shear heating in screw channel with a Newtonian fluid $\left(\times \frac{\eta W^2}{h^2} \mathrm{W\,m^{-3}}\right)$

y/h	Q/Wbh						
	0	0.1	0.2	0.3	0.4	0.5	0.6
0 to 0.05	3.769	1.985	0.851	0.366	0.531	1.346	2.811
0.05 to 0.15	2.159	1.045	0.390	0.189	0.457	1.192	2.384
0.15 to 0.25	0.705	0.257	0.056	0.078	0.425	1.034	1.892
0.25 to 0.35	0.044	0.0001	0.013	0.075	0.467	0.931	1.486
0.35 to 0.45	0.176	0.264	0.098	0.227	0.594	0.879	1.161
0.45 to 0.55	1.101	0.962	0.069	0.659	0.818	0.879	0.910
0.55 to 0.65	2.819	0.129	1.472	1.366	1.153	0.932	0.727
0.65 to 0.75	5.332	4.107	3.113	2.289	1.603	1.044	0.606
0.75 to 0.85	8.634	6.667	4.901	3.399	2.172	1.220	0.543
0.85 to 0.95	12.731	9.651	6.961	4.690	2.855	1.468	0.535
0.95 to 1.00	16.314	12.221	8.707	5.778	3.442	1.704	0.568

Table C.6 Cumulative shear heating per unit area $\left(\times \frac{\eta W^2}{h} \mathrm{W\,m^{-2}}\right)$

y/h	Q/Wbh						
	0	0.1	0.2	0.3	0.4	0.5	0.6
0 to 0.05	0.188	0.099	0.043	0.018	0.027	0.067	0.141
0 to 0.15	0.404	0.204	0.082	0.037	0.072	0.186	0.379
0 to 0.25	0.475	0.229	0.087	0.045	0.115	0.290	0.568
0 to 0.35	0.479	0.229	0.089	0.053	0.161	0.383	0.717
0 to 0.45	0.497	0.256	0.098	0.075	0.221	0.471	0.833
0 to 0.55	0.607	0.352	0.105	0.141	0.303	0.559	0.924
0 to 0.65	0.889	0.365	0.252	0.278	0.418	0.652	0.997
0 to 0.75	1.422	0.776	0.564	0.507	0.578	0.756	1.057
0 to 0.85	2.286	1.442	1.054	0.847	0.795	0.878	1.112
0 to 0.95	3.559	2.407	1.750	1.316	1.081	1.025	1.165
0 to 1.00[a]	4.374	3.018	2.185[b]	1.604	1.253	1.110	1.193

[a]Addition of the pumping power $Q\,dP$ accounts for much of the difference from the power calculated by equation (8.9), using the same values of viscosity. An unexplained discrepancy of 10–20% remains.
[b]Recalculation with 40 intervals gives a total only 0.6% greater.

Note that equation (C.62) cannot easily be integrated to give the cumulative shear heating from the screw root at $y/h = 0$, so a manual summation is used to give Fig. 8.6. Equation (C.62) is quite general for the assumptions of isothermal Newtonian conditions, whereas Fig. 8.6, in terms of watts per square metre of barrel surface, is specific to a channel depth of 0.01 m.

The shear heating per unit volume has been calculated from equation (C.62) for pitch and diameter equal, $\phi = 17.7°$ and $T = \tan\phi = 1/\pi$ for values of Q/Wbh from 0 to 0.6 at intervals of 0.1. As a first approximation, values have been calculated at $y/h = 0.025, 0.10, 0.20, \ldots, 0.90, 0.975$ to represent the

mean value for the ranges $0 < y/h < 0.05$, $0.05 < y/h < 0.15$, $0.85 < y/h < 0.95$, $0.95 < y/h < 1.00$, respectively. These values ($W\,m^{-3}$) are tabulated in Table C.5 and plotted in Fig. 8.5. The cumulative shear heating in watts per square metre of surface is tabulated in Table C.6 and plotted in Fig. 8.6. As a check on the approximation, the calculation was repeated at intervals of y/h of 0.025 (40 steps) for $Q/Wbh = 0.2$, since in this case a sudden change in curvature appears.

N Transverse circulation

The transverse velocity at y from the channel root is given by equation (6.26):

$$u_y = \frac{Uy}{h}\left(\frac{3y}{h} - 2\right) \tag{6.26}$$

noting that $u = 0$ at $y/h = 2/3$, and $u = -U/3$ (a maximum) at $y/h = 1/3$.

The transverse flow Q_x per unit helical length dz between $y = 0$ and $y = y_1$ is:

$$\begin{aligned} Q_x &= \int_0^{y_1} u\,dy\,dz \\ &= \left[\frac{U}{h}\left(\frac{y_1^3}{h} - y_1^2\right) + C\right]dz \end{aligned} \tag{C.63}$$

But $Q_x = 0$ at $y = 0$, therefore $C = 0$.

Similarly, the flow Q'_x between $y = y_2$ and $y = h$ is:

$$\begin{aligned} Q'_x &= \int_{y_2}^{h} u\,dy\,dz \\ &= -\frac{U}{h}\left(\frac{y_2^3}{h} - y_2^2\right)dz \end{aligned} \tag{C.64}$$

By continuity

$$Q_x = -Q'_x \tag{C.65}$$

therefore

$$\begin{aligned} Q_x &= \frac{Uhy_1^2}{h^2}\left(\frac{y_1}{h} - 1\right)dz \\ &= \frac{Uhy_2^2}{h^2}\left(\frac{y_2}{h} - 1\right)dz \end{aligned} \tag{C.66}$$

Table C.7 gives some values of y/h and the corresponding values of u/U and $Q_x/Uh\,dz = y^2(y/h - 1)/h^2$. This shows, for example, that the flow of $0.081Uh\,dz$ at an average velocity of $0.81U = 0.0772\,m\,s^{-1}$ in the lamina $0.9 < y/h < 1.0$ next to the barrel is approximately equal to that in the reverse direction in the region $0 < y/h < 0.355$ at a mean velocity of $0.081U/0.355 = 0.228U$.

Table C.7 Transverse velocities and flow rates

Fractional depth y/h	*Fractional velocity* u/U	*Cumulative flow rate 0–y* $Q_x/Uh\,\mathrm{d}z = y^2(y/h-1)/h^2$
0	0	0
0.05	−0.0925	−0.0024
0.1	−0.170	−0.0090
0.15	−0.232	−0.0191
0.2	−0.280	−0.0320
0.25	−0.312	−0.0469
0.3	−0.330	−0.0630
0.35	−0.332	−0.0796
0.4	−0.320	−0.0960
0.45	−0.292	−0.1114
0.5	−0.250	−0.1250
0.55	−0.192	−0.1361
0.6	−0.120	−0.1440
0.65	−0.032	−0.1479
0.667	0	−0.1481
0.7	+0.070	−0.1470
0.75	0.187	−0.1406
0.8	0.320	−0.1280
0.85	0.467	−0.1084
0.9	0.630	−0.0810
0.95	0.807	−0.0451
1.0	1.0	0

Each element in this lamina will be subjected to shear heating during its traverse across the channel. For example, at $Q/Wbh = 0.5$ and for $0.9 < y/h < 1.0$, from Fig. 8.6,

$$\text{shear heating} = 88.55\,\text{W/turn} \tag{C.67}$$

$$\text{lamina volume} = 0.001 \times 0.085\,76 \times 0.3297$$

$$= 2.83 \times 10^{-5}\,\text{m}^3/\text{turn (Table C.8)} \tag{C.68}$$

Thus 88.55 J are generated in 1 s in this volume, or $88.55/2.83 \times 10^{-5}\,\text{J m}^{-3}$. In 1 s, the volume flowing radially inward from this lamina is:

$$Q_x = Uh\frac{y^2}{h^2}\left(\frac{y}{h}-1\right)\mathrm{d}z$$

$$= 0.0953 \times 0.01 \times 0.081 \times 0.3297$$

$$= 2.545 \times 10^{-5}\,\text{m}^3\,\text{s}^{-1}\ \text{per turn} \tag{C.69}$$

Thus

$$\text{heat transferred out of lamina} = 88.55 \times \frac{2.545 \times 10^{-5}}{2.83 \times 10^{-5}}$$

$$= 79.7\,\text{J s}^{-1} \tag{C.70}$$

Table C.8 Radial elements for estimation of heat transfer

y/h	*Layer volume* ($\times 10^{-5}$ m^3)	*Transverse flow rate* Q_x ($\times 10^{-5}$ m^3 s^{-1})	*Mean transverse velocity (from* Q_x*)* (m s^{-1})	*Mean transit time across channel* (s)
0.9–1.0	2.827	2.545	0.0772	1.110
0.8–0.9	2.827	1.477	0.0448	1.915
0.7–0.8	2.827	0.597	0.0181	4.738
0.65–0.7	----------	Neglected	----------	
0.512–0.65	3.902	0.597	−0.0131	6.547
0.355–0.512	4.439	1.477	−0.0285	3.006
0–0.355	10.04	2.545	−0.0218	3.934

Inspection of equations (C.68) and (C.69) shows that they differ by b/u_y, the transit time of a particle in this lamina across the channel i.e.

$$t = \frac{0.085\,76}{0.0772}$$
$$= 1.11\,\text{s} \tag{C.71}$$

and

$$79.7\,\text{W} = \frac{88.55}{1.11}\,\text{J s}^{-1} \tag{C.72}$$

that is, the heat transferred radially is the shear heat in the source divided by the transit time across the channel. Similarly, the heat transferred radially outward, 54.4 W per turn, from the region $0 < y/h < 0.355$, is given by the shear heat of that region, 213.9 W per turn, divided by the transit time of 3.93 s. These values are calculated for several laminae and summed to give the total radial inward and outward heat flows, the difference being the net heat transferred inward e.g. 41.6 W at $Q/Wbh = 0.5$. From the cumulative shear heating (Fig. 8.6), the total shear heat is calculated as 620.0 W per turn and by graphical interpolation, that in the region of rightward flow, $0 < y/h < 0.67$, is estimated as 368.5 W per turn. Then the shear heating in the region of leftward flow, $0.67 < y/h < 1.0$, is by difference 251.5 W per turn. Because of the different masses involved, the equivalent average temperature rises, in the absence of circulation, are calculated as 1.077°C and 1.493°C, a difference of 0.416°C. When circulation is included, the net heating rate in the lower layer is increased by 41.6 W and that in the upper layer reduced by the same amount. Revised temperature increases are then calculated as 1.199°C and 1.246°C respectively, with a difference of 0.047°C. Thus it is estimated that the temperature difference between upper and lower regions of the channel is reduced through circulation by $(0.416 - 0.047)/0.416 = 89\%$.

Table C.9 Estimation of radial heat transfer in screw channel at speed 1 rps, temperature 150 °C

Q/Wbh	0	0.1	0.2	0.3	0.4	0.5	0.6
Viscosity ($N s m^{-2}$)	852.6	952.9	1088.4	1283.9	1596.7	2203.0	4126.0
Shear heat (W/turn)							
$0.9< y/h <1.0$	313.8	264.1	216.1	170.3	127.4	88.5	57.7
$0.8< y/h <0.9$	230.9	197.0	163.6	131.6	101.7	75.0	56.4
$0.7< y/h <0.8$	150.9	130.1	110.5	92.5	76.4	63.2	60.1
$0.512< y/h <0.65$	72.8	14.7	41.6	55.2	63.2	76.6	123.6
$0.355< y/h <0.512$	15.7	18.0	36.5	18.1	40.6	73.6	169.0
$0< y/h <0.355$	103.6	55.4	24.4	17.1	65.4	213.9	749.6
Heat transferred radially inward (W/turn)							
$0.9< y/h <1.0$	282.7	237.9	194.7	153.4	114.8	79.7	52.0
$0.8< y/h <0.9$	120.6	102.9	85.4	68.7	53.1	39.2	29.4
$0.7< y/h <0.9$	31.8	27.5	23.3	19.5	16.1	13.3	12.7
Total inward (W/turn)	435.1	368.3	303.4	241.6	184.0	132.2	94.1
Heat transferred radially outward (W/turn)							
$0.512< y/h <0.65$	11.1	2.2	6.3	8.4	9.6	11.7	18.9
$0.355< y/h <0.512$	5.2	6.0	12.2	6.0	13.5	24.5	56.2
$0< y/h <0.355$	26.3	14.1	6.2	4.3	16.6	54.4	190.5
Total outward (W/turn)	42.6	22.3	24.7	18.7	39.7	90.6	265.6
Net heat transferred inward (W/turn)	392.5	346.0	278.7	222.9	144.3	41.6	−171.5

The radial heat transfer is estimated for various values of Q/Wbh in Table C.9 and the reduction in temperature difference in Table C.10.

Although the main purpose of this appendix is to examine the variation of shear heating across the channel, the total shear heat, as shown by the bottom line of Table C.6, should be compared with the total calculated according to equation (8.7), using the same viscosities as mentioned on p. 245. The work of internal shearing appears as heat in the polymer, to which must be added the pressure energy produced at the end of the screw, as discussed on p. 227.

$$\begin{aligned}\text{pressure energy (pumping power)} &= Q\,\mathrm{d}p \text{ over length } \mathrm{d}z \\ &= Q\frac{\mathrm{d}P}{\mathrm{d}z}\cdot \mathrm{d}z\end{aligned}$$

Table C.10 Reduction of temperature difference in channel due to circulation

Q/Wbh	0	0.1	0.2	0.3	0.4	0.5	0.6
Total shear heat (W/turn)	945.3	729.0	602.8	522.1	507.1	620.0	1248.1
Approx. shear heat $0.67< y/h <1.0$ (W)	740.0	639.6	525.6	421.2	327.0	251.5	197.1
Approx. shear heat $0< y/h <0.67$ (W)	205.3	89.4	77.2	100.9	180.1	368.5	1051.0
Equivalent temperature rise without circulation							
$0.67< y/h <1.0$ (°C)	4.393	3.797	3.120	2.500	1.941	1.493	1.170
$0< y/h <0.67$ (°C)	0.600	0.261	0.226	0.295	0.527	1.077	3.073
Difference in temperature (°C) rise, no circulation	3.793	3.536	2.894	2.205	1.414	0.416	−1.903
Net energy with circulation (W/turn)							
$0.67< y/h <1.0$	345.5	293.6	246.9	198.3	182.7	209.9	368.6
$0< y/h <0.67$	599.8	435.4	355.9	323.8	324.4	410.1	879.5
Equivalent temperature rise with circulation							
$0.67< y/h <1.0$ (°C)	2.051	1.743	1.466	1.177	1.084	1.246	2.188
$0< y/h <0.67$ (°C)	1.754	1.273	1.041	0.947	0.948	1.199	2.571
Difference in temperature rise, with circulation (°C)	0.297	0.470	0.425	0.230	0.136	0.047	−0.383
Reduction in temperature difference (%)	92	87	85	90	90	89	80

(substituting from equation (6.16))

$$= \frac{\eta W}{h^2}\left(\frac{1}{2} - \frac{Q}{Wbh}\right) \cdot 12Q\,\mathrm{d}z$$

$$= \frac{\eta W^2}{h}\left(\frac{1}{2} - \frac{Q}{Wbh}\right) \cdot 12\,\frac{Q}{Wbh}\,b\,\mathrm{d}z \qquad \text{(C.73)}$$

For example, for $Q/Wbh = 0.2$,

$$\text{pressure energy} = 1088.4 \times \frac{0.2994^2}{0.01} \times 0.085\,76 \times 0.3297 \times 0.72$$

$$= 198.6\,\text{W/turn}$$

and

$$\frac{\mathrm{d}P}{\mathrm{d}z} = \frac{12\eta W}{h^2}\left(\frac{1}{2} - \frac{Q}{Wbh}\right)$$

$$= 11.73\,\text{MN m}^{-2} \text{ per metre}$$

$$\text{or } 3.87\,\text{MN m}^{-2} \text{ per turn}$$

The data for various values of Q/Wbh are given in Table C.11.

Table C.11 Comparison of channel power from equation (8.7) and section C.4 at speed 1 rps and temperature 150 °C

Q/Wbh	0	0.1	0.2	0.3	0.4	0.5	0.6
Shear rate $\dot{\gamma}_w$ (eqn (6.69)) (s^{-1})	119.8	101.8	83.8	65.9	47.9	29.9	12.0
Viscosity η_w ($N\,s\,m^{-2}$)	852.6	952.9	1088.4	1283.9	1596.7	2203.0	4126.0
Channel power, A (eqn (8.7))(W/turn)	952.0	919.1	884.2	847.8	811.5	784.7	842.2
Equivalent temperature rise (°C/turn)	∞	18.00	8.66	5.54	3.97	3.07	2.75
Shear heat, Table C.6 (W/turn)	945.3	729.0	602.8	522.1	507.1	620.0	1248.1
Pressure energy (W/turn)	0	115.9	198.6	234.3	194.2	0	−752.9
Total channel, power, B (W/turn)	945.3	844.9	801.4	756.4	701.3	620.0	495.2
$(B)/(A)$ (%)	99.3	91.9	90.6	89.2	86.4	79.0	58.8
Pressure rise ($MN\,m^{-2}$ per turn)	5.05	4.51	3.87	3.04	1.89	0	−4.89

C.5 TEMPERATURE VARIATION IN THE FLIGHT CLEARANCE

On p. 249 it is predicted that temperature differences and heat flows between the flight tip and adjacent polymer will be small; also that the latter represents a negligible heat sink. Thus the heat generated by shearing within the flight clearance will be dissipated by transient conduction in three dimensions within the barrel. However, inspection of Fig. C.3 shows that while at time t heat is conducted from a point opposite the leading flight face axially towards the die,

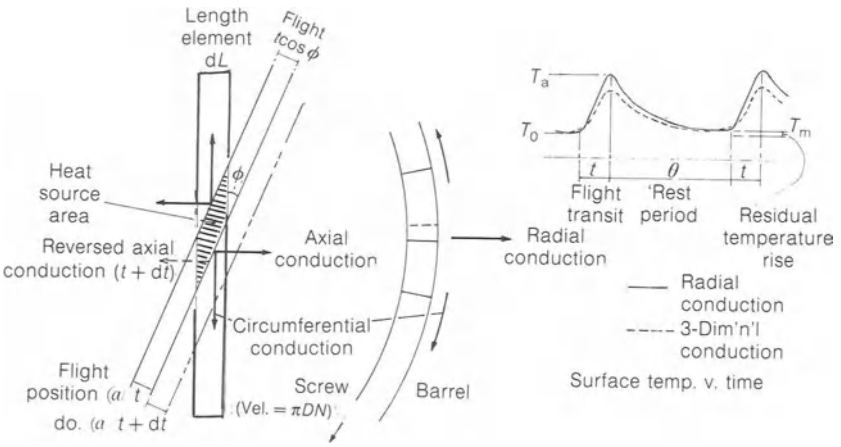


Figure C.3 Local heat flows in barrel from flight clearance.

at time $t + dt$ the same point on the barrel will be opposite the trailing flight face and heat will be conducted axially away from the die. Thus the heat conducted axially will be equal and opposite, though with a slight displacement in time. The same reasoning applies to circumferential conduction, so that one-dimensional (radial) transient conduction is a reasonable assumption, only slightly attenuated in practice.

The surface heat transfer coefficient in the flight clearance may be estimated by the method used for that in the screw channel **C**:

flight clearance $\delta = 0.000\,15\,\text{m}$

then equiv. slit $H = 0.0003\,\text{m}$

and equiv. dia $D_e = 0.0006\,\text{m}$

flight shear rate $$\dot{\gamma} = \frac{\pi DN}{\delta}$$
$$= 2094.4\,\text{s}^{-1}$$

equivalent flow rate Q for parabolic velocity distribution

$$= 2094.4 \times \frac{\pi \times 0.0003^3}{6}$$
$$= 29.61 \times 10^{-9}\,\text{m}^3\,\text{s}^{-1}$$

then mass flow $$w = 29.61 \times 10^{-9} \times 785$$
$$= 23.25 \times 10^{-6}\,\text{kg}\,\text{s}^{-1}$$

Graetz number $$Gz = \frac{wC_p}{kL}$$
$$= \frac{23.25 \times 10^{-6} \times 2300}{0.5 \times 0.03297}$$
$$= 3.24$$

McAdams (1954, equation (9.25a)) gives for this range of Graetz number,

Nusselt number $$Nu = \frac{2}{\pi} Gz$$
$$= 2.06$$

Then heat transfer coefficient,

$$h_a = \frac{2.06 \times 0.5}{0.0006}$$
$$= 1719\,\text{W}\,\text{m}^{-2}\,\text{K}^{-1}$$

Using the data of appendix C.3, the clearance volume per turn

$$= 0.3297 \times 0.009\,529 \times 0.000\,15$$
$$= 471.26 \times 10^{-9}\,\text{m}^3/\text{turn}$$

The shear heat developed will be a fuction of the mean temperature in the clearance, and since this is not predeterminable, it is calculated for various

temperatures in Table C.12. The barrel is assumed initially at a uniform temperature T_0, equal to that of the polymer in the channel, and it is in contact with the polymer in the flight clearance at a temperature T_a for a time $t = 0.1$ s at 1 rps. Because of simultaneous conduction of heat into the barrel, T_a is assumed constant during the very short heating time. Referring to McAdams (1954, p. 39) for one-dimensional transient heat conduction, if the surface resistance is negligible, then resistance ratio $m = k/hx = 0$.

Dimensionless group Z (related to Fourier number $\alpha t/r_m^2$)

$$= x/2\sqrt{\alpha t}$$
$$= x/2\sqrt{1.3 \times 10^{-5} \times 0.1}$$
$$= 438.5x$$

where t is time and x the distance below the surface.

Unaccomplished temperature change $Y = (T_a - T)/(T_a - T_0)$, where T is the temperature at position x and time t. This is obtained from the table of Y against Z, and for other values of x from McAdams (1954, equation (3.3))*.

The fractional temperature rise $(1 - Y)$ is given in Table C.13. The heat absorbed by the barrel in 0.1 s is given by McAdams (1954, equation (3.4)), where α is the thermal diffusivity and r_m is the half-thickness of an infinite slab. Then

$$X = \alpha t/r_m^2$$
$$= 1.3 \times 10^{-5} \times 0.1/0.01^2$$
$$= 0.013^*$$

giving a value of 0.128 68 to the right-hand side of McAdams (1954, equation (3.4)). Then

$$Q = 0.128\,68 r_m A \rho C_p (T_a - T_0)^\dagger$$
$$= 0.128\,68 \times 0.01 \times 0.3297 \times 0.009\,529 \times 7800 \times 503(T_a - T_0)$$
$$= 15.861(T_a - T_0)\ \text{J/turn}$$

Equating this to the shear work per turn in Table C.12 for a temperature of $150 + (T_a - T_0)$,

$$T_a - T_0 = 1.542°\text{C}$$
$$Q = 24.45\ \text{J/turn}$$

A finite surface heat transfer coefficient can be allowed for by McAdams (1954, equation (3.5)), which neglects the temperature gradient in the barrel for

*Convergence is very slow for the actual thickness of barrel i.e. $r_m = 0.05$ m. Since Table C.13 shows that in 0.1 s the temperature is unchanged beyond $x = 0.005$ m, r_m is taken as 0.01 m and X as 0.013 in McAdams (1954, eqn ((3.3)); agreement with McAdams (1954, p. 39) is still close.

†The factor 2 is omitted since the barrel is heated from one surface i.e. is semi-infinite.

large values of m (surface resistance controlling). If the surface heat transfer coefficient is $1719\,W\,m^{-2}\,K^{-1}$ (as above) and $r_m = 0.01\,m$, $X = 0.013$ and:

$$m = \frac{k}{r_m h}$$
$$= \frac{50}{0.01 \times 1719}$$
$$= 2.909$$

Then

$$-\ln Y = \frac{X}{m} \qquad \text{(McAdams, 1954, eqn (3.5))}$$
$$= \frac{0.013}{2.909}$$
$$= 0.004\,469$$

Table C.12 Shear heating in flight clearance

Mean temperature (°C)	$\beta(T - T_0)$	*Viscosity* ($N\,s\,m^{-2}$)	*Shear energy/ unit volume* ($MW\,m^{-3}$)	*Shear work per turn* (J/turn)	*Adiabatic temp. rise* (°C) *(insulated)*
1 rps					
140	−0.102	132.38	580.85	27.375	33.23
150	0	120.13	527.10	24.840	30.15
151	0.0102	118.90	521.70	24.586	29.84
152	0.0204	117.68	516.35	24.334	29.54
154	0.0408	115.23	505.60	23.827	28.92
156	0.0612	112.78	494.85	23.320	28.31
158	0.0816	110.33	484.10	22.814	27.69
160	0.102	107.88	473.35	22.307	27.08
170	0.204	95.62	419.56	19.772	24.00
180	0.306	83.37	365.81	17.239	20.93
190	0.408	71.12	312.06	14.706	17.85
200	0.510	58.86	258.26	12.171	14.77
2 rps					
140	−0.102	82.35	1445.3	34.05	41.33
150	0	74.73	1311.6	30.90	37.51
160	0.102	67.11	1177.8	27.75	33.69
170	0.204	59.48	1044.0	24.60	29.86
180	0.306	51.86	910.2	21.45	26.04
4 rps					
140	−0.102	51.23	3596.6	42.37	51.43
150	0	46.49	3263.8	38.45	46.67
160	0.102	41.75	2931.0	34.53	41.92
170	0.204	37.01	2598.0	30.61	37.16
180	0.306	32.26	2265.1	26.69	32.40

and

$$Y = 0.9955$$

then

$$(T - T_0) = (1 - Y)(T_a - T_0)$$
$$= 0.0045(T_a - T_0)$$

Table C.13 Radial temperature distribution in barrel when flight passes

Depth below inner surface, x (mm)	*Dimensionless depth* $Z = x/2\sqrt{(\alpha t)}$	*Unaccomplished temperature change* $Y = \frac{T_a - T}{T_a - T_0}$	*Fractional temperature rise* $\frac{T - T_0}{T_a - T_0}$
1 rps			
0	0	0	1.0
0.456	0.2	0.2227	0.7773
0.912	0.4	0.4284	0.5716
1.368	0.6	0.6039	0.3961
1.824	0.8	0.7421	0.2579
2.280	1.0	0.8427	0.1573
2.736	1.2	0.9103	0.0897
3.192	1.4	0.9523	0.0477
3.648	1.6	0.9763	0.0237[a]
4.104	1.8	0.9891	0.0109[a]
4.561	2.0	0.9953	0.0047
5.016	2.2	0.9981	0.0019[a]
5.472	2.4	0.9993	0.0007[a]
5.928	2.6	0.9998	0.0002[a]
6.384	2.8	0.9999	0.0001[a]
6.840	3.0	1.0	0[a]
2 rps			
0	0	0	1.0
1.14			0.3173[a]
2.28			0.0456[a]
3.42			0.0026[a]
4.56			0.0001[a]
5.70			0[a]
4 rps			
0	0	0	1.0
1.14			0.1552[a]
2.28			0.0044[a]
3.42			0.0001[a]
4.56			0[a]

[a]Calculated from equation (3.3).

and heat transferred

$$= A\rho C_p r_m (T - T_0)$$
$$= 0.3297 \times 0.009529 \times 7800 \times 503 \times 0.01 \times 0.0045(T_a - T_0)$$
$$= 0.5547(T_a - T_0)$$

The rise in temperature of the polymer in the clearance gap is now greater, so that the increase in its sensible heat becomes significant (with negligible surface resistance it is approximately 5% of the shear work). Increase in sensible heat,

$$\rho V C_p (T_a - T_0) = 760 \times 471.26 \times 10^{-9} \times 2300(T_a - T_0)$$
$$= 0.8238(T_a - T_0)$$

Then shear work,

$$24.45\,\text{J/turn} = (0.5547 + 0.8238)(T_a - T_0) \text{ at } 151.54°\text{C}$$
$$= 1.3785(T_a - T_0)$$

Comparing this with Table C.12 gives:

$$(T_a - T_0) = 15.2°\text{C}$$
$$T_a = 165.2°\text{C}$$
$$\text{shear work} = 1.3785(T_a - T_0)$$
$$= 20.98\,\text{J/turn}$$
$$\text{heat transferred} = 0.5547(T_a - T_0)$$
$$= 8.43\,\text{J/turn}$$

the remainder increasing sensible heat in the polymer.

For the assumed depth of heat penetration into the barrel of 0.01 m, the (uniform) increase in metal temperature,

$$T - T_0 = 0.0045(T_a - T_0)$$
$$= 0.068°\text{C}$$

The latter is strongly dependent on the value assumed for r_m, since this is also the thickness over which the heat is assumed to be uniformly distributed, e.g. for $r_m = 0.0036$ m, T_a and shear work remain virtually unchanged at 165.3°C and 20.97 J per turn, respectively, whereas the metal temperature rise, $T - T_0$, becomes 0.189°C. This approximation indicates that a finite surface heat transfer coeffcient will fractionally decrease the heat conducted into the barrel, and consequently also decrease the surface temperature, but the temperature of the polymer is greatly increased.

For the remaining 0.9 s of the revolution, this portion of the barrel is in contact with the polymer in the channel, and for a coefficient **C** of $300\,\text{W m}^{-2}\,\text{K}^{-1}$ (p. 441) may be treated as thermally insulated from the latter, so that the heat in the barrel, represented by the area under the initial temperature distribution in Fig. C.4 , will diffuse deeper into the barrel, with

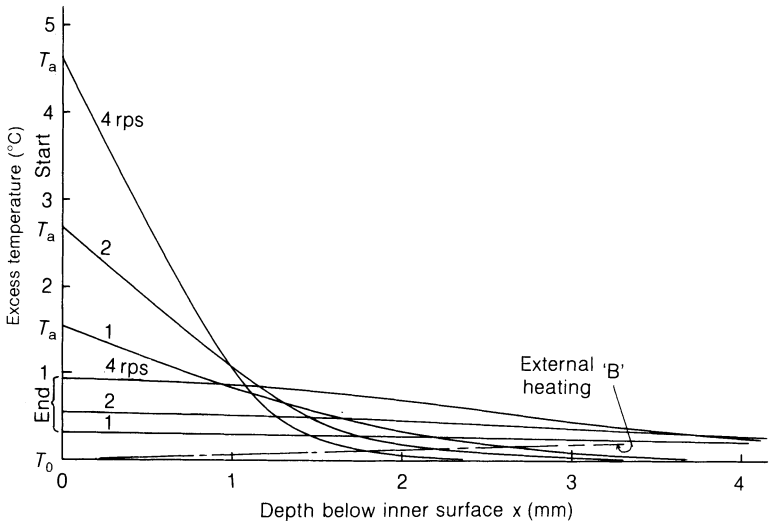


Figure C.4 Transient radial temperature distribution in barrrel at start and end of 'rest' period.

accompanying drop of surface temperature. Since this non-uniform temperature distribution is not represented by the standard graphs, it is necessary to resort to numerical methods, such as that due to Dusinberre (McAdams, 1954, p. 44). If the dimensionless ratio,

$$M = \frac{(\mathrm{d}x)^2}{\alpha\,\mathrm{d}t}$$

relates an element of thickness $\mathrm{d}x$ to a time interval $\mathrm{d}t$, then the temperature T'_n after time $\mathrm{d}t$ at the centre of element n from the surface is given by McAdams (1954, equation (3.6a)):

$$T'_n = \frac{T_{n-1} + (M-2)T_n + T_{n+1}}{M}$$

Table C.14 is calculated using the initial temperature ratios for $m = 0$ from Table C.13. The condition of thermal insulation from the polymer entails a zero temperature gradient at the surface. A rough calculation in which this condition was approximated by putting $T'_0 = T_1$ and taking $M = 4$, $\mathrm{d}x = 2.28\,\mathrm{mm}$ and $\mathrm{d}t = 0.1\,\mathrm{s}$ gives a surface temperature after 0.9 s of $0.1473(T_a - T_0)$, but with final heat content less than half that at the start. The heat content is given approximately by:

$$Q = \int C_p \rho A\,\mathrm{d}x\,\mathrm{d}T$$

$$= C_p \rho A\,\mathrm{d}x \Sigma\,\mathrm{d}T$$

for constant element thickness $\mathrm{d}x$.

Table C.14 Temperature profiles during 'rest' period in barrel

1 rps													
Depth x (mm)	0	2.28	4.56	6.84	9.12	11.40	13.68	15.96	18.24	20.52			
Times (s)													
0	0.8119	0.1573	0.0047	0									
0.1	0.4846	0.2828	0.0417	0.0012	0								
0.2	0.3838	0.2730	0.0918	0.0110	0.0003	0							
0.5	0.2658	0.2248	0.1355	0.0566	0.0155	0.0025	0.0002	0					
0.9	0.2050	0.1851	0.1370	0.0825	0.0400	0.0153	0.0045	0.0010	0.0001	0			
Final temperature = $0.205 \times 1.542 = 0.316$°C[a].													
2 rps													
Depth x (mm)	0	1.14	2.28	3.42	4.56	5.70	6.84	7.98	9.12	11.40	12.54	13.68	14.82
Time (s)													
0	0.8646	0.3173	0.0456	0.0026	0.0001	0							
0.05	0.4888	0.3665	0.1511	0.0322	0.0035	0.0002	0						
0.10	0.3858	0.3224	0.1871	0.0736	0.0188	0.0029	0.0002	0					
0.25	0.2660	0.2440	0.1884	0.1222	0.0661	0.0296	0.0108	0.0031	0.0006	0.0001	0		
0.45	0.2046	0.1942	0.1665	0.1290	0.0901	0.0566	0.0319	0.0161	0.0072	0.0028	0.0009	0.0003	0
Final temperature = $0.2046 \times 2.68 = 0.5483$°C													
4 rps													
Depth x (mm)	0	1.14	2.28	3.42	4.56	5.70	6.84	7.98	9.12	11.40	12.54	13.68	
Time (s)													
0	0.8116	0.1552	0.0044	0.0001	0								
0.025	0.4836	0.2816	0.0410	0.0011	0								
0.050	0.3826	0.2719	0.0912	0.0108	0.0003	0							
0.125	0.2644	0.2240	0.1349	0.0563	0.0154	0.0025	0.0002	0					
0.225	0.2040	0.1843	0.1364	0.0821	0.0398	0.0153	0.0045	0.0010	0.0001	0			
Final temperature = $0.2040 \times 4.61 = 0.9404$°C													

[a] When $dx = 0.912$ mm and $dt = 0.016$ s, giving 56 steps, the final temperature is 7% higher.

The heat content of the half-thickness element at the surface is reckoned as $\frac{1}{2} C_p \rho A \, dx(T - T_0)$, so that the total is $C_p \rho A \, dx(T - T_0)$ multiplied by the sum of the fractional temperature rises (last column of Table C.13) with the first element reckoned as 0.5. From this initial temperature distribution the heat content is calculated as:

$$= 503 \times 7800 \times 0.3297 \times 0.009\,529 \times 0.000\,456 \times 2.8398 \times 1.542$$
$$= 24.61 \text{ J/turn}^*$$

for an element thickness of 0.456 mm, compared with 24.45 J per turn calculated from McAdams (1954, equation (3.4)). To give this constant heat content, the surface temperature is adjusted at each step after the remaining temperatures have been estimated. To limit the number of steps, in Table C.14 the element thickness is increased to 2.28 mm (1 rps) or 1.14 mm (2 and 4 rps). Thus at 1 rps:

$$\frac{\Sigma \, dT}{1.542} = \frac{2.8398}{5}$$
$$= 0.5680$$

The corresponding values for 2 and 4 rps are 0.797 95 and 0.565 47, respectively. In each case, the temperature ratio calculated after 0.9 s, 0.45 s or 0.225 s lies between 0.204 and 0.205, which when multiplied by the initial temperature at the end of shearing gives the residual temperatures at the end of the 'rest' period in Table 8.2. With increased screw speed, the times of shearing and 'rest' are decreased, but with a constant ratio between them. The increased shear rate and shear work increase the surface temperatures at end of the shearing and at end of 'rest', in this case approximately as the 0.8 power of speed. With a constant thermal diffusivity, the heat does not penetrate as deeply as the time of shearing decreases with increase of screw speed. The decrease in the 'rest' period also localizes the diffusion of heat close to the inner surface of the barrel.

*Figure C.4 shows that the temperature falls rapidly from the surface and a value of 1.0 for T'_o/T_1 overestimates the mean temperature of the barrel close to the inner surface.

Appendix D
Stability of melt pumping section

In section 6.5 the total output was expressed in terms of speed N and pressure P by equation (6.50):

$$Q_{\text{Tot}} = AN - \frac{BP}{\eta} \tag{6.50}$$

where A and B are constants depending on the dimensions of the screw and die (equations (6.51) and (6.52)). For the present purpose it is convenient to define:

$$\begin{aligned} B' &= BZ \\ &= \frac{bh^3}{12} \end{aligned} \tag{D.1}$$

Equation (6.50) becomes:

$$Q_{\text{Tot}} = AN - \frac{B'P}{\eta Z} \tag{D.2}$$

and equation (6.58) becomes:

$$Q_{\text{Tot}}\left(1 + \frac{B'}{KZ}\right) = AN \tag{D.3}$$

or:

$$Q = \frac{ANKZ}{KZ + B'} \tag{D.4}$$

If, due to an external cause such as rearward movement of the 'gel' point, the melt length increases to $Z + \mathrm{d}z$, with the same die constant K, the output will change to $Q + \mathrm{d}q$ and pressure to $P + \mathrm{d}p$. Then:

$$Q + \mathrm{d}q = \frac{ANK(Z + \mathrm{d}z)}{K(Z + \mathrm{d}z) + B'} \tag{D.5}$$

Instantaneously, the rate of melting will remain at Q and the change of output represents an additional volume $bh\,\mathrm{d}z$. Therefore stable operation requires that the change of output for a given change of melt length should be minimized; this is represented by $\mathrm{d}q/Q\,\mathrm{d}t$.

Substituting from equation (D.4) in (D.5) gives:

$$\frac{\mathrm{d}q}{Q} = \frac{KZ + B'}{KZ} \cdot \frac{K(Z + \mathrm{d}z)}{K(Z + \mathrm{d}z) + B'} - 1 \tag{D.6}$$

Then:

$$\begin{aligned}
\frac{1}{Q}\frac{\mathrm{d}q}{\mathrm{d}t} &= \frac{\mathrm{d}}{\mathrm{d}t}\left(\frac{KZ + B'}{KZ} \cdot \frac{K(Z + \mathrm{d}z)}{K(Z + \mathrm{d}z) + B'}\right) \\
&= \frac{KZ + B'}{KZ} \cdot \frac{\mathrm{d}}{\mathrm{d}t}\left(\frac{K(Z + \mathrm{d}z)}{K(Z + \mathrm{d}z) + B'}\right) \\
&= \frac{KZ + B'}{KZ} \cdot \frac{\mathrm{d}}{\mathrm{d}t}\left(1 - \frac{B'}{K(Z + \mathrm{d}z) + B'}\right) \\
&= \frac{KZ + B'}{KZ}\left(\frac{B'K}{(K(Z + \mathrm{d}z) + B')^2}\right)\frac{\mathrm{d}(\mathrm{d}z)}{\mathrm{d}t}
\end{aligned} \tag{D.7}$$

For small values of $\mathrm{d}z/Z$:

$$\begin{aligned}
\frac{1}{Q} \cdot \frac{\mathrm{d}q}{\mathrm{d}t} &\simeq \frac{B'}{Z(KZ + B')} \cdot \frac{\mathrm{d}(\mathrm{d}z)}{\mathrm{d}t} \\
&= \frac{1}{Z\left(\dfrac{KZ}{B'} + 1\right)} \cdot \frac{\mathrm{d}(\mathrm{d}z)}{\mathrm{d}t}
\end{aligned} \tag{D.8}$$

Substituting for B':

$$\frac{1}{Q} \cdot \frac{\mathrm{d}q}{\mathrm{d}t} \simeq \frac{1}{Z\left(\dfrac{12KZ}{bh^3} + 1\right)} \cdot \frac{\mathrm{d}(\mathrm{d}z)}{\mathrm{d}t} \tag{D.9}$$

From equation (D.9) it is seen that if channel depth h is decreased, $\mathrm{d}q/\mathrm{d}t$ is reduced. Similarly, if channel length Z is increased, $\mathrm{d}q/\mathrm{d}t$ is reduced; both of these will tend to make the melt pumping section produce smaller amplitude oscillations of output and pressure (and also of power input) when subjected to disturbance, e.g. due to an imbalance between melting and pumping rates.

Appendix E
List of tables

2.1	Thermoplastics used in extrusion	5
2.2	Comparison of process requirements	25
3.1	Summary of flow equations	38
4.1	Thermal properties: conversion factors and typical values	55
5.1	Values of the damping constant, n	71
5.2	Effect of operational and geometrical variables on flow conditions in the die	122
5.3	Troubleshooting blown film, cast film, pipe and profile extrusion die related problems	124
6.1	Wall shear rate from equation (6.69) vs dimensionless output for screws of various tapers h_1/h_2, expressed as a ratio of the shear rate at the end of the screw in drag flow W/h_2	171
7.1	Materials used in feeding trials	177
7.2	Geometry of the screw used for computations	199
8.1	Heat flows in melt pumping section	238
8.2	Shear heating and temperature rises in flight clearance, neglible surface resistance	250
8.3	Output and power input as functions of dimensions (constant Q/Wbh), from equations (8.11), (8.12) and (8.24)–(8.27)	252
8.4	Variation in mechanical power with back pressure (kW/turn)	260
8.5	Change in energy balance with back pressure	264
8.6	Changes in energy balance with melt temperature and screw speed	267
9.1	Examples of screw types (90 mm diameter, single start, pitch equal to diameter (helix angle 17.6°))	294
9.2	Operational strategies: increased output required	296
9.3	Operational strategies: increased pressure required	297

9.4 Operational strategies: increased melt temperature required 298
9.5 Operational strategies: reduced melt temperature required 301
9.6 Operational strategies: reduced mechanical power input required 304
9.7 Operational strategies: reduced melt temperature variations required 307
9.8 Operational strategies: improved melting required 311
9.9 Operational strategies: improved mixing required 313
10.1 Gap areas between screws at axis plane and mid-plane 341
10.2 Comparison of single- and twin-screw extruders 349
11.1 Suggested conditions for individual processes 374
11.2 Scale-up of single-screw extruder: summary of effects of various scaling strategies with Q/Wbh as constant 378
12.1 Simple fault finding 385
12.2 Safety of operators 390
A.1 Thermal properties in the solid-state (room temperature) 406
B.1 Pressure gradients in a stepped screw 421
C.1 Static heat losses 434
C.2 Surface temperatures in heat loss tests (°C) 434
C.3 Surface heat transfer coefficient: barrel to polymer 442
C.4 Radial conduction in screw flight for several resistance ratios $m = k/hx$ 444
C.5 Shear heating in screw channel with a Newtonian fluid $\left(\times \frac{\eta W^2}{h^2} \mathrm{W\,m^{-3}}\right)$ 452
C.6 Cumulative shear heating per unit area $\left(\times \frac{\eta W^2}{h} \mathrm{W\,m^{-2}}\right)$ 452
C.7 Transverse velocities and flow rates 454
C.8 Radial elements for estimation of heat transfer 455
C.9 Estimation of radial heat transfer in screw channel at speed 1 rps, temperature 150 °C 456
C.10 Reduction of temperature difference in channel due to circulation 457
C.11 Comparison of channel power from equation (8.7) and section C.4 at speed 1 rps and temperature 150 °C 458
C.12 Shear heating in flight clearance 461
C.13 Radial temperature distribution in barrel when flight passes 462
C.14 Temperature profiles during 'rest' period in barrel 465

References

Abedi, P. (1975) Ph.D thesis, Loughborough University of Technology, Loughborough, UK.

Adamski, T. (1974) Unpublished work, Loughborough University of Technology, Loughborough, UK.

Agassant, J.F., Avenas, P. and Sergent, J.Ph. (1986) *La Mise en Forme des Matières Plastiques*. Lavoisier, Paris.

Allan, P.S. and Bevis, M.J. (1991) *Plast. Rubb. Compos. Proc. Appl.*, **16**, 133.

Allen, W.J. and Hillman, D.A (1957) *Plastics*, **22**, 423.

Amellal, K., Lafleur, P.G. and Arpin, B. (1990) Chapter 10 in *Polymer Rheology and Processing* (eds A.A. Collyer and L.A. Utracki). Elsevier, London.

Ast, W. (1976) *Kunstst.*, **66**, 186.

Barakos, G., and Mitsoulis, E. (1994) *PPS-10*, Akron, Ohio, USA.

Barnett, R.D., Klein, I. *et al.* (1966) *15th Annual Wire and Cable Symposium*, Atlantic City, NJ, USA.

Bauer, W., Ehrmann, G. and Schneider, W. (1981) *Conf. Filtration of Polymer Melts*. VDI-Verlag, Düsseldorf, 55.

Becker, J., Klason, C., Kubat, J. and Saha, P. (1990) *Plast. Rubb. Proc. Appl.*, **14**, 77.

Becker, J., Klason, C., Kubat, J. and Saha, P. (1991) *Int. Polym. Proc.*, **VI**, 326.

Beddus, D. (1989) in *Extrusion Technology for Tubing and Profiles*, Killion, Princeton, NJ, USA.

Benkhoucha, K. and Sebastian, D.H. (1989) *SPE-ANTEC*, 1774.

Benkreira, H., Shales, R.W. and Edwards, M.F. (1992) *Int. Polym. Proc.* **VII**, 126.

Berger, P. and Krämer, A. (1975) *Kunstst.* **65**, 2.

Bernhardt, E.C. (1956) *SPE J.*, **12**, 40.

Bernhardt, E.C. (ed.) (1959) *Processing of Thermoplastic Materials*, Reinhold, New York.

Beverloo, W.A., Leniger, H.A. and de Velde, V (1961) *Chem. Eng. Sci.*, **15**, 260.

Bigg, D.M. (1987) *Adv. Polym. Techn.*, **7**, 147.

Briston, J.H. (1974) *Plastic Films*, Iliffe-Butterworth, London.

Brown, R.J., Kim, H.T. and Summers, J.W. (1979) *SPE-ANTEC*, 130.

Broyer, E. and Tadmor, Z. (1972) *Polym. Eng. Sci.*, **12**, 12.

Brydson, J.A. (1981) *Flow Properties of Polymer Melts*, 2nd edn. Geo. Godwin, London.

Carley, J.F. and Smith, W.C. (1978) *Polym. Eng. Sci.*, **18**, 408.
Carneiro, O.S. (1994) Ph.D. thesis, University of Minho, Braga, Portugal.
Casulli, J., Clermont, J.R., Von Ziegler, A. and Mena, B. (1990) *Polym. Eng. Sci.*, **30**, 1551.
Chan, G.S.H. and Hon, K.K.B. (1990) *Computer-Aided Eng. J*, **7**, 37.
Charbonneaux, T.G. (1991) *Polym. Plast. Techn. Eng.*, **30**, 665.
Cheng, C.Y. (1990) *SPE-ANTEC*, 49.
Chung, C.I. (1970) *SPE J*, **26**, 32.
Cogswell, F.N. (1968) *Plast. Polym.* **36**, 109–111.
Cogswell, F.N. (1972) *Polym. Eng. Sci.*, **12**, 64.
Cogswell, F.N. (1977) *J. Non-Newtonian Fluid Mech.*, **2**, 37.
Cogswell, F.N. (1981) *Polymer Melt Rheology*. Geo. Godwin, London.
Cogswell, F.N. and Lamb, P. (1970) *Plast. Polym.*, **38**, 391.
Covas, J.A. (1985) Ph.D. thesis, Loughborough University of Technology, Loughborough, UK.
Covas, J.A., (1991) *J. Vinyl Techn.*, **13**, 123.
Covas, J.A. and Carneiro, O.S. (1992) *Polymer*, **33**, 4977.
Covas, J.A and Carneiro, O.S. (1993) *PPS-9*, Manchester, UK.
Covas, J.A. and Cunha, A.G. (1993) *Materiais 93*, Porto, Portugal.
Covas, J.A. and Gilbert, M. (1992) *Polym. Eng. Sci.*, **32**, 743.
Covas, J.A., Gilbert, M., Marshall, D.E. (1988) *Plast. Rubb. Proc. Appl.*, **9**, 107.
Covas, J.A., Carneiro, O.S. and Brito, A.M. (1991) *J. Elastom. Plast.*, **23**, 218.
Coyle, D.J. and Perdikoulias, J. (1991) *SPE-ANTEC*, 2445.
Darnell, W.H. and Mol, E.A.J. (1953) *SPE J*, **12**, 20.
Dekker, J. (1976) *Kunstst.*, **66**, 130.
Donovan, R.C. (1971) *Polym. Eng. Sci.*, **11**, 247.
Dooley, J. (1990) *SPE-ANTEC*, 168.
Duffo, P., Monasse, B. and Haudin, J.M. (1991) *J. Polym. Eng.*, **10**, 151.
Eccher, S. and Valentinotti, A. (1958) *Ind. Eng. Chem.*, **50**, 829–836.
Elbirli, B., Lindt, J.T. Gottgetreu, S.R. and Baba, S.M. (1984). *Polym. Eng. Sci.*, **24**, 988.
Fang, S., Chen, L. and Zhu, F. (1991) *Polym. Eng. Sci.*, **31**, 1117.
Fenner, R.T. (1970) *Extruder Screw Design*. Iliffe-Butterworth, London.
Fenner, R.T. (1977) *Polymer* **18**, 617.
Fenner, R.T., Cox, A.P.D. and Isherwood, D.P. (1979) *Polymer* **20**, 49.
Fisher, E.G. (1976) *Extrusion of Plastics*, 3rd edn. Newnes-Butterworth, London.
Forrest, G. and Wilkinson W.L. (1973) *Trans. Inst. Chem. Engrs*, **51**, 331–338.
Forrest, G. and Wilkinson W.L. (1974) *Trans. Inst. Chem. Engrs*, **52**, 10–16.
Garcia-Rejon, A. and Dealy, J.M. (1982) *Polym. Eng. Sci.*, **22**, 158.
Giacomin, A. and Doshi, S. (1988) *SPE-ANTEC*, 38.
Gitschner, H.W., and Lutterback, J. (1984) *Kunstst.* **74**, 12.
Grant, D. (1961) *Trans. Plast. Inst.***29**, 130.
Griffith, R.M. and Tsai, J.T. (1980) *Polym. Eng. Sci.*, **20**, 1181.
Grünschloss, E. (1990) PPS-6, Nice, France.
Halasz, L. (1993) *Control Methods in Polymer Processing*. Elsevier, London.
d'Halewyu, S., Agassant, J.F. and Demay, Y. (1990) *Polym. Eng. Sci.*, **30**, 335.
Han, C.D., Lee, K.Y. and Wheeler, N.C. (1990) *Polym. Eng. Sci.* **30**, 1557.

Hayward, I.F. (1977) The design of a model screw extruder for the examination of factors affecting the feed characteristics. Project for B. Tech. (Hons), Dept of Mechanical Engineering, Loughborough University of Technology, Loughborough, UK.
Helmy, H.A.A. (1987) *Adv. Polym. Techn.*, **7**, 59.
Helmy, H.A.A and Worth, R.A. (1980) in *Rheology* (eds G. Astarita, G. Marruci and L. Nicolais). Plenum Press, New York, **3**, 69.
Henson, F. (ed) (1988) *Plastics Extrusion Technology*. Hanser, Munich.
Huang, D. and White, J.L. (1979) *Polym. Eng. Sci.* **19**, 609.
Huneault, M.A., Lafleur, P.G. and Carreau, P.J. (1990) *Polym. Eng. Sci.*, **30**, 1544.
Huneault, M.A., Lafleur, P.G. and Carreau, P.J. (1992) *SPE-ANTEC*, 431.
Janssen, H.A. (1895) *Z. VDI* **39**, 1045.
Janssen, L.P.B.M. (1978) *Twin Screw Extrusion*, Elsevier, Amsterdam.
Jenike, A.W. (1961) Bull. 108, *Utah Eng. Exp. Station*, Salt Lake City, USA.
Kacir, L. and Tadmor, Z. (1972) *Polym. Eng. Sci.* **12**, 387.
Kamp, W. and Kurz, H.D. (1980) *Kunstst.* **70**, 257.
Kaplan, S.J., Morland, C.D. and Hsu, S.C. (1979) *Chem. Eng.*, **86**, 93.
Kay, J.M. and Nedderman, R.M. (1974) *An Introduction to Fluid Mechanics and Heat Transfer*, 3rd edn. Cambridge University Press, Cambridge, UK.
Kennaway, A. (1957) Some recent developments in extrusion in *Plastics Progress*. Iliffe, London.
Kirby, R.B. (1962) *SPE J.*, **18**, 1273.
Klein, I. (1972) *SPE J.*, **28**, 47.
Klein, J.H. (1973) *Plast. Polym.*, **41**, 286–291.
Keindienst, U. (1973) *Kunstst.*, **63** 7.
Kozicki, W., Chou, C.H. and Tiu, C. (1966) *Chem. Eng. Sci.*, **21**, 665.
Krein, H.L. (1983) *Polym. Eng. Sci.*, **23**, 285.
Kuo, S.H. and Chung, C.I. (1989) *Polym. Eng. Sci.*, **29**, 448.
Kurtz, S.J. (1984) in *Advances in Rheology* (ed B. Mena *et al.*). UNAM Press, Mexico, **3**, 399.
Kurz, H.D. (1988) *Kunstst.*, **78**, 1052.
Kurzbuch, W. (1974) *Plast. Eng*, **8**, 43.
Lahti, G.P. (1963) *SPE J.*, **7**, 619.
Lee, C.C. and Stevenson, J.F. (1992) *Int. Polym. Proc.*, **7**, 186.
Lee, K.Y. and Han, C.D. (1990) *Polym. Eng. Sci.*, **30**, 665.
Legat, V. and Marchal, J.-M. (1993) *Int. J. Num. Meth. Fluids*, **16**, 29.
Lenk, R.S. and Frankel, R.A. (1981) *J. Appl. Polym. Sci.*, **26**, 2801.
Levy, S. and Carley, J.F. (1989) *Plastics Extrusion Technology Handbook*. Ind. Press Inc., New York.
Lidor, G. and Tadmor, Z. (1976) *Polym. Eng. Sci.*, **16**, 450.
Lindt, J.T. (1976) *Polym. Eng. Sci.*, **16**, 284.
Lindt, J.T. (1981) *Polym. Eng. Sci.*, **21**, 1162.
Lindt, J.T. (1985) *Polym. Eng. Sci.*, **25**, 585.
Lindt, J.T. and Elbirli, B. (1985) *Polym. Eng. Sci.*, **25**, 412.
Lolley, R.A. and Wykes, H. (1966) *Plast. Polym.*, **34**, 187–188
Lovegrove, J.G.A. and Williams, J.G. (1973) *J. Mech. Eng. Sci.*, **15**, 114.
Maddock, B. (1959) *SPE J.*, **15**, 383.

Marshall, D.I., Klein, I. and Uhl, R.H. (1965) *SPE J.*, **21**, 1192–1202.
Martelli, F.G. (1983) *Twin-screw Extruders: A Basic Understanding*. Van Nostrand Reinhold, New York.
Masberg, U. (1981) *Conf. Filtration of Polymer Melts*. VDI-Verlag, Düsseldorf., 29.
Matsubara, Y. (1980) *Polym. Eng. Sci.*,**20**, 716.
McAdams, W.H. (1954) *Heat Transmission*, 3rd edn. McGraw-Hill, New York.
McKelvey, J.M. (1962) *Polymer Processing*. John Wiley, New York.
Menges, G. and Klenk, P. (1967) *Kunstst.*, **57**, 598.
Menges, G., Feistkorn, W. and Fischbach, G., (1984) *Kunstst.* **74**, 695.
Menges, G., Kalwa, M. and Schmidt, J. (1987) *Kunstst.* **77**, 797.
Michaeli, W. (1992) *Extrusion Dies for Plastics and Rubbers*, Hanser, Munich.
Miller, C. (1972) *Ind. Eng. Chem. Fundam.* **11**, 524.
Miller, W.H., Lee, C.C. and Stevenson, J.F. (1991) *Int. Polym. Proc.* **6**, 253.
Mohr, W.D., Saxton, R.L. and Jepson, C.H (1957) *Ind. Eng. Chem.*, **49**, 1857–1862.
Munstedt, H. (1978) *Kunstst.*, **68**, 92.
O'Brien, K.T. (ed.) (1992) *Computer Modelling for Extrusion and Other Continuous Polymer Processes*. Hanser, Munich.
Overeijnder, H. (1982) *Plast. Extrusion III*. Plast. and Rubb. Inst., London.
Pearson, C.E. (1944) *The Extrusion of Metals*, Chapman & Hall, London.
Pearson, J.R.A. (1976) *Int. J. Heat Mass Transf.*, **19**, 405.
Perdikoulias, J., Vlcek, J. and Vlachopoulos, J. (1987) *Adv. Polym. Techn.*, **7**, 333.
Pinto, G. and Tadmor, Z. (1970) *Polym. Eng. Sci.*, **10**, 270.
Pittman, J.F.T. and Sander, R. (1993) *PPS-9*, Manchester, UK.
Pittman, J.F.T., Whitham, G.P., Beech, S. and Gwynn, D. (1992) *Plastic Pipes VIII*. Plast. and Rubb. Inst., Eindhoven, Holland.
Potente, H. (1985) *Kunstst.*, **75**, 439.
Potente, H. (1991) *Int. Polym. Proc.*, **VI**, 297.
Powell, P.C. (1974) *Polym. Eng. Sci.*, **14**, 298–307.
Procter, B. (1972) *SPE J.*, **28**, 34.
Rakos, R. and Sebastian, D. (1990) *Adv. Polym. Techn.*, **10**, 297.
Rakos, R., Kiani, A. and Sebastian, D.H (1989) *SPE-ANTEC*.
Ramamurthy, A.V (1986) *J. Rheol.* **30**, 337.
Rauwendaal, C. (1987) *Polym. Eng. Sci.* **27**, 186.
Rauwendaal, C. (1990) *Polymer Extrusion*. Hanser, Munich.
Rauwendaal, C. (1991a) *Plast. World* **49** (4), 61
Rauwendaal, C. (1991b) *Plast. World* **49** (8), 85
Rauwendaal, C. (1991c) *Plast. World* **49** (11), 73
Rauwendaal, C. (1991-2) *Adv. Polym. Techn.*, **11**, 19.
Roberts, A.W. (1991) *Bulk Sol. Handl.*, **11**, 17.
Saillard, P. and Agassant, J.F. (1984) *Polym. Proc. Eng.*, **2**, 37.
Sakai, T. (1990) *Int. Polym. Proc.*, V, 229.
Schafer, K. (1994) *PPS-10*, Akron, Chio, USA.
Schenkel, G (1966) *Plastics Extrusion Technology and Theory*. Iliffe, London.
Schenkel, G. (1981) *Kunstst.*, **71**, 479.
Schenkel, G. and Kühnle, H. (1983) *Kunstst.* **73**, 17.
Schiedrum, H.O. (1975) *Kunstst.*, **65**, 250.
Sebastian, D.H and Rakos, R. (1985) *Adv. Polym. Techn.*, **5**, 333.

Shamlou, P.A. (1988) *Handling of Bulk Solids*. Butterworth, London.
Shenoy, A.V and Saini, D.R (1984) *Polym. Plast. Techn. Eng.*, **23**, 169.
Sirlereaux, S. and Loewen, K.W. (1983) *Kunstst.*, **73**, 114.
Sors, L. (1974) *Kunstst.*, **64**, 287.
Stevens, M.J. (1970) *Plast. Polym.*, **38**, 107–113.
Stevenson, J.F. (1985) *Plast. Rubb. Proc. Appl.*, **5**, 325.
Steward, E.L. (1989) *SPE-ANTEC*, 75.
Stokes, V.K. (1987) *Polym. Eng. Sci.*, **27**, 990.
Street, L.F. (1961) *Int. Plast. Eng.*, **1**, 289.
Sun, J., Luo, X.L. and Tanner, R.I. (1994) *Int. Polym. Proc.*, **9**, 168.
Tadmor, Z. and Broyer, E. (1972) *Polym. Eng. Sci.*, **12**, 378.
Tadmor, Z. and Gogos, C.G. (1979) *Principles of Polymer Processing*. John Wiley, New York.
Tadmor, Z. and Klein, I. (1970) *Engineering Principles of Plasticating Extrusion*. Van Nostrand Reinhold, New York.
Tanev, N. (1975) Brug af blandehoved i snekkesprøjtestøbemaskine. Report no. PT 75.63-A. AMT Danmarks tekniske Højskole, 2800 Lyngby, Denmark.
Tanner, R.I. (1970) *J. Polym. Sci.*, Part A2, **8**, 2067.
Teh, J.W., Rudin, A. and Schreiber, H.P. (1984) *Plast. Rubb. Proc. Appl.* **4**, 149–156.
Vergnes, B. and Agassant, J.F. (1986) *Adv. Polym. Techn.*, **6**, 441
Vergnes, B., Saillard, P. and Plantamura, B. (1980) *Kunstst.* **70**, 750.
Vincelette, A.R., Guerrero, C.S., Carreau, P.J. and Lafleur, P.G. (1989) *Int. Polym. Proc.*, **IV**, 232.
Vlachopoulos, J., Behncke, P. and Vlcek, J. (1989) *Adv. Polym. Techn.*, **9**, 147.
Vlcek, J., Kral, V. and Kouba, K. (1984) *Plast. Rubb. Proc. Appl.*, **4**, 309.
Vlcek, J., Vlachopoulos, J. and Perdikoulias, J. (1988) *Int. Polym. Proc.* **2**, 174.
Wagner, M.H. (1977) *Rheol. Acta*, **16**, 43.
Walker, D.M. (1966) *Chem. Eng. Sci.*, **21**, 975.
Wang, Y. (1991) *Polym. Eng. Sci.*, **31**, 204.
Weeks, D.J. (1958) *British Plast.*, **31**, 156.
Weeks, D.J. and Allen W.J. (1962) *J. Mech. Eng. Sci.*, **4**, 380–400.
Westover, R.F. (1961) *SPE Trans.* **1**, 14–20.
White, J.L. (1990) *Twin Screw Extrusion*. Hanser, Munich.
White, J.L and Huang, D. (1981) *Polym. Eng. Sci.* **21**, 1101.
Winter, H.H. and Fritz, H.G. (1986) *Polym. Eng. Sci.*, **26**, 543.
Wolf, D. and White, D.H. (1976) *AIChE J.* **22**, 122.
Wortberg, J. and Schmitz, K.F. (1982) *Kunstst.*, **72**, 198.
Worth, R.A. and Lai-Fook, R.A. (1978) *Plastics and Rubber Processing* 3 (June), 68–72.
Zemblowski, Z. and Sek, J. (1981) *Polym. Eng. Sci.*, **21**, 1194.
Zhu, F. and Chen, L. (1991) *Polym. Eng. Sci.*, **31**, 1113.

Index

Page numbers in **bold** refer to figures and page numbers in *italic* refer to tables.

Additives 6, 19, 22, 353–4
Adiabatic, *see* Operation, adiabatic; Temperature, adiabatic
Air trapping 178, 271–2, 287, 292
Ammeter, drive, *see* Drive ammeter
Analysis, hydrodynamic 128
  of delay zone 205–7
  of hoppers 201–4
  of melting 190, 210–24
  of solids conveying 190, 191–201
Analysis of variables, *see* Variables, analysis of
Application
  to individual machine 399
  of single-screw extruder 4
Approximations for flow and power
  Newtonian isothermal 158, 168, 229, 376
  pseudoplastic isothermal 167–72, 235
Assumptions, simplified flow, *see* Theory, simplified
Autogenous (autothermal), *see* Operation, autogenous; Speed, autogenous; Temperature, autogenous

Back pressure, *see* Pressure, back
Bagley end correction 52
Barrel, *see* Cooling, barrel; Heat flow in barrel; Heating, barrel; Temperature, set; Thermal conduction in barrel; Transient conduction in barrel
Barrier screw, *see* Screw, barrier
Bearing, thrust, *see* Thrust bearing
Bingham fluids 64
Blending
  feed 372
  melt, *see* Melt blending
Blow moulding 6, 23, 264, *375*
Blown film, *see* Product types, blown film
Breaker plate, *see* Filtering

Capillary
  circular 33
  flow 33
    in parallel 39
    in series 38
  viscometer, *see* Viscometer
Channel (screw)
  curvature 131, 164
  depth 155, 216, **222**, **254**, 292–4, *294*, *295–315*
    energy balance, effect on 254
    output, effect on 142–3, 150, **156**
  partial filling 145, 162, **166**, 361–2
  power input 230, 251–9, 260–9, 296–314
  velocities in, *see* Velocity
  width correction (shape factor), *see* Corrections, shape factor
  see also Screw
Characteristics
  energy balance **256**, **257**
    see also Energy balance
  graphical representation of, *see* Graphical representation
  output/pressure 135, **155**, **156**, 168–9, **424**
    see also Output, pressure, effect of
  output/speed 152, 155
    see also Output, speed, effect of
Circular capillary, *see* Capillary, circular
Cleaning 392

Cleaning *contd*
of dies, *see* Dies, cleaning
of granulators 398
safety, *see* Safety, in dismantling/cleaning
of screws 395–6
solvent 394
tools 393–6
Clearance, flight, *see* Flight clearance
Coating, *see* Product types, coating
Colour (pigments)
changing 388
compounding 6, 19, 349, 398
dispersion of 64, 282
see also Compounding; Mixing
Combined (pressure and drag) flow, *see* Flow, combined
Commercial processes, *see* Extrusion processes
Commercial products, *see* Products
Comparison
of machine types, *see* Types of machine, comparison
of requirements for processes, *see* Process requirements
of thermal properties, *see* Thermal properties, comparison
Compounding 6, 19, **25**, 349, 398
twin-screw, *see* Twin-screw, mixing
see also Melt blending; Mixing
Compression ratio, *see* Channel depth; Screw design
Computer control, *see* Control, computer
Condition changes, *see* Operating conditions
Conduction 56, 64
circumferential in barrel wall **458**, 459
longitudinal 228, 432
in barrel wall *238*, 242, 276, 356, 357
in polymer 448
in screw 276–7, 443–7
radial
in barrel wall 232, **233**, 237, *238*
in capillary 57–8
in flight 444
in polymer 64, 356, 357
in screw 444
steady 56
transient 58, 248–51, 458–66
in twin-screw, *see* Twin-screw, heating *see also* Heat flow
Conductivity, *see* Thermal conductivity
Constant depth screw, *see* Screw, constant depth
Contamination 22, **385**–6, 387–8, 397–8
Continuous operation, *see* Operation, continuous
Control 366
accuracy 371–6, *374–5*
action (temperature), *see* Control of temperature
computer 24, 79, 371, 373–6
die centering 79–83
external 367
indication for 368–70
loss of 371
methods 367–71
overall 371, 402
of power *374–5*
signal 368–70
for specific processes 371, *374–5*
of speed 362–3, 367–8, *374–5*
strategies 4, *296–314*, *374–5*
of temperature 232, 277–8, 287–8, 360, 369–70, *374–5*, 384–7
Controlled variables, effect of, *see* Variables, controlled, effect of
Conversion factors (units) *56*
Conveying, solids, *see* Solids conveying
Cooling 59
barrel 20, 173, 251, 255, 279–80, 366, 404
air- 360
for solids conveying 178, 198, 208
feed pocket 175, 228, 271, 276, 401
of product 7–17
screw 20, 228, *239*, 240, 280–1, 292, 356, 370, 395, 401, 404
effect of melting 183, 278
see also Control; Heating; Heat losses
Corrections
end (Bagley) 52
heat transfer 61–2
non-isothermal 173–4, 236–51
output 140–2, 164–7, 172–3, 173–4
power 235–6, 236–51
pseudoplastic 153, 168–71, **169**, 172, 235–6, 259
shape factor 128, 164, 273–4, 351
Corrosion 394–5
from PVC 394
Crosslinking 6, 24

Covering (wire), *see* Product types
Crystallinity 12, 14, 17–18, 54, 233, 290, 353, 372
  see also Post-extrusion operations

Data
  thermal properties, *see* Thermal properties
  viscosity, *see* Viscosity, experimental
Defects of flow, *see* Flow defects
Definition
  efficiency 225–6, 228–9
  energy terms 225–8
  product quality, *see* Quality, definition of
Deformation, *see* Strain
  rate, *see* Shear rate; Strain rate
Degassing 22, *25*
  see also Venting
Degradation 5, 22, 294, 350
  shear 21, 365–6
  thermal 7, 10–11, 21, 281, 289, 293, 366
    during dismantling and cleaning 392, 394
Delay zone 180, 182, 205–7, **206**
  forces in 182, 206
  pressure rise in 206
Density *56*, **407**
Derivation of equations, *see* Equations for flow, power, shear rate, stability; Strain energy; Temperature variations; Theory, simplified
Design
  for cleaning 397
  of dies 7–8, 11, 65
  of feed pocket 176–7, **176**, 271–2, 325–6, 341, 372
  of machines 1, 283, 291–5, 376
  of screw, *see* Screw design
Dewatering 23
Die
  adjustment 8, 10, 65, 68, 79–83, 120, 125, 391
    see also Control, die centering
  breaker plate/filter 98, 100
  cleaning 67, 393–5
  computer programs for
    annulus, parallel-plate approximation 93
    complex flows, elementary approximation 94
    die design, general purpose 93
    general strategy 95–102
    inverse formulation 95–102
    mean temperature approximation 93
    narrow-channel approximation 93
    specific die geometry 93
  construction 67
    adaptor (transition) 66, 85, 98, 109, 118–19
    choker bar 68, 83, 121–2
    coathanger 83
    entrance 66
    feed-block (modular) 89–90
    filter-basket 79
    fishtail 83
    flow dividers 121
    mandrel **8**, 16, 68, 78–9, 80, 120–1
    multistage 85
    oscillating 77, 81
    perforated ring 79
    rotating 81, 89
    spiral mandrel 66, 79, 81
    streamlined profile 80
    T-manifold 82
    torpedo 66
  defects (flow) 92, 114, 125
    die-lip build-up 69
    fish-eyes 69
    melt fracture 69, 125
    plate-out 69
    sharkskin 69, 125
    weld lines 78–9, 121
    see also Die, material rheology; Elastic effects; Melt fracture design
    case study 114–19
    coathanger 107–8
    manifold 106–7
    multilayer manifolds 88–9
    principles 91
    for profiles 76, 109–13, 120–1
    simplified geometry for 93
    specific aspects 103
  dismantling 393–5
  face relief, *see* Die, land length
  flow
    in arbitrary cross-section 98–9, 109–13
    convergent 69, 70
    defects, *see* Die, defects (flow)
    distribution 10–11, 68, 80–1, 82–3, 84
    extensional, *see* Flow, extensional
    path 69, 91

Die *contd*
plug 85
properties, *see* Die, material rheology
resistance 68, 82, 87, 120
stability 88
uniformity, *see* Die, velocity uniformity
heating (thermal) 67, 80, 102
land (lips) 66, 83, 109–13, 121
land length 68, 83, 85, 98, 109–13, 121
maintenance 67, 393–5
material rheology 67, 68–9, 114, 125
constitutive models 92
die swell 69–74, 85–6, 92, 115–17, 121
effect of die swell on product 7–8, 11, 50, 291
relaxation 68, 78
see also Die defects (flow); Elastic effects; Flow, extensional; Viscosity mechanical construction
deformation (clamshelling) 67, 83, 101, 108
sealing 67
surface finish 85
performance 67
pressure drop 68, 69, 81, 92, 125
in land 81, 85, 98, 109–13
transverse 110, 120–1
sub-sections 68, 79–80, 84, 95–6, 109–13, 114–15, 121
temperature
controlled variations (thermal systems) of gap 83
controlled variations of polymer 68, 80, 82–3
distribution 91
uniformity (homogeneity) 67
variations, effect on flow, 68
types
crosshead (lateral feeding) 7, **9**, **17**, 80, 86
heart-shaped distributor 87
oscillating 16, 77, 81
shear-controlled orientation 77
spinaret (multi-hole) **15**
spiral mandrel 79, 81,103–5
see also Product types
velocity
distribution 82–3, 84
streamlining 84, 85, 87, 89, 91
uniformity 68, 79, 80–1, 85, 121
variations (time) 81
Dimensionless output (Q/Wbh), *see* Output, dimensionless
Dismantling 392
of die 393–5
of screw 395–6
safety in, *see* Safety in dismantling
Dispersive mixing, *see* Mixing, dispersive
Distribution, *see* Energy; Flow; Mixing; Temperature; Velocity
Distributive mixing, *see* Mixing, distributive
Double-parallel screw, *see* Screw, stepped
Drag flow 4, 9, 132–3, 151, 164, 251
power in **262**
shear heating **244**, 244–5
shear rate 133, *171*
velocity distribution 133
Drawdown, *see* Post-extrusion operations
Drawing, *see* Post-extrusion operations
Drive
ammeter 369, 387, 391, 402
efficiency 229, 368, 428–9
motor 226, 229, 278, 284, 287, 376
characteristic 360, **363**, 367–8
load 391
losses 226, 428
speed regulation 363, 367–8
stability 363
torgue measurement, *see* Torque measurement
Drying
of feed 158, 290, *385–6*
process 22

Effective melt length, *see* Melt length, effective
Efficiency 5, 225, 228–9, 353
definition, *see* Definition, efficiency
of drive, *see* Drive efficiency
pumping, *see* Pumping efficiency
Elastic effects 27, 48, 351, 372
in die 6–7, 46–7, 67, 68–72, 74, 91
measurement of 51–2
in product 23, 289, 291, 353, 373
see also Flow defects; Melt fracture
Elastic melter, *see* Weissenberg extruder
Energy
balance 4, 226, 346–7, 377
determination 226–9, 400–1

heating, effect of 254–6, 265–9, 279, 284
pressure, effect of 263–5, *264*, 284
pseudoplastic 259, **261**, **262**
at solids/film interface 213, 215–16
speed, effect of 256–9, **257**, 265–9, **268**, 283–4, 289–90, 401
variables, effect of 251–60, 282, 288
wall shear rate, effect of 259
dissipation (absorption) 236–7, 242–6, 248–51, 278–9, 349–50
distribution 42–5, 242–6, **244**, 349–50
in feed 227, 272–3
heater 226–7, 429
input (specific) 225, 228, 251–60, *301–14*
losses 228, 256, 400–1
mechanical 226, 229–31, *304–6*, 377–81, 401
pressure 227
properties 54–5
strain, *see* Strain energy
transfer, *see* Energy balance
see also Power
Enthalpy, *see* Heat content
Equations for
die flow *38*, 68, 93, 103–4, 106, 151–2, **157**
drag flow 133
flow *38*, 135, 274
leakage flow 417
output 135, 142–8, 168–9, 377
twin-screw 320, 340, 342, 383
power 230, 234–5, 377–80
twin-screw 383
pressure flow *38*, 134
shear heating 450–3
shear rate 27–32, 33–7, *38*, 133, 168
stability 362, 467–8
transverse flow 138–9, 414–15
Experimental determination of
elastic properties 52, 70–2
energy balance 400–1, 427–35
heat losses 433–5, **434**
heater energy 429
mechanical power 427–9
melt length (gel point) 165, 185–9
melting process 179, 182–3, 185–9, 210, **211**, 275–6
melt properties, *see* Experimental determination of elastic/viscous properties
output 368, 430–1
pressure 165, 368
solids feeding 176–7
temperature variations at die 165, 358–9, 362, 402–3
torque 427–9
viscous properties 32, 51, 372, 376, 399–400
Experimental screw nose, *see* Screw nose
Extensional flow, *see* Flow, extensional
Extraction, vacuum, *see* Vacuum extraction; Venting
Extruder
comparison of single- and twin–screw 349
and die interactions, *see* Output
operation *296–314*, 352
ram 350
single-screw 127, 175, 225, 270
scale-up, *see* Scale-up of machines
smooth disc, *see* Weissenberg extruder
spiral disc 351
twin-screw, *see* Twin-screw
vented, *see* Venting; Vacuum extraction
Extrusion processes 4, 352, *385–6*

Fault finding *123–5*, *385–6*
Feed
blending 372
enthalpy, *see* Heat content
grooved bush 177, 207–10
hopper 271–2
gravity flow 175, 201–4, **204**
vibration 175
see also Pressure in feed
properties 372
stirrer 271
throat, *see* Feed-pocket
variations 19, 271–3, 371, 372, 387
see also Feeding
Feeding 4, 128, 284, 293, *385–6*, 387, 391
deblending 21, 271, 281, 372
force 273
gravity 271
melt 227, 269, 349
powder, *see* Solids conveying
preheating, *see* Preheating of feed
pressure, effect of 273, 275
rubber 23, 176, 272
scrap 176–7, 271, 272, 372, 387, 398
segregation 21, 164, 271, 272, 281, 372

Feeding *contd*
starve 273, 370
temperature, effect of 271–2, 287
see also Solids conveying
Feed-pocket 23, 176, 271–2
air trapping, *see* Air trapping
cooling 175, 226, 271, 276
design 175, **176**, 271–2, 276
heating 269
Fibres, *see* Product types
Filling, partial of screw channel, *see* Channel, partial filling
Film, *see* Product types
Filtering 13, 15, 22, *297*, *307–10*, 395
see also Contamination; Die, breaker plate
Flat film, *see* Product types
Flat sheet, *see* Product types
Flight clearance 19, 49, 129, 140–2, 353, 365
power in 237, 248–51, **261**, **262**, 279–80, 356, 373
temperature variations in 237, 250, 458–66
Flow
behaviour 27–32
capillary 33–4
combined (pressure and drag) 135, 139–40, 167–8, 243
defects 9, 17–18, 50, 353, 354
see also Die, defects (flow)
dimensionless, *see* Output, dimensionless
drag 4, 9, 132–3, 151, **262**
equations, *see* Equations for flow
extensional 27, 47–8, 52–3, 70, 74–6, 114
fluctuations (with time) 127, 166–7, 367, 372
in infinite slit 36
isothermal 60, 156–7, **158**
approximation 167–73, 376
leakage 19, 140–1, 174
power in 230, 237, 248–51, *260*, 279–80, 356
temperature variations in 237, 248–51
in twin-screw, *see* Twin-screw
variables 141–2
melt, *see* Melt flow
in melting, *see* Melting rate
Newtonian, *see* Newtonian flow
non-isothermal, *see* Non-isothermal flow
non-Newtonian, *see* Pseudoplastic flow
index, *see* Pseudoplasticity index
patterns **137**, **138**, **140**
pressure 33–40, 133–4, 164–5, 167–8
properties 29–32, 51–2, 372, 373, 399–400
pseudoplastic, *see* Pseudoplastic flow
index, *see* Pseudoplasticity index
rate 6, 35–7, *38*, 39–40, 127, 135
of solids, *see* Solids conveying
stability in melting, *see* Stability in melting
transverse, *see* Transverse flow
see also Measurement; Properties; Shear rate; Viscosity
Fluctuations with time, *see* Flow; Material flow; Output; Pressure; Speed; Temperature
Foams, *see* Product types
Force feeding, *see* Feeding, force
Forces in solids conveying and melting, *see* Delay zone; Melting forces; Solids conveying, forces in
Fourier number (transient conduction) 460
Functions of the single-screw extruder, *see* Single-screw extruder

Gaps between screws, *see* Twin-screw, gap areas
Gear pump 15
combination with extruder 424–6
Gearing 376, 427–8
Gelation of PVC 187–8
'Gel point', *see* Melt length, effective
Grade of polymer 32, 51–2, 254, 288–9, 387–8
changing 387–8
Gradient, temperature, *see* Temperature gradients
Graetz number 61, 408, 441, 459
Granulators 398
cleaning, *see* Cleaning
safety of, *see* Safety of granulators
Graphical representation
energy balance **253–8**, **265**, **266**, **268**
output/pressure/speed **152**, **155**, **158**, **424**, **425**
see also Characteristics
Grooved feed bush, *see* Feed, grooved bush

Haul-off, *see* Post-extrusion operations
Hazards 389, *390*
  burns *385–6*, *390*, 392, 393
  contamination 387–8, 397–8
  decomposition *385–6*, 389, 391–2, 394, 397
  electric shock *390*, 392, 393, 398
  excess pressure *385–6*, 387, *390*, 391
  fire *390*, 394, 397–8
  leakage *390*
  powders *390*, 397–8
  static electricity *390*, 397–8
  see also Safety
Heat
  balance, *see* Energy balance
  from/to barrel 356
  capacity of barrel 360, 429
  conduction, *see* Conduction
  content (enthalpy) 227, 233, 253, 278–9
  of crystallisation 54
  flow 56–7
    in barrel 241–2, 248–51, 276–7, 279–80, 284–7, 355
    in melt pumping section 236–42, *238–9*, **240**
    in screw 240–1, 281, *444*
  flux 57
  history 372
    in melting 185, 187–8, 188
  losses 228, 233, 256, 400–1
  radiation 59
  from/to screw 356
  specific, *see* Specific heat
  transfer 59, 60–2
    coefficient *56*, 58–9, 60–1
    through barrel 277–80, 355–6
    in channel (radial) *456*
    from heaters 440
    non-isothermal 60–2
    to polymer 440–2
    to screw 281, 356, 443–7
    to solid bed 211, 212, 213, 215
  see also Conduction; Thermal conductivity; Thermal degradation; Thermal diffusivity; Thermal properties
Heater(s)
  energy 226–7, 278–9
    change with temperature 430
  handling 393
  induction 241, 256, 430
Heating 60, 226–7, 278–9
  barrel 173, 205–6, 224, 241–2, 278–9, 284–7, 356
  in die 67–8, 79–80, 102, *390*
  of feed, *see* Preheating of feed
  of feed-pocket, *see* Feed-pocket heating
  shear (viscous), *see* Shear heating
  space 226
  at start-up, *see* Start-up
Hollow sections, *see* Product types
Hopper, *see* Feed hopper
Hot feeding, *see* Feeding, melt; Preheating

Individual machine 399
Injection moulding 6, 24, 350, 371, 374–5
Input, *see* Feed; Heater; Power
Instruments 165, 364, 369, 384, 399
  pressure 368
  temperature 358–9, 402
  viscosity 51–3
Insulation, longitudinal 287, 358
Internal energy, *see* Heat content (enthalpy)
Internal melt mixer, *see* Mixing, internal melt mixer
Isothermal flow, *see* Flow, isothermal
Isothermal power, *see* Power consumption, isothermal

Leakage flow, *see* Flow, leakage
Length, effective melt, *see* Melt length, effective
Limiting factors 352–3
Limits, *see* Control of speed; Control of temperature; Drive motor load; Output limit for quality; Pressure maximum; Quality of product; Speed fluctuations
Lips, *see* Die lips
Longitudinal conduction, *see* Conduction; Insulation; Mixing; Temperature gradients
Losses, *see* Drive motor; Energy; Heat; Scrap

Machine
  comparison of types, *see* Types of machine, comparison of
  individual, *see* Individual machine
  single-screw, *see* Single-screw extruder

Machine *contd*
twin-screw, *see* Twin-screw
variables, *see* Operational strategies; Operational variables
Material flow 128–9, 271–2
fluctuations (time) 127, 166–7, 366–7, 372
see also Feeding; Flow; Output
Mean temperature difference 60–1, 440–1
Measurement, *see* Experimental determination; Melt temperature; Pressure; Speed
Mechanical construction 1, 348
Mechanical power, input, *see* Power consumption
Mechanism of solids conveying, *see* Solids conveying
see also Analysis
Melt
blending 21
elasticity, *see* Elastic effects
feeding, *see* Feeding, melt
film 182, 277, 279–80
in delay zone 205–6
in melting zone 210
thickness 213
flow 127–8
fracture 9, 18, 50, 52, 291, 354
see also Elastic effects
length, effective 148, 149, 155, 269, 291–2, 294, 360–2
variation 165–7, 231, 233, 358, 360–1, 403
effect on energy balance 252–3, **253**
mixing, *see* Mixing
pool (stream) 178, 180, 183–4, 273–4, 277, 360
cross-section **181**, 210
width 180, 183, 186
properties, *see* Elastic effects; Experimental determination; Variations; Viscosity
pumping
effective length, *see* Melt length, effective
equations for, *see* Equations for flow
heat flows 236–42, *238–9*
temperature 231–2, 254, 287–8, *298–300*, *301–3*, 353, 358, *367*
measurement 165, 232, 358, 368–9
viscosity 21, 29–32, 51–3, 288–9, 372–6
in screw channel 167–9, 232, 235, *260*, **261**, **262**
Melt Flow Rate 10, 22, 52, 289, 387, 400
Melting 128, 283–4, *311–2*, 377
after bed break-up 165, 277–8, 284, 354–5,
channel depth changes, effect of 183–4, 217, 220–2, **223**
delay zone *see* Delay zone
forces, transverse 188
mechanism 178, 187–8, 273–4, 287–8, 357
melt film, *see* Melt film
mixing in, *see* Mixing in melting
point, *see* Melting temperature
powder 277
power consumption, *see* Power consumption in melting
pressure, effect of 275
pressure rise in melting, *see* Pressure profile in melting
process 273–4, 277–8, 279, 361–2, 403
description 179–89, **181**, **186**
experimental, *see* Experimental determination
improvement *311–12*, 362, 403
length 178, 188, 211, 216, 219, **221**, 222
solid bed, effect of 179
speed, effect of **187**, 198, 216, **219**, 219–20
temperature at interface, *see* Temperature at interface
see also Experimental determination
rate 182, 211, 213, 216, 217, 224
region 130
residence time distribution (RTD) in, *see* Time, residence
screw cooling, effect of 183
of solid bed, *see* Solid bed
temperature (crystalline) 54, 290, 405, *406*
transverse flow, *see* Transverse flow in melting
velocities in
flight clearance 188
melt film 182, 211, 213
melt pool 182, 183, 184–5
solid, bed 182, 211
Mesh, *see* Product types

Metering section, *see* Melt pumping
Mixing 5, 18, 19–21, 62–4
  continuous mixer 350
  dispersive 4, 19, 64
    in single-screw 128, 281–2, 349–50, 353, 365
    in twin-screw 354, 366
  distribution 349
  distributive 4, 19, 63
    in single-screw 281–2, 291–2, 350, 353, 365, 377
    in twin-screw 354, 366
  improvement *313–14*
  'intensive' powder mixer 20, 350
  internal melt mixer 21, 349
  longitudinal 281–2, 357
  in melting 188–9, 281
  pressure, effect of 282
  radial 247, 277–82, 365–6
  scale of 19, 282, 350, 353
  in single-screw 128, 281–2, *313–14*, 377
  in twin-screw, *see* Twin-screw
  units, *see* Units
Modelling 353, 371, 373–6, 404
Modulus of elasticity 27
Molecular weight 21, 288–9
  effect on fluctuations 372
  effect on power 254
Molecular weight distribution 21, 22, 23, 290, 373
  effect on operation 372
Monofilaments, *see* Product types
Motor, *see* Drive motor
Moulding
  blow, *see* Blow moulding
  injection, *see* Injection moulding
Multilayer extrusion, *see* Product types

Navier–Stokes equation 413
Netting, *see* Product types
Newtonian
  approximation for flow 131, 156, 229, 376–7
  flow 29, 33–7, *38*
  power 229, 380–1
  viscosity 29, **30**
Non-isothermal
  corrections 127, 173, 235, 236
  flow 59–60, 173–4, 235
  heat transfer, *see* Heat transfer, non-isothermal
  power 235, 236
  shear rate **55**, 60
Non-Newtonian flow, *see* Pseudoplastic flow
Nusselt number 61, 441, *442*

Objectives 1
  operational changes to achieve 295, *296–314*
Operating conditions 352, 363–4, 372, *374–5*, 384, 391
  changes to achieve objectives 295, *296–314*
  transients from changes 352, 363–4, 371, 391
Operation 270, 282
  adiabatic 255, 258
  autogenous 255, 258
  continuous 6, 19, 350, 384
  molecular weight distribution, effect of 372
  as part of a total process 352
  practical 384
  of single-screw, *see* Single-screw extruder
  steady 271, 352, 384
  of twin-screw, *see* Twin-screw
  viscosity, effect of 372
Operational strategies 4, 76–7, 119–26, 282, 295, *296–314*
Operational variables 282
Orientation 12, 14, 17–18, 50, 353
  see also Post-extrusion operations
Output 135, *296*
  corrections 127, 164–7, 167–73, 173–4
  dimensionless (Q/Wbh) 135–7, 143, 146–8, 149–50, 156, *171*
    applications of 286, 377, 399
  dimensions, effect of 142–3, *252*, *378–9*
  equations, *see* Equations for output
  fluctuations (with time) 127, 166–7, 367, 372
  limit for quality 352–3, 402
  measurement of 368, 430–1
  output/pressure diagrams **155**, **156**, **158**, 423, **424**
  output/pressure stability, *see* Stability, output/pressure
  pressure, effect of 127–8, **155**, **156**, **158**
  with screw/die combinations 151–6, **158**, 171–2
  speed, effect of 151, **152**, 153–4, **155**, 252, 378–9

Output *contd*
temperature, effect of 285–6, 367
viscosity, effect of 143, 168, **169**, **174**
see also Flow; Pressure; Speed; Viscosity
Overall performance, *see* Performance, overall

Paper coating, *see* Product types
Parallel screw, *see* Screw, constant depth; Screw, stepped
Partial filling of screw channel, *see* Channel (screw), partial filling
Performance
overall 270, 352, 371
variables, effect on 2, 376–7
Pigments, *see* Colour (pigments)
Pipe, *see* Product types
Polymer
changing 387–8
for extrusion, *see* Thermoplastics
properties 51–3, 54–5, *56*, 288–91, 405
effect on operation 289–91, 372
see also Experimental determination
types 5
Polymer Supply and Characterisation Centre (PSCC) 410
Polymerisation 5, 23
Post-extrusion operations 2–3, 67, 278
annealing 76
calibration/sizing 7–8, 17, 68, 73, 74
computer simulation 92–5
cooling 68, 73, 75, 76, 81–2, 84, 102
cutting 73
drawdown 7, 12–13, 14, 15, 278
in relation to die 73, 74, 92, 97, 102, 115, 121
effects
die swell, *see* Die, material rheology
distortion 73, 102
neck-in 102
residual stress, *see* Product properties
shrinkage 97
slump (gravity) 74–6
haul-off 7–18, 73, 372, 391
Powder, *see* Feeding; Melting; Seals; Solids conveying
Power 225, 229–30, 401
consumption (input) 226, 229–30, 231, *304–6*, 380–1
calculation, temperature for 232
in channel 230, 234, 253–9, 283–90, *296–314*, 380–1
cooling, effect of 279–81
depth, effect of 231, 234, 292–4
dimensions, effect of *252*
equations, *see* Equations for power
over flight 230, 235, 237, 248–51, 259–60, 279–80, 289, 356
isothermal 229, 235
in melting 223, 231
pressure, effect of 234, 235–6, 260–3, *260*
speed, effect of 234, 235, 256–9, 289, 401
see also Energy, mechanical
law 30–2, *38*, 39–40
measurement, *see* Experimental determination
molecular weight, effect of 234
Newtonian, *see* Newtonian power
non-isothermal, *see* Non-isothermal power
pseudoplastic, *see* Pseudoplastic flow, power in
specific 225, 251–60, *252*, *301–14*, 380–3, 401
temperature, effect of 234, 254, **256**
Practical extrusion processes, *see* Extrusion processes
Practical operation, *see* Operation, practical
Prandtl number *56*, 407
Preheating of feed 216, 220, 227, 276, 290
Pressure 33, 133–4, 275–6, *297*
back 4, 8, 284
energy 227, 278, *390*
energy balance, effect on 263–5, **265**, 284
in feed 175, 181, 201–4, **204**, 272, 275
flow, *see* Flow, pressure
fluctuation (with time) at die 127, 276, 361–2, 367, 387
gradient 34–9, 291, 377
maximum 150
in screw 135–6, **137**, 143–50, 168–71
effect on shear heating 245
maximum 136, 145, 149–50
measurement, *see* Experimental determination
melting, effect on 275–6
mixing, effect on 282
power, effect on 235–6, 260–3, **261**, 284

pressure/output diagrams **155**, **156**, **158**, **424**
pressure/output stability, *see* Stability, output/pressure
profile 127
longitudinal 144–50, **145**, **147**, **149**, 165, **170**, 172
in melting 186–7, **187**, 190, 220, **221**
in venting, *see* Venting, pressure profile in
speed, effect of 289, 424–5
venting, effect on 161, 163
viscosity, effect on 33
Principles
energy balance 225–6
of single-screw 128
of twin-screw, *see* Twin-screw
Procedures, safe, *see* Safety procedures
Process(es)
control 76, 79–80, 81–2, 402
see also Control
control for specific, *see* Control for specific processes
fault-finding *385–6*
modelling 404
practical, *see* Extrusion processes
requirements 1, 4, 25, 26, 352, 371, *374–5*
non-shaping 19
shaping 6
subsidiary 3
total 2, 352
Product 2
dimensions, *see* Die materials rheology, die swell; Post-extrusion operations; Product shape
properties 290, 353–4, 372, 391
residual stress 68, 76, 84, 92
in specific products 9–10, 14, 15, 17–18, 21–2, 24
quality, *see* Quality of product
range 79, 83–4, 86–7, 88–9, 120
requirements, *see* Process requirements
shape 76–7, 92, 391
distortion 68, 70, 86
multilayer thickness 88, 90
thickness 72, 82–3
thickness variations 126
width 72
surface finish 7–8, 11–12, 17–18, 69, 78, 88, 391
see also Die, flow defects in; Die, material rheology
tolerances 79, 92
types *25*
blown film 16, 80, 103, *123*, 278
cable 9, 86
coating on paper/textiles 14, 83, 158, 264
fibre spinning 15, 367, 424
flat film 12, 82, 105, *123*, 367
flat sheet 10, 82, 105, *123*
foams 18
monofilaments, *see* Product types, fibre spinning
multilayer film/sheet 12, 14, 88
netting/mesh 16
pipes 7, 77, 94, 114, *123*
profiles, hollow 7, 85, 108, *123*
profiles, solid 6, 83, 108
tape 14
tubing 7
wire covering 9, 86
uniformity, *see* Uniformity of product
velocity 81, 86
void formation 87
see also Post-extrusion operations
Profile
pressure, *see* Pressure profile
pressure in venting, *see* Venting, pressure profile in
products, *see* Product types
screw, *see* Screw types
temperature
radial at die, *see* Experimental determination
set, *see* Temperature, set
velocity, *see* Velocity distribution
Properties
energy, *see* Energy properties
feed, *see* Feed properties
flow, *see* Flow properties
melt, determination of, *see* Elastic effects; Experimental determination; Viscosity
polymer, *see* Experimental determination of elastic/viscous properties
product, *see* Product properties; Product shape
thermal, *see* Thermal properties
Protection of metal surfaces 393–6
see also Corrosion; Wear

Pseudoplastic flow **30**, **55**, 60, 167, 289–90, 376, 382
corrections 152–3, 167–73
energy balance, effect on **257**, 259
power in 235–6
shear rate in 168–9
Pseudoplasticity index 21, 32, 289, 373, 400
Pump, gear, *see* Gear pump
Pumping efficiency 5, 227, 350
see also Pressure; Flow
Purging 388, 391–2
see also Cleaning

Quality of product ix, 3, 353, 373, 377, 403–4
definition 353
at die 353, 364, 372, *374–5*, 377, *378–9*, 402–3
screw type, effect of 291–5, 404
see also Product properties
Q/Wbh, *see* Output, dimensionless

Regulation
of drive 362–3, 428–9
self-, of process
Requirements of processes, *see* Process requirements
Residence time, *see* Mixing; Time
Residual strain, *see* Strain, residual
Residual stress, *see* Stress, residual
Restrictor
adjustable 403
bar (ring) 10, 68, 83, 120, 284
Reynolds number 61
Rheology 27
see also Elastic effects; Flow properties; Viscosity
Rubber
extrusion 6, 128, 164, 292, 365
feeding 23, 176, 272

Safety
of compounding machines 398
in dismantling/cleaning 392–6
dust masks 398
ear muffs 398
gloves 393
goggles *390*
of granulators 398
housekeeping 397–8
of operators *390*
procedures 389, 392–3
in shut down 391–2
in start up 389
see also Hazards
Scale of mixing, *see* Mixing, scale of
Scale up of machines 3, 234–5, 376, *378–9*
Scrap 22, 387–8, 397–8
feeding 271, 272, 372, 387, 398
losses 387, 397
recovery 22–3, 387, 397–8
Screen, *see* Filtering
Screw
barrier 20, 178, 295
channel depth, *see* Channel (screw) depth
cleaning and storage 396
constant depth (parallel) 135, 144, 168–9, 230
conveying of solids 128, 145, 179–80, 191–201, 271–3, 360
cooling, *see* Cooling, screw
design 271–5, *294*, 376, 399
double-parallel, *see* Screw, stepped
flight, *see* Flight clearance; Flow, leakage
gap areas between *341*
see also Twin-screw
length 24, 144–5, 163, 291–2
effective, *see* Melt length, effective
nose (tip) 281
output equations, *see* Equations for output
partial filling, *see* Channel (screw), partial filling
power input, *see* Channel (screw), power input
pressure profiles, *see* Pressure profiles
quality, effect on, *see* Quality of product, effect of screw type
removal, *see* Dismantling of screw
sections 130, 292–4
in parallel 157–8
in series 157
for specific processes *294*, *374–5*
speed, *see* Speed
stepped (double parallel) 146–7, 169–71, 293–4, 361–2
effects in melting 179, 209, 290
surface finish, *see* Surface finish
taper 148–50, 169–72, **170**, *171*, 278, 292–4, 362
effects in melting 179, 209, 272–4
velocity in 274–5

taper-parallel 148–50, 418–20
torsional strength 287, 292, 293, 348, 351, 364
twin, *see* Twin-screw
types 291–5, *294*
for venting, *see* Venting, screw types
wear, *see* Wear
Screw/die combinations 127
output 151–7, **158**, 423–6
Seals, powder 271, 273, 395, 396
Sections 2
hollow, *see* Product types
of screw, *see* Screw sections
solid, *see* Product types
Segregation of feed, *see* Feeding, segregation
Set temperature, *see* Temperature, set
shape factor, *see* Corrections, shape factor
Shaping processes 6–25
see also Process requirements
Shear
degradation, *see* Degradation, shear
flow 33, 41
drag flow in screw 133
simple shear 33, 42
heating (viscous) 20, 24, 43, 61, 173
in channel 242–6, **244**, **246**, 356, 366
in die 45, 46, 47, 66, 72, 119, 126
over flight 248–51, *250*, 356
in melting 214, 217, 219–20, 279
history 127, 353, 364, 366, 372, 376
rate 29, 33, 34, *38*, 63, 167–8
apparent 52
capillary 35
drag flow 133
energy balance, effect on 259
equation for, *see* Equation for shear rate
non-isothermal, *see* Non-isothermal shear rate
pseudoplastic, *see* Pseudoplastic shear rate
slit 37
wall 35, 37, *38*, 136, 167–8, *171*, 377
wall, effect of taper 169–70, *171*
strain 29, 63, 364–5, 377
units of, *see* Units
variation 365
stress 29, 33–4, 36, 64, 230, 353, 364
Sheathing, *see* Wire covering
Sheet, flat, *see* Product types
Shut-down
safety in, *see* Safety in shut-down
Simplified theory, *see* Theory, simplified
Single-screw extruder 2
comparison with twin-screw 348, 349
comparison with other machines 348
control 366
energy balance 225, 251, 427
functions 4–6, 19, 127–8, 130
operation 270
output 135
power consumption 230
principles, *see* Principles of single-screw
processes, *see* Extrusion processes
quality, *see* Quality of product
scale-up, *see* Scale-up of machines
stability, *see* Stability, inherent
Sizing, *see* Post-extrusion operations
see also Die adjustment; Die swell
Slit flow, *see* Flow, infinite slit; Shear rate, slit
Solid bed
break-up 178, 180, 183, 191, 355–6
cross section **181**, **210**
heat transfer to, *see* Heat transfer
interface, solid bed/melt
shape 212
temperature 211
re-shaping 179, 183
width 180, 183, **187**, 210, 214, **222**
Solids conveying 128, 175, 177, 272
air trapping, *see* Air trapping
compacted plug 177, 182
description 180
forces in 177, 182, 193–4, **195**, 196–7, 200
granules 175
size and shape, effect of 179
length 196
mechanism 191–201, **199**
powders 175, 208, 272–3
pressure 178, 194–6, **199**, 200–1
rate 178
stability, *see* Stability
surface friction 177, 193–4, 196–7, 200, 207, 210
velocity **184**, 192–3
see also Feed; Feeding
Solid sections, *see* Product types
Solvent cleaning, *see* Cleaning, solvent
Specific energy input, *see* Energy input, (specific); Power, specific
Specific heat 54, *56*, 227, 290–1, **409**
Specific processes, *see* Control for specific processes; Process requirements; Screws for specific processes

Specific volume 54, **407**
Speed 142–3, 283–4, 328, 349, 351, 380–1, *378–9*
  alteration 386, 391
  autogenous 258
  control, *see* Control of speed
  energy balance, effect on 256–9, **257**, 265–9, 283
  fluctuations 127, 363, 367, *374–5*
  haul-off, *see* Post-extrusion operations
  measurement 427
  melting, effect on, *see* Melting process
  output, effect on 151–4, **152**, **155**, 167–8
  power, effect on 235–6, 256–9
  pressure, effect on 424–6
  regulation of drive, *see* Regulation of drive
  stability, *see* Stability, speed
  temperature variations, effect on 165, 284
Spinning, *see* Product types
Stability 291, 359, 377, 467–8
  in condition changes 363–4
  equation for *see* Equations for stability
  inherent 367
  loss of 371
  in melting 178, 179, 183–4, 188, 208
  output/pressure 178, 179, 367, 382
  output/temperature 367
  speed 362–3
  in start-up 363–4
  surging, *see* Surging
Start-up 384, 389
  heating 242, 364
  safety in, *see* Safety in start-up
  stability, *see* Stability in start-up
  transients 363, 391
Steady operation, *see* Operation, steady
Steady-state, *see* Operation, steady
Stepped screw, *see* Screw, stepped
Strain 27, 29, 63, 364–5, 377
  energy 41–6, 242–6
    in capillary 42, 44
    distribution **43**, 62, 242–6
    in elongational flow 45–6
    in screw channel 43–4, **244**, **246**
    in slit 43
  rate 14, 27–9
    elongational 47–8
    see also Shear rate
  recovery 48–9
  residual 353
Strategy 353
  for operation, *see* Operational strategies
  for scale-up, *see* Scale-up of machines
Strength of screw, *see* Screw, torsional strength
Stress 27–30, 33–4, 36, 64
  residual 7, 353
Surface finish
  of barrel 195, 196–7, 207
  in die, *see* Die, mechanical construction
  in product, *see* Product surface finish
  of screw 195
Surface heat transfer, *see* Heat transfer
Surface protection, *see* Protection of metal surfaces
Surging 166–7, 354, 359, 403
  origin 360–2
  in venting 162–3
  see also Stability
Swell ratio, *see* Die, materials rheology

Tape, *see* Product types
Taper
  die, *see* Die, taper
  -parallel screw, *see* Screw, taper-parallel
  screw, *see* Screw, taper
  wall shear rate, effect on, *see* Shear rate, wall
Temperature 276
  adiabatic 255, 377, 382
  autogenous (autothermal) 255, 258, 360
  barrel, *see* Temperature, set
  coefficient of viscosity, *see* Viscosity, temperature coefficient
  control, *see* Control of temperature
  controllers 254, 279, 369–70, 389
    adjustment 360, 387
    stability 364
    time-proportioning 360
  difference 56–9, 60–2, 278, 351
    between flight clearance and channel 356, 458–66
    mean 60
    in melting 277, 279, 355–6, 357–8
    in melt pumping 279, 377, *457*
    in solids conveying 199, 208, **209**

distribution from screw 10–11, 246, 277–8, 282, 284, 287–8, 358–9, 403
feed, effect on, *see* Feeding, temperature, effect of
fluctuations (time) 127, 165, *250*, *307–10*, 362, 366, 372, 404
over flight 248–51, 458–66
in melting 179, 355, 361–2
gradients 56–7
longitudinal 4, 174, 232, 236, 276, 287–8, 357, 364
radial 173, 174, 232, 236, 245–8, 277–8, 355–6, 360
history, *see* Heat history
at interface of solid/melt film 211
measurement, *see* Melt temperature measurement
melt, *see* Melt temperature
in melting, *see* Melting temperature
output, effect on, *see* Output, temperature effect of
for power calculation 232, 236
power, effect on, *see* Power, temperature, effect of
profile **288**, 358–9, 387
in melting 277–8, 279, 287–8, 402
in melt pumping 279–80, 287–8, 369
rise, *see* Temperature difference
set (barrel) 284–5, 287–8, 357–8, 369, 387
in melting 211, 215, 216, 220, **221**, 279–80, 284–5, 287–8, 402
in melt pumping 232, 279–80, 284–5, 287–8, 357
variations (space) 165, 173–4, 280, 356
at die 10, 245–8, 284, 287, *307–10*, 357–8
over flight 248–51, *250*, 279
in injection moulding 24–5
in length (screw) 165, 174
measurement, *see* Experimental determination
from melting 178–9, 277, 354, 360
reduced by transverse flow, *see* Transverse flow
speed, effect of 165, 278, 283–4, 291, 351, 354, 362, 376–7, 382, 402
viscosity, effect on, *see* Viscosity
Theory, simplified 2, 127, 130–1, 152–4, 164, 229, 353, 376
Thermal conduction, *see* Conduction; Heat flow
Thermal conductivity 55, *56*, 291
Thermal degradation, *see* Degradation, thermal
Thermal diffusivity 55, *56*, 407
Thermal properties 54, *56*, 400, 405, *406*
comparison *56*
conversion factors *56*
typical values *56*, 405
Thermocouple
control 369, *385–6*, 389
experimental array 358–9, 402
melt 369
position 232
Pyrotenax 358
Thermoplastics
abbreviations *5*
for extrusion 5
products, *see* Product types
Thrust
bearing 284, 348, 376
load 229, 284, 351
Thyristor
fast cycling 430
phase angle firing 430
speed control 363, 367
Time
fluctuations of temperature, *see* Temperature fluctuations (time)
reaction, for process control 386
residence 5, 10, 20, 47, 82, 282, 291, 377
distribution (RTD) in melting 188, **189**
distribution (RTD) in die 81, 84, 91
Tools, cleaning, *see* Cleaning tools
Torque measurement 369
A.S.E.A. Torductor 428
belt tension 428
reaction 427
strain gauge 427
Torsional strength of screw, *see* Screw, torsional strength
Total process, *see* Process, total
Transient conduction in barrel, *see* Conduction, transient
Transients, from condition changes, *see* Operating conditions, transients
Transverse flow 137–9, 247, 274
in melting 188–9
reducing temperature variations 247, 278, 356
see also Die flow, distribution
Trouble shooting, *see* Fault finding
Tube, *see* Product types

Tubular film (blown), *see* Product types
Twin-screw 2, 5–6, 19–20, 23
  air release 325, 341
  applications *25*, 326–7, 345
  cleaning, self 327, 343
  clearances, mechanical 322, 323, 344
    see also Twin-screw, interference
  comparison of machine types 348–51
  compounding, *see* Twin-screw, mixing
  conduction, *see* Twin-screw, heating
  conjugation 323, 330–1, 337–8
    loss of 327, 330–1, 333, 337–8
  co-rotation 319, 322, 330–7
  counter-rotation 319, 320, 323–30
  definitions 316–18
    conjugation 323
  degradation 327, 328, 345
  degree of filling
    co-rotation 340, 341, 345
    counter-rotation 325–6
  energy balance
    co-rotation 346–7
    counter-rotation 330
  Erdmenger 322, 339
  feeding 325–6, 341
  feed rate 325, 347
    flood 325
    fluctuations 326, 341
  fibre-reinforced polymers 327
  filled length
    co-rotation 331, 342, 343, 344–5, 346–7
    counter-rotation 325, 330
  flight
    clearances, *see* Twin-screw clearances
    dimensions 324–7, 331, 334, 336–7, 340–1
    leakage over, *see* Twin-screw, flow pattern
  flow
    from back pressure 327–8, 340
    between channels of two screws 322, 324, 326–7, 331, 337–8
    over flight tip 333, 343, 344
    in gashed flights 342
    in interrupted flights 327, 329, 340
    in kneading discs 340, 343
    restriction by flight of other screw 320, 322
    in reverse flights 340, 342
    in slotted flights, *see* Twin-screw flow, gashed
    in unflighted sections 340, 342
  flow patterns 325, 338
    in calendar gap 321
    in channel, circumferential 319, 320, 323, 325
    in channel, transverse 319, 325
    through clearance between screws 320–1, 322, 323, 335
    by division within channel 320
    overall, axial in co-rotation 319, 343–4
    overall, axial in counter-rotation 319, 323, 327–8
  forces, lateral on screw 322
  gap(s)
    areas 335–9, 341
    axial between flanks 323
    radial, channel to barrel 325
    radial, flight tip to barrel 343, 344
  heating 326, 341, 346
    length to melt 326
    length to final temperature 326
  interference, mechanical 320, 322, 331–7
    curves 333, 336
  intermeshing, degree of
    full co-rotation 330–8
    full counter-rotation 323–30
    non- 318–19
    partial 320–3
  leakage, *see* Twin-screw, flow patterns
  length, *see* Twin-screw, heating length; Twin-screw, pressure, length, effect on
  mechanical clearances, *see* Twin-screw clearances
  mechanical power 329–30, 345
  mechanism
    of melting 318, 326, 341–2
    of mixing 318, 326–7
    of pumping 318, 327–8
  melting, *see* Twin-screw mechanism
  methods of operation, *see* Twin-screw operation
  mixing
    between channels of two screws 324–5, 338–9, 342
    dispersive 327
    distributive 326, 331, 337
    from division of flow 324, 337,342
    in interrupted flights 327, 329–30, 340
    longitudinal 324

local distributive 325, 342
from relative screw velocity 319, 343
in reverse flights 340, 342
operation 318, 347–8
output capacity
co-rotation 340, 347–8
counter-rotation 325–6, 327–8
output/speed relations 325, 328, 346
partial filling, *see* Twin-screw degree of filling
performance 5–6, 318, 323, 325, 327–8, 336, 339–40, 346
polymerisation 23
power, *see* Twin-screw mechanical power
pressure difference
in calendar gap 321–2, 323
circumferentially in channel 321–2, 322, 328, 344
at die 322
over flight tip 343–4
length, effect on 323, 327–8, 331
output, effect on 340
overall axial 325, 327–8, 343
principles, *see* Twin-screw mechanisms
reclaim 326
residence time 328–9, 331, 345
screw speed, effect of 329, 345
screw
areas, *see* Twin-screw gap areas
channel depth 325, 341
clearances, *see* Twin-screw clearances
conjugation, *see* Twin-screw conjugation
constraints, *see* Twin-screw, interference
degree of filling, *see* Twin-screw, degree of filling
degree of intermeshing, *see* Twin-screw intermeshing
flank 'angle' 333
flight tip width, *see* Twin-screw flight dimensions
gaps, axial and radial, *see* Twin-screw gaps
restriction, *see* Twin-screw flow restriction
rotation, *see* Twin-screw definitions; Twin-screw speed
sections, *see* Twin-screw, sections of screw
speed, *see* Twin-screw speed
velocity, relative, *see* Twin-screw speed
sections of screw
diameter reduction 341
feed 325
flight width variation 325, 331
longitudinal variation 325
mixing 326–7, 342–3
pitch variation 325, 340
starts, number of 327
shear 319, 320
rate 326, 328, 330
speed 325, 329, 330, 345, 347
energy balance, effect on 348
stability 326, 341
trapped air, *see* Twin-screw, air release
temperature, energy balance, effect on 346
velocity, *see* Twin-screw speed
venting 326, 327, 343
wear on flight tips 322, 333, 344
Two stage screw, *see* Screw, stepped
Types of screw, *see* Screw types
Types of machine, comparison of 348–51, *349*

Uniformity
of conditions *25*
of product 19, 353, 371, 372
see also Operating, conditions; Output; Pressure; Temperature
Units 29
conversion factors *56*
of shear strain (mixing) 365
Unmolten material (particles) at die 353–4, 402
see also Die temperature, distribution at; Melting; Mixing; Temperature

Vacuum extraction 22, 158–63, 289, 326–7, 343
die pressure, effect of **160**, 161–2, **162**, 163
pressure profile **159**, **161**, 161–3
see also Venting
Variables
analysis of
output equation 142–3
parallel screw 144–5

Variables *contd*
power equation 233–5
controlled, effect of 282
dependent 4
energy balance, effect on, *see* Energy balance
in leakage flow, *see* Flow, leakage
machine (operational) 283
performance, effect on, *see* Performance, variables effect on
Variations
in feed, *see* Feed variations
in melt properties 372
in pressure with speed, *see* Pressure, effect of speed
in temperature, *see* Temperature variations
see also Output, fluctuations (with time); Pressure, fluctuations (with time)
Velocity
distribution
barrel cooling, effect of 279–80
in capillary 35
in combined flow 136, **137**, 167–9
in drag flow **132**, 133, 164–5
non-isothermal **55**, 60, 173
in pressure flow 35, 37, 136
in pseudoplastic flow 169
in simple shear **33**
in slit 37
mean *38*, 40
in melting, *see* Melting, velocity in
in screw channel 132–3, 354
longitudinal 135–7, 274–5, 357
tapered 275
transverse 139
in solids conveying, *see* Solids conveying
Venting 158–63, 167, 291, 326–7, 343
screw types **159**, 160–3, **161**, 291
see also Vacuum extraction
Viscometer, capillary 52
Viscosity 10, 21, 27, 29–32, *56*, 288–90
apparent 52
changing 387–8
in die 66–7, 68–72, 114
experimental determination, see Experimental determination
extensional 27, 48
matching in multilayer die 14, 90
Newtonian, *see* Newtonian viscosity
operation, effect on 288–90, 373
output, effect on 143, 167
pressure, effect of 33
pseudoplastic 30–2, 69, 167–9, 288–90
shear 29–32
temperature
coefficient of 21, 289, 290
effect of 32, 52, 232, 289–90, 387–8
see also Melt viscosity
Viscous heating (dissipation), *see* Shear heating (viscous)
Viscous history, *see* Shear heating
Vulcanisation, *see* Crosslinking

Wall shear rate, *see* Shear rate, wall
Warm-up, *see* Start up, heating
Waste
heat 225
recovery 397–8
see also Scrap
Wear 129, 141–2
Weissenberg extruder 351
Wire covering, *see* Product types

Yield stress 64